Submitted by:

Applied Science Associates
A member of the RPS Group plc
55 Village Square Drive
South Kingstown, RI 02879 USA
Tel: +1 (401) 789-6224
Fax: +1 (401) 789-1932
www.rpsgroup.com
http://www.asascience.com/

and

Environmental Research Consulting (ERC)
41 Croft Lane
Cortlandt Manor, NY 10567-1160 USA
Tel: +1 (914) 734-7511
www.environmental-research.com

Draft Report

SIMAP Modelling of Hypothetical Oil Spills in the Beaufort Sea for World Wildlife Fund (WWF)

AUTHOR(S): Melanie Schroeder Gearon, Deborah French McCay (Ph.D.), Emily Chaite, Stefanie Zamorski, Danielle Reich, Jill Rowe (RPS ASA); and Dagmar Schmidt-Etkin (Ph.D.) (ERC)

Project Manager: Melanie Schroeder Gearon
mschroeder@asascience.com

PROJECT NUMBER: ASA 13-235

VERSION: *FINAL DRAFT*

DATE: April 17, 2014

CLIENT:

Daniel Slavik,
Canadian Arctic Program, WWF-Canada
dslavik@wwfcanada.org, 867-777-5343

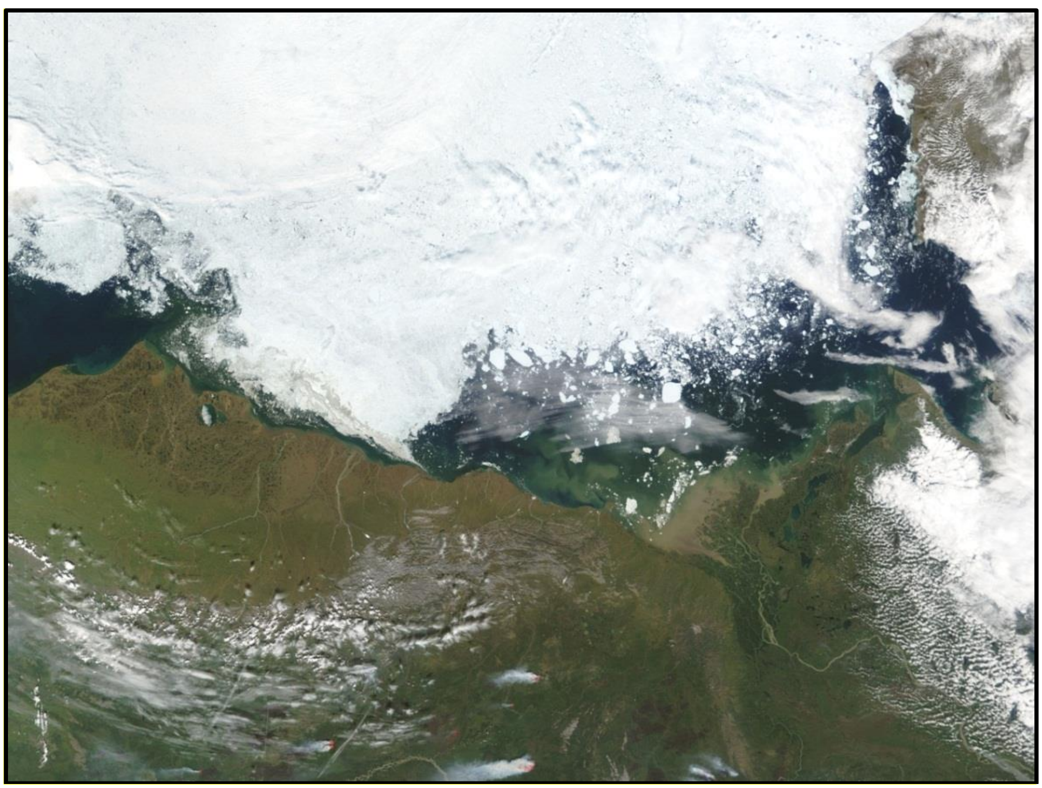

Document Control Form

Title:
"SIMAP Modelling of Hypothetical Oil Spills in the Beaufort Sea for World Wildlife Fund (WWF)"
Location:
Beaufort Sea
ASA Project Number:
13-235 WWF Beaufort Sea
Main Point of Contact:
Melanie Schroeder Gearon
Internal Reviewer(s):
Danielle Reich, Jill Rowe, Deborah French McCay

Release	File Name	Date Submitted	Notes
V1. Draft	13-235_WWF_Beaufort_SIMAP_Modeling_DRAFT_REPORT_Feb24.docx	February 24, 2014	No modelling results, place holders for executive summary/conclusions, submitted for WWF preliminary review, final internal RPS ASA review still necessary.
V2. Draft	13-235_WWF_Beaufort_SIMAP_Modeling_DRAFT_REPORT_Mar21.docx	March 21, 2014	Stochastic modelling results, place holders for executive summary/conclusions, submitted for WWF preliminary review, final internal RPS ASA review still necessary.
V3. Draft	13-235_WWF_Beaufort_SIMAP_Modeling_DRAFT_REPORT_Apr1.docx	April 1, 2014	Stochastic and individual modelling results, submitted for WWF final draft review, final internal RPS ASA review still necessary.
V4. Final	13-235_WWF_Beaufort_SIMAP_Modeling_FINAL_REPORT_Apr17.docx	April 17, 2014	Internal RPS ASA review complete. Changes from V3 submission are tracked in _tracked copy.

Disclaimer

This oil spill modelling report document contains information intended for use and review by the client (WWF,) and is not intended for third party use without prior written consent from the client (WWF). Client understands that modelling is predictive in nature and while this report is based on information from sources that RPS ASA considers reliable, the accuracy and completeness of said information cannot be guaranteed. Therefore, RPS ASA and its directors, agents, assigns, and employees accept no liability for the result of any action taken or not taken on the basis of the information given in this report, nor for any negligent misstatements, errors, and omissions. This study was conducted with consideration of the client's specified objectives and needs. This report is intended to convey only the methodology and results of the study. This report was authored by RPS ASA and does not represent the views of the client (WWF).

Executive Summary

World Wildlife Foundation (WWF), Canada contracted RPS Applied Science Associates, Inc. (dba RPS ASA) to evaluate the extent of hypothetical, generalized oil spills originating in the Canadian Beaufort Sea. The study investigated possible spill events associated with potential increased ship traffic and offshore petroleum exploration and development. The results of the analysis were intended to inform local risk perception, prepare for oil spill response planning, and inform integrated ocean management and planning. The goals of the work included assessing the best available model input data (e.g., currents and winds); projecting the probable behaviour of spilled oil using best modelling practices; and producing modelled output such as statistics (e.g., average length of shoreline oiled, habitat types affected), mass balance graphs, and visual representations (e.g., probability of oiling maps) for various scenarios.

The project involved the analysis of multiple types of oil spill scenarios that could occur in the Beaufort Sea. The goal was to assess the transport, fates, and effects of oil on nearby surface water and shorelines from potential crude, heavy fuel, and light fuel oil spills. Modelling investigated both surface and subsea releases. Four different generalized "spill analyses" were evaluated for this study: a shipping spill analysis in the eastern region of the Beaufort Sea in the Amundsen Gulf; a trans-boundary analysis of various spill types (shipping and pipeline leaks) on the coastal Beaufort Shelf near the U.S./Canadian border; a shallow blowout analysis close to shore on the Beaufort shelf in an area potentially subject to exploratory drilling; and a deep blowout analysis on the Beaufort shelf break in an area potentially subject to exploratory drilling. Each spill analysis consisted of multiple varied scenarios. For the blowout analyses, both worst case discharge (WCD) and maximum most probable discharge (MMPD) volumes were evaluated. For the other analyses, mostly the MMPD was considered. Spills were simulated during both the ice free season (July to October) and throughout the ice season (November to June). Response measures were considered for various events (subsea and surface dispersant application, and *in situ* burning).

Near-field plume dynamics for the subsurface deep blowout scenario were estimated using RPS ASA's OILMAPDeep model. Both stochastic and individual trajectory results were attained for each spill scenario using RPS ASA's Spill Impact Modelling Application (SIMAP). SIMAP results were used to analyze expected far-field surface, shoreline, and water column oil contamination. The stochastic approach sampled the various meteorological and oceanographic conditions in the study area and provided insight into the probable behaviour of the potential oil spills. A stochastic scenario was comprised of many individual trajectories (i.e., 100 trajectories) of the same spill scenario, each run with a different start time, to develop an expectation of risk. Individual or "deterministic" trajectories that were identified as the 95th percentile for degree of surface area and shoreline oiled, or water column contamination were selected from the stochastic ensemble of results. The individual trajectory simulations provided estimates of the oil's fate and transport for a *specific set* of environmental conditions, whereas the stochastic output provided overall probability of oiling extent and travel time given a *wide range* of environmental conditions.

Oil interactions with ice involve several processes that affect transport and fate of the oil. Modelling needs to account for oil interactions with mobile sea ice or immobile landfast ice. When oil interacts with mobile sea ice, some fraction becomes contained (either on top, in, or underneath the ice) and then travels with the ice floe (Drozdowski et al., 2011). To simplify the problem in the model approach, the ice coverage or concentration information provided in the hydrodynamic model was used as an

indicator of whether oil follows the surface currents or the ice currents. Immobile or fixed landfast ice which seasonally extends out from the coast acts as a natural barrier where oil collects. In the model, when oil encountered landfast ice at the surface of the ocean it was assumed to trap along the ice edge and remain immobile until ice retreats. The presence of ice can shelter oil from the wind and waves (Drozdowski et al., 2011). Thus, oil weathering processes in the model such as evaporation and emulsification, and behaviours such as spreading and entrainment were slowed (Spaulding, 1988).

Environmental Conditions, Geographic Location and Environmental Model Input Data

Summarizing a full literature review regarding the environmental conditions and circulation of the Beaufort Sea, ocean circulation is dominated by the anticyclonic motion of the Beaufort Gyre, which results in a westward movement of the near-surface waters. The gyre transports some of the oldest and thickest ice in the Arctic from the region north of the Canadian Archipelago into the Beaufort Sea. The strength of the gyre can fluctuate annually and the ice motion can reverse for short time periods. The average winter drift is typically parallel to the coastline. A major influence on general circulation in this area is a region of high pressure normally located over the Beaufort Sea, known as the Beaufort High. Since 1996, the Beaufort High has become stronger and has enhanced the predominant easterly winds in the Beaufort Sea, with larger increases seen at more offshore locations (Schulze, 2012). On the Beaufort Shelf, wind direction is primarily from the east and west-northwest. Landfast ice, sea ice that forms and remains fixed along a coast, covers the shelf area for four to eight months each year.

Geographic and environmental input data required for modelling include bathymetry, shoreline and shore type, long-term wind and hydrodynamic records, and average temperature/salinity water column profiles. Bathymetry data for the study area were obtained from the General Bathymetric Chart of the Oceans (GEBCO) Digital Atlas (GEBCO, 2009). A habitat grid containing both shore and subtidal habitat types was constructed for the study area and used as an input to the SIMAP modelling system. Mapped shoreline classification data from the “Environmental Atlas for Beaufort Sea Oil Spill Response” (AXYS, 2004) and the National Oceanic and Atmospheric Administration (NOAA) Office of Response and Restoration (OR&R) Environmental Sensitivity Index (ESI) was used to define habitat types. The Canadian and Alaskan Arctic coastline were composed of primarily gravel and sand beaches, and some rocky shore. Areas behind barrier islands, inlets, bays, and coastal estuaries consisted of mud flats, saltmarsh wetlands, and intertidal macroalgal beds. Mapped subtidal marine substrate types (e.g. rock, gravel, sand, silt-mud) were acquired from Audubon Alaska’s “Arctic Marine Synthesis” database. Given the magnitude and volume of the spills modelled, the SIMAP habitat grid had to encompass a very large area.

Wind is one of the primary forcing factors used in surface pollutant modelling (e.g., oil spill simulations) as it is a dominant force in circulation and surface transport. For this study data was obtained from the ERA-40 (ECMWF RE-ANALYSIS) wind model. This model was developed and is operated by the European Center for Medium-range Weather Forecast (ECMWF). This model has global domain coverage with 0.75° resolution. A long-term (April 2008-March 2013) gridded wind data record was extracted from the ECMWF database and used as input to the SIMAP model.

Two datasets were merged (BOEM, Mahoney et al., 2012 and the National Snow and Ice Data Center (NSIDC)) to create monthly average continuous landfast ice coverage polygons for the entire area of interest. Water, ice circulation and coverage data generated from the TOPAZ4 (Towards an Operational Prediction system for the North Atlantic European coastal Zones) hydrodynamic model were used in this modelling study. TOPAZ4 is a coupled ocean-sea ice data assimilation system for the North Atlantic and the Arctic, developed by the Nansen Environmental and Remote Sensing Center (NERSC) and publically available through the Norwegian Meteorological Institute. Daily mean 3-dimensional current speed and direction, surface sea ice drift speed and direction, ice thickness, and ice coverage fraction were acquired for the time period April 2008 – March 2013 and used as input to the SIMAP model. Coastal hydrodynamic features were not well resolved in the TOPAZ4 data including the influence of the Mackenzie River discharge and the eastward flowing shelf counter current. For this study, data defining the vertical structure of the water column, temperature and salinity, were obtained from the publicly available World Ocean Atlas 2001 (WOA01) (Boyer et al., 2004).

Oil Spill Scenarios

RPS ASA, with subcontractor ERC, worked with the client to develop the oil spill scenarios to be investigated in this modelling study. The client requested that four generalized "spill analyses" be conducted: eastern shipping spills; a trans-boundary analysis having multiple spill types; a shallow blowout analysis; and a deep blowout analysis. Each spill analysis consisted of multiple scenarios, varied in some way (e.g., season, oil type, etc.).

ERC reviewed worldwide literature and data on plausible discharge volumes and incident probability for each spill analysis. For blowouts and pipeline leaks, discharge volumes selected for modelling were based on a review of historical blowout and leakage events. For shipping related accidents, discharge volumes were based on a review of vessel types and associated fuel carrying capacities that currently, or are proposed to, operate in Canadian and U.S. Arctic waters.

RPS ASA, with the client, developed modelling assumptions for the study regarding release time frames, model duration, and response measures. Release time frames and model duration for each analysis were based on activity type (e.g., drilling, shipping) and location-specific constraints from environmental conditions such as sea ice cover. Response measures were modelled in the larger deep and shallow blowout analyses only. RPS ASA reviewed proposed O&G project documents and other technical reports addressing potential response options in the Arctic (IORVL, 2013; Sørstrøm et. al., 2010; Potter et. al., 2012; NEB, 2011; SL Ross et. al., 2010; BREA, Trudel, 2012; WWF 2011 comment/critique memorandum of S.L. Ross's Spill Response Gap Study). It was determined that subsea dispersant application (deep blowout only), in situ burning and surface dispersant (surface response) were the most appropriate measures to include for modelled spills in the Arctic. Specific response assumptions and inputs (e.g., plausible amount of response time estimated for Arctic and dispersant and burning efficiency) were based on client-provided memorandums (WWF comments on S.L. Ross's Spill Response Gap Study) and on RPS ASA expert opinion/past experience.

Three representative oil types were examined in the various spill analyses modelled: 1.) a crude oil that either released from an exploratory drill site, from a large tanker, or from a pipeline leak (Alaska North Slope Crude); 2.) a heavy fuel oil utilized by bulk carrier vessels (Intermediate Fuel Oil 380, and 3.) a light fuel oil carried by a re-supply barge (Marine Diesel).

Eastern Shipping Analysis

The eastern shipping release site was located in the Amundsen Gulf, approximately 45 km north of Baillie Island, along the shipping route (Figure ES-1).

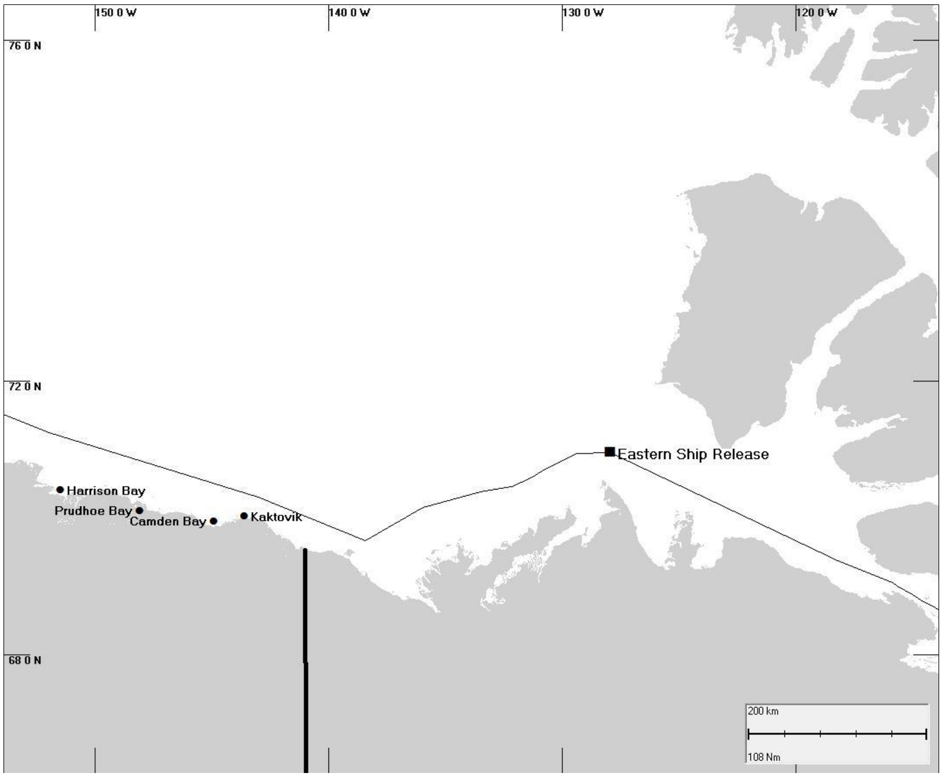

Figure ES-1. Location of the eastern shipping release site in the Amundsen Gulf, along the shipping route (thin black line). Thick black line represents U.S./Canadian border.

The release type simulated was an instantaneous surface release from a shipping accident (e.g., collision, grounding, etc.). The release time frame analysed was the active shipping months (July-October), when the route is relatively ice free. Table ES-1 summarizes the variations or scenarios investigated for the eastern shipping analysis.

Table ES-1. Summary of scenarios simulated for the eastern shipping analysis (2 scenarios total).

Source Type	Release Location	Water Depth (m)	Release Type	Oil Type	Spill Duration (days)	Total Volume (bbl)	Release Time Frame
Bulk Ore Carrier	Amundsen Gulf, shipping route, approx. 45 km N Baillie Island, single point release	40 - 100	Surface MMPD	IFO 380	0.25	21,000	July – October
Resupply Tank Barge	Amundsen Gulf, shipping route, approx. 45 km N Baillie Island, single point release	40 - 100	Surface MMPD	Diesel	0.25	5,400	July – October

Trans-boundary Analysis

The trans-boundary analysis spill locations were on the Beaufort shelf near the U.S./Canadian border (Figure ES-2). Two release regions were investigated and were situated on either side of the border: Canadian Beaufort coast from Herschel Island to east of the U.S./Canadian border, and U.S. Beaufort Coast from Kaktovik to Prudhoe Bay to the west of the U.S./Canadian border.

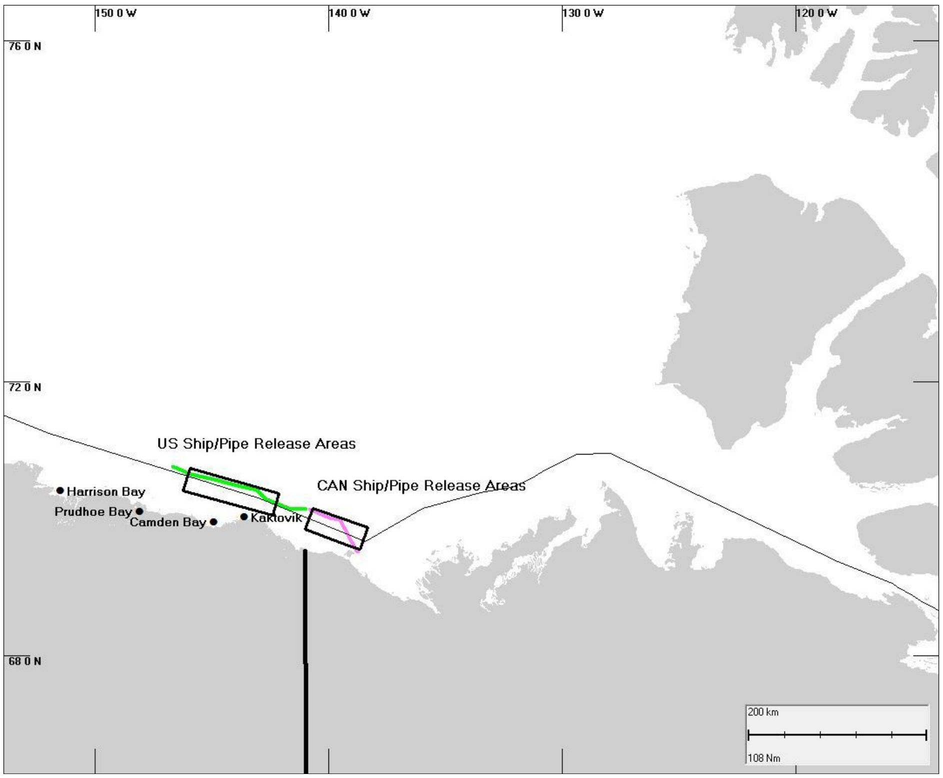

Figure ES-2. Location of the trans-boundary release sites near the U.S./Canadian border (thick black line). Shipping route is indicated by thin black line. Spill release sites associated with shipping incidents were randomly distributed inside each of the black rectangles. Rectangle to the east of the border represented the release region along the Canadian Beaufort coast, and the rectangle to the west of the border represented the release region along the U.S. Beaufort coast. Release sites for spills originating from the pipeline occurred along the coloured lines; pink for the Canadian Beaufort coast, and green for the U.S. Beaufort coast.

Two release types were simulated for the trans-boundary analysis: an instantaneous surface release originating from a shipping accident (e.g., grounding, etc.) and a subsea pipeline leak.

Table ES-2 summarizes the variations or scenarios investigated for the trans-boundary analysis.

Table ES-2. Summary of scenarios simulated for the trans-boundary analysis (6 scenarios total).

Source Type	**Release Location**	**Water Depth (m)**	**Release Type**	**Oil Type**	**Spill Rate (bbl/day)**	**Spill Duration (days)**	**Total Volume (bbl)**	**Release Time Frame**
Bulk Ore Carrrier	Shipping route, Canadian Beaufort coast Herschel Island to US/Can Border	40 - 100	Surface MMPD	IFO 380	NA	0.25	21,000	July - October
Bulker Ore Carrier	Shipping route, US Beaufort coast Kaktovik to Prudhoe Bay	40 - 100	Surface MMPD	IFO 380	NA	0.25	21,000	July - October
Tanker	Shipping route, Canadian Beaufort coast Herschel Island to US/Can Border	40 - 100	Surface WCD	Crude	NA	0.50	533,000	January-December
Tanker	Shipping route, US Beaufort coast Kaktovik to Prudhoe Bay	40 - 100	Surface WCD	Crude	NA	0.50	533,000	January-December
Offshore Pipeline	Pipeline route, Canadian Beaufort coast Herschel Island to US/Can Border	60	Shallow subsurface MMPD	Crude	4,800	6	28,800	May – November
Offshore Pipeline	Pipeline route, US Beaufort coastline from US/Canadian Border Prudhoe Bay	60	Shallow subsurface MMPD	Crude	4,800	6	28,800	May – November

Shallow Blowout Analysis

The shallow blowout release site was located in the Amauligak lease area on the Beaufort shelf (Figure ES-3).

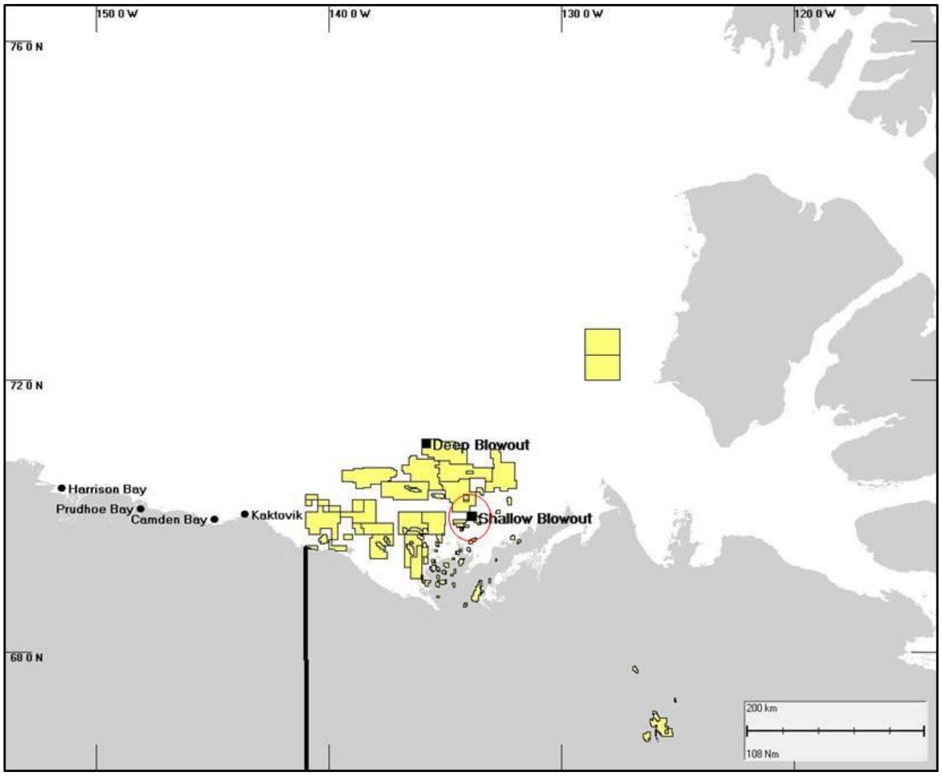

Figure ES-3. Location of the shallow blowout release site (circled in red), in the Amauligak lease area on the Beaufort shelf. Yellow polygons outline all lease areas in Canadian Beaufort. Thick black line represents U.S./Canadian border.

The release type simulated was a shallow-water subsurface well blowout. The release time frames analysed were “Early Operating Season (June-July)” and “Late Operating Season (August-October)”. Table ES-3 summarizes the variations or scenarios investigated for the shallow blowout analysis.

Table ES-3. Summary of scenarios simulated for the shallow blowout analysis (6 scenarios total). *Note: Surface response measures were only simulated in iterations of the 95th percentile trajectory for surface and shoreline from the base case or parent stochastic scenario. Therefore, surface response was not simulated in a full stochastic analysis.

Source Type	Release Location	Water Depth (m)	Release Type	Oil Type	Spill Rate (bbl/day)	Spill Duration (days)	Total Volume (bbl)	Response Measures	Release Time Frame
Well	Amauligak Lease Area	32	Shallow Subsurface WCD	Crude	30,000	60	1,800,000	None	June – July
Well	Amauligak Lease Area	32	Shallow Subsurface WCD	Crude	30,000	60	1,800,000	Surface*	June – July
Well	Amauligak Lease Area	32	Shallow Subsurface WCD	Crude	30,000	90	2,700,000	None	August – October
Well	Amauligak Lease Area	32	Shallow Subsurface WCD	Crude	30,000	90	2,700,000	Surface*	August – October
Well	Amauligak Lease Area	32	Shallow Subsurface MMPD	Crude	3,000	30	90,000	None	June – July
Well	Amauligak Lease Area	32	Shallow Subsurface MMPD	Crude	3,000	60	180,000	None	August – October

Deep Blowout Analysis

The deep blowout release site was located in the deepest portion of what is referred to as the Pokak lease area on the Beaufort slope (Figure ES-4).

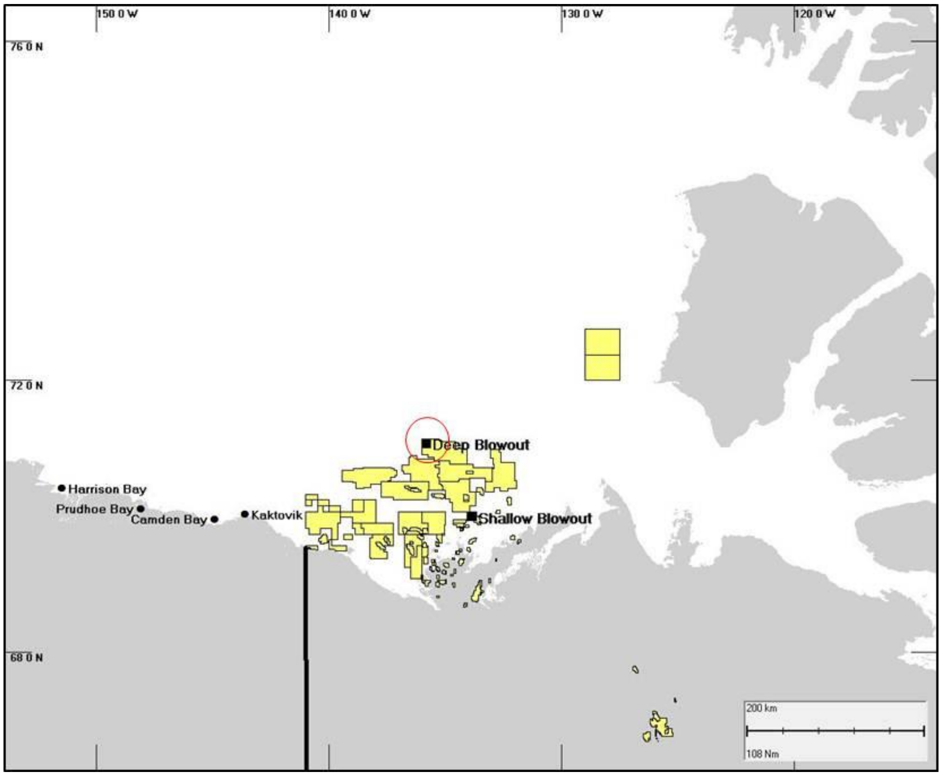

Figure ES-4. Location of the deep blowout release site (circled in red), in the deeper portion of the Pokak lease area on the Beaufort slope. Yellow polygons outline all lease areas in Canadian Beaufort. Thick black line represents U.S./Canadian border.

The release time frames analysed were the same as the shallow blowout analysis; “Early Operating Season (June-July)”, and “Late Operating Season (August-October)”.

ES-4 summarizes the variations or scenarios investigated for the deep blowout analysis.

Table ES-4. Summary of scenarios simulated for the deep blowout analysis (8 scenarios total). *Note: Surface response measures were only simulated in iterations of the 95th percentile trajectories for surface and shoreline from the base case or parent stochastic scenario. Therefore, surface response was not simulated in a full stochastic analysis.

Source Type	Release Location	Water Depth (m)	Release Type	Oil Type	Spill Rate (bbl/day)	Spill Duration (days)	Total Volume (bbl)	Response Measures	Release Time Frame
Well	Pokak Lease Area	1,008	Deep subsurface WCD	ANS Crude	60,000	90	5,400,000	None	June – July
Well	Pokak Lease Area	1,008	Deep subsurface WCD	ANS Crude	60,000	90	5,400,000	Surface*	June – July
Well	Pokak Lease Area	1,008	Deep subsurface WCD	ANS Crude	60,000	90	5,400,000	Subsurface	June – July
Well	Pokak Lease Area	1,008	Deep subsurface WCD	ANS Crude	60,000	120	7,200,000	None	August - October
Well	Pokak Lease Area	1,008	Deep subsurface WCD	ANS Crude	60,000	120	7,200,000	Surface*	August - October
Well	Pokak Lease Area	1,008	Deep subsurface WCD	ANS Crude	60,000	120	7,200,000	Subsurface	August - October
Well	Pokak Lease Area	1,008	Deep subsurface MMPD	ANS Crude	6,000	60	360,000	None	June – July
Well	Pokak Lease Area	1,008	Deep subsurface MMPD	ANS Crude	6,000	90	540,000	None	August - October

<u>Oil Spill Modelling Results and Conclusions</u>

Stochastic footprints from the lower thresholds investigated (surface oil ≥0.01 g/m^2, shoreline oil ≥1 g/m^2) were fairly large for most of the scenarios and suggest that transport of oil over long distances in the region is possible. Stochastic output corresponding to these lower thresholds included surface oil as thin as sheen. Oil weathering processes, including spreading, evaporation, emulsification, entrainment, and volatilization, were slowed as higher ice coverage was encountered. This inherently increased the residence time of oil on the sea surface, which undoubtedly contributed to increased distance traveled while "trapped" in and/or under moving sea ice, even for lower volume spills. In open water conditions where wind heavily influences oil transport and fate, residence time of oil at the surface would be shorter.

The most common surface oiling trajectory pattern observed, for the 5-year (spring 2008-spring 2013) wind and current record at all spill sites evaluated in this region of the Beaufort, was transport to the west along the shelf break with the westward flowing Beaufort Gyre current. This movement pattern coincides with the observed prevailing wind pattern as well (coming from the east, blowing towards the west).

Net sea ice flow followed the prevailing westward surface current near and on the shelf. Many of the spill analyses investigated began in open water conditions (summer) and continued throughout months where ice coverage increased (fall into winter). In most cases oil collected or became trapped in areas of high percent ice coverage in the late fall. Oil was modelled as travelling long distances from the Canadian Beaufort west to the Alaskan coast and Chukchi Sea throughout the entire simulation because of being trapped under high ice cover, which moved westward at a relatively fast rate according to the TOPAZ4 ice current data. However, Sakov et al. (2012) found that modelled ice drift velocities in TOPAZ4, when compared to field data, were generally too fast by approximately 3 km/day. Even so, these results suggest that spills originating from the Canadian Beaufort and resulting coastal oiling could be an international issue.

The spreading of oil on the water surface was limited as ice coverage increased. This was apparent in model output starting in open water and continuing throughout the freeze up. Oil released in open water spread into larger and wider surface slicks than when surfacing in ice. When subsequently encountering high ice coverage, these wider slicks continued to be transported in the ice in a more spread out patchy pattern. Oil that was directly released into high sea ice coverage appeared as long thin continuous and highly concentrated streaks of oil contained in ice floes.

With respect to inter-annual variability, the wind, current, and ice patterns in 2012 were overall somewhat different from other years. A positive shift in the Arctic Oscillation has been reported for the years 2011-2012 (NSIDC), which may in part account for the observed variation. There were some less common trajectories observed that flowed to the north and eastward, and traveled into the channels between the islands in the Canadian archipelago. These trajectories, though less likely, often resulted in high shoreline oiling. Many of the less common eastward and northward trajectories occurred in 2012, although some were also observed in 2009.

Similar to sea ice, landfast ice was least present in the months of August and September. It began to build out from the coast in October, mainly in areas of Mackenzie Bay and along the North Slope up to Point Barrow. Landfast ice growth increased throughout the fall and winter months, peaking in extent from the coastline in March, and began to recede in May. Shoreline oiling was highest in cases that started early in the summer when coastlines were the most free of landfast ice. For cases that continued into or started in the landfast freeze up period, oil coming in contact with this “artificial shoreline” became “entrapped” in the ice.

Eastern Shipping Analysis

Spills of the IFO oil type resulted in greater distance travelled and more extensive shoreline oiling to the west, as compared to spills of diesel. In both cases the areas closest to the spill site, around Bailee Island and the Amundsen Gulf, were affected the most. IFO is a very heavy viscous product that typically does not readily entrain into the water column, doing so only under highly turbulent conditions. In open water, IFO surface slicks may travel long distances. If IFO trajectories encounter ice, such as those occurring in the later months of the active shipping season, this travel time can be extended. Diesel will entrain into the water column much easier than a heavier oil product such as IFO. Highest probabilities of diesel surface oiling were localized around the spill site. Surface and shoreline oiling of the diesel cases was less extensive due to overall lower volume released, the high evaporation associated with light fuel oils, and the tendency of the oil to entrain into the water and disperse. Figure ES-5 shows the stochastic model output for surface oiling probabilities (oil ≥0.01 g/m^2) for spills originating from the Eastern Shipping spill site, bulk ore carrier IFO 380. Note that oil <1 g/m^2 would appear as sheen, scattered pockets of oil under ice, or scattered tarballs.

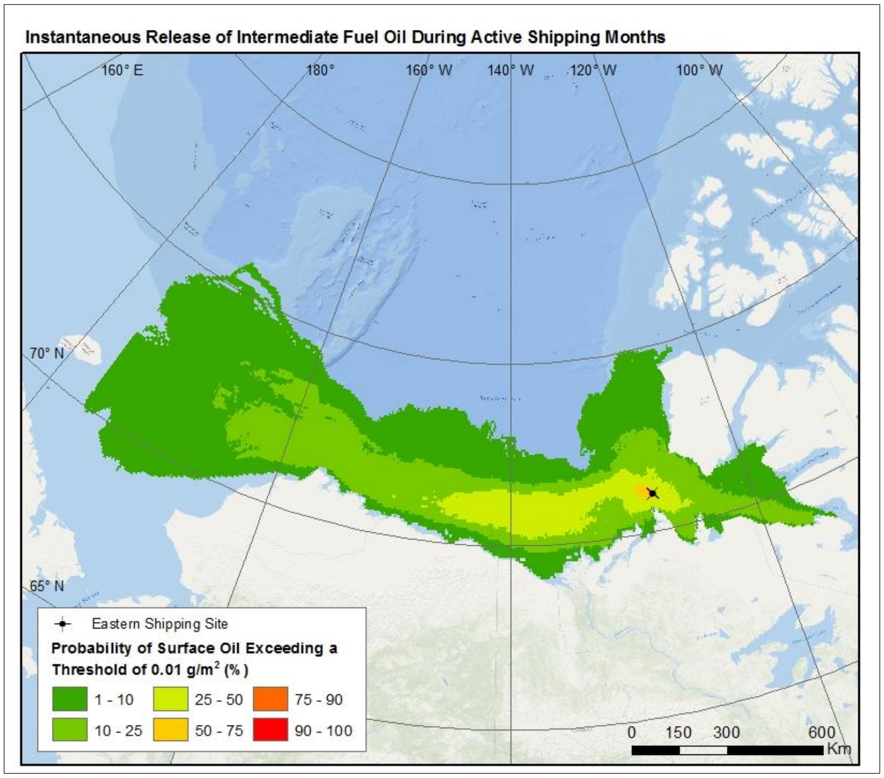

FigureES-5. EastShip_IFO - Water surface oiling probabilities for floating oil ≥0.01 g/m^2. Note: Oil <1 g/m^2, covering much of the affected area, would appear as sheen, scattered oil pockets under ice, or scattered tarballs.

Trans-boundary Analysis

The Trans-boundary analysis confirmed that most oil from spills originating from around the US/Canadian border would travel westward and affect the Alaskan coastline. The results suggested that some eastward movement of oil was possible along the Canadian coast and Mackenzie River Delta, but this would be much less probable than the prevailing westward drift. Regardless of varying release periods and years, the general probability patterns of all scenarios investigated were similar suggesting that the surface current, ice current, and wind regime throughout the year, and between years, exhibited low variability and were relatively consistent. Figure ES-6 shows the stochastic model output for surface oiling probabilities (oil ≥0.01 g/m^2) for spills originating from the Trans-boundary Canadian Shipping spill region, crude tanker.

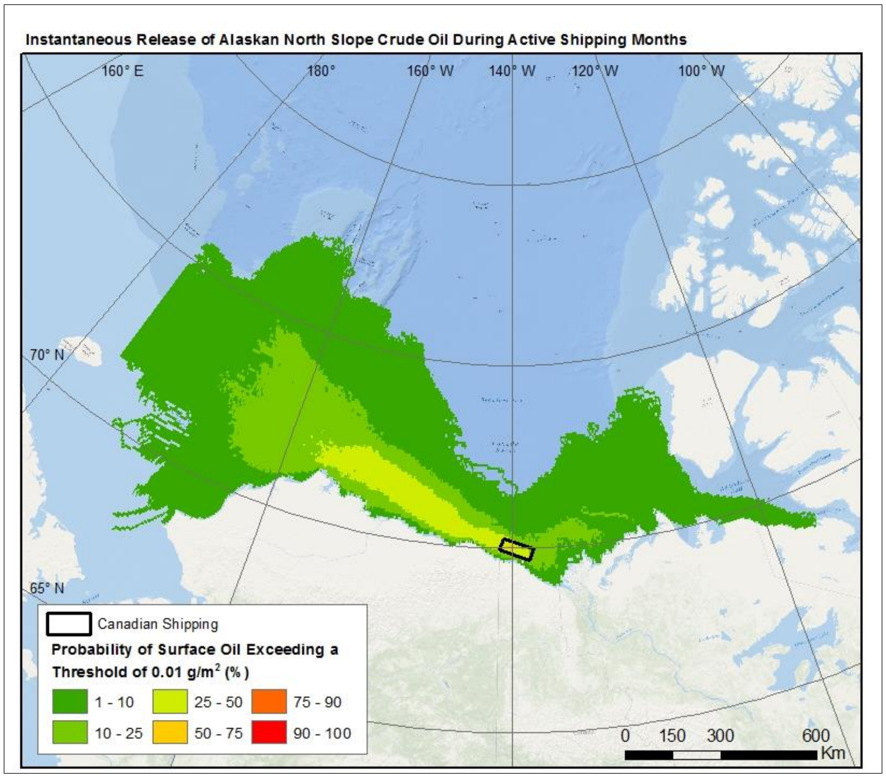

Figure ES-6. TB_Ship_Crude_CAN - Water surface oiling probabilities for floating oil ≥0.01 g/m^2. Note: Oil <1 g/m^2, covering much of the affected area, would appear as sheen, scattered oil pockets under ice, or scattered tarballs.

Shallow Blowout Analysis

Like the other analyses investigated in this study, 60-and 90-day spills from the shallow blowout site primarily travelled westward towards Alaska and into the Chukchi Sea. There were some trajectories (low occurrence) that travelled eastward into the channels of the Canadian archipelago. For all scenarios, some surface oil exited the western boundary of the model domain. Model output appears to be cut-off in a straight line were oil left the boundary (Figure ES-7).

Modelling results suggested that 60-day WCD and 30-day MMPD blowouts originating from the shallow spill site located in the Amauligak lease area, early in the operating season, would result in extensive surface oiling to the west, as far as Point Barrow. There was a high probability that shorelines to the south of the spill site along the Mackenzie River delta, and to the west along the Canadian Beaufort coast up the North Slope would get moderately to heavily oiled. Blowouts occurring later in the operating season (90-day WCD, and 60-day MMPD) would exhibit extensive westward surface oiling, although less extensive to the north as compared to spills spreading for longer periods of time in ice free open water (early season). Late season spills would result in lower shoreline oiling due to landfast ice build-up into the winter months. Persistent water contamination by dissolved aromatics (1-100 ppb) may result from long blowout releases, but these would be relatively localized around the spill site area. Surface response scenarios in the early season showed dramatic differences in surface and shoreline effects as compared to the no response base cases. Late season response cases showed less of a difference as compared to the no response base cases. These differences were primarily driven by the assumed high efficiency of *in situ* burning, as opposed to surface dispersant application. Figure ES-7 shows the stochastic model output for surface oiling probabilities (oil ≥0.01 g/m^2) for spills originating from the Shallow Blowout site, crude shallow blowout, early operating season.

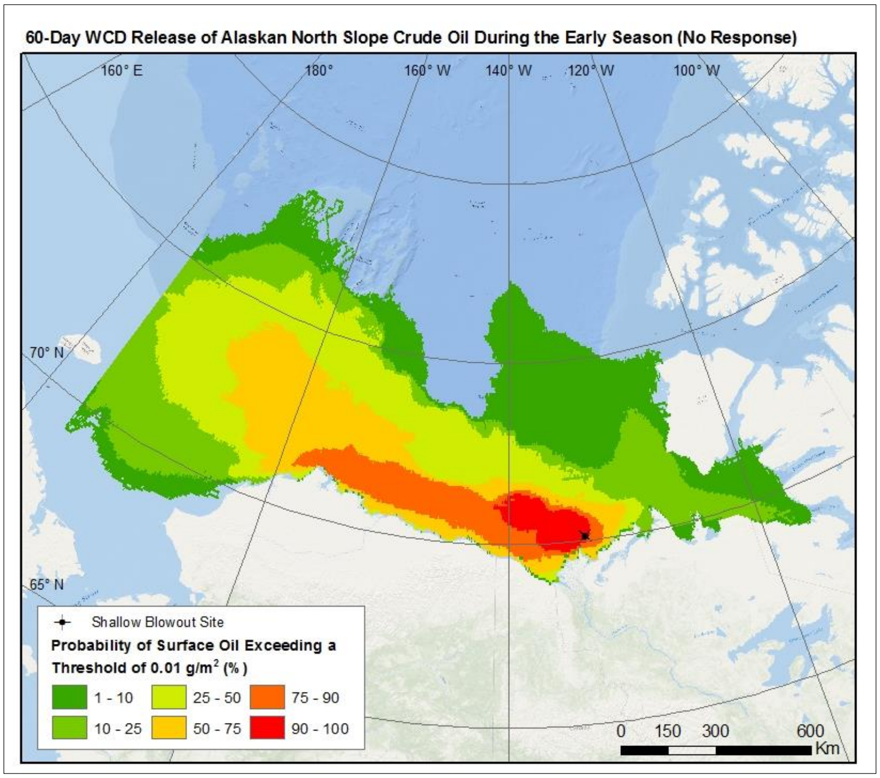

Figure ES-7. ShalWCD_60rel_noresp_early - Water surface oiling probabilities for floating oil ≥0.01 g/m^2. Note: Oil <1 g/m^2, covering much of the affected area, would appear as sheen, scattered oil pockets under ice, or scattered tarballs.

Deep Blowout Analysis

Like the shallow blowout analysis, 90- to 120-day spills from the deep blowout site primarily travelled westward towards Alaska and into the Chukchi Sea. There were some trajectories (low occurrence) that travelled eastward into the channels of the Canadian archipelago. Some trajectories exhibited northward movement before travelling west. The deep blowout site was located just south of a shelf break eddy feature. In several trajectories, oil was initially swept up into this feature and swirled before getting transported to the west (or east, lower occurrence). In general, deep blowout scenarios resulted in higher surface oiling probabilities and slightly higher overall extent as compared to the shallow blowout scenarios. The deeper location allowed for oil to spread in wider slicks that extended to the west, especially during the early season when there was more open water. For all scenarios some surface oil exited the western boundary of the model domain. Model output appears to be cut-off in a straight line were oil left the boundary (Figure ES-8).

Modelling results suggested that 90-day WCD and 60-day MMPD blowouts originating from the deep spill site located in the Pokak lease area, early in the operating season would result in extensive surface oiling to the west, as far as Point Barrow (occasionally further west). There was a high probability that shorelines along the US coast of the North Slope and Point Barrow would become moderately to heavily oiled. Blowouts occurring later in the operating season would exhibit extensive westward surface oiling.

Contamination from later season blowouts would be less extensive to the north when compared to spills spreading for longer periods of time in ice free open water (early season). Late season spills would result in lower shoreline oiling due to landfast ice build-up into the winter months. Persistent water contamination by dissolved aromatics (1-100 ppb) may result from long blowout releases, and could travel far distances from the spill site. If no dispersants are used, oil surfaces within a day and may become trapped in sea ice in the later operating season and winter. Use of subsea dispersants at the deep release site may cause subsurface oil to concentrate at depth along the Beaufort shelf. Figure ES-8 shows the stochastic model output for surface oiling probabilities (oil ≥0.01 g/m^2) for spills originating from the Deep Blowout site, crude deep subsurface blowout, late operating season. Surface response scenarios in the early season showed differences in surface and shoreline effects as compared to the no response base cases. Late season response cases showed less of a difference as compared to the no response base cases. These differences were primarily driven by the assumed high efficiency of *in situ* burning, as opposed to surface dispersant application. Figure ES-9 shows the stochastic model output for subsurface oil concentration probabilities for spills originating from the Deep Blowout site, crude deep subsurface blowout, late operating season, subsurface dispersants.

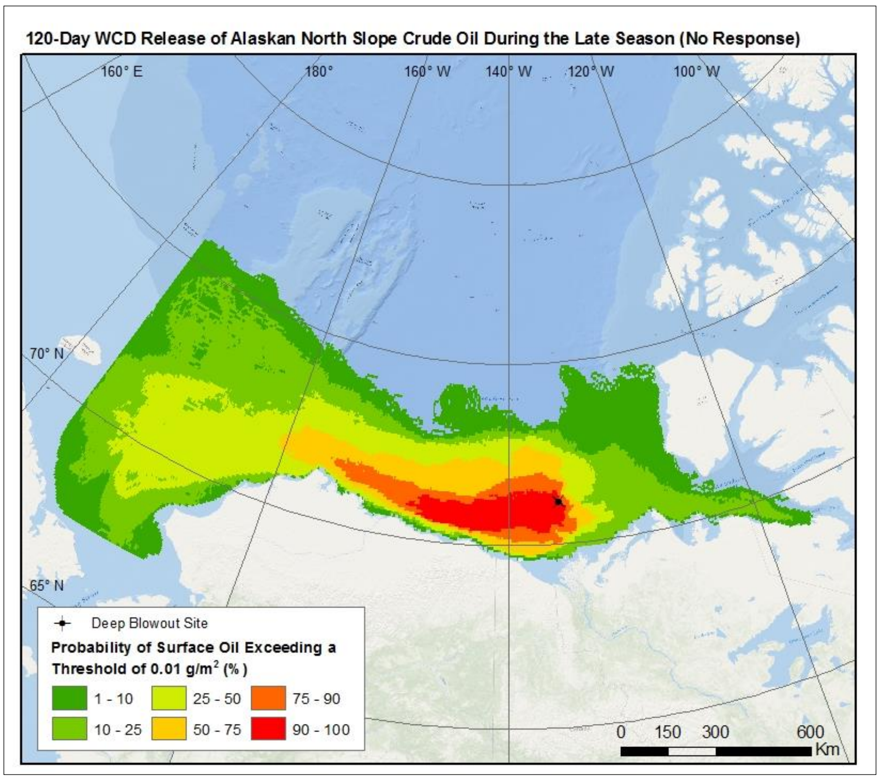

Figure ES-8. DeepWCD_120rel_noresp_late - Water surface oiling probabilities for floating oil ≥0.01 g/m^2. Note: Oil <1 g/m^2, covering much of the affected area, would appear as sheen, scattered oil pockets under ice, or scattered tarballs.

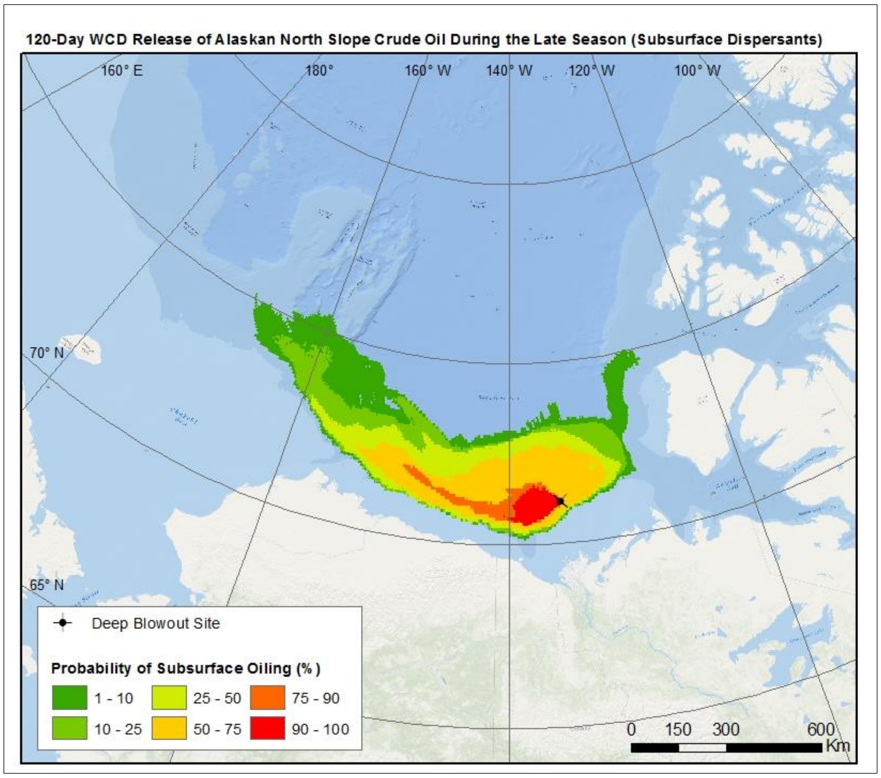

Figure ES-9. DeepWCD_120rel_noresp_late - Subsurface contamination probabilities for total oil in the water column.

Table of Contents

List of Figures

List of Tables

1 Introduction

World Wildlife Foundation (WWF), Canada contracted RPS Applied Science Associates, Inc. (dba RPS ASA) to evaluate the extent of hypothetical, generalized oil spills originating in the Canadian Beaufort Sea (Figure 1). The study investigated possible spill events associated with potential increased ship traffic and offshore petroleum exploration and development. The results of the analysis were intended to inform local risk perception, prepare for oil spill response planning, and inform integrated ocean management and planning. The goals of the work included assessing the best available model input data (e.g., currents and winds); projecting the probable behaviour of spilled oil using best modelling practices; and producing modelled output such as statistics (e.g., average length of shoreline oiled, habitat types affected), mass balance graphs, and visual representations (e.g., probability of oiling maps) for various scenarios.

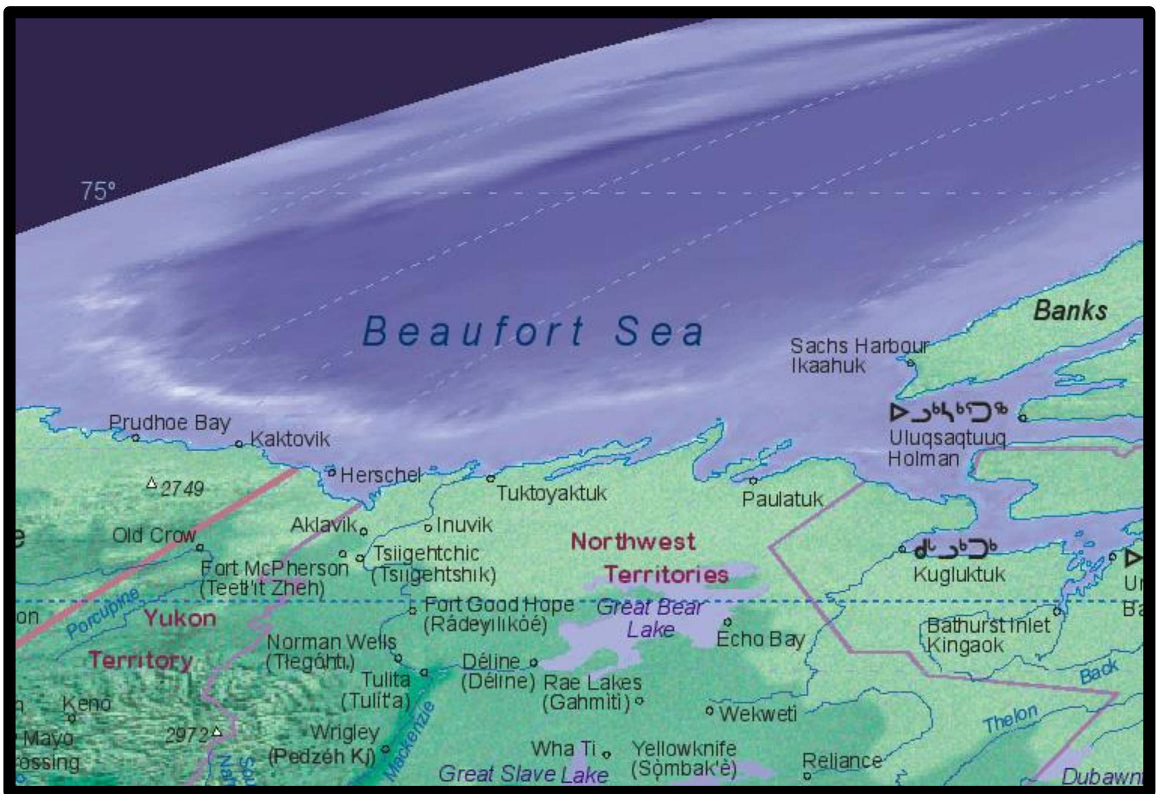

Figure 1. Map of the region of interest for this modelling study, the Canadian Beaufort Sea and coastline.

The project involved the analysis of multiple types of oil spill scenarios that could occur in the Beaufort Sea. The goal was to assess the transport, fates, and effects of oil on nearby surface water and shorelines from potential crude, heavy fuel, and light fuel oil spills. Modelling investigated both surface and subsea releases. RPS ASA and subcontractor Environmental Research Consulting (ERC) worked with the client to develop the suite of spill scenarios to be modelled. The scenario specifications consisted of:

- Spill locations,
- Spill release types,
- Oil types,
- Spill volumes and durations,
- Seasons or time frames, and

- Response actions.

Four different generalized “spill analyses” were evaluated for this study: a shipping spill analysis in the eastern region of the Beaufort Sea in the Amundsen Gulf; a trans-boundary analysis of various spill types (shipping and pipeline leaks) on the coastal Beaufort Shelf near the U.S./Canadian border; a shallow blowout analysis closer to shore on the Beaufort shelf in an area potentially subject to exploratory drilling; and a deep blowout analysis on the Beaufort shelf break in an area potentially subject to exploratory drilling. Each spill analysis consisted of multiple varied scenarios. For the blowout analyses, both worst case discharge (WCD) and maximum most probable discharge (MMPD) volumes were evaluated. For the other analyses, mostly the MMPD was considered. Spills were simulated during both the ice free season (July to October) and throughout the ice season (November to June). Response measures were considered for various events (subsea and surface dispersant application, and *in situ* burning).

This was a comprehensive oil spill trajectory modelling study for the Canadian Arctic, and encompassed the following components, in agreement with those suggested by Drozdowski, et al., (2011):

- A blowout plume model to determine the distribution of the oil in the water column for spills occurring at depth.
- Models for the physical environment (wind, ocean currents, sea ice and waves).
- An oil spill model to address weathering, evaporation, ice-oil interactions, and other details of the oil’s interplay with the environment.

RPS ASA’s data input requirements for this oil spill modelling study included:

- Description of the spill scenarios (e.g., volume and duration of the oil releases);
- Description of the oil properties;
- Geo-referenced shoreline (definition of the land and water boundaries) and classified shore types/habitats;
- Characterization of the winds for the area of interest (long-term wind time series);
- Characterization of the major circulation features of the water body (long-term wind time series);
- Characterization of typical sea ice conditions, and
- Characterization of the vertical structure of the water column.

Near-field plume dynamics for the subsurface deep blowout scenario were estimated using RPS ASA’s OILMAPDeep model. Both stochastic and individual trajectory results were attained for each spill scenario using RPS ASA’s Spill Impact Modelling Application (SIMAP). SIMAP results were used to analyze expected far-field surface, shoreline, and water column oil contamination. The stochastic approach sampled the various meteorological and oceanographic conditions in the study area and provided insight into the probable behaviour of the potential oil spills. A stochastic scenario was comprised of many individual trajectories (i.e., 100 trajectories) of the same spill scenario, each run with a different start time, to develop an expectation of risk. Individual or “deterministic” trajectories that were identified as the 95th percentile for degree of surface area and shoreline oiled, or water column contamination were selected from the stochastic ensemble of results. The individual trajectory simulations provided estimates of the oil’s fate and transport for a *specific set* of environmental conditions, whereas the stochastic output provided overall probability of oiling extent and travel time given a *wide range* of environmental conditions.

This report presents a summary of the modelling methodology (Section 2); the general environmental effects of oil in the marine environment (Section 3); a literature review of the environmental conditions of the Beaufort Sea (Section 4); the environmental and geographic input data utilized for modelling (Section 5), a description of the spill scenarios and oil types (Section 6); and model results and conclusions (Sections 7 & 8). Additional supporting information including a detailed description of the SIMAP and OILMAPDeep modelling system is provided in Appendices A & B. Appendix C (delivered as a separate electronic document file) contains the report compiled by ERC addressing spill volumes, incident types and probabilities. This document outlines and provides the basis for spill scenario modelling inputs. Appendix D provides a full list of the modelled scenarios and provides a key for the scenario naming convention. Appendix E contains figures of stochastic output for the higher set of thresholds examined for surface and shoreline oiling.

2 Oil Spill Fates and Transport Modelling Approach

Model descriptions, modelling approach, methodologies, assumptions, and limitations are summarized in Section 2. OILMAPDeep was used to model near-field plume dynamics for the deep blowout analysis only. The output from OILMAPDeep was used as the initial conditions for the far-field fates and trajectory model (SIMAP). For all other spill analyses, deriving initial conditions from a separate modelling effort was not necessary because releases were either at the surface or at shallow depths. The effects of ice interactions with oil are described in addition to the standard open water fates and transport processes accounted for in the SIMAP model.

2.1 OILMAPDeep Blowout Modelling (Near-field)

To reproduce near-field dynamic and complex processes associated with the deep subsurface blowout scenario (Section 6.5), a near-field analysis using OILMAPDeep was performed prior to simulating the far-field movement of the oil with SIMAP. The objective of this first step in modelling was to characterize the plume mixture (oil, gas and water) discharged from the wellhead blowout (Figure 2). In most blowout cases, the near-field region occurs only within a few hundred meters of the wellhead. The blowout model solved equations for the conservation of water mass, momentum, buoyancy, and gas mass using integral plume theory, following work outlined in McDougall (1978). An additional description of the OILMAPDeep modelling system is provided in Appendix B.

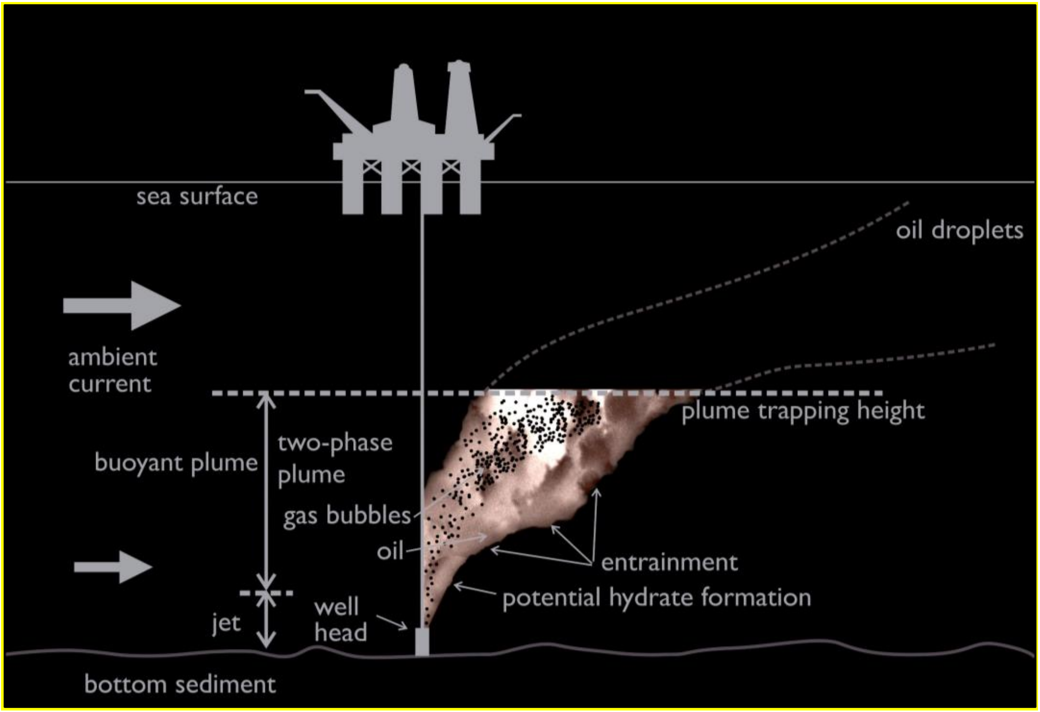

Figure 2. General schematic showing profile and associated dynamics or characteristics of a deep well blowout.

The inputs to the model include flow rate, gas-to-oil ratio (GOR), and aperture or pipe diameter. In cases where subsea dispersant injection was modelled, a dispersant-to-oil ratio (DOR) was applied. For a summary of blowout model inputs used for the study, see Section 7.4.1.

The results of the near-field model provided a description of the behaviour of the blowout plume, its evolution within the water column, and the expected initial dilution (concentration decrease) with distance from the wellhead (seafloor). It provided information about the termination height of the plume and the oil droplet size distribution associated with the release.

The oil droplet size distribution has a profound effect on how oil is transported after the initial plume, as the size dictates how long the oil droplet will remain suspended in the water column. Large droplets will reach the surface faster, potentially generating a floating oil slick that will drift much quicker due to surface winds and currents. Small droplets will remain in the water column longer and be subjected to the subsurface advection-diffusion transport. As the oil is transported by subsurface currents away from the well site, natural dispersion of the oil droplets quickly reduces hydrocarbon component concentrations in the water column, with decreasing concentration at increasing distance away from the well site. However, lower rise velocities of the oil droplets correspond to longer residence times of oil suspended in the water column and thus a larger volume of affected water.

Depending on the environmental conditions near the spill location, there may also be significant degradation (decay) of the oil before surfacing occurs. The oil decay rate is typically higher in warm water environments where biological productivity is high and microbial organisms may play an active role in the breakdown of oil. Thus, if the oil remains in the water column longer, there may be significantly less oil by mass that eventually surfaces.

From a response perspective, a turbulent blowout that results in the formation of very small oil droplets essentially acts as a natural dispersion mechanism, as these smaller size particles effectively keep the oil from surfacing. On the other hand, with large particle sizes, there will be quick surfacing of oil which will limit the subsurface volume exposed to oil, but result in a larger surface oil slick.

The droplet size distribution predicted by OILMAPDeep was calculated based on an estimate of a characteristic diameter (d_{95}) and the Rosin-Rammler distribution. In the absence of dispersant application, the predicted d_{95} was most heavily influenced by the exit velocity of the discharge, which is an indicator of the energy associated with the release. The interfacial tension (IFT) of the oil also affected the droplet size distribution where lower IFT results in smaller droplets. The use of dispersants reduces IFT to values much lower than the range typically associated with untreated oils.

The results obtained in the near-field analysis that were used as initial conditions of the far-field modelling conducted in SIMAP include the:

- location and size of the plume at the termination height, and
- characterization of the oil droplet size distribution.

Section 7.4.1 & 7.4.2 presents the assumptions, model inputs, and results of the blowout modelling for this study.

2.2 SIMAP Stochastic and Individual Trajectory Modelling

RPS ASA's oil spill modelling system, SIMAP (French McCay, 2004 & 2009), was used to determine far-field transport and weathering of the released oil in Beaufort Sea. SIMAP used site specific wind data and current data, and state-of-the-art transport and oil weathering algorithms (Figure 3) to quantify areas swept by floating surface oil of varying thicknesses, fates and concentrations of subsurface oil components (dissolved and particulate), areas of shoreline affected to varying degrees, and areas/volumes where biological effects would occur for habitats and wildlife. SIMAP is a 3-dimensional Lagrangian model, and each component of the spilled oil is represented by an ensemble of independent mathematical particles or "spillets". Each spillet is a sub-set of the total mass spilled and is transported by both currents and surface wind drift. Various response actions can be modelled including oil removal from skimming, burning, or collection booms, and surface and subsurface dispersant application. A detailed description of SIMAP is presented in Appendix A.

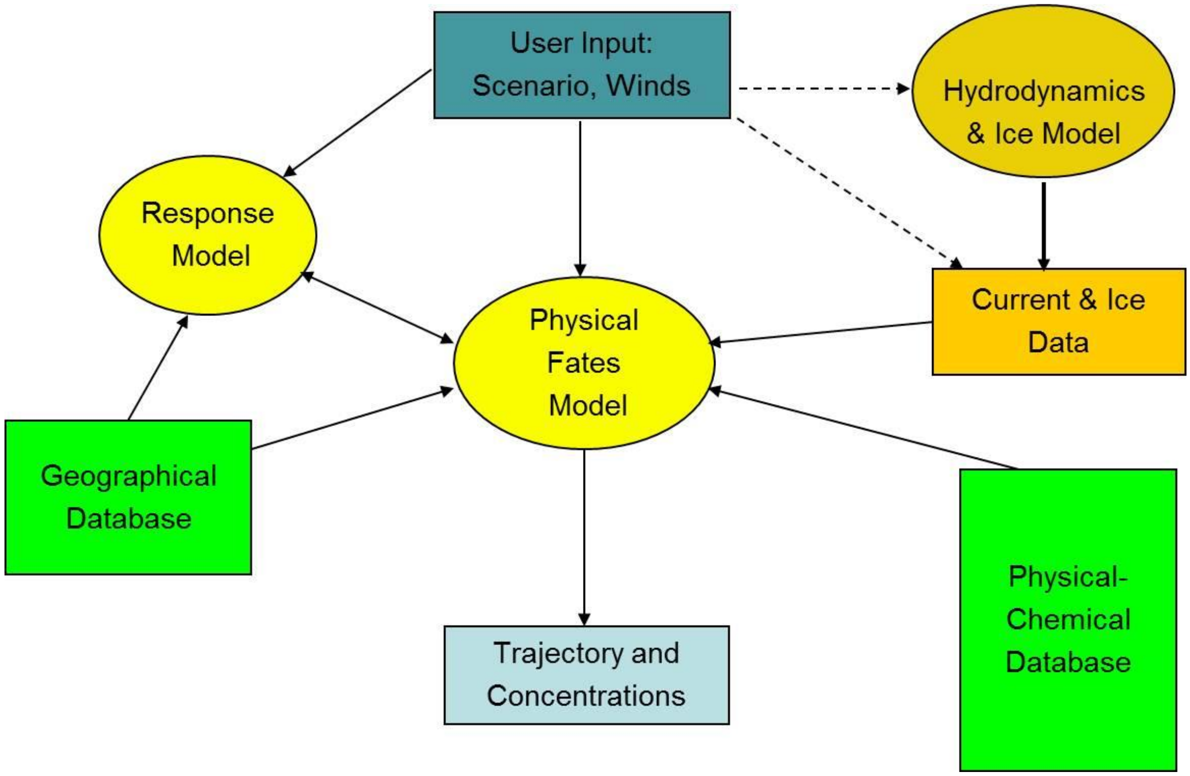

Figure 3. SIMAP Oil Fate model components and inputs flow diagram.

Processes simulated in the SIMAP physical fates model include oil spreading (gravitational and by shearing), evaporation, transport, vertical and horizontal dispersion, emulsification, entrainment (natural and facilitated by dispersant), dissolution, volatilization of dissolved hydrocarbons from the surface water, adherence of oil droplets to suspended sediments, adsorption of soluble and sparingly-soluble aromatics to suspended sediments, sedimentation, and degradation (Figure 4). SIMAP is unique in that it not only models particulate oil content at the surface and in the water column, but it also accounts for the dissolved component. After oil is spilled, soluble polynuclear aromatic hydrocarbons (PAHs) and monoaromatic hydrocarbons (MAHs) may dissolve into the water column potentially causing toxicity. SIMAP calculates the dissolved in-water concentrations and tracks them over time.

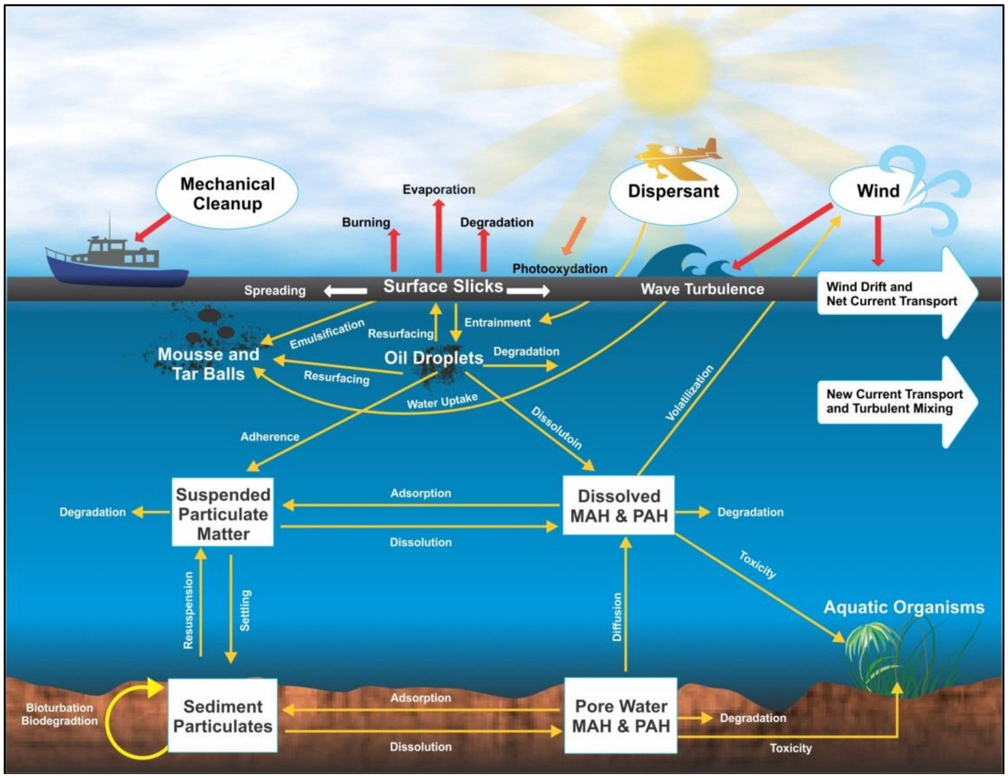

Figure 4. Open water oil fates and behaviour processes simulated in the SIMAP modelling system.

In the first phase of this study, SIMAP's stochastic model was used to determine risks of various resources being oiled. The stochastic analysis was a statistical analysis of results generated from many different individual trajectories of the same spill event (characteristics) with each trajectory having a different spill start time selected at random from a relatively long term window. The random start time allows for the same type of spill to be analyzed under varying conditions. In order to reproduce the natural variability of winds, the model required wind data which can vary both spatially (multiple points) and temporally (changing with time). The favored approach was to use historical observed multiple-year wind record(s) and perform the simulations within the coinciding time period, as this allowed reproduction of the natural variability of the wind direction and speed. Optimally, the minimum time window for stochastic analysis is at least five years, therefore a minimum of five years of observed winds was required.

The stochastic analysis provided two types of information: 1) areas associated with probability of oiling, and 2) the shortest time required for oil to reach any point within the areas predicted to be oiled. The following figures illustrate the stochastic modelling process for a generic example spill scenario. The left panel of Figure 5 shows four individual trajectories predicted by SIMAP for the example scenario. Because these trajectories started on different dates/times, they were exposed to varying environmental conditions, and thus traveled in different directions. To compute the stochastic results, all 100+ individual trajectories (like the four shown) were overlain and the number of times that a given location is reached by different trajectories was used to calculate the probability of oiling for that location. This is shown as the stacked runs in the right panel of Figure 5. The predicted cumulative footprint or area and probabilities of oiling were generated by a statistical analysis of all the individual trajectories. It is important to note that a single trajectory encountered only a relatively small portion of the overall probability footprint. This information was presented for surface oil, shoreline oil, and subsurface oil (Section 7).

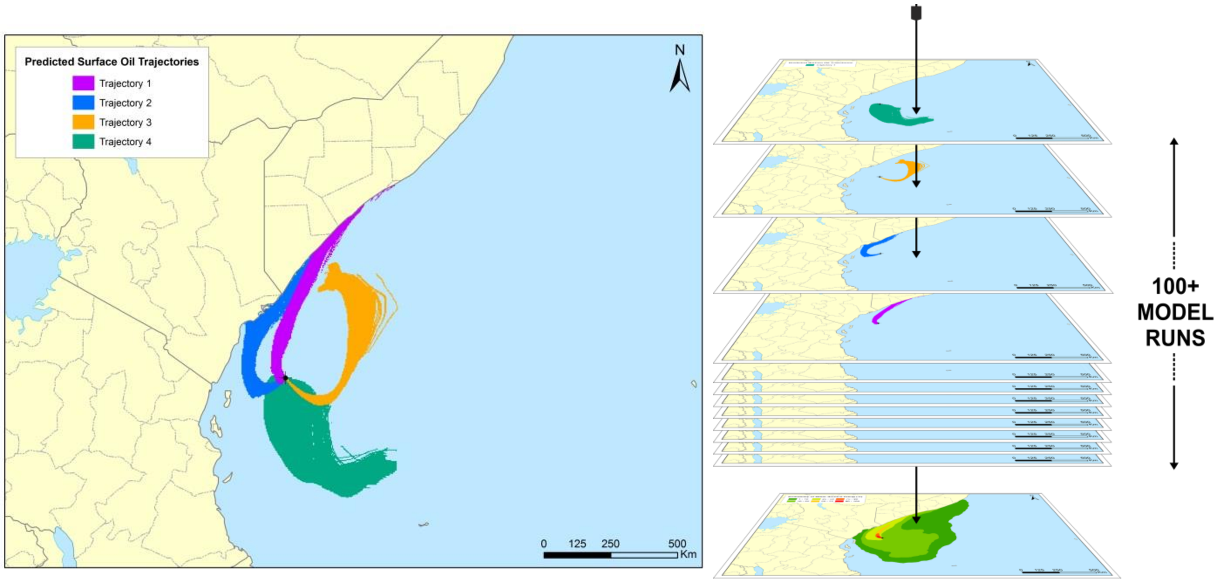

Figure 5. Examples of four individual spill trajectories predicted by SIMAP for a generic spill scenario. All 100+ individual trajectories are overlain (shown as the stacked runs on the right), and the frequency of contact with given locations is used to calculate the probability of being affected during a spill.

The stochastic model is capable of evaluating areas affected and concentrations over a prescribed minimum threshold value. Often these thresholds are based on response requirements or environmental impact assumptions. For this study, the following thresholds were assessed in the stochastic analysis:

- Floating Surface Oil Thickness Threshold: **≥0.01 g/m²**
    - The threshold is for barely visible sheen; oil sheens are generally 0.01-1 g/m^2 on average.
    - Effects on socioeconomic resources (i.e., fishing may be prohibited)
    - French McCay et al. (2011)
- Shoreline Thickness Threshold: **≥1 g/m^2**
    - The threshold represents an oil amount that would appear as a dull brown colour
    - Effects on socioeconomic resources (i.e. need for shoreline cleanup)
    - French McCay et al. (2011)

Stochastic results for the lower thresholds are presented in Section 7 of this report. A second set of higher thresholds, where potential effects on wildlife and shoreline biota may occur, were also analysed.

- Floating Surface Oil Thickness Threshold: **≥10 g/m^2**
    - Dark brown oil
    - Potential effects on ecological resources on the water surface (coating, smothering)
    - French McCay (2009); French McCay et al. (2011)
- Shoreline Thickness Threshold: **≥100 g/m^2**
    - Black Oil
    - Potential effects on ecological resources on the shoreline (coating, smothering)
    - French McCay (2009); French McCay et al. (2011)

Stochastic results for the higher thresholds are presented in Appendix E of this report.

While the stochastic analysis provides insight into the probable behaviour of oil spills given historic wind and current data for the region, it does not provide oil weathering information or mass balance. Therefore, for the second phase of the study, individual 3-D or “deterministic” trajectories were rerun to produce fates and weathering information for particular runs, representative of specific conditions, selected from the stochastic parent scenario. An individual trajectory and fate simulation was performed for each 95th percentile for degree of sea surface and shoreline oiling, and water column contamination as identified in the stochastic analysis.

The results of the deterministic simulations provide a time history of oil weathering over the duration of the spill (mass balance), expressed as the percentage of spilled oil on the water surface, on the shoreline, evaporated, entrained in the water column, and decayed. In addition, times series snapshots of the individual trajectories showing concentration of floating surface oil, shoreline oil, and the concentration of total hydrocarbons in the water column are provided (Section 7).

2.3 Modelling Oil Interactions in Ice

Oil interactions with mobile sea ice or immobile landfast ice involve several processes that affect transport and fate of the oil. If oil is released at or above the water surface, it may spill into water and/or onto the surface of the ice. Oil deposited on ice may absorb into surface snow, run off and become trapped between cracks or in open water fields between floes, and/or become encapsulated in the ice. Oil released into and under water may become trapped under the ice in ridges and keels, or build up along and become trapped in sea or landfast ice edges (Figure 6) (Drozdowski et al., 2011). For more description of landfast ice and sea ice, please refer to Sections 4.4, 5.4.1, and 5.4.2. Many of these interactions and processes are at a finer scale than can be captured in oil spill models using inputs from large scale meteorological, hydrodynamic and coupled ocean-ice models. However, the influence of ice on net transport and fate processes is simulated by considering potential reduction in surface area of the oil and the water in contact with the atmosphere, which changes the wave environment, spreading, movements, volatilization, and mixing.

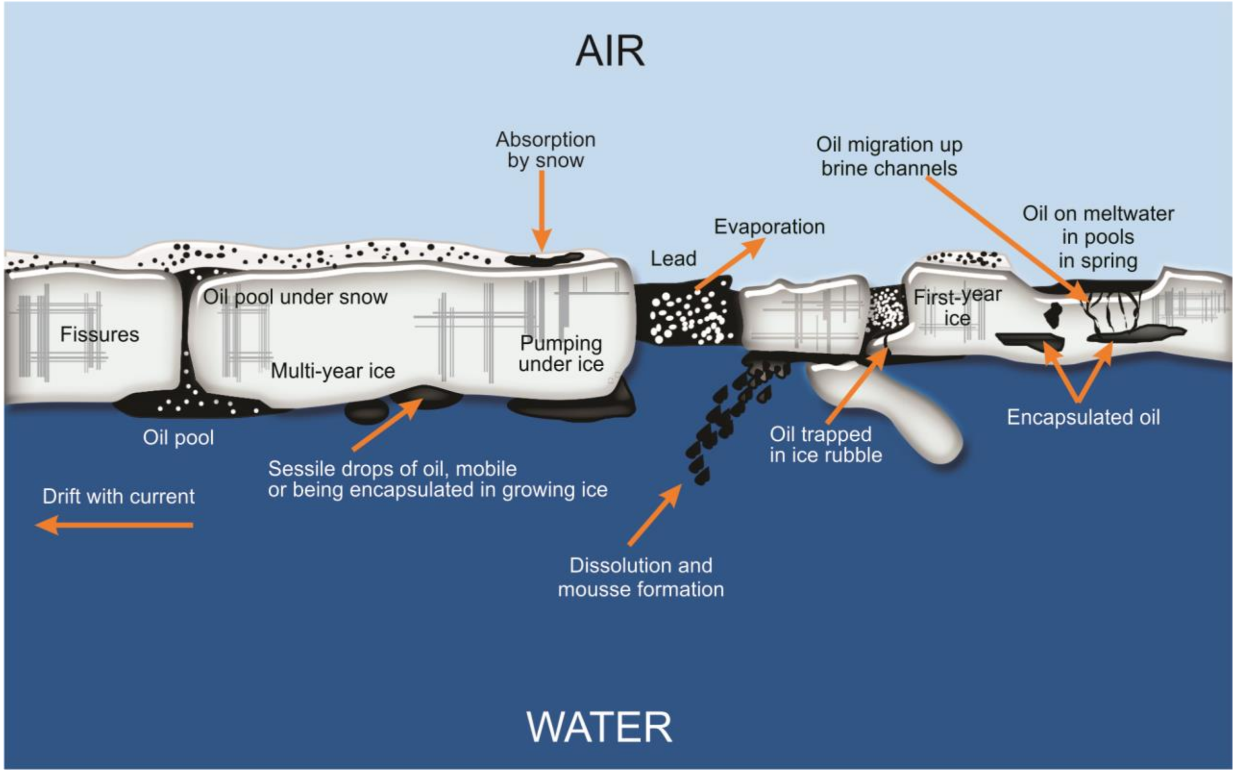

Figure 6. General schematic showing dynamics and characteristics of sea ice and oil interaction at the sea surface. (Source: Original figure by Alan A. Allen).

2.3.1 Oil Transport in Sea Ice

When oil interacts with mobile sea ice, some fraction of that oil will become contained (either on top, in, or underneath the ice) and will then travel with the ice floe (Drozdowski et al., 2011). Sea ice fields can drift rapidly and over great distances in the Arctic (Peterson et al., 2008). The fraction of oil moving with the ice verses in open water depends on conditions and specifics of the release. In some cases, all of the oil becomes completely frozen in the ice and remains there until it melts. This scenario is readily modelled (i.e., 100% of oil drifts with ice). However, in most cases since sea ice can be patchy (Figure 7), only partial amounts may become either encapsulated or trapped (e.g., between ice fragments or under ice sheet in small cavities) (Drozdowski et al., 2011), depending on ice coverage, subsurface roughness, winds and currents, and ice formation/melting dynamics.

To simplify the problem, the ice coverage or concentration information provided by the ice data or model can be used as an indicator of whether oil follows the surface currents or the ice currents. Ice coverage information available in coupled hydrodynamics and ice models typically comes from remotely sensed satellite data. A rule of thumb followed by past modelling studies is oil will generally drift with ice when ice coverage is greater than 30% (Drozdowski et al., 2011; Venkatesh et al., 1990). For more description of the ice coverage information and ice currents utilized in this modelling study please see Section 5.4.2.

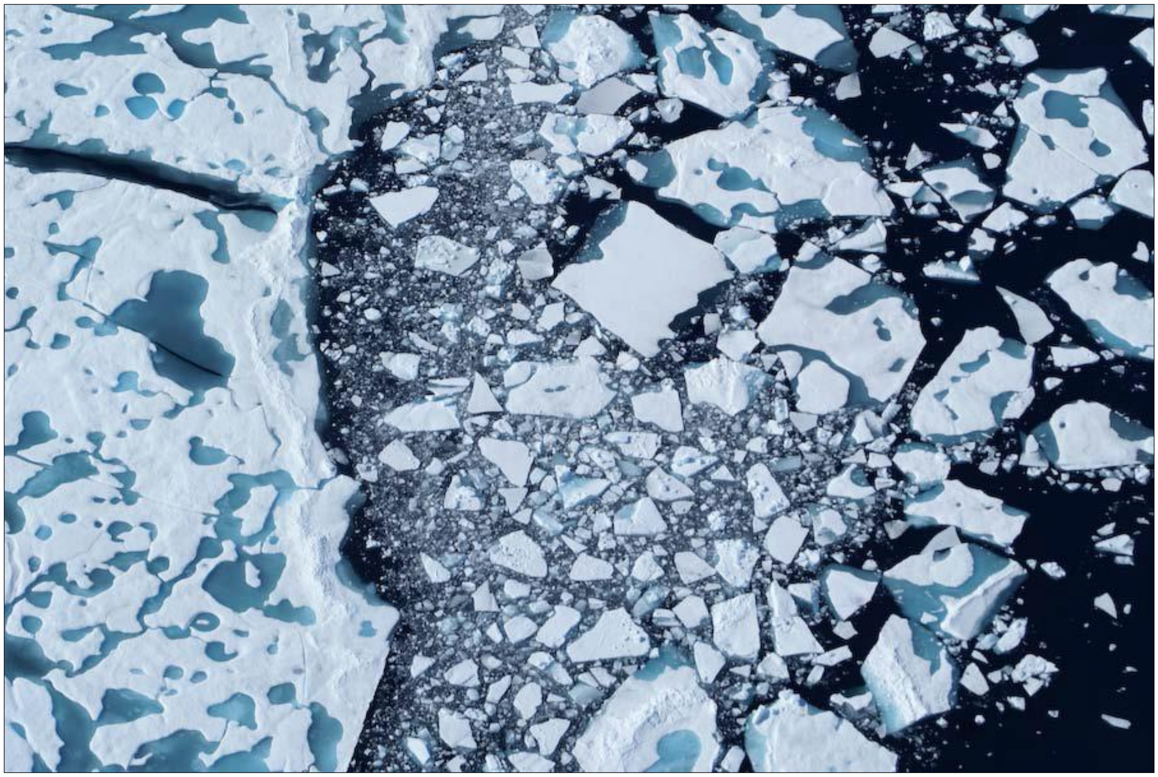

Figure 7. Aerial photograph of late July 2009 ice conditions in the Canadian Beaufort Sea, Ajurak-Pokak license area, resolution of a 2-3 m. Sea ice on the ocean surface is often patchy and fragmented which allows oil to accumulate in the surface water between. Photo Source: ASL Borstad Remote Sensing.

When a coupled ocean-ice model is available and provides water currents and ice velocities, the SIMAP model uses the ice coverage data to determine whether floating (or ice-trapped) oil moves with the surface water currents or the ice. If the ice coverage is <30%, the oil is assumed not to be trapped and moves with surface water currents. If ice coverage exceeds this threshold, the ice is assumed to have ample spatial coverage to trap the oil in it or between floes, and oil is transported along with the ice using the ice velocities from the ocean-ice model.

In areas and at times where ice cover <30%, floating oil is transported with surface water currents and a wind drift algorithm to account for wind-induced drift current not resolved by the hydrodynamic model plus Stokes drift caused by wave motions. Wind drift is predicted in SIMAP based on the modelling analysis of Stokes drift and Ekman flow by Youssef (1993) and Youssef and Spaulding (1993, 1994). According to this algorithm, at moderate wind speeds, floating oil drifts 20^{o} to the right of downwind at about 3.5% of wind speed. Alternatively, a constant drift speed percentage and angle may be used in simulations; however, the modelled drift is used in the examples herein. In areas where ice exceeds 30%, and an ice drift model provides transport velocities, the ice drift model has accounted for wind drift, and so no additional wind drift is added in SIMAP.

To simulate oil transport in this study, the SIMAP model used the ice coverage variable, and both the regular water currents and the ice currents or ice velocities available in the hydrodynamics and ice model TOPAZ4 (Section 5.4.2).

2.3.2 Oil Transport and Interaction with Landfast Ice

Immobile or fixed landfast ice which seasonally extends out from the coast may act as a natural barrier where oil collects. The ice edge is complex with ridges, keels, cracks and crevices where oil can become trapped. During landfast ice melt, oil that has been stored along the edge may either release back into open water, or may retreat back with the ice towards the coast (Drozdowski et al., 2011).

In the model, when oil encounters landfast ice at the surface of the ocean it is assumed to trap along the ice edge and remain immobile until ice retreats. When landfast ice is no longer present at trapped oil's location, the oil is released back into the water as floating oil. In areas deep enough for landfast ice to have subsurface open channels (i.e., where the ice sheet may not extend completely to the seabed in all areas), entrained oil is allowed to circulate underneath the surface ice using subsurface current data for transport. The thickness of landfast ice is typically about 2 m in the Beaufort Sea; thus, in deeper waters subsurface oil spillets continue to move with currents, whereas in shallower areas, subsurface oil spillets remain stationary for the time where landfast ice is present. Monthly representations of the landfast edge along the entire coast (capturing average growth and retreat patterns) where prepared as data inputs (Section 5.4.1).

2.3.3 Effects of Ice on Oil Fates and Behaviour Processes

The presence of ice can shelter oil from the wind and waves (Drozdowski et al., 2011). Thus, weathering processes such as evaporation and emulsification, and behaviours such as spreading and entrainment are slowed (Spaulding, 1988). Field data show evaporation, dispersion, and emulsification significantly slowed in ice leads, contrary to some laboratory experiments. Wave-damping, the limitations on spreading dictated by the presence of sea ice, and temperature appear to be the primary factors governing observed spreading and weathering rates (Sørstrøm et al., 2010).

As with transport, the ice coverage or concentration variable provided in the ice model is used as an index to control oil weathering and behaviour processes (Table 1). Oil behaves as it would in open water in <30% ice coverage. Ice coverage exceeding 80% is assumed fast ice and effectively continuous ice cover. Evaporation and volatilization of oil under/in ice, as well as spreading, emulsification, and entrainment into the surface water are zeroed in fast ice. Oil spilled on top of fast ice is allowed to evaporate, but does not spread from the initial condition of the release. Degradation of subsurface and ice-bound oil occurs during all ice conditions, at rates occurring at the location (i.e., floating versus subsurface) without ice present. Dissolution of soluble aromatics proceeds for subsurface oil and oil under ice using the normal open-water algorithm (French McCay, 2004).

In ice coverage between 30% and 80%, a linear reduction in wind speed from the open-water value (used in <30% ice) to zero in fast ice (>80% ice coverage) is applied to simulate shielding from wind effects. This reduces the evaporation, volatilization, emulsification, and entrainment rates due to reduced wind and wave energy. Terminal thickness of oil is increased in proportion to ice coverage in this range (i.e., oil is thickest at >80% ice coverage).

Table 1. Percent ice coverage thresholds for oil fates and behaviour processes applied in the SIMAP model.

Ice Cover (Percent)	Advection	Evaporation & Emulsification	Entrainment	Spreading
0 – 30 (Drift Ice)	Surface oil moves as in open water	As in open water	As in open water	As in open water
30 – 80 (Ice Patches and Leads)	Surface oil moves with the ice	Linear reduction with ice cover (i.e., none at 80% ice cover)	Linear reduction with ice cover (i.e., none at 80% ice cover)	Terminal thickness increased in proportion to ice coverage
80 – 100 (Pack Ice)	Surface oil moves with the ice	None	None	None

Assumptions applied to fates and behaviour processes are not well quantified by field experiments or other studies. Also, the coupled ocean-ice models available to date do not resolve the details of leads, fractures, and ice roughness. This presents a major modelling limitation. The applied thresholds, or the discrete bands of 0 to 30, 30 to 80, and 80 to 100%, may not reflect what happens to the fate of oil in real ice cover, particularly at fine scales.

3 Potential Effects of Oil and Subsea Dispersant

Oil can affect flora and fauna in the marine environment in several ways. This section briefly summarizes these effects in general terms and is based on the review in French McCay (2009).

Floating and shoreline oil can affect biota via smothering or coating. In birds and mammals, oil contamination can inhibit thermal regulation by fouling fur and feathers. Coating can lead to mechanical effects such as prevention of uptake or depuration (e.g., intertidal vegetation) and interference with motility. When coated with oil, absorption of toxic compounds via skin or gut is possible leading to chronic and acute effects. Floating and shoreline oil can also cause behavioural interference. Animals may avoid or leave the area, or, if immobile, shut down. It is hypothesized that some species may be attracted to oil which would result in higher exposure.

Dissolved aromatics in the water column resulting from spills may reach toxic concentrations. The uptake of dissolved components into tissues and can result in chronic and acute effects. Subsurface oil droplets (in the particulate form) can cause clogging of feeding appendages and gills, and can impede movement. Organisms at highest risk of water column effects include planktonic invertebrates, larval and juvenile fish.

As a result of the Deepwater Horizon incident, subsea dispersant application is now considered by many entities an effective response tool during a catastrophic blowout. Dispersants are composed of surfactants, as are detergents. Dispersants themselves have very low toxicity to aquatic biota, but when applied to oil, water column effects can increase. These chemicals can reduce the interfacial tension of oil, facilitating increased entrainment of oil into water as microscopic droplets. This leads to more oil in water column, increased dissolution rates of soluble hydrocarbons (mostly aromatics), and enhanced biodegradation rates due to more surface area than if a floating slick. Application of subsea dispersants reduces the effects of surface floating oil on birds and other wildlife, and on shorelines. However, dispersant use is a trade-off with increased risks to fish and invertebrates in the water column.

4 Literature Review: Beaufort Sea Environmental Conditions

The following section provides a literature review on the ocean currents, wind regimes and patterns, and ice circulation and conditions observed in the Beaufort Sea.

4.1 Large-Scale Arctic Ocean Circulation

Ocean circulation in the western Arctic Ocean is complex, consisting of multiple currents, gyres and sea ice. The Chukchi and Beaufort Seas are the northernmost shelves bordering Alaska in the western Arctic Ocean (Mahoney, 2012). The predominantly northward movement of water through the Bering Strait represents the flow of Pacific water from the Bering Sea towards the Arctic Ocean and exhibits considerable spatial and temporal structure (Coachman, 1975). The inflow of Pacific water through the Bering Strait into the Chukchi and Beaufort Seas separates into three main bathymetrically constrained currents (Pickart, 2011). The most eastern branch is the Alaskan Coastal Current that transports relatively warm Alaska Coastal Water (ACW) north and hugs the Alaskan coast. When this current reaches the edge of the Chukchi shelf, some portion of the Alaskan Coastal Current turns eastward as a shelf break jet (Pickart 2009). To the east of Barrow Canyon (northern tip of Alaska), this eastward current is referred to as the Beaufort shelf break jet or the western Arctic boundary current (Schulze, 2012) (Figure 8). This jet consists of a narrow core, on the order of 10-15 km wide, flowing eastward with an average speed of 15-20 cm/s. During the late-fall and winter, the current frequently develops a deep “tail”, extending down to about 250 m, which arises during the relaxation phase of easterly wind events (Pickart, 2011). The Beaufort shelf break jet is present year-round, advecting both summer and winter Pacific water to the east when the winds are weak (Nikolopoulos, 2009). The middle branch flows northward along the Central Channel. Hanna Shoal lies between the Barrow Canyon and the Central Channel current, and part of the Central Channel current turns eastward and enters the head of Barrow Canyon to join the Beaufort shelf break jet (Jia, 2008). The most western branch (Herald valley branch) flows northwestward into the Chukchi Sea through a deep channel between the Wrangel Island and Herald Shoal (Figure 8) (Jia, 2008). The heat flux associated with the northward flow enhances the early loss of ice in the Chukchi Sea (Mahoney, 2012).

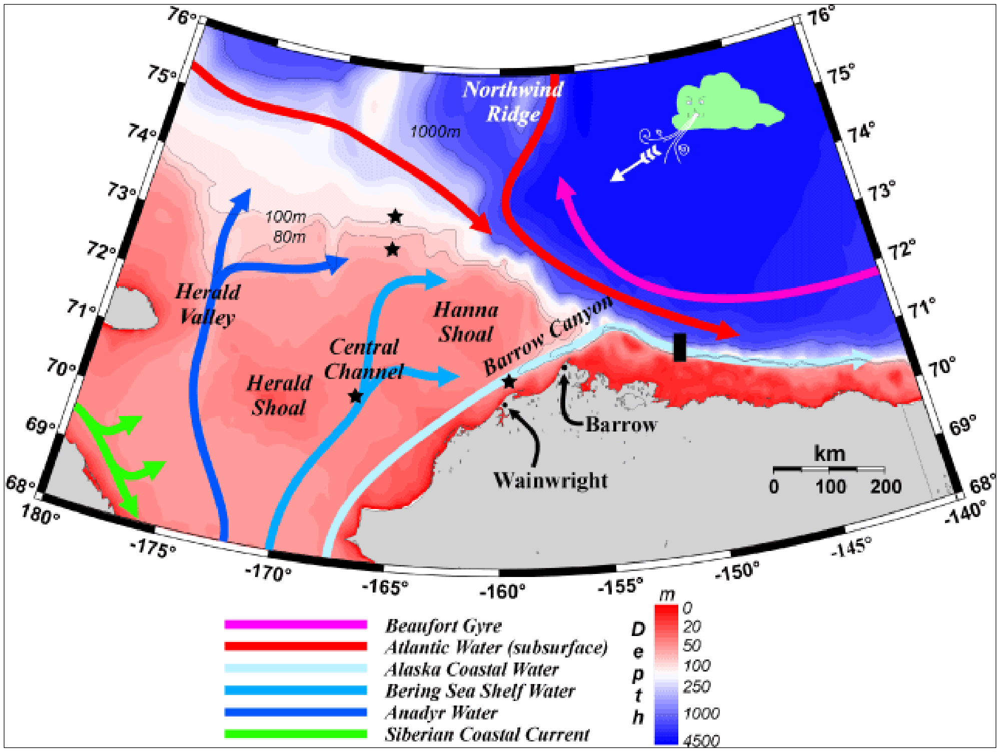

Figure 8. Main currents in Chukchi and Beaufort Seas. The three inflowing Pacific branches are color-coded with navy blue being the most nutrient-rich waters and light blue being the least nutrient-rich. The Siberian Coastal Current (green) is present in summer and fall, but absent or weak in winter and spring (Source: WHOI, 2013).

4.2 Currents in the Beaufort Sea

The currents in the Beaufort Sea are driven by a combination of various oceanographic processes, such as, large-scale circulation features, winds, Mackenzie River discharges, and tidal forcing (IORVL, 2013). There are several large-scale circulation features in the Beaufort Sea, namely the anticyclonic Beaufort Gyre (BG) and the Beaufort Shelf break/Slope Current. Circulation is dominated by the anticyclonic motion of the Beaufort Gyre that is driven by the Beaufort High (described in Section 4.3), which results in a westward movement of the near-surface waters. The gyre transports some of the oldest and thickest ice in the Arctic from the region north of the Canadian Archipelago into the Beaufort Sea. The strength of the gyre can fluctuate annually and the ice motion can reverse for short time periods. The average winter drift is typically parallel to the coastline. The Beaufort Sea has a greater extent of landfast sea ice than the Chukchi Sea and is the largest freshwater storage area of the Arctic Ocean (Proshutinsky, 2009).

The principal circulation feature of the outer shelf and slope of the Beaufort Sea is the Beaufort shelf break jet, which flows along the edge of the shelf at depths of 50-200 m. This eastward flowing current transports Pacific-origin water towards the Canadian Arctic Archipelago, however, under enhanced easterly winds the current is subject to reversals to the west with current speeds up to 1 m/s (Schulze, 2012). In waters deeper than 200 m, there is an eastward movement of Atlantic Ocean water. It underlies a shallow flow regime, where the ice and upper ocean moves westward and represents the southern limb of the clockwise Beaufort gyre (Aagaard, 1989). These reversals are normally associated with upwelling onto the outer shelf and are basin-scale circulation within the Arctic Ocean. The currents over the shelf edge and continental slope are periodic with events occurring over a few days. This is due largely to the response to wind forcing as modulated by the local sea-ice cover, topographic waves, and mesoscale eddies (Carmack, 1998). Current measurements from 2009 to 2011 FDCPs identified current speeds as high as 99 cm/s in the upper 200 m of the water column and up to 47 cm/s in depths greater than 250 m (Osborne, 2012). These strong events are associated with northeasterly winds and resulted in ocean upwelling along the Beaufort Shelf edge and slope. Near the Mackenzie Trough, upwelling is enhanced and thus influences the currents along the shelf-break area.

On the inner shelf (landward of ~50 m isobaths), the circulation has a largely wind driven component, particularly in summer. During winter, the flow over the inner shelf is less energetic but still exhibits some wind influence. The main subsurface flow influence on the shelf is primarily ocean influence, while wind is of secondary importance and accounts for less than 25% of flow variance below 60 m (Aagaard, 1989). Proshutinsky (2002) hypothesized that during winter, the wind drives the ice and ocean in an anticylonic direction so that the Beaufort Gyre accumulates fresh water mechanically through a deformation of the salinity field. The strength of the horizontal salinity gradient and resultant geostrophic circulation depend on the intensity and duration of the anticyclonic winds. During summer, winds are weaker and sometimes will reverse direction, although the mean ice still rotates anticylonically. This means that in summer the ocean geostrophic circulation prevails and may drive the ice against the wind motion (Proshutinsky, 2002).

The inner shelf surface currents are also influenced by the Mackenzie River plume and topography. The westerly winds result in strong alongshore currents, while easterly winds result in an offshore displacement of water from the Mackenzie River and pack ice (Carmack, 2002). The large discharges of fresh water from the Mackenzie River onto the shelf areas and beyond, plus the wind-dependent advection of these rivers waters, leads to frontal features with distance scales of tens of meters to tens of kilometers over the shelf and outer slope regions. Water from the Mackenzie River has been observed in the southern Canada Basin, as well as constrained to the coastline. The horizontal dispersion of this water depends upon the strength, frequency, and duration of northeasterly (upwelling-favorable) winds over the shelf, and has been detected along the continental slope as far west as 160°W. However, during years of frequent or strong downwelling winds, the Mackenzie River's summer discharge is likely advected northeastward into the Canadian Archipelago (Melling, 1993). In winter, the Mackenzie shelf water is more saline due to enhanced ice production, which can alter the along-slope density gradient (Melling, 1993). Measurements related to Mackenzie River plume waters indicated strong horizontal gradients in the currents in relation to large horizontal salinity, temperature and turbidity gradients. The upper 250 m of the water column consists of relatively cold, fresh Arctic Ocean surface water. Below the surface, from about 250 to 900 m, there is warmer and salty Atlantic water, while beneath 900 m, the water is cold and salty (Figure 9). Arctic surface water is composed of water from the Mackenzie River, melted sea ice, winter polar or surface mixed layer water, and upper halocline water that can include Pacific water (Lansard, 2012). Pacific summer water is warmer and fresher than Pacific winter water, with water temperatures reaching up to 1°C and salinity values range from 31 to 33 PSU (Lansard, 2012). The surface water is fresher in summer than winter due to the fresh water from melted sea ice and river runoff.

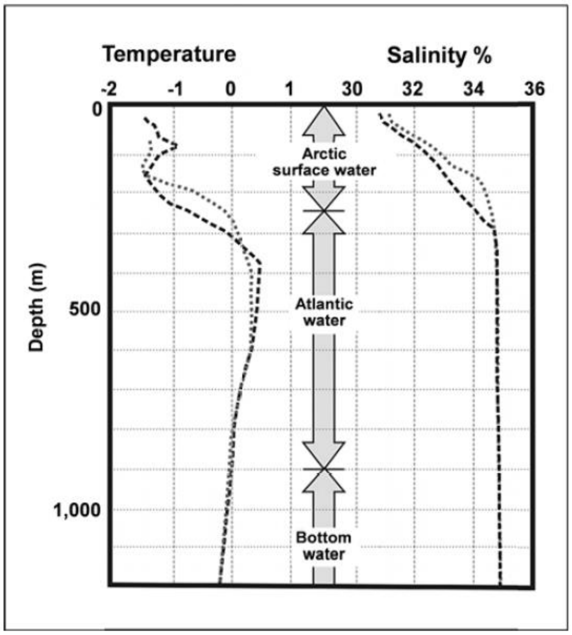

Figure 9. Water properties of Arctic surface water, Atlantic water, and bottom water. Summer profiles are indicated by the dashed black line, while winter profiles are illustrated by the light dotted line (Source: IORVL, 2013).

4.3 Winds in the Beaufort Sea

A major influence on general circulation in this area is a region of high pressure normally located over the Beaufort Sea, known as the Beaufort High. Since 1996, the Beaufort High has become stronger and enhances the predominant easterly winds in the Beaufort Sea, with larger increases seen at more offshore locations (Schulze, 2012). On the Beaufort Shelf, wind direction is primarily from the east and west-northwest. During winter, the high pressure system drives easterly winds across the North Slope and northeasterly winds offshore at Icy Cape (Aagard, 1989). At Cape Lisburne, there are topographic effects from the mountains, thus the mean winter wind is southeasterly. The Siberian high pressure system is southwest of the Beaufort High and occasionally the two systems form a saddle over the central and western Chukchi Sea, resulting in light winds (Aagard, 1989). The winter anticyclonic wind stress associated with the Beaufort High has many important effects, such as: surface Ekman drift that advects the Beaufort coastal freshwater into the Beaufort Gyre; sub-surface upwelling that brings the warm, saline Arctic intermediate water into the Beaufort Sea shelf break; melting surface sea ice; and the formation of landfast ice (Jia, 2008). During summer, the wind stress is relatively weak due to the weakened Beaufort High and there is often a low pressure system occupying the same spot over the Beaufort Sea. Thus, winds are largely zonal year-round over the Beaufort Sea and westward in all seasons, except when in summer there are weak eastward flows. The northward propagating summer storms occasionally move to the Chukchi Sea via the Bering Strait, producing strong wind and mixing. Maximum wind speeds occur in November-December and April-May, and are centered over the western Beaufort slope (Eicken et al., 2006). Data obtained at Pelly Island in the Beaufort Sea indicates that wind direction is most frequently from the east; however, speeds exceeding 12 m/s are most common from the west-northwest (Figure 10). The surface currents generated by the two dominate wind directions generally follow the wind direction with a 15-30 degree deflection to the right. Current speeds were found to typically by 2 to 3% of the wind speed, with average velocities of 0.25 to 0.4 m/s, with maximum velocity around 0.8 m/s (IORVL, 2013).

Cyclonic low-pressure systems are also important in the Arctic, particularly during summer and fall. The majority of the cyclones tend to follow the sea ice-ocean interface, which causes ice edges to retreat as the storms move further offshore (Moore, 2012). Polar lows are low-level, small-scale features that form near the ice edge or in coast regions where cold air flows from ice or land surfaces over open water. These features are uncommon in the Beaufort Sea, but these lows create cyclonic circulation and generate strong winds (IORVL, 2013).

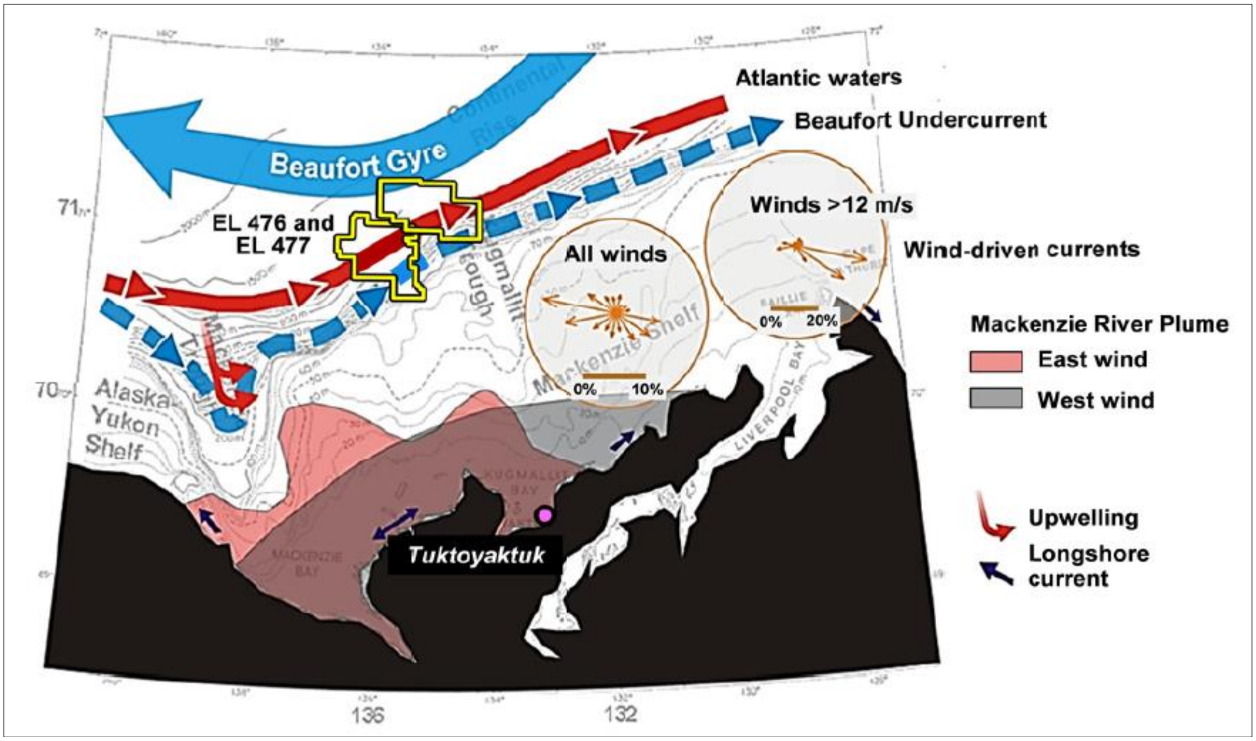

Figure 10. Ocean currents and winds in the Canadian Beaufort Sea (Source: IORVL, 2013).

4.4 Ice in the Beaufort Sea

The sea ice in the Beaufort Sea can be divided into four different regimes: (1) landfast ice zone, (2) active shear zone, (3) transition zone, and (4) offshore polar pack zone (IORVL, 2013) (Figure 11). The seasonal first-year landfast ice cover forms in the shallow portions of the continental shelf in the fall, and disperses and melts in the following summer. The large-scale atmospheric circulation over the Western Arctic Ocean is the most dominant influence in determining oceanographic and sea ice movement patterns and landfast ice break up (Divine, 2004).

Landfast ice is classified as sea ice that forms and remains fixed along a coast, where it is attached to the shore or held between shoals or grounded icebergs. Thus, it forms a rigid, immobile boundary that isolates the coastal ocean from the atmosphere and affects the fate of river inflow when it enters the marine environment (Kasper, 2012). The typical thickness of landfast ice is about one to two meters, and its appearance is normally smooth and level in the inner part of the landfast ice pack but can be highly deformed rubbles at its seaward boundary. Landfast ice modifies the momentum exchange between the atmosphere and ocean due to its lack of mobility. Since it covers the shelf area for four to eight months each year, the heat and fresh water exchange is greatly affected. In addition, the freezing and melting of landfast ice makes an important contribution to the salt and fresh water budgets, thus influencing water circulation, dense water production and the location of upwelling and downwelling zones (Macdonald, 1999). The landfast ice edge is marked by open water or drifting pack ice. Landfast ice is known to form every year along the inner Beaufort shelf and varies seasonally in the Beaufort Sea. On a broad scale, the ice cycle can be characterized by gradual seaward advance from the coast beginning in late fall or early winter and reaches its widest extent during April or May, followed by a rapid retreat in May-June. Landfast ice in the Beaufort Sea usually extends to approximately the 20 m isobath (roughly 20 km offshore), where it grounds in the Stamukhi zone due to ridging (Mahoney, 2007). The Stamukhi zone marks the boundary between the moving arctic pack ice and more stable landfast ice, and it is composed of abundant coast-parallel, shear and pressure ridges of sea ice in water depths of 15–50 m. Since the shelf break is on the order of 50 km offshore, it means that, under normal conditions, there is no landfast ice in the vicinity of the shelf edge. However, using Synthetic Aperture Radar (SAR) imagery, Mahoney (2007) revealed that there are times when landfast ice can extend well offshore into the southern Beaufort Sea, to areas where water depths are as great as 3,500 m. These episodes are referred to as “stable extensions”, and were found to occur most frequently during March and April in the Beaufort Sea (Schulze, 2012).

The shear zone represents the shoreward edge of the transition zone. The ice deformation is driven by strong winds that are usually from the northwest, which result in high ice stresses as the drifting ice of the polar pack zone encounters the landfast ice and the shallower waters. The transition zone lies landward of the polar pack ice and is typically associated with high concentrations of first-year ice and a gradual decrease of the anticyclonic average flow. Degradation appears most strongly in the form of higher variability and lower average ice drift in the most southern areas. A dynamic shear zone is often separately designated to denote regions of intense ice deformation near the flow discontinuity, which defines the offshore edge of the landfast ice zone. The offshore, mobile polar pack ice describes a large anticyclonic pattern of ice movement related to the Beaufort Gyre (IORVL, 2013).

Typically, the sea ice starts to release fresh water during May and fresh water from ice reaches a maximum in September-October. If thermodynamic processes (i.e. solar radiation) were the only forcing considered on seasonal freshwater content, the Arctic would become a two-layer ocean with a completely fresh upper layer and a salty lower layer. However, in the real ocean, seasonal variability is also influenced by Ekman pumping, ocean mixing, and by changes in fresh water sources and sinks, including precipitation, evaporation, river runoff and fresh water fluxes (Pickart, 2011). Therefore, it has been surmised that there are two fresh water content maxima and minima throughout the year in the Beaufort Sea. The Beaufort Gyre Exploration Project, conducted by Woods Hole Oceanographic Institution, found one maximum in December-January and a second smaller maximum during June-August. The two minimum fresh water content periods were found during April-May, with a less pronounced minimum during September-October.

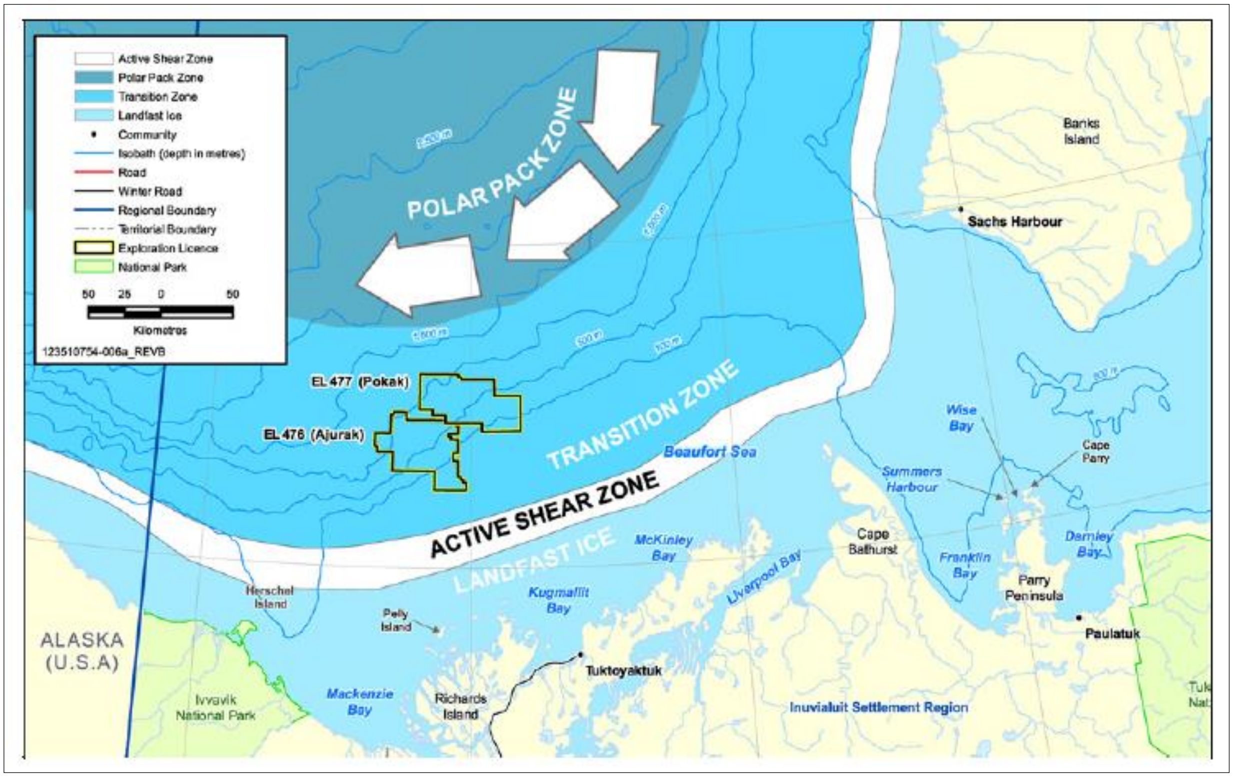

Figure 11. Schematic representation of zones of ice dynamics in the Beaufort Sea (Source: IORVL, 2013).

5 Geographic Location and Environmental Model Input Data

Geographic and environmental input data required for modelling include bathymetry, shoreline and shore type, long-term wind and hydrodynamic records, and average temperature/salinity water column profiles. This data was compiled and mapped in gridded format for the Beaufort Sea study location. The following sections describe the geographic location and metocean input data used for modelling.

5.1 Bathymetry

Point Barrow is typically considered the coastal separation point between the Chukchi and Beaufort Seas. Away from the coast, the boundary between these two bodies is defined by bathymetry. The Barrow Canyon forms a connection between the Beaufort and Chukchi seas and is a 250 km long depression in the northeastern most Chukchi Sea that runs parallel to the coast. The Chukchi Sea has a broad, shallow shelf mostly less than 50 m deep, while the Beaufort Sea is characterized by a relatively narrow continental shelf, a narrow and steep shelf slope, and a deep basin (Figure 12). The Beaufort Sea is typically more than 1,000 m deep with only a narrow strip of waters shallower than 50 m located within 100 km of the coast.

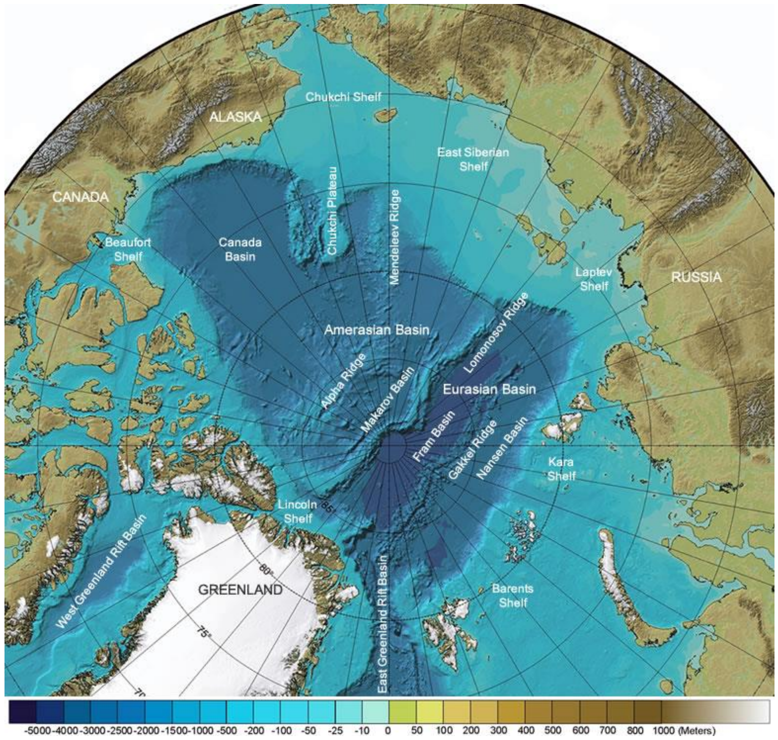

Figure 12. Bathymetry throughout the Arctic Ocean (From: geology.com).

Bathymetry is an important input for oil spill modelling. Data for the study area were obtained from the General Bathymetric Chart of the Oceans (GEBCO) Digital Atlas (GEBCO, 2009). The GEBCO Digital Atlas consists of a global one arc-minute grid. The grid is largely generated by combining quality-controlled ship depth soundings with interpolation between points guided by satellite-derived gravity data. A subset of the gridded GEBCO data was extracted to generate the depth grid used for an input to the SIMAP model (Figure 13).

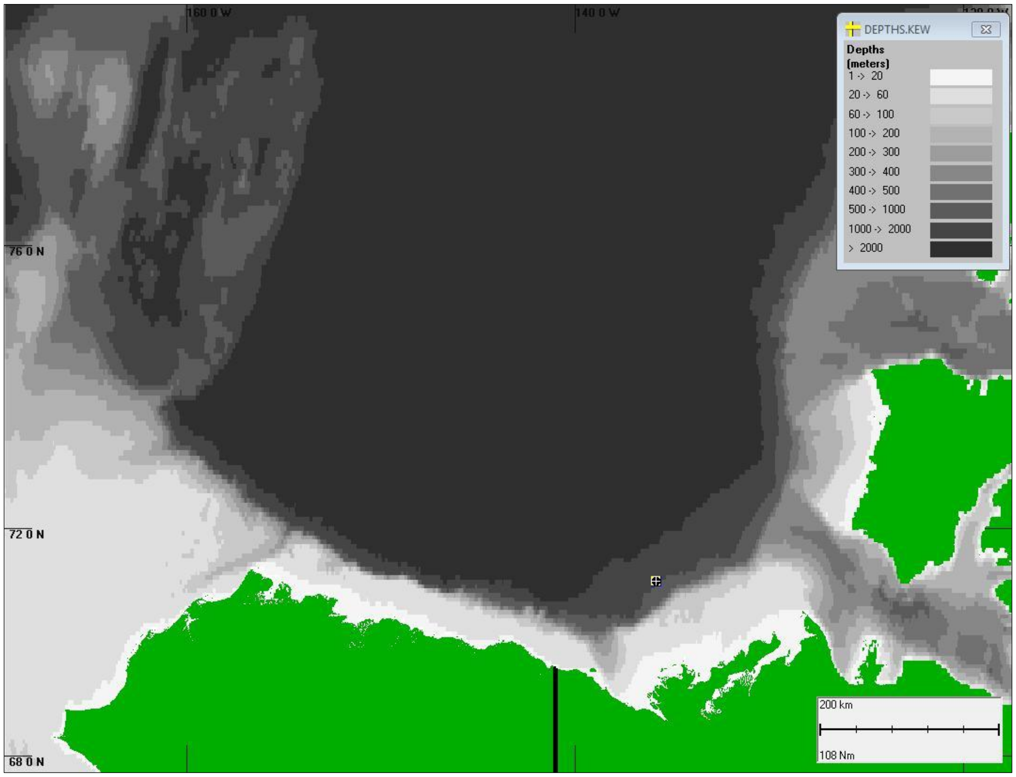

Figure 13. Depth grid used for Beaufort Sea modelling (m). Bathymetry data source: General Bathymetric Chart of the Oceans (GEBCO).

5.2 Shoreline and Habitat Mapping

Coastline geometry definition (i.e. distinction of the land and water boundary) for the Canadian coastline was obtained from the “Atlas of Canada Reference Map” for Northern Canada (http://atlas.nrcan.gc.ca/site/english). The Canadian coastline was merged with the Alaskan “hydro” polygon shape file from the National Oceanic and Atmospheric Administration (NOAA) Environmental Sensitivity Index (ESI) database (http://response.restoration.noaa.gov/esi). Together these two data sources created the land basemap used for SIMAP modelling.

A habitat grid containing both shore and subtidal habitat types was constructed for the study area and used as an input to the SIMAP modelling system. Mapped shoreline classification data from the “Environmental Atlas for Beaufort Sea Oil Spill Response” (AXYS, 2004) was used to characterize the shore habitat types along the Canadian coastline. This resource was provided to RPS ASA by the client in PDF format. Spatial data in the Physical Environment and Logistics maps of this Atlas were interpreted and integrated into the SIMAP habitat grid. Habitat classifications in the Atlas were recategorized into existing SIMAP habitat type codes. For example, areas coded as “Tidal Flats with Low Tundra/Marsh” in the Atlas were categorized as “Seaward Fringing Wetland” for the SIMAP grid. Available data coverage for the Canadian coastline extended from the Canadian/U.S. Border east to Baillie Island. Where data were available, the dominant habitat type was gravel beach, so all shoreline east of Baillie Island in the domain of the habitat grid were defaulted to the Seaward Gravel Beach habitat type.

For the U.S. Alaskan coastline, data from the National Oceanic and Atmospheric Administration (NOAA) Office of Response and Restoration (OR&R) Environmental Sensitivity Index (ESI) was used to define the habitat type. The ESI data is in geospatial format and contains shoreline and polygonal information for much of the U.S. This includes delineations of sand, rock, gravel shore, and wetland, among other classifications for habitats. Alaskan ESI shoreline data was reclassified to match SIMAP's habitat classification, similar to what was done for the Canadian coastline.

The Canadian and Alaskan Arctic coastline in the area of interest for this oil spill modelling study were composed of primarily gravel and sand beaches, and some rocky shore. Areas behind barrier islands, inlets, bays, and coastal estuaries consisted of mud flats, saltmarsh wetlands, and intertidal macroalgal beds.

Mapped subtidal marine substrate types (e.g. rock, gravel, sand, silt-mud) were acquired from Audubon Alaska's "Arctic Marine Synthesis" database, available online at NOAA's Arctic ERMA website https://www.erma.unh.edu/arctic/ERMA/metadata?layer_id=13356. Data coverage for subtidal habitats included the Alaskan Chukchi/Beaufort Shelf and most of the Canadian Beaufort Shelf. Where no subtidal habitat data was available, the default habitat type "Subtidal Sand Bottom" was used. Silt-mud and gravel bottom were the most abundant substrate types in the subtidal data set.

Given the magnitude and volume of the spills modelled, the SIMAP habitat grid had to encompass a very large area. The grid was rectilinear, expanding from approximately 176°W to 103°W, and from 67°N to 79°N (approximately 1,800 km W-E by 1,300 km S-N). The grid consists of 1,000 (W-E) by 164 (S-N) rectangular cells. Each cell was approximately 3.135 by 8.104 km, having a total area of 25.4 km^2 (Figure 14).

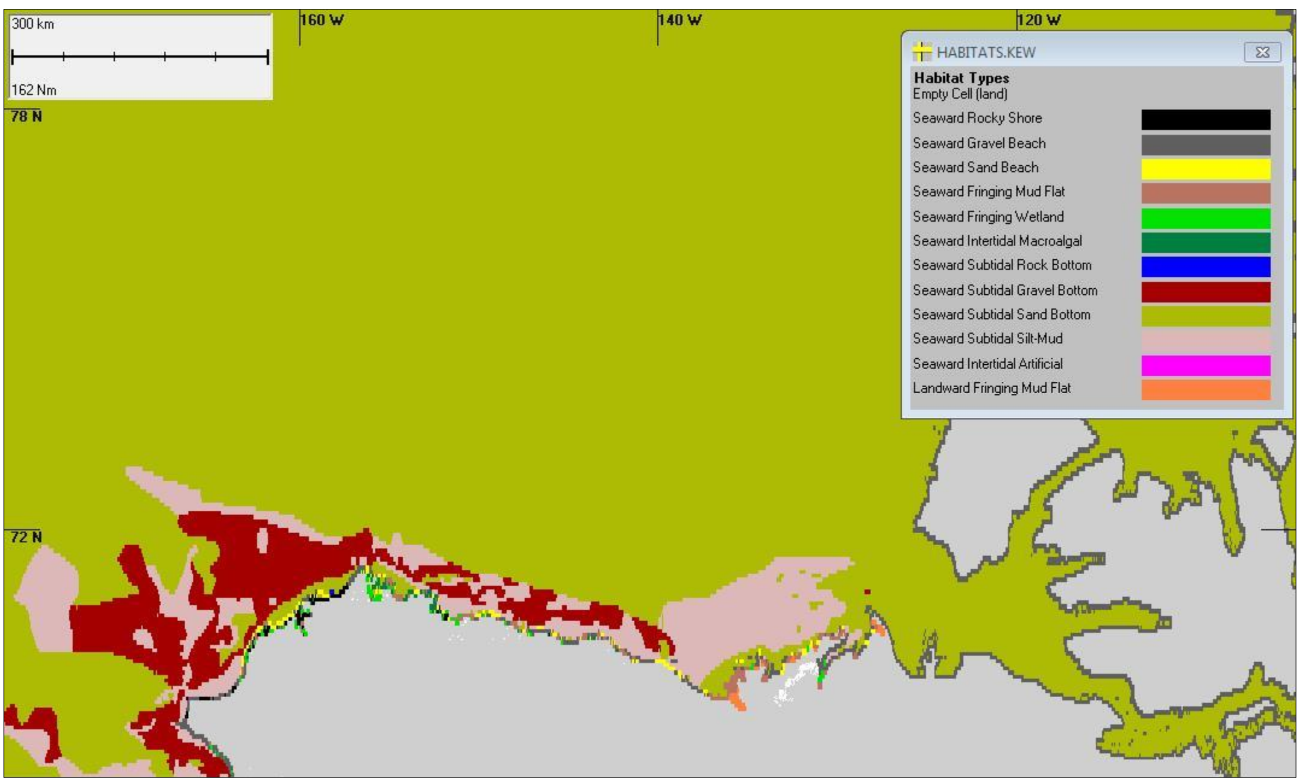

Figure 14. SIMAP habitat grid used for Beaufort Sea oil spill modelling.

The SIMAP model includes an oil-shoreline interaction algorithm which is used to estimate the amount of oil retained onshore based on shoreline type. For example, flat sandy beaches typically retain much more oil than steep rocky coast, and furthermore, oil that cannot be retained on the shore is susceptible to being further transport, thereby potentially affecting other regions. Table 2 outlines the holding capacities for shore types included in this study.

Table 2. Modelled shore widths and oil holding capacities for each shore type (French et al., 1996).

Type of Shore	**Width (m)**	**Oil Holding Capacity (mm)**		
		Oil Viscosity < 30 cSt	Oil Viscosity 30 – 2,000 cSt	Oil Viscosity > 2,000 cSt
Rocky Shore	2	1.0	2.0	2.0
Gravel Beach	3	2.0	9.0	15.0
Sand Beach	10	4.0	17.0	25.0
Mud Flat (Seaward)	10	3.0	6.0	10.0
Mud Flat (Landward)	140	6.0	30.0	40.0
Wetland (Saltmarsh)	140	6.0	30.0	40.0
Intertidal Macroalgal	2	1.0	2.0	2.0
Artificial Shore	0.1	0.01	0.1	0.1

5.3 Wind Data

Wind is one of the primary forcing factors used in surface pollutant modelling (e.g., oil spill simulations) as it is a dominant force in circulation and surface transport. The greatest surface oil movement results from persistent winds from the same general direction, where as highly variable winds promote spreading and dispersion of the spill slick into multiple directions and patches. RPS ASA's oil spill models incorporate a transport term due to the wind stress applied on the oil slick floating on the water surface. This wind drift factor has been observed to range between 2.0 and 4.5% of the wind speed. For this study, the effect of the wind stress on surface oil is reduced as ice cover increases (and open water decreases). See Section 2.3.1 for further discussion on how transport of surface oil is modelled when sea ice is present. A long-term wind record is needed to carry out an appropriate stochastic analysis, effectively sampling a wide range of environmental conditions.

5.3.1 Wind Dataset – ECMWF

For this study, wind data was obtained from the ERA-40 (ECMWF RE-ANALYSIS) wind model. This model was developed and is operated by the European Center for Medium-range Weather Forecast (ECMWF). This model has global domain coverage with 0.75° resolution (Figure 15). A long-term (April 2008-March 2013) gridded wind data record was extracted from the ECMWF database (http://www.ecmwf.int/products/data/archive/descriptions/e4/) and processed into a file format compatible with the SIMAP modelling system. This dataset contains 3 hourly (8 times a day) wind speed and direction readings at all grid nodes included in the region of interest. The data subset of grid points used for this study spans from approximately 170°W to 120°W (Figure 16).

ERA-40 is the wind forcing dataset that is used in the TOPAZ4 ocean circulation model (see section 5.4.2). Therefore the ECMWF RE-ANALYSIS wind dataset was the most appropriate choice for forcing surface oil. Other datasets, both modelled and observed, such as the Navy Operational Global Atmospheric Prediction System (NOGAPS) and from the Pelly Island meteorological station were acquired and compared to the ECMWF winds. General seasonal trends, direction, and velocities compared well between each data source.

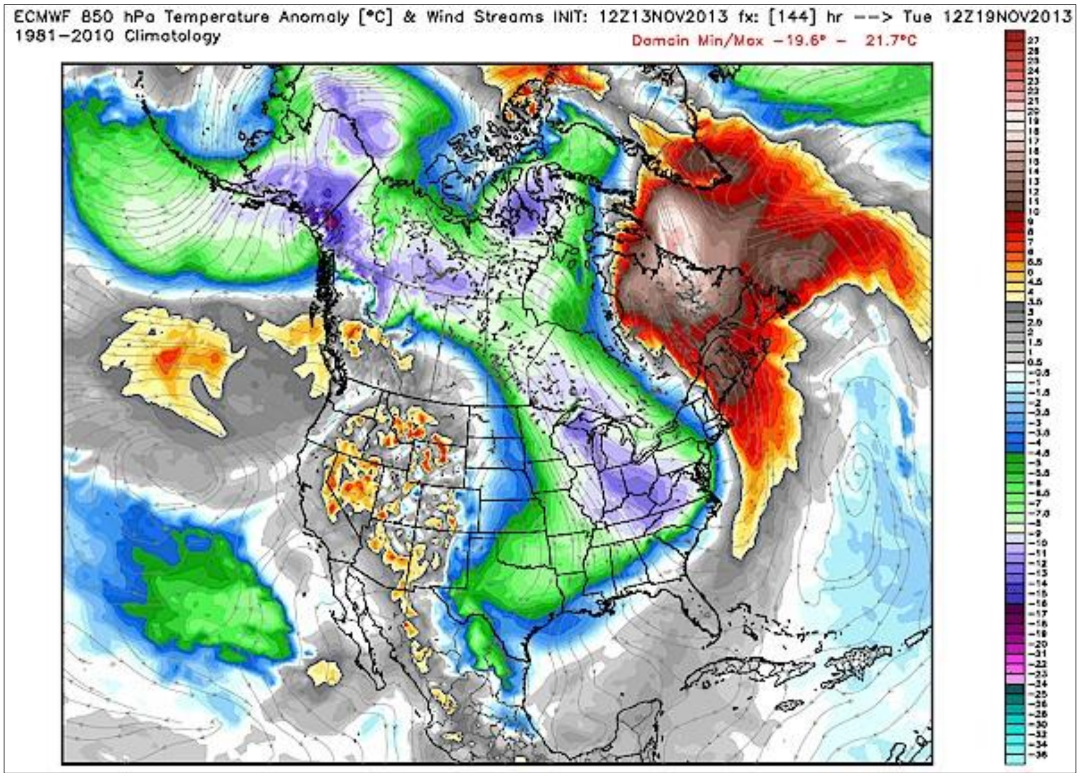

Figure 15. Map showing ECMWF RE-ANALYSIS wind data coverage over the North American Continent.

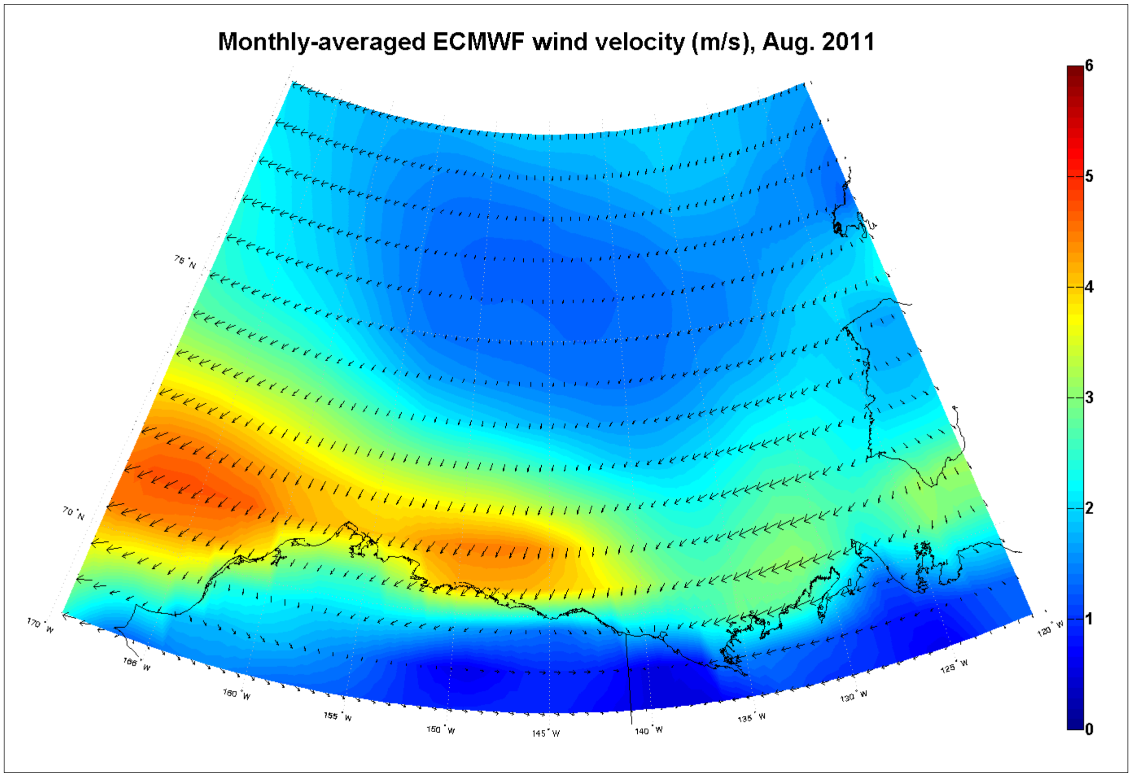

Figure 16. Figure showing region and coverage of data extracted for this oil spill modelling study. Arrow vectors are present at all grid nodes in the data set. Arrow vectors and velocity contours represent the monthly average from August 2011.

Wind rose plots are provided below for ECMWF average monthly wind speed and direction from years 2008-2013 from the deep blowout site on the Beaufort Shelf (Figure 17). In addition, a wind rose plot was generated for the yearly average 2008-2013 at the same site (Figure 18). Wind speed in rose plots are presented in knots, using meteorological convention (i.e., direction from which wind originates, i.e., easterly is from the east). Wind trends observed in the ECMWF data set compare well with what is described in the literature about the Beaufort Shelf. Wind direction is primarily from the east and west-northwest. During winter, high pressure drives easterly winds across the North Slope. During the late summer (August and September), the easterly wind speed is relatively weak and direction is more variable, compared to other months, due to the weakened Beaufort High. Thus, winds are largely zonal year-round and toward the west in all seasons, except in summer when there are weaker flows toward the east.

Figure 17 provides monthly wind speed statistics (average, maximum, and 95th percentile) near the deep blowout site (Section 6.5), from years 2008-2013 of the ECMWF dataset. Average wind speeds are relatively consistent throughout the year at between approximately 10 and 15 knots, with peak average speeds occurring in October.

Wind trends between years in the ECMWF dataset compare well with the exception of 2012. The highest variability in speed and direction occurs in 2012 with noticeable differences in the fall months. Wind direction in the fall of 2012 was more variable and more often from the northwest. A positive shift in the Arctic Oscillation has been reported for the years 2011-2012 (NSIDC), which may contribute to the observed variation.

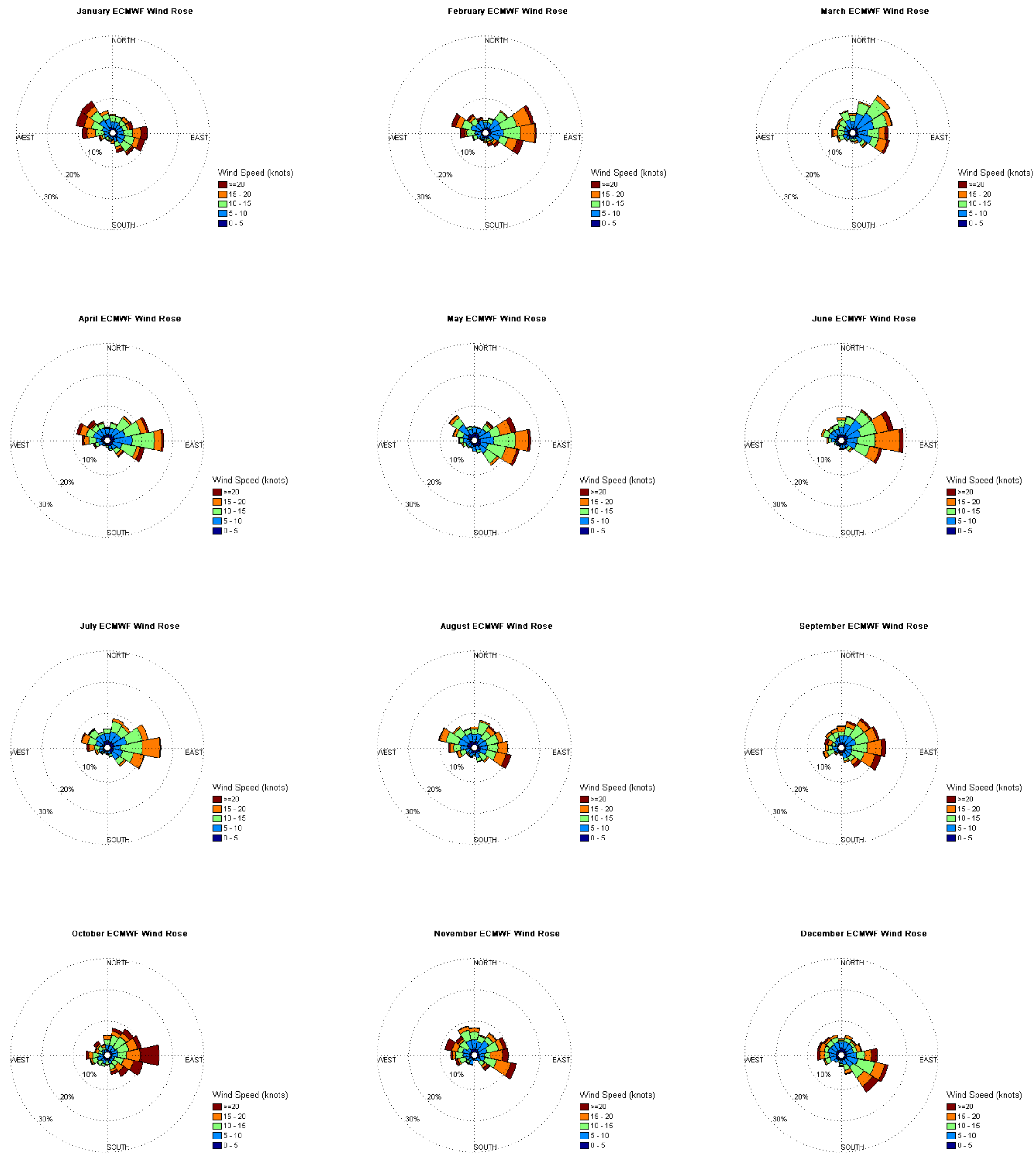

Figure 17. Monthly wind rose plots showing speed (knots) and direction at the deep blowout site averaged from years 2008-2013 from the ECMWF data set.

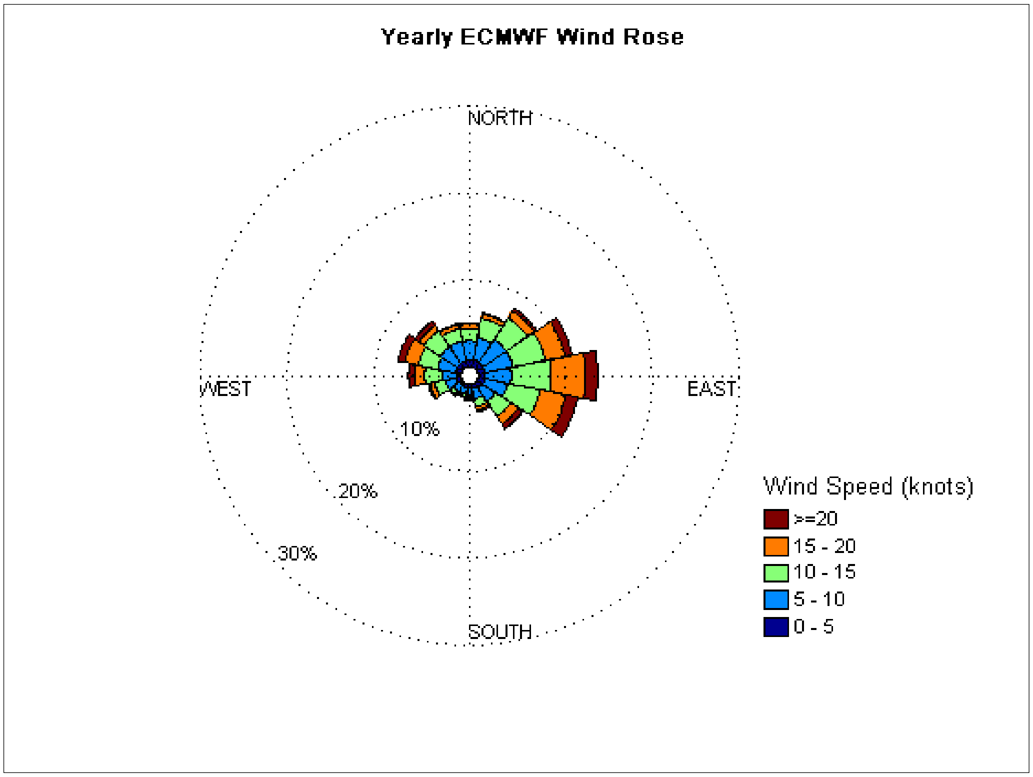

Figure 18. Yearly wind rose plot showing speed (knots) and direction at the deep blowout site averaged from years 2008-2013 from the ECMWF data set.

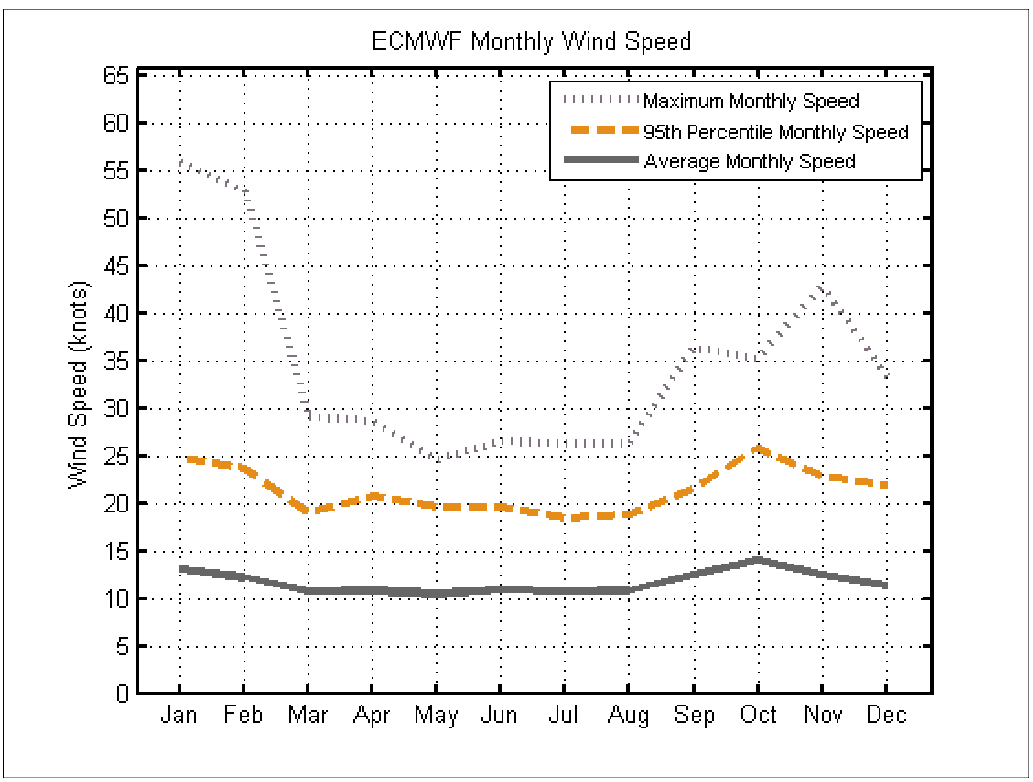

Figure 19. Chart showing monthly wind speed statistics: average, 95th percentile, and maximum speed (knots) from 2008-2013 of the ECMWF data set.

5.4 Ocean Circulation, Water Column Structure, and Ice Data

While winds are important for transporting floating oil in the marine environment, currents transport discharged pollutants at all water depths. Physical properties of the water column influence behaviour and weathering processes of discharged pollutants, especially for subsurface releases such as blowouts. In the Beaufort Sea during the late fall through the winter months much of the sea surface is covered in polar pack ice. This pack ice moves with the currents and can act as a sink or trap for discharged pollutants at the surface. Both transport and weathering of oil are influenced by the presence of sea ice. Landfast ice accumulates and grows along the coastline of the Beaufort Sea throughout the colder seasons. Landfast ice creates a temporary barrier where surface oil can accumulate until thaw. The following sections describe the data sources used in this modelling study for each of these important inputs.

5.4.1 Landfast Ice Data

Numerous general definitions of landfast ice can be found in the literature (see review in Eicken et al., 2006). Barry et al. (1979) provided a clear list of criteria to distinguish landfast ice from other forms of sea ice: "(i) the ice remains relatively immobile near the shore for a specified time interval; (ii) the ice extends from the coast as a continuous sheet; (iii) the ice is grounded or forms a continuous sheet which is bounded at the seaward edge by an intermittent or nearly continuous zone of grounded ridges." Though this definition thoroughly describes the attributes of landfast ice, for the purposes of this modelling study a more concrete definition of landfast was required. In the interest of accurately and consistently identifying landfast ice, Eicken et al. (2006) define landfast ice as sea ice contiguous with the shoreline and lacking motion detectable in satellite imagery for approximately 20 days. Using this definition, Mahoney et al. (2012) quantified the coverage of landfast ice along the Alaskan Arctic coast.

A BOEM study (Mahoney et al., 2012) quantified the extent of landfast ice along the Arctic coast of Alaska including the Chukchi and Beaufort Seas. Publically available shapefiles were extracted from the project website (http://boemre-new.gina.alaska.edu/beaufort-sea/landfast-summary). Monthly averaged means (1996-2008) were utilized as baseline data for the Alaskan Arctic landfast ice coverage.

Landfast ice coverage was available for more eastern portions (east of the Mackenzie River delta) of the modelling zone through the National Snow and Ice Data Center (NSIDC) (Konig Beatty, 2012). Monthly data from the years 1991 through 1998 were composited into mean monthly landfast ice coverage. This dataset included ice concentration percentages for each raster cell. Cells with a concentration of greater than 15% were considered to have landfast ice. This concentration level most strongly corresponded with the higher resolution shapefile data available through BOEM (Mahoney et al., 2012). These mean raster datasets were converted into shapefile extents.

These two datasets (BOEM and NSIDC) were then merged to create continuous landfast ice coverage (monthly average) for the entire area of interest. The BOEM dataset (1996-2008) provided higher resolution and more recent years than the NSIDC dataset (1991-1998). Therefore, the BOEM dataset served as the reference dataset for merging. Figure 20 through Figure 22 show the composited monthly average landfast ice coverage used in this modelling study.

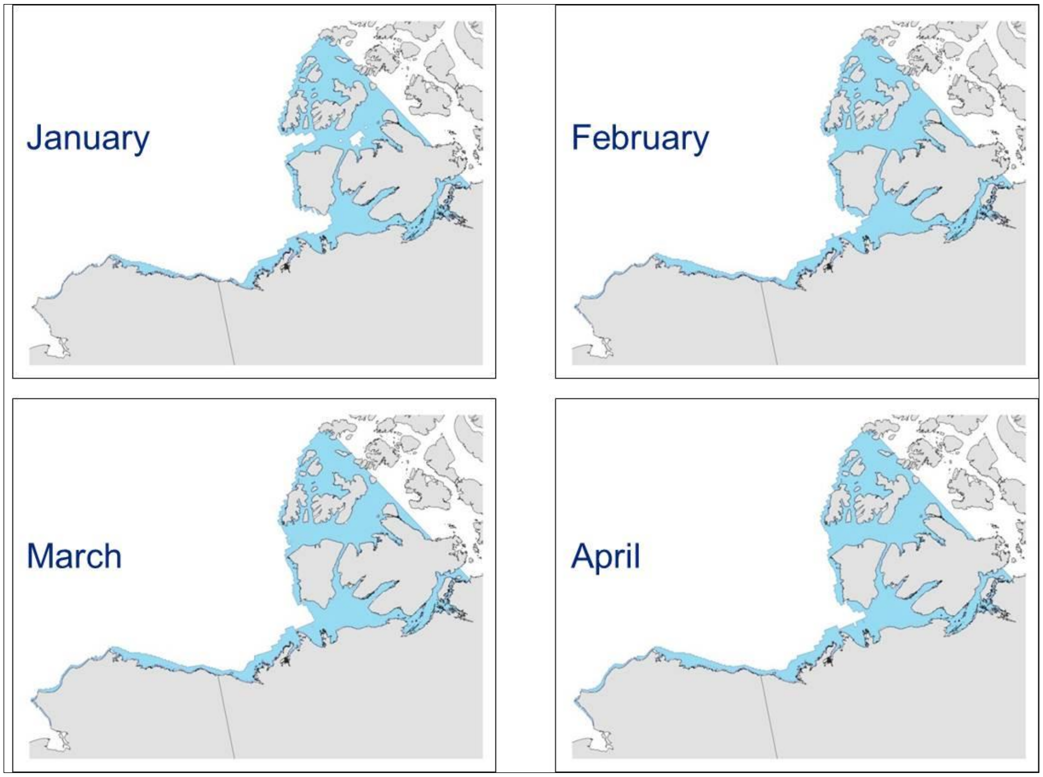

Figure 20. Monthly average landfast ice coverage January–April.

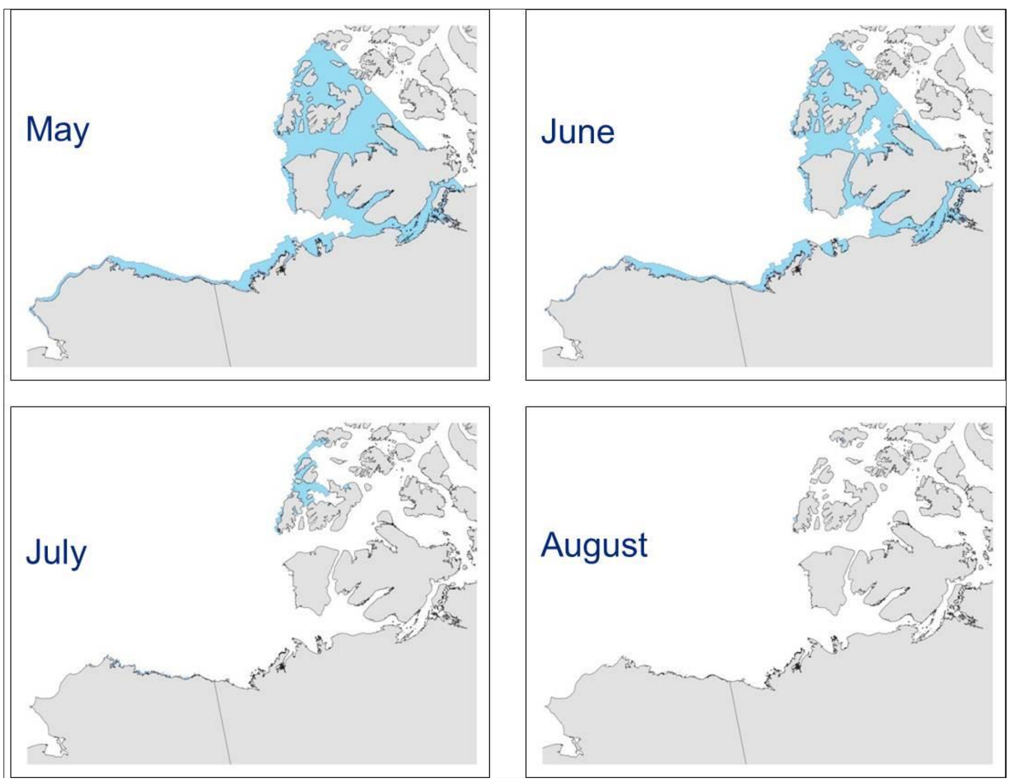

Figure 21. Monthly average landfast ice coverage May–August.

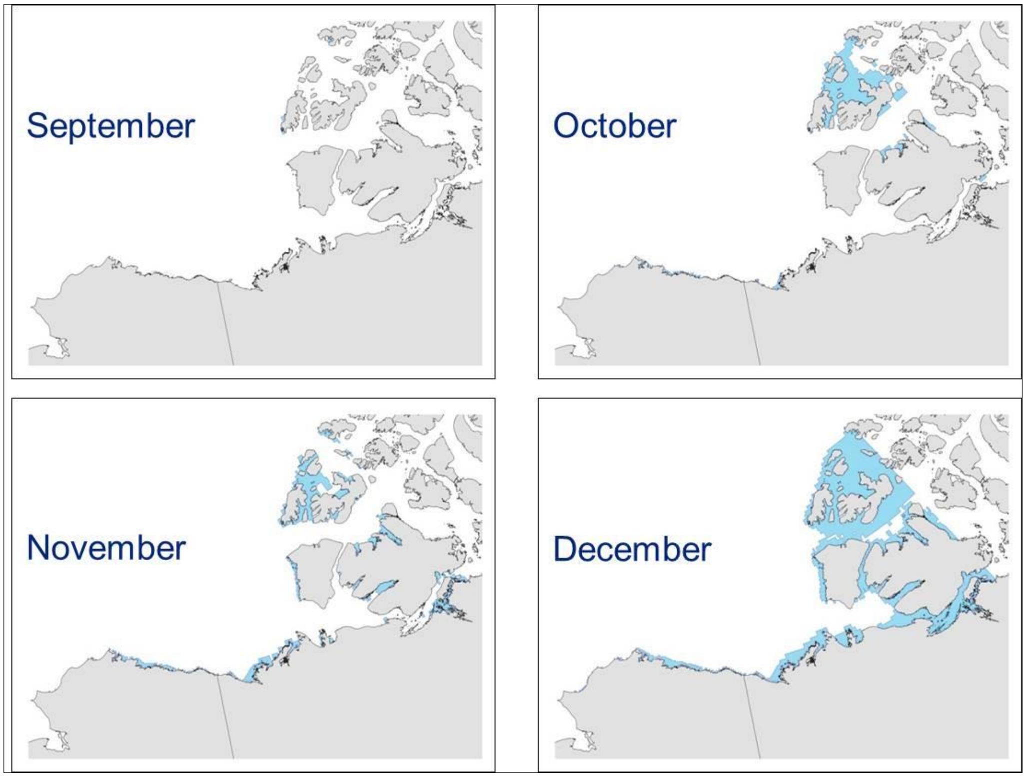

Figure 22. Monthly average landfast ice coverage September–December.

5.4.2 Circulation Data for Water and Ice Currents – TOPAZ4 Model

Model Description

Water and ice circulation data generated from the TOPAZ4 hydrodynamic model were used in this modelling study. TOPAZ stands for (Towards) an Operational Prediction system for the North Atlantic European coastal Zones. TOPAZ4 is a coupled ocean-sea ice data assimilation system for the North Atlantic and the Arctic. The dataset was developed by the Nansen Environmental and Remote Sensing Center (NERSC) and is publically available through the Norwegian Meteorological Institute. TOPAZ4 incorporates the hybrid coordinate ocean model (HYCOM, version 2.2) (Bleck, 2002) coupled with a sea-ice model (Hunke and Dukowicz, 1997), and a 100-member ensemble Kalman filter (EnKF) (Evensen, 1994) assimilating both *in situ* observations and satellite data. Wind stress for the TOPAZ4 model is from the ERA-40 (ECMWF RE-ANALYSIS) wind model (described in Section 5.3.1). TOPAZ is the only operational, large-scale, eddy-resolving ocean data assimilation system that uses a deterministic formulation of the EnKF in the Arctic region. The EnKF assimilates remotely-sensed sea level anomalies, sea surface temperature, sea ice concentration, Lagrangian sea ice velocities (winter only), as well as temperature and salinity profiles from Argo floats. From the results of a 6-year pilot reanalysis, TOPAZ4 has been shown to produce a realistic estimate of the mesoscale ocean circulation in the North Atlantic, as well as the sea ice variability within the Arctic (Sakov et al., 2012).

In the implementation of HYCOM for the TOPAZ4 system, the vertical coordinate is isopycnal in the stratified open ocean and z-coordinate in the unstratified surface mixed layer (Sakov et al., 2012). HYCOM was found to be the most suitable model for the large-scale Arctic water masses that span the stratified open ocean, regions of steep topography, and extensive sea ice. HYCOM is also flexible in that it provides sigma coordinates in coastal regions. However, sigma coordinates were not adopted because resolving coastal areas was not a primary objective of the TOPAZ4 project.

The model domain covers the North Atlantic and Arctic Ocean basins (Figure 23). The model grid is horizontal and created by a conformal mapping with the poles shifted to the side of the globe. This allows for a quasi-homogeneous grid size (Bentsen et al., 1999, Sakov et al., 2012). The model grid has 880 x 800 horizontal grid points and with horizontal spacing of approximately 12-16 km in the open ocean (about 12.5 km at the north pole, equivalent to 1/8 degree). There are 28 hybrid layers (or z layers) in the vertical from the surface to a depth of 5,500 m. Z-layer thickness can range from a minimum of 3 m to a maximum of 450 m (to resolve the deep mixed layer of the sub-polar gyre). The model bathymetry is based on the General Bathymetric Chart of the Oceans database (GEBCO) at 1-min resolution (GEBCO, 2009).

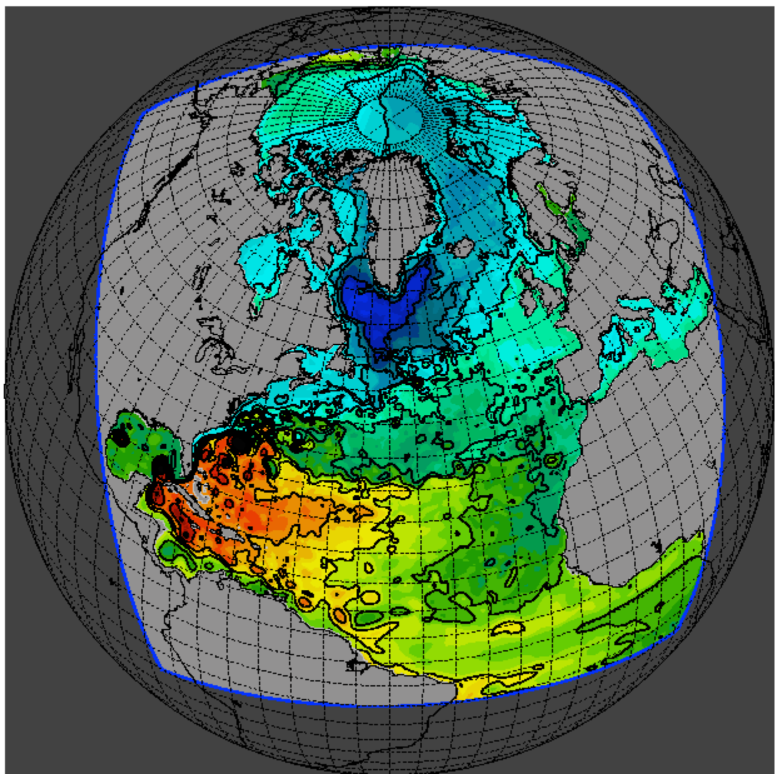

Figure 23. The entire domain of the outer model of TOPAZ4 Arctic and Atlantic Oceans, coloration shows snapshot of sea surface height. (Source: Samuelsen and Bertino, 2013).

TOPAZ4 is coupled with a sea-ice model based on elastic-viscous-plastic (EVP) rheology (Hunke and Dukowicz, 1997). EVP is the standard fluid dynamics model used to predict the behaviour of free moving sea ice. The EVP treats pack ice as a visco-plastic material that flows plastically under typical stress conditions, but behaves as a linear viscous fluid where strain rates are small and the ice becomes nearly rigid (Hunke and Dukowicz, 1997). Predicted currents and wind stress, together with the EVP accounting for behaviour, are used to derive modelled sea ice velocities. These ice currents are then assimilated with remotely-sensed sea ice concentration (CRESAT) and Lagrangian sea ice velocities (winter only) using the EnKF.

For more information, refer to Sakov et al. (2012) for detailed documentation of the complete TOPAZ4 Data Assimilation System.

Data Processing

The TOPAZ4 Reanalysis dataset provides daily mean data from 1991-2010, whereas daily mean data from 2011 to present is available through the operational TOPAZ4 system. Reanalysis data from years earlier than 2008 were found to have spotty and inconsistent coverage in the area of interest. Overall, temporal and spatial data quality was highest from spring of 2008 to present.

The TOPAZ4 Arctic Reanalysis hindcast data product (2008-2011), and daily mean data product from the TOPAZ4 operational system (2011-2013) was downloaded from the MyOcean web portal (http://myocean.met.no/). Raw data was in netcdf format. Daily mean 3-dimensional current speed and direction, surface sea ice drift speed and direction, ice thickness, and ice coverage fraction were acquired and processed for the time period April 2008 – March 2013. Only a subset of the Arctic grid was retrieved for the region of interest (Beaufort and Chukchi Seas). The geographical coordinates of the subset are approximately 61° N to 90° N, and 170° W to 110° W.

Raw TOPAZ4 data was provided using a polar stereographic projection with velocity vectors orthogonal to the curvilinear grid. An inversion projection was applied to get the coordinates of the grid in latitude and longitude. The raw velocity data was transformed using an inverse polar stereographic vector projection for an eastward northward reference frame for the SIMAP model.

Hydrodynamic Model Output

Water and Ice Currents

Figure 24 through Figure 27 show the TOPAZ4 grid, ice and current vectors, and general extent of the subset of TOPAZ4 data used in this modelling study. Each figure shows the monthly average current and ice velocities, in addition to ice coverage, of various months in 2011.

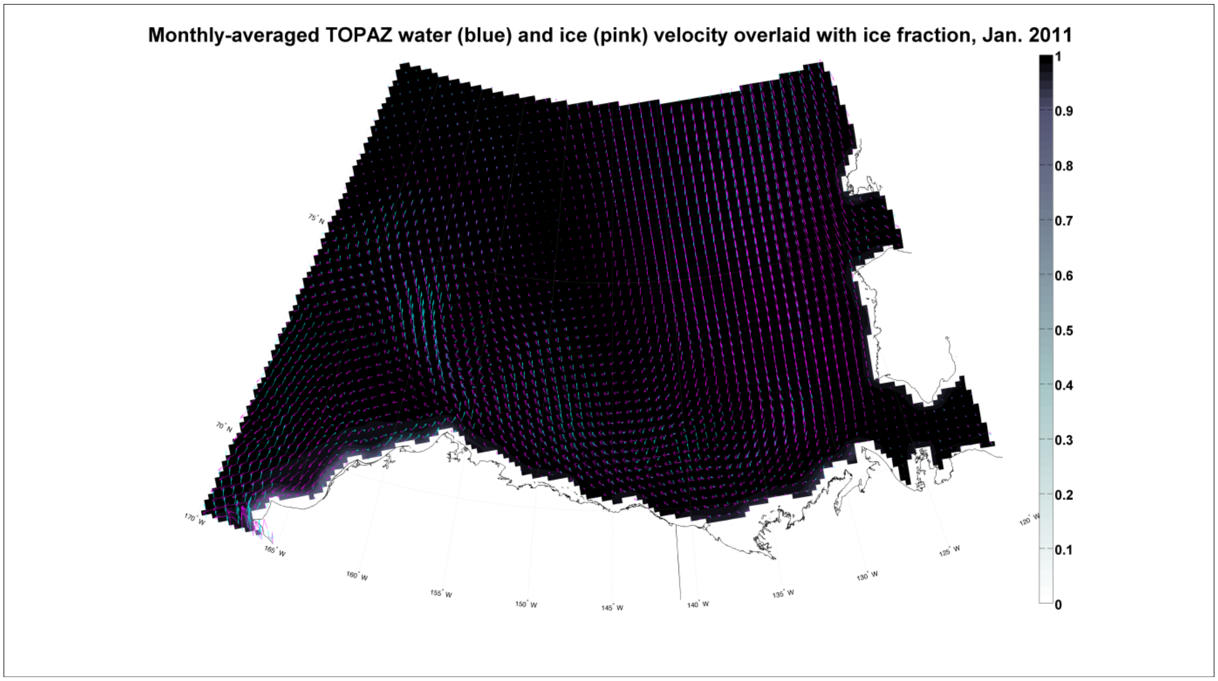

Figure 24. TOPAZ4 data domain and grid node resolution. Vector arrows show direction of the average monthly surface currents (blue) and ice currents (pink) for January of 2011. Arrows are scaled by size to represent the average speed observed each grid node. The grey contours overlaid on the vector arrows represent the average ice coverage fraction for January 2011.

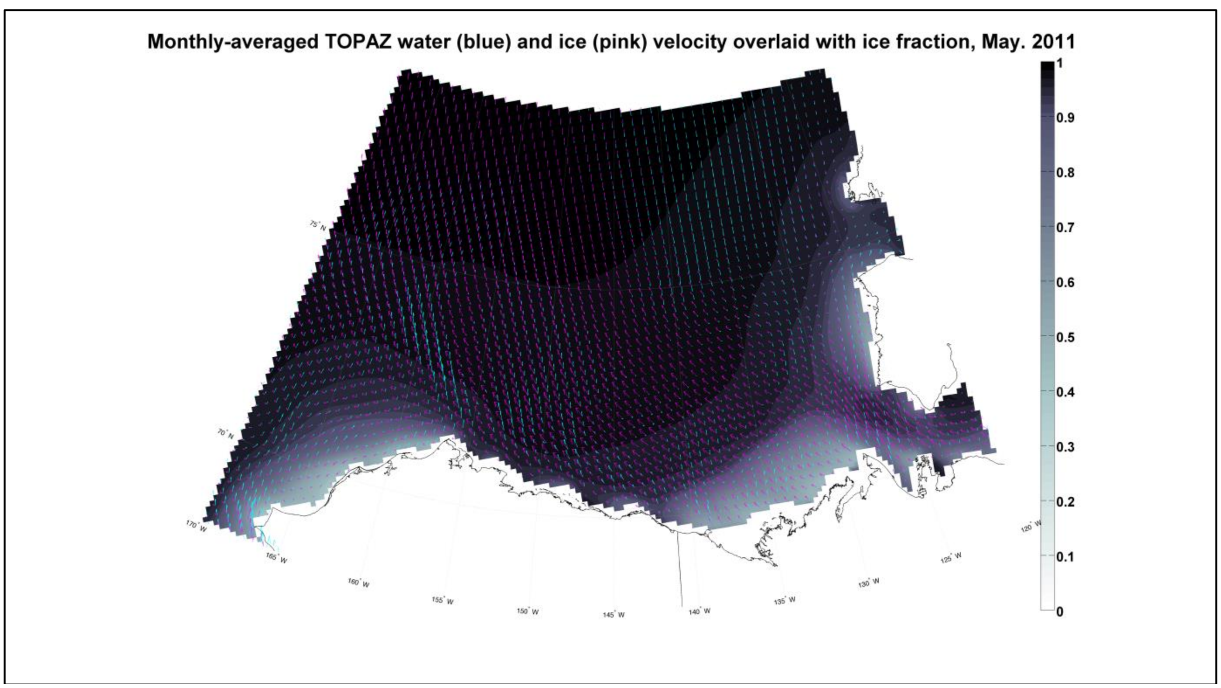

Figure 25. TOPAZ4 data domain and grid node resolution. Vector arrows show direction of the average monthly surface currents (blue) and ice currents (pink) for May of 2011. Arrows are scaled by size to represent the average speed observed each grid node. The grey contours overlaid on the vector arrows represent the average ice coverage fraction for May 2011.

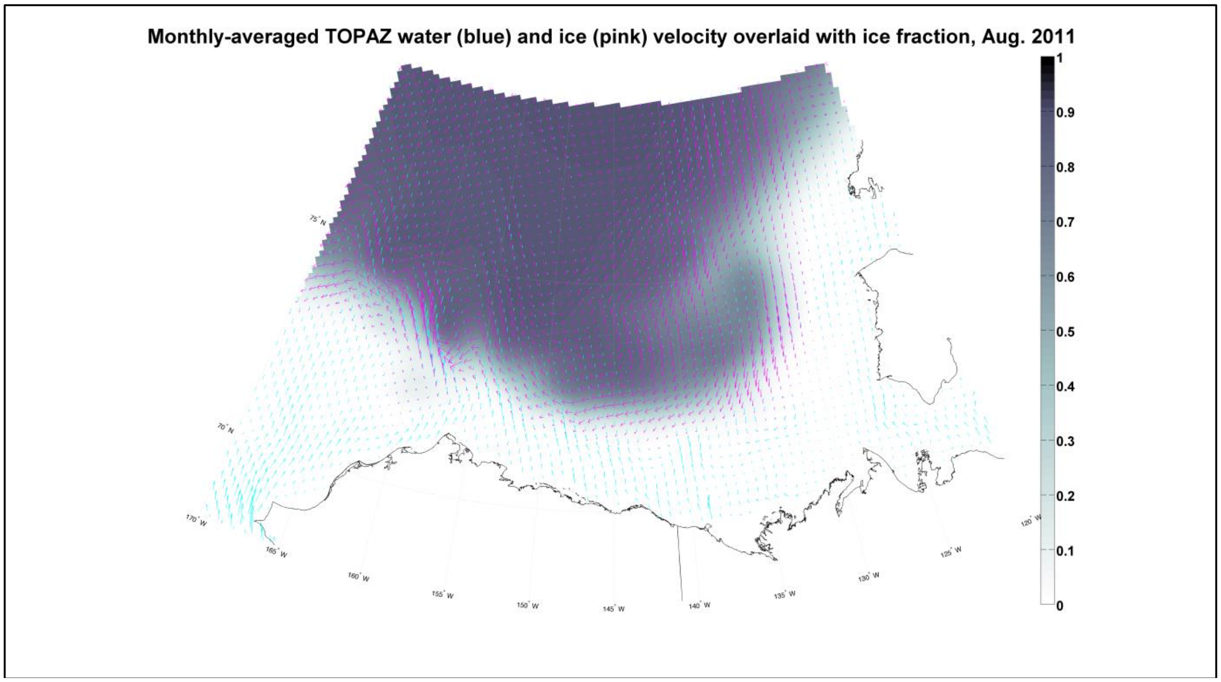

Figure 26. TOPAZ4 data domain and grid node resolution. Vector arrows show direction of the average monthly surface currents (blue) and ice currents (pink) for August of 2011. Arrows are scaled by size to represent the average speed observed each grid node. The grey contours overlaid on the vector arrows represent the average ice coverage fraction for August 2011.

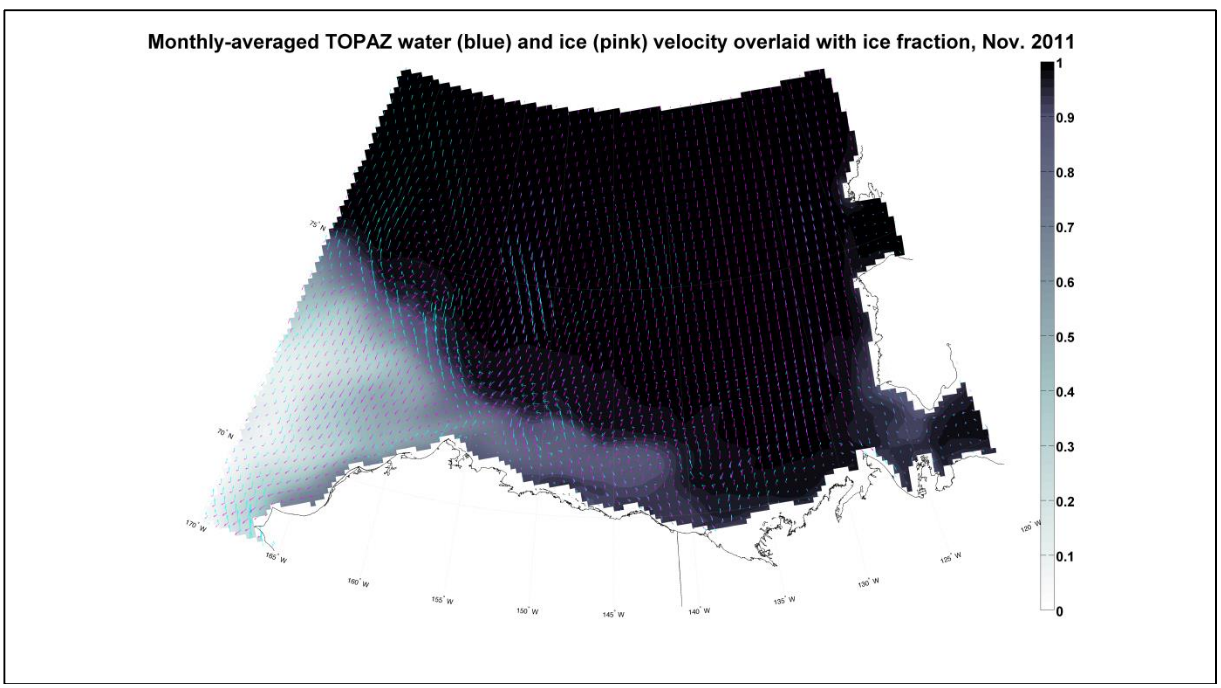

Figure 27. TOPAZ4 data domain and grid node resolution. Vector arrows show direction of the average monthly surface currents (blue) and ice currents (pink) for November of 2011. Arrows are scaled by size to represent the average speed observed each grid node. The grey contours overlaid on the vector arrows represent the average ice coverage fraction for November 2011.

Figure 28 shows the average surface currents speed and direction near the deep blowout site (Section 6.5) for each month from the TOPAZ4 dataset. In the current rose plots speed is shown as cm/s and direction is shown using oceanographic convention (i.e., direction currents are flowing towards). For most months at the deep blowout site the dominant direction of the surface current is towards the west and southwest, with the strongest velocities occurring during the ice free months.

Figure 28. Monthly surface current rose plot showing speed (cm/s) and direction at the deep blowout site averaged from years 2008-2013 from the TOPAZ4 data set.

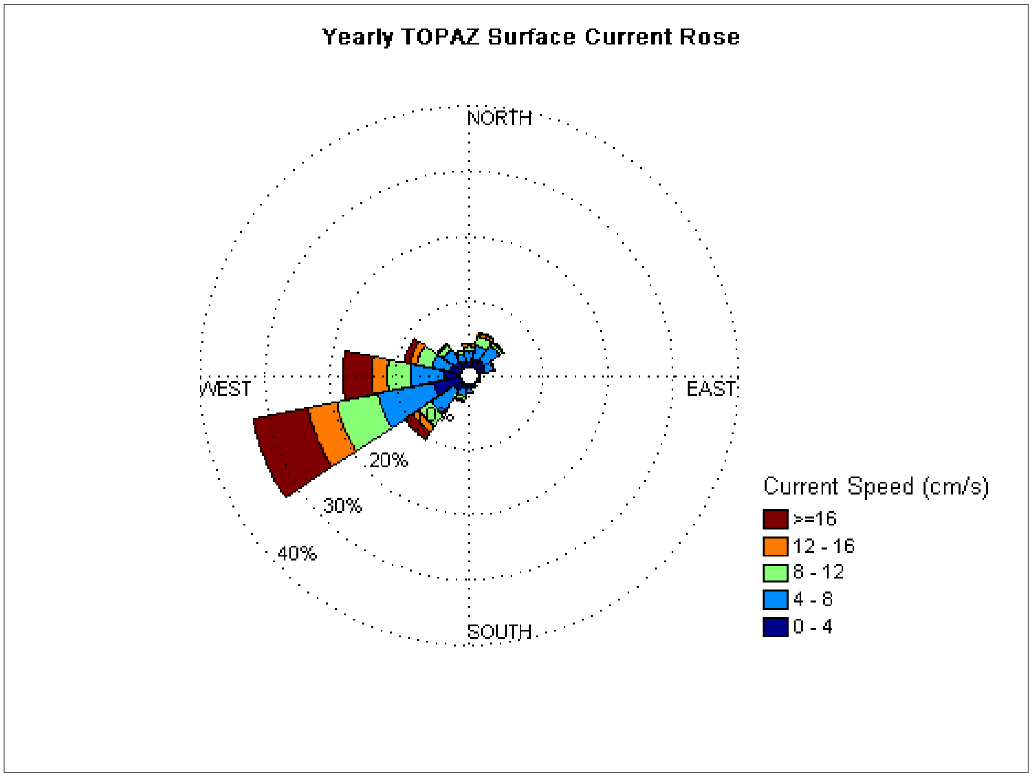

Figure 29. Yearly surface current rose plot showing speed (cm/s) and direction at the deep blowout site averaged from years 2008-2013 from the TOPAZ4 data set.

Figure 30 presents monthly statistics (average, 95th percentile, and maximum) of the TOPAZ4 surface current speeds location near the deep blowout site. Average monthly speeds are highest in September and October, at approximately 16 cm/s. Lowest average speeds are in February-April, at about 4 to 5 cm/s.

For the subsurface blowout simulations, a characterization of the vertical profile of currents is also needed to appropriately evaluate the transport of oil released near the seabed through the water column. Thus, a vertical profile of currents was also obtained from the TOPAZ4 model. Figure 31 shows the yearly average vertical profile of current velocities near the deep blowout site, 2008-2013. Near the surface, the current velocity can reach 35 cm/s. However, surface speeds average around 10 cm/s. Velocity decreases with depth to an average of about 1 cm/s at 1,000 m deep.

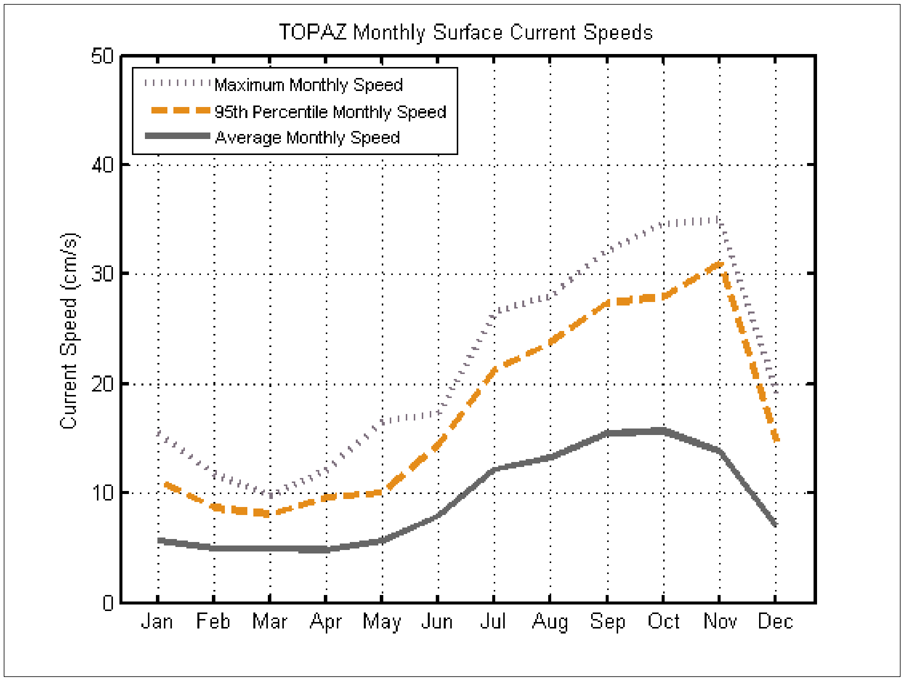

Figure 30. Chart showing monthly surface current speed statistics at the deep blowout site: average, 95th percentile, and maximum speed (cm/s) from 2008-2013 from the TOPAZ4 data set.

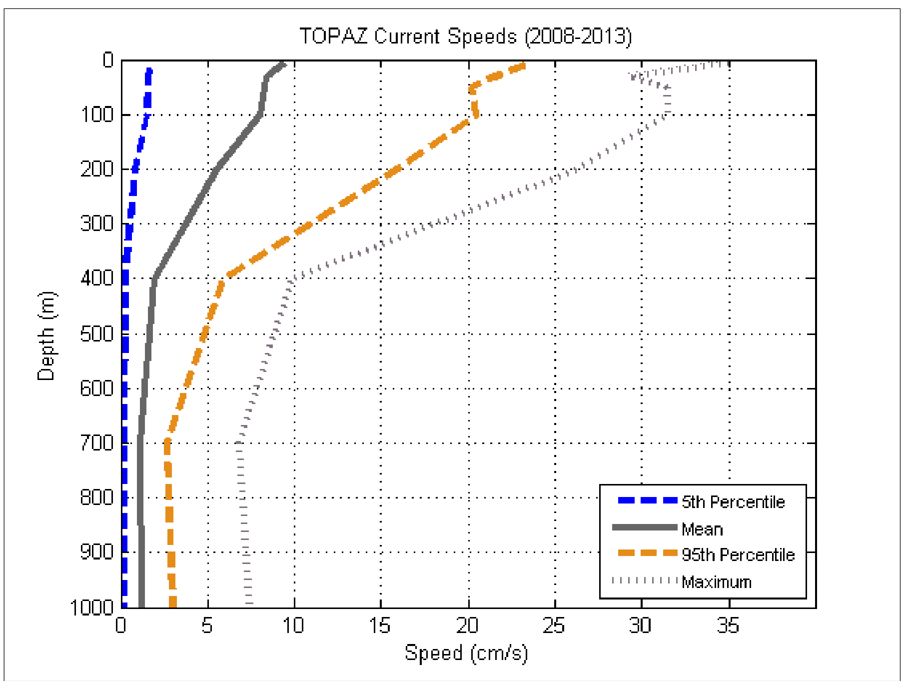

Figure 31. Chart showing vertical profile of yearly average current speed statistics throughout the water column at the deep blowout site: 5th percentile, average, 95th percentile, and maximum speed (cm/s) from 2008-2013 from the TOPAZ4 data set.

Figure 32 show the average surface sea ice current speed and direction for the months where ice coverage was typically greater than 30% at the deep blowout site (November to June) (Section 6.5). In the current rose plots, speed is shown as cm/s and direction is shown using oceanographic convention (i.e., direction currents are flowing towards).

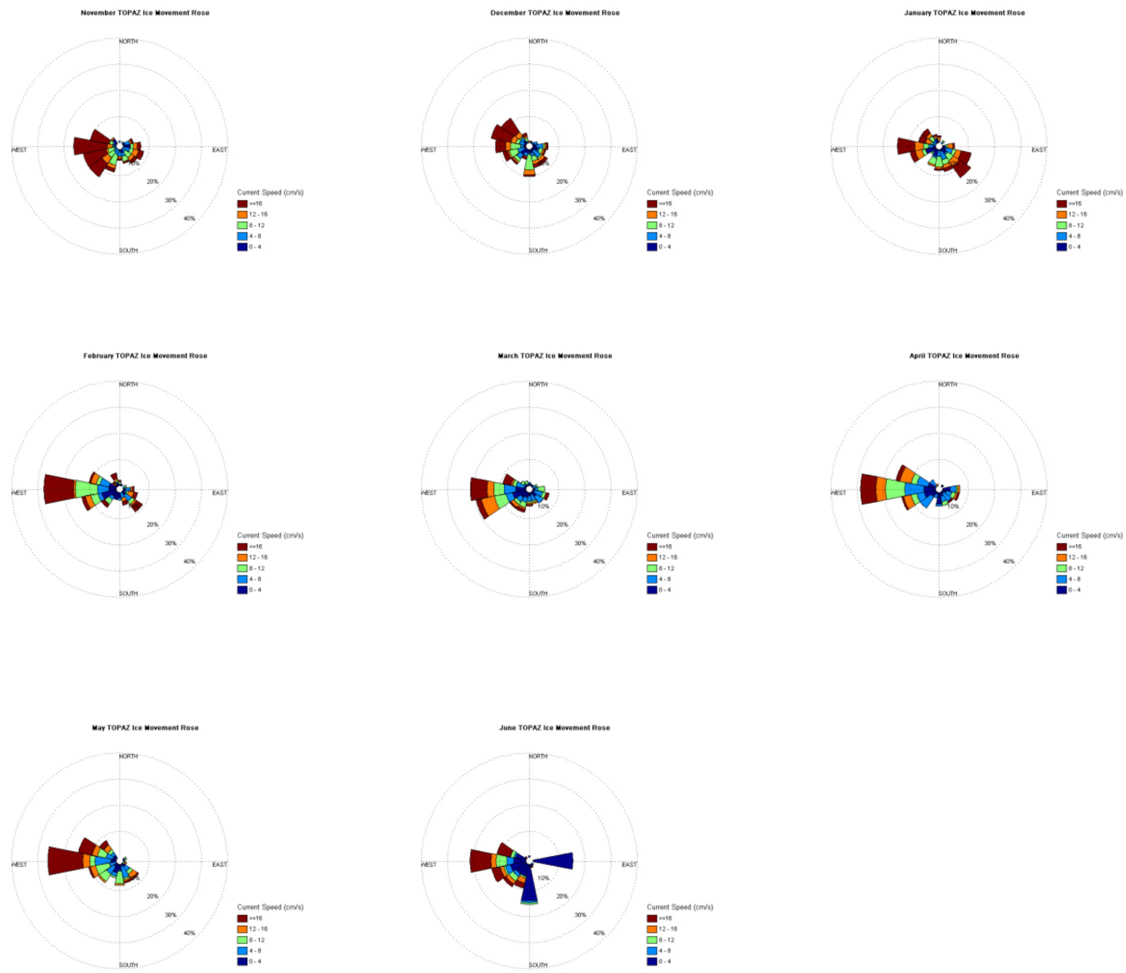

Figure 32. Monthly ice current rose plot showing speed (cm/s) and direction at the deep blowout site averaged from years 2008-2013 from the TOPAZ4 data set.

Figure 33 shows monthly statistics (average, 95th percentile, and maximum) of the TOPAZ4 ice movement speeds near the deep blowout site (Section 6.5) for the years 2008-2013. Average ice movement speeds were highest in November, at about 17 cm/s. Ice velocities were low or none July to September when there is no ice present at the deep blowout site. Dominant direction of flow is towards the west in most months except January.

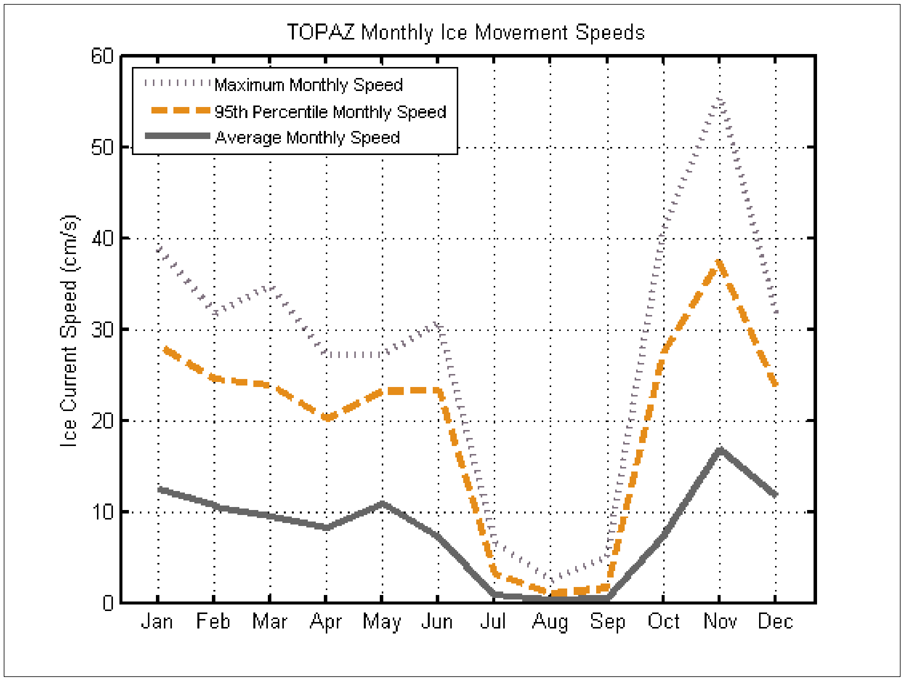

Figure 33. Chart showing monthly ice current speed statistics at the deep blowout site: average, 95th percentile, and maximum speed (cm/s) from 2008-2013 from the TOPAZ4 data set.

Percent Ice Coverage

The TOPAZ4 model output also contains a variable for fraction of ice coverage, which was translated into percent ice coverage for this modelling study. Figure 34 through Figure 36 show contours in grey scale of the average spatial ice coverage for each month of 2011. All years in the TOPAZ4 dataset contain ice coverage information, but 2011 was selected to show monthly examples in this section as it best represented the general ice coverage observed across all years. In addition, the landfast ice polygons described in Section 5.4.1 are overlaid in each figure (shown in pink).

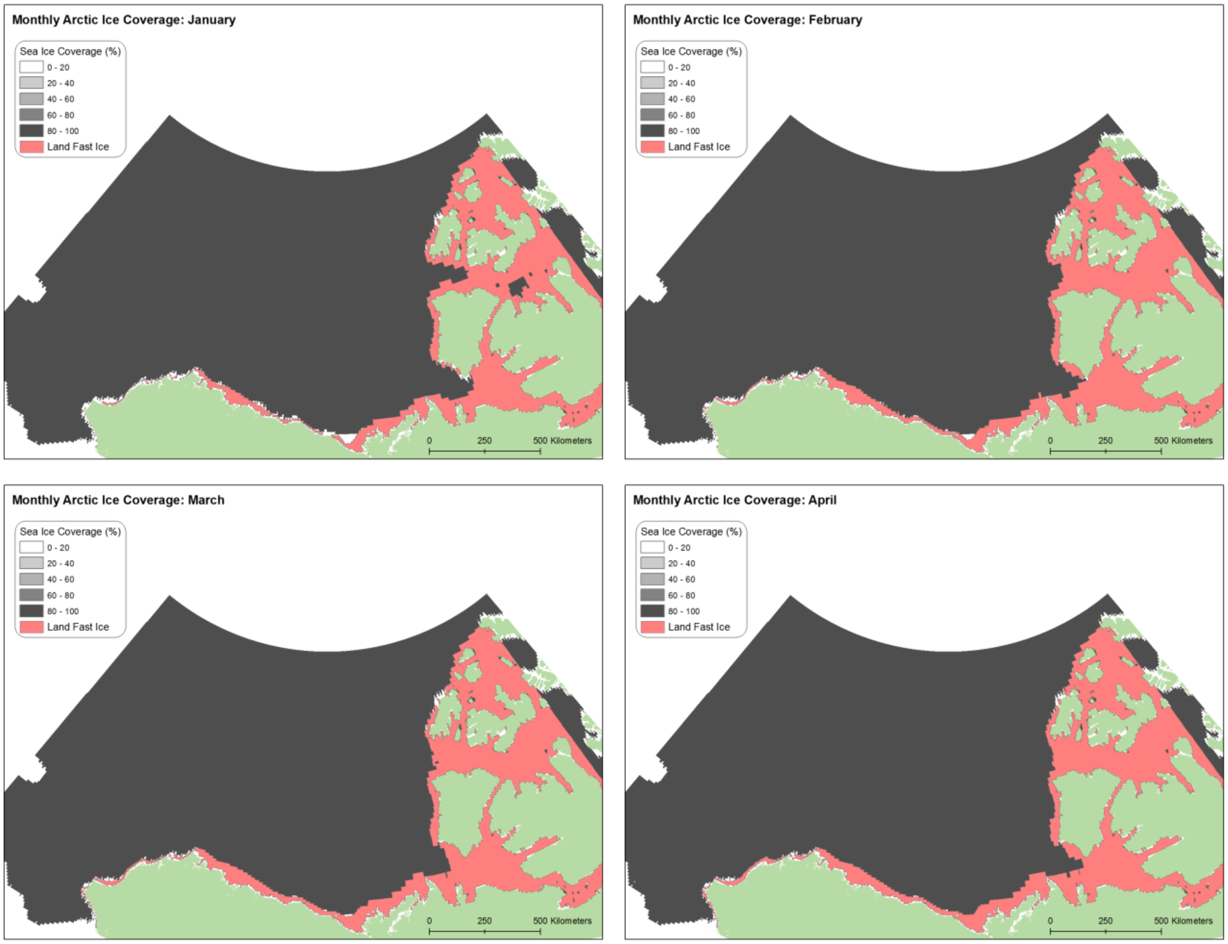

Figure 34. Map showing 2011 monthly average sea ice coverage and landfast ice polygons January -April.

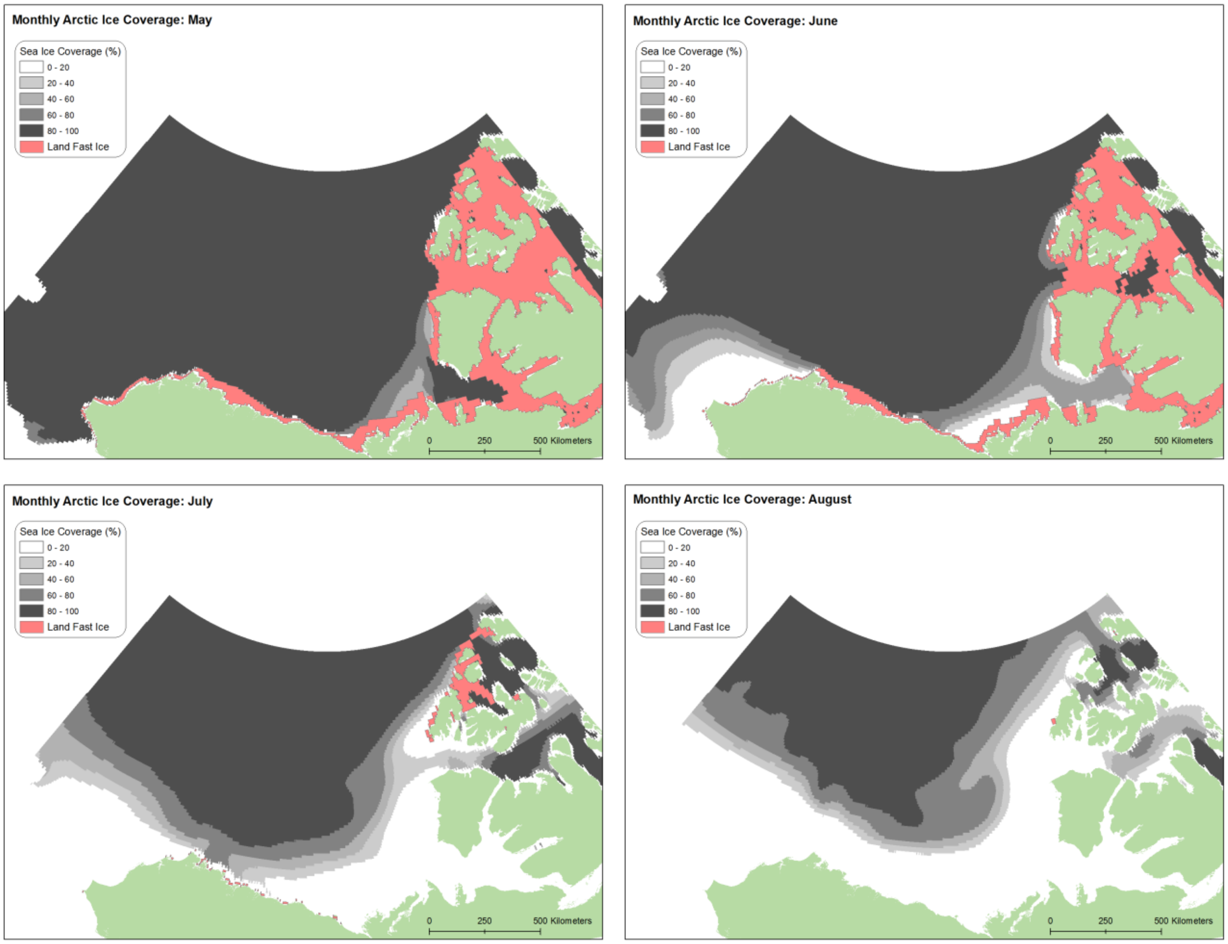

Figure 35. Map showing 2011 monthly average sea ice coverage and landfast ice polygons for May - August.

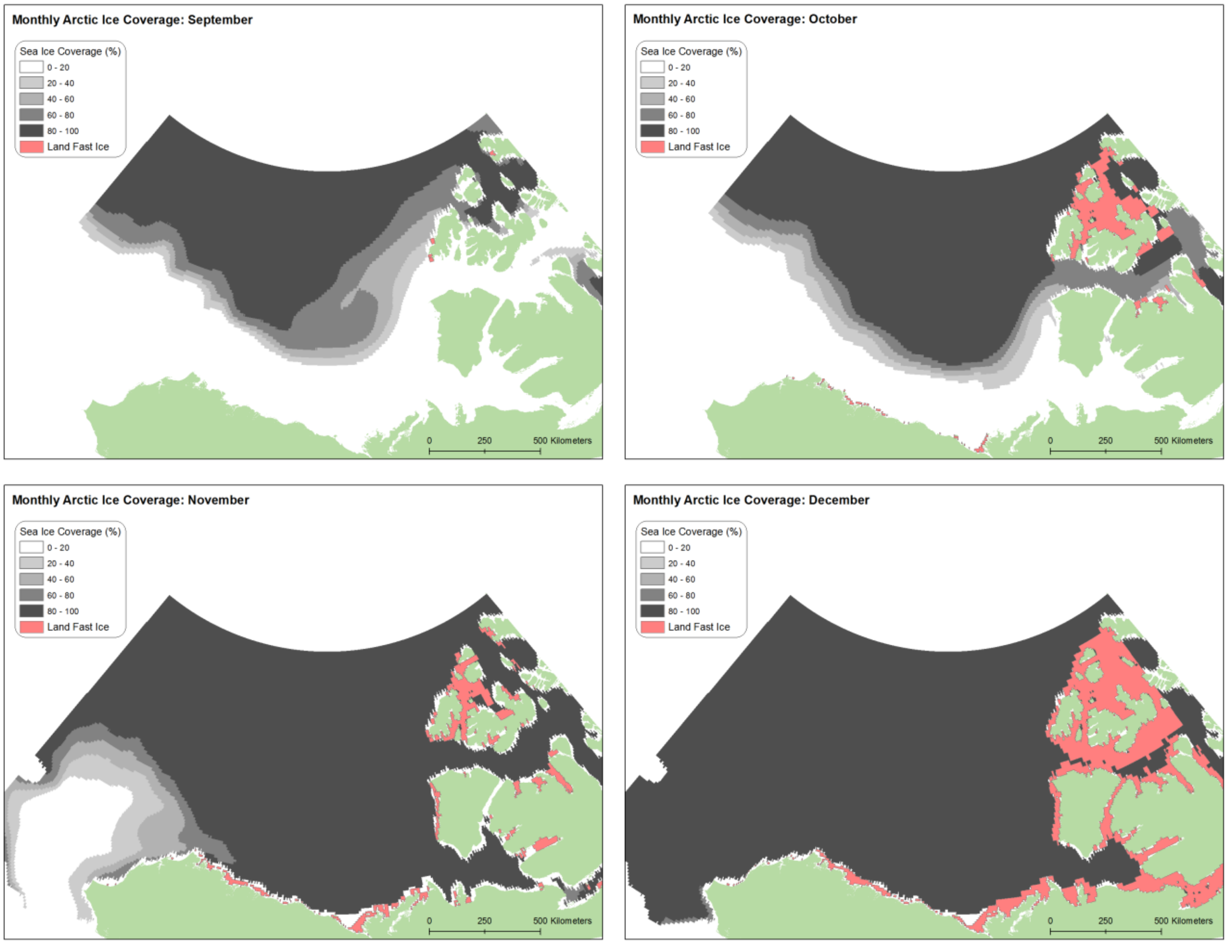

Figure 36. Map showing 2011 monthly average sea ice coverage and landfast ice polygons for September - December.

TOPAZ4 Hydrodynamic Model Limitations

The TOPAZ4 model was selected for this modelling study because it was one of the only publically available large-scale, multi-year hindcast datasets for the Arctic containing 3-dimensional current fields as well as surface ice velocities and coverage. The spill locations in this study ranged from deep areas on the shelf break, to shallower regions closer to the coast, therefore a large-scale hydrodynamic model was required for oil spill modelling. However, the hydrodynamic model does have limitations that need to be considered while interpreting the results of this study. The primary objective of TOPAZ4 project was to resolve large-scale Arctic Ocean circulation. Coastal hydrodynamic features are not well resolved in the model, because the Z-coordinates used in the unstratified shelf regions do not resolve coastal dynamics. The Beaufort shelf, as compared to other continental shelves, is relatively narrow and the area does exhibit complex coastal features and dynamics (e.g. counter currents and eddies).

Some of the complex features that were unresolved in the TOPAZ4 data include the influence of the Mackenzie River discharge and the eastward flowing shelf counter current. The coastal counter current does occur in the modelled data but was variable in speed and direction and its presence was highly erratic throughout the years. Inspection of local surface currents in TOPAZ4 compared well with local wind stress in various coastal areas along the North Slope, but fluctuated often in direction. Schulze

(2012) found that the eastward flowing current, under enhanced easterly winds, is subject to reversals to the west with current speeds up to 1 m/s. Reversal of the shelf break current in the TOPAZ4 data may not be completely unjustified, but this pattern was still assumed by the authors to be somewhat suspect.

Overall, the general Beaufort shelf and shelf break circulation was westward in direction for both water and ice currents. In open waters, a shelf break eddy feature was often observed around the 600-1,000 m bathymetry contours, directly north of the Mackenzie River delta. This was occurring on the shelf break between the Beaufort Gyre and the coastal counter current. Average current velocities in the TOPAZ4 model compared well with data reported in the literature, on average 10-20 cm/s with maximum velocities up to 1 m/s. During a reanalysis study of the TOPAZ4 system it was found that modelled ice drift velocities are generally too fast by approximately 3 km/day, as compared to drifter field data (Sakov et al., 2012). Comparison to other ice cover data from NASA confirmed that TOPAZ4 seasonal trends were reliable.

5.4.3 Nearshore Tidal Currents Model - HYDROMAP

The TOPAZ4 model grid did extend to the coastline, but in various coastal areas null values were observed in the grid cells (Figure 37). Due to this limitation in the TOPAZ4 dataset, RPS ASA created a coastal tidal model using the HYDROMAP system to account for some current forcing in these null areas in addition to wind forcing at the ocean surface.

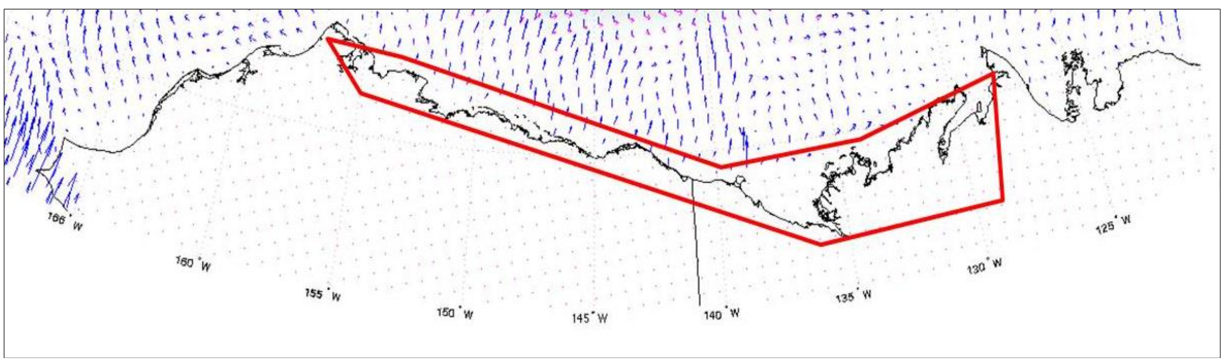

Figure 37. Close-up of TOPAZ4 grid and current vectors (blue arrows) along the Beaufort coastline. The red box highlights the areas of null values (red grid nodes) found in certain coastal features in the TOPAZ4 dataset.

HYDROMAP is a globally re-locatable three-dimensional hydrodynamic model (Isaji, et al., 2001a, 2001b) capable of simulating complex circulation patterns due to tidal forcing, wind stress, and fresh water flows. HYDROMAP employs a novel step-wise-continuous-variable rectangular gridding strategy with up to six levels of resolution. The term “step-wise continuous” implies that the boundaries between successively smaller and larger grids are managed in a consistent integer step. The numerical solution methodology follows that of Owen (1980). Isaji, et al. (2001a, 2001b) provide a detailed description of the model. HYDROMAP incorporates spatially-variable global tidal database characterization of tidal constituents for use in specifying water surface elevation (tidal) boundary conditions. Alternatively, boundary specific water level records can be used to generate water surface elevation boundary conditions. HYDROMAP creates harmonic models that are not time-stamped.

The HYDROMAP model created for this project only accounted for tidal constituents M2, S2, N2, K2, O1, K1, and P1. Fresh water flows and wind stress were not included in the simulation. The HYDROMAP grid extent is shown in Figure 38. The grid had a successive resolution from 5.0 km to 1.26 km. Tidal currents in HYDROMAP merged with TOPAZ4 forcing where overlap occurred. Overall, HYDROMAP had very little influence over net circulation in the oil spill modelling results.

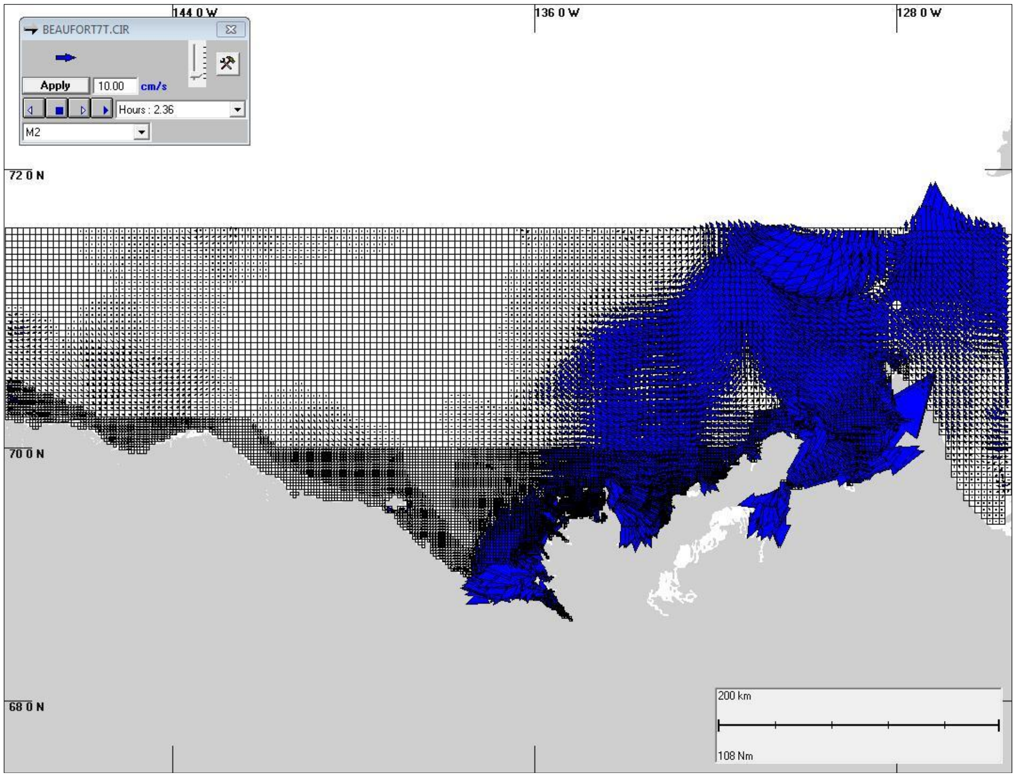

Figure 38. HYDROMAP model domain and successive grid resolution. Blue vectors indicate direction and speed at one time step in the harmonic model.

5.4.4 Water Column Structure: Temperature and Salinity Data

A definition of the physical properties of the water column in the area of interest is an important input for oil spill modelling, especially for subsurface releases. Water temperature dictates many physical attributes and weathering processes including the viscosity and evaporation rate of the spilled oil. Temperature and salinity also dictate the density of the surrounding water body, which influences the speed at which entrained oil can re-surface. Similarly, these physical attributes play an important role in the near-field mechanics of a subsurface blowout.

For this study, data defining the vertical structure of the water column, temperature and salinity, were obtained from the publicly available World Ocean Atlas 2001 (WOA01) (Boyer et al., 2004). The WOA01 dataset is compiled and maintained by the US National Oceanographic Data Center (www.nodc.noaa.gov). The dataset consists of decades of observations from various global data management projects. The WOA originated from the Climatological Atlas of the World Ocean (Levitus, 1982) and was updated with new records in 1994, 1998, and 2001 (Conkright et. al., 2002). Records have been obtained using a variety of oceanographic instruments from millions of collection stations. After a comprehensive quality control process, the remaining data were averaged yearly, seasonally, and monthly and interpolated to fit a grid with ¼ degree horizontal resolution. The yearly dataset, used in this study, includes up to 33 depth bins from the surface down to depth.

Seasonal temperature and salinity profiles were calculated for winter, spring, summer, and fall (average over multiple years) at six designated points, creating a coarse grid (2 by 3 cells) across the area of interest (Figure 39). Seasons included the following months: Winter -January, February, March; Spring – April, May, June; Summer – July, August, September; and Fall – October, November, December. Each seasonal profile was then applied to the entire corresponding grid cell. While this approach created a coarse representation of the temporal and spatial variation in temperature and salinity in the Chukchi and Beaufort Seas, it is sufficient for this hypothetical risk assessment modelling. Point 2 (Figure 39) was closest to the spill sites investigated in this study.

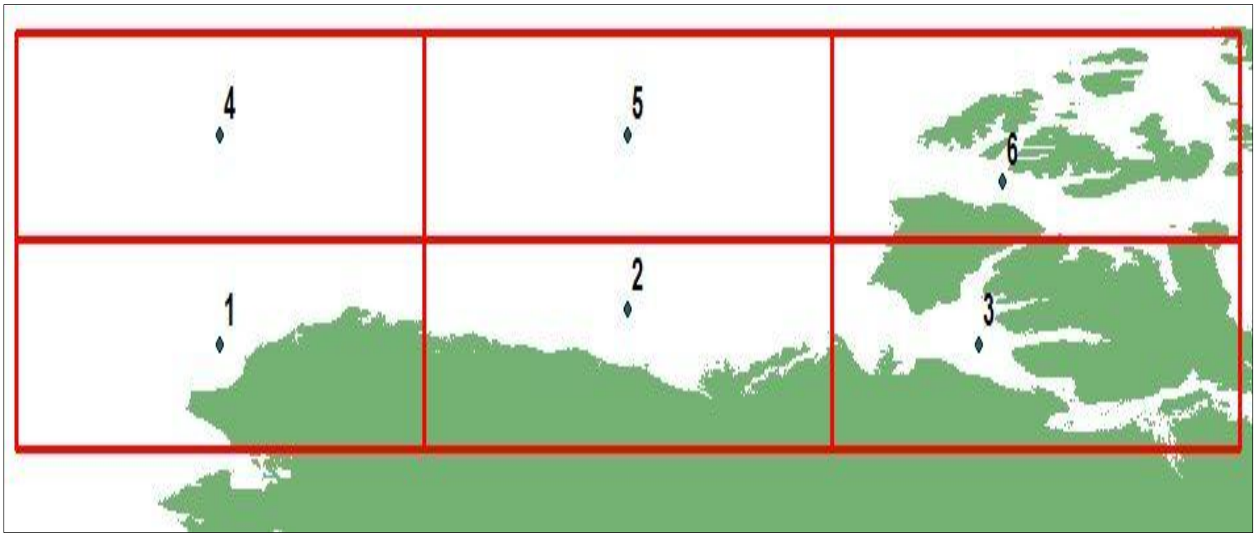

Figure 39. Six points across Chukchi and Beaufort Seas where temperature and salinity profiles were extracted from the WOA01 data set. Seasonal average temperature and salinity was calculated from several years of data for each of these points.

Figure 40 through Figure 45 show the seasonal temperature and salinity profiles used in this study for each point/grid cell.

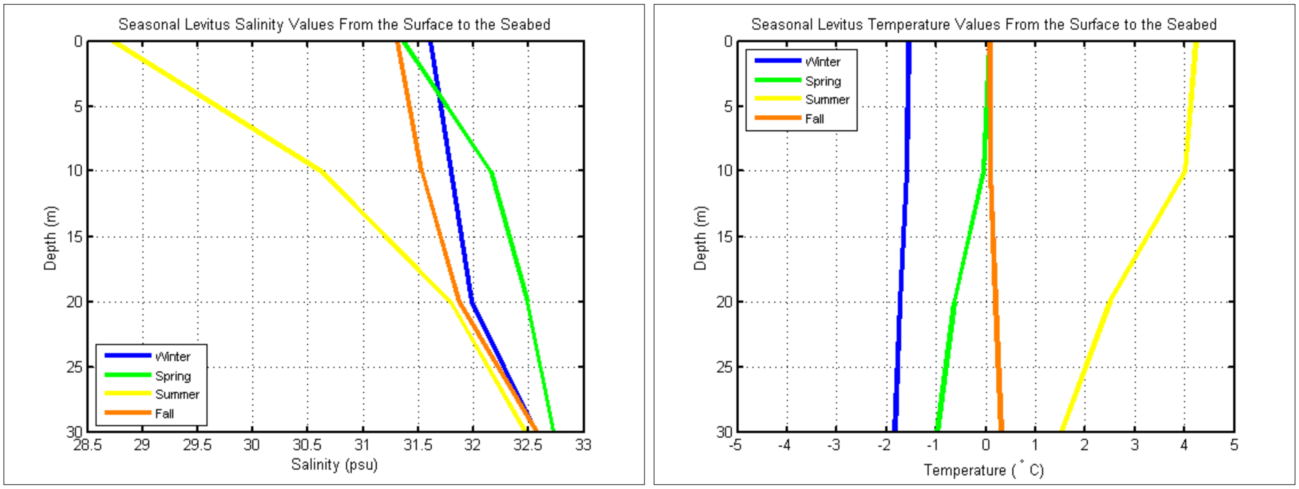

Figure 40. Seasonal salinity (psu) and temperature (°C) profiles at Point 1.

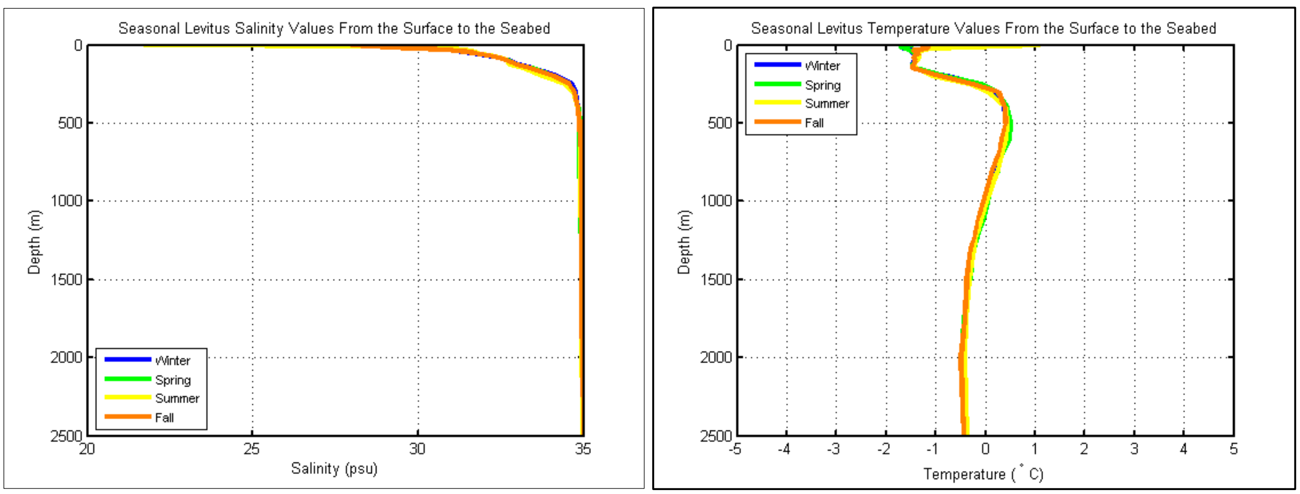

Figure 41. Seasonal salinity (psu) and temperature (°C) profile at Point 2.

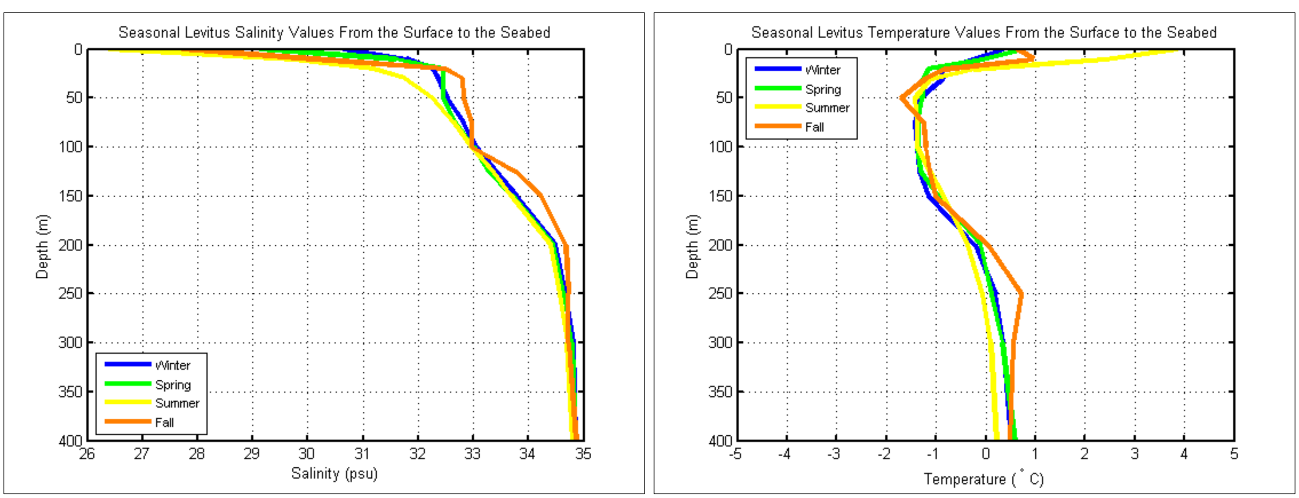

Figure 42. Seasonal salinity (psu) and temperature (°C) profile at Point 3.

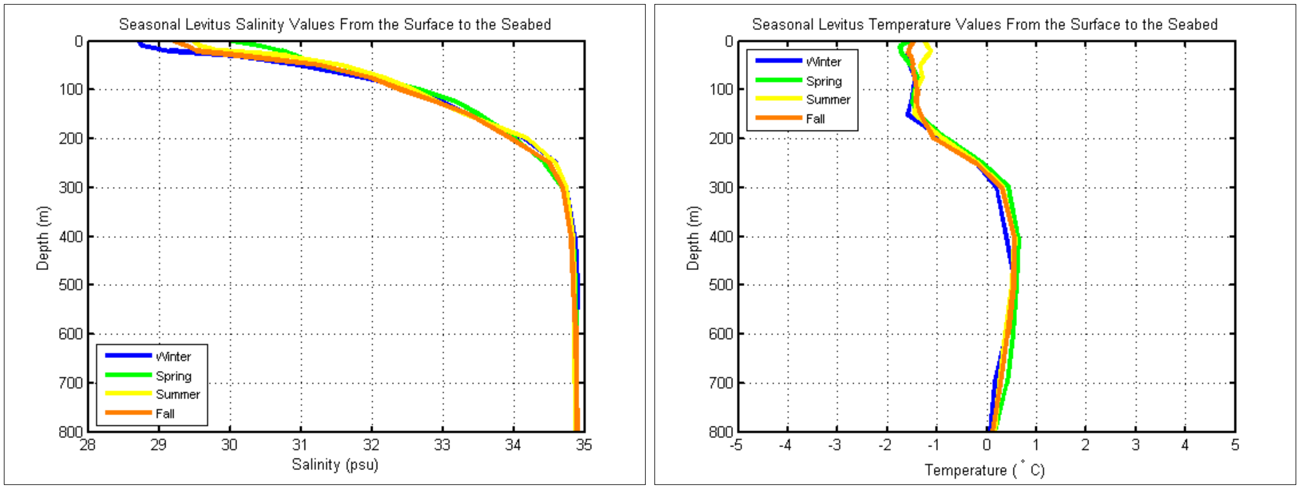

Figure 43. Seasonal salinity (psu) and temperature (°C) profile at Point 4.

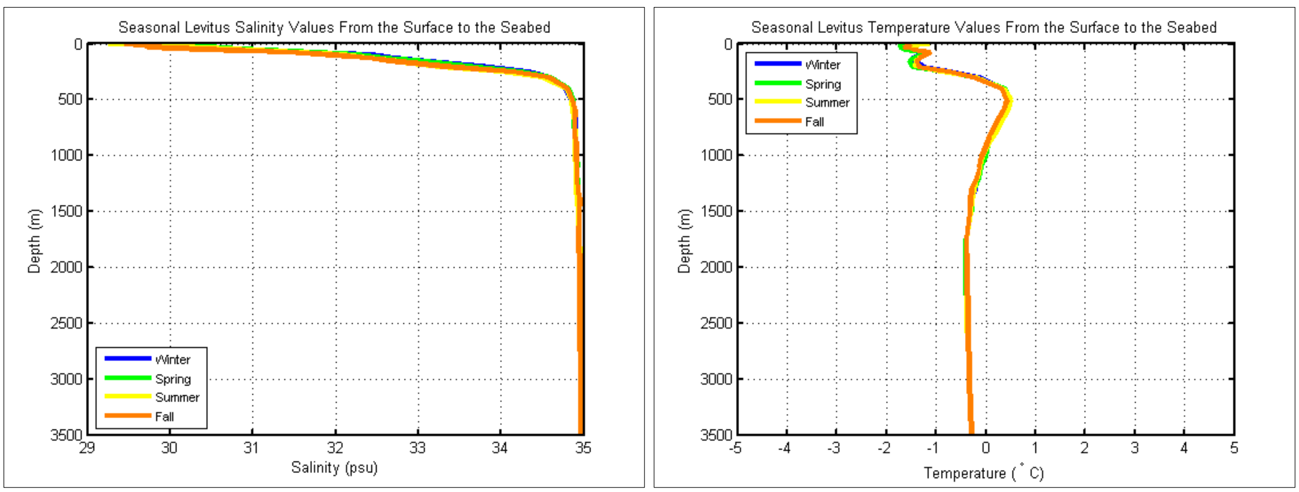

Figure 44. Seasonal salinity (psu) and temperature (°C) profile at Point 5.

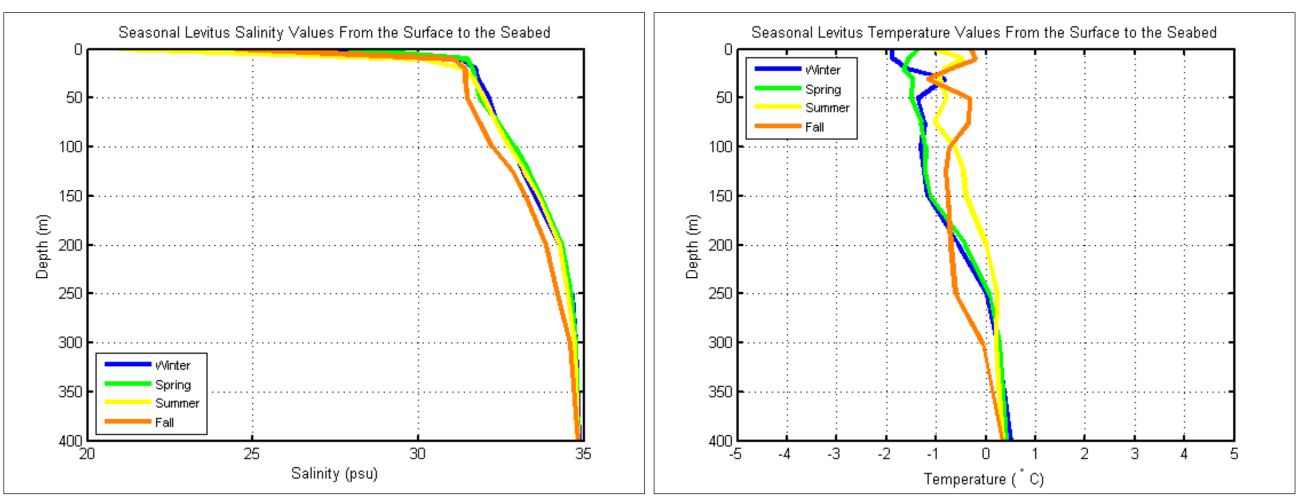

Figure 45. Seasonal salinity (psu) and temperature (°C) profile at Point 6.

6 Oil Spill Scenarios

RPS ASA, with subcontractor ERC, worked with the client to develop the oil spill scenarios to be investigated in this modelling study. The client requested that four generalized "spill analyses" be conducted: eastern shipping spills; a trans-boundary analysis having multiple spill types; a shallow blowout analysis; and a deep blowout analysis. Each spill analysis consisted of multiple scenarios, varied in some way (e.g., season, oil type, etc.). These analyses were based around the client's knowledge of various proposed oil and gas (O&G) development projects, increased shipping resulting from O&G activity, and from other development projects in the Canadian Beaufort.

ERC reviewed worldwide literature and data on plausible discharge volumes and incident probability for each spill analysis. For blowouts and pipeline leaks, discharge volumes selected for modelling were based on a review of historical blowout and leakage events. For shipping related accidents, discharge volumes were based on a review of vessel types and associated fuel carrying capacities that currently, or are proposed to, operate in Canadian and U.S. Arctic waters.

For vessel traffic, grounding incidents were found to be the most likely event to cause massive spillage in this region (e.g., tankers and bulk carriers). ERC estimated one grounding spill incident in over 400 years for a tanker, whereas for a bulk carrier one grounding spill incident in over 81 years. The probability of a pipeline spill incident is associated with the length of the pipeline. In general, for approximately 400 miles of offshore pipeline, one pipeline spill every 8 years was predicted. The probability that a pipeline spill in the Beaufort Sea will be 10,000 bbl or more is 0.0096, or about once in over 104 years. Additional analyses on more comprehensive worldwide blowout data, indicated that the probability of an individual well blowout is very small with the probability decreasing with increasing spillage volume.

Overall, ERC's review of incident probability found that, for all spill types, the worst case discharge (WCD) was not the most likely event. The maximum most probable discharge (MMPD) volumes selected for modelling represent the most likely events. For all analyses, MMPD volumes were modelled. A WCD volume was only modelled for the larger blowout analyses in addition to the MMPD.

Please see Appendix C for the full report compiled by ERC addressing spill volumes and event probability. This report contains the supporting information used to determine the spill volumes modelled in the study (e.g., review of worldwide blowout volumes, vessel type descriptions and fuel capacities). Appendix C, due to size, is provided as an external electronic document file.

RPS ASA, with the client, developed modelling assumptions for the study regarding release time frames, model duration, and response measures. Release time frames and model duration for each analysis were based on activity type (e.g., drilling, shipping) and location specific constraints from environmental conditions such as sea ice cover. Response measures were modelled in the larger deep and shallow blowout analyses only. RPS ASA reviewed proposed O&G project documents and other technical reports addressing potential response options in the Arctic (IORVL, 2013; Sørstrøm et. al., 2010; Potter et. al., 2012; NEB, 2011; SL Ross et. al., 2010; BREA, Trudel, 2012). It was determined that subsea dispersant application (deep blowout only), in situ burning and surface dispersant (surface response) were the most appropriate measures to include for modelled spills in the Arctic. Specific response assumptions and inputs (e.g., plausible amount of response time estimated for Arctic and dispersant and burning efficiency) were based on client-provided memorandums (WWF comments on S.L. Ross's Spill Response Gap Study) and on RPS ASA expert opinion/past experience.

The following sections contain a characterization of the oils used in each spill analysis (Section 6.1), and for each analysis, spill location and reasoning, summary of spill scenario assumptions, and modelling inputs (including discharge amount, spill duration, incident release time frame, and response measures, if any) are discussed (Sections 6.2, 6.3, 6.4, & 6.5).

6.1 Oil Characterization and Chemistry

Three different oil types were examined in the various spill analyses modelled: 1.) a crude oil that either released from an exploratory drill site, from a large tanker, or from a pipeline leak; 2.) a heavy fuel oil utilized by bulk carrier vessels, and 3.) a light fuel oil carried by a re-supply barge. RPS ASA developed modelling inputs for each oil type from an in-house oil property database. This database is comprised of information from Environment Canada, from published literature sources, and from past client/project provided information approved for consulting use. The tables below list the oil properties utilized by the SIMAP modelling system, the values assumed, and comments and references associated with each.

Alaska North Slope Crude (2002):

Alaska North Slope Crude (2002) was selected as the representative crude oil (
Table 3). This oil was characterized as a light to medium crude with high aromatic content and was assumed to have oil properties typical of oil potentially extracted from the region of interest.

Table 3. Oil properties of the crude oil (Alaska North Slope Crude 2002) used in the model simulations.

Oil Property	Value	Comments/References
Density @ 16 deg. C (g/cm^3)	0.87131	Calculated density from API
Viscosity @ 15 deg. C (cp)	11.5	Environment Canada Oil Property Database, as described in Jokuty et al. (1999).
API Gravity	30.9	Environment Canada characterization of Alaska North Slope (2002)
Interfacial Tension (dyne/cm)	27.3	Environment Canada characterization of Alaska North Slope (2002)
Pour Point (deg. C)	-32.0	Environment Canada characterization of Alaska North Slope (2002)
Adsorption Rate to Suspended Sediment	0.010080	From Kolpack et al. (1977)
Adsorption Salinity Coefficient (/ppt)	0.023000	From Kolpack et al. (1977)
Fraction monoaromatic hydrocarbons (MAHs)	0.02192	Value calculated by RPS ASA from Environment Canada characterization of Alaska North Slope (2002)
Fraction 2-ring aromatics	0.003076	Value calculated by RPS ASA from Environment Canada characterization of Alaska North Slope (2002)
Fraction 3-ring aromatics	0.007284	Value calculated by RPS ASA from Environment Canada characterization of Alaska North Slope (2002)
Fraction Non-Aromatics: boiling point < 180^{o}C	0.20408	Value calculated by RPS ASA from Environment Canada characterization of Alaska North Slope (2002)
Fraction Non-Aromatics: boiling point 180-264^{o}C	0.121224	Value calculated by RPS ASA from Environment Canada characterization of Alaska North Slope (2002)
Fraction Non-Aromatics: boiling point 265-380^{o}C	0.186616	Value calculated by RPS ASA from Environment Canada characterization of Alaska North Slope (2002)
Minimum Oil Thickness (mm)	0.05	Based on McAuliffe, 1987 (1987 Oil Spill Conference, API, pp.

Oil Property	Value	Comments/References
		275 - 288) who provided information on typical minimum slick thicknesses.
Maximum Mousse Water Content (%)	72.9	Value estimated by RPS ASA from Environment Canada characterization of Alaska North Slope (2002)
Degradation Rate (/day), Surface & Shore	0.01	From French et al. (1996)
Degradation Rate (/day), Hydrocarbons in Water (1-200 m)	0.1	From French et al. (1996)
Degradation Rate (/day), Hydrocarbons in Water (>200 m)	0.01	From French et al. (1996)
Degradation Rate (/day), Oil in Sediment	0.001	From French et al. (1996)

Intermediate Fuel Oil 380 (IFO 380):

Intermediate Fuel Oil 380 (IFO 380) was selected as representative of the heavy fuel oil used by vessels commonly found in the Beaufort region of the Arctic (Table 4).

Table 4.Oil properties of the intermediate fuel oil (IFO 380) used in the model simulations.

Oil Property	Value	Comments
Density @ 16 deg. C (g/cm^3)	0.99298	Prestige spill off the western coast of Spain. Nov 2002. (French McCay et al., 2013)
Viscosity @ 25 deg. C (cp)	14,470	Environment Canada Oil Property Database as described in Jokuty et al. (1999).
API Gravity	11	Prestige spill off the western coast of Spain. Nov 2002. (French McCay et al., 2013)
Interfacial Tension (dyne/cm)	32.6	Environment Canada Oil Property Database as described in Jokuty et al. (1999).
Pour Point (deg. C)	-6	Environment Canada Oil Property Database as described in Jokuty et al. (1999).
Adsorption Rate to Suspended Sediment	0.01008	From Kolpack et al. (1977)
Adsorption Salinity Coefficient (/ppt)	0.023	From Kolpack et al. (1977)
Fraction monoaromatic hydrocarbons (MAHs)	0.00064	Environment Canada Oil Property Database as described in Jokuty et al. (1999).
Fraction 2-ring aromatics	0.00197	Environment Canada Oil Property Database as described in Jokuty et al. (1999).
Fraction 3-ring aromatics	0.00719	Environment Canada Oil Property Database as described in Jokuty et al. (1999).
Fraction Non-Aromatics: boiling point < 180^{o}C	0.004355	Environment Canada Oil Property Database as described in Jokuty et al. (1999).
Fraction Non-Aromatics: boiling point 180-264^{o}C	0.04653	Environment Canada Oil Property Database as described in Jokuty et al. (1999).
Fraction Non-Aromatics: boiling point 265-380^{o}C	0.08331	Environment Canada Oil Property Database as described in Jokuty et al. (1999).
Minimum Oil Thickness (mm)	0.001	Based on McAuliffe, 1987 (1987 Oil Spill Conference, API, pp. 275 - 288) who provided information on typical minimum slick thicknesses.

Oil Property	Value	Comments
Maximum Mousse Water Content (%)	0	ADIOS (Automated Data Inquiry for Oil Spills). NOAA/HMRAD.
Degradation Rate (/day), Surface & Shore	0.01	From French et al. (1996)
Degradation Rate (/day), Hydrocarbons in Water (1-200 m)	0.1	From French et al. (1996)
Degradation Rate (/day), Hydrocarbons in Water (>200 m)	0.01	From French et al. (1996)
Degradation Rate (/day), Oil in Sediment	0.001	From French et al. (1996)

Diesel Fuel:

A typical marine diesel fuel was selected to represent the light fuel oil carried by re-supply vessels in the area (Table 5). This diesel fuel was non-biodiesel based.

Table 5. Oil properties of the diesel oil used in the model simulations.

Oil Property	Value	Comments
Density @ 16 deg. C (g/cm^3)	0.83089	Environment Canada Oil Property Database as described in Jokuty et al. (1999).
Viscosity @ 15 deg. C (cp)	2	Environment Canada Oil Property Database as described in Jokuty et al. (1999).
API Gravity	38.8	Environment Canada Oil Property Database as described in Jokuty et al. (1999).
Interfacial Tension (dyne/cm)	27.4	Environment Canada Oil Property Database as described in Jokuty et al. (1999).
Pour Point (deg. C)	-36	Environment Canada Oil Property Database as described in Jokuty et al. (1999).
Adsorption Rate to Suspended Sediment	0.01008	From Kolpack et al. (1977)
Adsorption Salinity Coefficient (/ppt)	0.023	From Kolpack et al. (1977)
Fraction monoaromatic hydrocarbons (MAHs)	0.023336	Environment Canada Oil Property Database as described in Jokuty et al. (1999).
Fraction 2-ring aromatics	0.010175	From Lee et al. (1992)
Fraction 3-ring aromatics	0.001976	From Lee et al. (1992)
Fraction Non-Aromatics: boiling point < 180°C	0.186664	Subtracted the Aromatic Hydrocarbons from the Total Hydrocarbons to obtain the fraction of Aliphatic Hydrocarbons.
Fraction Non-Aromatics: boiling point 180-264°C	0.426825	Subtracted the Aromatic Hydrocarbons from the Total Hydrocarbons to obtain the fraction of Aliphatic Hydrocarbons.
Fraction Non-Aromatics: boiling point 265-380°C	0	Environment Canada Oil Property Database as described in Jokuty et al. (1999). (Boiling Point data stopped before 380° C. Assumed Aliphatic for boiling points >265° C and <380° C to be 0. Therefore the Total Hydrocarbons is equal to the Aromatic Hydrocarbons for boiling points >265° C and < 380° C.)
Minimum Oil Thickness (mm)	0. 00001	Based on McAuliffe, 1987 (1987 Oil Spill Conference, API, pp. 275 - 288) who provided information on typical minimum slick thicknesses.

Oil Property	Value	Comments
Maximum Mousse Water Content (%)	0	From Whiticar et al. (1992)
Degradation Rate (/day), Surface & Shore	0.01	From French et al. (1996)
Degradation Rate (/day), Hydrocarbons in Water (1-200 m)	0.1	From French et al. (1996)
Degradation Rate (/day), Hydrocarbons in Water (>200 m)	0.01	From French et al. (1996)
Degradation Rate (/day), Oil in Sediment	0.001	From French et al. (1996)

6.2 Eastern Shipping Analysis

The eastern shipping release site was located in the Amundsen Gulf, approximately 45 km north of Baillie Island, along the shipping route (Figure 46). The site was approximately 77 m deep. This site was selected for its position along a known shipping route at the mouth of the passage to the east through the Canadian archipelago. Vessels carrying ore from the Izok mine and re-supply barges may utilize this route.

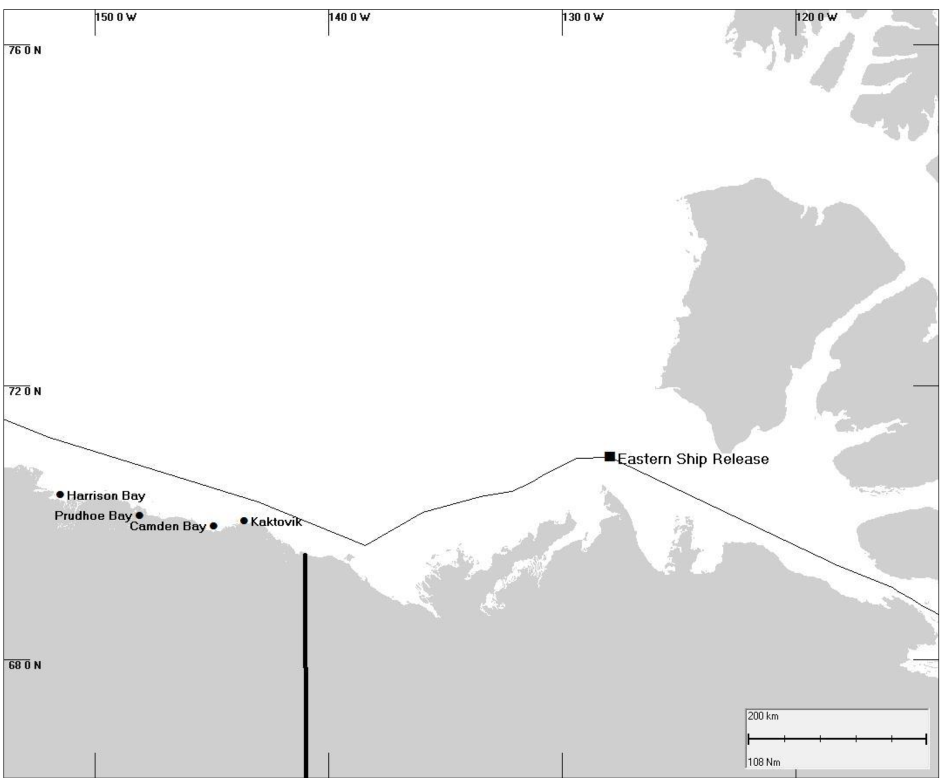

Figure 46. Location of the eastern shipping release site in the Amundsen Gulf, along the shipping route (thin black line). Thick black line represents U.S./Canadian border.

The release type simulated was an instantaneous surface release from a shipping accident (e.g., collision, grounding, etc.). The release time frame analysed was the active shipping months (July-October), when the route is relatively ice free. Discharge volumes were based on ERC review of vessel types described in Appendix C. Spills of both Intermediate Fuel Oil 380 (IFO 380) and Diesel Fuel were simulated. The MMPD for IFO 380 was 21,000 bbls and based on the fuel capacity of the bulk ore carriers considered for the Izok mine. The MMPD for Diesel Fuel was 5,400 bbls and based on the fuel capacity of a typical resupply barge servicing coastal communities. No response measures were modelled in the eastern shipping analysis. Table 6 summarizes the variations or scenarios investigated for the eastern shipping analysis. This matrix lists all of the stochastic scenarios. For every stochastic "parent" scenario, several representative individual (deterministic) trajectories were identified (typically up to 3). For this study the results of the 95th percentile run for degree of surface and shoreline oiling, and water column contamination (where applicable), was presented.

Table 6. Summary of scenarios simulated for the eastern shipping analysis (2 scenarios total).

Source Type	Release Location	Water Depth (m)	Release Type	Oil Type	Spill Duration (days)	Total Volume (bbl)	Release Time Frame
Bulk Ore Carrier	Amundsen Gulf, shipping route, approx. 45 km N Baillie Island, single point release	40 - 100	Surface MMPD	IFO 380	0.25	21,000	July – October
Resupply Tank Barge	Amundsen Gulf, shipping route, approx. 45 km N Baillie Island, single point release	40 - 100	Surface MMPD	Diesel	0.25	5,400	July – October

6.3 Trans-boundary Analysis

The trans-boundary analysis spill locations were on the Beaufort shelf near the U.S./Canadian border (Figure 47).The release sites ranged in depth from approximately 30-70 m. These sites were selected based on known shipping routes, and a proposed subsea oil pipeline route following the 60 m bathymetric contour. Two release regions were investigated and were situated on either side of the border: Canadian Beaufort coast from Herschel Island to east of the U.S./Canadian border, and U.S. Beaufort Coast from Kaktovik to Prudhoe Bay to the west of the U.S./Canadian border.

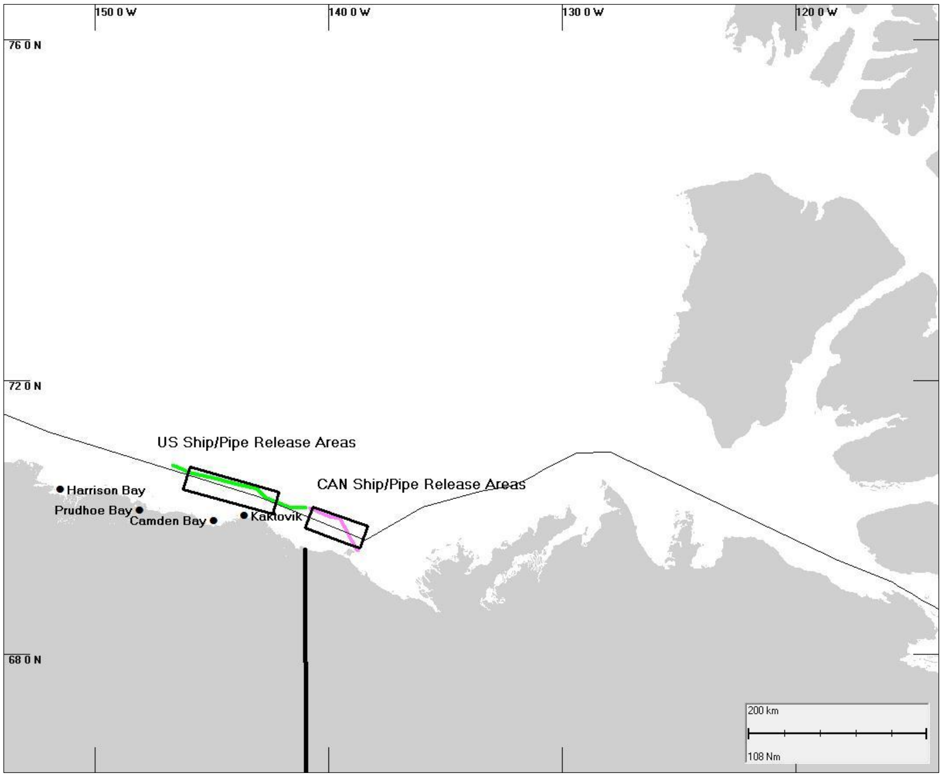

Figure 47. Location of the trans-boundary release sites near the U.S./Canadian border (thick black line). Shipping route is indicated by thin black line. Spill release sites associated with shipping incidents were randomly distributed inside each of the black rectangles. Rectangle to the east of the border represented the release region along the Canadian Beaufort coast, and the rectangle to the west of the border represented the release region along the U.S. Beaufort coast. Release sites for spills originating from the pipeline occurred along the coloured lines; pink for the Canadian Beaufort coast, and green for the U.S. Beaufort coast.

Two release types were simulated for the trans-boundary analysis: an instantaneous surface release originating from a shipping accident (e.g., grounding, etc.) and a subsea pipeline leak. Two ship types, a bulk ore carrier and an ice class oil tanker, were considered for the shipping accident scenarios. The bulk ore carrier was based on those considered for use at the Izok mine. The release time frame for the bulk ore carrier was the active shipping months when the route is relatively ice free (July – October). The MMPD release volume for the bulk ore carrier was 21,000 bbls, and the oil type released was Intermediate Fuel Oil 380 (IFO 380). The specifications for the ice class vessel used for this study were based on those proposed by Imperial Oil for future use at the Pokak lease site (IORVL, 2013). The release time frame for the ice class tanker was year round (January - December). The MMPD release volume for the tanker was 533,000 bbls, and the oil type released was Alaska North Slope Crude (ANS).

A shallow, slow, non-turbulent subsea release was simulated for the pipeline scenarios (60 m depth). Release of oil was initialized at the seabed. The release duration was assumed to be 6 days, and based on response time for cutting off the section of pipe leaking. The MMPD flow rate assumed was 4,800 barrels per day, totalling a discharge volume of 28,800 bbls. The oil type released was Alaska North Slope Crude (ANS).

All discharge volumes were based on ERC review of vessel types and incidents described in Appendix C. No response measures were modelled in the trans-boundary analysis. Table 7 summarizes the variations or scenarios investigated for the trans-boundary analysis. This matrix lists all of the stochastic scenarios.

For every stochastic "parent" scenario, several representative individual (deterministic) trajectories were identified (typically up to 3). For this study the results of the 95th percentile run for degree of surface and shoreline oiling, and water column contamination (where applicable) was presented.

Table 7. Summary of scenarios simulated for the trans-boundary analysis (6 scenarios total).

Source Type	Release Location	Water Depth (m)	Release Type	Oil Type	Spill Rate (bbl/day)	Spill Duration (days)	Total Volume (bbl)	Release Time Frame
Bulk Ore Carrrier	Shipping route, Canadian Beaufort coast Herschel Island to US/Can Border	40 - 100	Surface MMPD	IFO 380	NA	0.25	21,000	July - October
Bulker Ore Carrier	Shipping route, US Beaufort coast Kaktovik to Prudhoe Bay	40 - 100	Surface MMPD	IFO 380	NA	0.25	21,000	July - October
Tanker	Shipping route, Canadian Beaufort coast Herschel Island to US/Can Border	40 - 100	Surface WCD	Crude	NA	0.50	533,000	January-December
Tanker	Shipping route, US Beaufort coast Kaktovik to Prudhoe Bay	40 - 100	Surface WCD	Crude	NA	0.50	533,000	January-December
Offshore Pipeline	Pipeline route, Canadian Beaufort coast Herschel Island to US/Can Border	60	Shallow subsurface MMPD	Crude	4,800	6	28,800	May – November
Offshore Pipeline	Pipeline route, US Beaufort coastline from US/Canadian Border Prudhoe Bay	60	Shallow subsurface MMPD	Crude	4,800	6	28,800	May – November

6.4 Shallow Blowout Analysis

The shallow blowout release site was located in the Amauligak lease area on the Beaufort shelf (Figure 48). The site was approximately 32 m deep. The Amauligak lease area was selected because of the close proximity to the sensitive shoreline habitats of the Mackenzie River delta, and for its past exploratory drilling history.

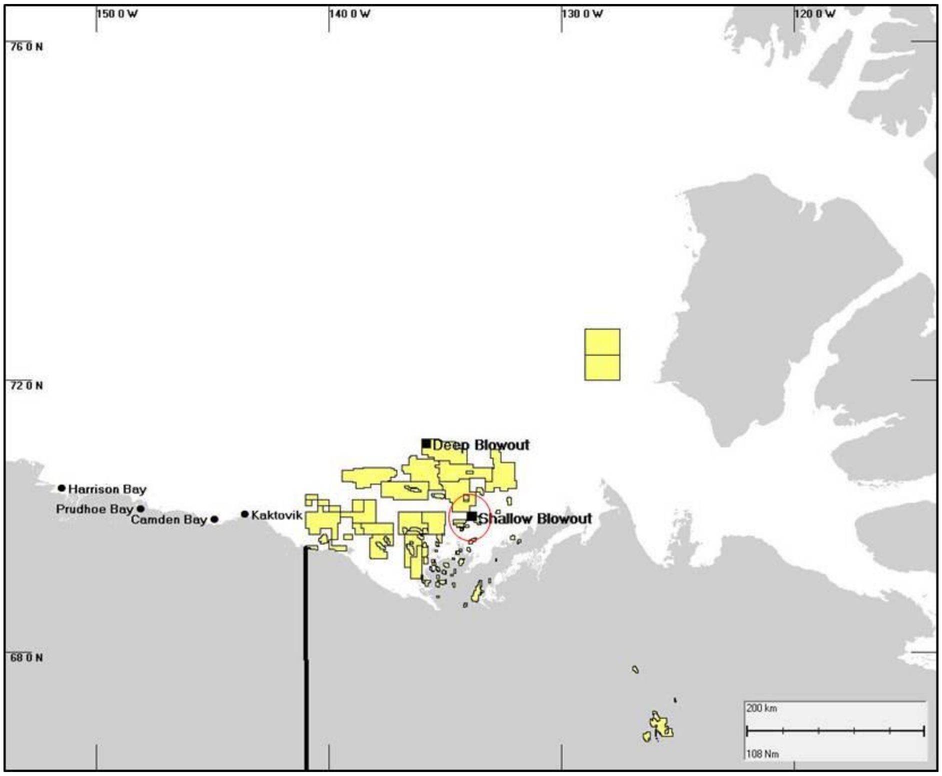

Figure 48. Location of the shallow blowout release site (circled in red), in the Amauligak lease area on the Beaufort shelf. Yellow polygons outline all lease areas in Canadian Beaufort. Thick black line represents U.S./Canadian border.

The release type simulated was a shallow subsurface well blowout. At shallow depths in a less turbulent or mixed water column, typically oil will quickly rise to the surface. At high exit velocities and high gas content in shallow water, oil is shot up to the surface causing a "boiling over" or "bubbling up" effect. Under these turbulent release conditions, a turbulent plume results and oil does not trickle up through the water column in a steady stream. For the WCD scenarios in this analysis, oil was initialized 1-2 meters below the sea surface in a cylinder having a diameter associated with the probable plume dimensions calculated using the high flow rate. For the lower MMPD flow rates, oil was initialized from the seabed and assumed not to cause a subsurface turbulent plume, but rose up as a trickle.

The release time frames analysed were "Early Operating Season (June-July)" and "Late Operating Season (August-October)". "Operating season" is an industry definition for the partial- to open-ice season whereby drilling operations can commence (typically defined as June-October in the Beaufort and Chukchi Seas). Release dates for the stochastic analyses were randomly selected within each of these time frames (early and late operating season). Oil was tracked for two months after the end of the total release duration. For example, a shallow blowout occurring in August (late season) would release for 90 days (August – October), and then oil would be tracked through December.

It was assumed that more response activity to a well blowout occurring early in the operating season would be possible due to more favourable environmental conditions (e.g., less ice, more daylight). Whereas, response mobilization and wellhead shutdown might be more difficult nearing ice freeze up and colder fall conditions, potentially leading to spillage into the winter and beyond. Based on this reasoning, the entire operating season was broken into two release time frames. Release duration for the late operating season was assumed to be longer than that for the early operating season. The release duration was shorter at the shallow blowout site than at the deep blowout site due to the shallow location (i.e., easier to stop spill). In a comment/critique memorandum of S.L. Ross's Spill Response Gap Study in the Arctic, WWF states that it would not be possible to conduct response actions (e.g., capping well, dispersant application) after October 31st due to harsh environmental conditions in the Beaufort.

Flow rates and spill durations assumed for the shallow blowout analysis were based on U.S. Bureau of Ocean Energy Management (BOEM) guidance for blowouts and are described in Appendix C. The WCD flow rate was 30,000 barrels per day (bpd), while the MMPD was 3,000 bpd. Flow rate was assumed to be continuous and non-varying throughout the release. Release duration for the Early Operating Season was assumed to be 60 days for the WCD, and 30 days for the MMPD. For the Late Operating Season, release duration was assumed to be to 90 days for the WCD, and 60 days for the MMPD. Alaska North Slope Crude (ANS) 2002 was the oil type released in this analysis.

Only surface response measures were modelled in the shallow blowout analysis (no subsurface dispersant). It was assumed that because the release location was in productive shallow shelf waters, that subsea dispersant application would not be considered a plausible response measure. Critical assumptions were made about response capabilities in the Beaufort region. Assumptions have not been tested or reviewed by response experts, considering Arctic conditions. Surface response assumptions were based around observed rates from previous incidents, hours of daylight in the Arctic region during the time periods of interest, and various thresholds from well-established response documents. Overall, favourable and beneficial response outcomes were incorporated into the modelling. For example, *the in situ* burn rate observed during the Deepwater Horizon in the Gulf of Mexico was applied. This was a generous assumption considering conditions in the Arctic would be more inclement and the presence of ice would present difficulty. In addition, the number of daylight hours when response could take place was extended during the summer months in the Arctic. Below are the outlined assumptions:

Surface Response (Burning + Surface Dispersant)

a. *In situ* Burning – Removal of Surface Oil Mass
    - Assumed mid-range burn rate (midpoint of average minimum and maximum) observed during Deepwater Horizon Incident in the Gulf of Mexico:
        - 551.5 bbls of oil burned per hour (Source: NIC Oil Budget Calculator DWH, 2010)
    - Assumed minimum oil thickness threshold for burning 13 µm (Source: API et al., 2001)
    - Corrected for plausible amount of response time estimated in Arctic
        - Average hours of light per day by month for June-October (Source: Based on 2013 daylight hours at West Kavik Airport, North Slope, AK http://worldtime.io)
        - No response activity possible after October 31st (Source: WWF 2011 comment/critique memorandum of S.L. Ross's Spill Response Gap Study).

b. Surface Dispersant Application – Entrainment of Surface Oil Mass
    - Assumed 1000 bbls/day of surface dispersant available during response (aerial or vessel) (Source: IORVL, 2013)
    - Assumed mid-range dispersant to oil ratio (DOR), 20 bbls of oil to 1 bbl of dispersant (Source: API et al., 2001):
        - 833.3 bbls of oil dispersed per hour

- Assumed minimum oil thickness threshold for dispersal 13 µm (Source: API et al., 2001)
- Assumed maximum oil viscosity threshold for burning 20,000 cP (Source: API et al., 2001)
- Corrected for plausible amount of response time estimated in Arctic:
  - Average hours of light per day by month for June-October (Source: Based on 2013 daylight hours at West Kavik Airport, North Slope, AK http://worldtime.io)
- No response activity possible after October 31st (Source: WWF (2011) comment/critique memorandum of S.L. Ross's Spill Response Gap Study).

Table 8 summarizes the variations or scenarios investigated for the shallow blowout analysis. This matrix lists all of the stochastic scenarios. For every stochastic "parent" scenario, several representative individual (deterministic) trajectories were identified (typically up to 3). For this study the results of the 95th percentile run for highest surface and shoreline oiling, and water column contamination (where applicable) was presented. Surface response measures were *only* simulated for the 95th percentile individual trajectories for degree of surface and shoreline oiling from the base case or parent stochastic scenario (no response). Therefore, surface response was not simulated in a full stochastic analysis. The authors felt that investigating the surface response at the individual trajectory level was more appropriate, since mass balance and metrics of overall shoreline effects could be compared with and without surface response.

Table 8. Summary of scenarios simulated for the shallow blowout analysis (6 scenarios total). *Note: Surface response measures were only simulated in iterations of the 95th percentile trajectory for surface and shoreline from the base case or parent stochastic scenario. Therefore, surface response was not simulated in a full stochastic analysis.

Source Type	Release Location	Water Depth (m)	Release Type	Oil Type	Spill Rate (bbl/day)	Spill Duration (days)	Total Volume (bbl)	Response Measures	Release Time Frame
Well	Amauligak Lease Area	32	Shallow Subsurface WCD	Crude	30,000	60	1,800,000	None	June - July
Well	Amauligak Lease Area	32	Shallow Subsurface WCD	Crude	30,000	60	1,800,000	Surface*	June - July
Well	Amauligak Lease Area	32	Shallow Subsurface WCD	Crude	30,000	90	2,700,000	None	August - October
Well	Amauligak Lease Area	32	Shallow Subsurface WCD	Crude	30,000	90	2,700,000	Surface*	August - October
Well	Amauligak Lease Area	32	Shallow Subsurface MMPD	Crude	3,000	30	90,000	None	June - July
Well	Amauligak Lease Area	32	Shallow Subsurface MMPD	Crude	3,000	60	180,000	None	August – October

6.5 Deep Blowout Analysis

The deep blowout release site was located in the deepest portion of what is referred to as the Pokak lease area on the Beaufort slope (Figure 49). The site was approximately 1,008 m deep. RPS ASA used its OILMAPDeep model to define the associated blowout plume and oil droplet size distribution for scenarios included in the analysis of deep subsurface blowouts. For the assumed OILMAPDeep model parameters, please see Section 7.4.1. This site was selected because it is deep and the Pokak lease area was recently proposed for an exploratory drilling project. Deeper releases are more difficult to respond to and have more complex subsurface plume dynamics.

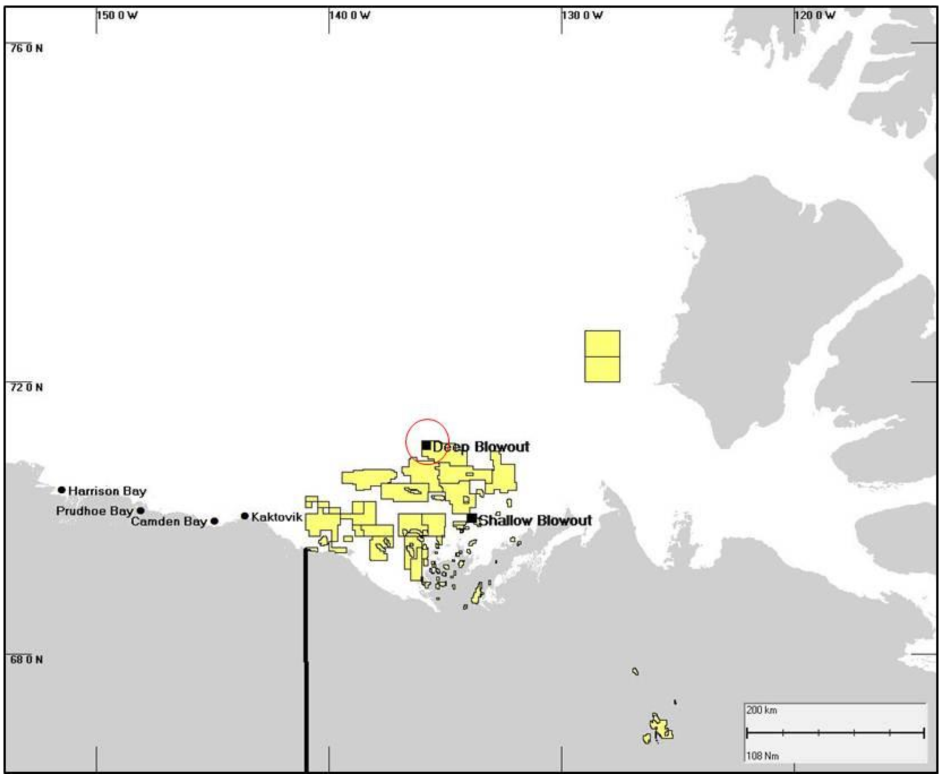

Figure 49. Location of the deep blowout release site (circled in red), in the deeper portion of the Pokak lease area on the Beaufort slope. Yellow polygons outline all lease areas in Canadian Beaufort. Thick black line represents U.S./Canadian border.

The release time frames analysed were the same as the shallow blowout analysis; “Early Operating Season (June-July)”, and “Late Operating Season (August-October)”. See Section 6.4 for details. The release duration for the late operating season was assumed to be longer than the early operating season. The release duration was longer at the deep blowout site than at the shallow blowout site (Section 6.4), also due to the deep offshore location (i.e., more difficult to stop spill). In a comment/critique memorandum of S.L. Ross’s Spill Response Gap Study in the Arctic, WWF states that it would not be possible to conduct response actions (e.g., capping well, dispersant application) after October 31st due to harsh environmental conditions in the Beaufort.

Flow rates and spill durations assumed for the deep blowout analysis were based on U.S. Bureau of Ocean Energy Management (BOEM) guidance for blowouts and are described in Appendix C. The WCD flow rate was 60,000 barrels per day (bpd), while the MMPD was 6,000 bpd. Flow rate was assumed to be continuous and non-varying throughout the release. Release duration for the Early Operating Season was assumed to be 90 days for the WCD, and 60 days for the MMPD. For the Late Operating Season, release duration was assumed to be to 120 days for the WCD, and 90 days for the MMPD. Alaska North Slope Crude (ANS) 2002 was the oil type released in this analysis.

Both subsurface and surface response measures were modelled in the deep blowout analysis. Critical assumptions were made about response capabilities in the Beaufort region. Assumptions have not been tested or reviewed by response experts, considering Arctic conditions. Surface response assumptions were based around observed rates from previous incidents, hours of daylight in the Arctic region during the time periods of interest, and various thresholds from well-established response documents. Overall, favourable and beneficial response outcomes were incorporated into the modelling. For example, *the in situ* burn rate observed during the Deepwater Horizon in the Gulf of Mexico was applied. This was a generous assumption considering conditions in the Arctic would be more inclement and the presence of ice would present difficulty. In addition, the number of daylight hours when response could take place was extended during the summer months in the Arctic. It was assumed that the subsurface dispersant application was 100% efficient. Response measures included in the deep blowout analysis were modelled two ways following the below outlined assumptions:

1. Subsurface Response (Subsea Dispersant)
    - Subsea dispersant injection (e.g., applied inside pipe).
    - 100% of oil treated for entire release duration (all oil remains subsurface).
    - Assumed subsea dispersant application can continue into winter regardless of environmental conditions (e.g., dispersant pipeline is set up from shore).

2. Surface Response (Burning + Surface Dispersant)
    a. *In situ* Burning – Removal of Surface Oil Mass
        - Assumed mid-range burn rate (midpoint of average minimum and maximum) observed during Deepwater Horizon Incident:
            - 551.5 bbls of oil burned per hour (Source: NIC Oil Budget Calculator DWH, 2010)
        - Assumed minimum oil thickness threshold for burning 13 µm (Source: API et al., 2001)
        - Corrected for plausible amount of response time estimated in Arctic
            - Average hours of light per day by month for June-October (Source: Based on 2013 daylight hours at West Kavik Airport, North Slope, AK http://worldtime.io)
            - No response activity possible after October 31st (Source: WWF 2011 comment/critique memorandum of S.L. Ross's Spill Response Gap Study).

    b. Surface Dispersant Application – Entrainment of Surface Oil Mass
        - Assumed 1000 bbls/day of surface dispersant available during response (aerial or vessel) (Source: IORVL, 2013)
        - Assumed mid-range dispersant to oil ratio (DOR), 20 bbls of oil to 1 bbl of dispersant (Source: API et al., 2001):
            - 833.3 bbls of oil dispersed per hour
        - Assumed minimum oil thickness threshold for dispersal 13 µm (Source: API et al., 2001)
        - Assumed maximum oil viscosity threshold for dispersing 20,000 cP (Source: API et al., 2001)

- Corrected for plausible amount of response time estimated in Arctic:
    - Average hours of light per day by month for June-October (Source: Based on 2013 daylight hours at West Kavik Airport, North Slope, AK http://worldtime.io)
    - No response activity possible after October 31st (Source: WWF (2011) comment/critique memorandum of S.L. Ross's Spill Response Gap Study).

Table 9 summarizes the variations or scenarios investigated for the deep blowout analysis. This matrix lists all of the stochastic scenarios. For every stochastic "parent" scenario, several representative individual (deterministic) trajectories were identified (typically up to 3). For this study the results of the 95th percentile run for degree of surface and shoreline oiling, and water column contamination (where applicable), was presented. Surface response measures were *only* simulated for the 95th percentile individual trajectories for degree of surface and shoreline oiling from the base case or parent stochastic scenario (no response). Therefore, surface response was not simulated in a full stochastic analysis. Again, the authors felt that investigating the surface response at the individual trajectory level was more appropriate, since mass balance and metrics of overall shoreline effects could be compared with and without surface response.

Table 9. Summary of scenarios simulated for the deep blowout analysis (8 scenarios total). *Note: Surface response measures were only simulated in iterations of the 95th percentile trajectories for surface and shoreline from the base case or parent stochastic scenario. Therefore, surface response was not simulated in a full stochastic analysis.

Source Type	Release Location	Water Depth (m)	Release Type	Oil Type	Spill Rate (bbl/day)	Spill Duration (days)	Total Volume (bbl)	Response Measures	Release Time Frame
Well	Pokak Lease Area	1,008	Deep subsurface WCD	ANS Crude	60,000	90	5,400,000	None	June - July
Well	Pokak Lease Area	1,008	Deep subsurface WCD	ANS Crude	60,000	90	5,400,000	Surface*	June - July
Well	Pokak Lease Area	1,008	Deep subsurface WCD	ANS Crude	60,000	90	5,400,000	Subsurface	June - July
Well	Pokak Lease Area	1,008	Deep subsurface WCD	ANS Crude	60,000	120	7,200,000	None	August - October
Well	Pokak Lease Area	1,008	Deep subsurface WCD	ANS Crude	60,000	120	7,200,000	Surface*	August - October
Well	Pokak Lease Area	1,008	Deep subsurface WCD	ANS Crude	60,000	120	7,200,000	Subsurface	August - October
Well	Pokak Lease Area	1,008	Deep subsurface MMPD	ANS Crude	6,000	60	360,000	None	June - July
Well	Pokak Lease Area	1,008	Deep subsurface MMPD	ANS Crude	6,000	90	540,000	None	August - October

7 Oil Spill Modelling Results

In this section modelling results are presented for the four spill analyses. See Appendix D for a complete list of stochastic and deterministic scenarios (or model runs) and a guide to the scenario naming convention. Results for each analysis are organized in the following general order:

Stochastic Analysis Results

The figures presented in the stochastic modelling results sections illustrate the spatial extent of surface oiling, shoreline oiling, and water column contamination probabilities and associated minimum travel times for the spills. Certain scenarios did not affect every environmental compartment (surface, shoreline, water column). Only output for an affected compartment is presented herein. These maps present model output in gridded format. For each scenario:

> **Probability of Oil Contamination**: The map defines the area and the associated probability in which sea surface and shoreline oiling above the defined thresholds, or total water column contamination, would be expected. The coloured area in the stochastic maps indicates areas that *may* receive oil pollution in the event of that particular spill scenario. The 'hotter' the colour (i.e., reds), the more likely an area would be affected; the cooler the colours (greens), the less likely an area would be affected. The probability of oil contamination was based on a statistical analysis of the resulting ensemble of individual trajectories for each spill scenario. These figures do not imply that the entire contoured area would be covered with oil in the event of a spill. The map also does not provide any information on the quantity of oil in a given area. **Note that only probabilities of 1% or greater were included in the map output.** Stochastic maps showing *total* water column contamination indicate frequency that a given area experienced any oil contamination (i.e., not limited by concentration threshold, unlike surface and shoreline oiling). Total oil mass in the water column was used to generate the map (all components of oil).
>
> **Minimum Travel Times**: The footprint on this map corresponds to the probability map, and illustrates the shortest time required for oil to reach any point within the footprint at a thickness or concentration exceeding the defined threshold (shore and surface oiling). For water column contamination, minimum travel times illustrate the shortest time required for oil to reach any point within the footprint (no threshold). These results were also based on the ensemble of all individual trajectories.

Oil contamination exceeding the following thresholds for surface and shoreline oiling are provided in Section 7:

- Floating Surface Oil Thickness Threshold: **≥ 0.01 g/m^2**
  - The threshold is for barely visible sheen; oil sheens are generally 0.01-1 g/m^2 on average.
  - Effects on socioeconomic resources (i.e., fishing may be prohibited)
  - French McCay et al. (2011)
- Shoreline Thickness Threshold: **≥ 1 g/m^2 (or 1 μm)**
  - The threshold represents an oil amount that would appear as a dull brown colour
  - Effects on socioeconomic resources (i.e. need for shoreline cleanup)
  - French McCay et al. (2011)

A second set of higher thresholds were also analysed. These thresholds are summarized, and stochastic results are presented in Appendix E of this report.

Representative Individual Trajectory Results

Representative deterministic trajectories for the 95th percentile trajectory with respect to degree of surface, shoreline, and water column contamination were identified from each parent stochastic analyses conducted with the lower thresholds summarized above. The figures presented in the individual trajectory modelling results sections include mass balance charts; time series maps of gridded floating surface oil and vertical maximum concentration of dissolved aromatics in the water column; and tables and maps summarizing shoreline effects. Only corresponding mapped results are presented for each type of representative deterministic trajectory (i.e., maps of surface oil contamination only for 95th percentile run for degree of surface oiling, maps of shoreline effects only for 95th percentile run for degree of shoreline oiling). Mass balance charts are presented for *all* representative deterministic trajectories.

1.) **Mass Balance**: The mass balance charts provide an estimate of the oil's weathering and fate for a specific run for the entire model duration. Components of the oil tracked over time include amount of oil on the sea surface, amount of oil ashore, total hydrocarbons in the water column (or water column concentration), oil in subsea sediments, oil evaporated into the atmosphere, oil burned, and decay (accounts for both photo-oxidation and biodegradation).

2.) **Surface and Water Column Contamination Time Series Maps**: Maps showing the footprint of floating surface oil concentration (g/m^2), or maximum water column concentration of aromatics (ppb), at various times steps during the individual spill simulation. Unlike the stochastic water column contamination results (showing *total* or *all* components of oil), only the resulting dissolved aromatic concentrations are shown in the individual trajectory time series maps. Dissolved aromatics are the portion of the oil most likely to affect water column biota. Dissolved aromatic concentration footprints were typically smaller than total oil water column contamination footprints. Water column contamination figures show only concentrations ≥1 ppb, the screening threshold used in this analysis.

3.) **Shoreline Effects**: Tables showing total length of shoreline oiled (km) by shoreline type/habitat for each representative deterministic trajectory. Map showing overall effects to shorelines as mass of oil deposited on shore per unit of area (g/m^2).

Note that deterministic trajectory output maps may show oil contamination outside of the predicted stochastic analysis footprint, as the stochastic results only show probabilities ≥1%.

7.1 Eastern Shipping Analysis

This section contains the stochastic analysis and individual trajectory results for the Eastern Shipping Analysis (Section 6.2). There were a total of two stochastic scenarios and four individual trajectories run for this analysis. Table 10 provides the scenario names. Please see Appendix D for full scenario list and naming conventions. Please note that IFO scenarios did not result in subsurface contamination exceeding 1 ppb of dissolved aromatics (at the model resolution), therefore no results are presented.

Table 10. List of scenario names and types for the Eastern Shipping Analysis.

Scenario Name	Scenario Type	Start Date/Range
EastShip_IFO	Stochastic	July- October
EastShip_Diesel	Stochastic	July- October
EastShip_IFO_r98_95surf	Individual	9/29/2009
EastShip_Diesel_r60_95surf	Individual	10/17/2011
EastShip_IFO_r59_95shore	Individual	8/26/2012
EastShip_Diesel_r22_95shore	Individual	10/11/2008

7.1.1 Stochastic Analysis Results

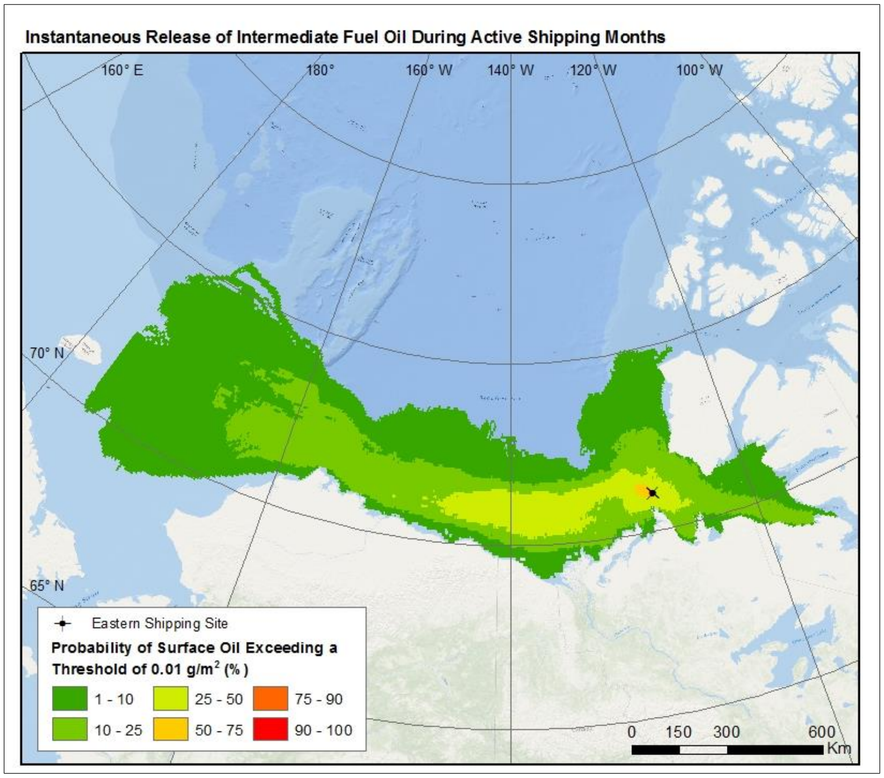

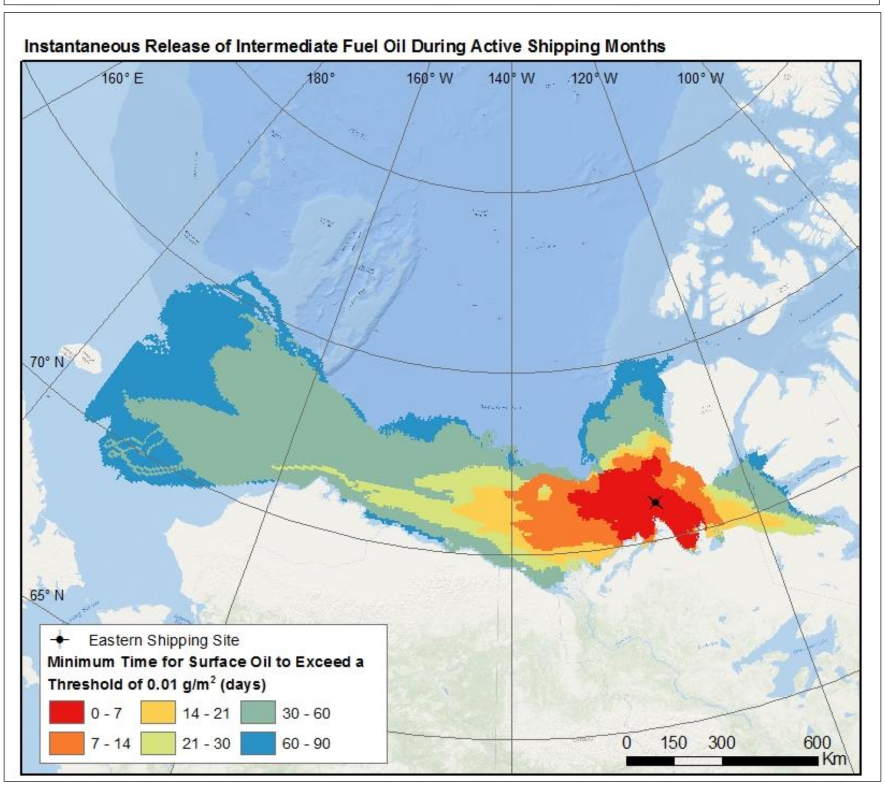

Figure 50. EastShip_IFO - Water surface oiling probabilities and minimum travel times for floating oil ≥0.01 g/m².

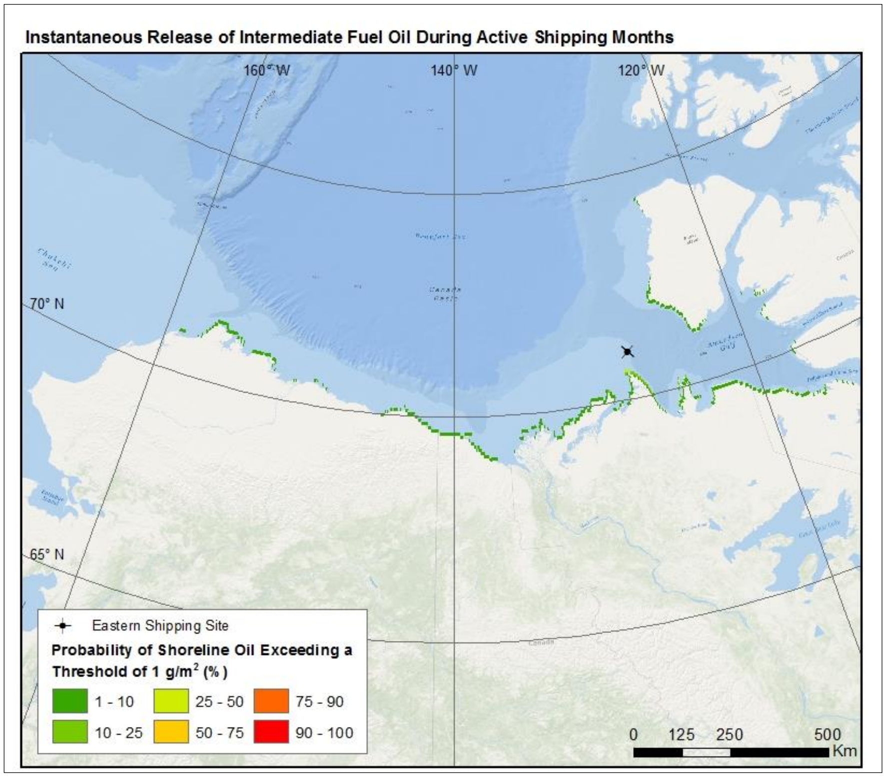

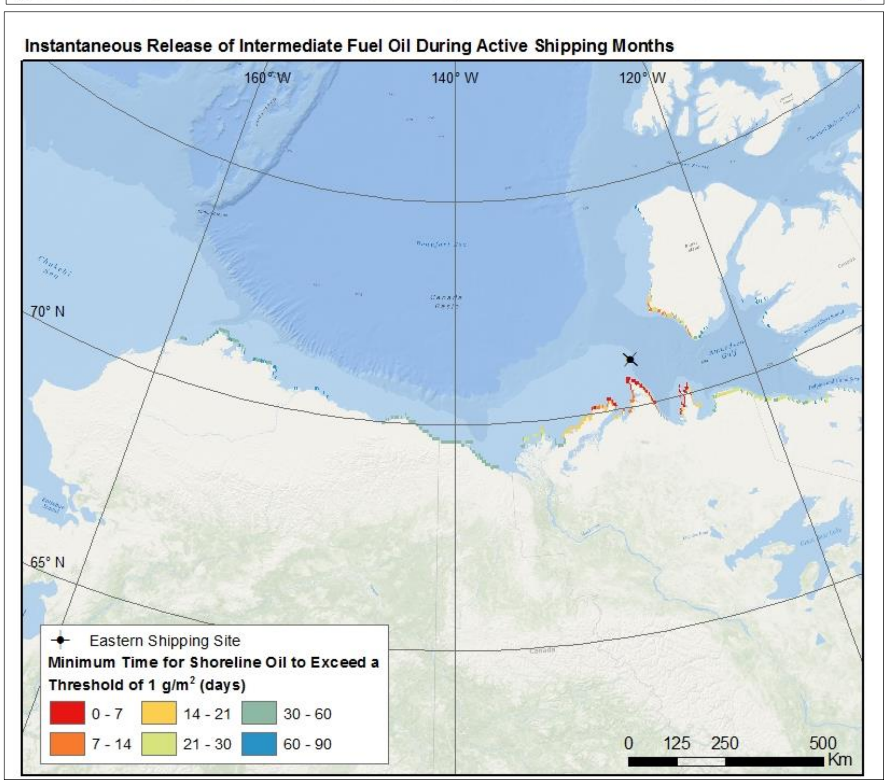

Figure 51. EastShip_IFO - Shoreline oiling probabilities and minimum travel times for shoreline oil ≥1 g/m^2.

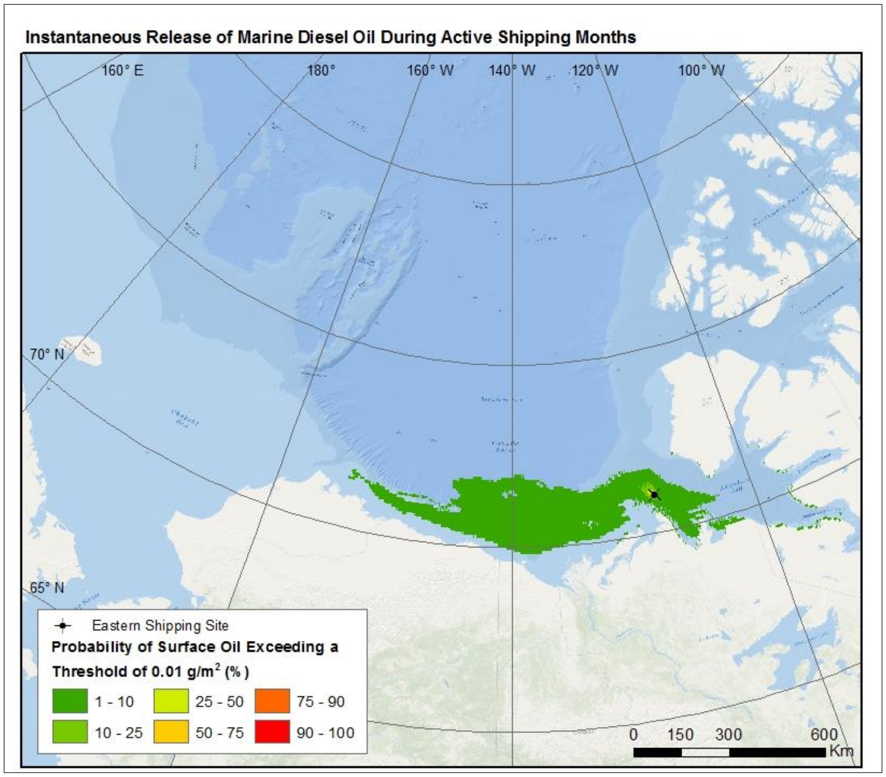

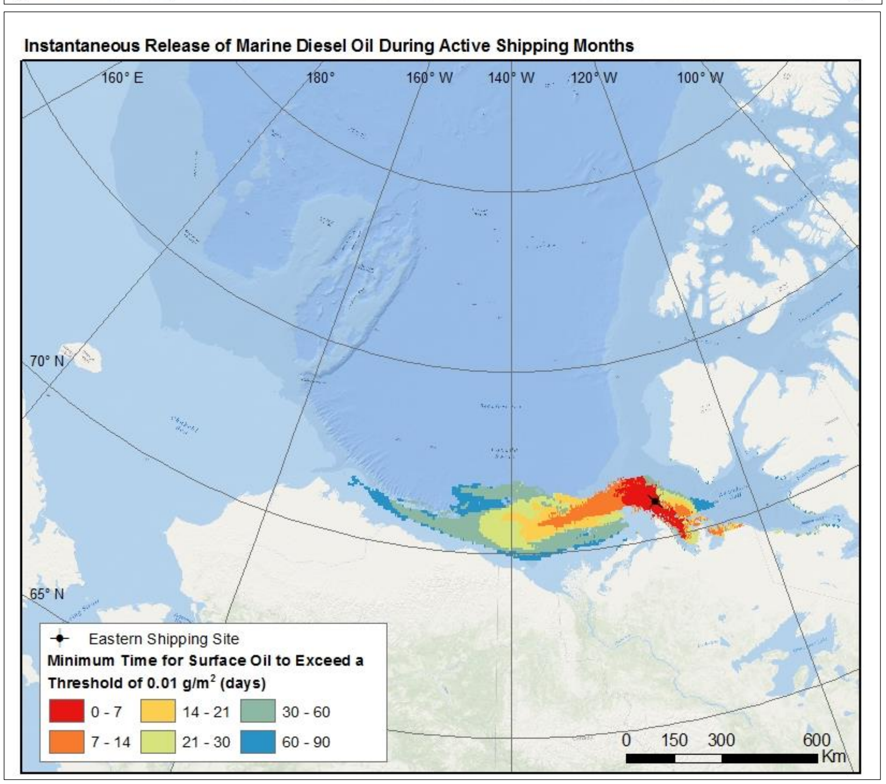

Figure 52. EastShip_Diesel - Water surface oil contamination probabilities and minimum travel times for floating oil ≥0.01 g/m^2.

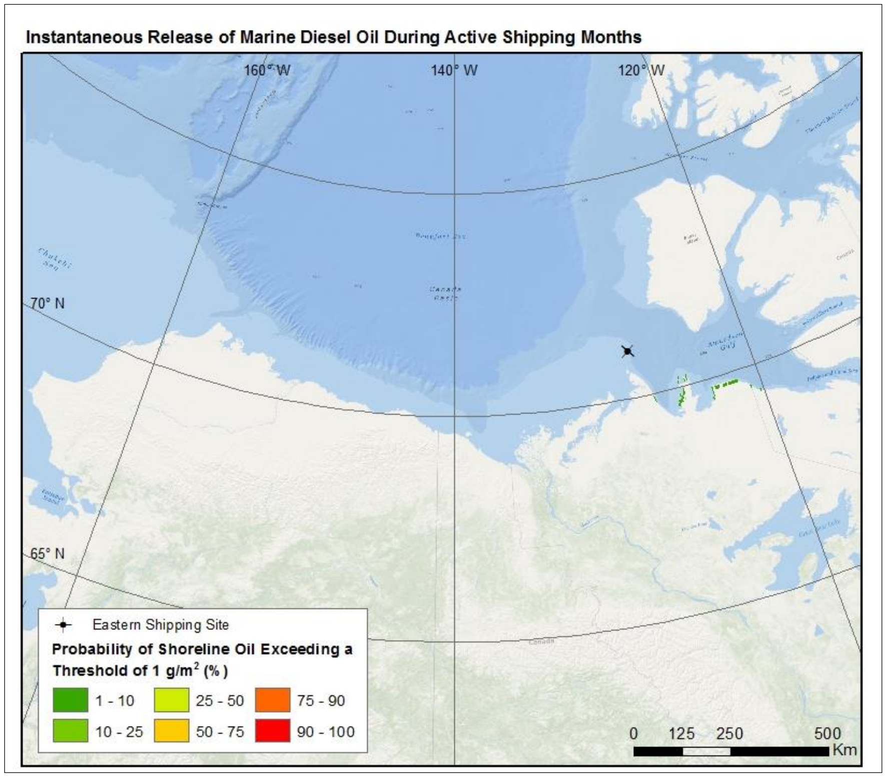

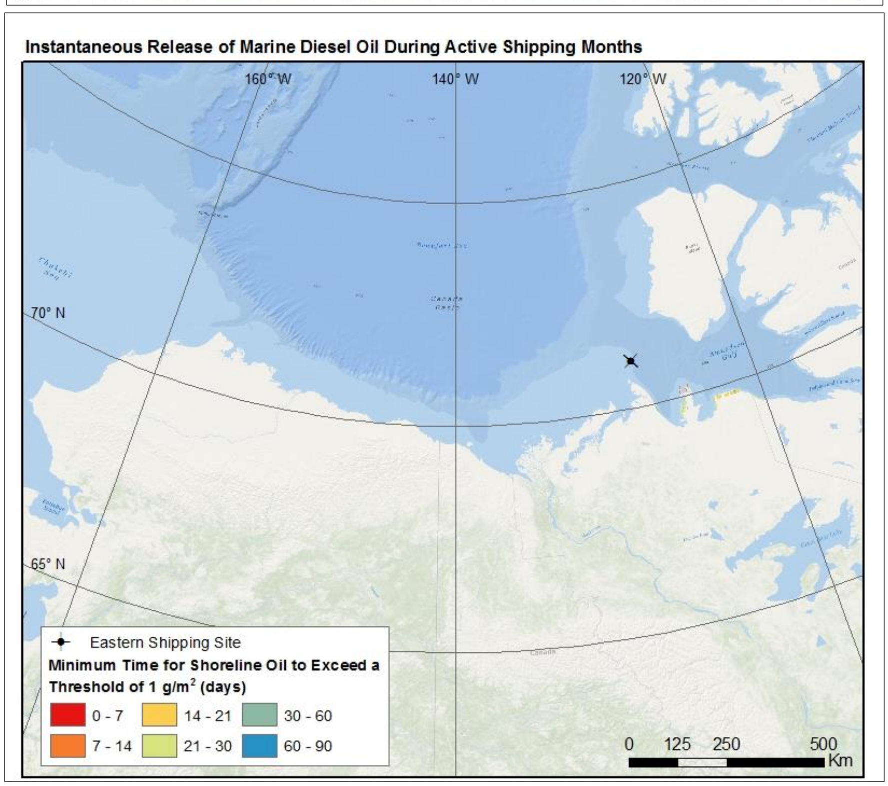

Figure 53. EastShip_Diesel - Shoreline oiling probabilities and minimum travel times for shoreline oil ≥1 g/m^2.

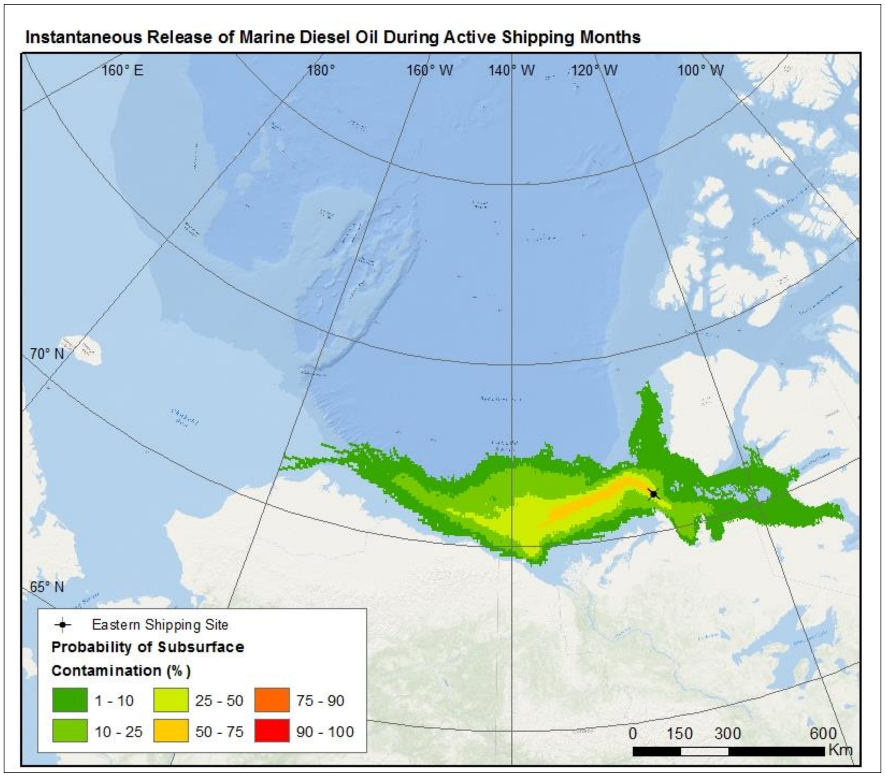

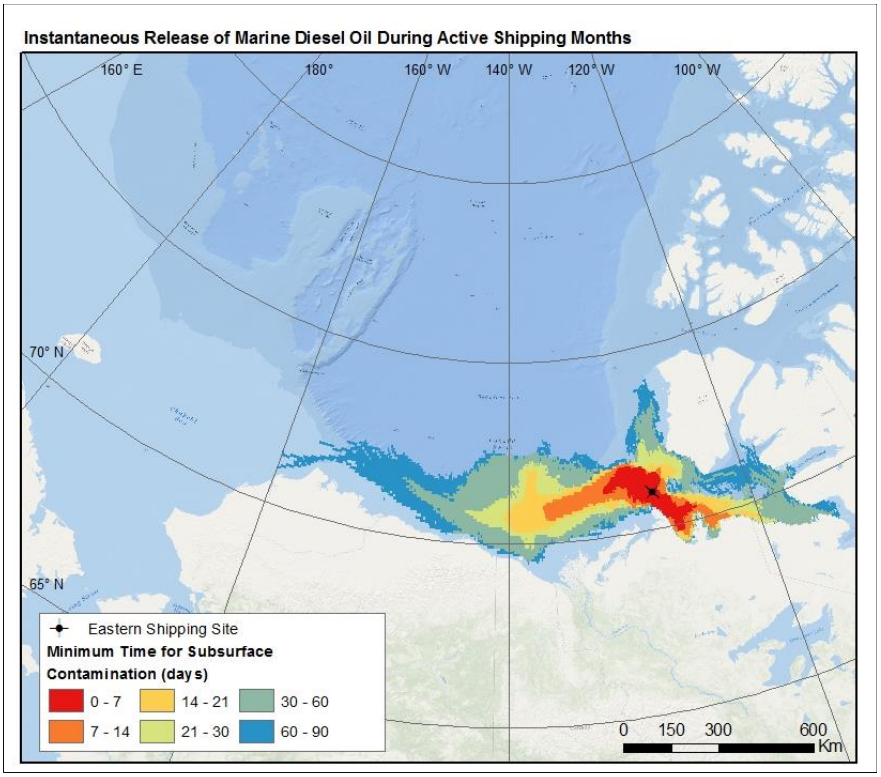

Figure 54. EastShip_Diesel - Subsurface contamination probabilities and minimum travel times for total oil in the water column.

7.1.2 Individual Trajectory Model Results

Note: Only 95th percentile surface and shoreline oiling runs were evaluated for the Eastern Shipping Analysis. In the mass balance charts, surface oil is either floating or trapped under and in ice.

95th Percentile Surface Oiling

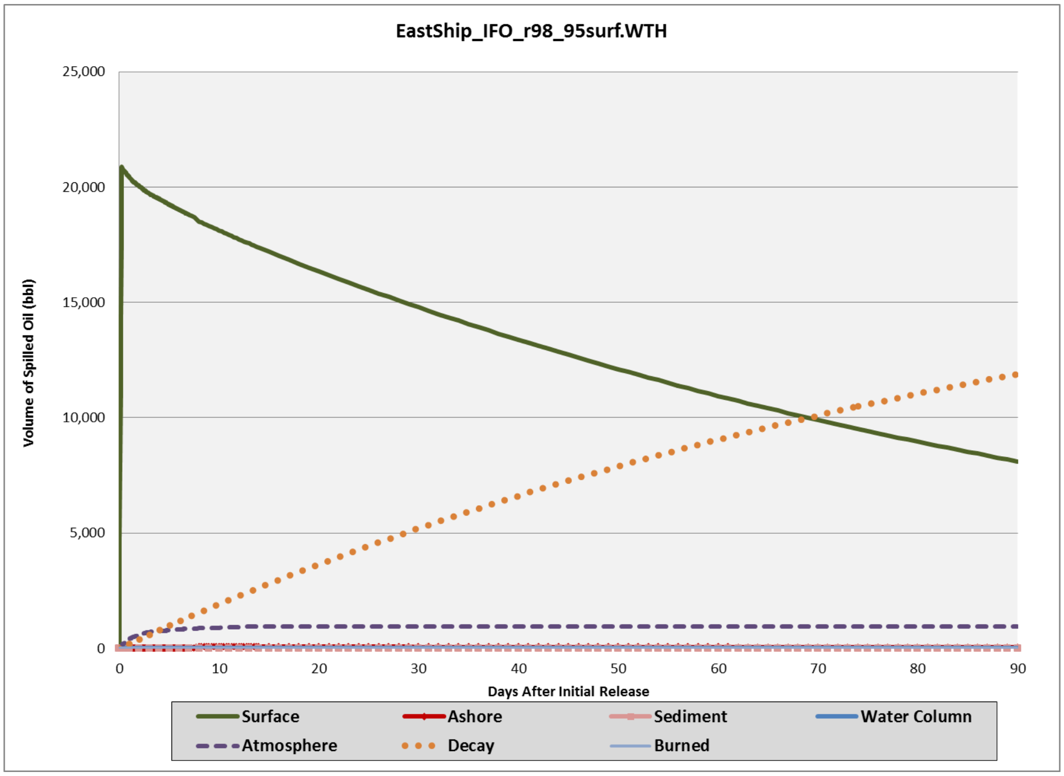

Figure 55. EastShip_IFO_r98_95surf - Mass balance chart. Start Date: 9/28/2009.

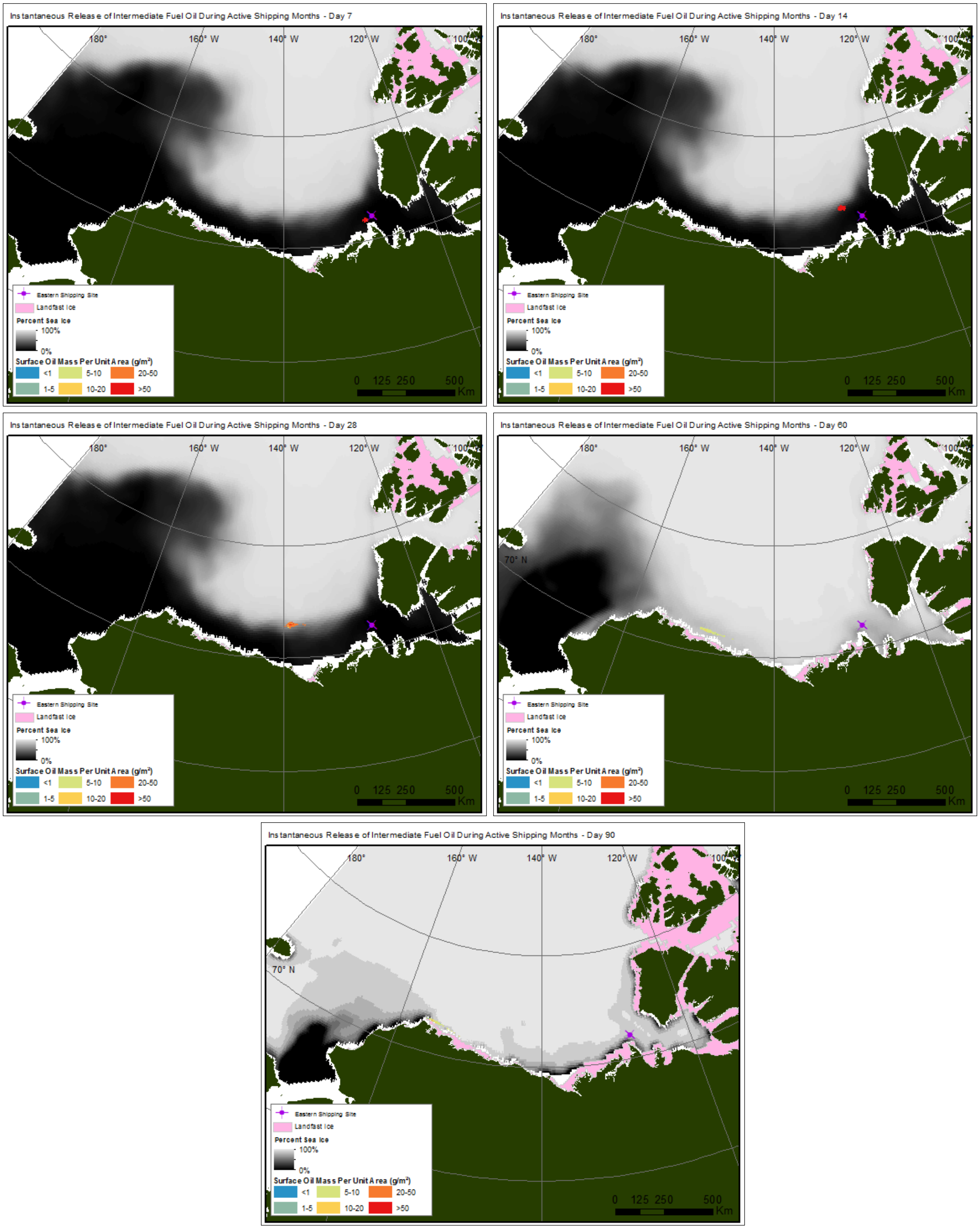

Figure 56. EastShip_IFO_r98_95surf – Time series maps of spill floating surface oil mass per unit area (g/m^2) (day 7, 14, 28, 60, 90; September – December 2009). Pink polygons represent monthly average landfast ice. Grey scale contours represent ice percent coverage for that month from TOPAZ4 model. White indicates areas of no data for ice coverage. Start Date: 9/28/2009.

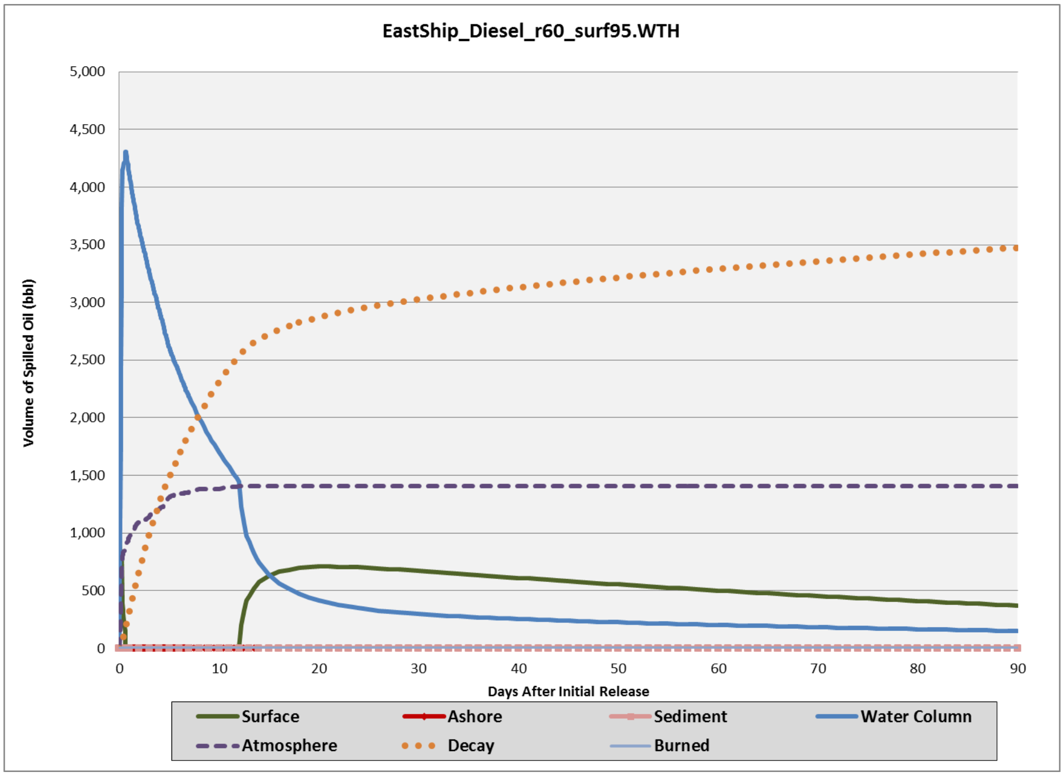

Figure 57. EastShip_Diesel_r60_95surf - Mass balance chart. Start Date: 10/17/2011.

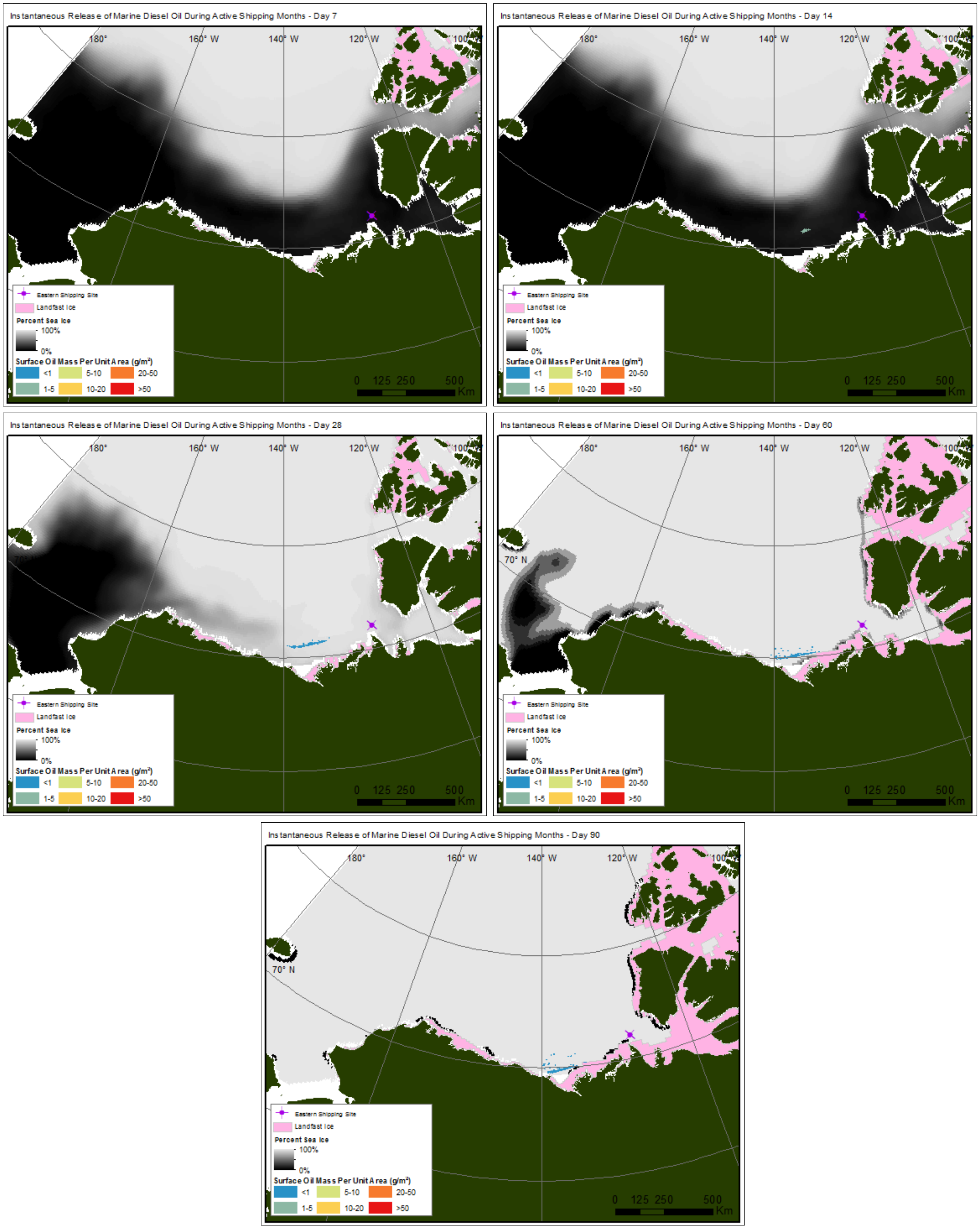

Figure 58. EastShip_Diesel_r60_95surf – Time series maps of spill floating surface oil mass per unit area (g/m^2) (day 7, 14, 28, 60, 90; October 2011 – January 2012). Pink polygons represent monthly average landfast ice. Grey scale contours represent ice percent coverage for that month from TOPAZ4 model. White indicates areas of no data for ice coverage. Start Date: 10/17/2011.

95th Percentile Shoreline Oiling

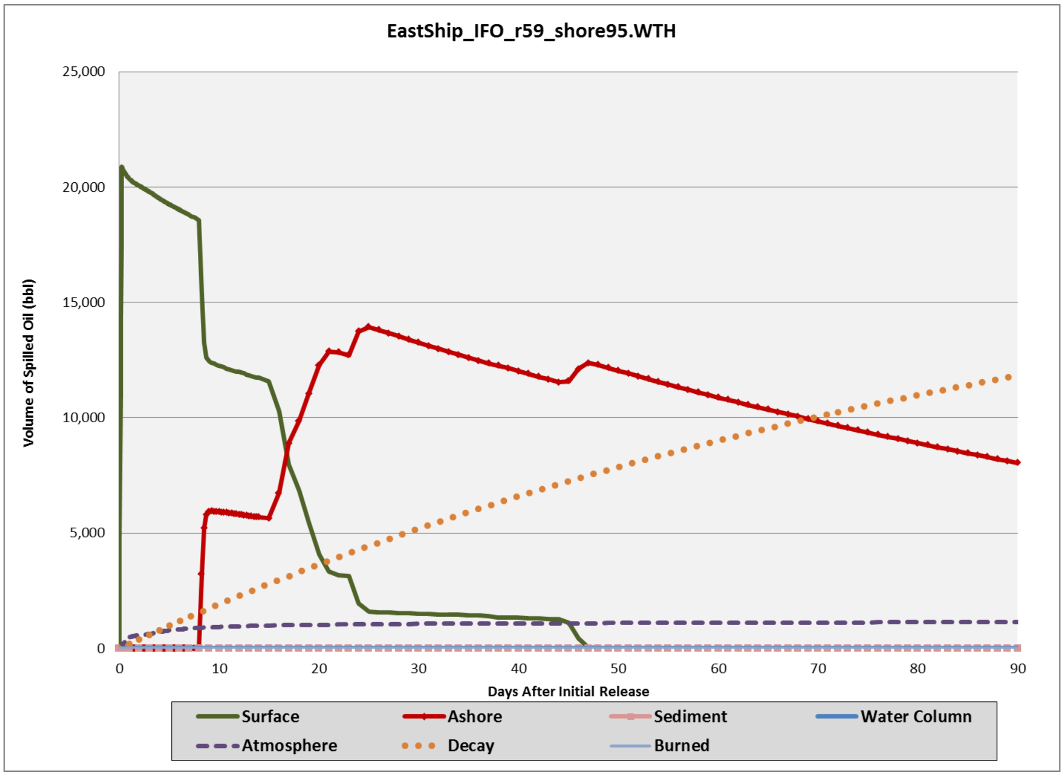

Figure 59. EastShip_IFO_r59_95shore - Mass balance chart. Start Date: 8/26/2012.

Table 11. EastShip_IFO_r59_95shore – Shoreline length oiled (km) by habitat type, for both shore oiling thresholds. Start Date: 8/26/2012.

Shore Type	Shore Length Oiled (km)	
	> 100 micrometers	> 1 micrometer
Seaward Gravel Beach	267.2	418.4
Total Shoreline	**267.2**	**418.4**

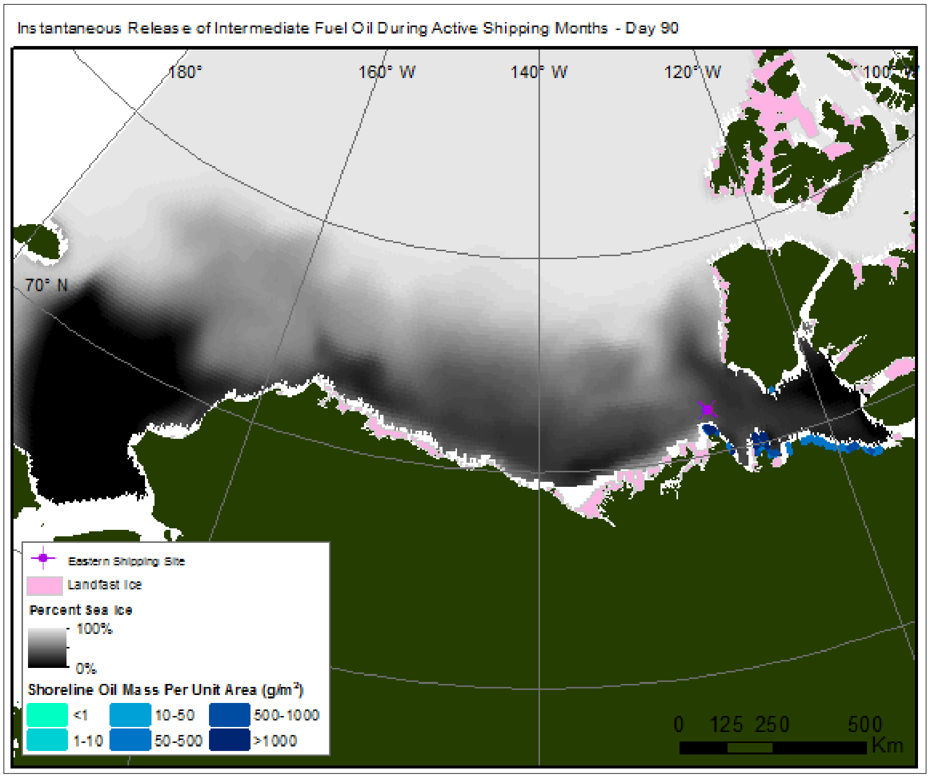

Figure 60. EastShip_IFO_r59_95shore – Map of overall effects to shorelines as mass of oil deposited on shore per unit of area (g/m^2) (day 90, November 2012). Pink polygons represent monthly average landfast ice. Grey scale contours represent ice percent coverage for that month from TOPAZ4 model. White indicates areas of no data for ice coverage. Start Date: 8/26/2012.

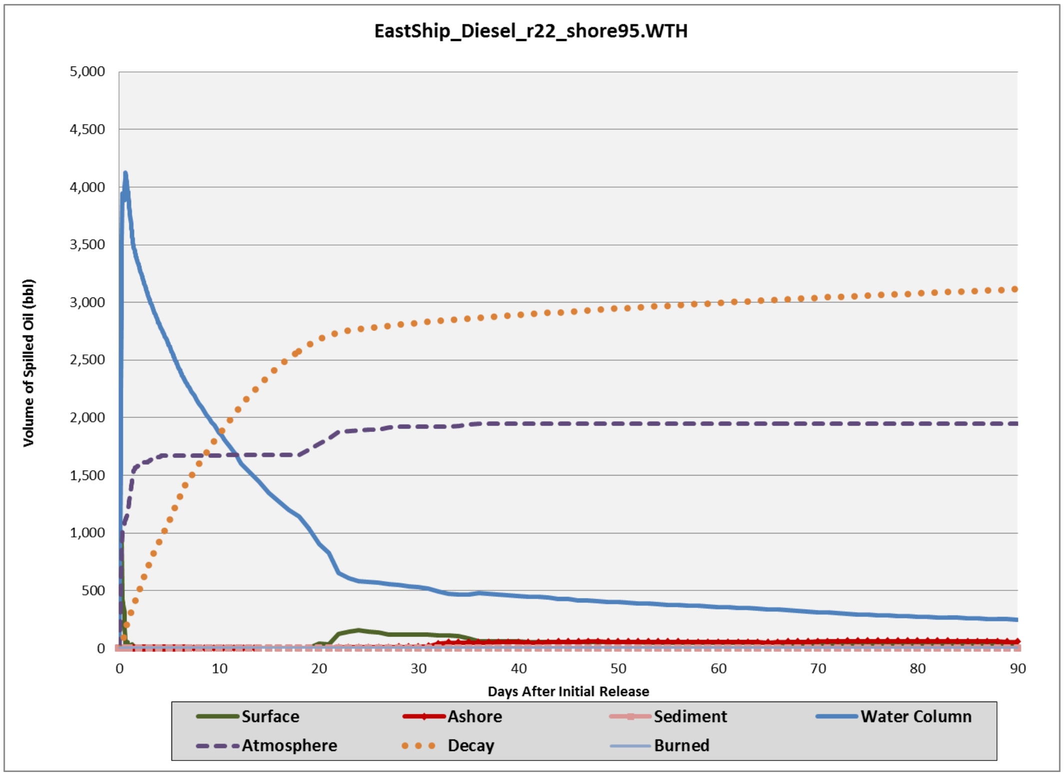

Figure 61. EastShip_Diesel_r22_95shore- Mass balance chart. Start Date: 10/11/2008.

Table 12. EastShip_Diesel_r22_95shore – Shoreline length oiled (km) by habitat type, for both shore oiling thresholds. Start Date: 10/11/2008.

Shore Type	Shore Length Oiled (km)	
	> 100 micrometers	> 1 micrometer
Seaward Gravel Beach	0.0	25.2
Total Shoreline	**0.0**	**25.2**

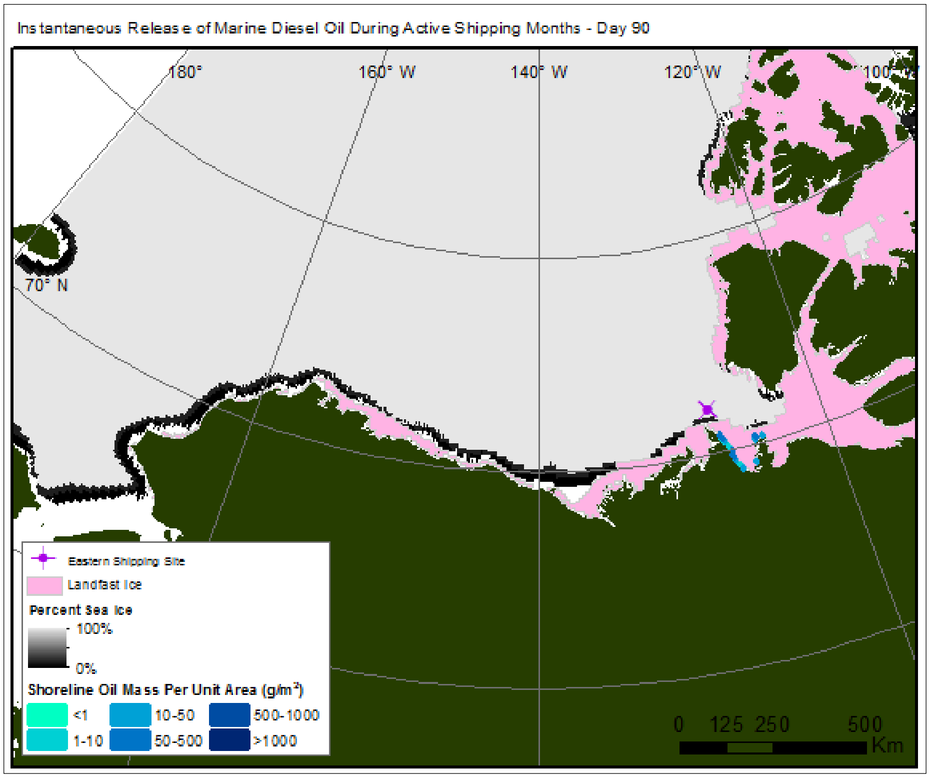

Figure 62. EastShip_Diesel_r22_95shore – Map of overall effects to shorelines as mass of oil deposited on shore per unit of area (g/m^2) (day 90; January 2009). Pink polygons represent monthly average landfast ice. Grey scale contours represent ice percent coverage for that month from TOPAZ4 model. White indicates areas of no data for ice coverage. Start Date: 10/11/2008.

7.2 Trans-boundary Analysis

This section contains the stochastic analysis and individual trajectory results for the Trans-boundary Analysis (Section 6.3). There were a total of six stochastic scenarios and sixteen individual trajectories run for this analysis. Table Table 13 provides the scenario names. Please see Appendix D for full scenario list and naming conventions. Please note that IFO scenarios did not result in subsurface contamination exceeding 1 ppb of dissolved aromatics (at the model resolution), therefore no results are presented.

Table 13. List of scenario names and types for the Trans-boundary Analysis.

Scenario Name	Scenario Type	Start Date/Range
TB_Ship_IFO_CAN	Stochastic	July - October
TB_Ship_Crude_CAN	Stochastic	January-December
TB_Ship_IFO_US	Stochastic	July - October
TB_Ship_Crude_US	Stochastic	January-December
TB_Pipeline_CAN	Stochastic	May - November
TB_Pipeline_US	Stochastic	May - November
TB_Ship_IFO_CAN_r85_95surf	Individual	10/16/2008
TB_Ship_Crude_CAN_r80_95surf	Individual	8/24/2010
TB_Ship_IFO_US_r65_95surf	Individual	9/26/2011
TB_Ship_Crude_US_r65_95surf	Individual	6/28/2012
TB_Pipeline_CAN_r57_95surf	Individual	7/19/2011
TB_Pipeline_US_r23_95surf	Individual	6/1/2012
TB_Ship_IFO_CAN_r87_95shore	Individual	8/30/2008
TB_Ship_Crude_CAN_r71_95shore	Individual	5/17/2012
TB_Ship_IFO_US_r23_95shore	Individual	9/4/2008
TB_Ship_Crude_US_r33_95shore	Individual	6/12/2008
TB_Pipeline_CAN_r15_95shore	Individual	7/27/2008
TB_Pipeline_US_r54_95shore	Individual	7/8/2008
TB_Ship_Crude_CAN_r70_95WC	Individual	7/5/2012
TB_Ship_Crude_US_r60_95WC	Individual	4/4/2008
TB_Pipeline_CAN_r60_95WC	Individual	8/29/2010
TB_Pipeline_US_r85_95WC	Individual	9/12/2008

7.2.1 Stochastic Analysis Results

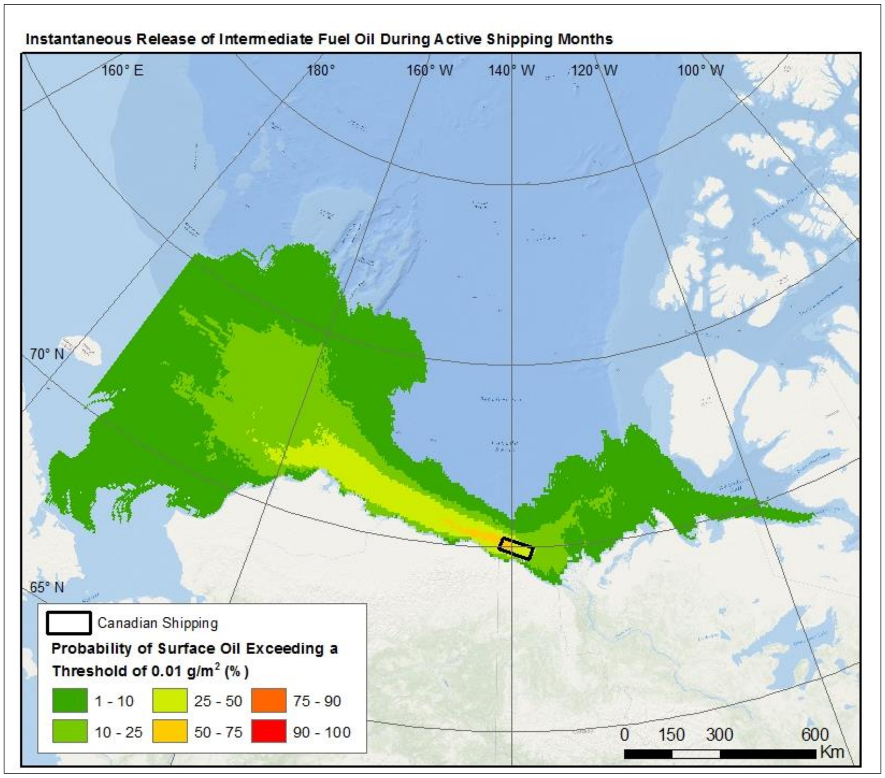

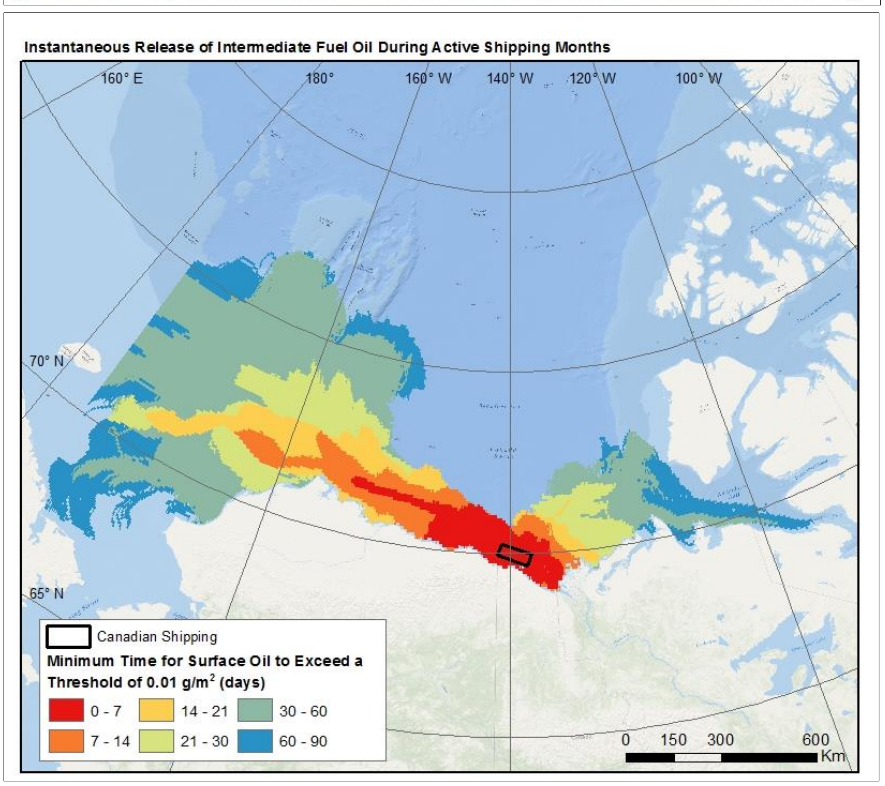

Figure 63. TB_Ship_IFO_CAN - Water surface oiling probabilities and minimum travel times for floating oil ≥0.01 g/m^2.

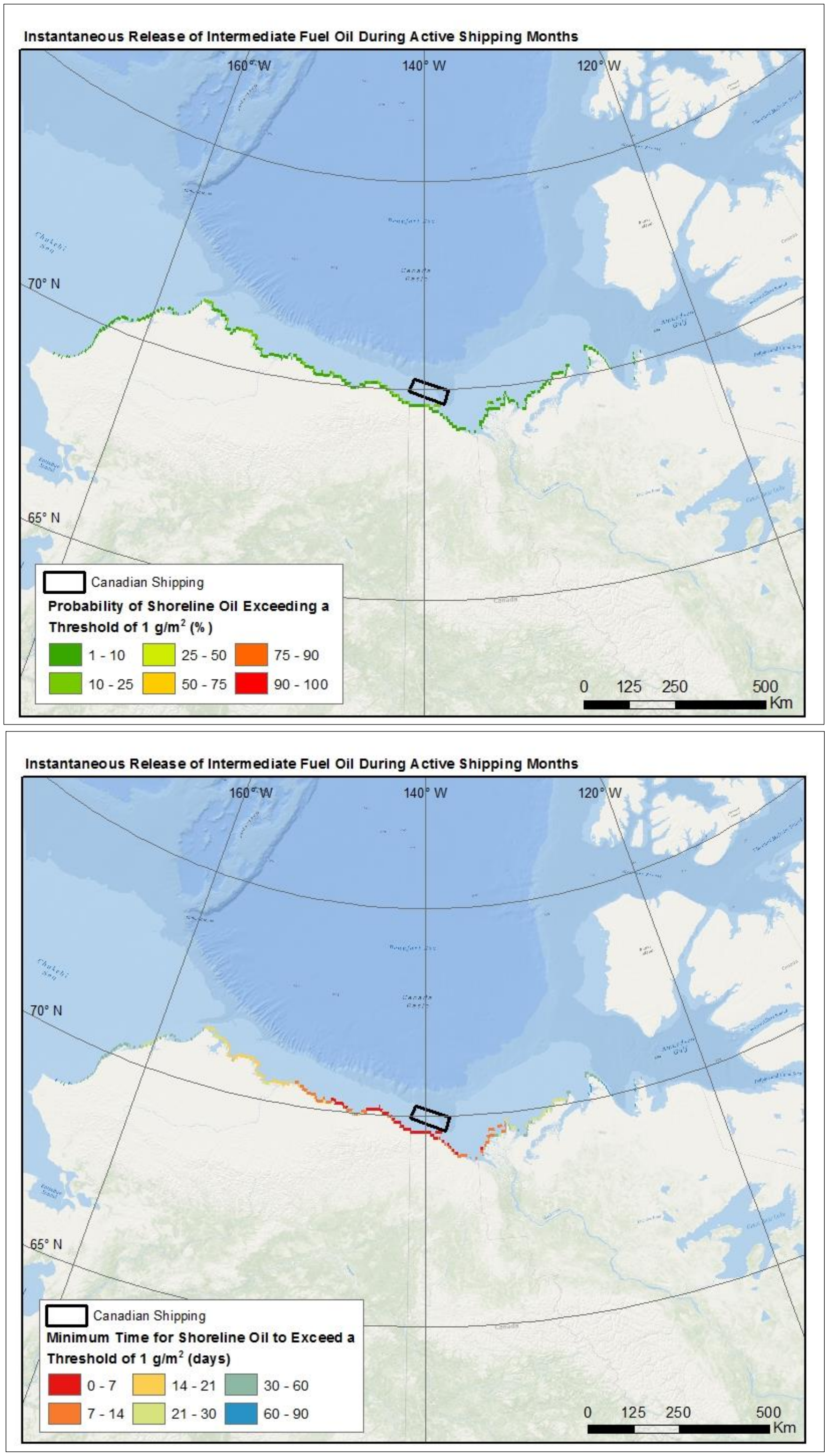

Figure 64. TB_Ship_IFO_CAN - Shoreline oiling probabilities and minimum travel times for shoreline oil ≥1 g/m^2.

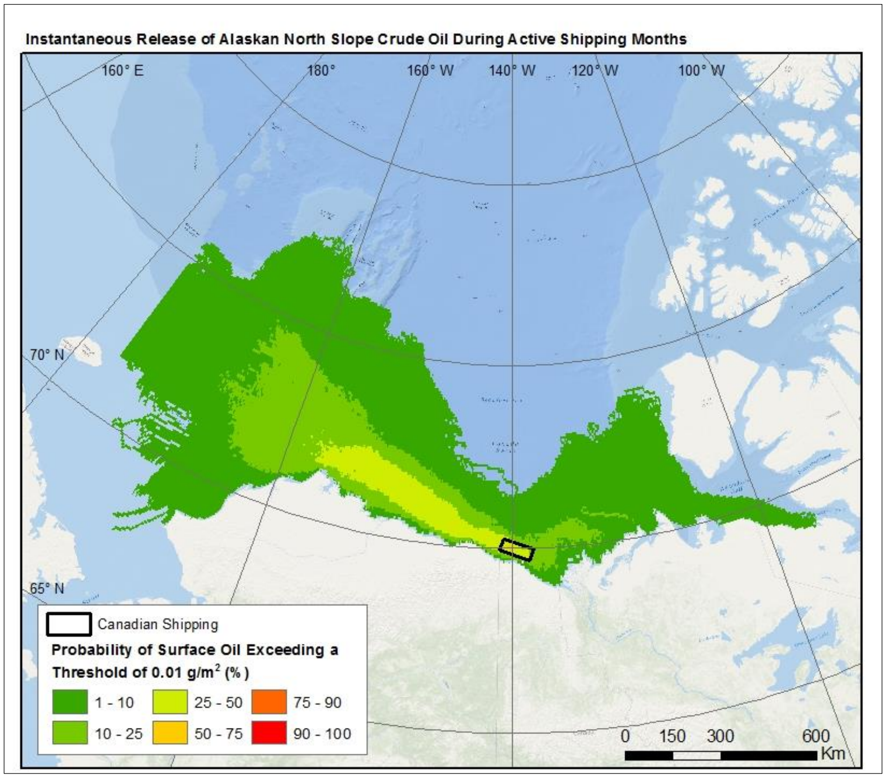

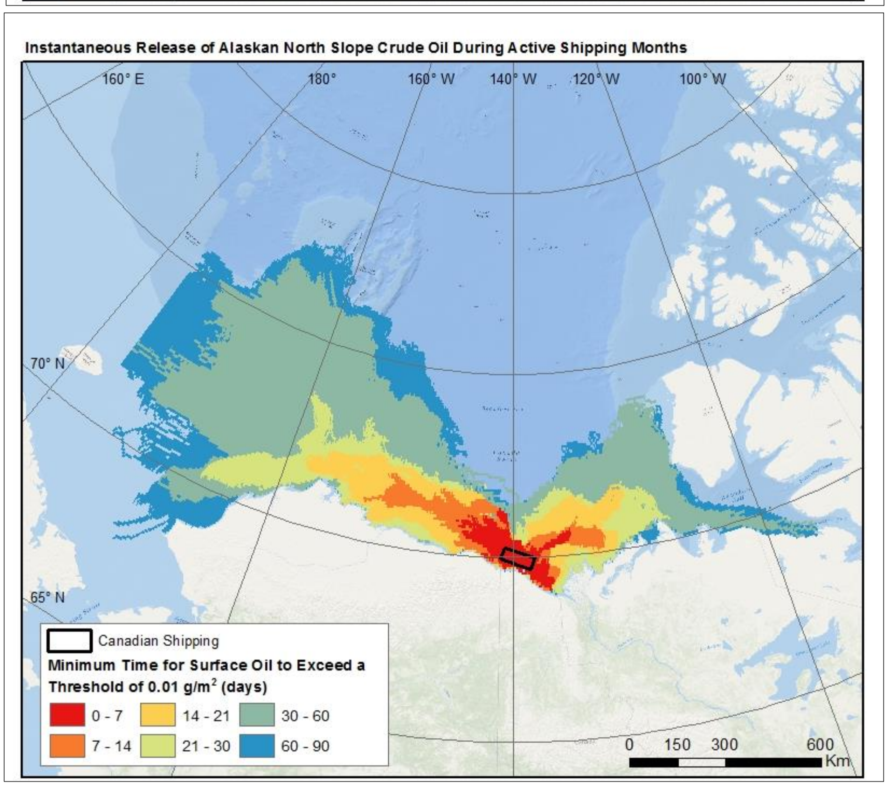

Figure 65. TB_Ship_Crude_CAN - Water surface oiling probabilities and minimum travel times for floating oil ≥0.01 g/m^2.

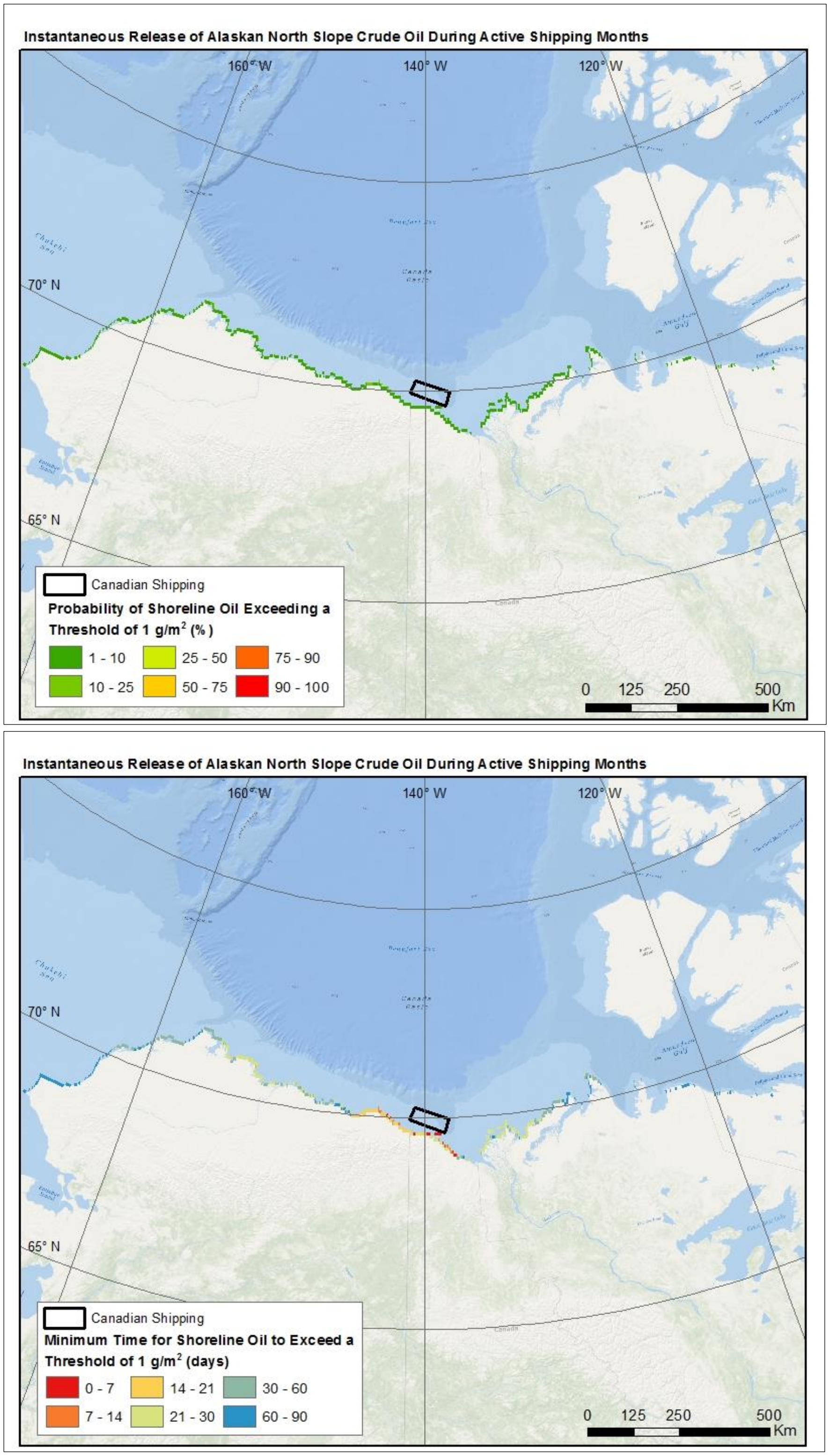

Figure 66. TB_Ship_Crude_CAN - Shoreline oiling probabilities and minimum travel times for shoreline oil ≥1 g/m^2.

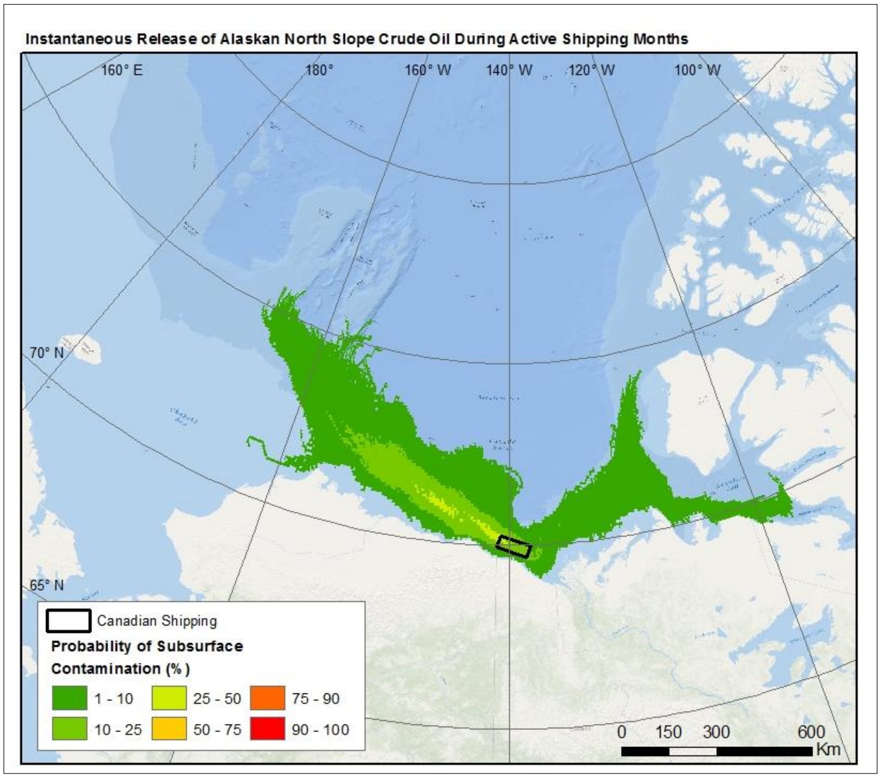

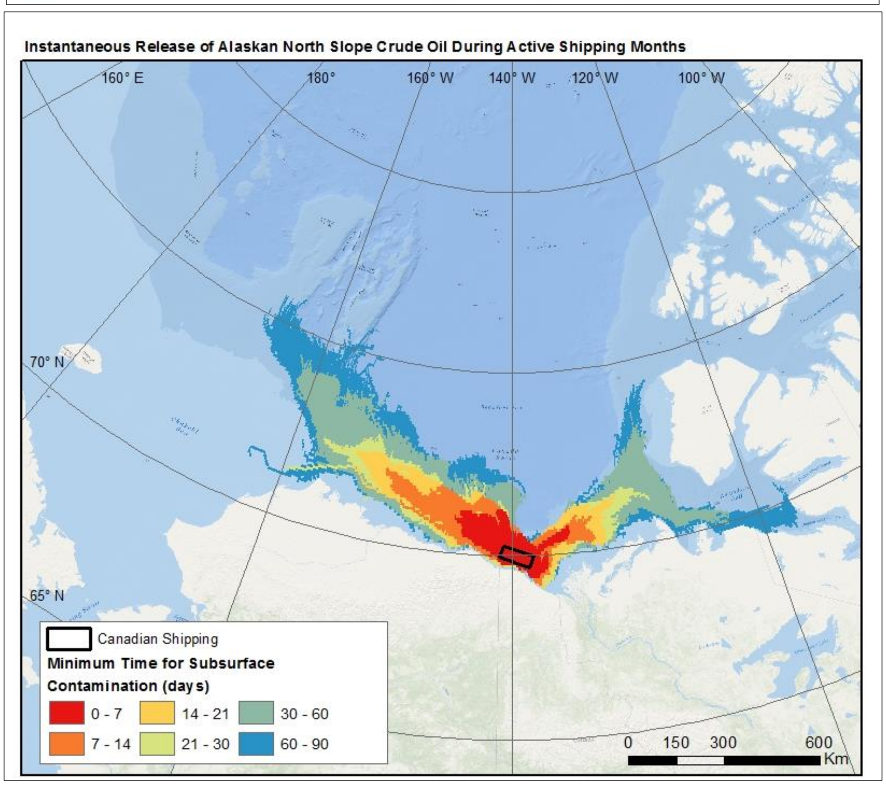

Figure 67. TB_Ship_Crude_CAN - Subsurface contamination probabilities and minimum travel times for total oil in the water column.

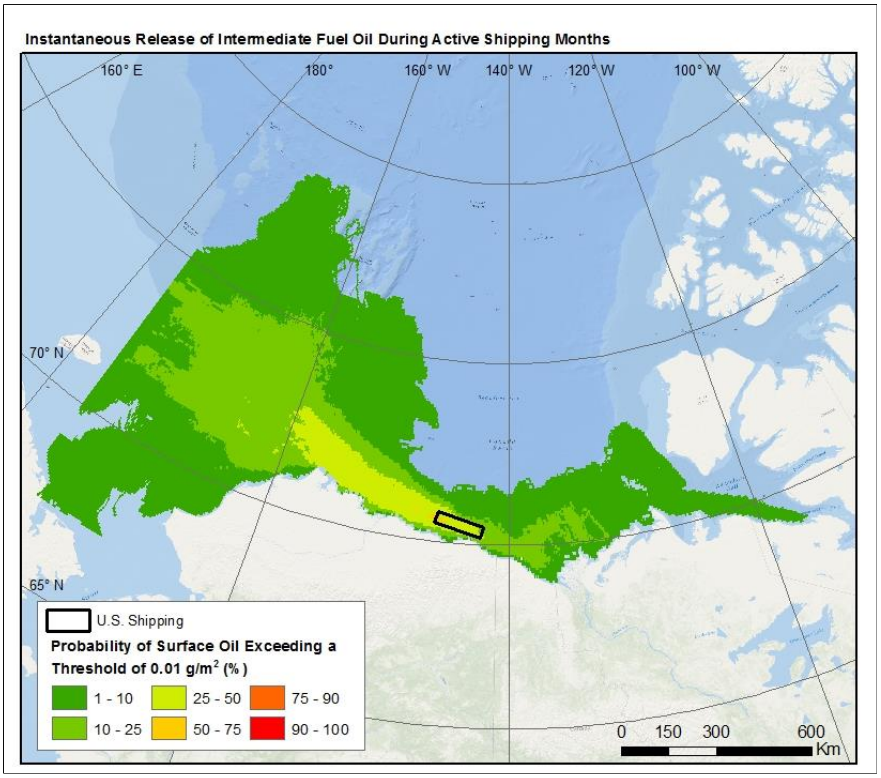

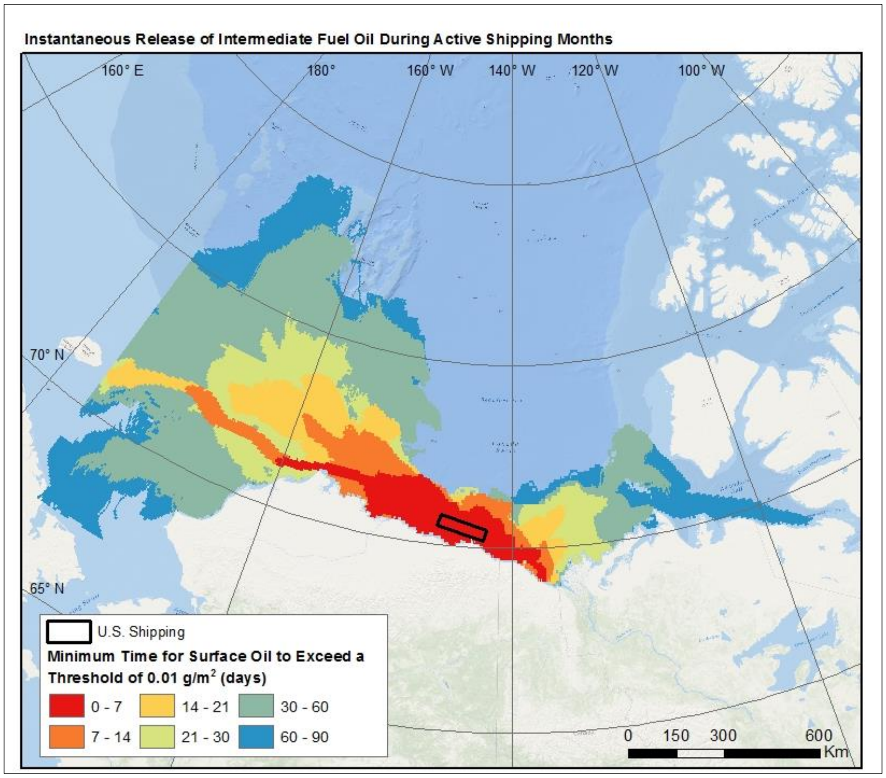

Figure 68. TB_Ship_IFO_US - Water surface oiling probabilities and minimum travel times for floating oil ≥0.01 g/m^2.

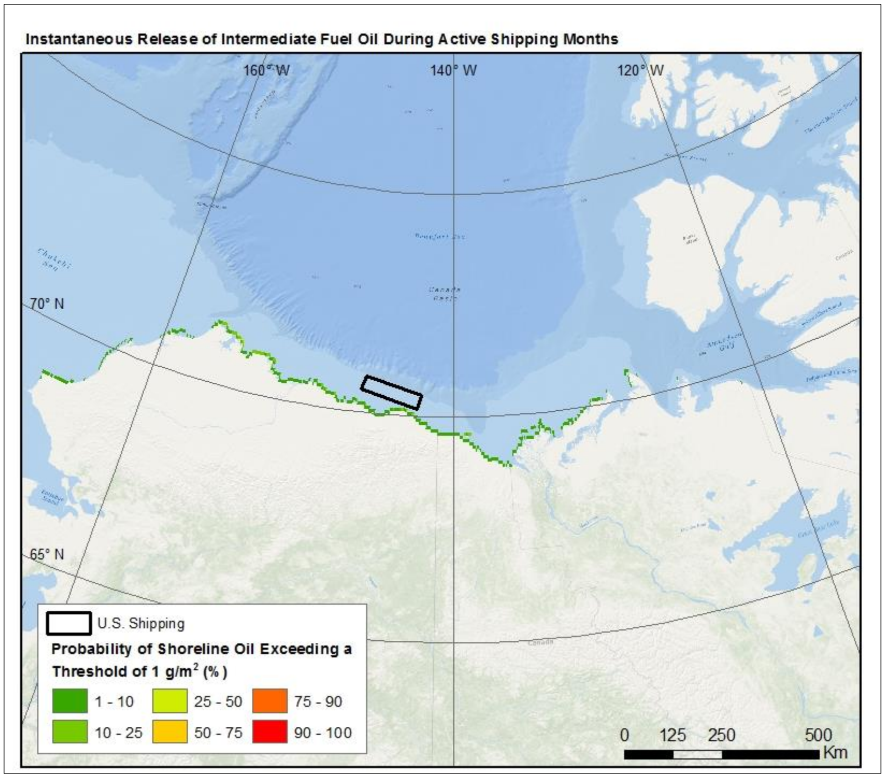

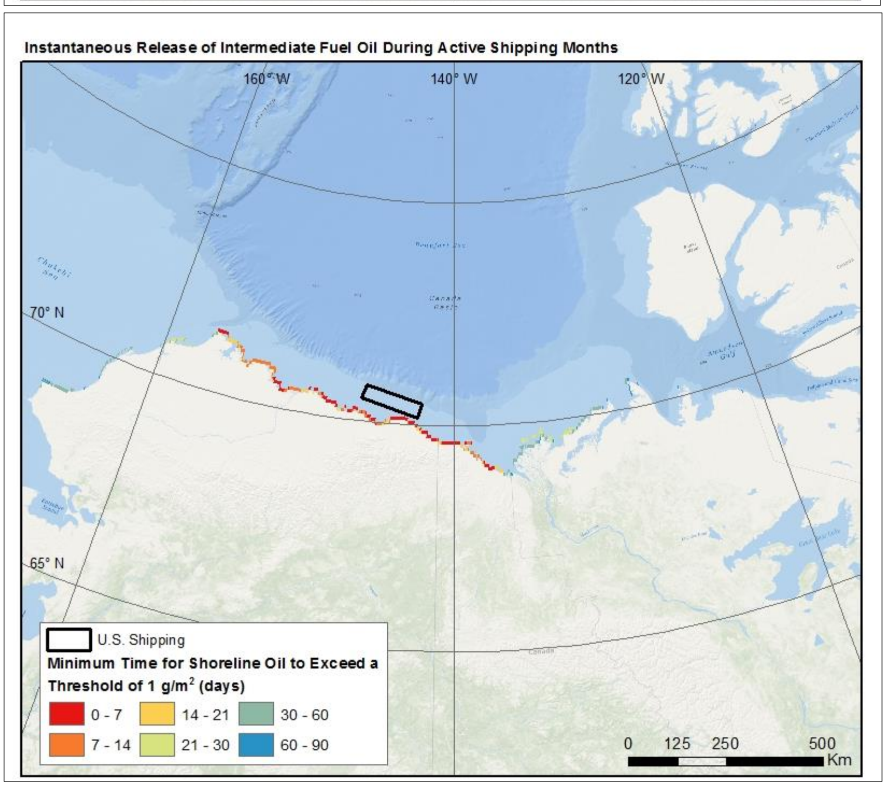

Figure 69. TB_Ship_IFO_US - Shoreline oiling probabilities and minimum travel times for shoreline oil ≥1 g/m^2.

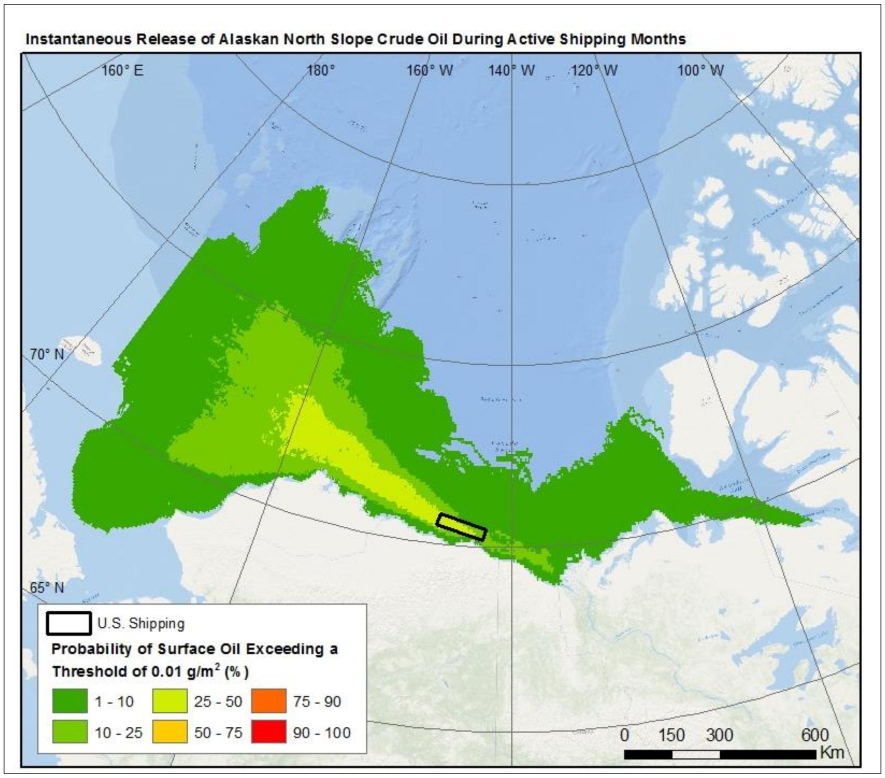

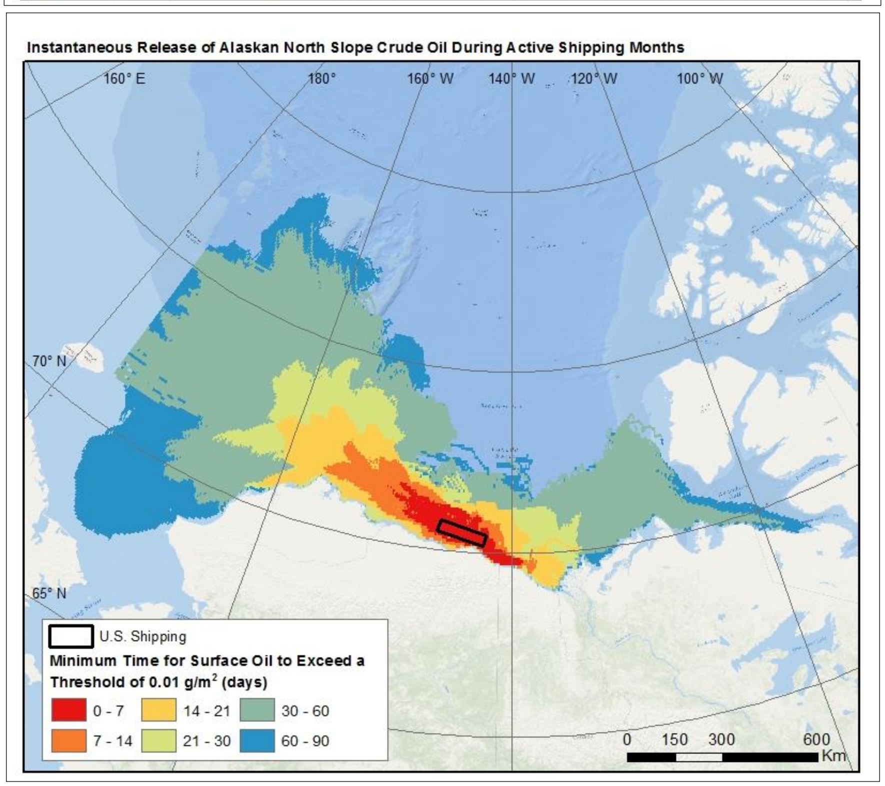

Figure 70. TB_Ship_Crude_US - Water surface oiling probabilities and minimum travel times for floating oil ≥0.01 g/m^2.

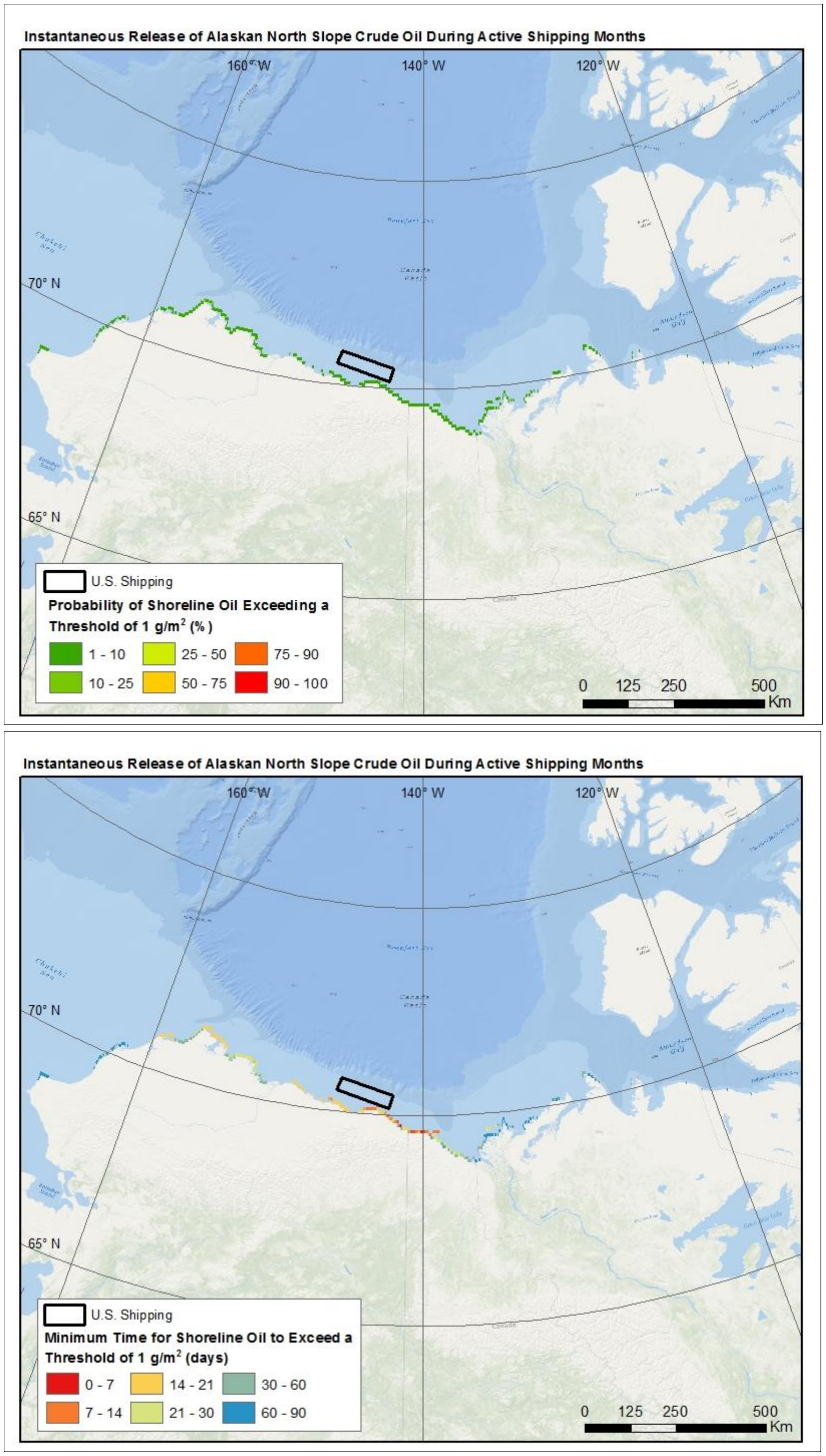

Figure 71. TB_Ship_Crude_US – Shoreline oiling probabilities and minimum travel times for shoreline oil ≥1 g/m².

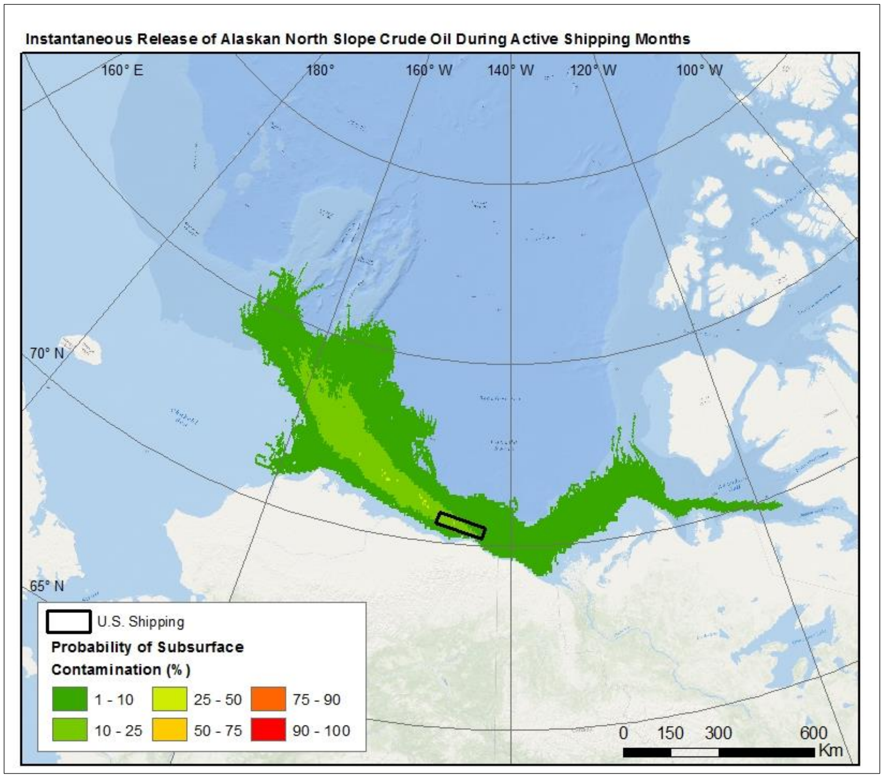

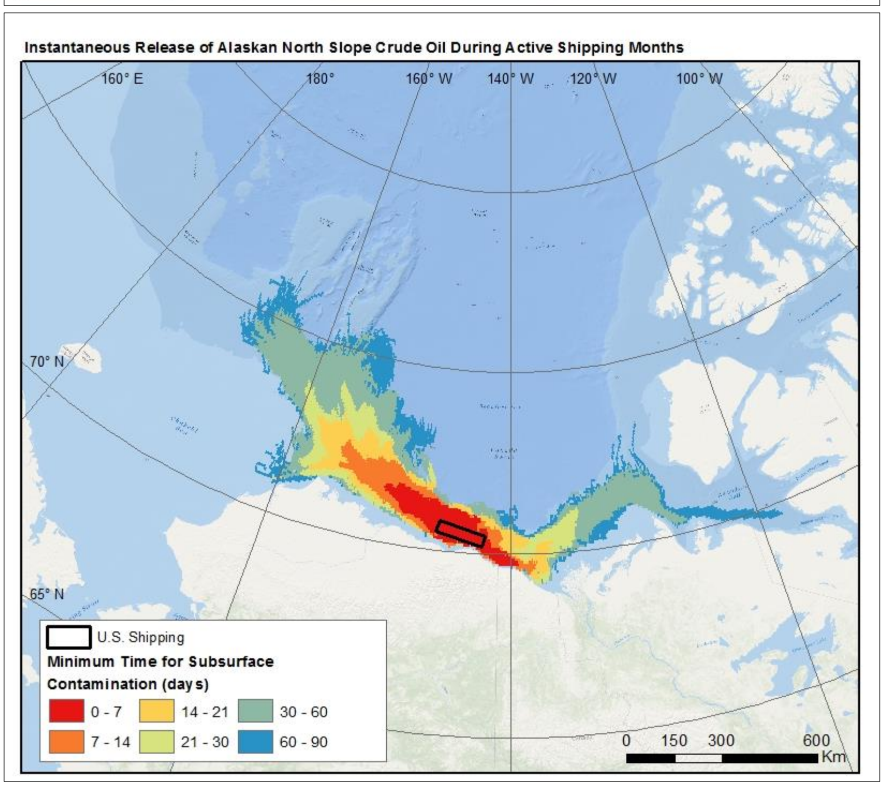

Figure 72. TB_Ship_Crude_US - Subsurface contamination probabilities and minimum travel times for total oil in the water column.

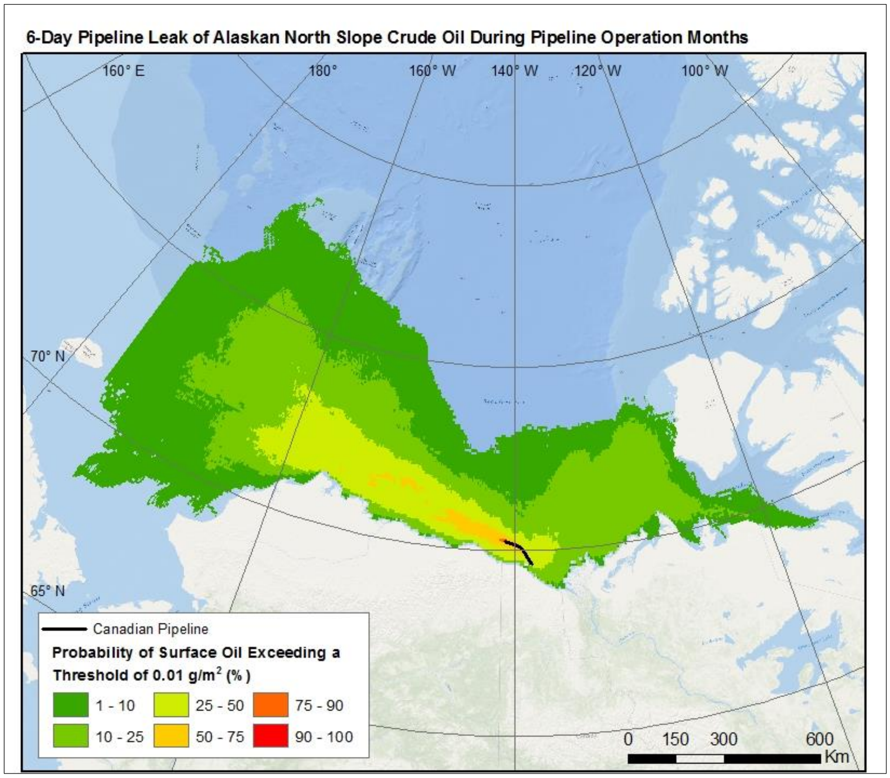

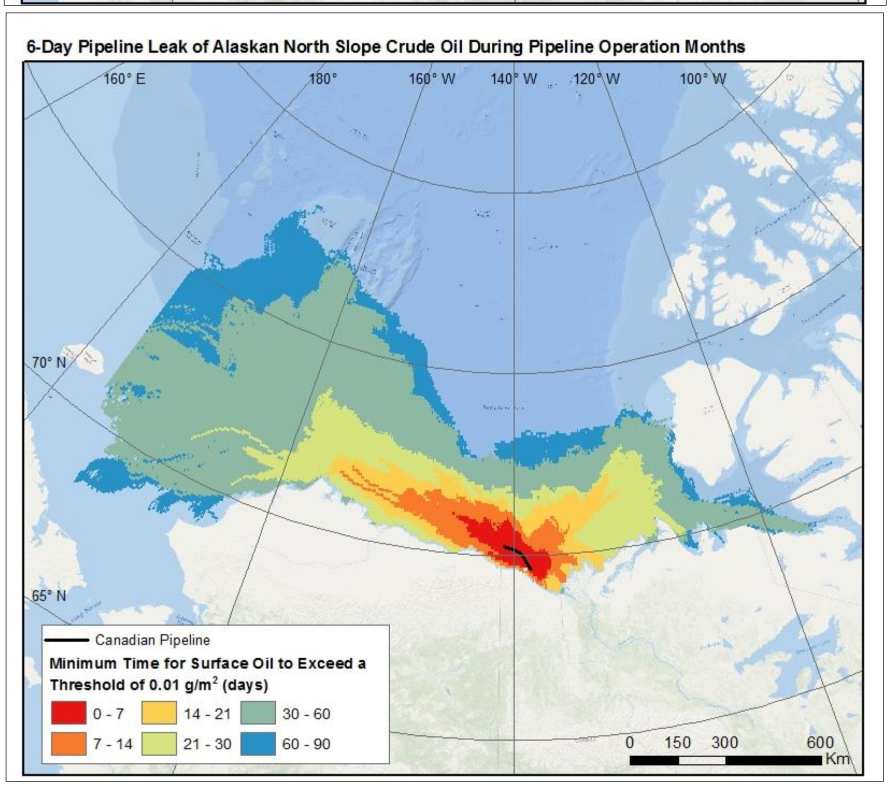

Figure 73. TB_Pipeline_CAN - Water surface oiling probabilities and minimum travel times for floating oil ≥0.01 g/m^2.

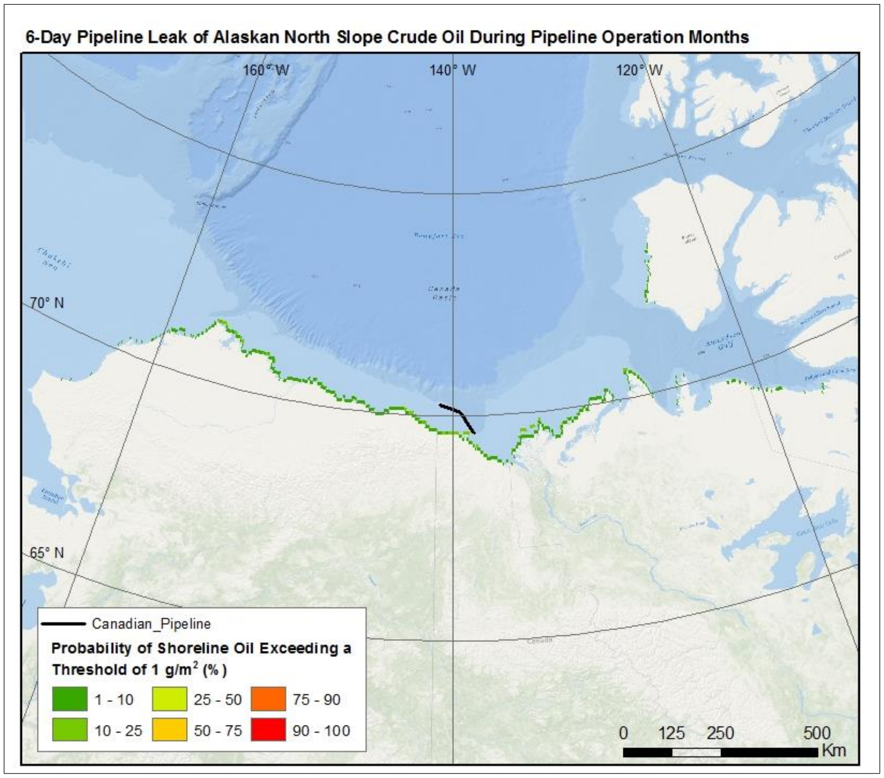

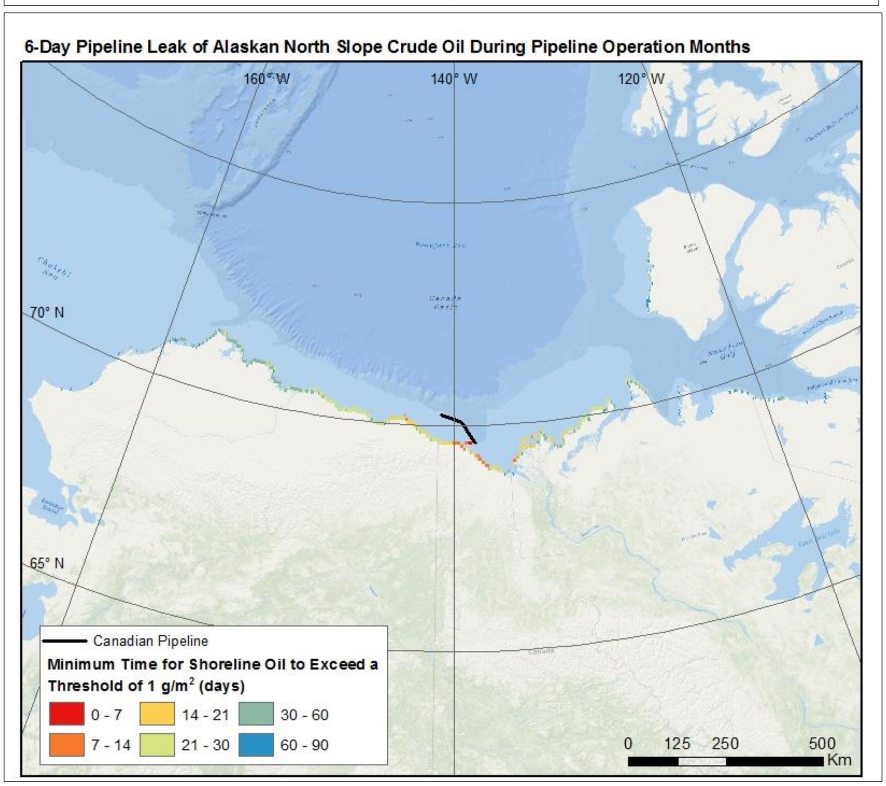

Figure 74. TB_Pipeline_CAN - Shoreline oiling probabilities and minimum travel times for shoreline oil ≥1 g/m^2.

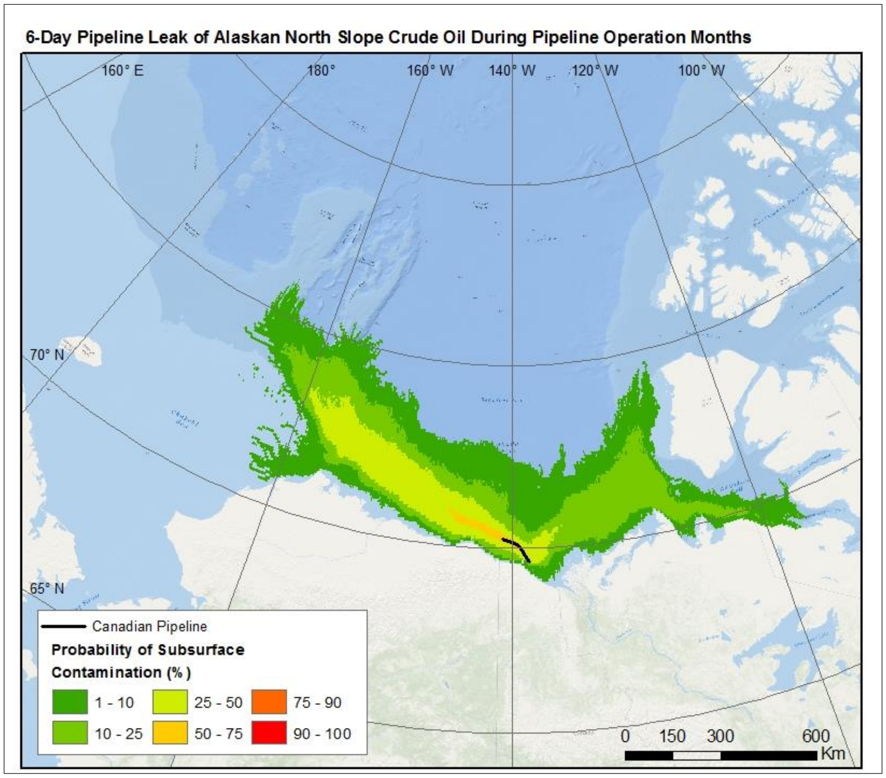

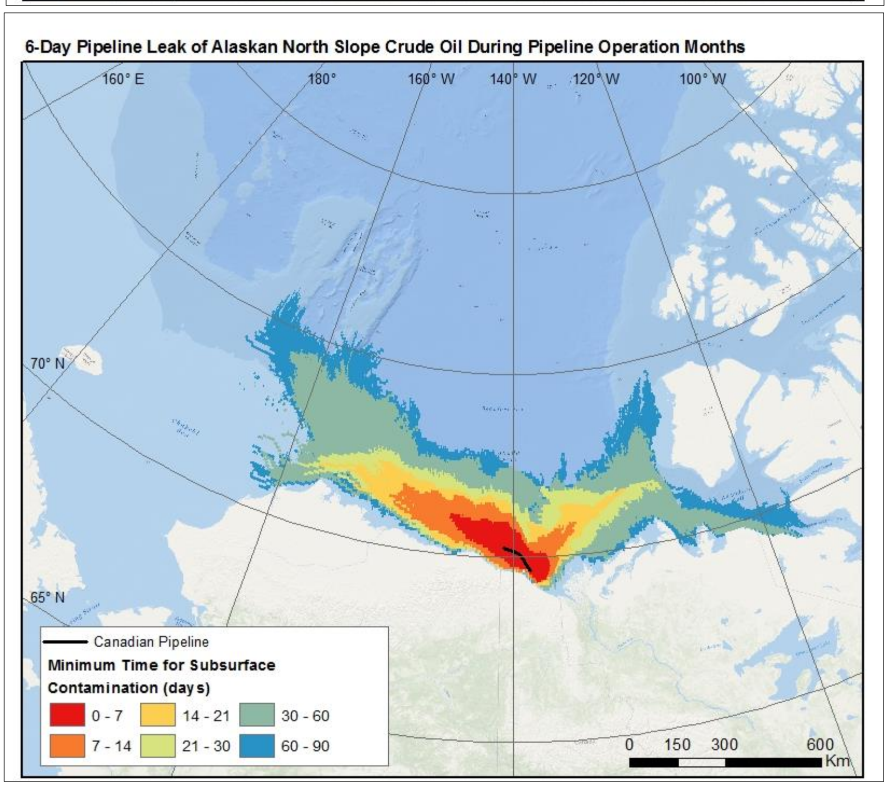

Figure 75. TB_Pipeline_CAN - Subsurface contamination probabilities and minimum travel times for total oil in the water column.

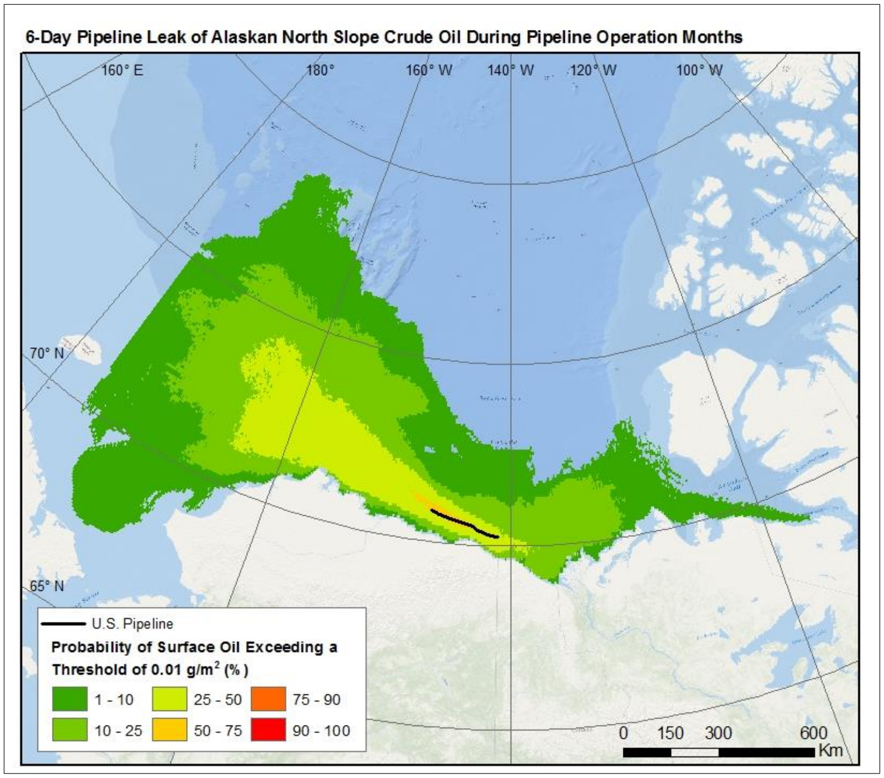

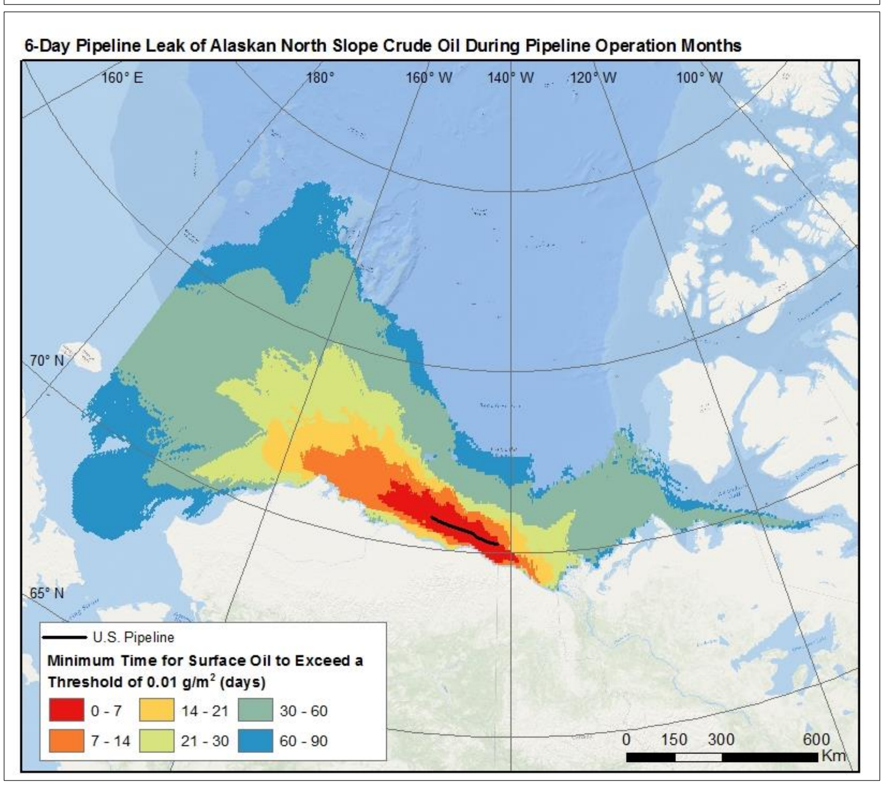

Figure 76. TB_Pipeline_US - Water surface oiling probabilities and minimum travel times for floating oil ≥0.01 g/m^2.

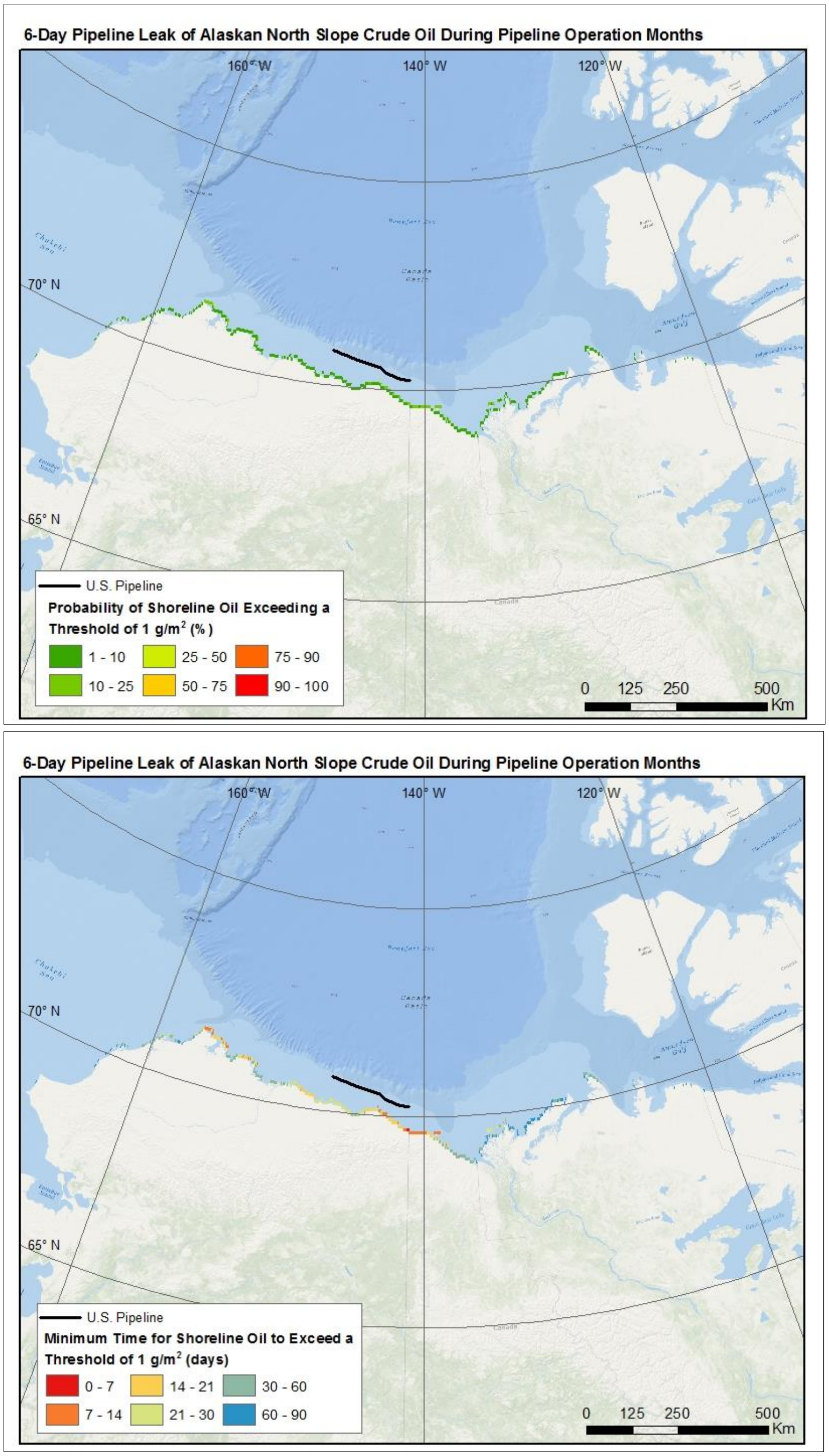

Figure 77. TB_Pipeline_US - Shoreline oiling probabilities and minimum travel times for shoreline oil ≥1 g/m^2.

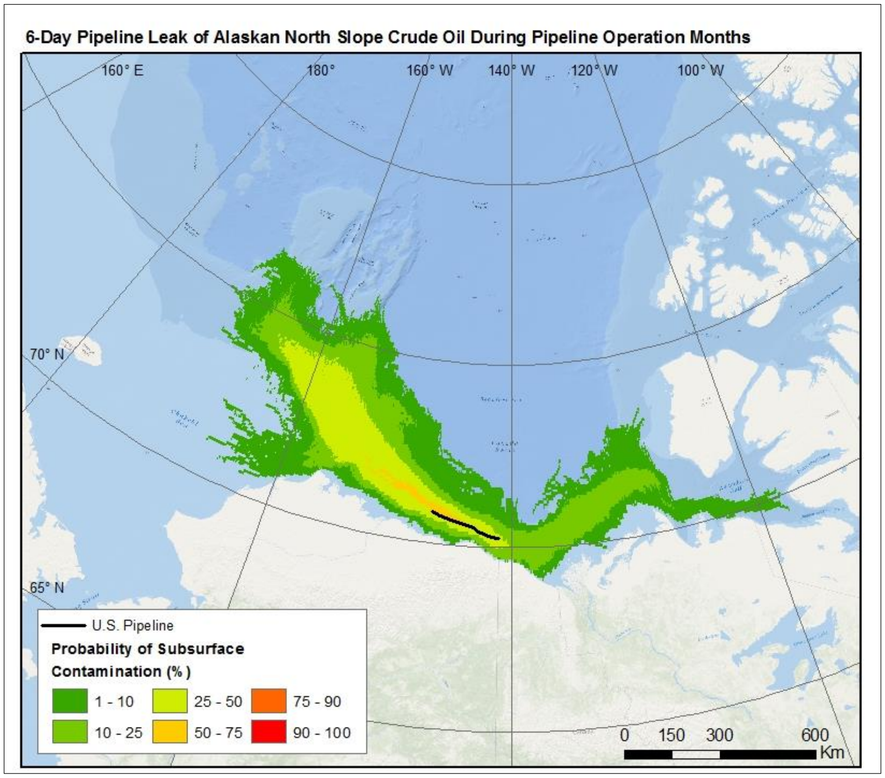

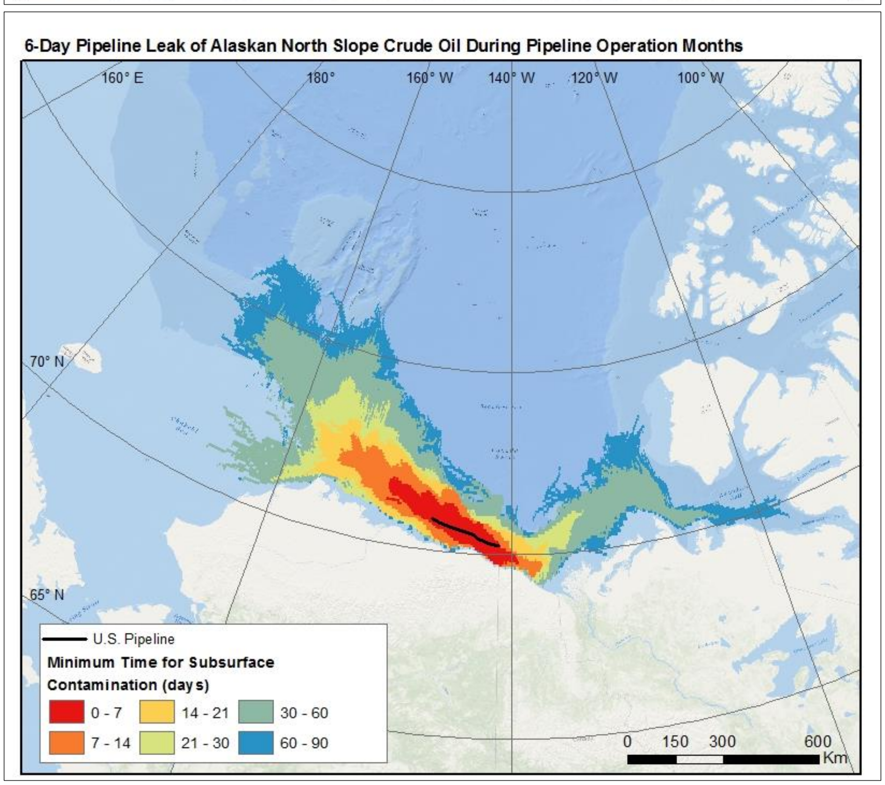

Figure 78. TB_Pipeline_US - Subsurface contamination probabilities and minimum travel times for total oil in the water column.

7.2.2 Individual Trajectory Model Results

Note: Water column contamination or dissolved aromatics results are presented for crude runs only (no IFO) for the Trans-boundary Analysis.

95th Percentile Surface Oiling

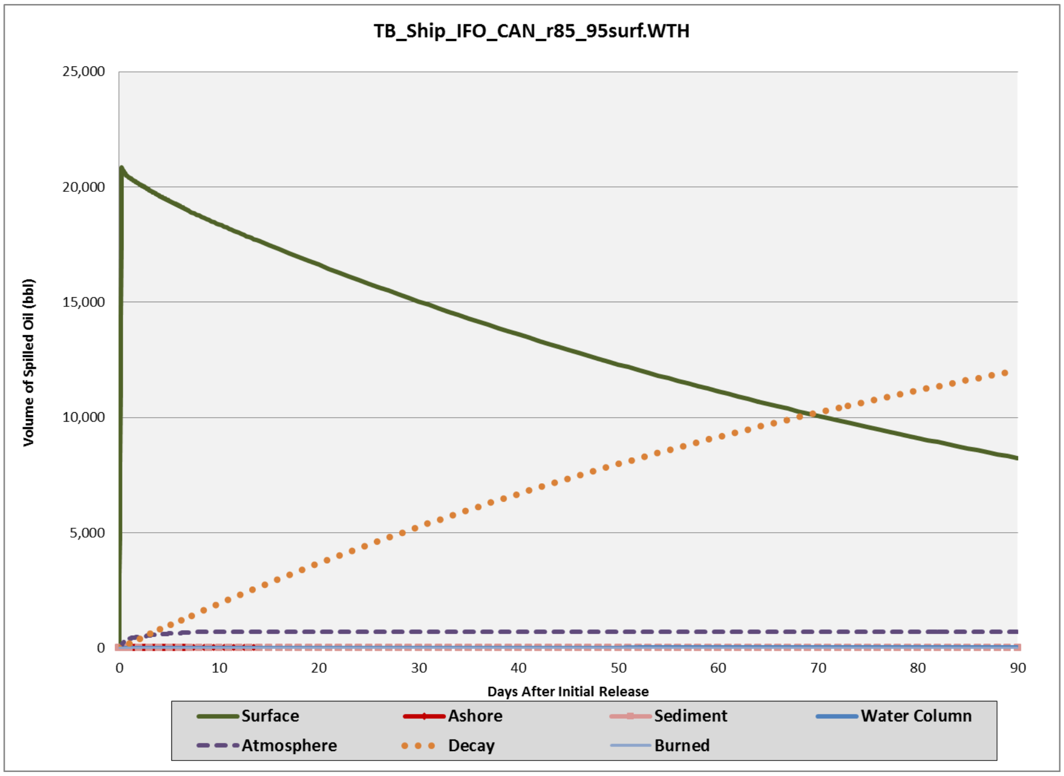

Figure 79. TB_Ship_IFO_CAN_r85_95surf - Mass balance chart. Start date: 10/16/2008.

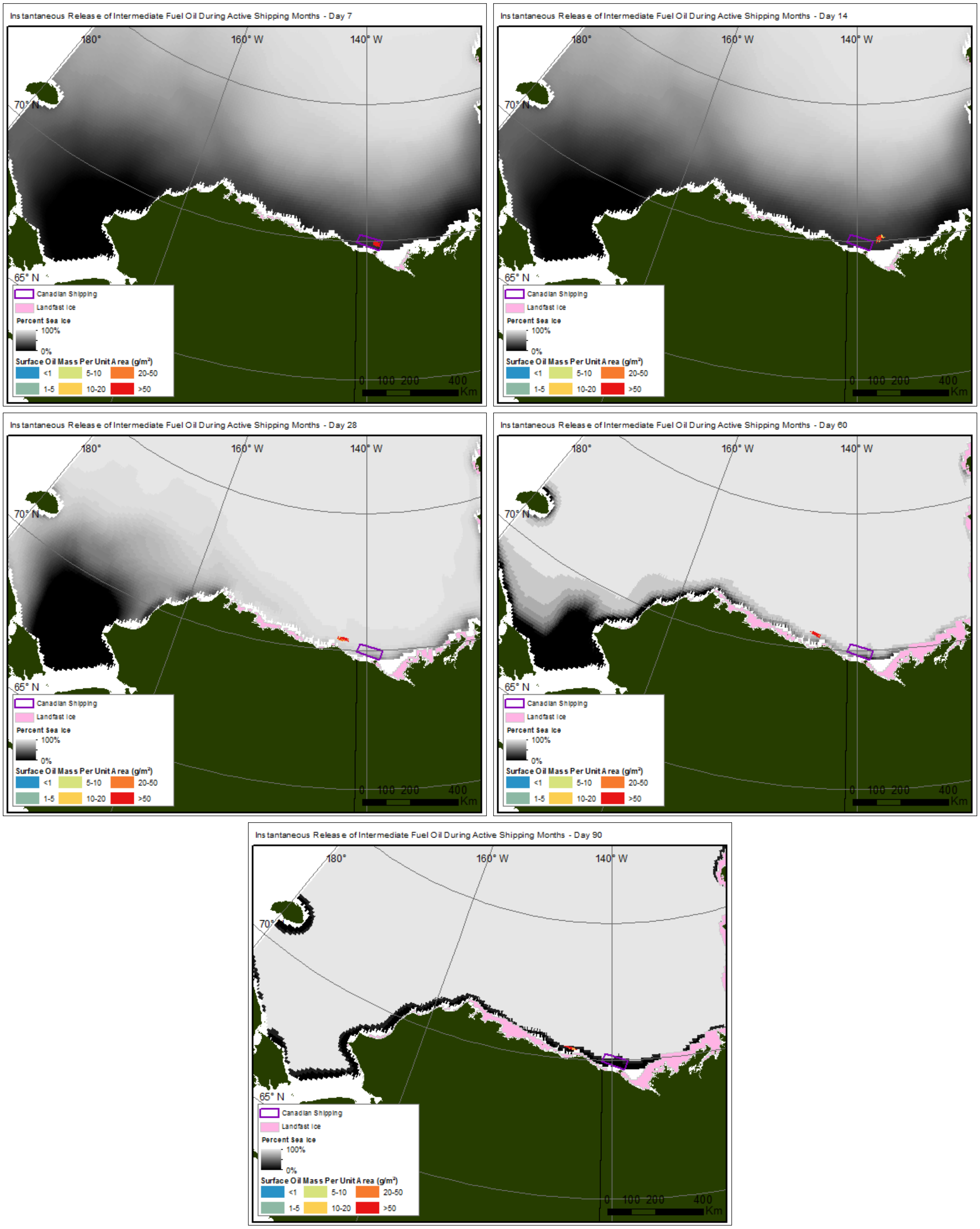

Figure 80. TB_Ship_IFO_CAN_r85_95surf – Time series maps of spill floating surface oil mass per unit area (g/m^2) (day 7, 14, 28, 60, 90; October 2008 – January 2009). Pink polygons represent monthly average landfast ice. Grey scale contours represent ice percent coverage for that month from TOPAZ4 model. White indicates areas of no data for ice coverage. Start date: 10/16/2008.

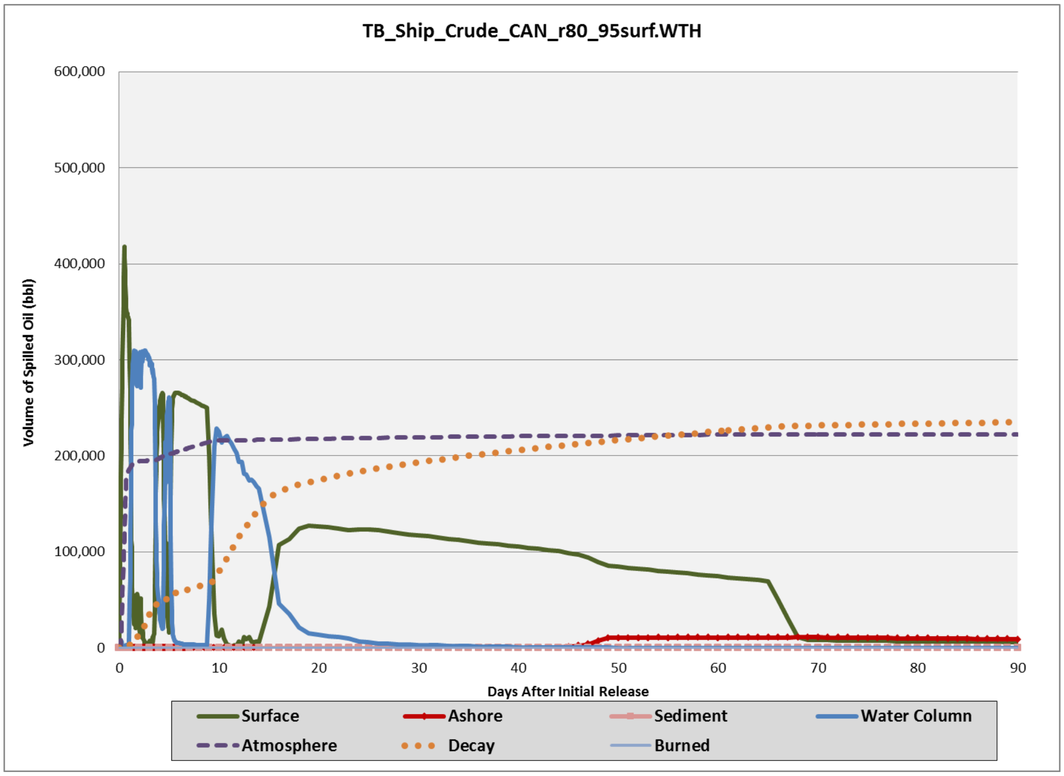

Figure 81. TB_Ship_Crude_CAN_r80_95surf - Mass balance chart. Several strong wind events occurred early in this scenario run, entraining most of the floating oil, whereupon the oil resurfaced in subsequent calm periods. By day 20, the oil is trapped in and under ice. Start date: 8/24/2010.

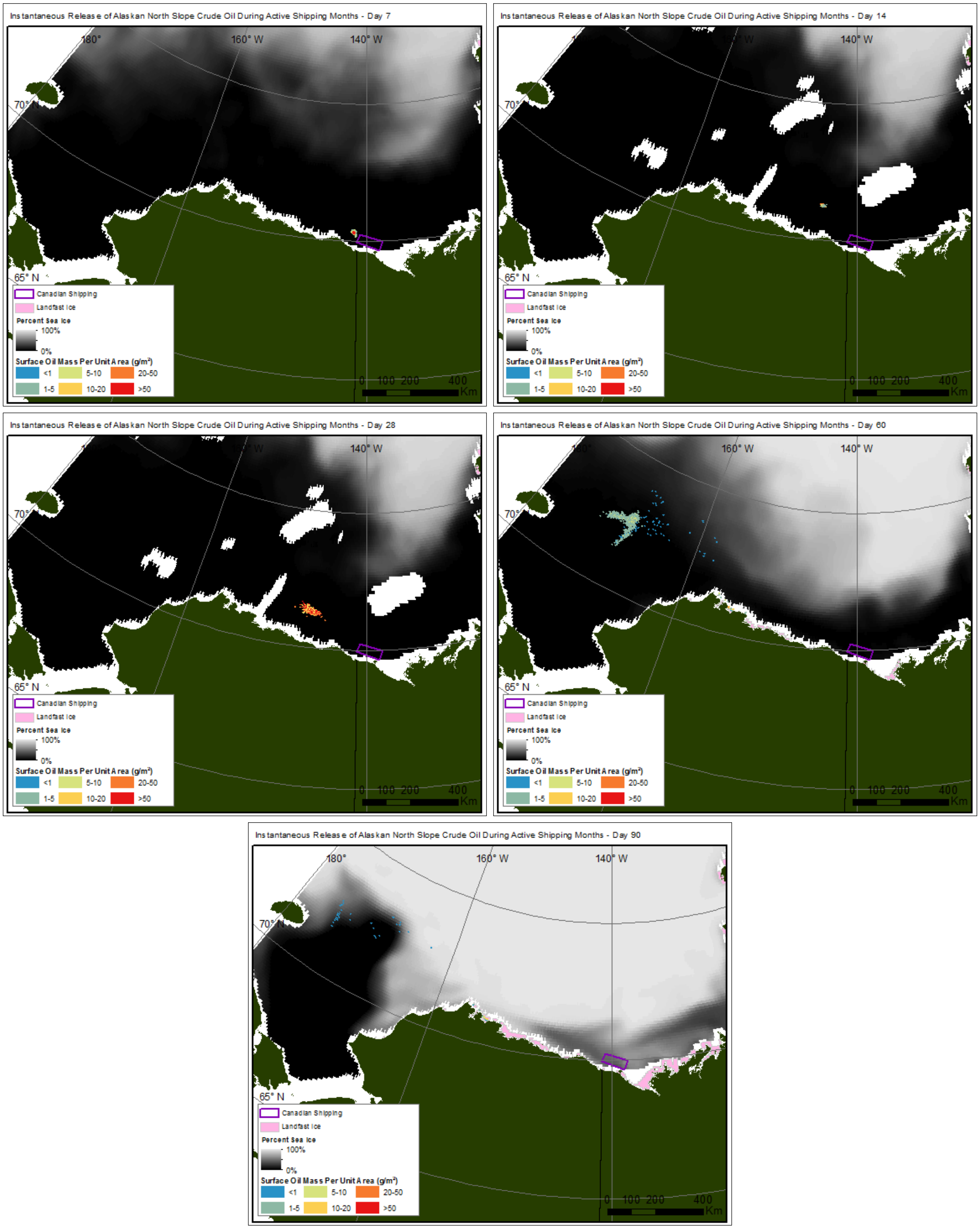

Figure 82. TB_Ship_Crude_CAN_r80_95surf – Time series maps of spill floating surface oil mass per unit area (g/m^2) (day 7, 14, 28, 60, 90; August – November 2010). Pink polygons represent monthly average landfast ice. Grey scale contours represent ice percent coverage for that month from TOPAZ4 model. White indicates areas of no data for ice coverage. Start date: 8/24/2010.

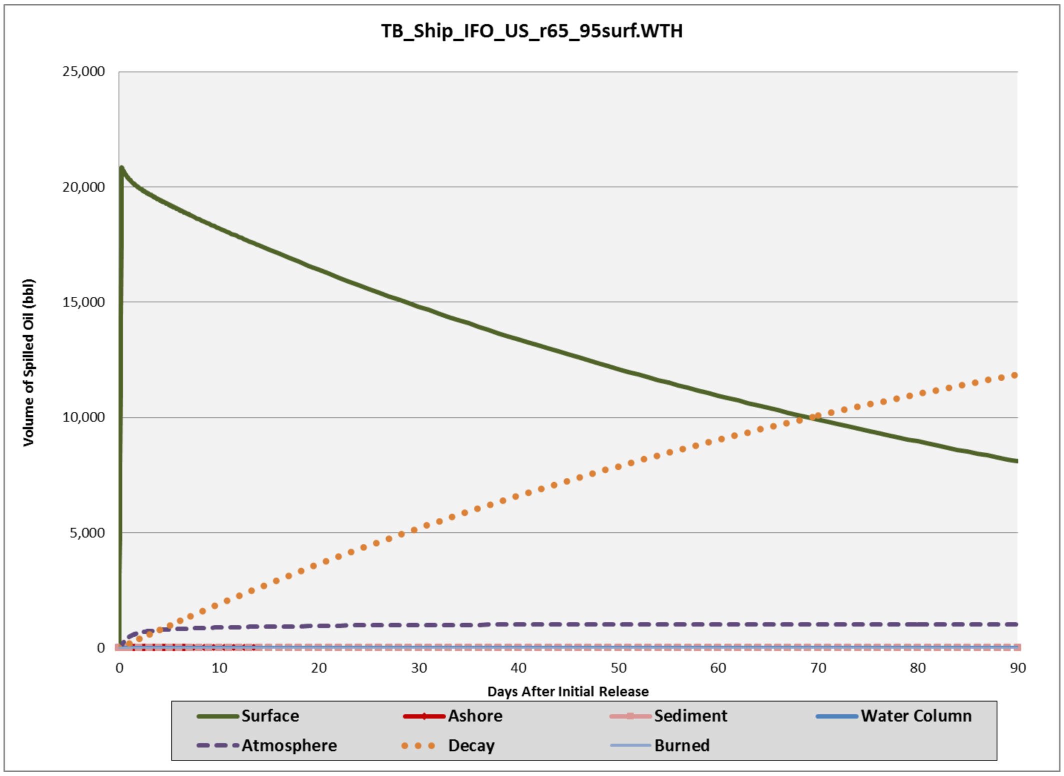

Figure 83.TB_Ship_IFO_US_r65_95surf - Mass balance chart. Start date: 9/26/2011.

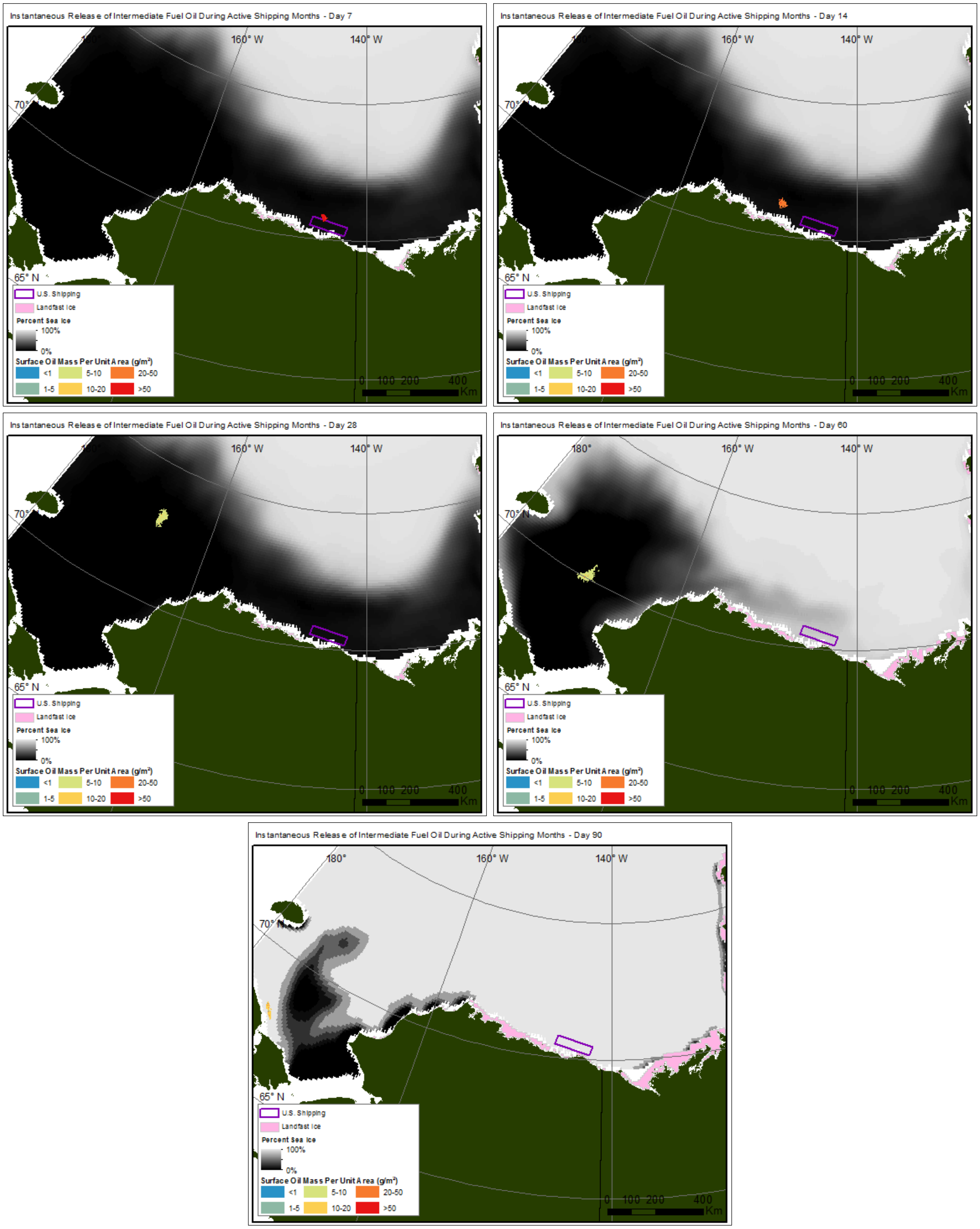

Figure 84.TB_Ship_IFO_US_r65_95surf – Time series maps of spill floating surface oil mass per unit area (g/m^2) (day 7, 14, 28, 60, 90; September – December 2011). Pink polygons represent monthly average landfast ice. Grey scale contours represent ice percent coverage for that month from TOPAZ4 model. White indicates areas of no data for ice coverage. Start date: 9/26/2011.

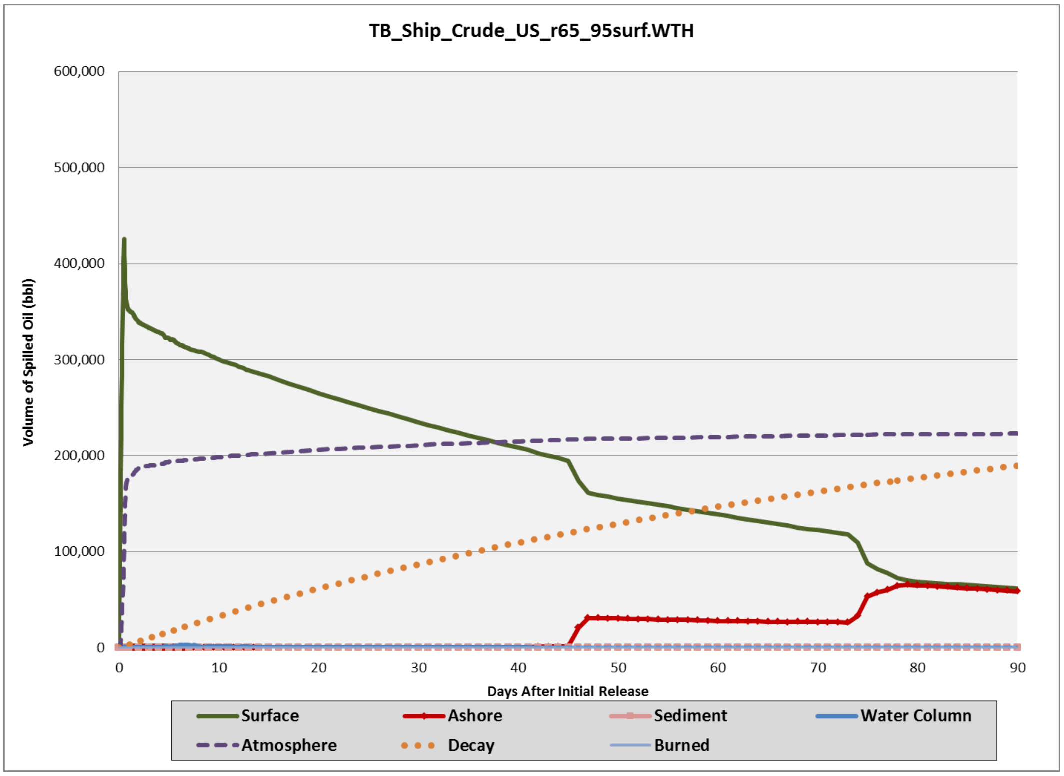

Figure 85. TB_Ship_Crude_US_r65_95surf - Mass balance chart. Start date: 6/26/2012.

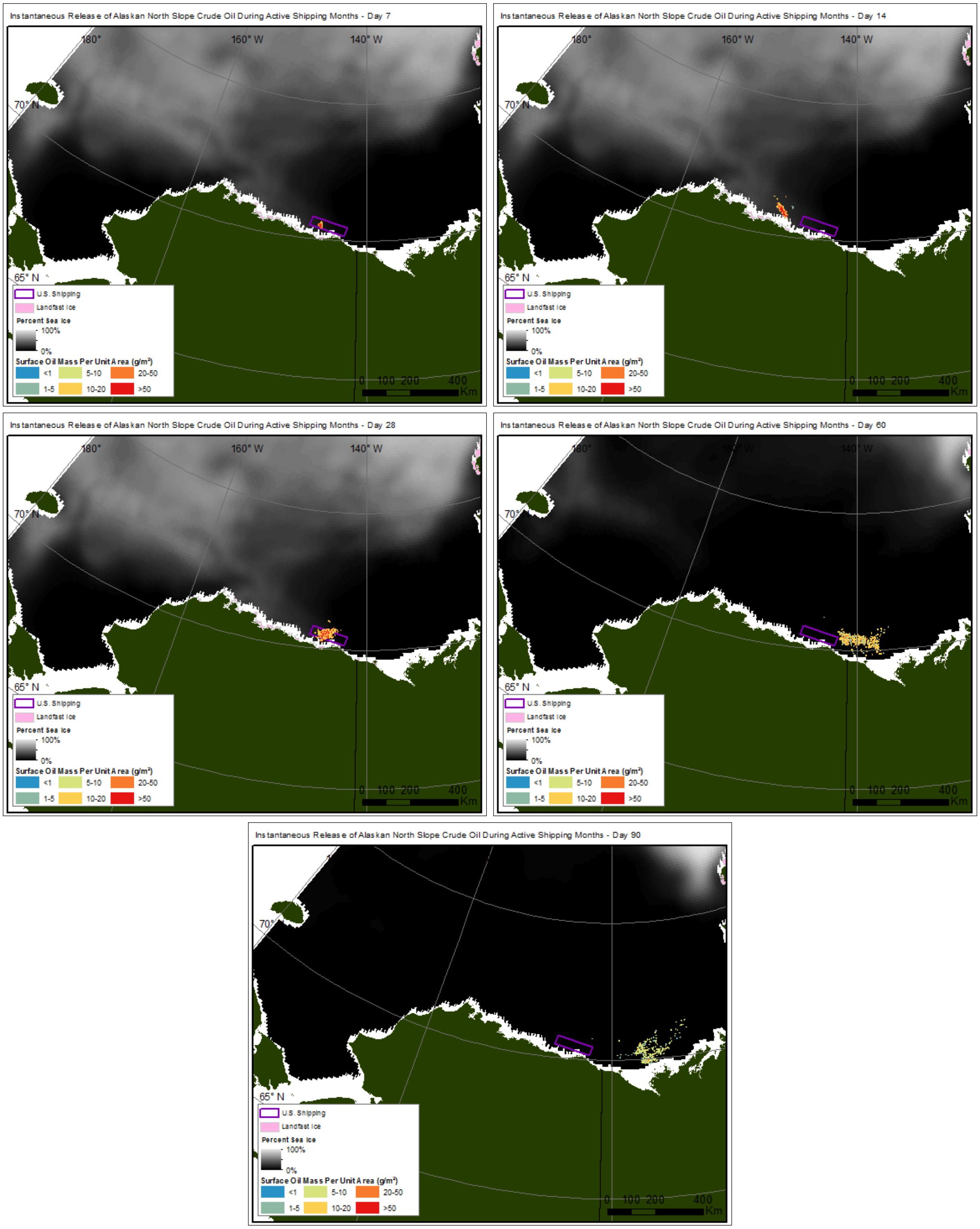

Figure 86.TB_Ship_Crude_US_r65_95surf – Time series maps of spill floating surface oil mass per unit area (g/m^2) (day 7, 14, 28, 60, 90; June – September 2012). Pink polygons represent monthly average landfast ice. Grey scale contours represent ice percent coverage for that month from TOPAZ4 model. White indicates areas of no data for ice coverage. Start date: 6/26/2012.

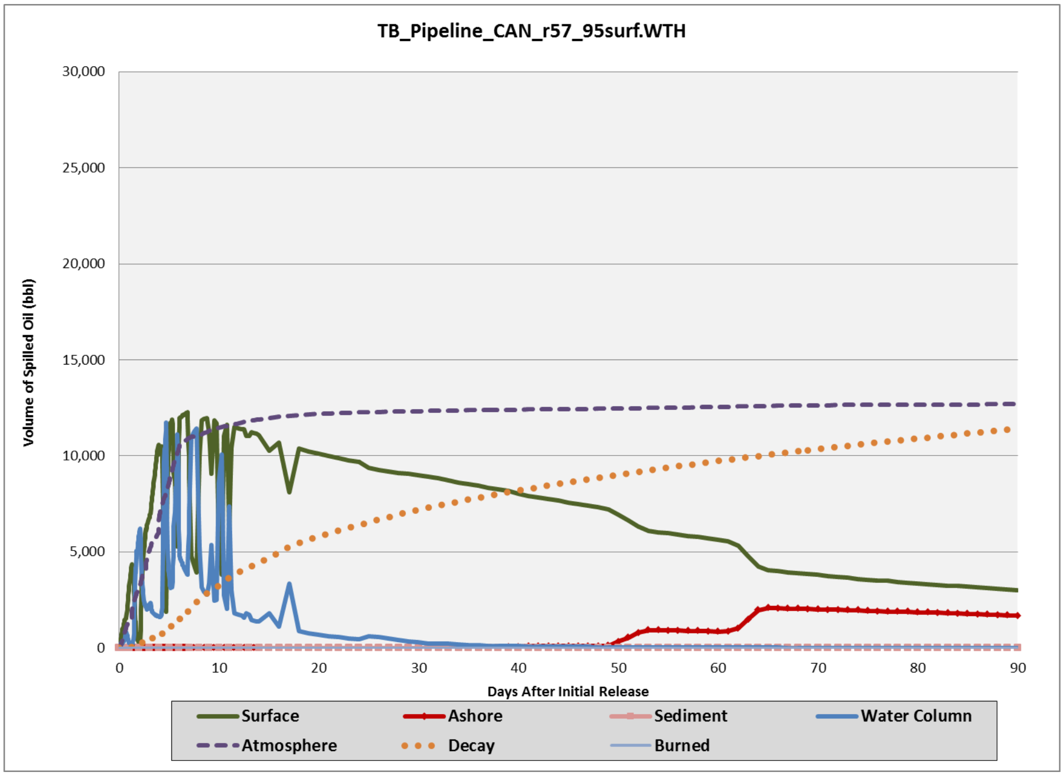

Figure 87. TB_Pipeline_CAN_r57_95surf - Mass balance chart. Several strong wind events occurred early in this scenario run, entraining most of the floating oil, whereupon the oil resurfaced in subsequent calm periods. Eventually, the oil weathers and becomes too viscous to be entrained by wind events. Start date: 7/19/2011.

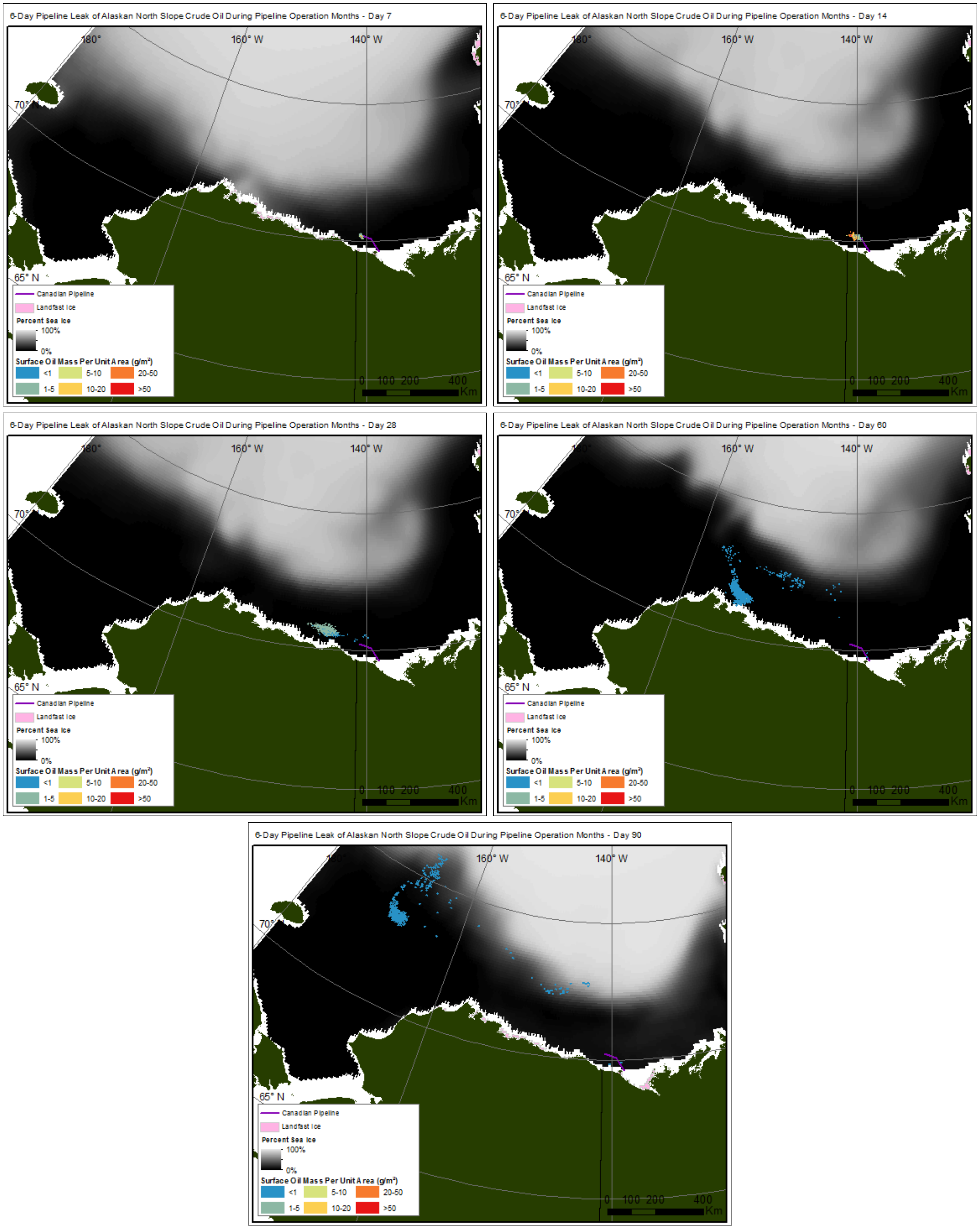

Figure 88. TB_Pipeline_CAN_r57_95surf – Time series maps of spill floating surface oil mass per unit area (g/m^2) (day 7, 14, 28, 60, 90; July – October 2011). Pink polygons represent monthly average landfast ice. Grey scale contours represent ice percent coverage for that month from TOPAZ4 model. White indicates areas of no data for ice coverage. Start date: 7/19/2011.

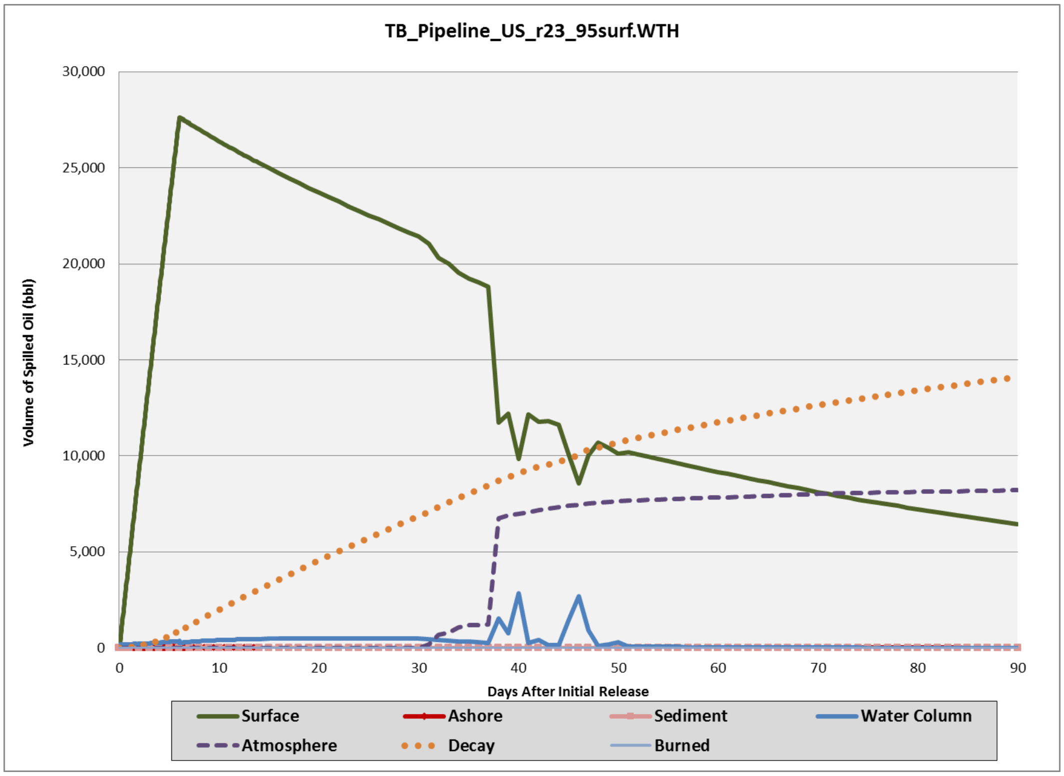

Figure 89.TB_Pipeline_US_r23_95surf - Mass balance chart. In this model run, oil was trapped under ice for most of the period simulated, except for about 36-50 days after the spill. Start date: 6/1/2012.

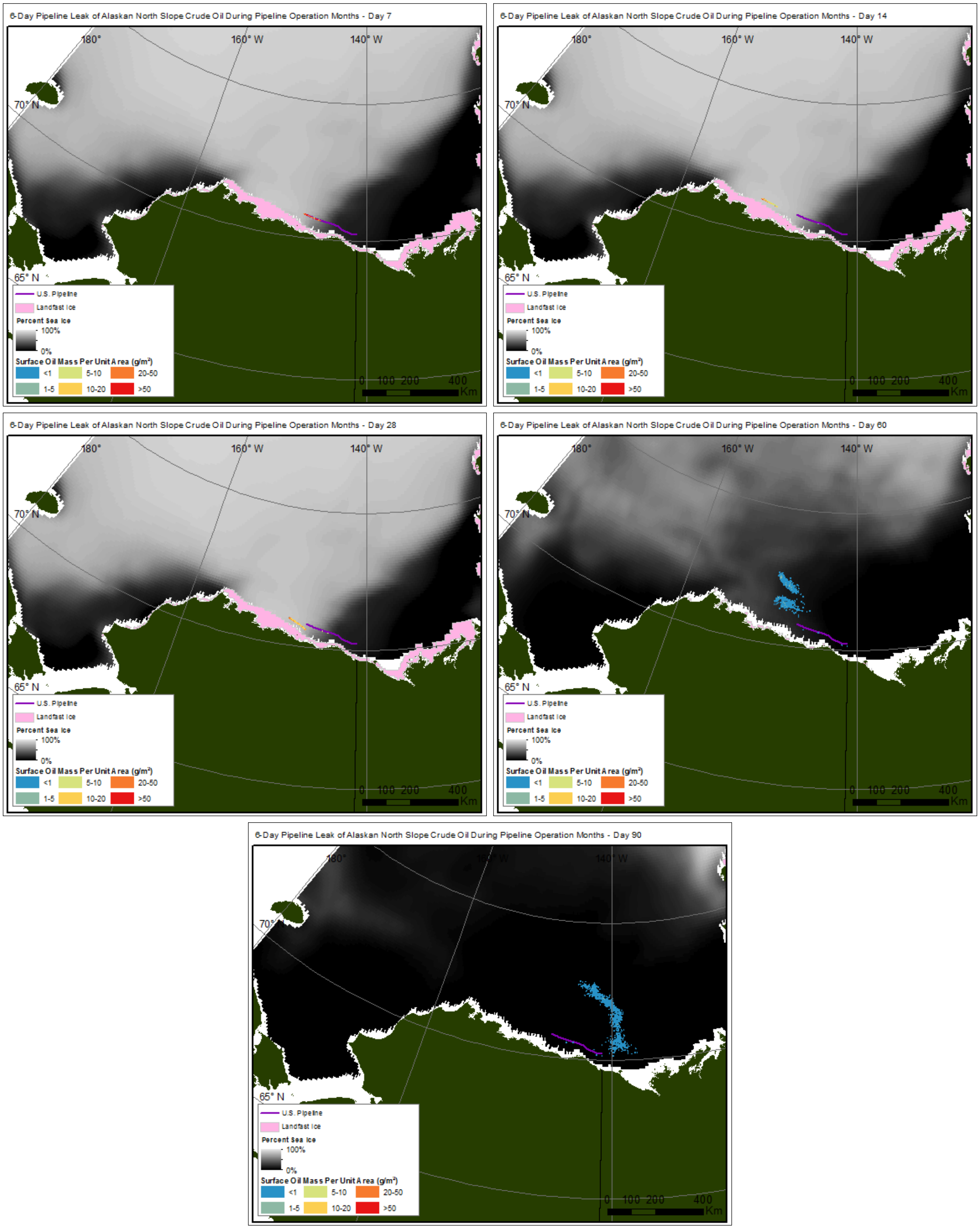

Figure 90. TB_Pipeline_US_r23_95surf – Time series maps of spill floating surface oil mass per unit area (g/m^2) (day 7, 14, 28, 60, 90; June – September 2012). Pink polygons represent monthly average landfast ice. Grey scale contours represent ice percent coverage for that month from TOPAZ4 model. White indicates areas of no data for ice coverage. Start date: 6/1/2012.

95th Percentile Shoreline Oiling

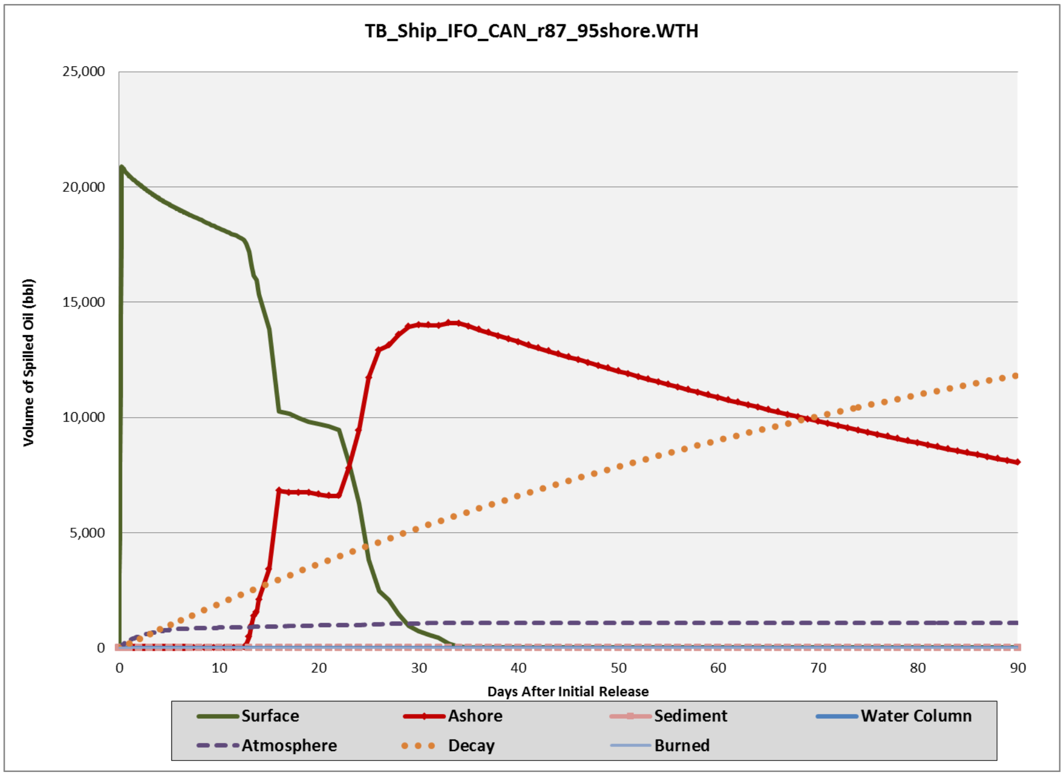

Figure 91.TB_Ship_IFO_CAN_r87_95shore - Mass balance chart. Start date: 8/30/2008.

Table 14.TB_Ship_IFO_CAN_r87_95shore – Shoreline length oiled (km) by habitat type, for both shore oiling thresholds. Start date: 8/30/2008.

Shore Type	Shore Length Oiled (km)	
	> 100 micrometers	> 1 micrometer
Seaward Rocky Shore	15.1	15.1
Seaward Gravel Beach	50.4	55.5
Seaward Sand Beach	90.7	136.1
Seaward Fringing Mud Flat	40.3	85.7
Seaward Fringing Wetland	5.0	40.3
Seaward Intertidal Macroalgal Bed	90.7	95.8
Total Shoreline	**292.2**	**428.5**

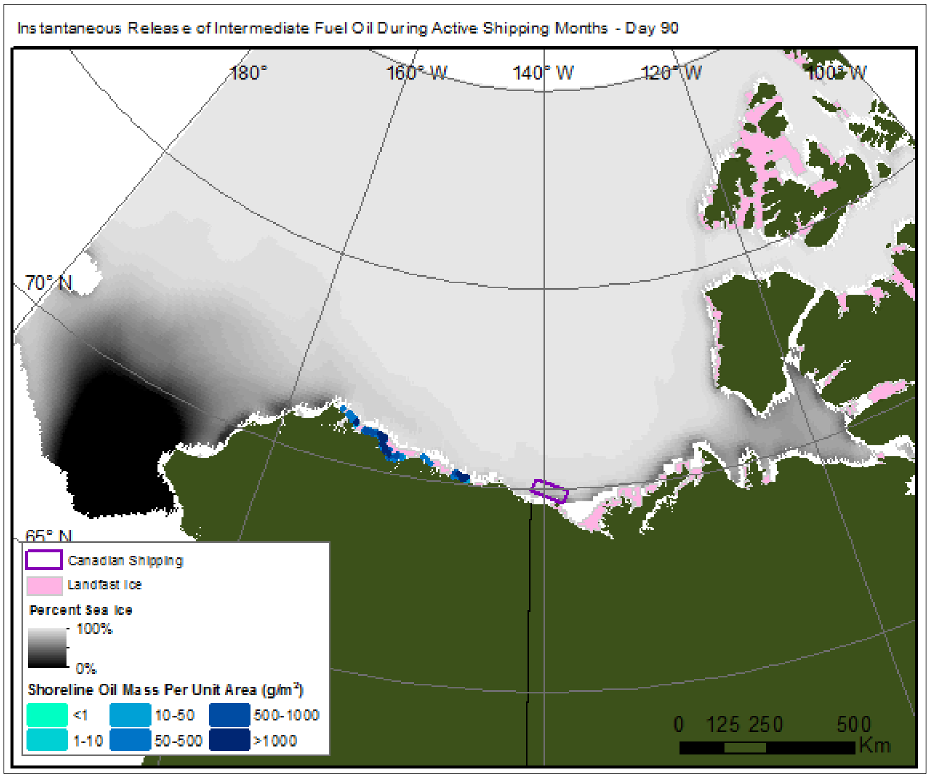

Figure 92.TB_Ship_IFO_CAN_r87_95shore – Map of overall effects to shorelines as mass of oil deposited on shore per unit of area (g/m^2) (day 90 – November 2008). Pink polygons represent monthly average landfast ice. Grey scale contours represent ice percent coverage for that month from TOPAZ4 model. White indicates areas of no data for ice coverage. Start date: 8/30/2008.

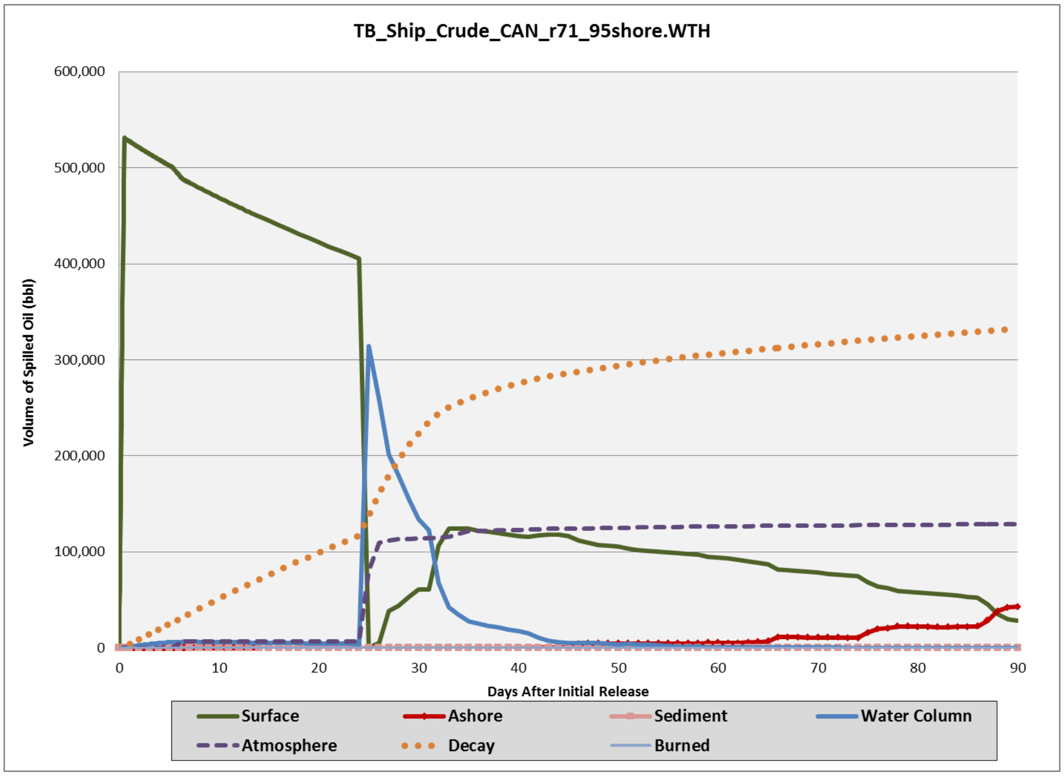

Figure 93.TB_Ship_Crude_CAN_r71_95shore - Mass balance chart. For the first 24 days after the spill, oil was trapped at the surface under ice. Start date: 5/17/2012.

Table 15. TB_Ship_Crude_CAN_r71_95shore – Shoreline length oiled (km) by habitat type, for both shore oiling thresholds. Start date: 5/17/2012.

Shore Type	Shore Length Oiled (km)	
	> 100 micrometers	> 1 micrometer
Seaward Gravel Beach	267.2	267.2
Seaward Sand Beach	126.0	146.2
Seaward Fringing Mud Flat	80.7	95.8
Seaward Intertidal Macroalgal Bed	5.0	5.0
Total Shoreline	**478.9**	**514.2**

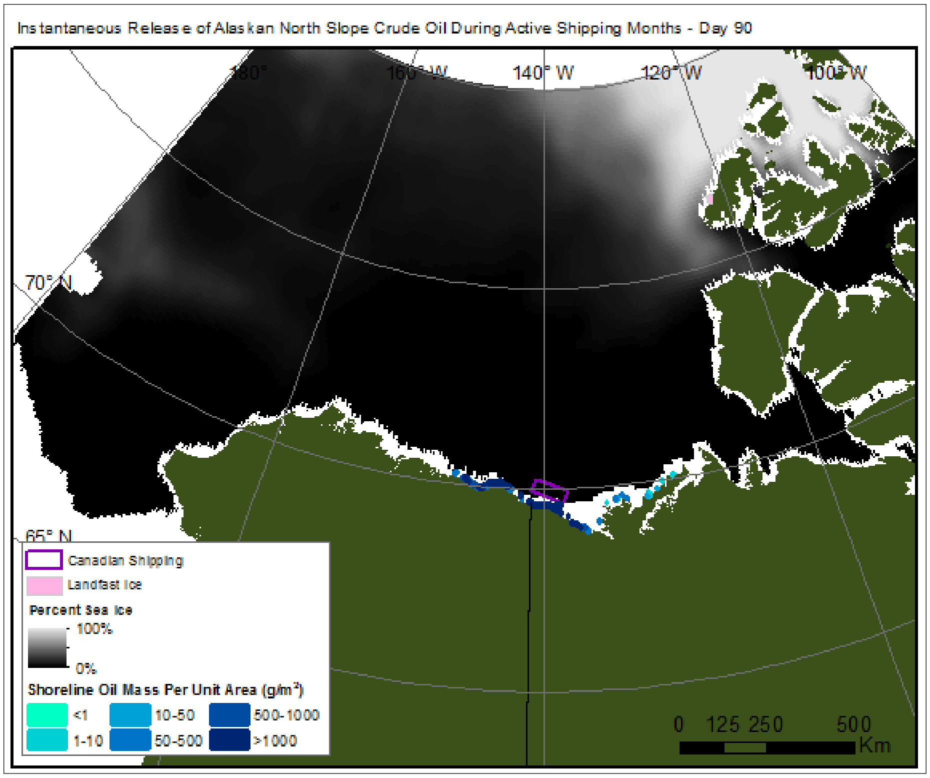

Figure 94. TB_Ship_Crude_CAN_r71_95shore – Map of overall effects to shorelines as mass of oil deposited on shore per unit of area (g/m^2) (day 90 – August 2012). Pink polygons represent monthly average landfast ice. Grey scale contours represent ice percent coverage for that month from TOPAZ4 model. White indicates areas of no data for ice coverage. Start date: 5/17/2012.

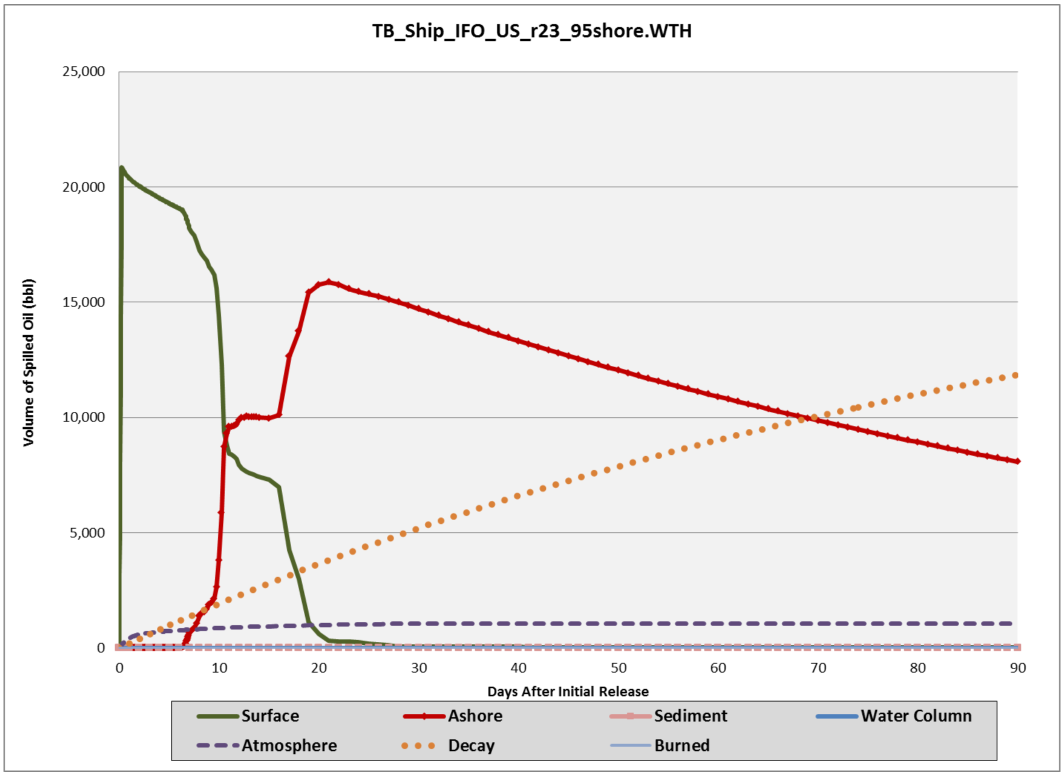

Figure 95. TB_Ship_IFO_US_r23_95shore - Mass balance chart. Start date: 9/4/2008.

Table 16. TB_Ship_IFO_US_r23_95shore – Shoreline length oiled (km) by habitat type, for both shore oiling thresholds. Start date: 9/4/2008.

Shore Type	Shore Length Oiled (km)	
	> 100 micrometers	> 1 micrometer
Seaward Rocky Shore	10.1	10.1
Seaward Gravel Beach	85.7	131.1
Seaward Sand Beach	70.6	126.0
Seaward Fringing Mud Flat	50.4	110.9
Seaward Fringing Wetland	0.0	15.1
Seaward Intertidal Macroalgal Bed	10.1	10.1
Total Shoreline	**226.9**	**403.3**

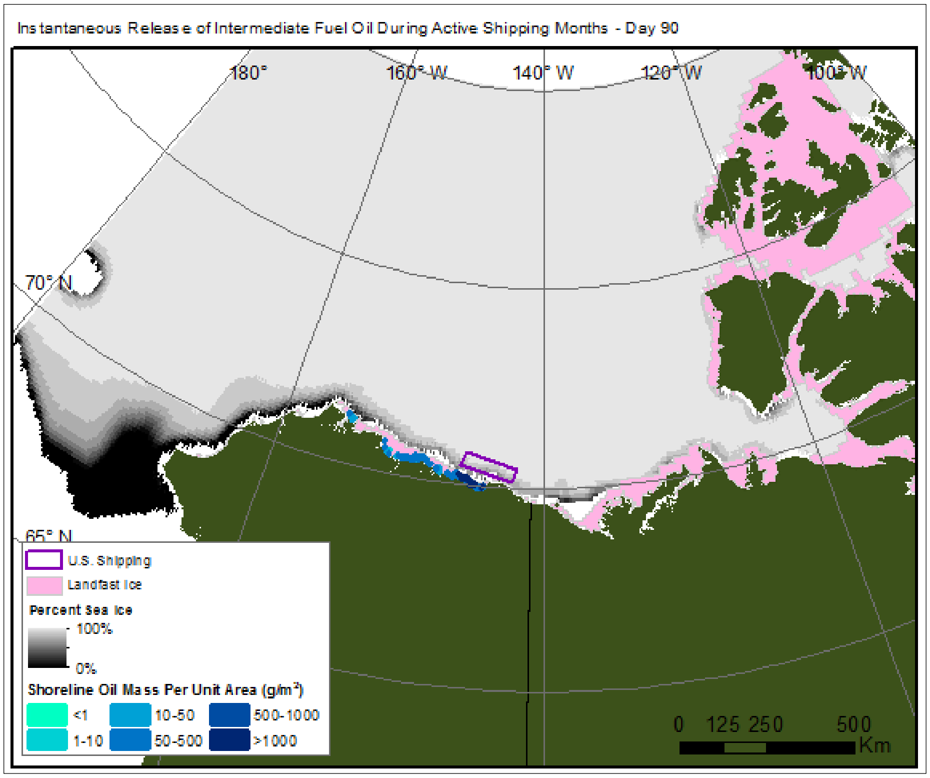

Figure 96. TB_Ship_IFO_US_r23_95shore – Map of overall effects to shorelines as mass of oil deposited on shore per unit of area (g/m^2) (day 90 – December 2008). Pink polygons represent monthly average landfast ice. Grey scale contours represent ice percent coverage for that month from TOPAZ4 model. White indicates areas of no data for ice coverage. Start date: 9/4/2008.

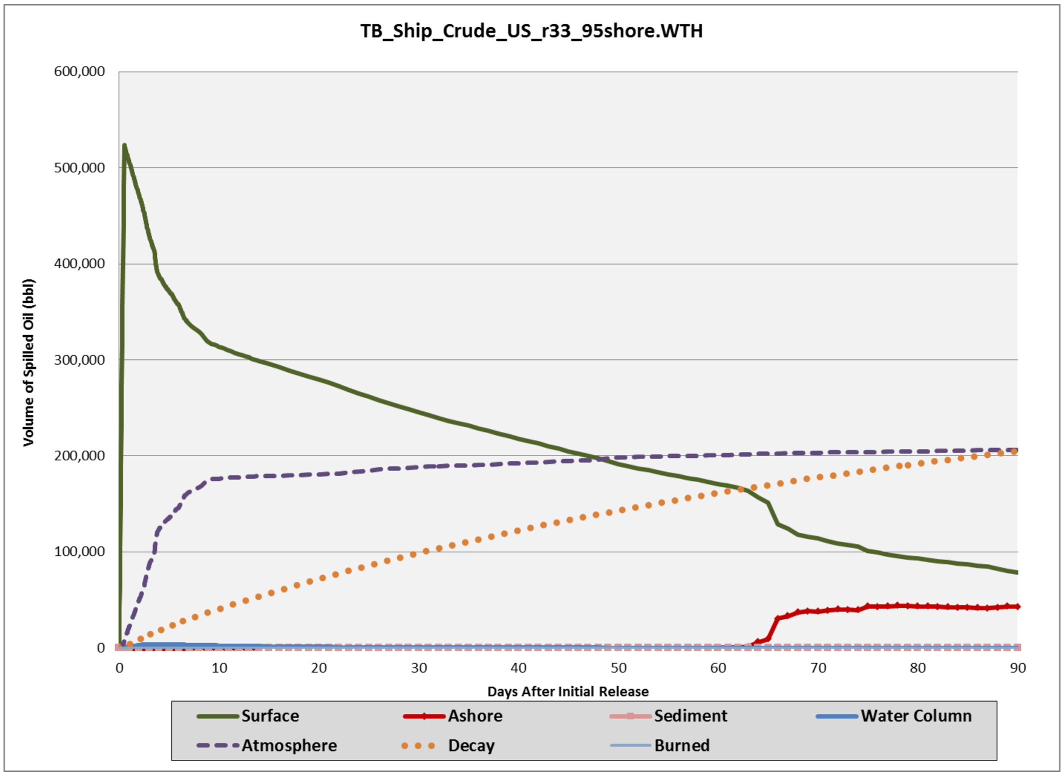

Figure 97. TB_Ship_Crude_US_r33_95shore - Mass balance chart. Start date: 6/12/2008.

Table 17. TB_Ship_Crude_US_r33_95shore – Shoreline length oiled (km) by habitat type, for both shore oiling thresholds. Start date: 6/12/2008.

Shore Type	Shore Length Oiled (km)	
	> 100 micrometers	> 1 micrometer
Seaward Rocky Shore	5.0	5.0
Seaward Gravel Beach	115.9	115.9
Seaward Sand Beach	100.8	100.8
Seaward Fringing Mud Flat	90.7	95.8
Seaward Intertidal Macroalgal Bed	100.8	100.8
Total Shoreline	**413.2**	**418.3**

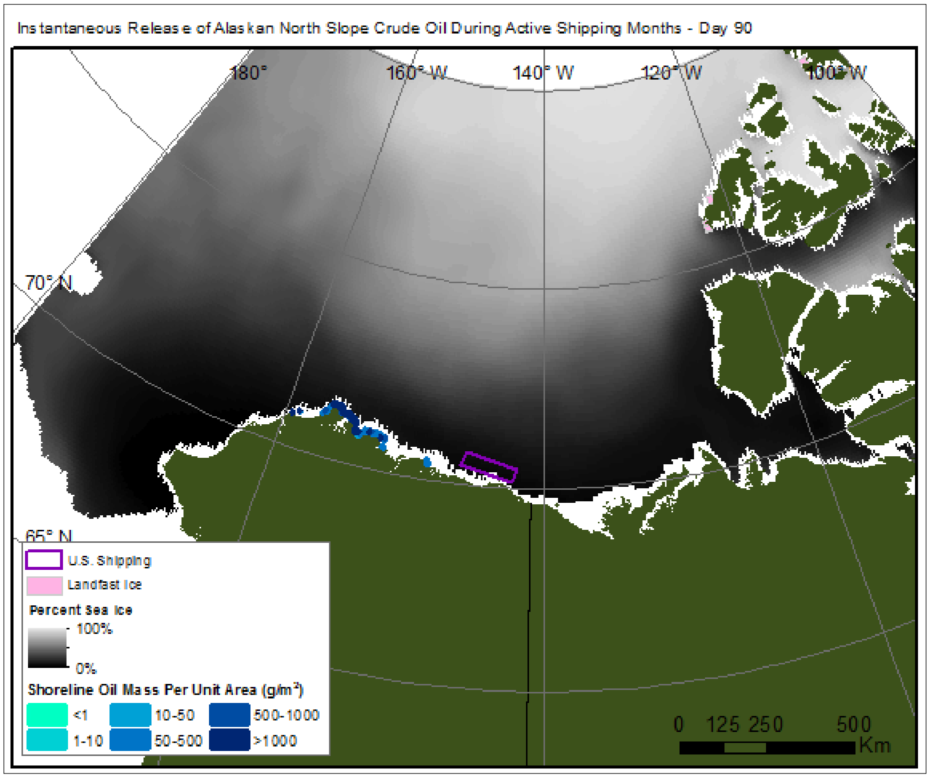

Figure 98. TB_Ship_Crude_US_r33_95shore – Map of overall effects to shorelines as mass of oil deposited on shore per unit of area (g/m^2) (day 90 – September 2008). Pink polygons represent monthly average landfast ice. Grey scale contours represent ice percent coverage for that month from TOPAZ4 model. White indicates areas of no data for ice coverage. Start date: 6/12/2008.

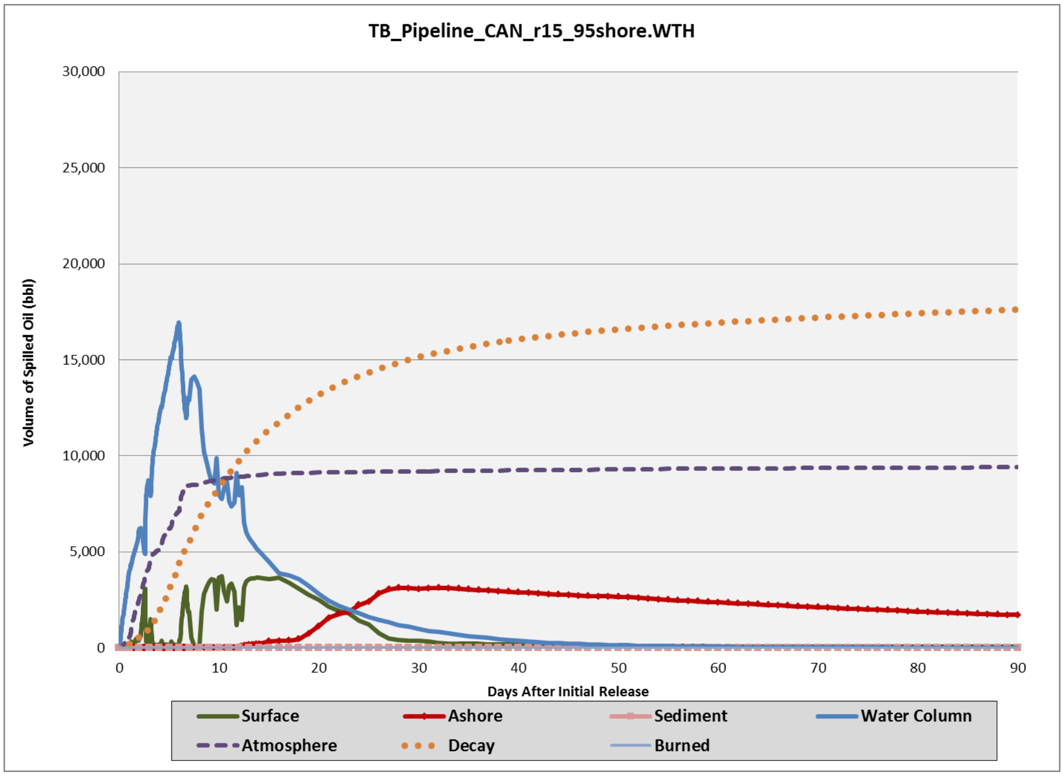

Figure 99. TB_Pipeline_CAN_r15_95shore - Mass balance chart. This spill scenario occurs in open water. Strong wind events entrain floating oil, which subsequently resurface. Start Date: 7/27/2008.

Table 18. TB_Pipeline_CAN_r15_95shore – Shoreline length oiled (km) by habitat type, for both shore oiling thresholds. Start Date: 7/27/2008.

Shore Type	Shore Length Oiled (km)	
	> 100 micrometers	> 1 micrometer
Seaward Rocky Shore	0.0	5.0
Seaward Gravel Beach	181.5	236.9
Seaward Sand Beach	45.4	161.3
Seaward Fringing Mud Flat	45.4	156.3
Seaward Fringing Wetland	0.0	5.0
Seaward Intertidal Macroalgal Bed	35.3	35.3
Shoreline Total	**307.6**	**599.8**

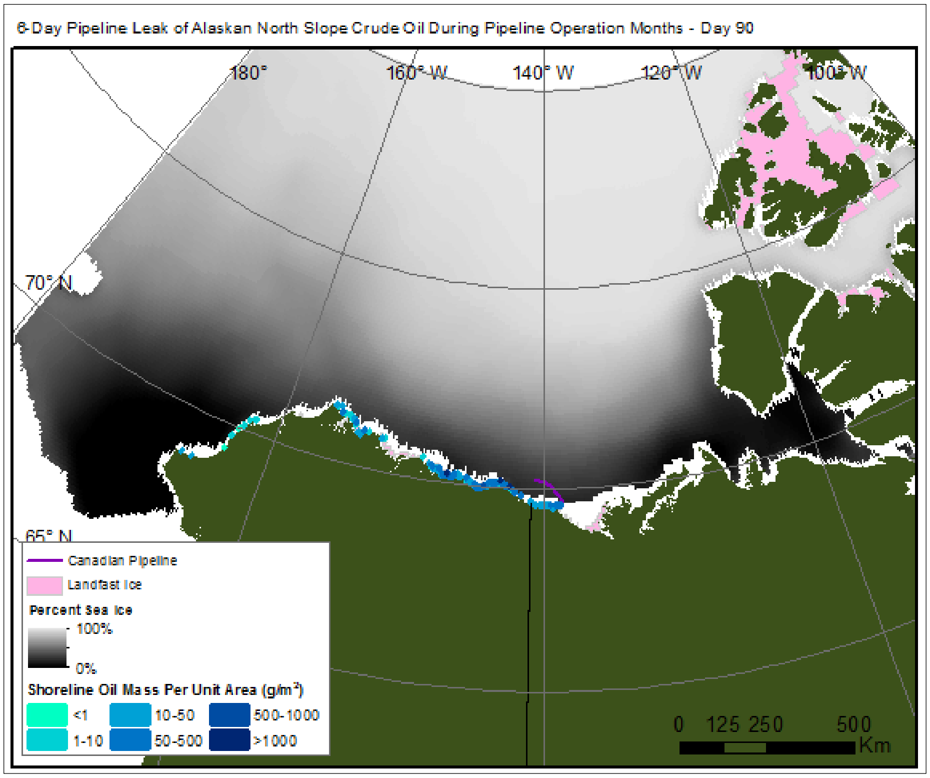

Figure 100. TB_Pipeline_CAN_r15_95shore – Map of overall effects to shorelines as mass of oil deposited on shore per unit of area (g/m^2) (day 90 – October 2008). Pink polygons represent monthly average landfast ice. Grey scale contours represent ice percent coverage for that month from TOPAZ4 model. White indicates areas of no data for ice coverage. Start Date: 7/27/2008.

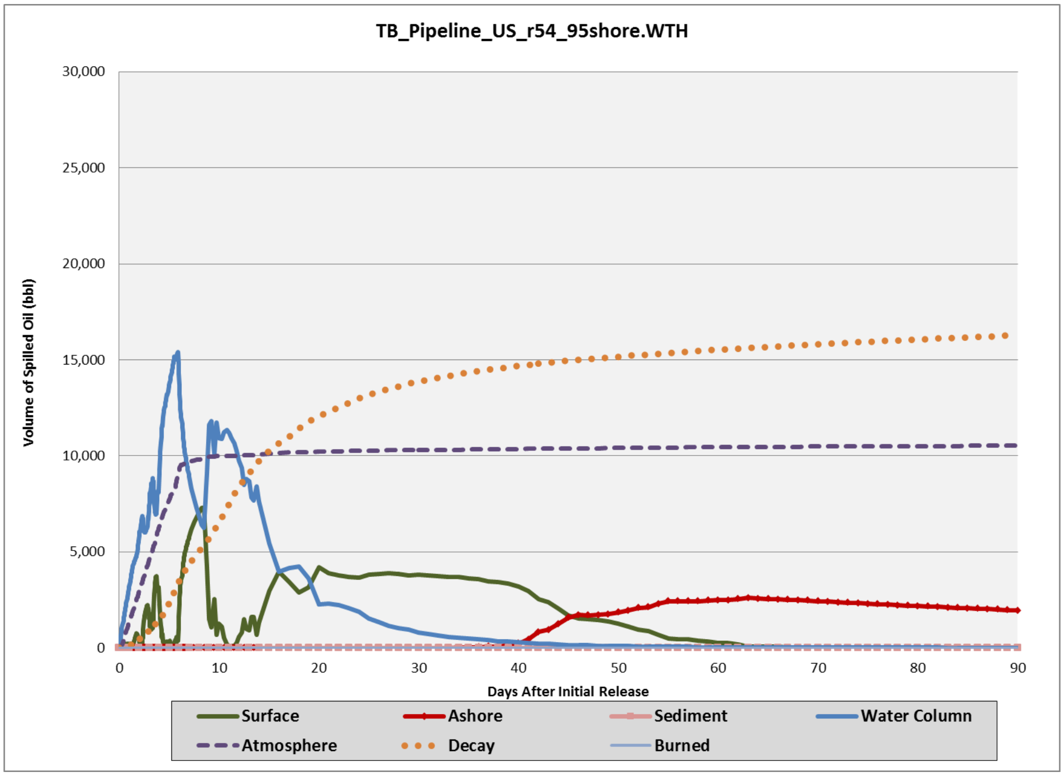

Figure 101. TB_Pipeline_US_r54_95shore - Mass balance chart. This spill occurs in open water. Strong wind events entrain floating oil, which subsequently resurfaces. Eventually, much of the floating oil goes ashore. Start Date: 7/8/2008.

Table 19. TB_Pipeline_US_r54_95shore – Shoreline length oiled (km) by habitat type, for both shore oiling thresholds. Start Date: 7/8/2008.

Shore Type	Shore Length Oiled (km)	
	> 100 micrometers	> 1 micrometer
Seaward Rocky Shore	30.2	45.4
Seaward Gravel Beach	20.2	40.3
Seaward Sand Beach	60.5	136.1
Seaward Fringing Mud Flat	30.2	136.1
Seaward Fringing Wetland	0.0	30.2
Seaward Intertidal Macroalgal Bed	110.9	115.9
Shoreline Total	**252**	**504**

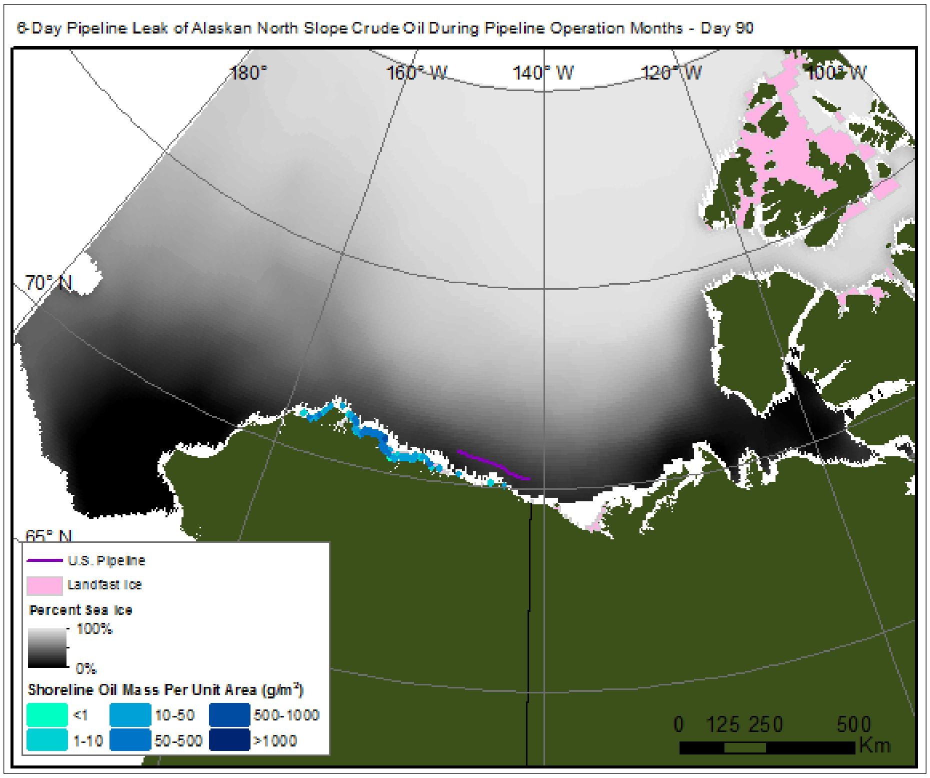

Figure 102. TB_Pipeline_US_r54_95shore – Map of overall effects to shorelines as mass of oil deposited on shore per unit of area (g/m^2) (day 90 – October 2008). Pink polygons represent monthly average landfast ice. Grey scale contours represent ice percent coverage for that month from TOPAZ4 model. White indicates areas of no data for ice coverage. Start Date: 7/8/2008.

95th Percentile Water Column Contamination

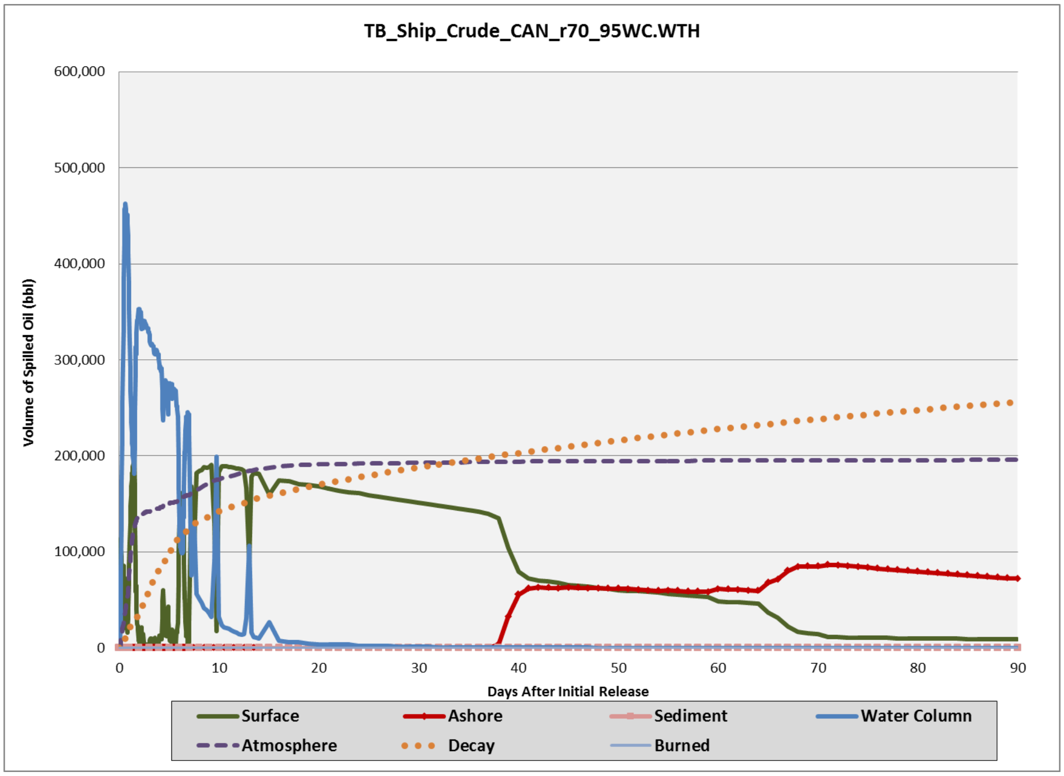

Figure 103. TB_Ship_Crude_CAN_r70_95WC - Mass balance chart. Wind events entrain the floating oil, which subsequently resurfaces in calm periods. Start Date: 7/5/2012.

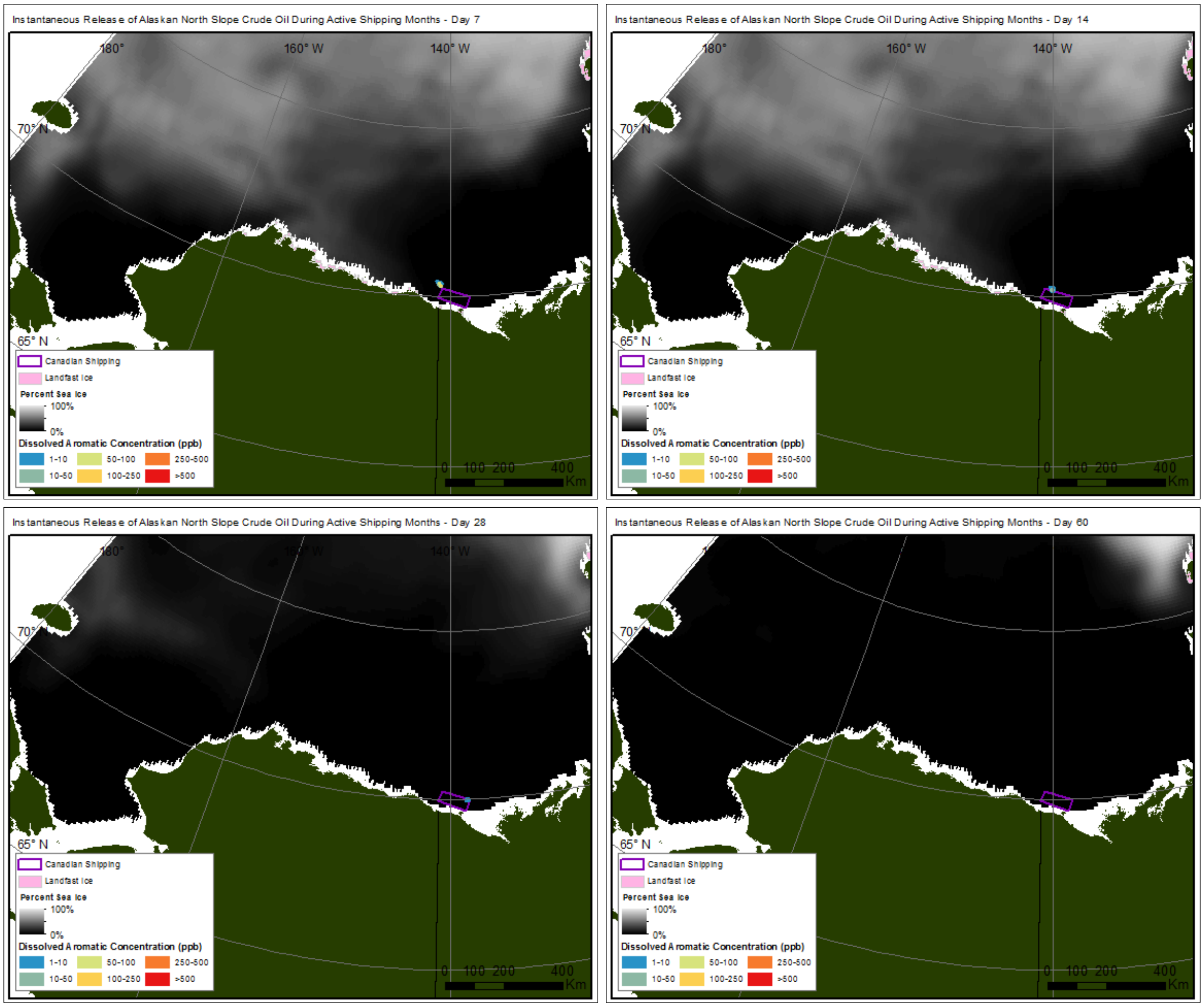

Figure 104. TB_Ship_Crude_CAN_r70_95WC – Time series maps of spill dissolved aromatics ≥ 1 ppb (day 7, 14, 28, 60, no aromatics in later time steps; July – September 2012). Pink polygons represent monthly average landfast ice. Grey scale contours represent ice percent coverage for that month from TOPAZ4 model. White indicates areas of no data for ice coverage. Start Date: 7/5/2012.

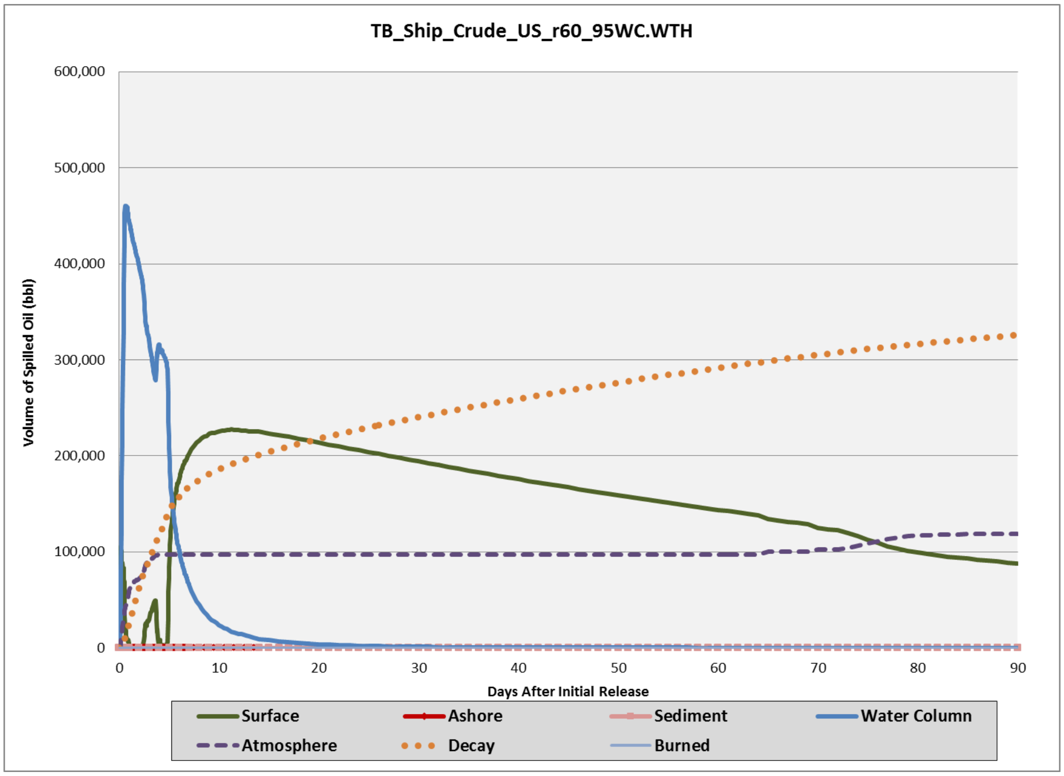

Figure 105. TB_Ship_Crude_US_r60_95WC - Mass balance chart. The spilled oil becomes trapped in ice in this model run. Start Date: 4/4/2008.

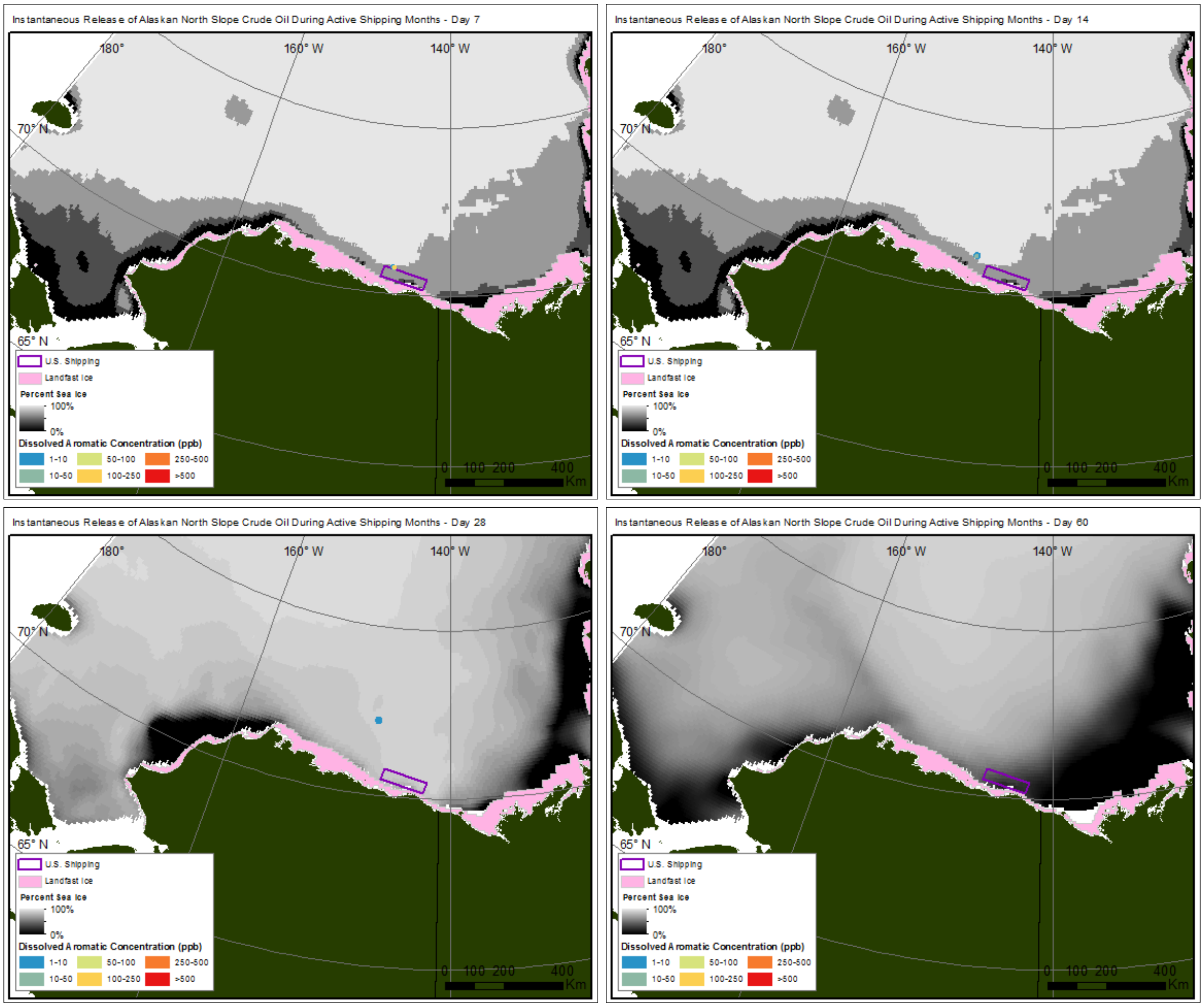

Figure 106. TB_Ship_Crude_US_r60_95WC – Time series maps of spill dissolved aromatics ≥ 1 ppb (day 7, 14, 28, 60, no aromatics in later time steps; April – June 2008). Pink polygons represent monthly average landfast ice. Grey scale contours represent ice percent coverage for that month from TOPAZ4 model. White indicates areas of no data for ice coverage. Start Date: 4/4/2008.

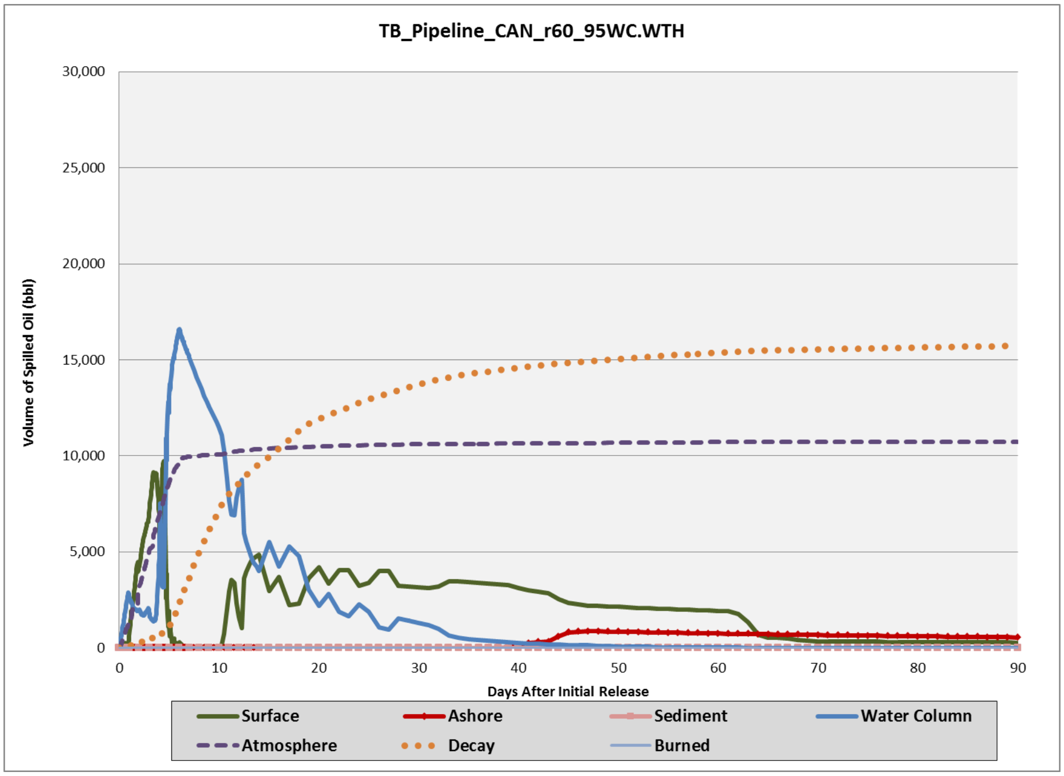

Figure 107. TB_Pipeline_CAN_r60_95WC - Mass balance chart. This scenario in open water shows the effects of strong wind events entraining the floating oil. Start Date: 8/29/2010.

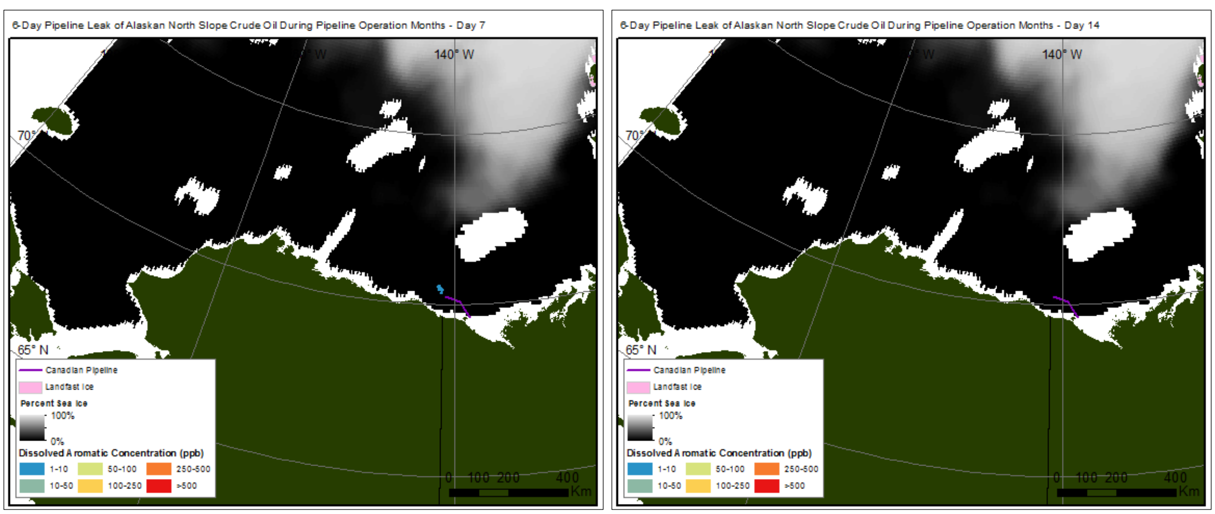

Figure 108. TB_Pipeline_CAN_r60_95WC – Time series maps of spill dissolved aromatics ≥ 1 ppb (day 7, 14, no aromatics in later time steps; September 2010). Pink polygons represent monthly average landfast ice. Grey scale contours represent ice percent coverage for that month from TOPAZ4 model. White indicates areas of no data for ice coverage. Start Date: 8/29/2010.

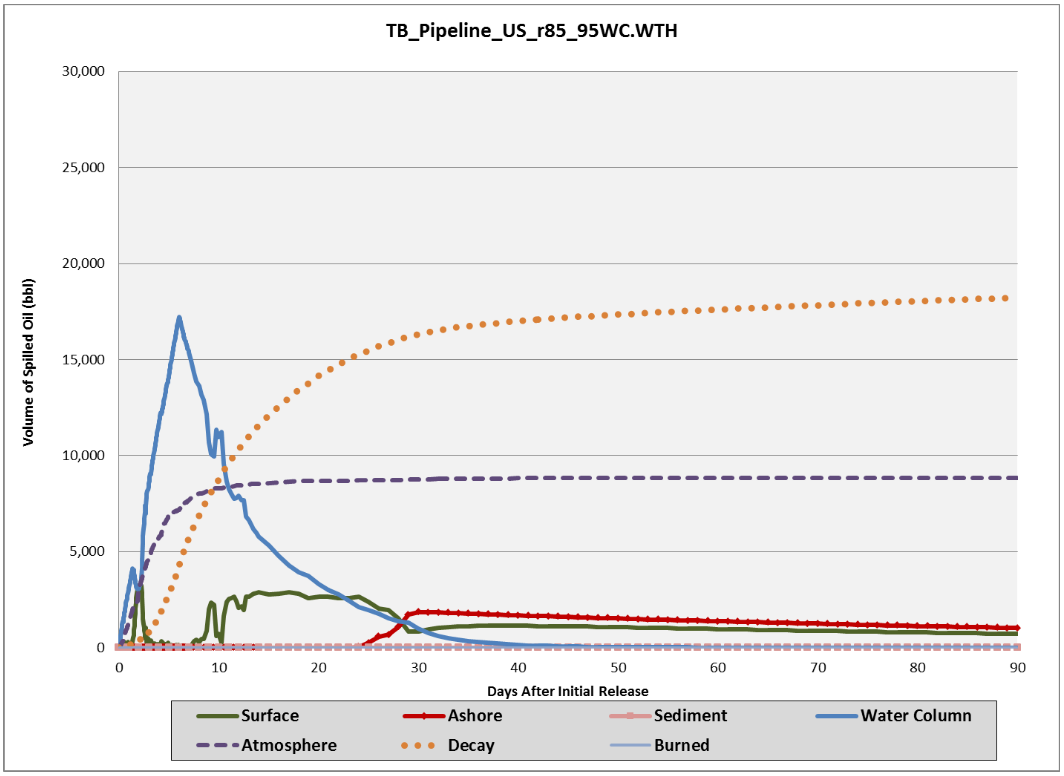

Figure 109. TB_Pipeline_US_r85_95WC - Mass balance chart. Start Date: 9/12/2008.

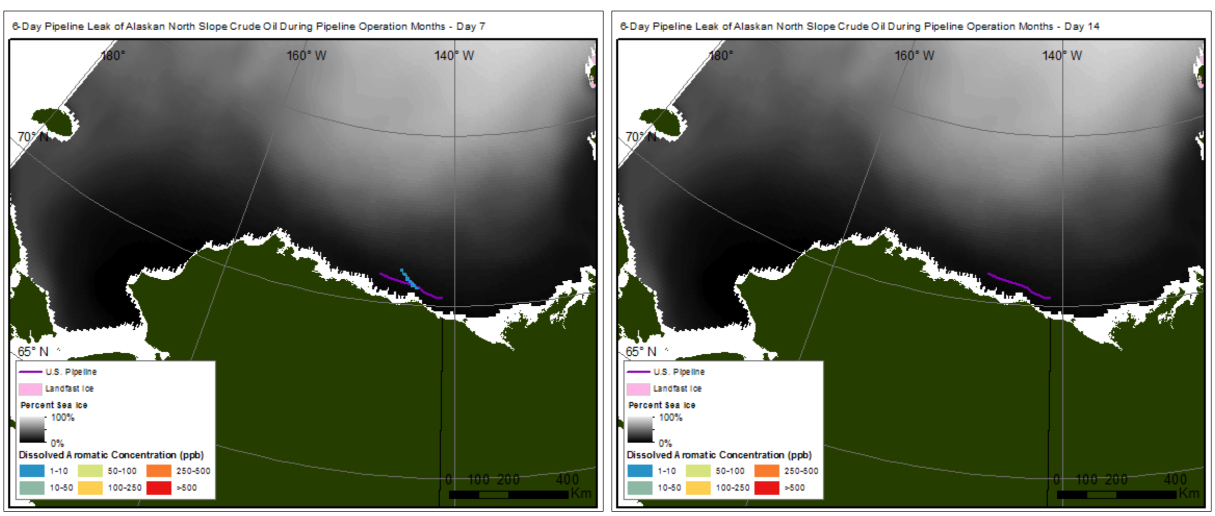

Figure 110. TB_Pipeline_US_r85_95WC – Time series maps of spill dissolved aromatics ≥ 1 ppb (day 7, 14, no aromatics in later time steps; September 2008). Pink polygons represent monthly average landfast ice. Grey scale contours represent ice percent coverage for that month from TOPAZ4 model. White indicates areas of no data for ice coverage. Start Date: 9/12/2008.

7.3 Shallow Blowout Analysis

This section contains the stochastic analysis and individual trajectory results for the Shallow Blowout Analysis (Section 6.4). There were a total of four stochastic scenarios and fourteen individual trajectories run for this analysis. Table Table 20 provides the scenario names. Please see Appendix D for full scenario list and naming conventions.

Table 20. List of scenario names and types for the Shallow Blowout Analysis.

Scenario Name	Scenario Type	Start Date/Range
ShalWCD_60rel_noresp_early	Stochastic	June-July
ShalWCD_90rel_noresp_late	Stochastic	August-October
ShalMMPD_30rel_noresp_early	Stochastic	June-July
ShalMMPD_60rel_noresp_late	Stochastic	August-October
ShalWCD_60rel_noresp_early_r32_95surf	Individual	6/3/2009
ShalWCD_60rel_surfresp_early_r32_95surface	Individual	6/3/2009
ShalWCD_90rel_noresp_late_r72_95surf	Individual	8/6/2012
ShalWCD_90rel_surfresp_late_r72_95surf	Individual	8/6/2012
ShalMMPD_30rel_noresp_early_r31_95surf	Individual	6/23/2009
ShalMMPD_60rel_noresp_late_r13_95surf	Individual	8/14/2010
ShalWCD_60rel_noresp_early_r98_95shore	Individual	6/18/2008
ShalWCD_60rel_surfresp_early_r98_95shore	Individual	6/18/2008
ShalWCD_90rel_noresp_late_r8_95shore	Individual	8/8/2012
ShalWCD_90rel_surfresp_late_r8_95shore	Individual	8/8/2012
ShalMMPD_30rel_noresp_early_r20_95shore	Individual	7/17/2008
ShalMMPD_60rel_noresp_late_r50_95shore	Individual	8/19/2008
ShalWCD_60rel_noresp_early_r81_95WC	Individual	7/22/2010
ShalWCD_90rel_noresp_late_r30_95WC	Individual	10/26/2008

7.3.1 Stochastic Analysis Results

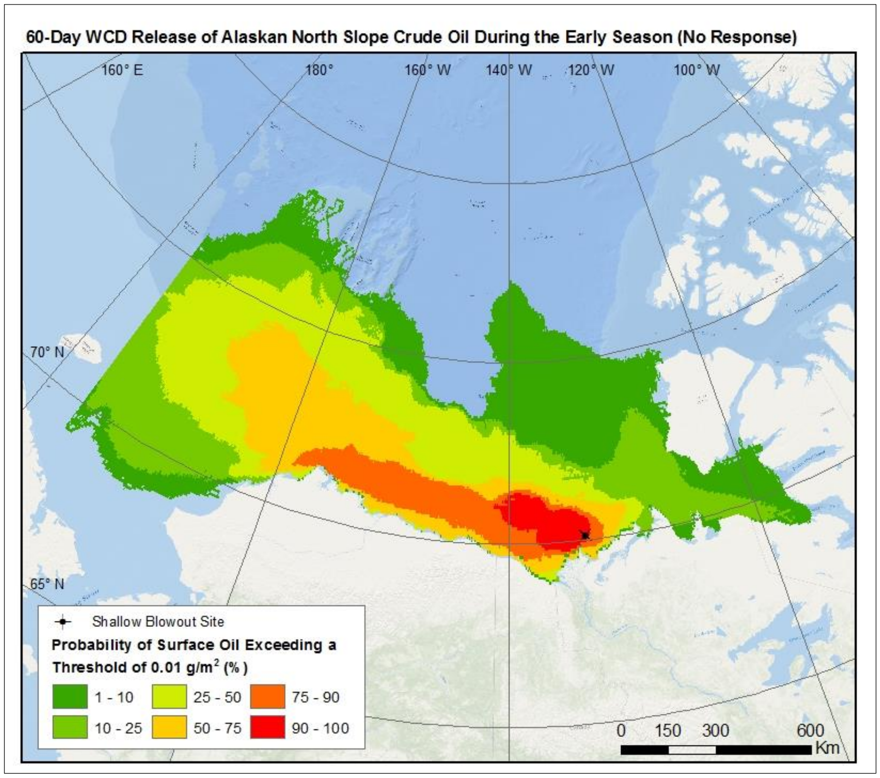

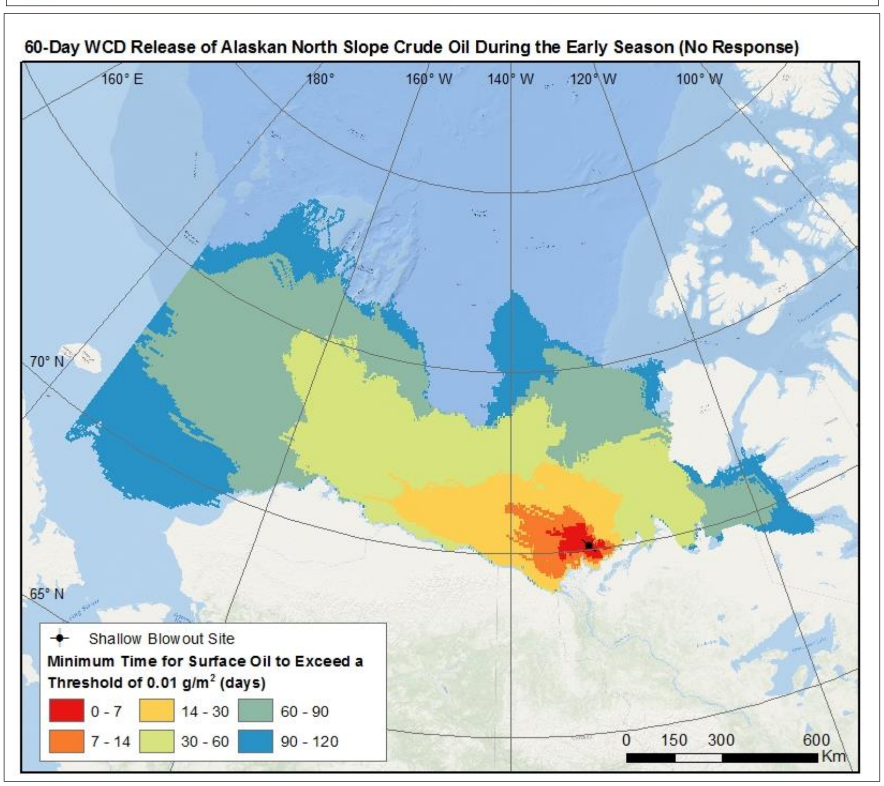

Figure 111. ShalWCD_60rel_noresp_early - Water surface oiling probabilities and minimum travel times for floating oil ≥0.01 g/m^2.

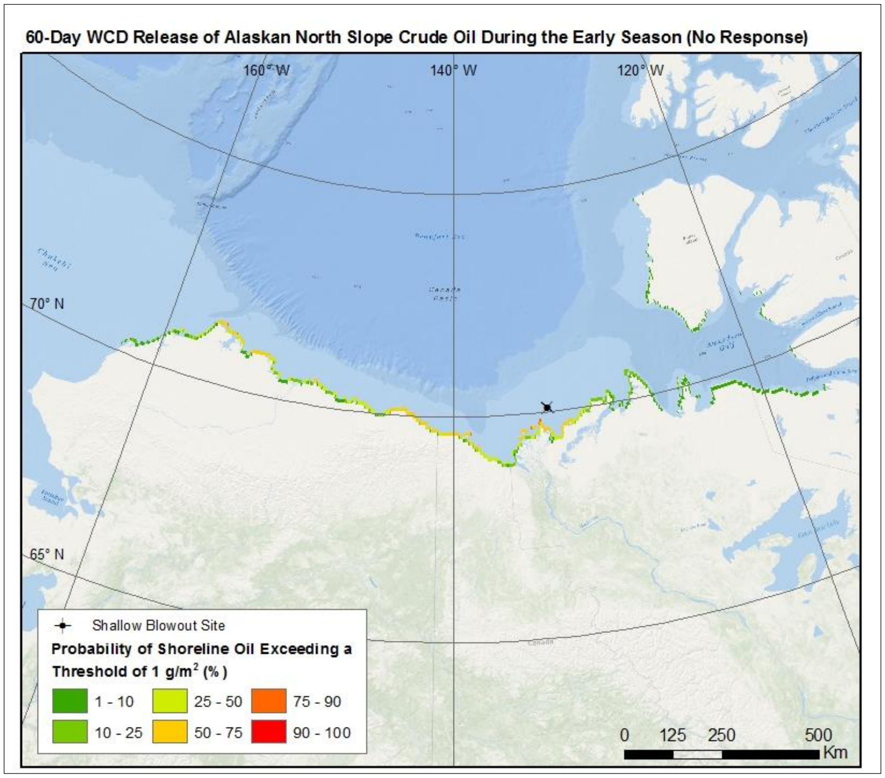

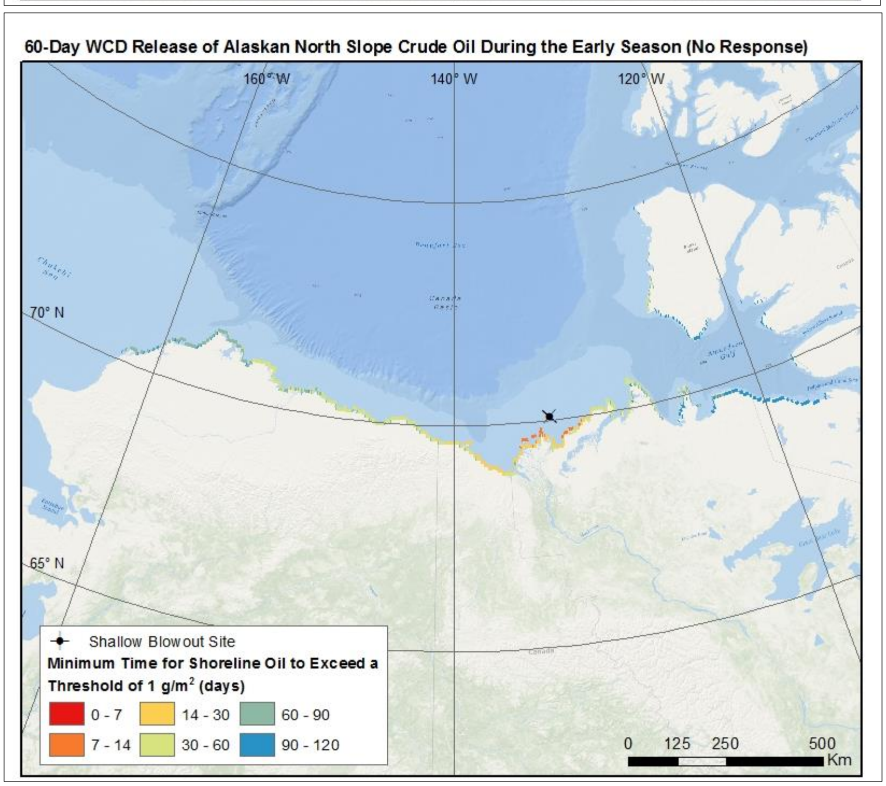

Figure 112. ShalWCD_60rel_noresp_early - Shoreline oiling probabilities and minimum travel times for shoreline oil ≥1 g/m².

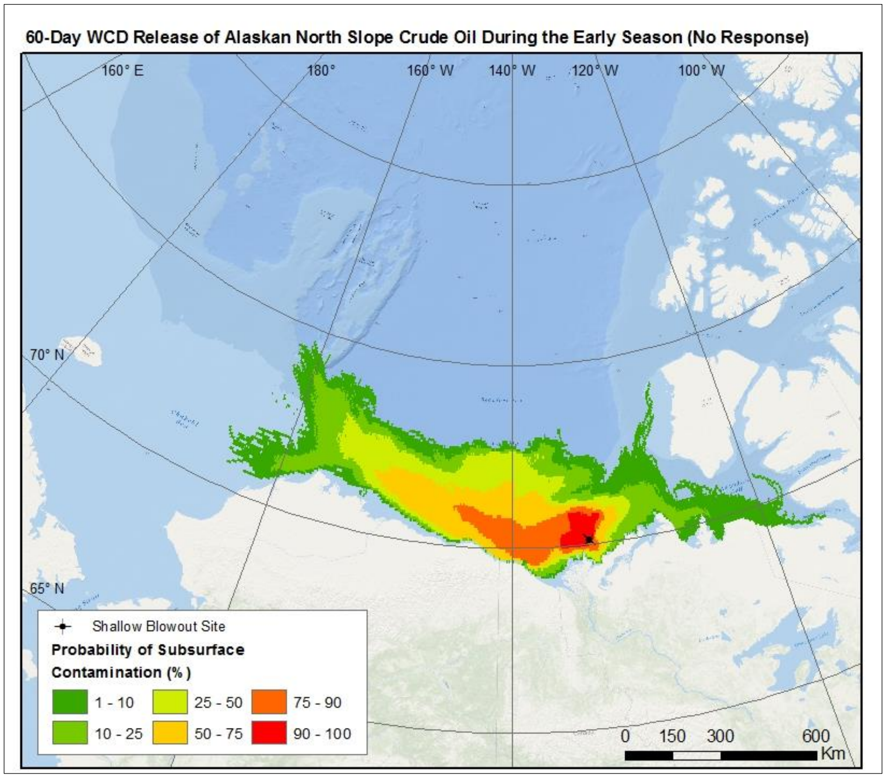

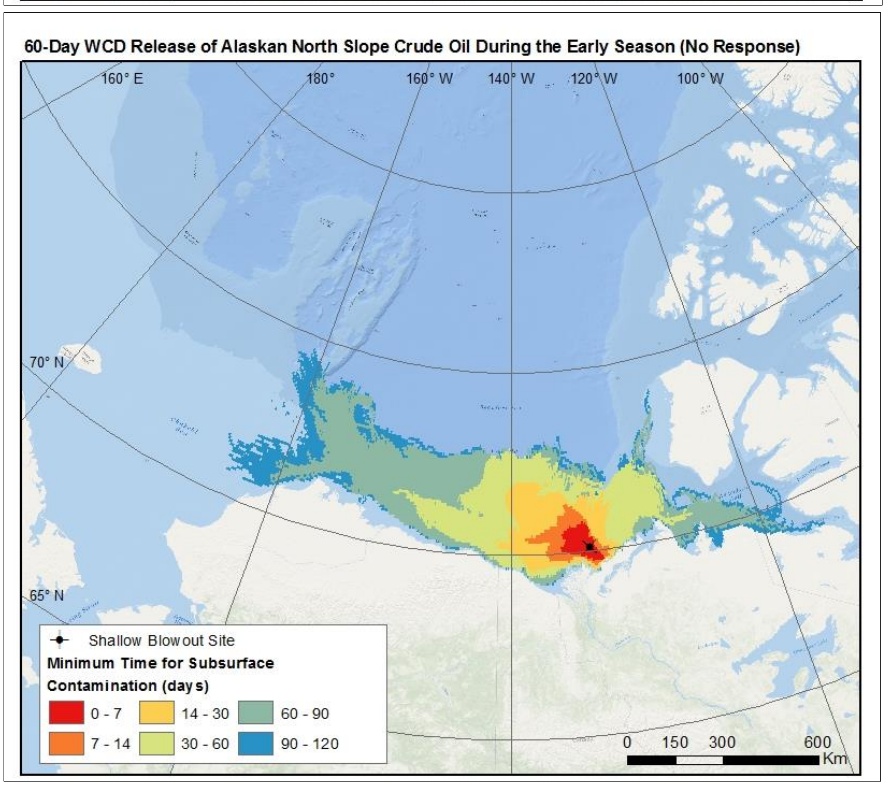

Figure 113. ShalWCD_60rel_noresp_early - Subsurface contamination probabilities and minimum travel times for total oil in the water column.

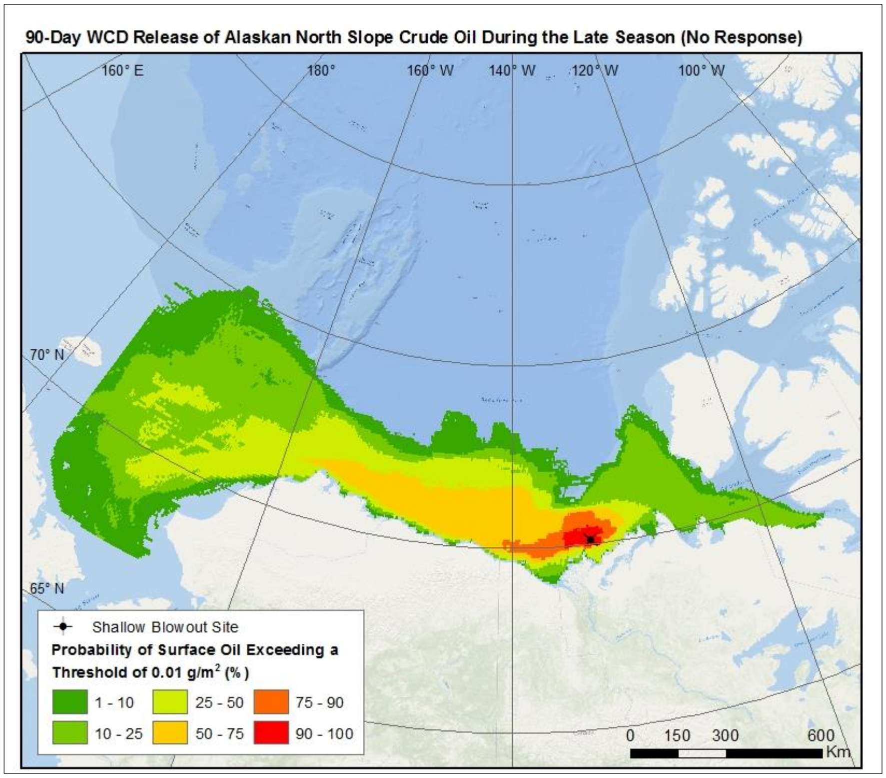

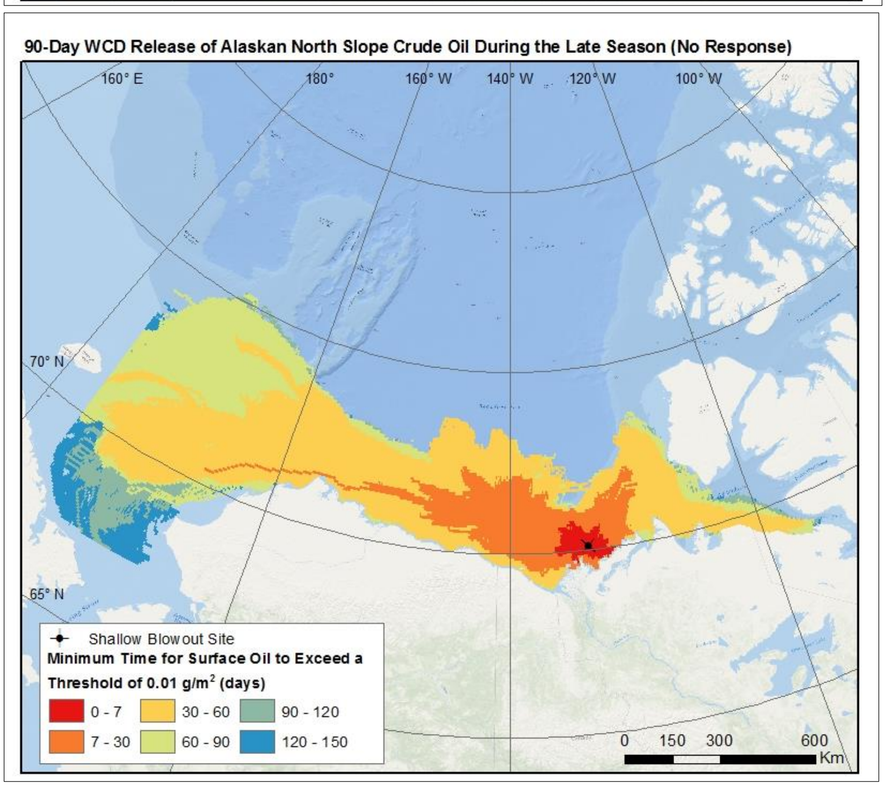

Figure 114. ShalWCD_90rel_noresp_late - Water surface oiling probabilities and minimum travel times for floating oil ≥0.01 g/m^2.

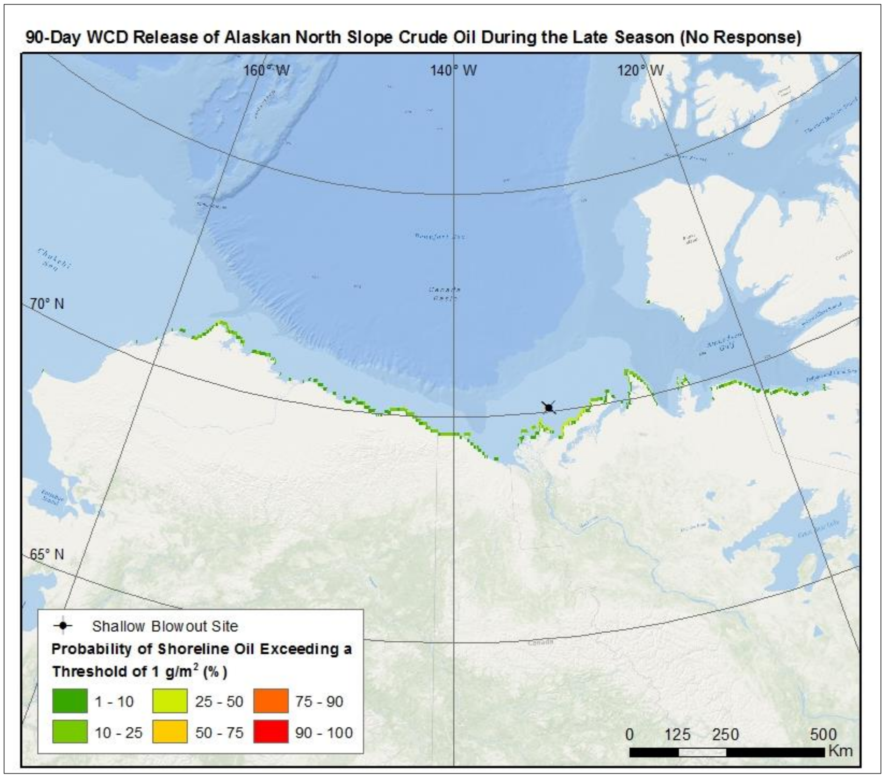

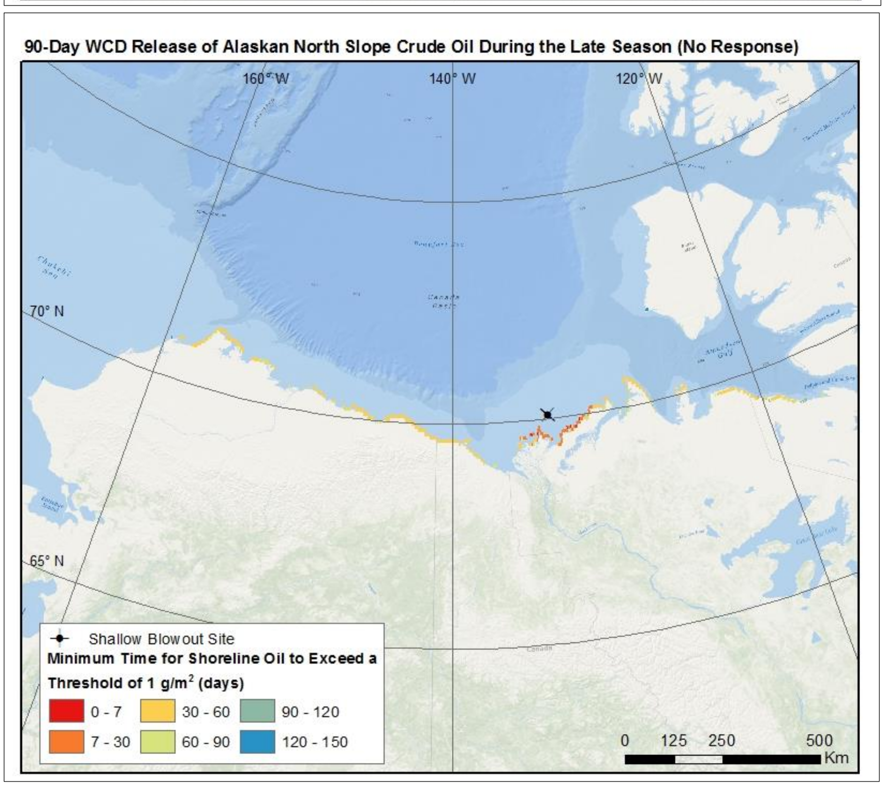

Figure 115. ShalWCD_90rel_noresp_late - Shoreline oiling probabilities and minimum travel times for shoreline oil ≥1 g/m^2.

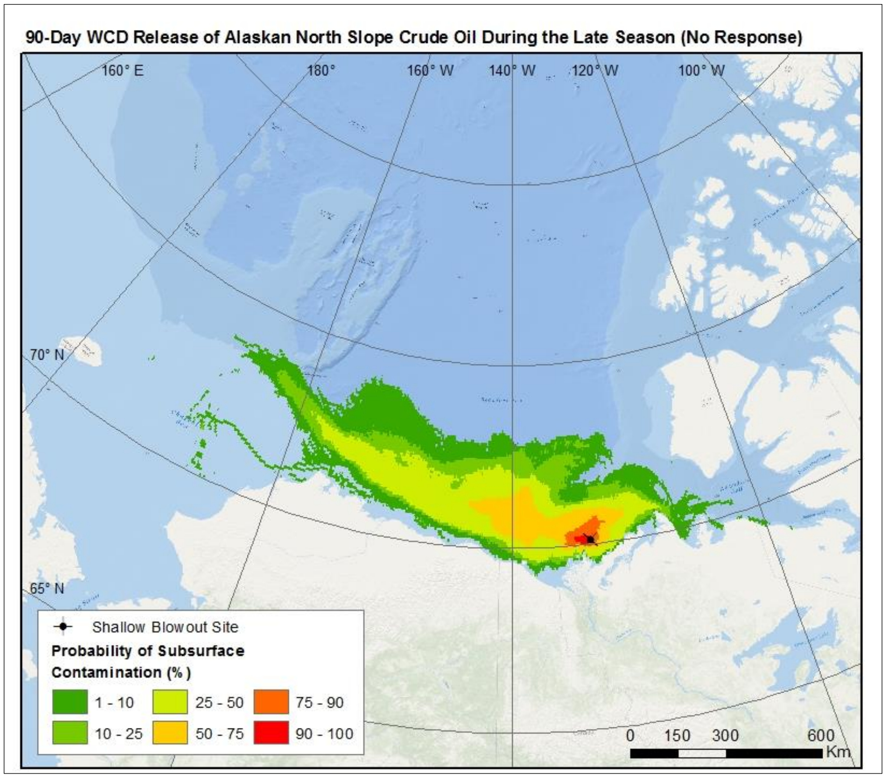

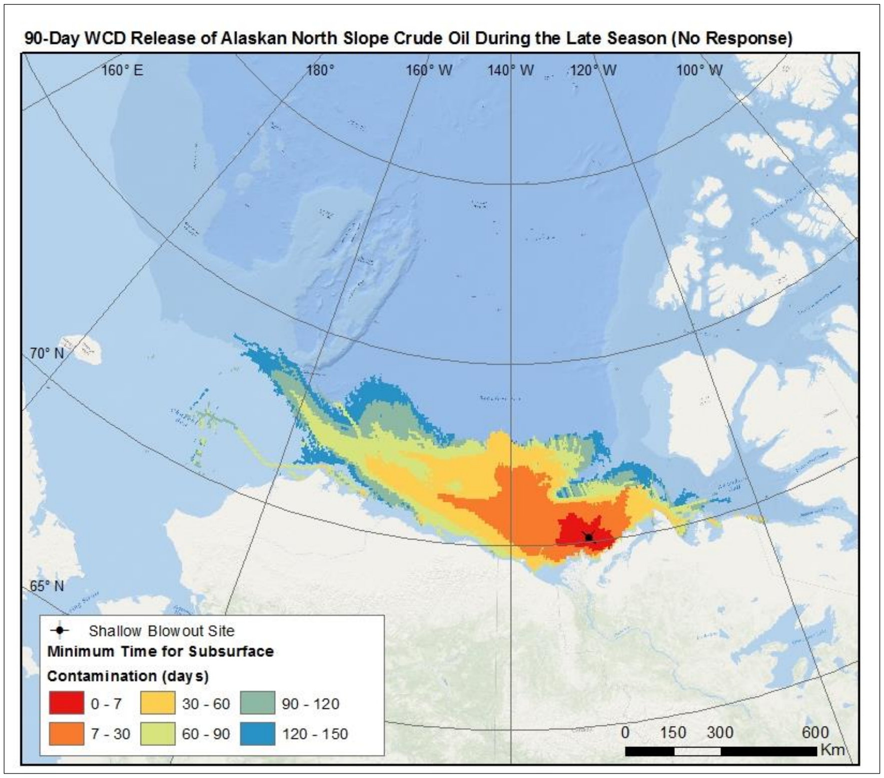

Figure 116. ShalWCD_90rel_noresp_late - Subsurface contamination probabilities and minimum travel times for total oil in the water column.

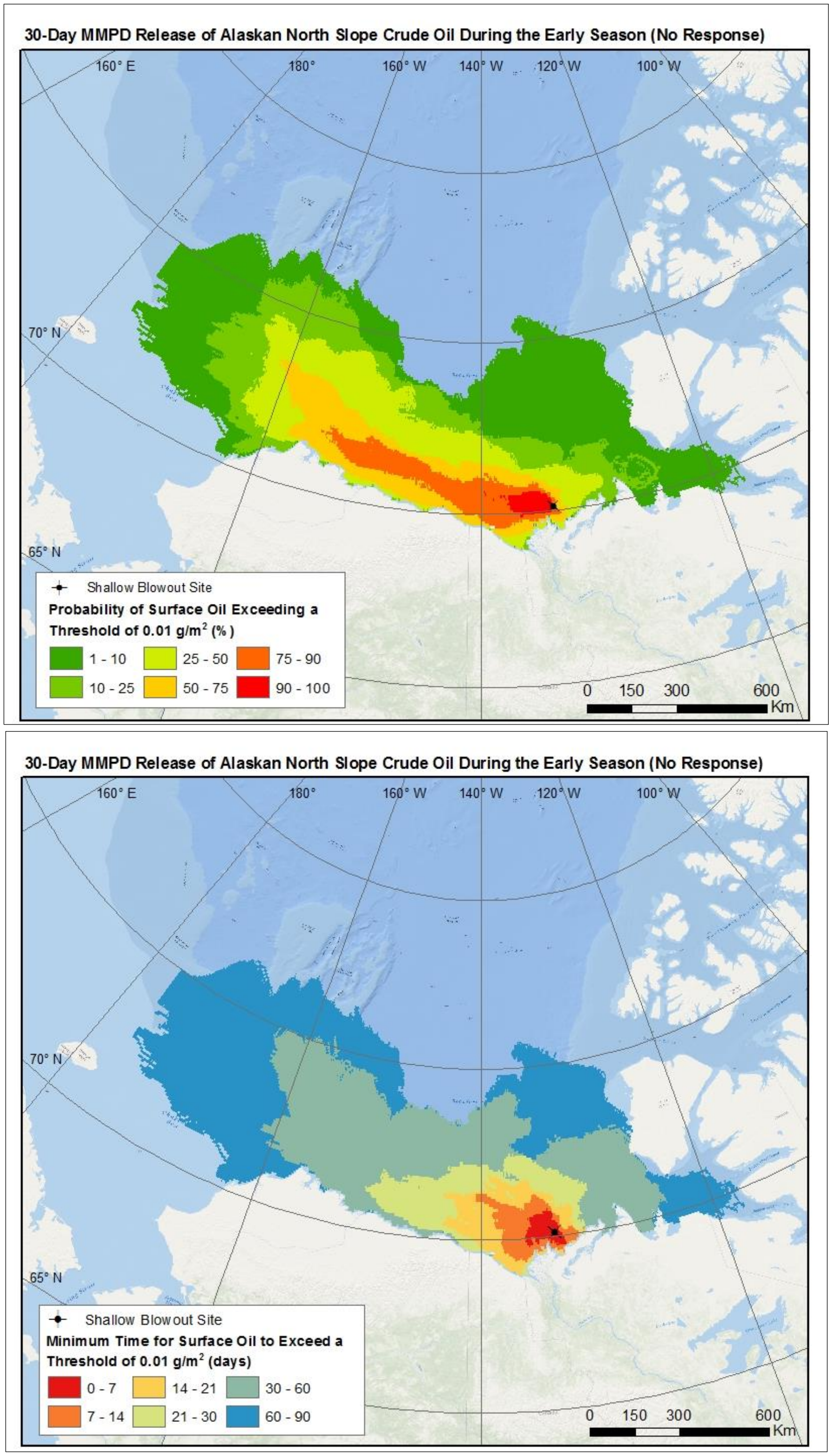

Figure 117. ShalMMPD_30rel_noresp_early - Water surface oiling probabilities and minimum travel times for floating oil ≥0.01 g/m^2.

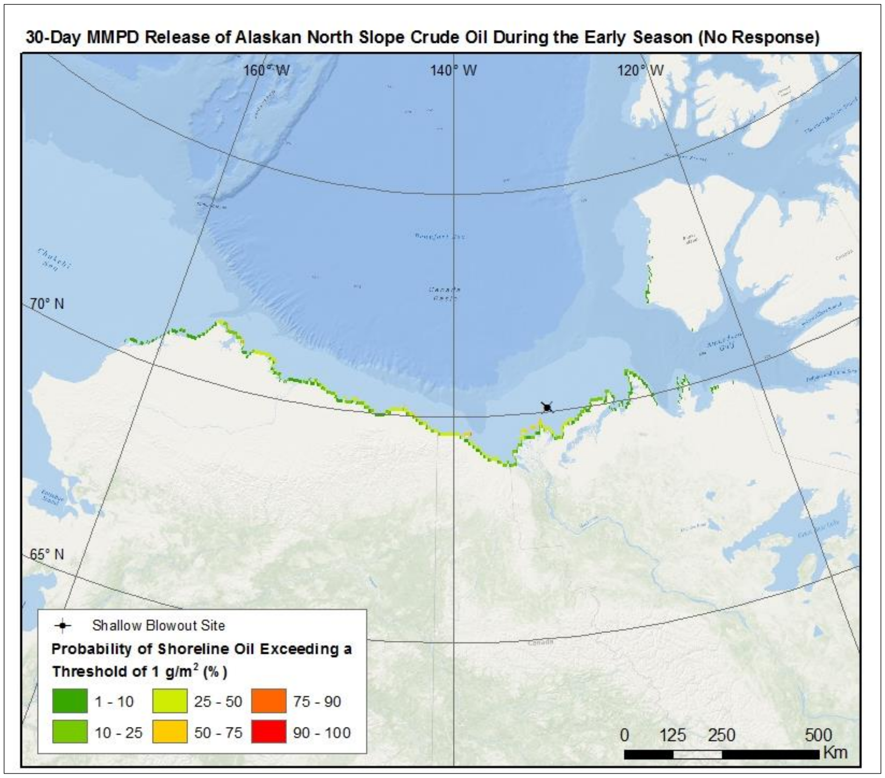

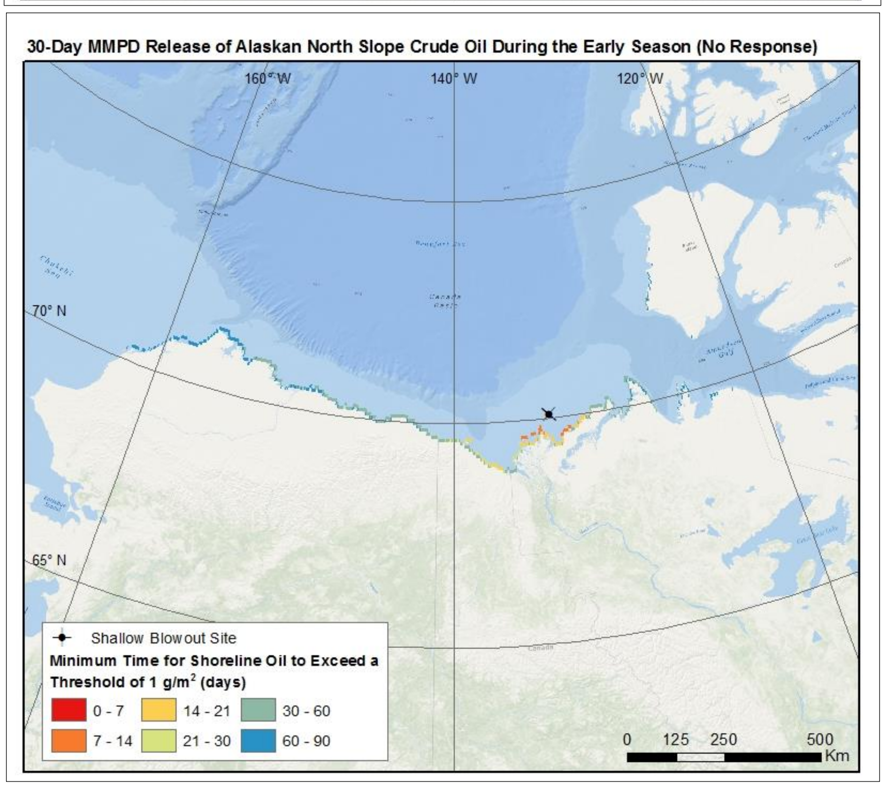

Figure 118. ShalMMPD_30rel_noresp_early - Shoreline oiling probabilities and minimum travel times for shoreline oil ≥1 g/m^2.

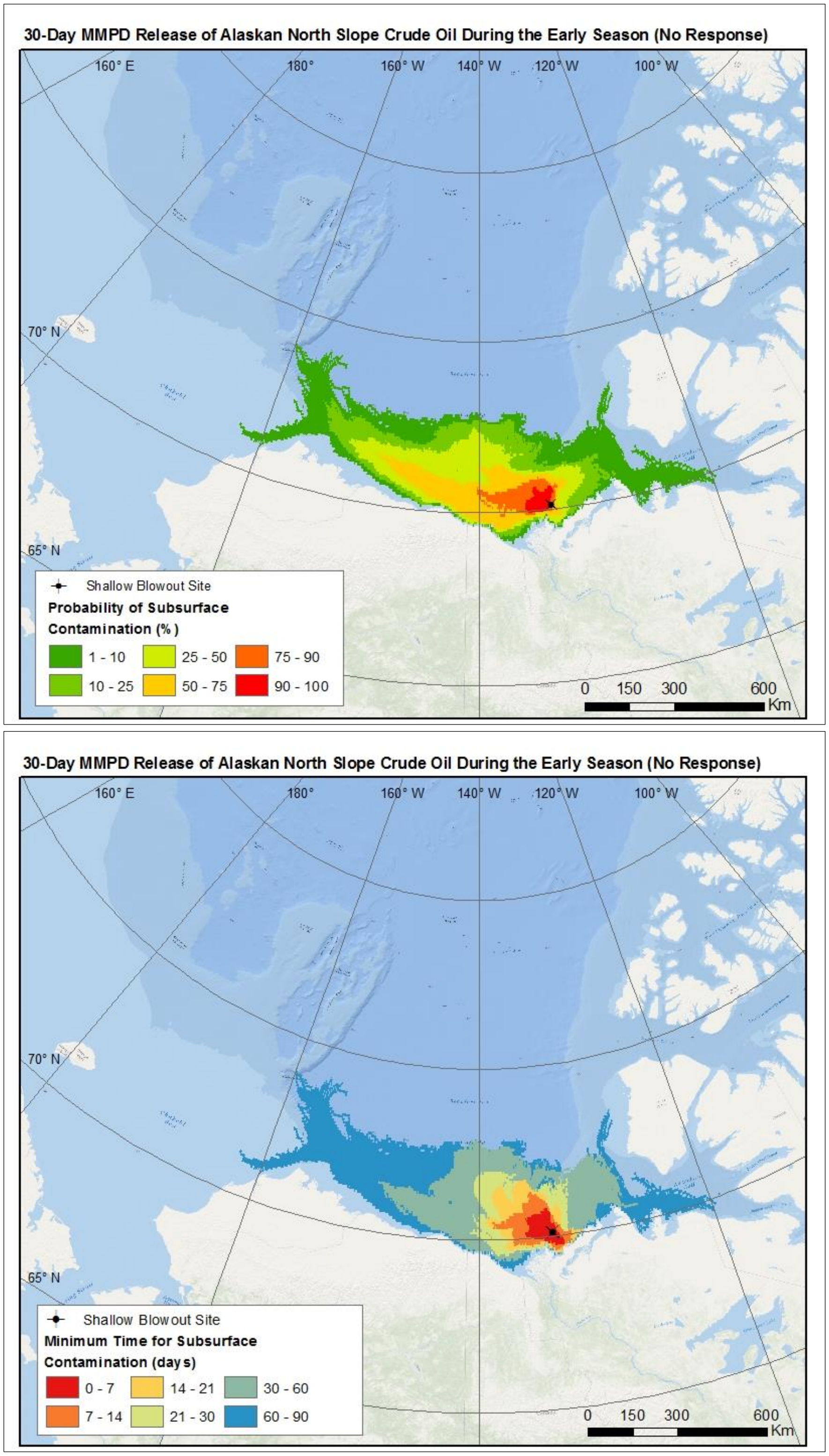

Figure 119. ShalMMPD_30rel_noresp_early - Subsurface contamination probabilities and minimum travel times for total oil in the water column.

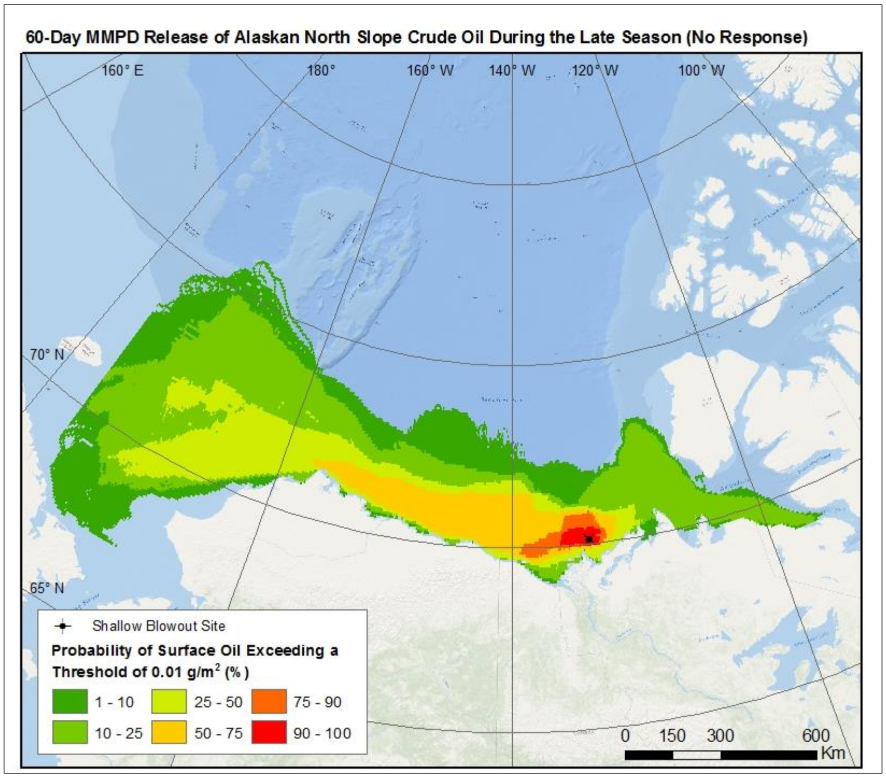

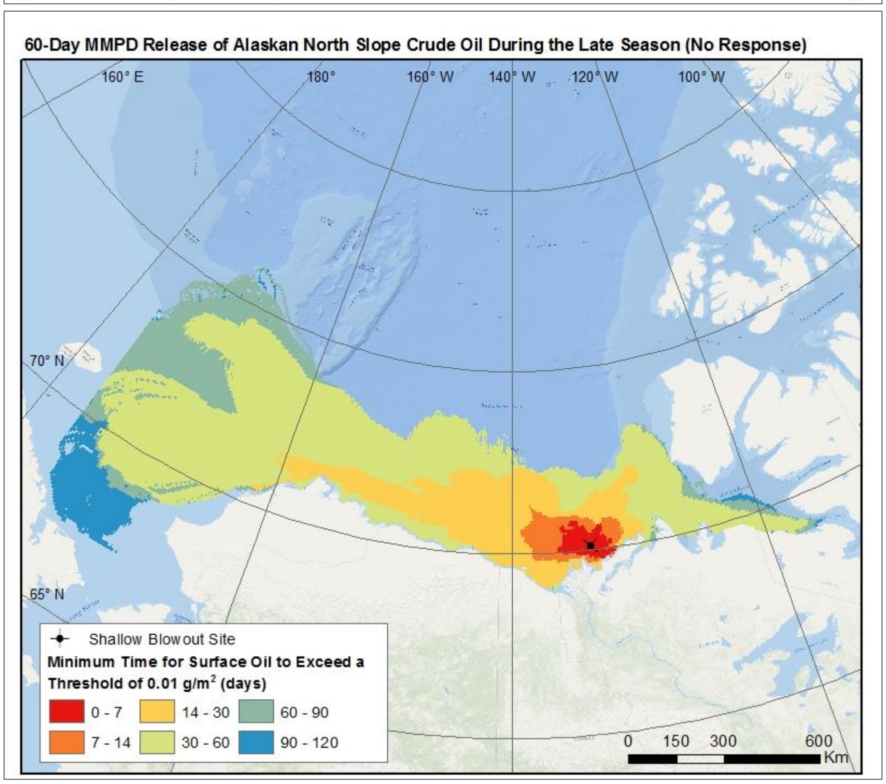

Figure 120. ShalMMPD_60rel_noresp_late - Water surface oiling probabilities and minimum travel times for floating oil ≥0.01 g/m^2.

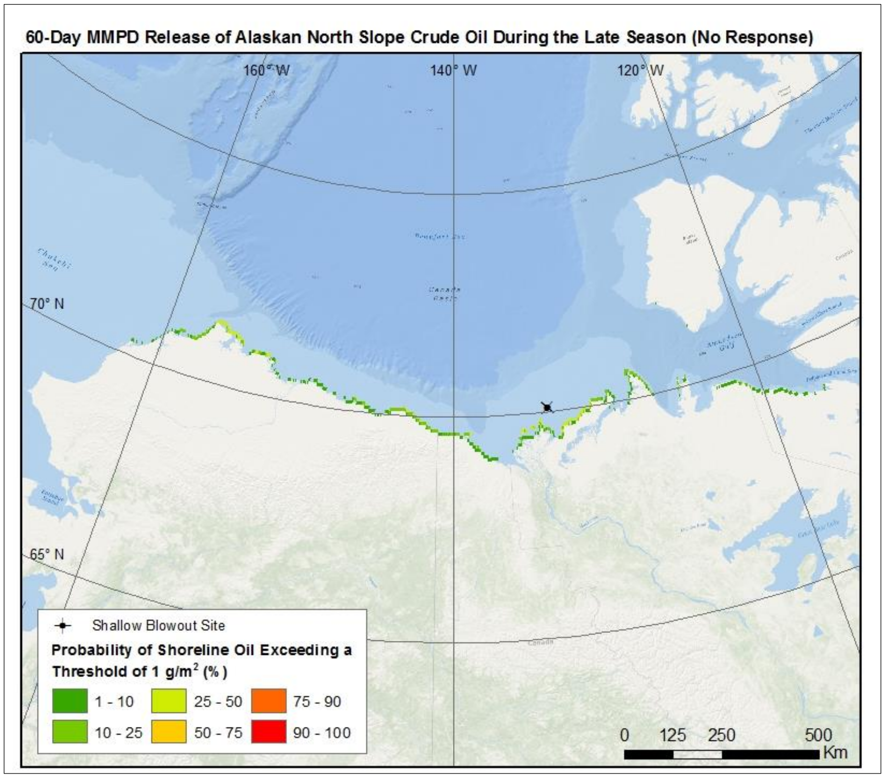

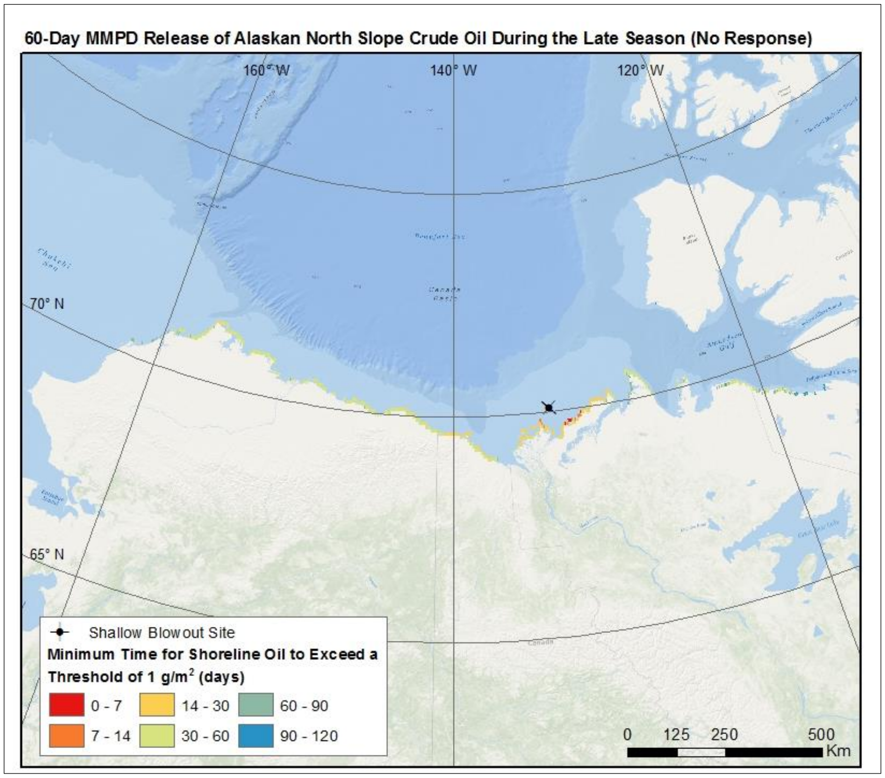

Figure 121. ShalMMPD_60rel_noresp_late - Shoreline oiling probabilities and minimum travel times for shoreline oil ≥1 g/m^2.

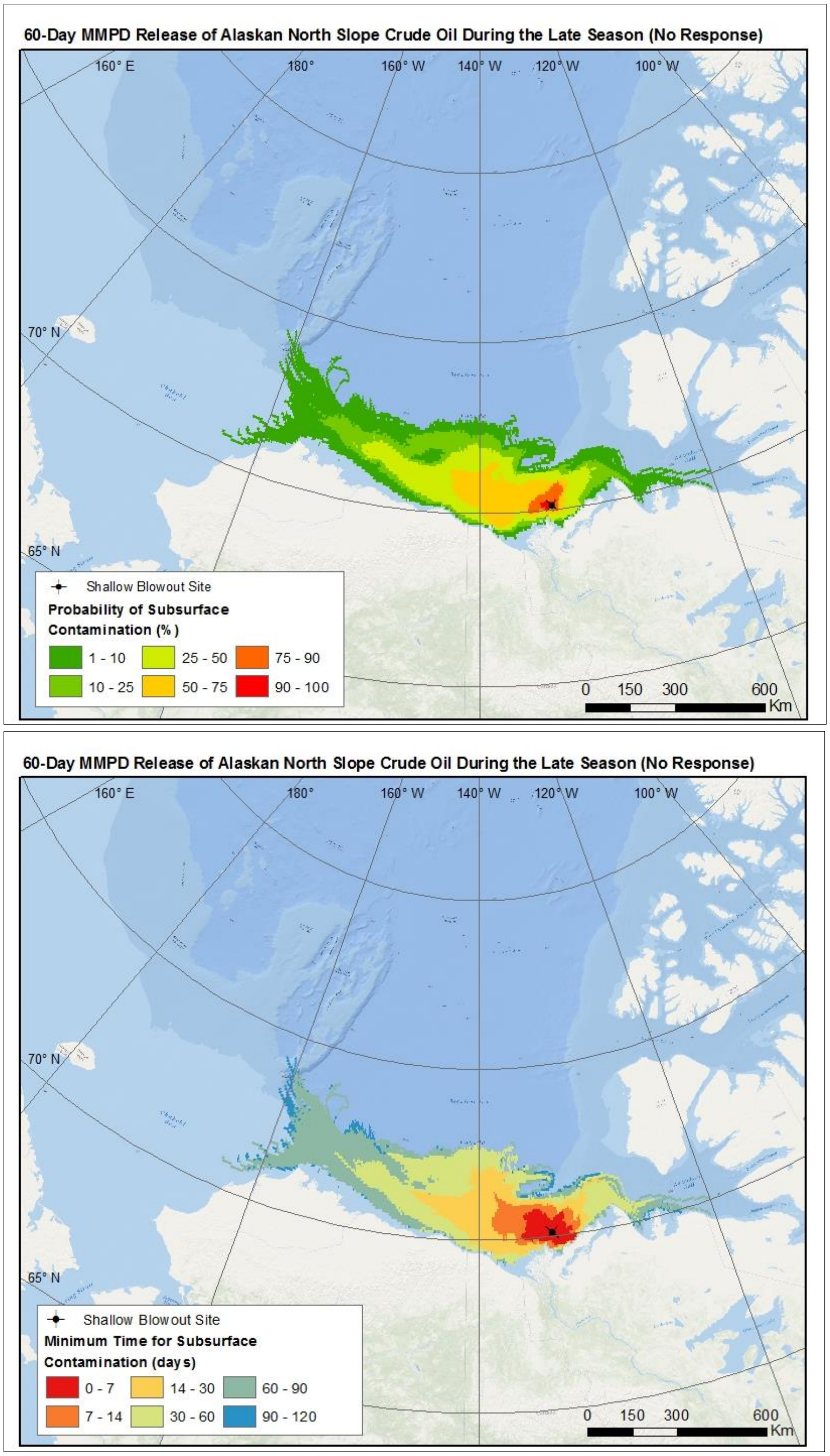

Figure 122. ShalMMPD_60rel_noresp_late - Subsurface contamination probabilities and minimum travel times for total oil in the water column.

7.3.2 Individual Trajectory Model Results

Note: Only 95th percentile surface and shoreline oiling runs were evaluated for the MMPD Shallow Blowout scenarios. Surface response measures were *only* simulated for the 95th percentile individual trajectories for surface and shoreline oiling from the base case or parent stochastic scenario (no response).

95th Percentile Surface Oiling

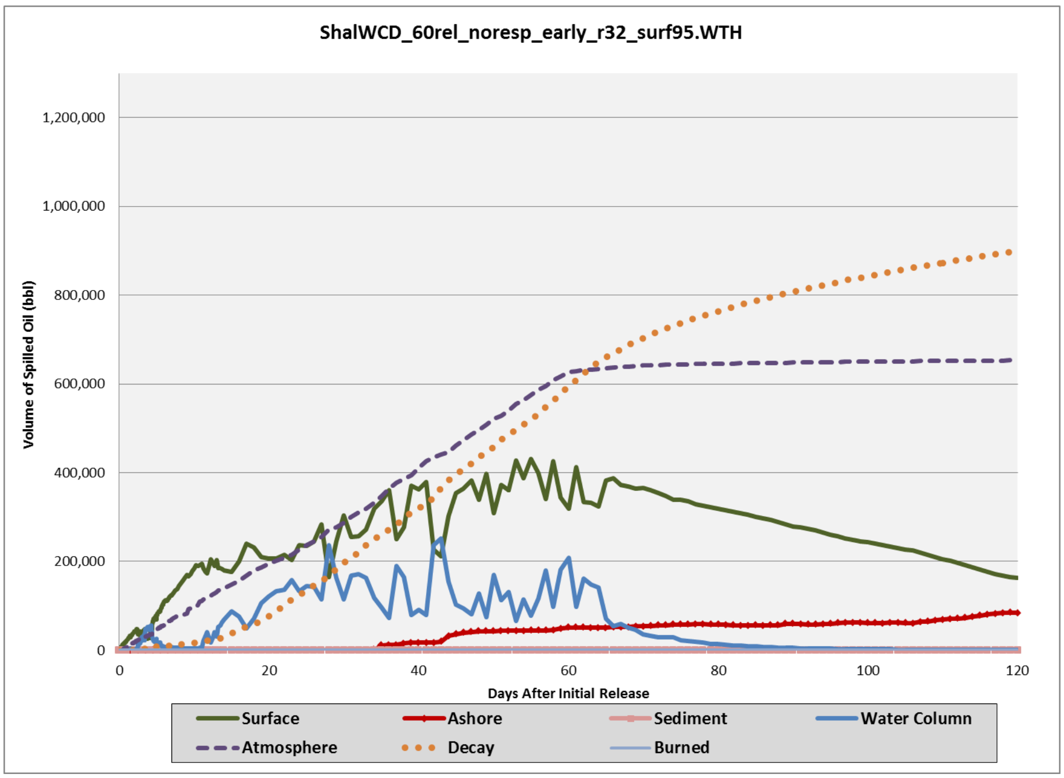

Figure 123. ShalWCD_60rel_noresp_early_r32_95surf - Mass balance chart. Start date: 6/3/2009.

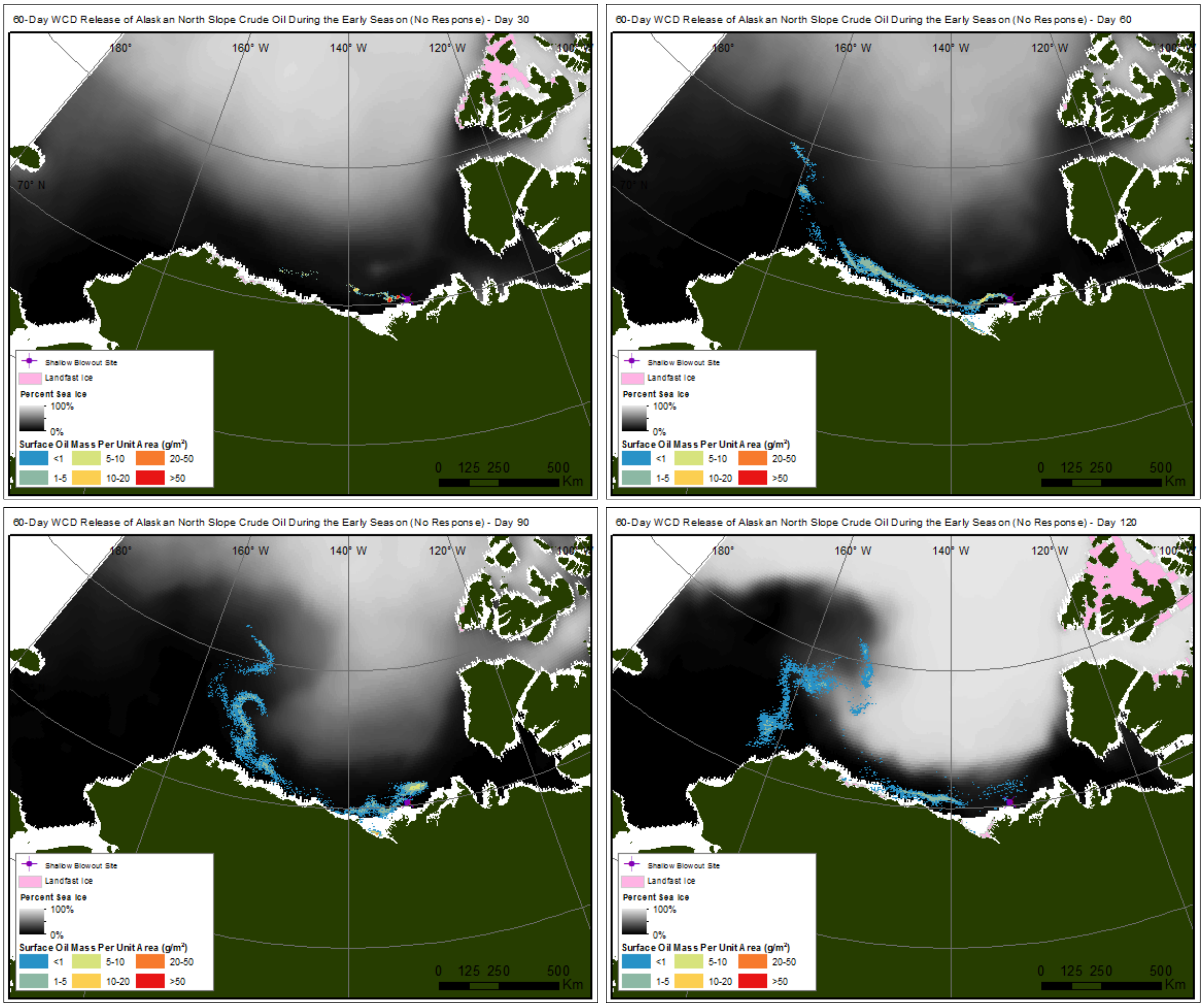

Figure 124. ShalWCD_60rel_noresp_early_r32_95surf – Time series maps of spill floating surface oil mass per unit area (g/m^2) (day 30, 60, 90, 120; July – October 2009). Pink polygons represent monthly average landfast ice. Grey scale contours represent ice percent coverage for that month from TOPAZ4 model. White indicates areas of no data for ice coverage. Start date: 6/3/2009.

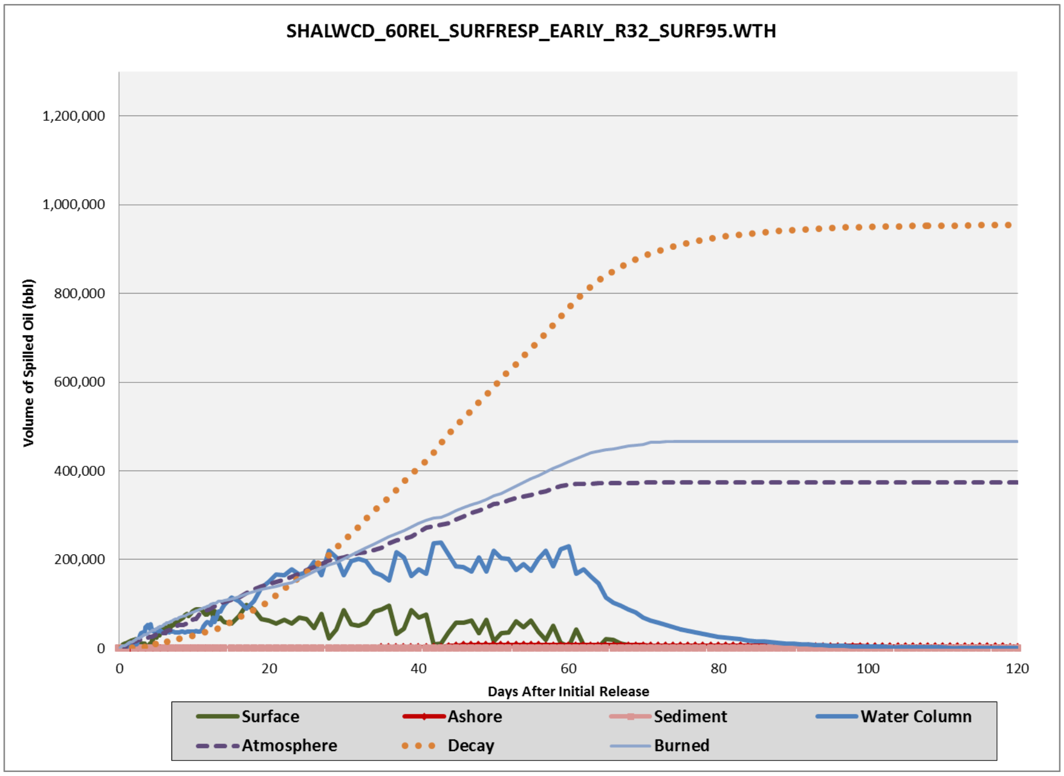

Figure 125. ShalWCD_60rel_surfresp_early_r32_95surface - Mass balance chart. **Surface response case including dispersant application and *in situ* burning.** Start date: 6/3/2009.

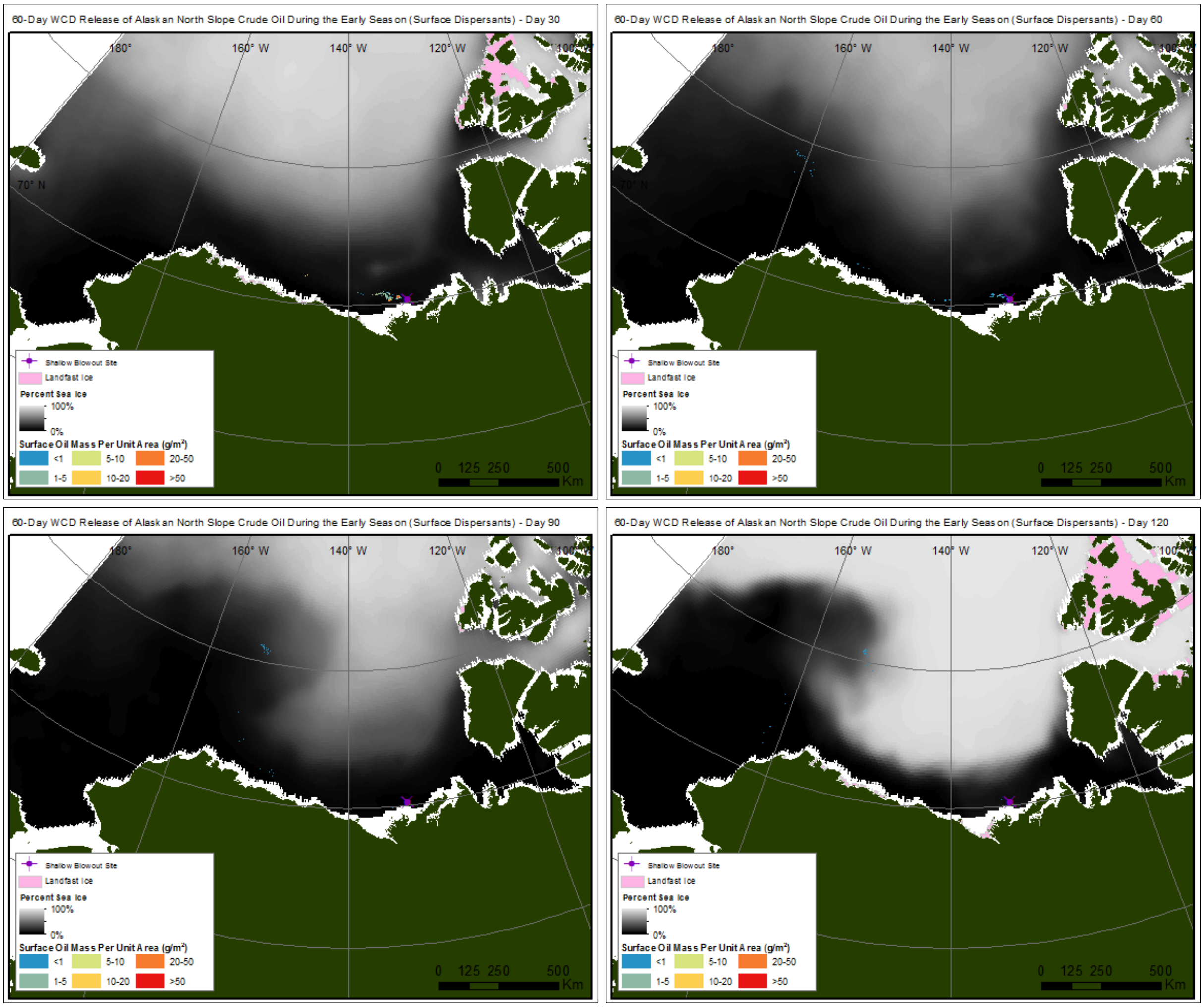

Figure 126. ShalWCD_60rel_surfresp_early_r32_95surface – Time series maps of spill floating surface oil mass per unit area (g/m^2) (day 30, 60, 90, 120; July –October 2009). **Surface response case including dispersant application and *in situ* burning**. Pink polygons represent monthly average landfast ice. Grey scale contours represent ice percent coverage for that month from TOPAZ4 model. White indicates areas of no data for ice coverage. Start date: 6/3/2009.

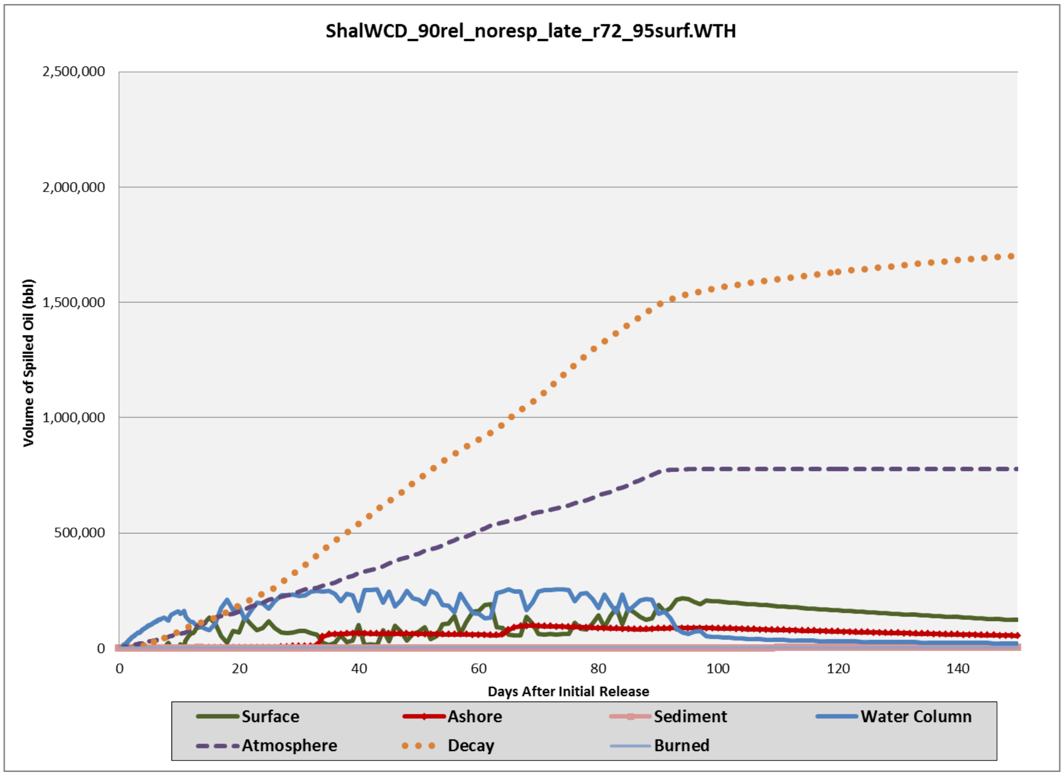

Figure 127. ShalWCD_90rel_noresp_late_r72_95surf - Mass balance chart. Start date: 8/6/2012.

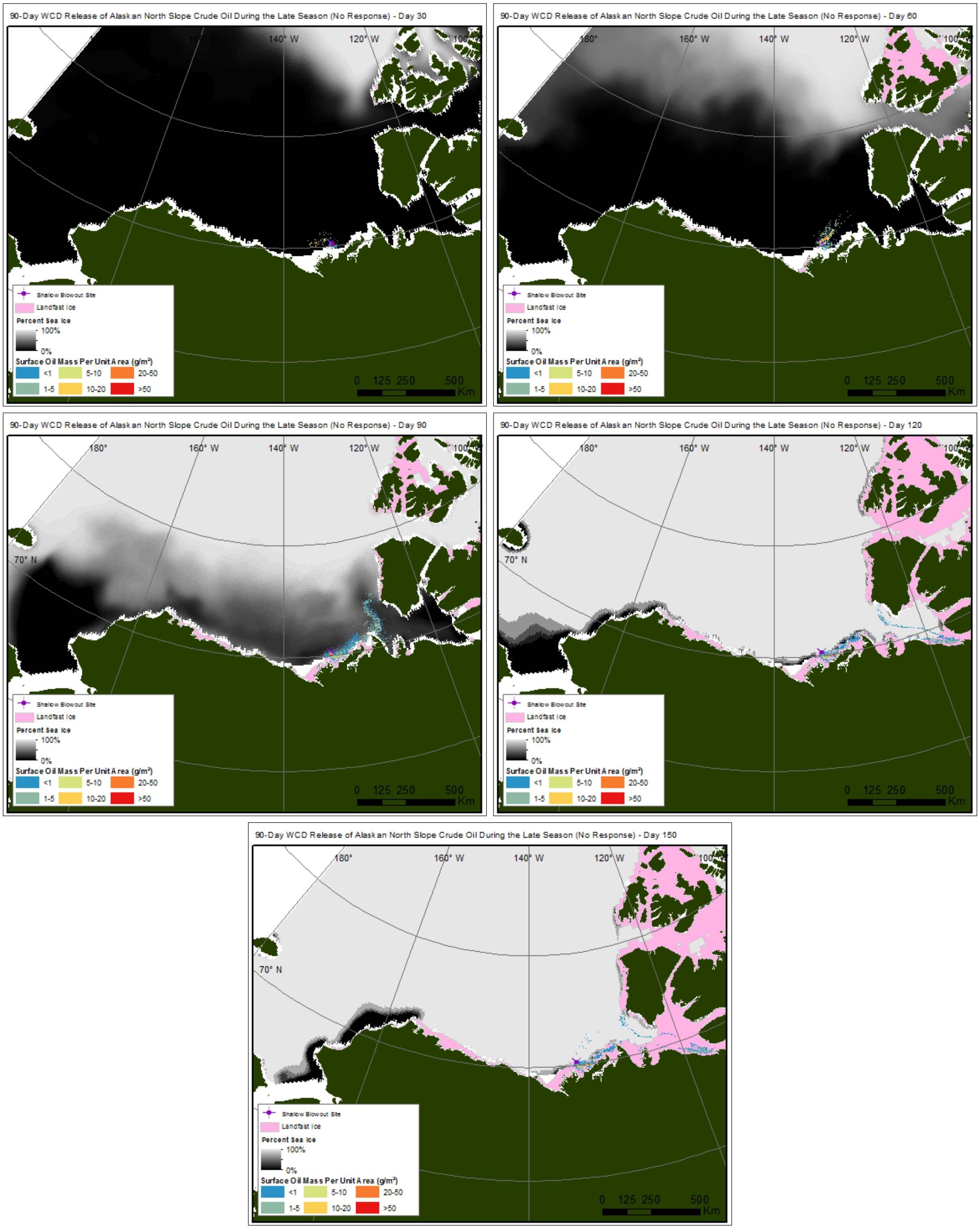

Figure 128. ShalWCD_90rel_noresp_late_r72_95surf – Time series maps of spill floating surface oil mass per unit area (g/m^2) (day 30, 60, 90, 120, 150; September 2012 – February 2013). Pink polygons represent monthly average landfast ice. Grey scale contours represent ice percent coverage for that month from TOPAZ4 model. White indicates areas of no data for ice coverage. Start date: 8/6/2012.

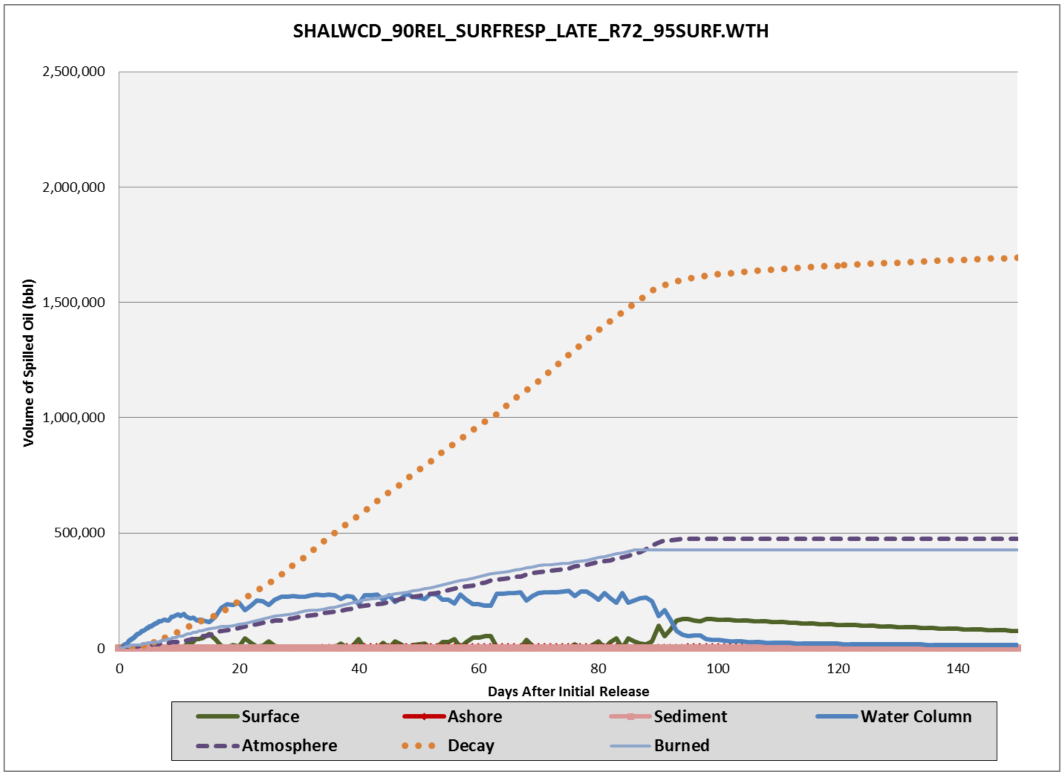

Figure 129. ShalWCD_90rel_surfresp_late_r72_95surf - Mass balance chart. **Surface response case including dispersant application and *in situ* burning**. Start date: 8/6/2012..

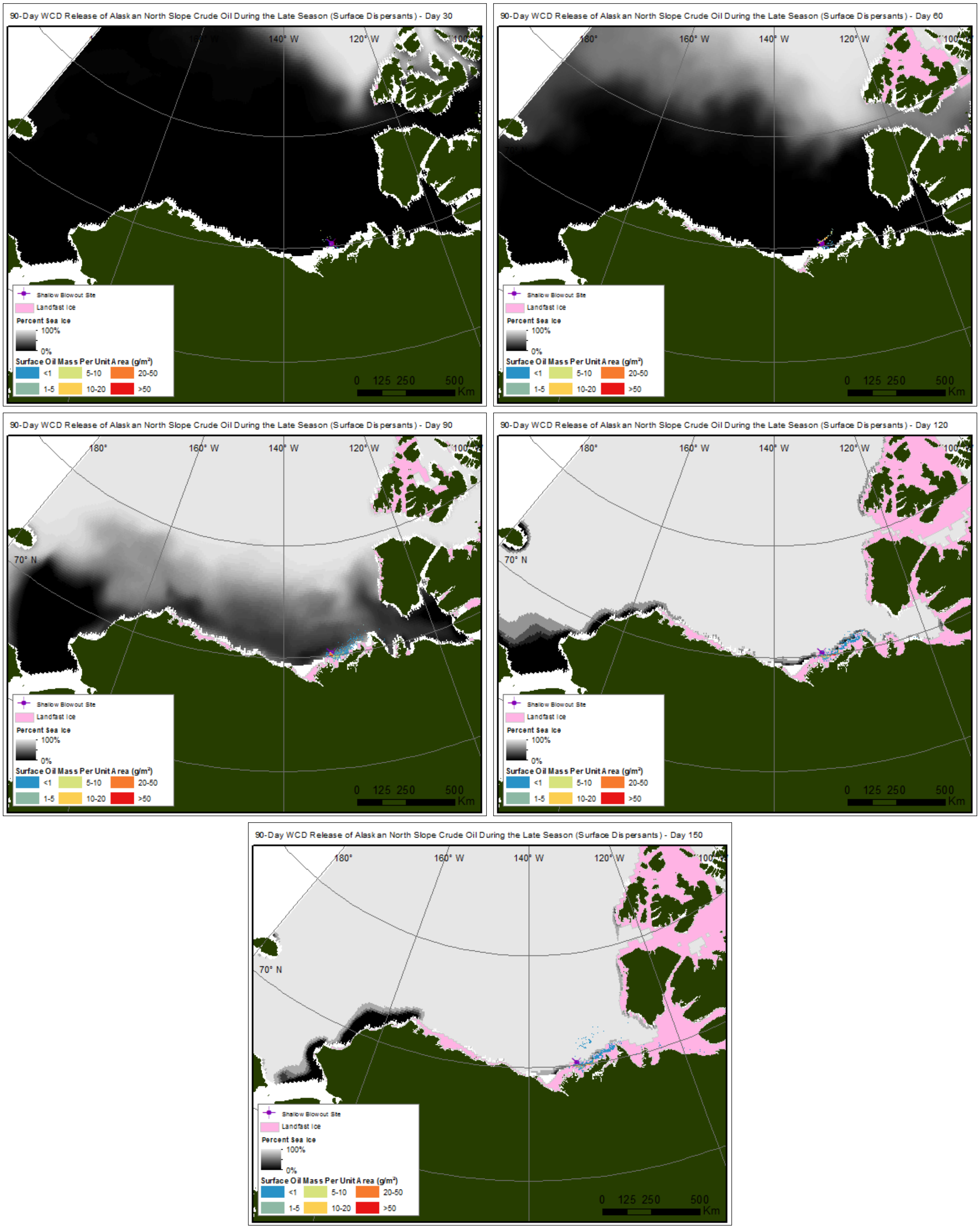

Figure 130. ShalWCD_90rel_surfresp_late_r72_95surf – Time series maps of spill floating surface oil mass per unit area (g/m^2) (day 30, 60, 90, 120, 150; September 2012 – February 2013). **Surface response case including dispersant application and *in situ* burning**. Pink polygons represent monthly average landfast ice. Grey scale contours represent ice percent coverage for that month from TOPAZ4 model. White indicates areas of no data for ice coverage. Start date: 8/6/2012.

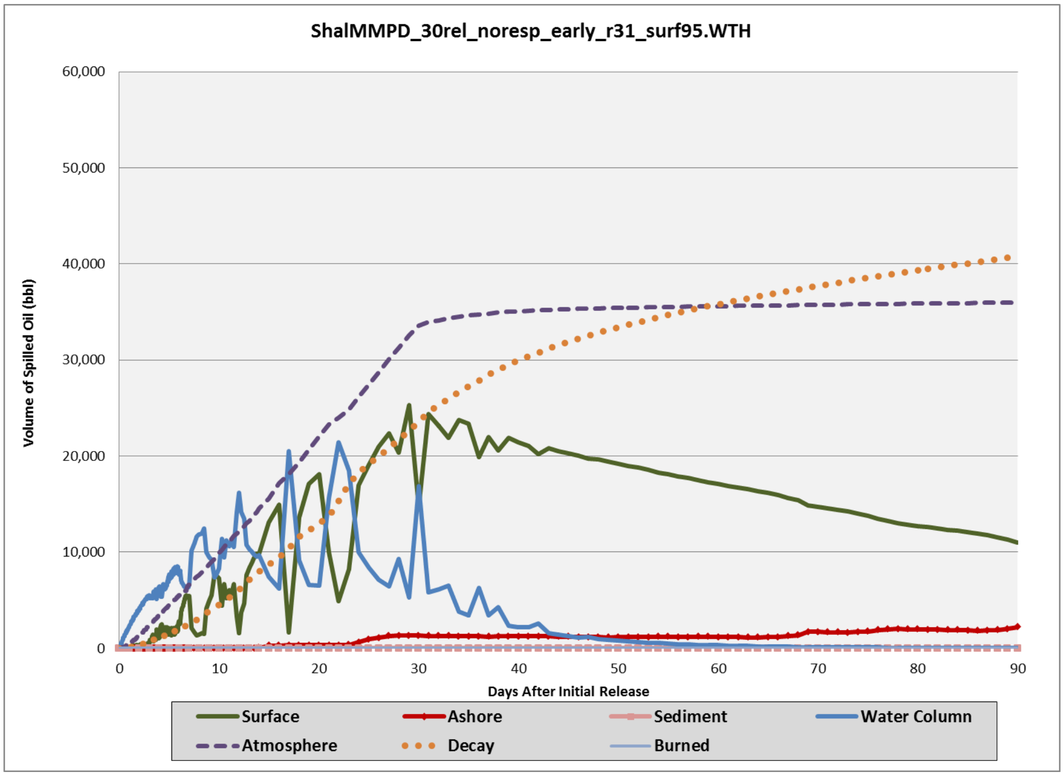

Figure 131. ShalMMPD_30rel_noresp_early_r31_95surf - Mass balance chart. Start date: 6/23/2009.

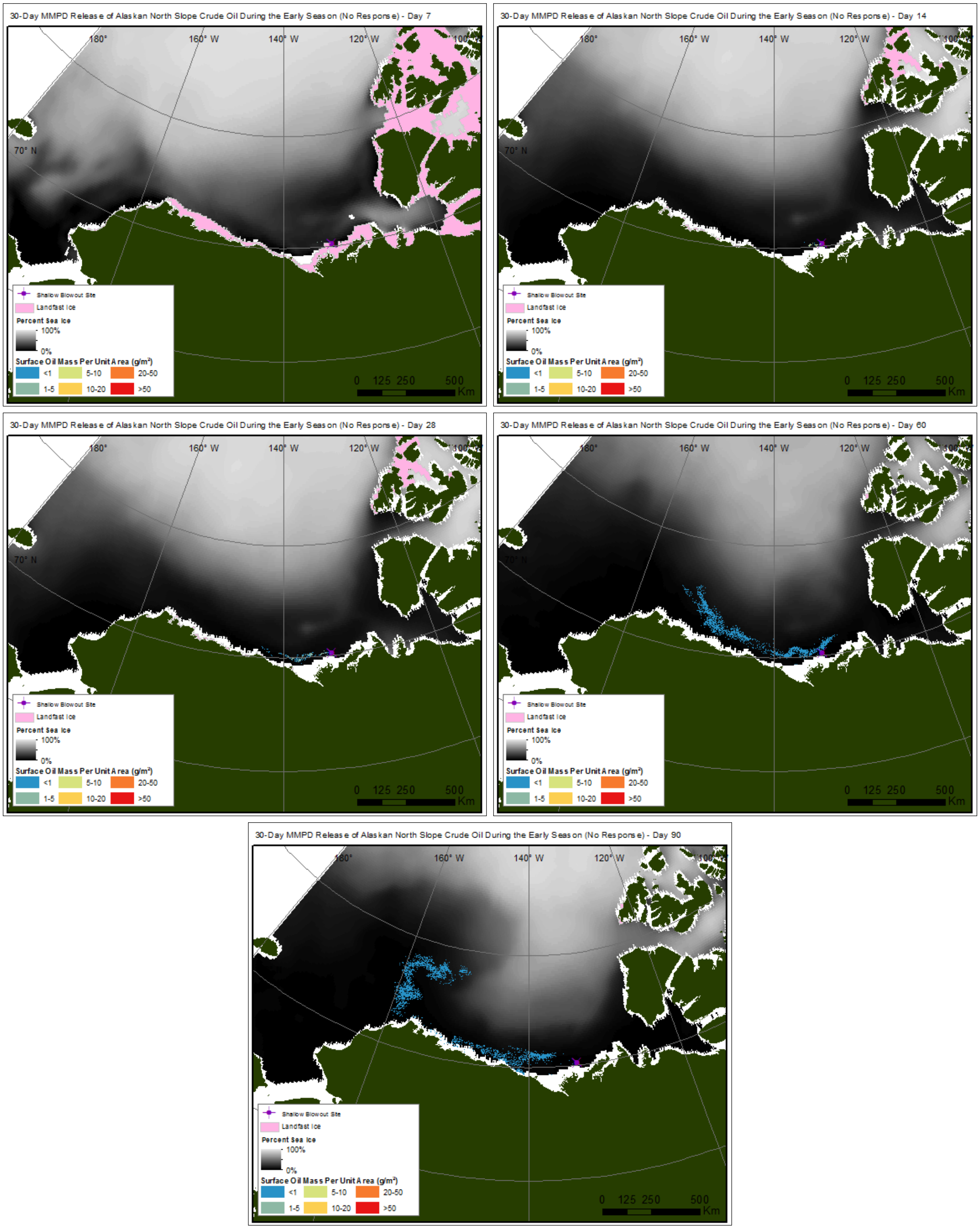

Figure 132. ShalMMPD_30rel_noresp_early_r31_95surf – Time series maps of spill floating surface oil mass per unit area (g/m^2) (day 7, 14, 28, 60, 90; June – September 2009). Pink polygons represent monthly average landfast ice. Grey scale contours represent ice percent coverage for that month from TOPAZ4 model. White indicates areas of no data for ice coverage. Start date: 6/23/2009.

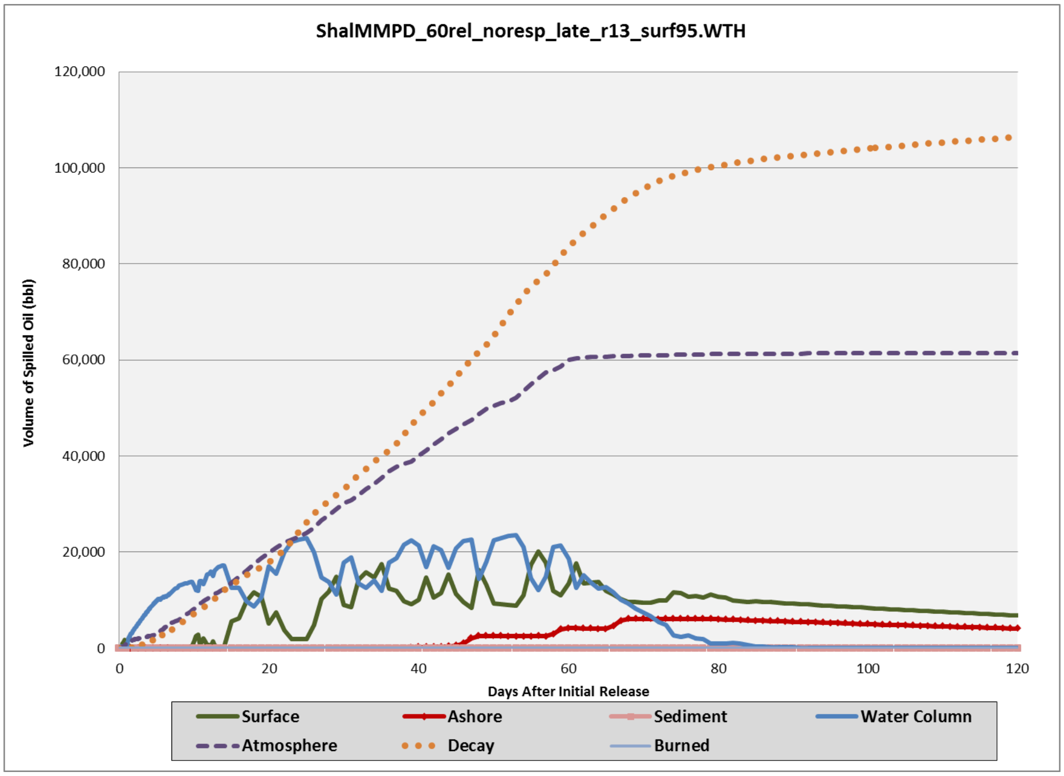

Figure 133. ShalMMPD_60rel_noresp_late_r13_95surf - Mass balance chart. Start date: 8/14/2010.

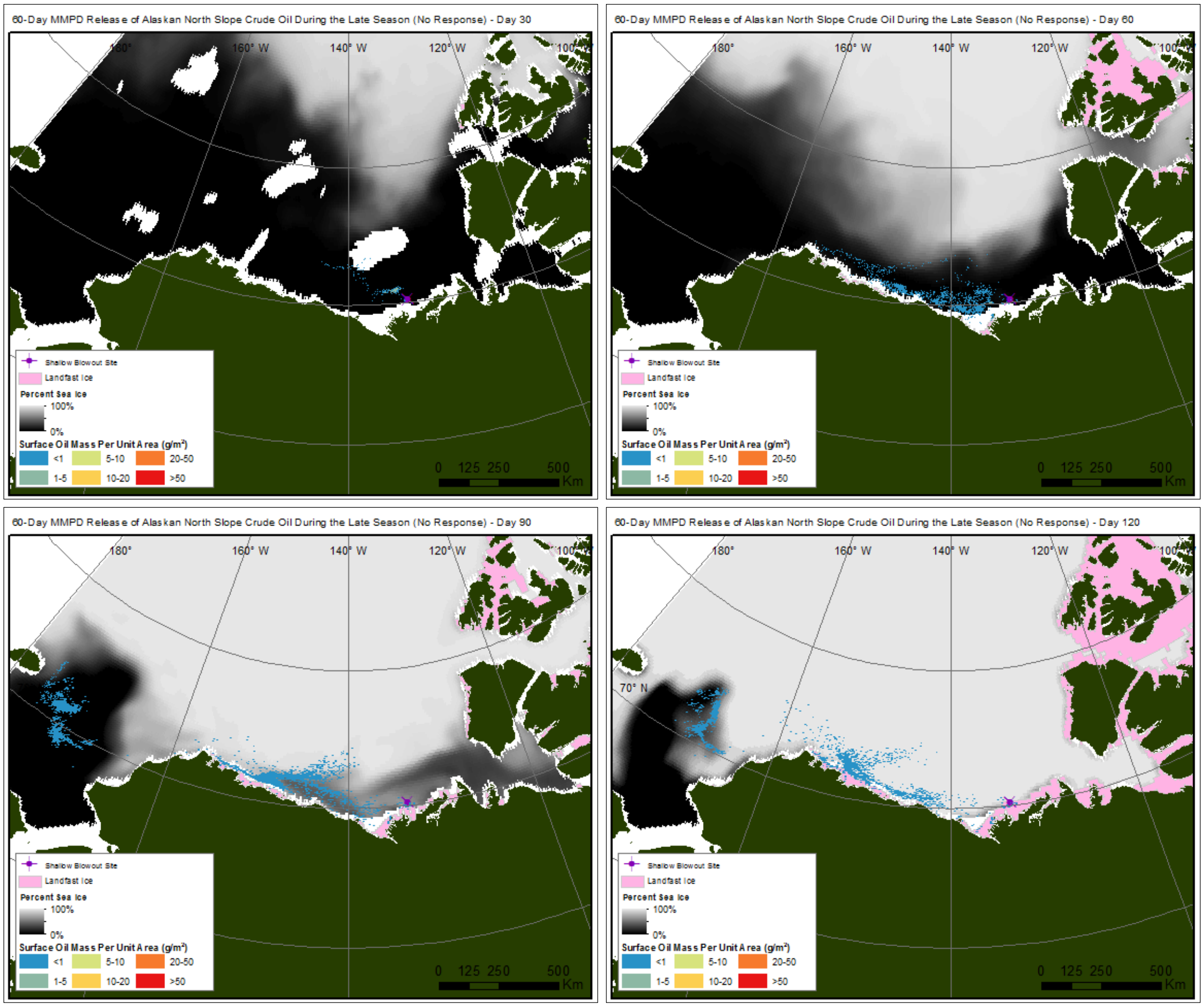

Figure 134. ShalMMPD_60rel_noresp_late_r13_95surf – Time series maps of spill floating surface oil mass per unit area (g/m^2) (day 30, 60, 90, 120; September – December 2010). Pink polygons represent monthly average landfast ice. Grey scale contours represent ice percent coverage for that month from TOPAZ4 model. White indicates areas of no data for ice coverage. Start date: 8/14/2010.

95th Percentile Shoreline Oiling

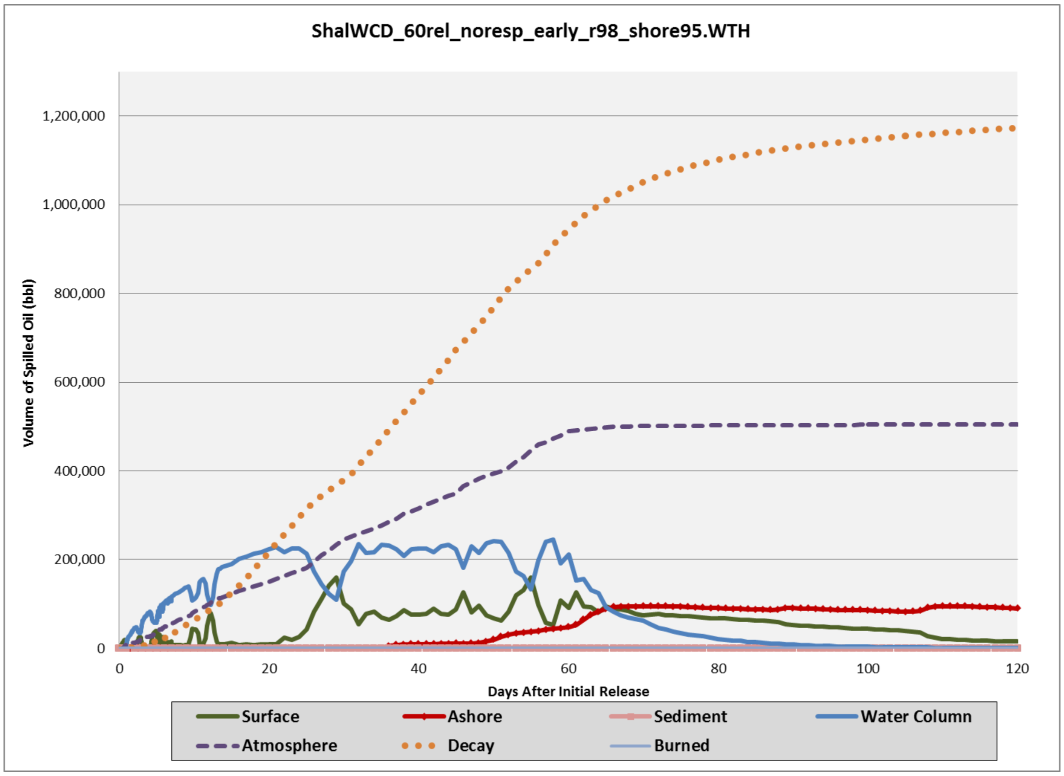

Figure 135. ShalWCD_60rel_noresp_early_r98_95shore - Mass balance chart. Start date: 6/18/2008.

Table 21. ShalWCD_60rel_noresp_early_r98_95shore – Shoreline length oiled (km) by habitat type, for both shore oiling thresholds. Start date: 6/18/2008.

Shore Type	Shore Length Oiled (km)	
	> 100 micrometers	> 1 micrometer
Seaward Rocky Shore	65.5	65.5
Seaward Gravel Beach	741.0	756.1
Seaward Sand Beach	423.4	453.7
Seaward Fringing Mud Flat	418.4	489.0
Seaward Fringing Wetland	15.1	55.5
Seaward Intertidal Macroalgal Bed	146.2	146.2
Shoreline Total	**1,809.6**	**1,966.0**

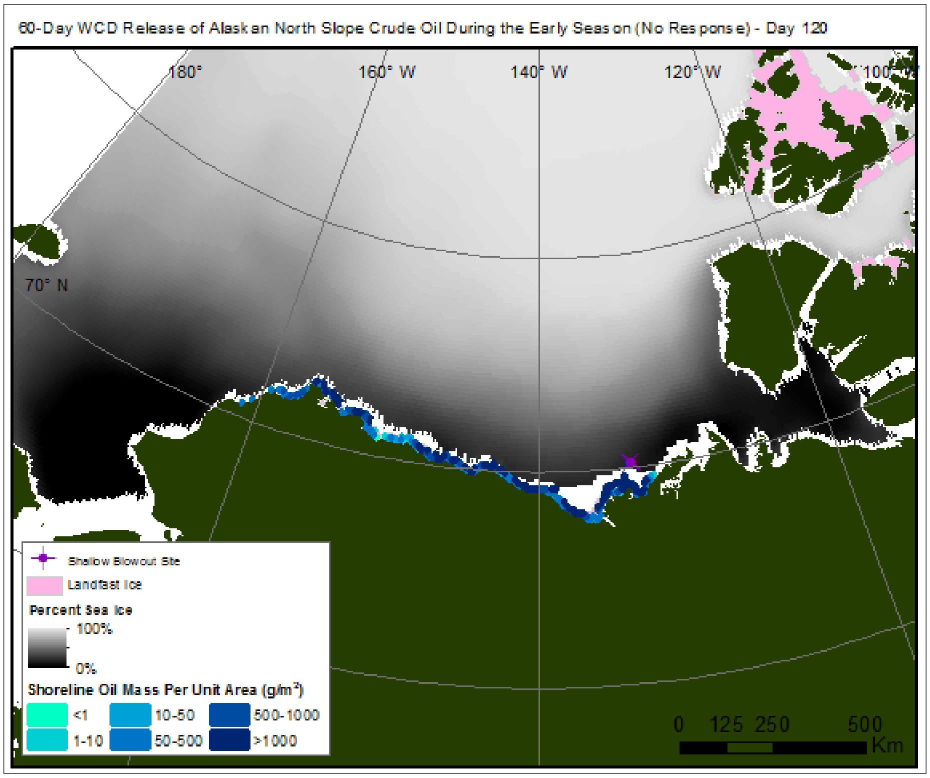

Figure 136. ShalWCD_60rel_noresp_early_r98_95shore – Map of overall effects to shorelines as mass of oil deposited on shore per unit of area (g/m^2) (day 120 – October 2008). Pink polygons represent monthly average landfast ice. Grey scale contours represent ice percent coverage for that month from TOPAZ4 model. White indicates areas of no data for ice coverage. Start date: 6/18/2008.

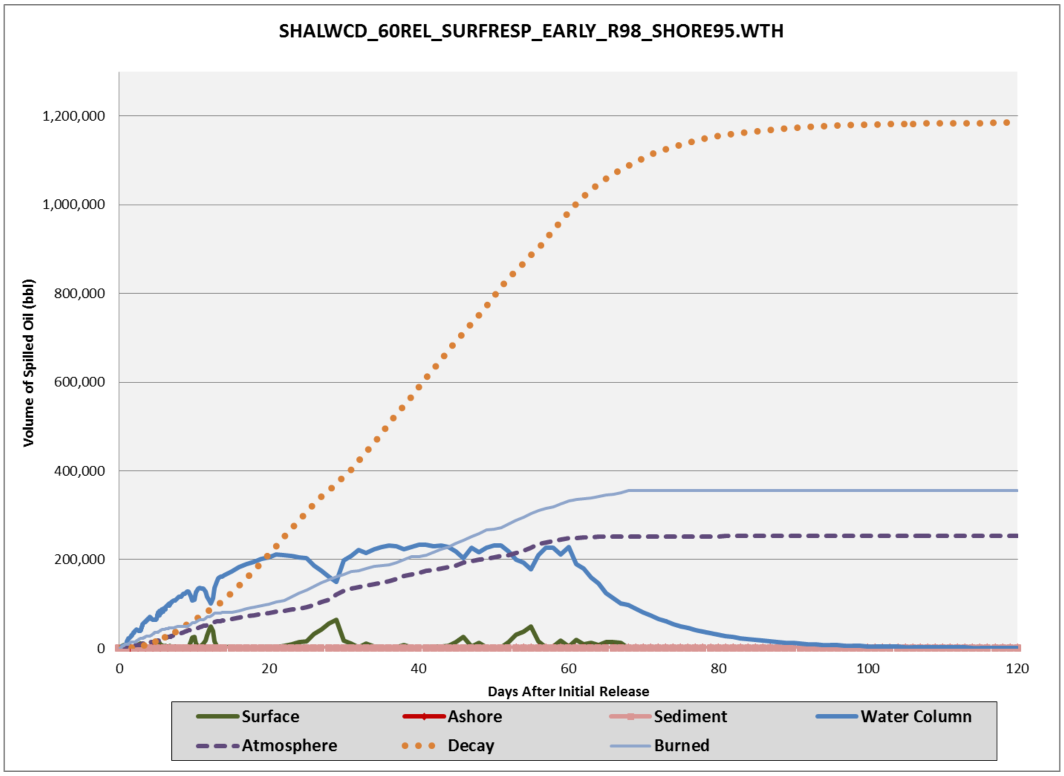

Figure 137. ShalWCD_60rel_surfresp_early_r98_95shore - Mass balance chart. **Surface response case including dispersant application and *in situ* burning**. Start date: 6/18/2008.

Table 22. ShalWCD_60rel_surfresp_early_r98_95shore – Shoreline length oiled (km) by habitat type, for both shore oiling thresholds. **Surface response case including dispersant application and *in situ* burning**. Start date: 6/18/2008.

Shore Type	Shore Length Oiled (km)	
	> 100 micrometers	> 1 micrometer
Seaward Gravel Beach	55.5	85.7
Seaward Sand Beach	15.1	15.1
Seaward Fringing Mud Flat	10.1	35.3
Shoreline Total	**80.7**	**136.1**

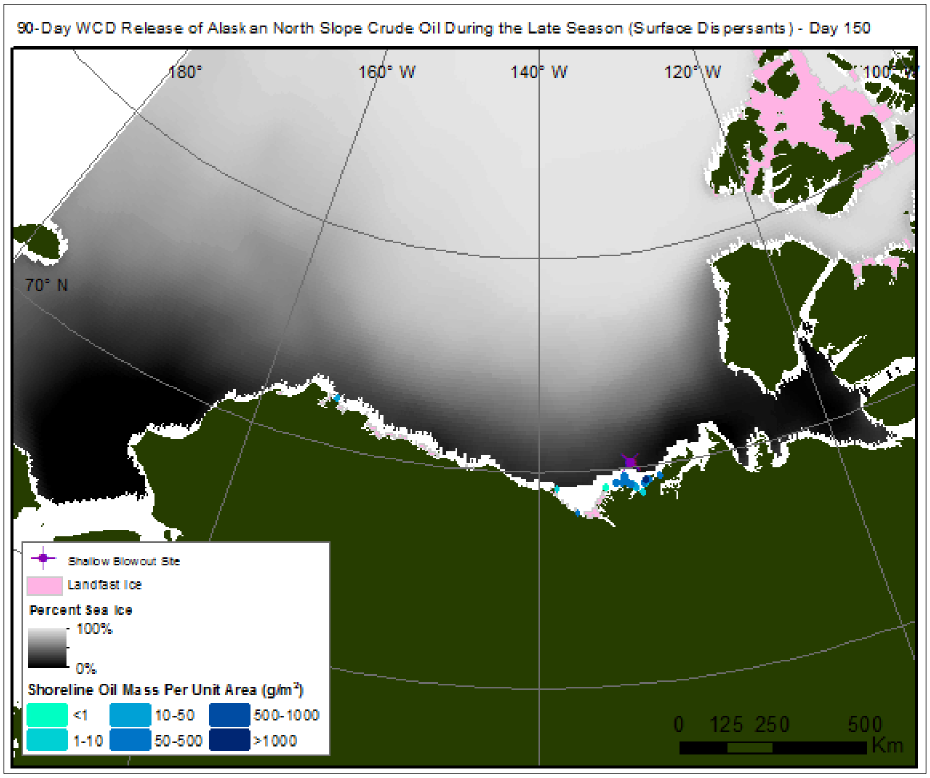

Figure 138. ShalWCD_60rel_surfresp_early_r98_95shore – Map of overall effects to shorelines as mass of oil deposited on shore per unit of area (g/m^2) (day 150 – October 2008). **Surface response case including dispersant application and *in situ* burning**. Pink polygons represent monthly average landfast ice. Grey scale contours represent ice percent coverage for that month from TOPAZ4 model. White indicates areas of no data for ice coverage. Start date: 6/18/2008.

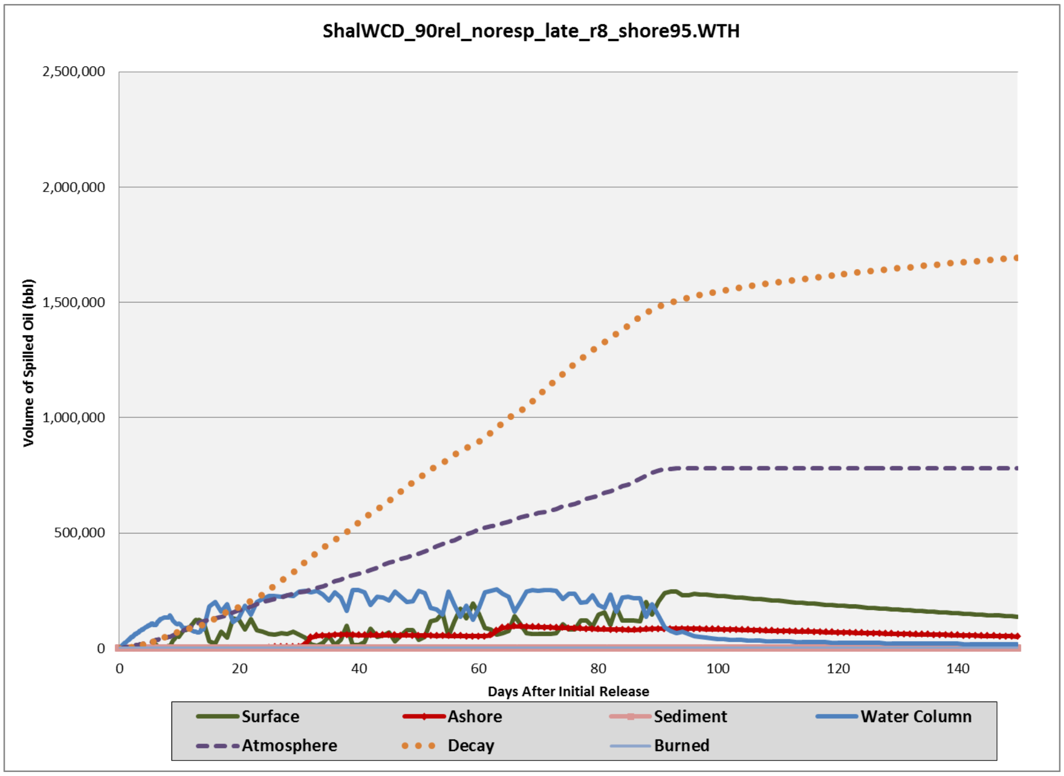

Figure 139. ShalWCD_90rel_noresp_late_r8_95shore - Mass balance chart. Start date: 8/8/2012.

Table 23. ShalWCD_90rel_noresp_late_r8_95shore – Shoreline length oiled (km) by habitat type, for both shore oiling thresholds. Start date: 8/8/2012.

Shore Type	Shore Length Oiled (km)	
	> 100 micrometers	> 1 micrometer
Seaward Gravel Beach	483.9	534.3
Seaward Sand Beach	105.9	105.9
Seaward Fringing Mud Flat	201.6	201.6
Seaward Fringing Wetland	10.1	15.1
Total Shoreline	**801.5**	**856.9**

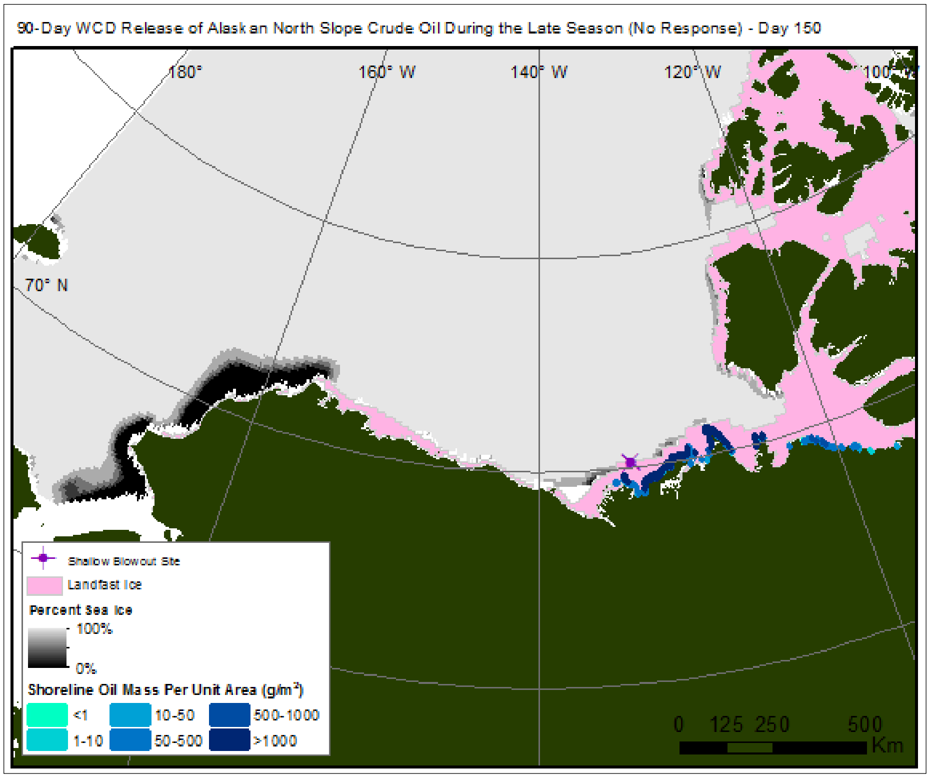

Figure 140. ShalWCD_90rel_noresp_late_r8_95shore – Map of overall effects to shorelines as mass of oil deposited on shore per unit of area (g/m^2) (day 150 – December 2012). Pink polygons represent monthly average landfast ice. Grey scale contours represent ice percent coverage for that month from TOPAZ4 model. White indicates areas of no data for ice coverage. Start date: 8/8/2012.

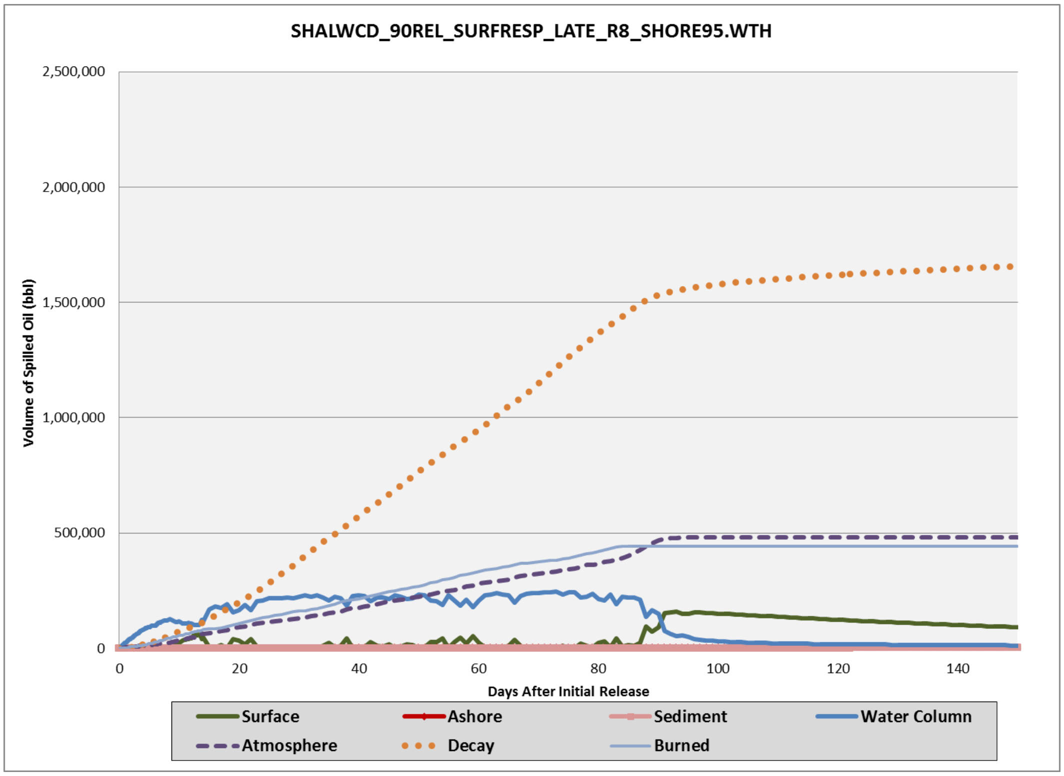

Figure 141. ShalWCD_90rel_surfresp_late_r8_95shore - Mass balance chart. **Surface response case including dispersant application and *in situ* burning**. Start date: 8/8/2012.

Table 24. ShalWCD_90rel_surfresp_late_r8_95shore – Shoreline length oiled (km) by habitat type, for both shore oiling thresholds. **Surface response case including dispersant application and *in situ* burning**. Start date: 8/8/2012.

Shore Type	Shore Length Oiled (km)	
	> 100 micrometers	> 1 micrometer
Seaward Gravel Beach	85.7	156.3
Seaward Sand Beach	15.1	40.3
Seaward Fringing Mud Flat	55.5	65.5
Seaward Fringing Wetland	0.0	10.1
Total Shoreline	**156.3**	**272.2**

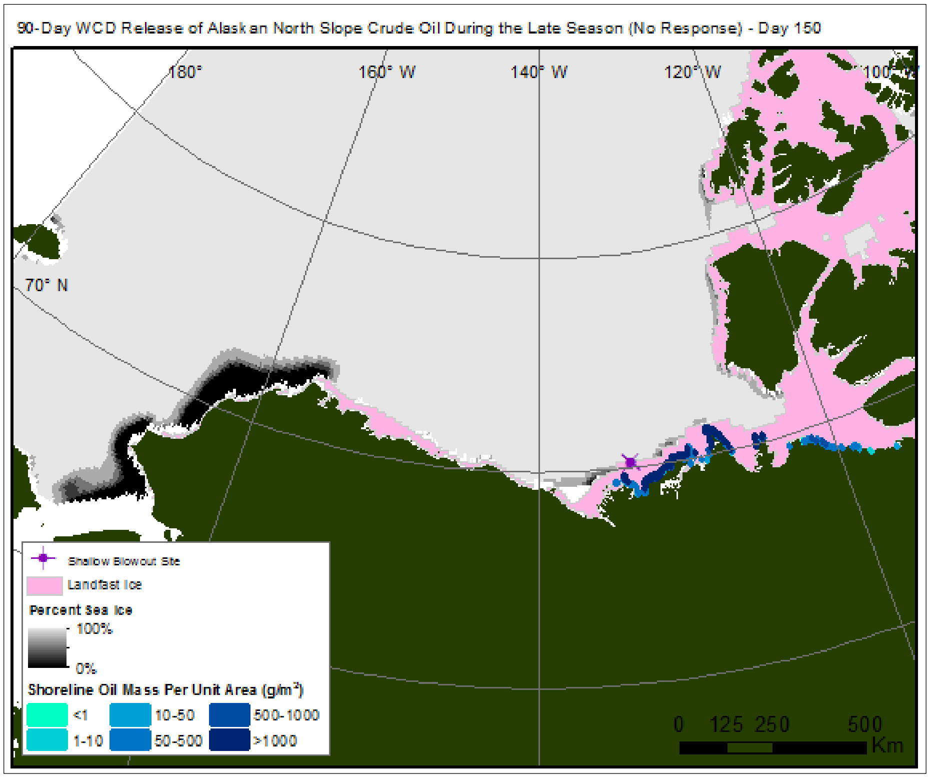

Figure 142. ShalWCD_90rel_surfresp_late_r8_95shore – Map of overall effects to shorelines as mass of oil deposited on shore per unit of area (g/m^2) (day 150 – December 2012). **Surface response case including dispersant application and *in situ* burning**. Pink polygons represent monthly average landfast ice. Grey scale contours represent ice percent coverage for that month from TOPAZ4 model. White indicates areas of no data for ice coverage. Start date: 8/8/2012.

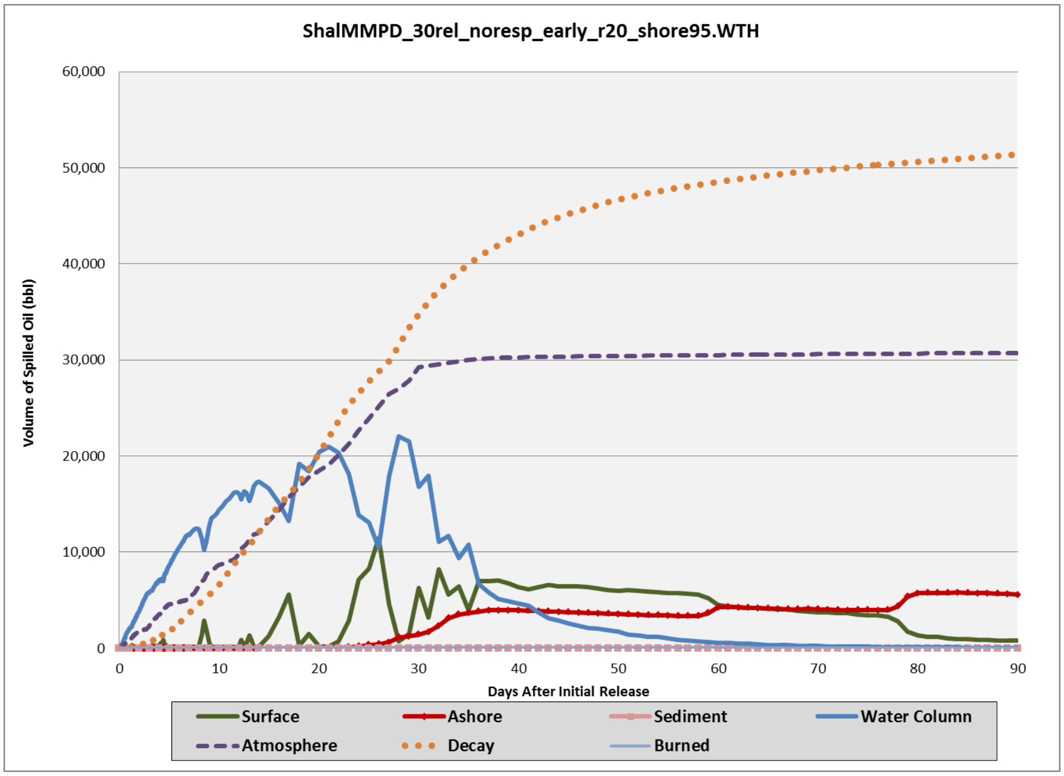

Figure 143. ShalMMPD_30rel_noresp_early_r20_95shore - Mass balance chart. Start date: 7/17/2008.

Table 25. ShalMMPD_30rel_noresp_early_r20_95shore – Shoreline length oiled (km) by habitat type, for both shore oiling thresholds. Start date: 7/17/2008.

Shore Type	Shore Length Oiled (km)	
	> 100 micrometers	> 1 micrometer
Seaward Rocky Shore	60.5	60.5
Seaward Gravel Beach	327.7	499.1
Seaward Sand Beach	131.1	363.0
Seaward Fringing Mud Flat	95.8	322.6
Seaward Fringing Wetland	0.0	10.1
Seaward Intertidal Macroalgal Bed	100.8	105.9
Total Shoreline	**715.9**	**1,361.2**

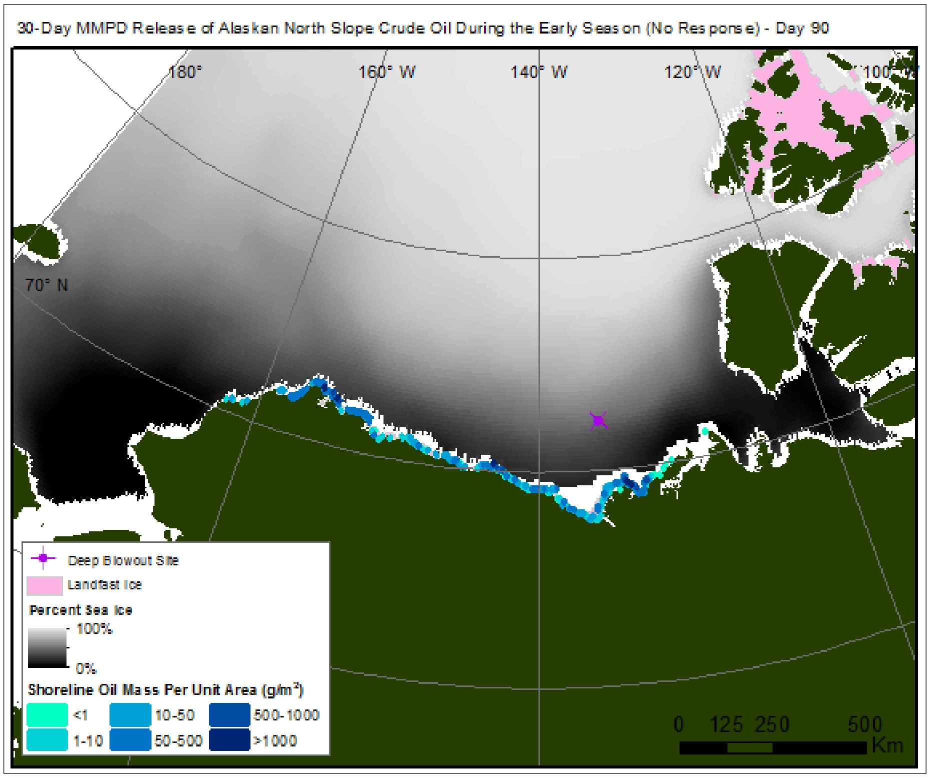

Figure 144. ShalMMPD_30rel_noresp_early_r20_95shore – Map of overall effects to shorelines as mass of oil deposited on shore per unit of area (g/m^2) (day 90 – October 2008). Pink polygons represent monthly average landfast ice. Grey scale contours represent ice percent coverage for that month from TOPAZ4 model. White indicates areas of no data for ice coverage. Start date: 7/17/2008.

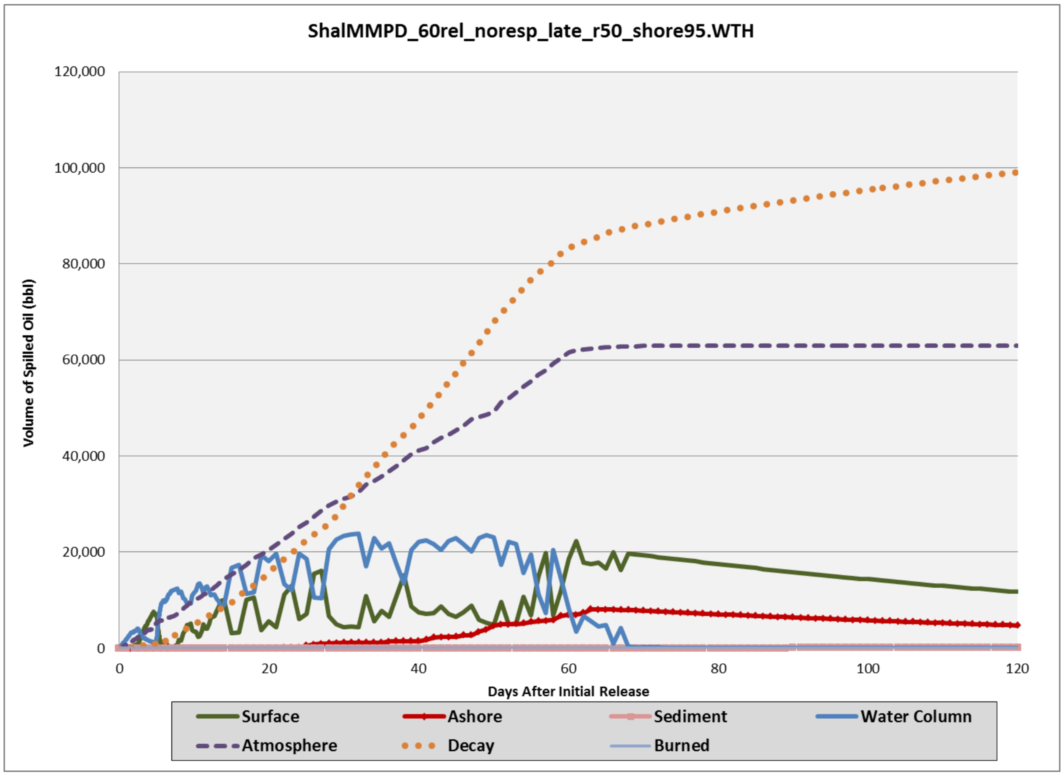

Figure 145. ShalMMPD_60rel_noresp_late_r50_95shore - Mass balance chart. Start date: 8/19/2008.

Table 26. ShalMMPD_60rel_noresp_late_r50_95shore – Shoreline length oiled (km) by habitat type, for both shore oiling thresholds. Start date: 8/19/2008.

Shore Type	Shore Length Oiled (km)	
	> 100 micrometers	> 1 micrometer
Seaward Gravel Beach	357.9	499.1
Seaward Sand Beach	151.2	352.9
Seaward Fringing Mud Flat	75.6	236.9
Seaward Fringing Wetland	5.0	15.1
Seaward Intertidal Macroalgal Bed	65.5	65.5
Total Shoreline	**655.2**	**1,169.5**

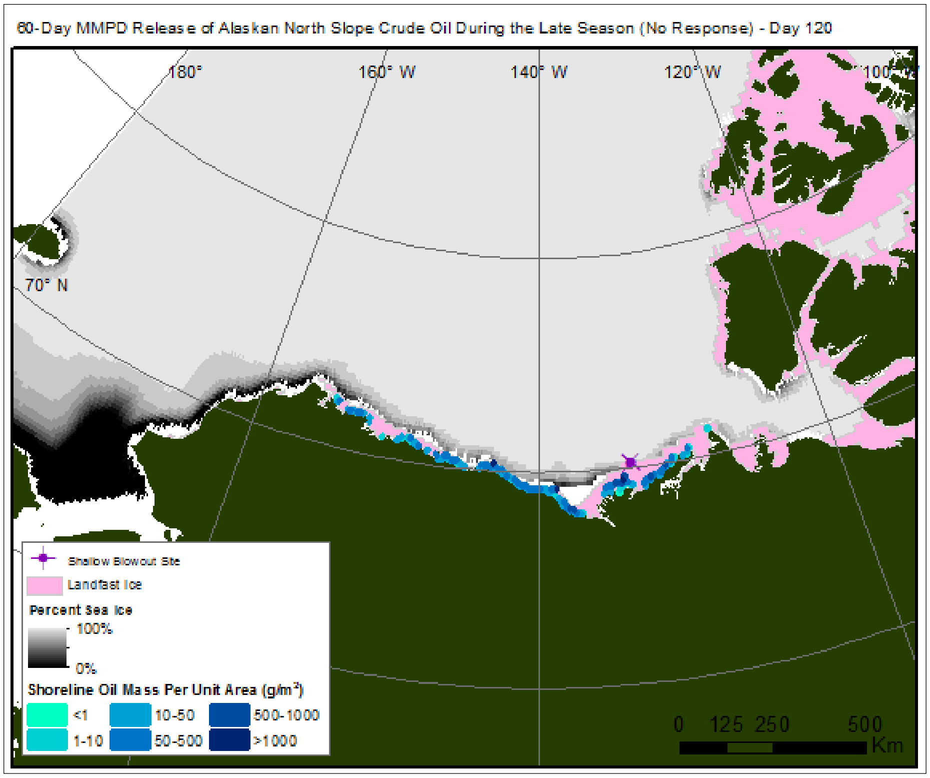

Figure 146. ShalMMPD_60rel_noresp_late_r50_95shore – Map of overall effects to shorelines as mass of oil deposited on shore per unit of area (g/m^2) (day 120 – December 2008). Pink polygons represent monthly average landfast ice. Grey scale contours represent ice percent coverage for that month from TOPAZ4 model. White indicates areas of no data for ice coverage. Start date: 8/19/2008.

95th Percentile Water Column Contamination

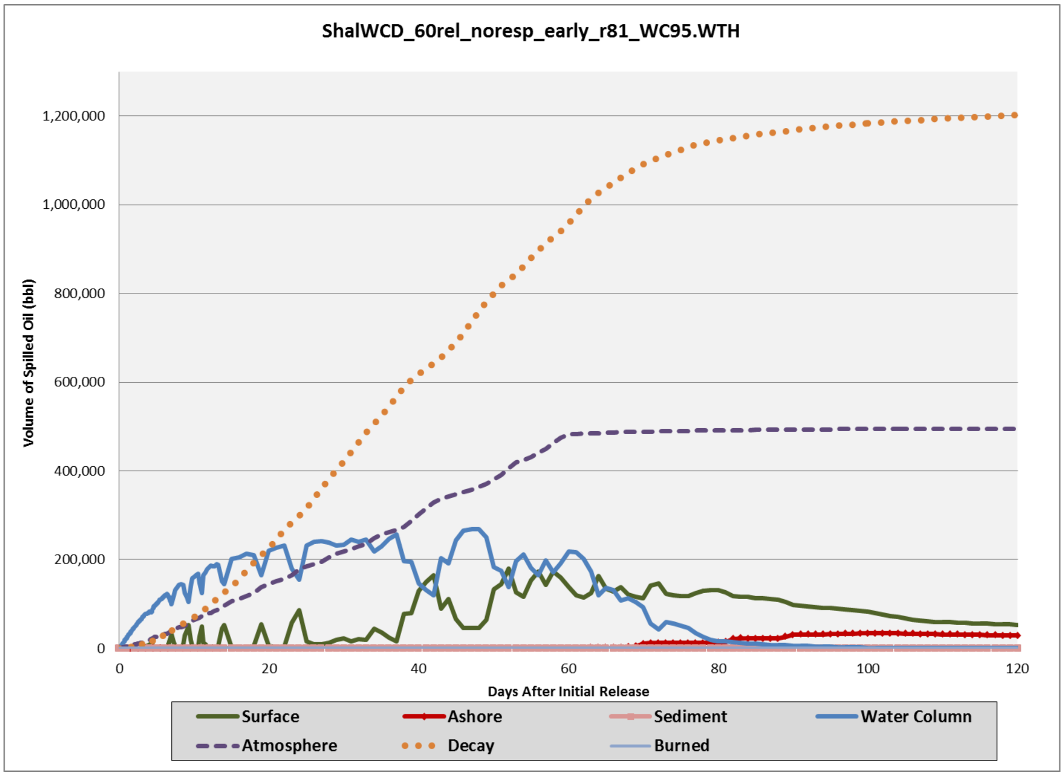

Figure 147. ShalWCD_60rel_noresp_early_r81_95WC - Mass balance chart. Start date: 7/22/2010.

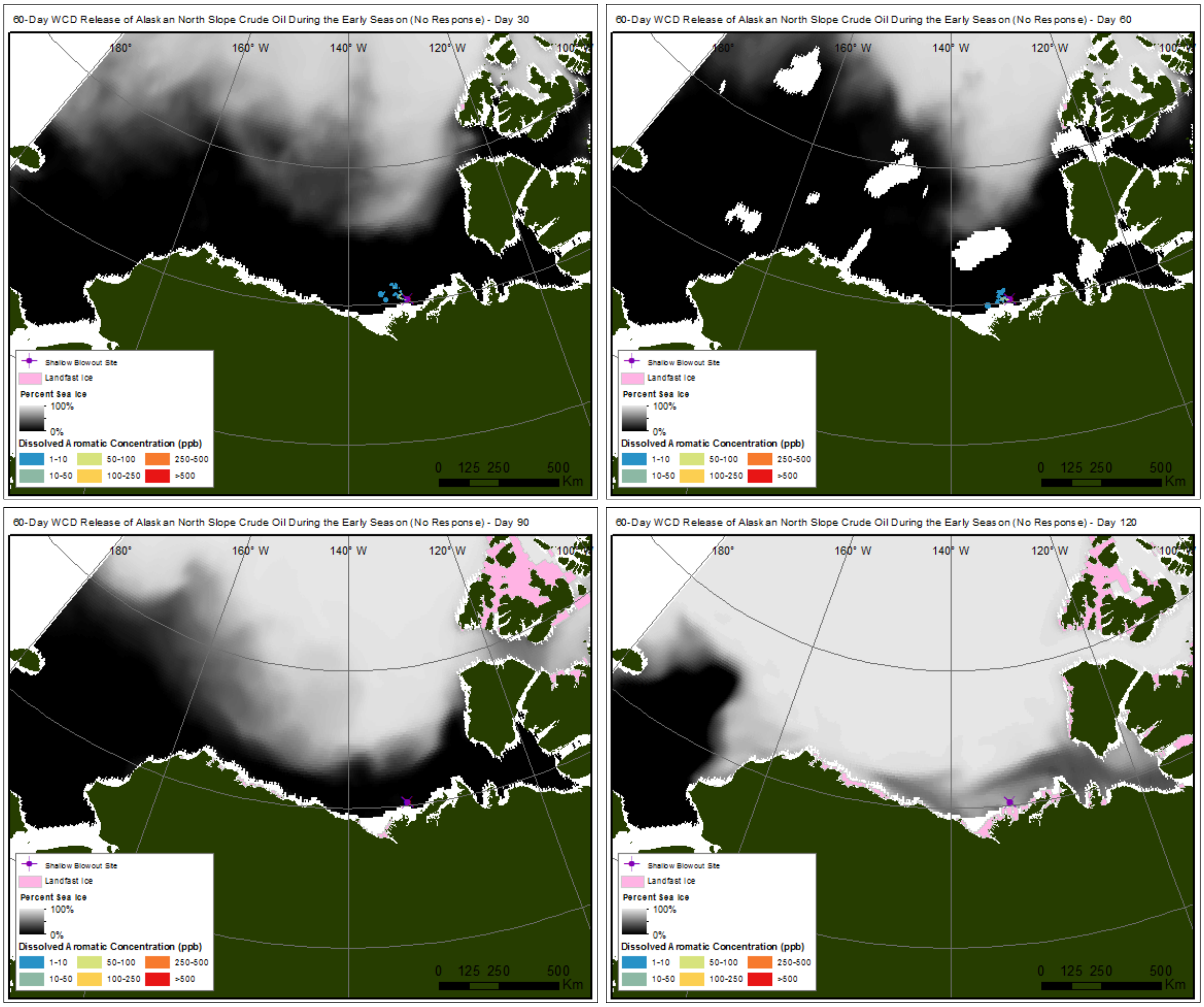

Figure 148. ShalWCD_60rel_noresp_early_r81_95WC – Time series maps of spill dissolved aromatics ≥1 ppb (day 30, 60, 90, 120; August – November 2010). Pink polygons represent monthly average landfast ice. Grey scale contours represent ice percent coverage for that month from TOPAZ4 model. White indicates areas of no data for ice coverage. Start date: 7/22/2010.

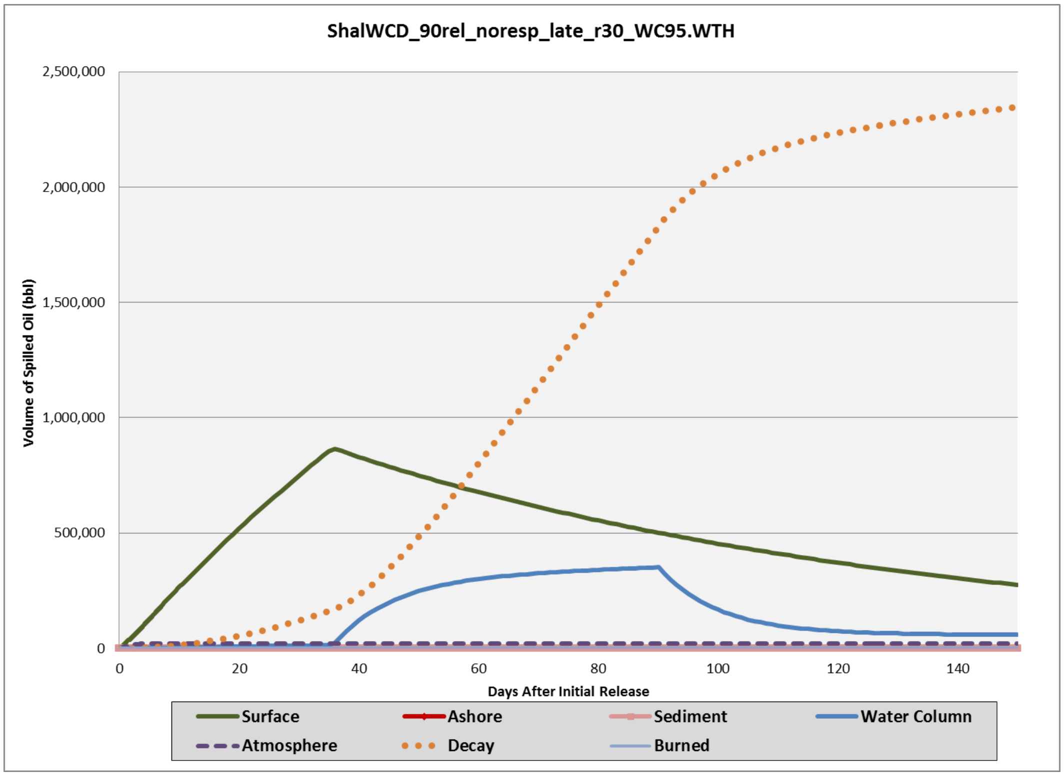

Figure 149. ShalWCD_90rel_noresp_late_r30_95WC - Mass balance chart. Start date: 10/26/2008.

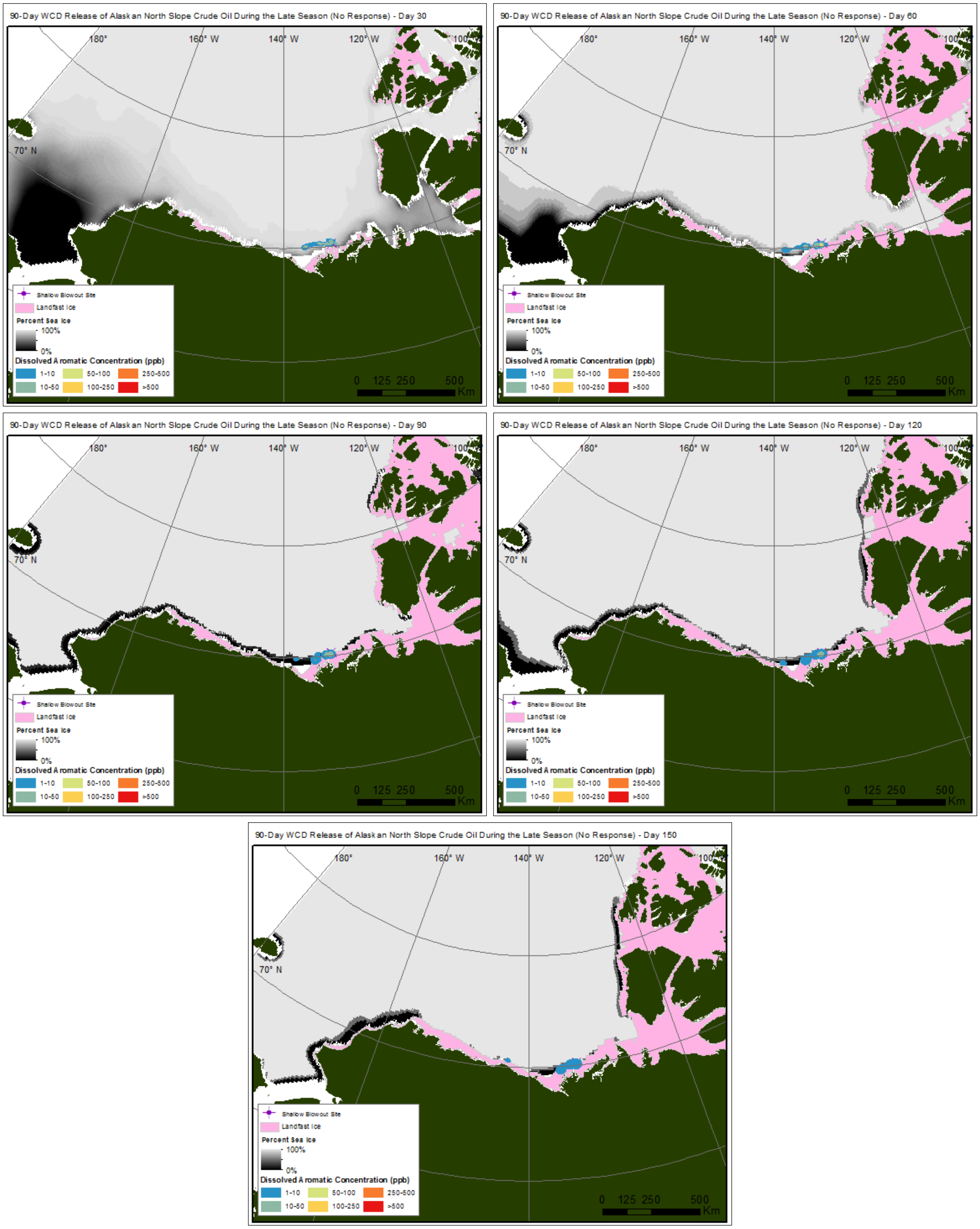

Figure 150. ShalWCD_90rel_noresp_late_r30_95WC – Time series maps of spill dissolved aromatics ≥1 ppb (day 30, 60, 90, 120, 150; November 2008 - March 2009). Pink polygons represent monthly average landfast ice. Grey scale contours represent ice percent coverage for that month from TOPAZ4 model. White indicates areas of no data for ice coverage. Start date: 10/26/2008.

7.4 Deep Blowout Analysis

This section contains the model inputs and results of the blowout plume modelling conducted at the deep blowout site (near-field). This modelling provided the conditions for which the stochastic analysis and individual trajectory models were initialized at. This section also contains the stochastic analysis and individual trajectory results (far-field) for the Deep Blowout Analysis (Section 6.5). There were a total of six stochastic scenarios and sixteen individual trajectories run for this analysis. Table 27 provides the scenario names. Please see Appendix D for full scenario list and naming conventions.

Table 27. List of scenario names and types for the Deep Blowout Analysis.

Scenario Name	Scenario Type	Start Date/Range
DeepWCD_90rel_noresp_early	Stochastic	June-July
DeepWCD_90rel_subresp_early	Stochastic	June-July
DeepWCD_120rel_noresp_late	Stochastic	August-October
DeepWCD_120rel_subresp_late	Stochastic	August-October
DeepMMPD_60rel_noresp_early	Stochastic	June-July
DeepMMPD_90rel_noresp_late	Stochastic	August-October
DeepWCD_90rel_noresp_early_r97_95surf	Individual	6/29/2009
DeepWCD_90rel_surfresp_early_r97_95surf	Individual	6/29/2009
DeepWCD_120rel_noresp_late_r21_95surf	Individual	8/16/2009
DeepWCD_120rel_surfresp_late_r21_95surf	Individual	8/16/2009
DeepMMPD_60rel_noresp_early_r32_95surf	Individual	6/3/2009
DeepMMPD_90rel_noresp_late_r40_95surf	Individual	9/4/2009
DeepWCD_90rel_noresp_early_r98_95shore	Individual	6/18/2008
DeepWCD_90rel_surfresp_early_r98_95shore	Individual	6/18/2008
DeepWCD_120rel_noresp_late_r91_95shore	Individual	8/12/2008
DeepWCD_120rel_surfresp_late_r91_95shore	Individual	8/12/2008
DeepMMPD_60rel_noresp_early_r7_95shore	Individual	6/22/2008
DeepMMPD_90rel_noresp_late_r37_95shore	Individual	8/4/2009
DeepWCD_90rel_noresp_early_r61_95WC	Individual	6/2/2010
DeepWCD_90rel_subresp_early_r3_repsub	Individual	7/29/2008
DeepWCD_120rel_noresp_late_r32_95WC	Individual	8/7/2010
DeepWCD_120rel_subresp_late_r19_repsub	Individual	9/2/2010

7.4.1 Blowout Plume Model Inputs (Near-Field)

Near-field blowout modelling was performed to determine the near-field plume characteristics to be used to initialize the far-field modelling simulations. The objectives of the near-field modelling were to determine the extent of the blowout plume and to characterize the associated droplet size distributions.

The near-field results of a blowout are constant for continuous release conditions, in other words the plume termination height and droplet size distribution associated with a particular release essentially remains the same whether the release occurs for 2 days or 20 days; slight changes in the water column profile could change the results; however, often this effect is negligible. The approach used in this study was to use the most conservative representation of the water column in the near-field modelling, with conservative meaning the profile that would promote further vertical ascent of the plume. Furthermore the use of subsurface dispersants does not affect the plume characteristics, only the droplet size characteristics. Therefore for a given release condition, with the exception of dispersant treatment methodology, the resulting plume dimension is the same. Due to the nature of these processes each of the far-field simulations did not necessarily have a unique set of near-field results. The unique near-field scenarios are summarized in Table 28 including the pertinent near-field blowout modelling inputs that characterize the scenario.

The treated scenario assumed that the release would be treated with dispersant at a ratio of 1:60 (1 bbl of dispersant for every 60 bbl of oil). The Oil Budget Calculator for Deepwater Horizon (NIC Oil Budget Calculator DWH, 2010) suggests that a dispersant to oil ratio (DOR) of 1:60 is plausible, but on the higher end of the efficiency range. The dispersant treatment algorithm in OILMAPDeep employs a modified Weber number (dimensionless number in the droplet size calculation) based on an adjusted interfacial tension (IFT) determined by the relationship between IFT and the dispersant to oil ratio (DOR). This relationship is based on findings from laboratory experiments (Khalifa and So, 2009). The empirical findings from the different studied oil/dispersant mixtures were averaged to develop a singular proxy for the IFT reduction function; this relationship, shown in Figure 151, is nonlinear and highly sensitive (both axes use a logarithmic scale).

The gas-to-oil ratio or GOR and pipe diameter used for this analysis was based on a review of RPS ASA's past blowout modelling projects (2009-2014). 1000 scf/stb and 0.381 m is the most common GOR and pipe diameter that the authors have been requested to model, therefore felt these values were good proxies for this study.

Table 28. Summary of blowout plume analyses conducted at the deep blowout site (6 model runs total).

Scenario	Oil Type	GOR (scf/stb)	Release Depth (m)	Oil Release Rate (Reference)	Oil Release Rate (bbl/day)	Subsurface Dispersant Treatment	Release Pipe Diameter (m)
WCD	ANS Crude	1000	1008	WCD	60,000	Untreated	0.381
WCD, subsurface response	ANS Crude	1000	1008	WCD	60,000	Treated DOR 1:60	0.381
MMPD	ANS Crude	1000	1008	MMPD	6,000	Untreated	0.381
MMPD	ANS Crude	1000	1008	MMPD	6,000	Untreated	0.381

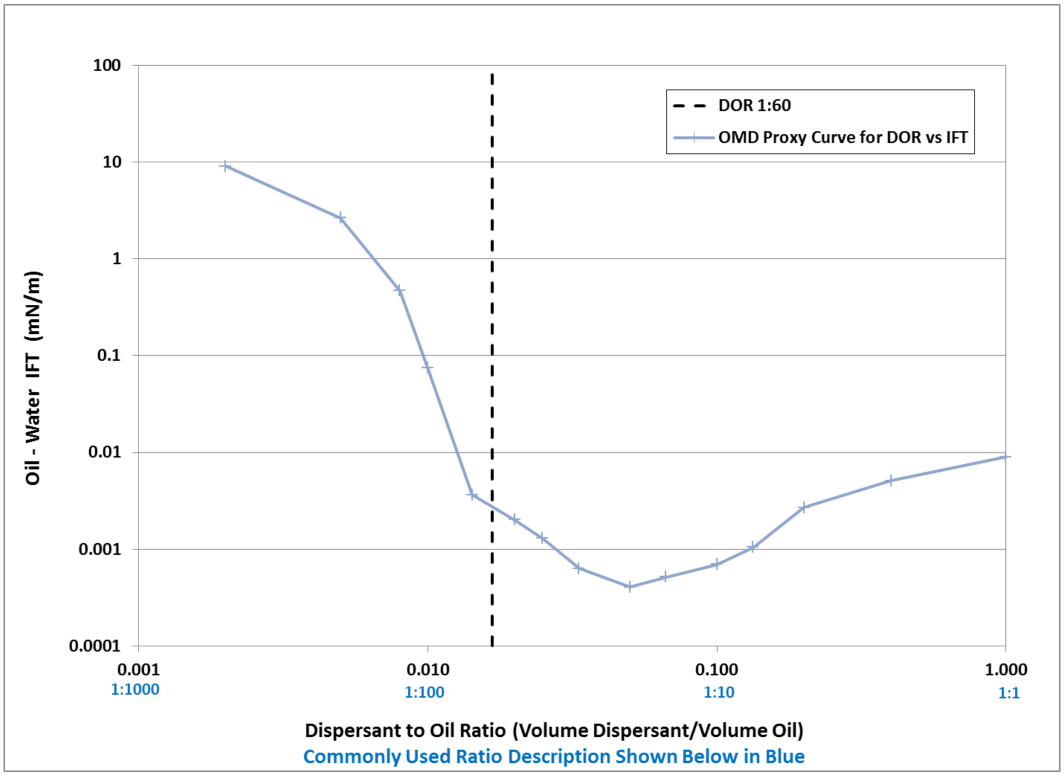

Figure 151. Illustration of proxy curve representing DOR vs IFT in OILMAPDeep (OMD).

7.4.2 Blowout Plume Modelling Results (Near-Field)

Termination Height and Radius

The results of the near-field modelling provided information about the formation of the blowout plume including the three dimensional extent of the mixture of gas/oil/water, and a characterization of the initial dispersion/mixing of the oil discharged during the blowout. Key factors in this analysis were the release conditions (depth, opening diameter, oil release rate, gas to oil ratio (GOR)) and water column conditions (profile of temperature and density). Subsurface releases of oil are accompanied by gas; the GOR for the source oil (reservoir) defines this relationship. The gas, which is primarily methane, is compressible and therefore the volumetric rate of the gas released is a function of the oil release rate as well as the pressure (hydrostatic pressure as a function of depth) and temperature of the water column which together dictate the state of gas at the release. For a given reservoir specification of oil release rate and GOR, the volumetric rate of gas release would be much greater at a shallower depth (lower pressure) than at deeper depths. The depth dependent volumetric flow rate has a large effect on the release exit velocity and therefore the droplet sizes associated with the release.

Figure 152 presents the OILMAPDeep plume modelling results. This figure shows:

- Plume radius plotted as a function of the height above the sea floor (well-head).
- Plume velocity along the centerline of the blowout as a function of the height above the seafloor. Plume centerline velocity defines the vertical movement of the mixture of gas, oil and water along the centre of the plume.

Figure 152 shows that the deep release would trap within the water column. The model predictions for the deep blowout cases showed that the plume will trap between 300–420 m above the seabed for both the lower flow rates and higher flow rates respectively (Figure 152). The lower flow (6,000 K BPD) will have relatively low plume centerline velocity starting at approximately 0.4 m/s and decreasing to zero as the plume entrains water. This entrainment will also serve to increase the plume radius which will be less than 60 m over most of the water column but expand to over 150 m where it traps. The higher flow (60,000 BPD) release shows similar trend in behaviour though with higher centerline velocities and larger plume radius; the centerline velocity starts at approximately 1 m/s and decreases to zero and the radius is less than 80 m over most of the water column but expands to just above 180 m where it traps.

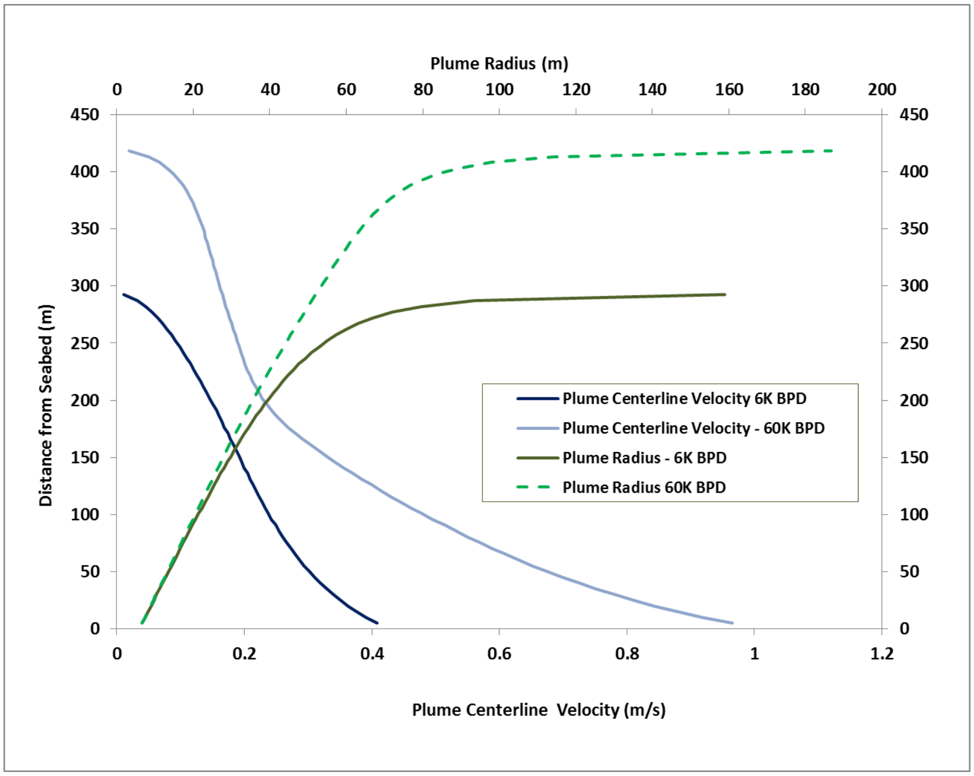

Figure 152. Plume radius and centerline velocity from deep blowout site (~ 1,008 m depth).

Figure 153 presents the OILMAPDeep droplet size results for the deepwater blowout site. There are three unique cases of droplet size distributions for the deep location; the high flow untreated, high flow treated at a DOR of 1:60; and low flow untreated. For each of these three cases the figure shows two results:

- Cumulative droplet size distribution.
- Free rise velocity of droplets associated with the predicted droplet size distribution.

Figure 153 illustrates that the low flow untreated has the largest droplets, ranging from 2,000 um to 10,000 um which have free rise velocities between 6-12 cm/s. The high flow 60,000 bpd untreated has droplets ranging from 1,200 to 6,400 um which have associated free rise velocities ranging between 3.4 –12 cm/s. And the high flow treated at a DOR of 1:60 has the smallest droplets ranging from 5-30 um with associated free rise velocities between 0.0002 – 0.0042 cm/s. Due to the large differences in droplet size and rise velocities a logarithmic scale was use for the axis displaying these parameters. The droplets associated with the untreated release will rise much faster than the treated droplets. The untreated droplets would reach the surface on the order of a few hours whereas the treated droplets would take months based on free rise velocity alone, however in reality would likely not surface due to other processes at play within that time scale (e.g., vertical turbulence and biodegradation or decay).

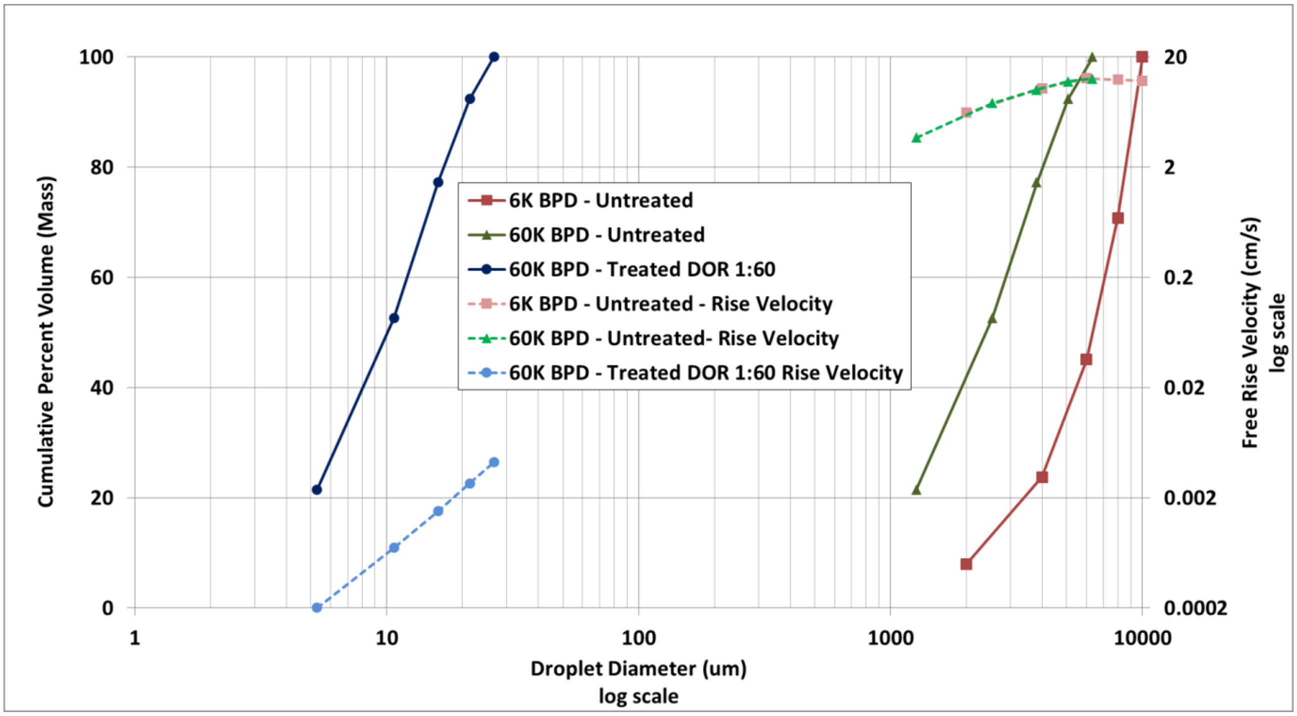

Figure 153. Cumulative percent mass and free rise velocity for droplet size distributions associated with blowouts at deep blowout site (~1,008 m depth).

7.4.3 Stochastic Analysis Results

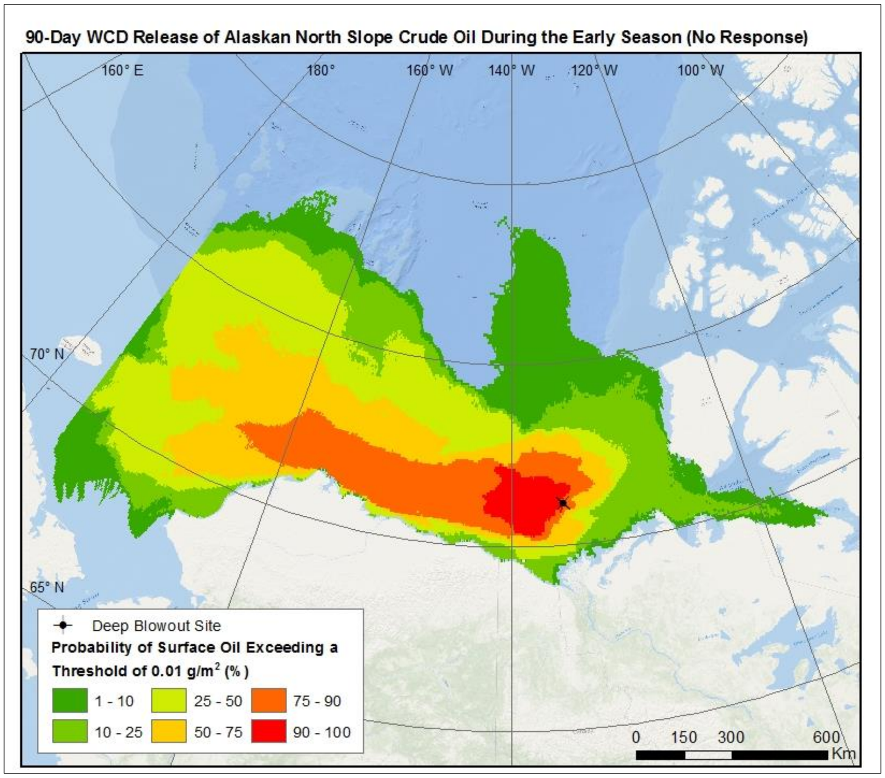

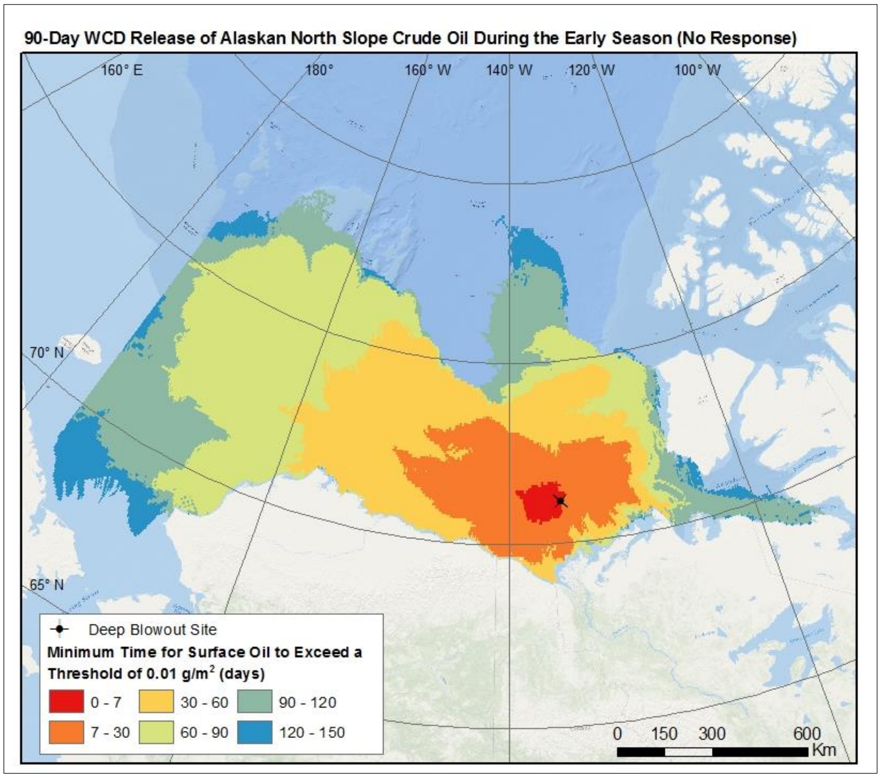

Figure 154. DeepWCD_90rel_noresp_early - Water surface oiling probabilities and minimum travel times for floating oil ≥0.01 g/m^2.

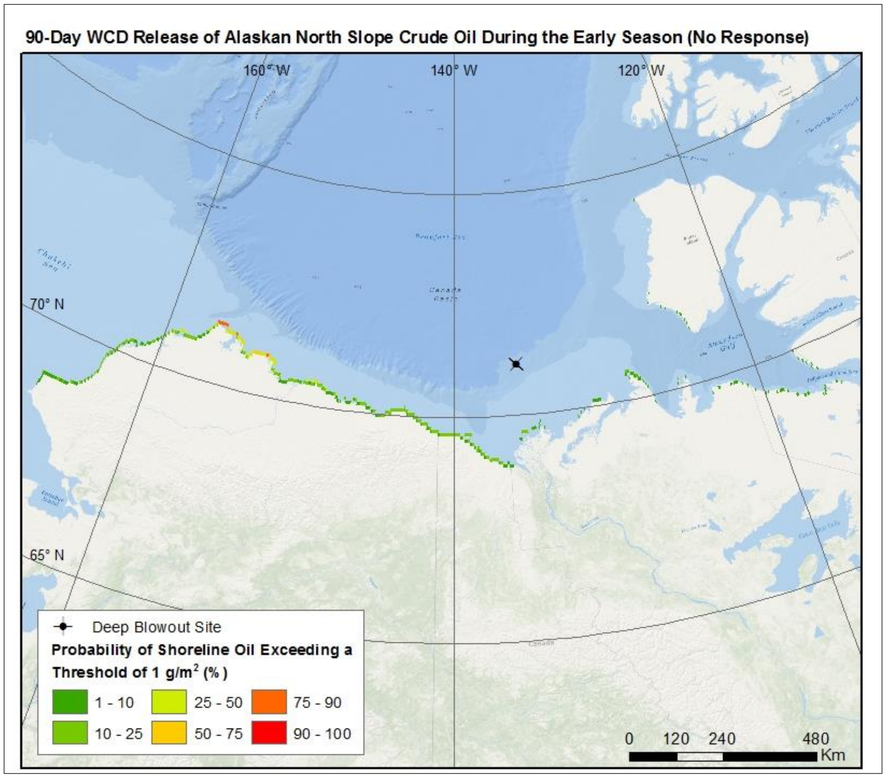

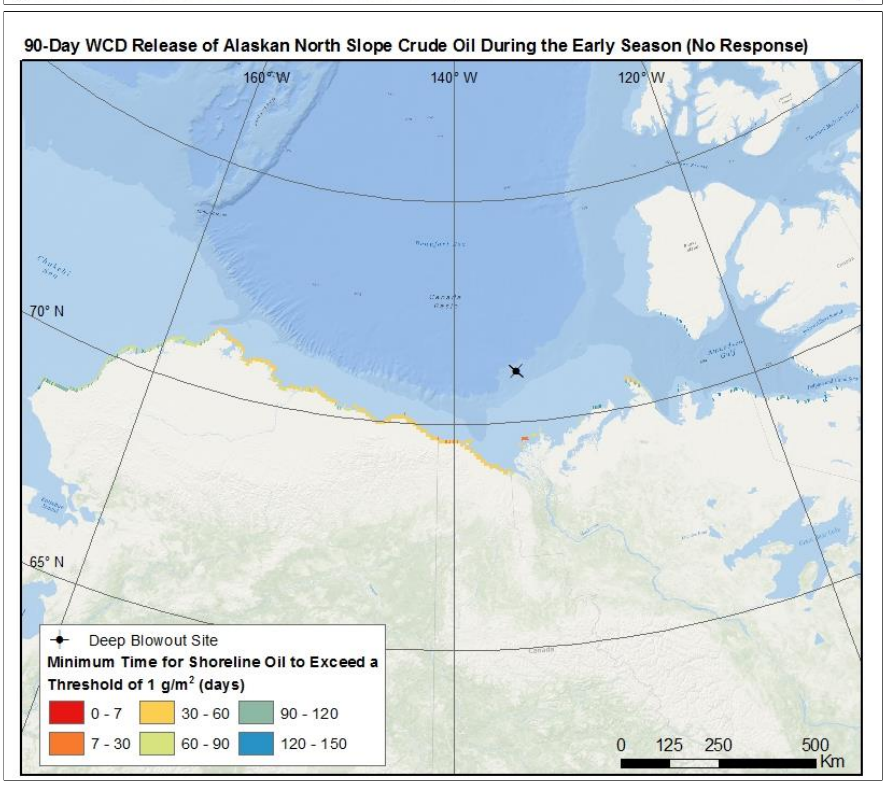

Figure 155. DeepWCD_90rel_noresp_early - Shoreline oiling probabilities and minimum travel times for shoreline oil ≥1 g/m^2.

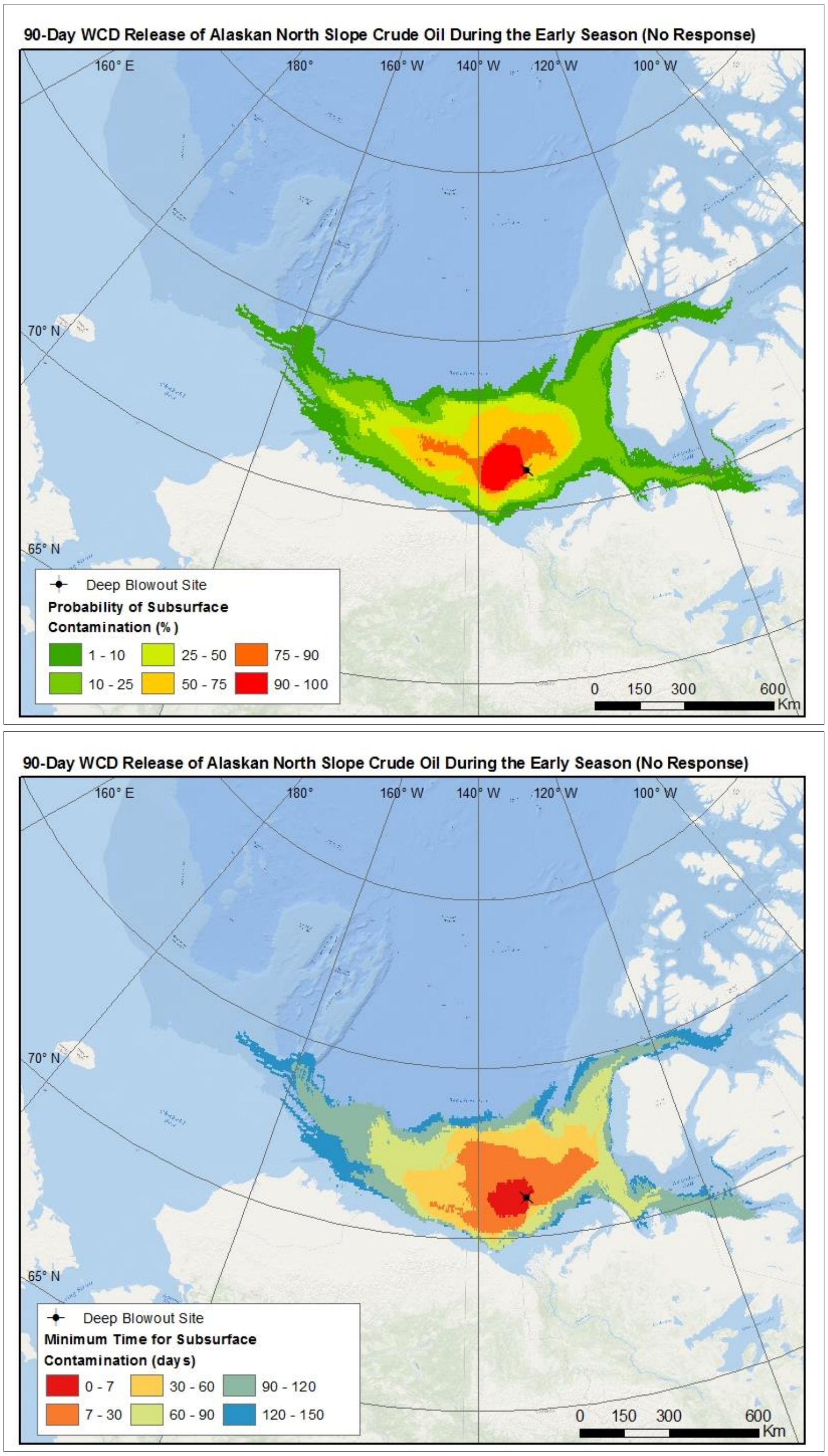

Figure 156. DeepWCD_90rel_noresp_early - Subsurface contamination probabilities and minimum travel times for total oil in the water column.

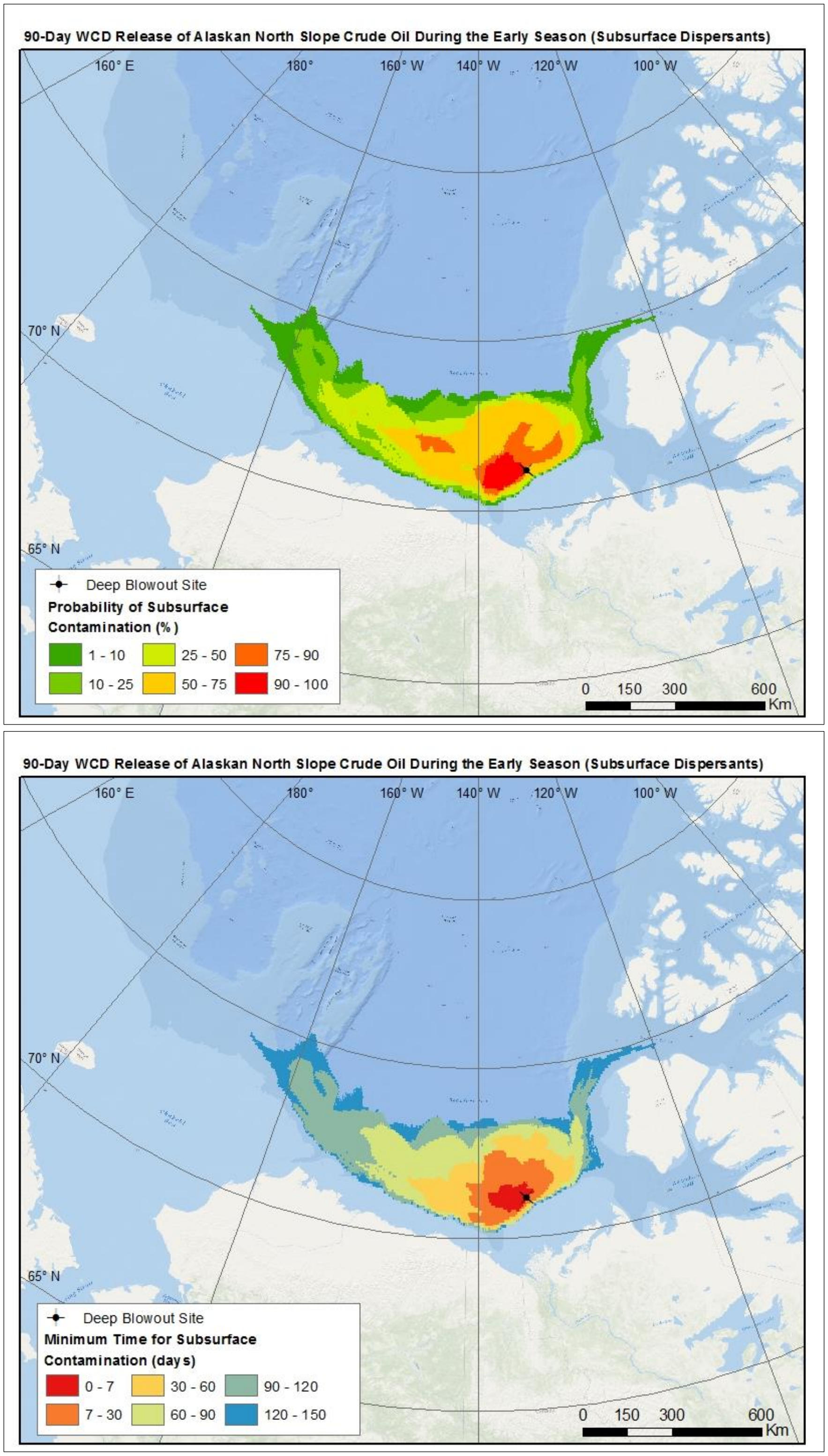

Figure 157. DeepWCD_90rel_subresp_early - Subsurface contamination probabilities and minimum travel times for total oil in the water column.

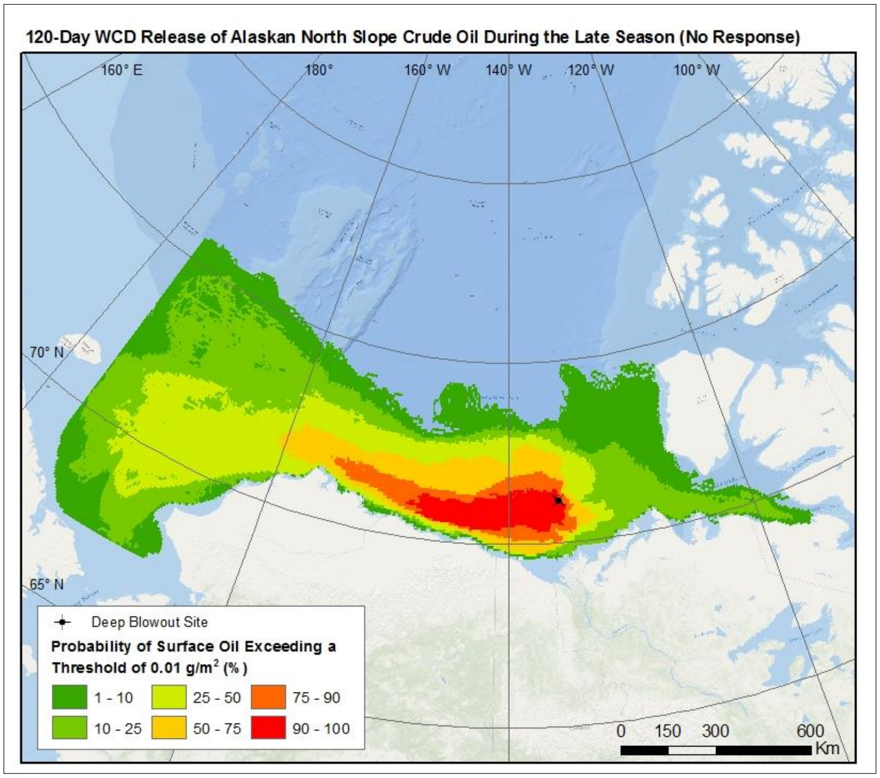

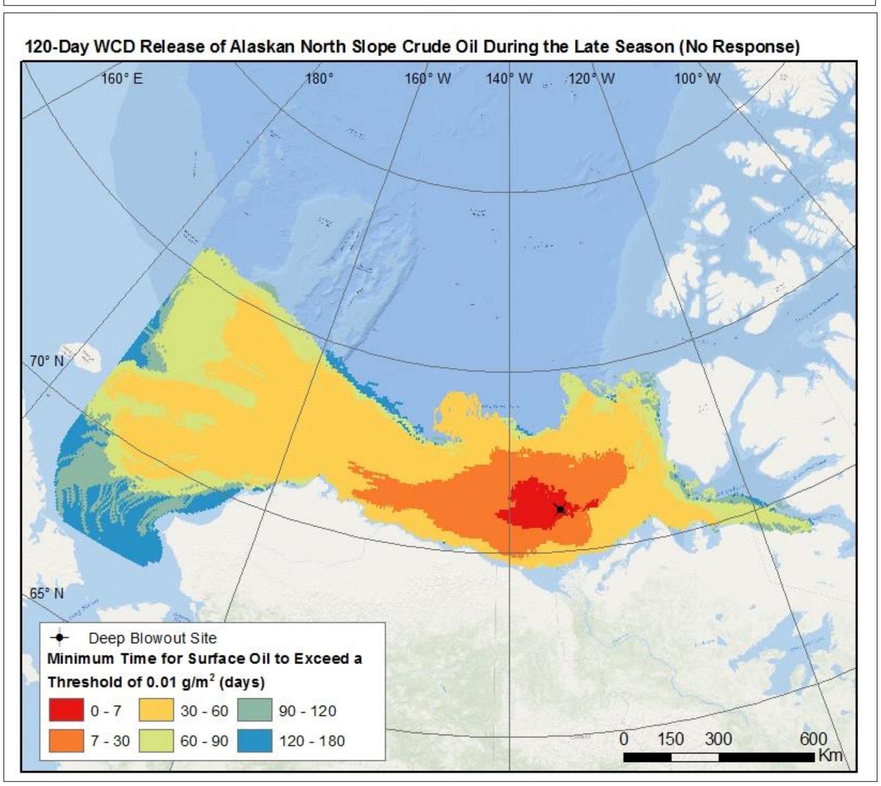

Figure 158. DeepWCD_120rel_noresp_late - Water surface oiling probabilities and minimum travel times for floating oil ≥0.01 g/m^2.

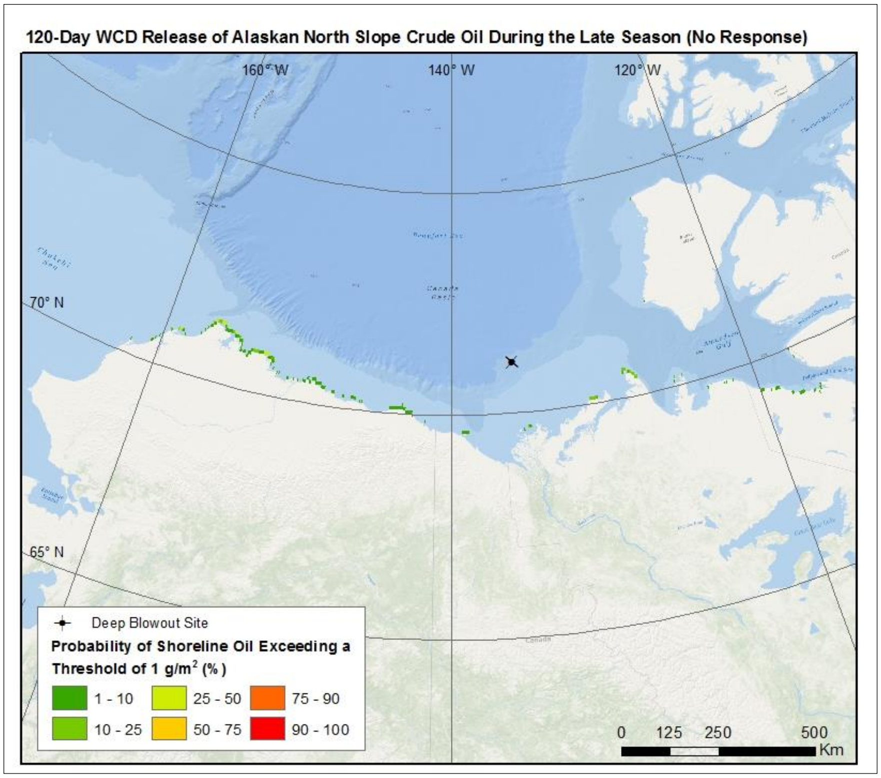

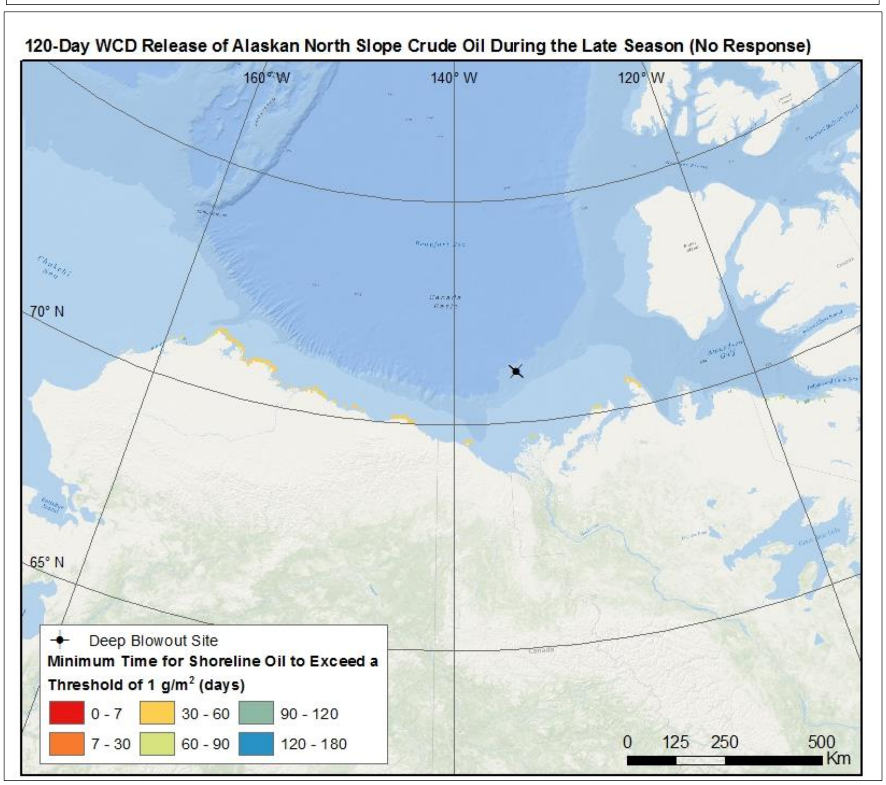

Figure 159. DeepWCD_120rel_noresp_late - Shoreline oiling probabilities and minimum travel times for shoreline oil ≥1 g/m².

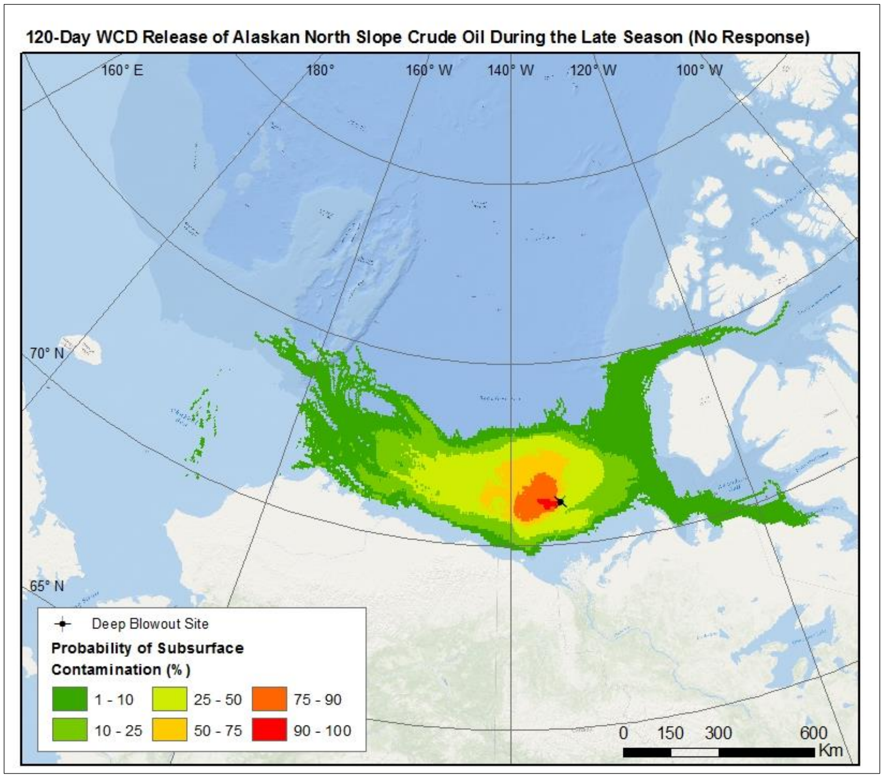

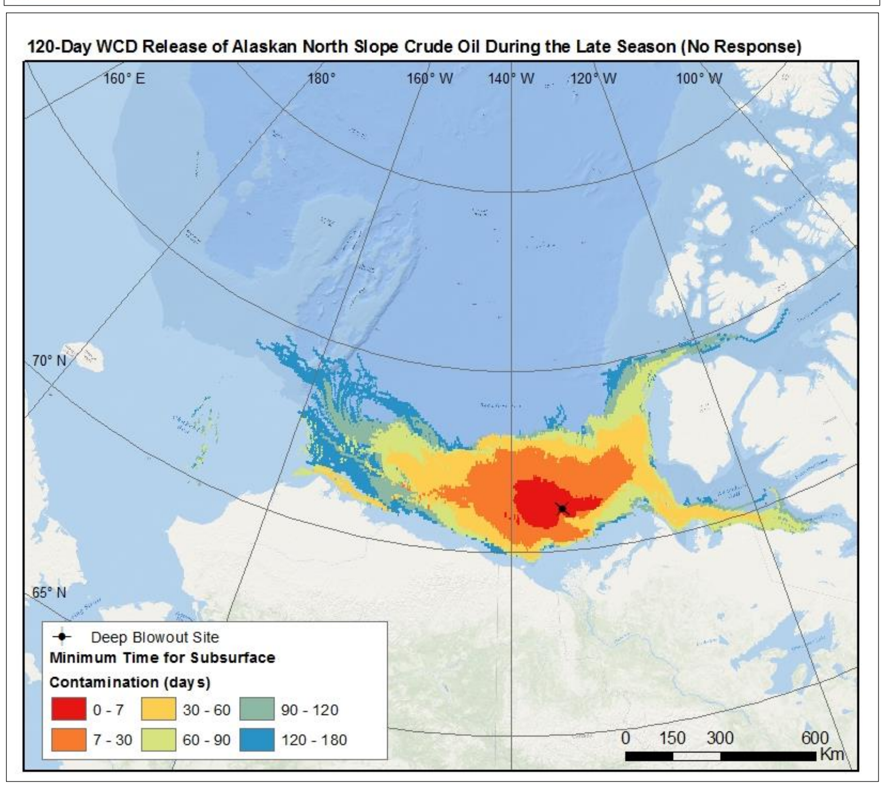

Figure 160. DeepWCD_120rel_noresp_late - Subsurface contamination probabilities and minimum travel times for total oil in the water column.

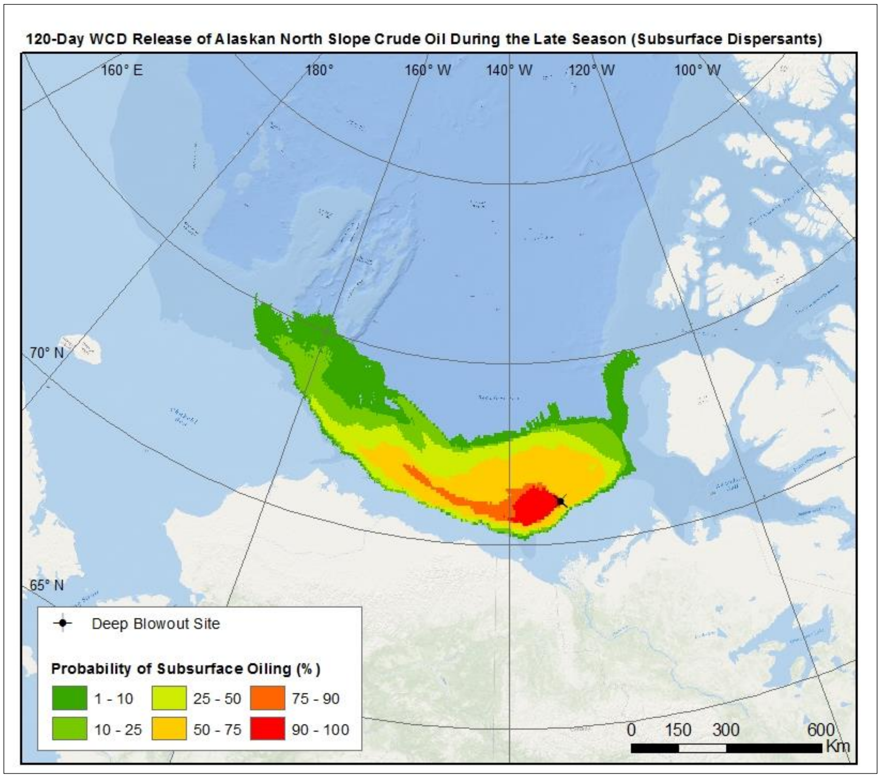

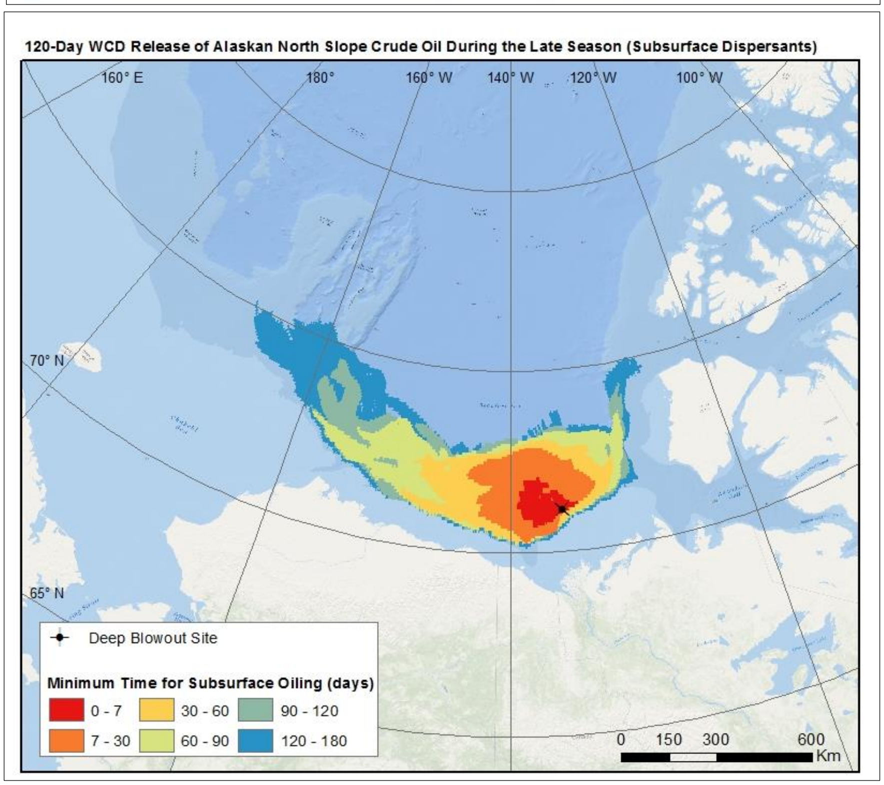

Figure 161. DeepWCD_120rel_subresp_late - Subsurface contamination probabilities and minimum travel times for total oil in the water column.

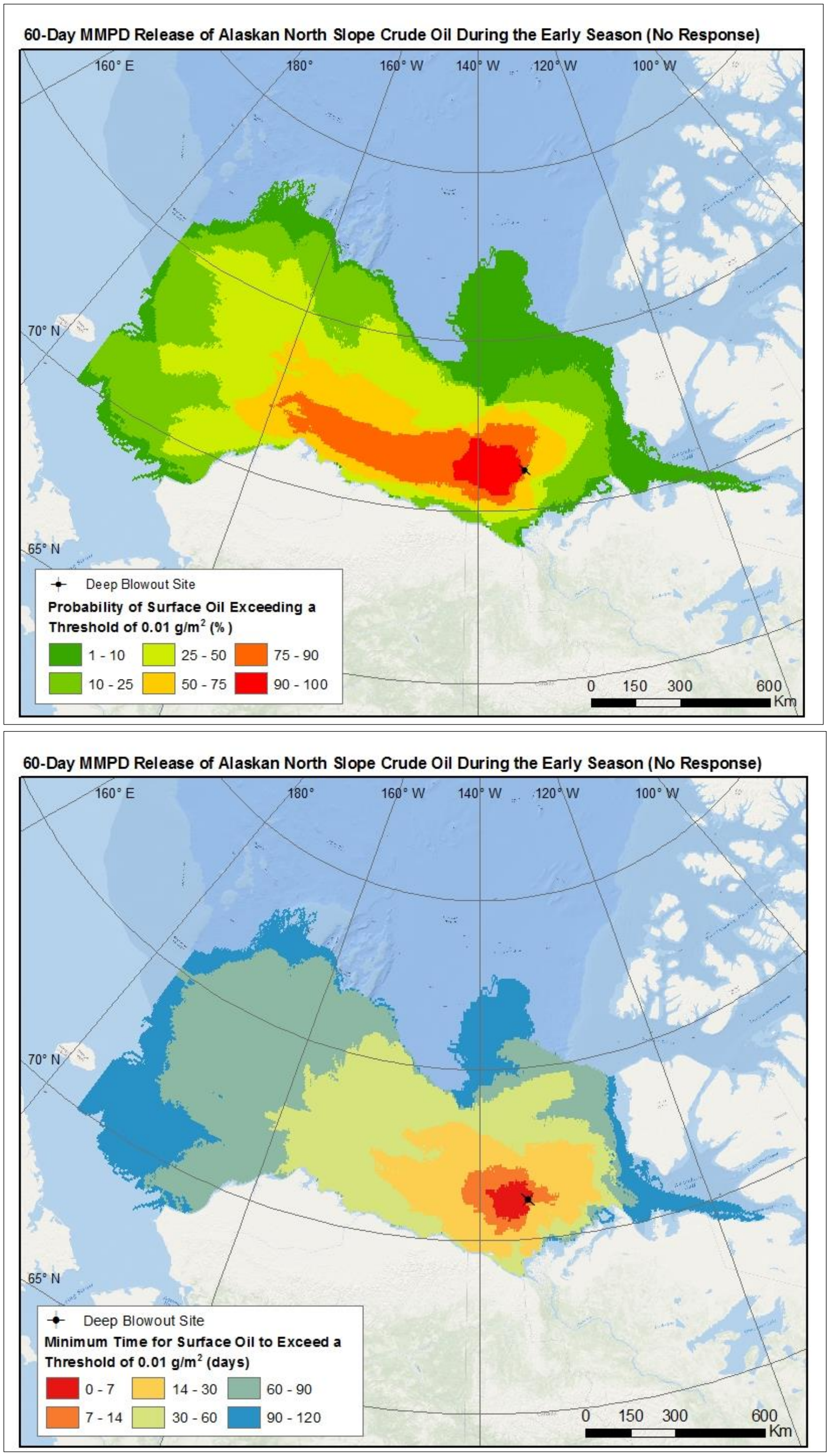

Figure 162. DeepMMPD_60rel_noresp_early - Water surface oiling probabilities and minimum travel times for floating oil ≥0.01 g/m^2.

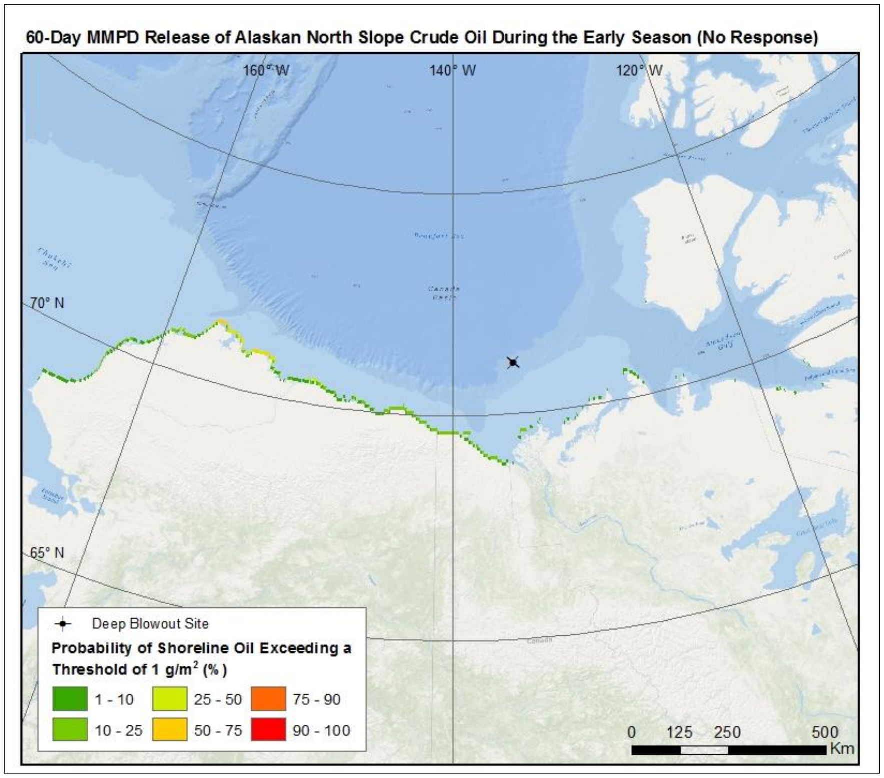

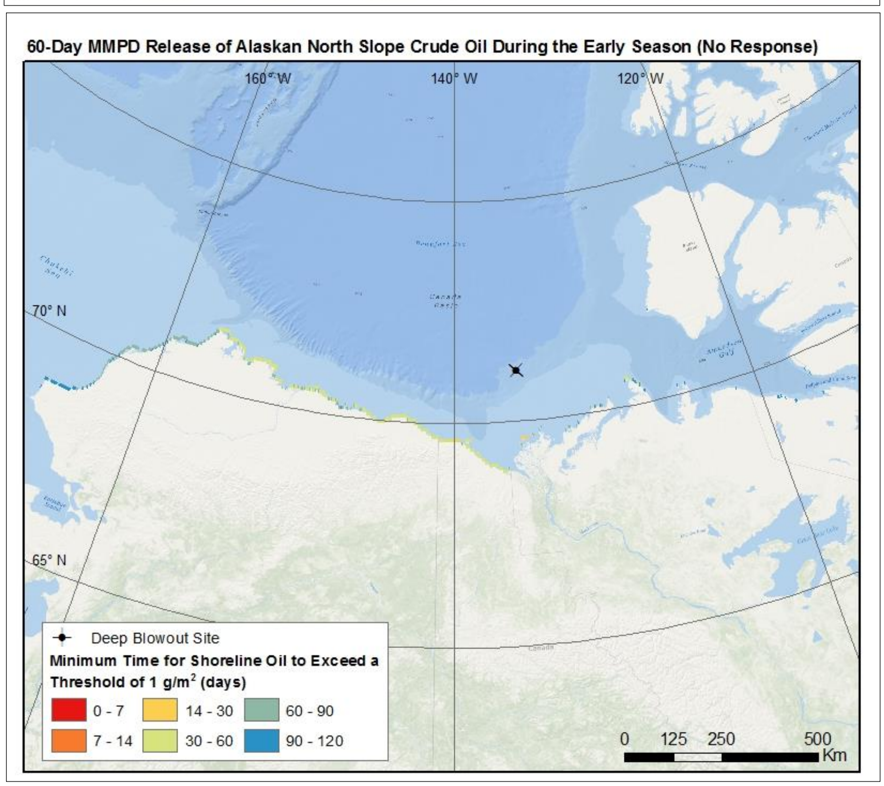

Figure 163. DeepMMPD_60rel_noresp_early - Shoreline oiling probabilities and minimum travel times for shoreline oil ≥1 g/m^2.

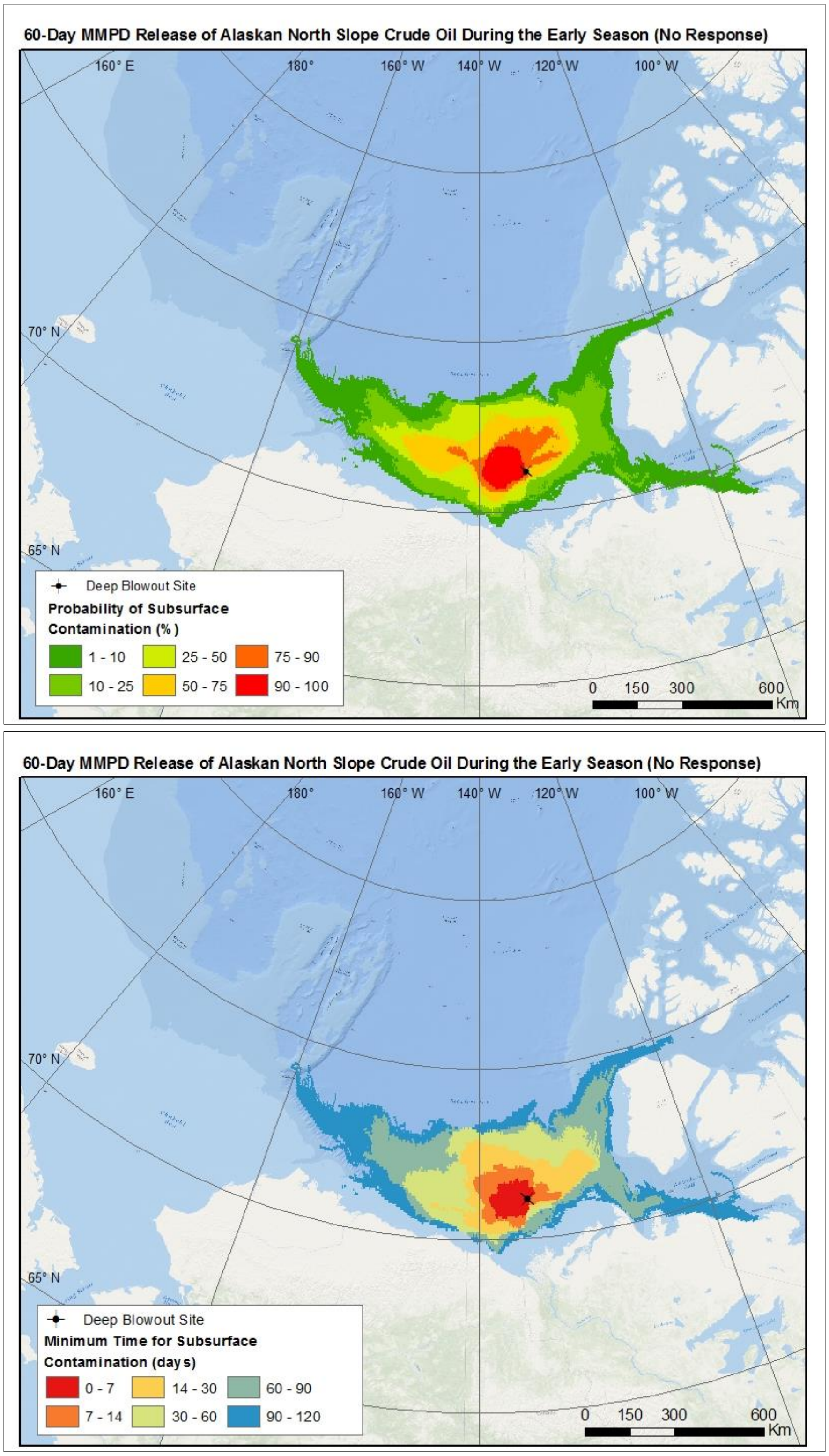

Figure 164. DeepMMPD_60rel_noresp_early - Subsurface contamination probabilities and minimum travel times for total oil in the water column.

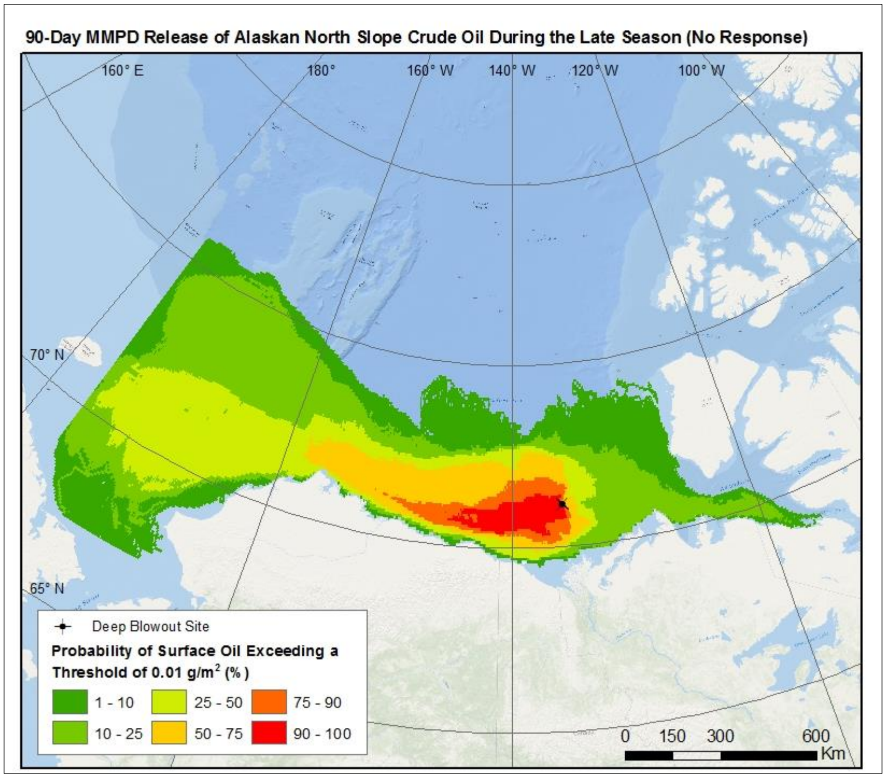

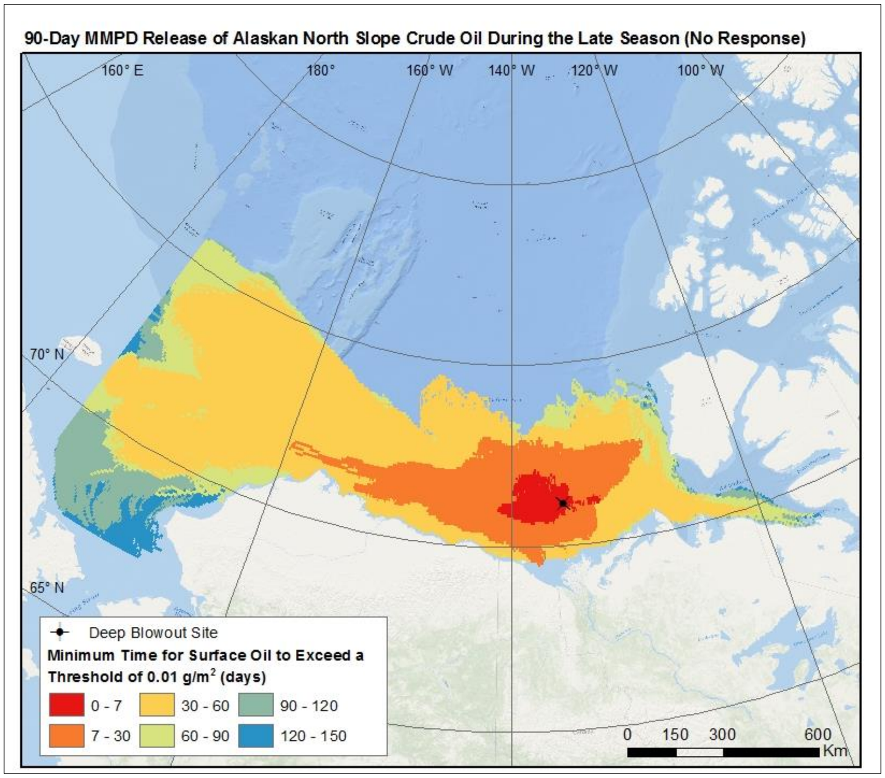

Figure 165. DeepMMPD_90rel_noresp_late - Water surface oiling probabilities and minimum travel times for floating oil ≥0.01 g/m^2.

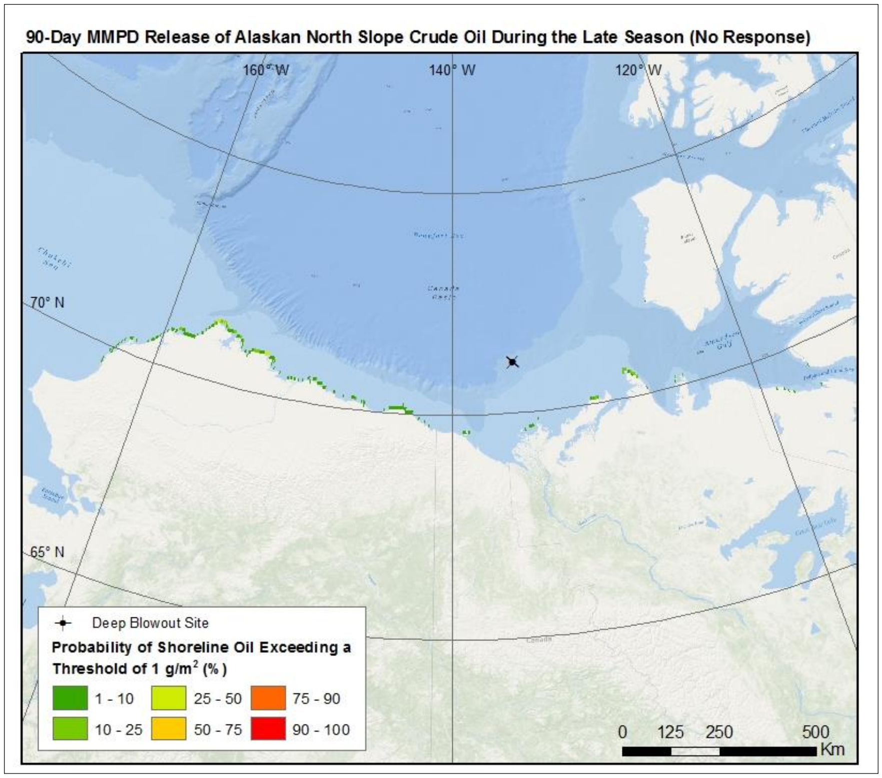

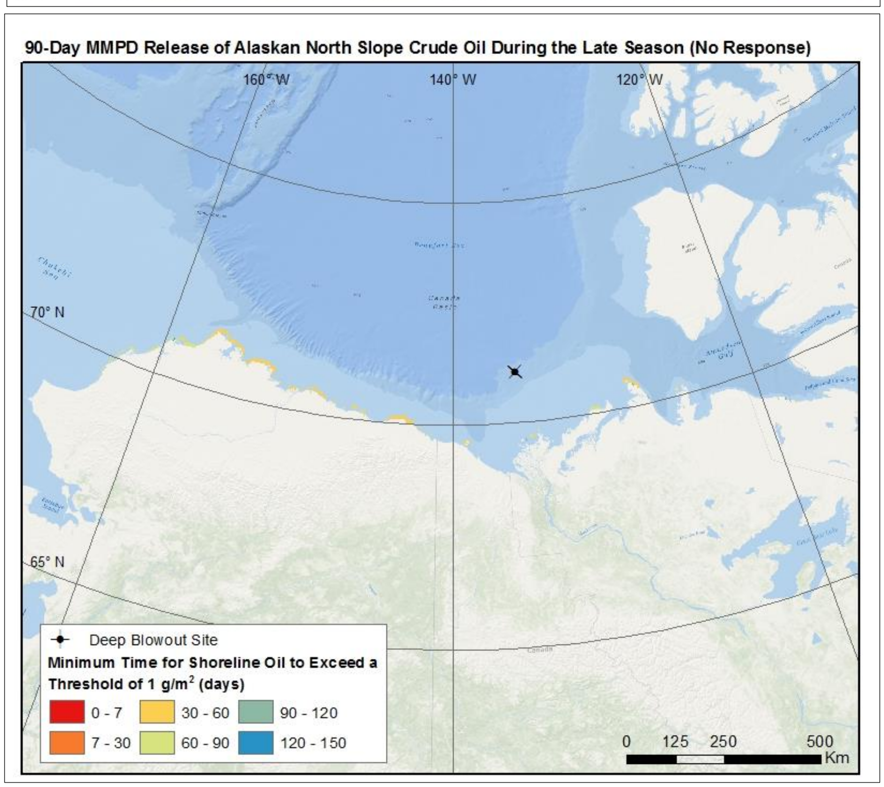

Figure 166. DeepMMPD_90rel_noresp_late - Shoreline oiling probabilities and minimum travel times for shoreline oil ≥1 g/m^2.

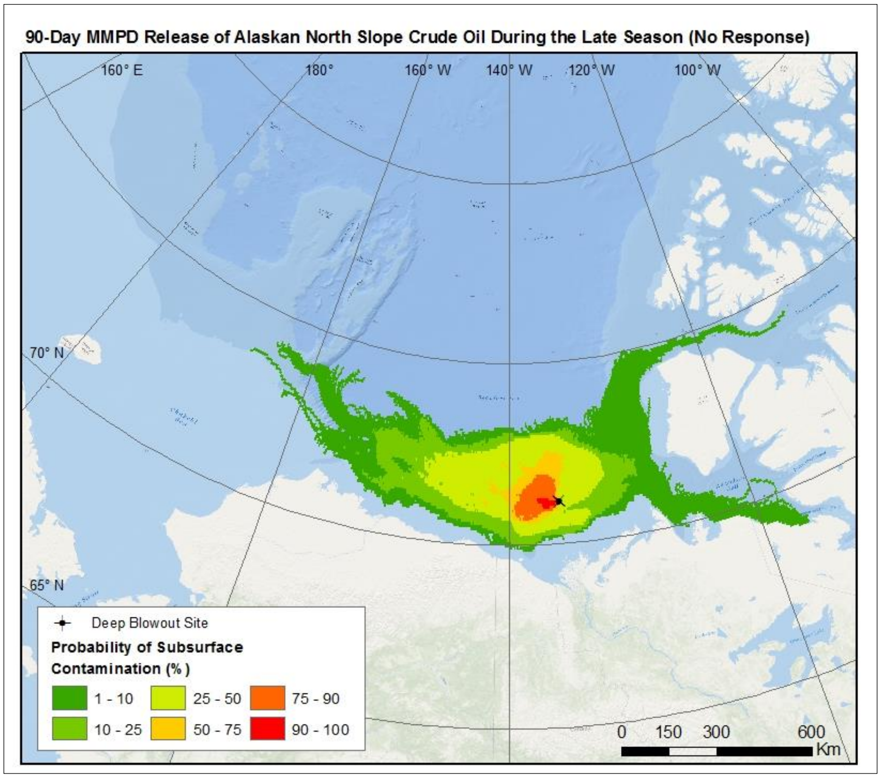

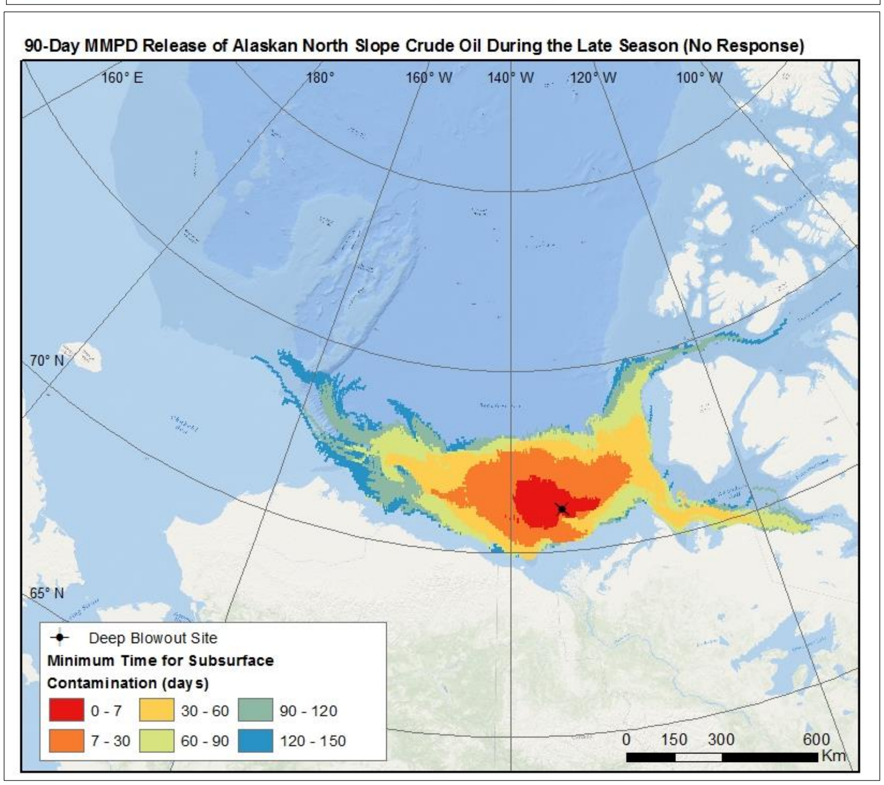

Figure 167. DeepMMPD_90rel_noresp_late - Subsurface contamination probabilities and minimum travel times for total oil in the water column.

7.4.4 Individual Trajectory Model Results

Note: Only 95th percentile surface and shoreline oiling runs were evaluated for the MMPD Deep Blowout scenarios. Surface response measures were *only* simulated for the 95th percentile individual trajectories for degree of surface and shoreline oiling from the base case or parent stochastic scenario (no response). Individual subsurface response scenarios that travelled to the southwest and exhibited the most extensive subsea contamination that lingered the longest along the Beaufort Shelf were selected to be the representative worst-case individual runs. Identifying the 95th percentile run was not possible since all runs resulted in the same amount of subsurface oil contamination (i.e., all oil dispersed). It was assumed that the runs where oil built up along the shelf would have higher effects on productive coastal waters as opposed to those that travelled west and to the north of the spill site, water column contamination remaining in deep slope waters.

95th Percentile Surface Oiling

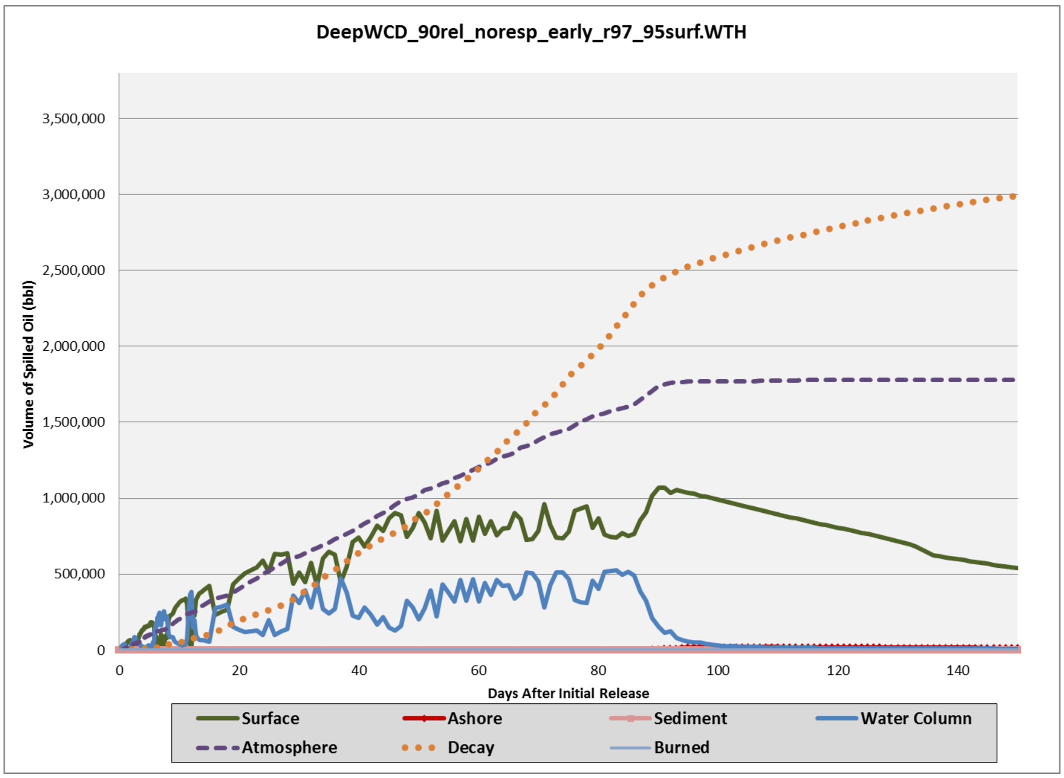

Figure 168. DeepWCD_90rel_noresp_early_r97_95surf - Mass balance chart. The blowout begins during the ice-free period and collects under ice beginning at about day 90. Start date: 6/29/2009.

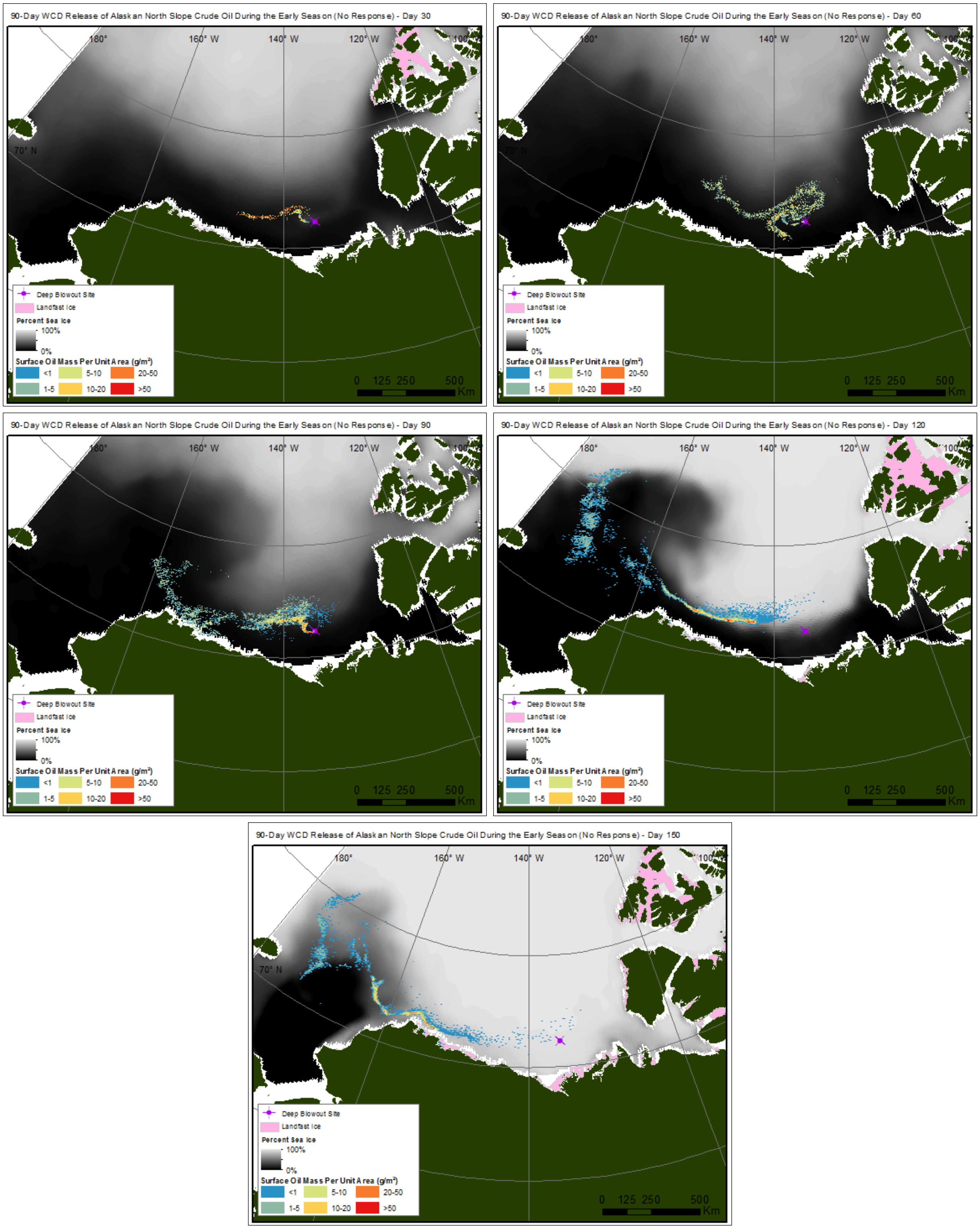

Figure 169. DeepWCD_90rel_noresp_early_r97_95surf – Time series maps of spill floating surface oil mass per unit area (g/m^2) (day 30, 60, 90, 120, 150; July – December 2009). Pink polygons represent monthly average landfast ice. Grey scale contours represent ice percent coverage for that month from TOPAZ4 model. White indicates areas of no data for ice coverage. Start date: 6/29/2009.

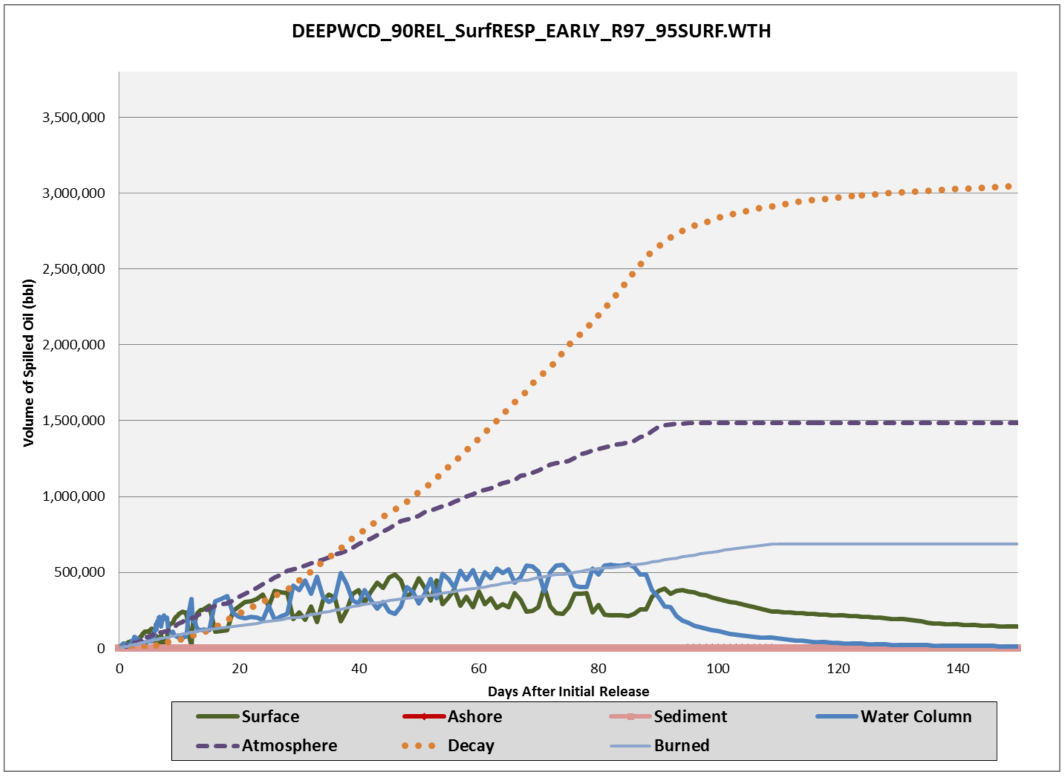

Figure 170. DeepWCD_90rel_surfresp_early_r97_95surf - Mass balance chart. **Surface response case including dispersant application and *in situ* burning**. Start date: 6/29/2009.

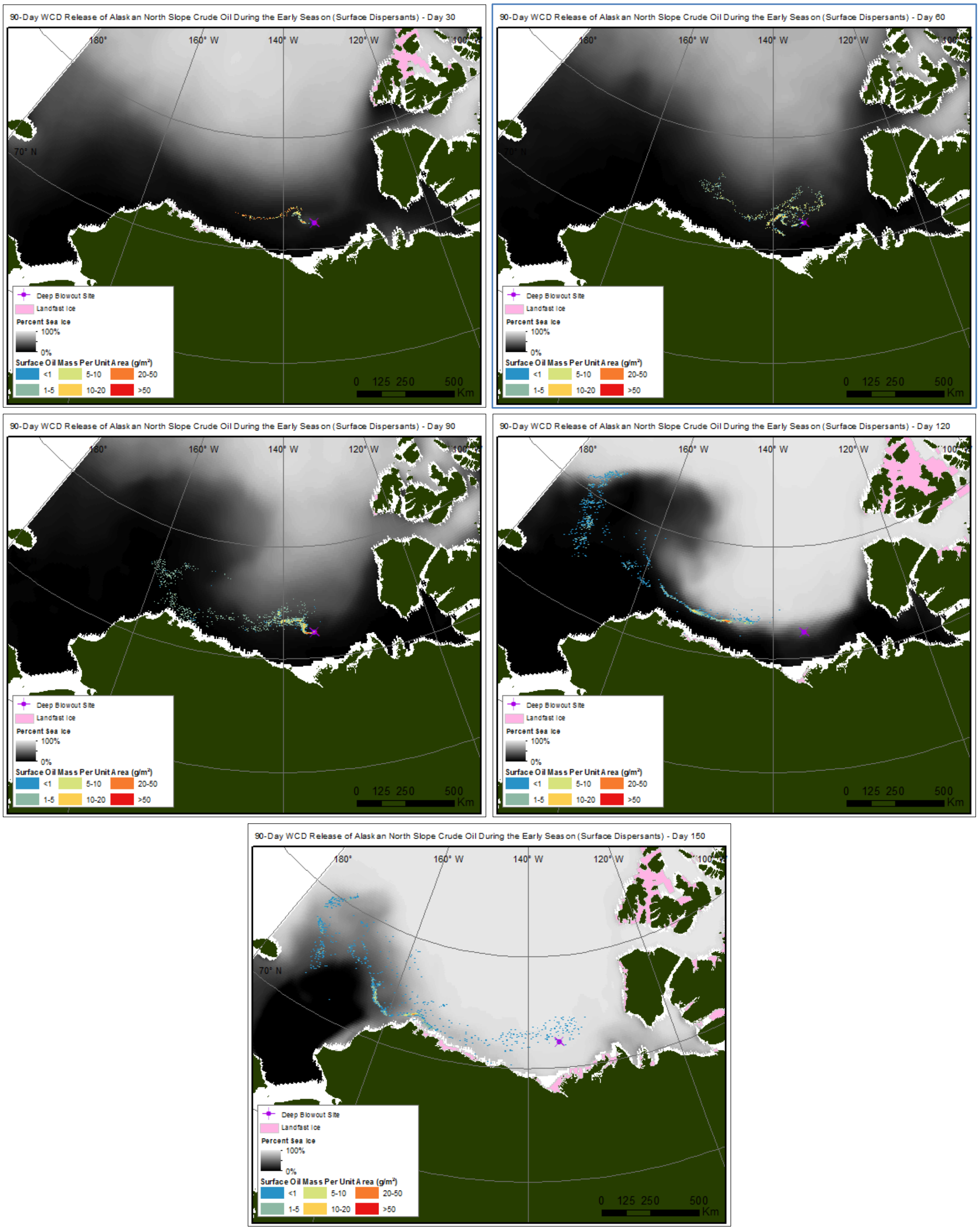

Figure 171. DeepWCD_90rel_surfresp_early_r97_95surf – Time series maps of spill floating surface oil mass per unit area (g/m^2) (day 30, 60, 90, 120, 150; July – December 2009). **Surface response case including dispersant application and *in situ* burning**. Pink polygons represent monthly average landfast ice. Grey scale contours represent ice percent coverage for that month from TOPAZ4 model. White indicates areas of no data for ice coverage. Start date: 6/29/2009.

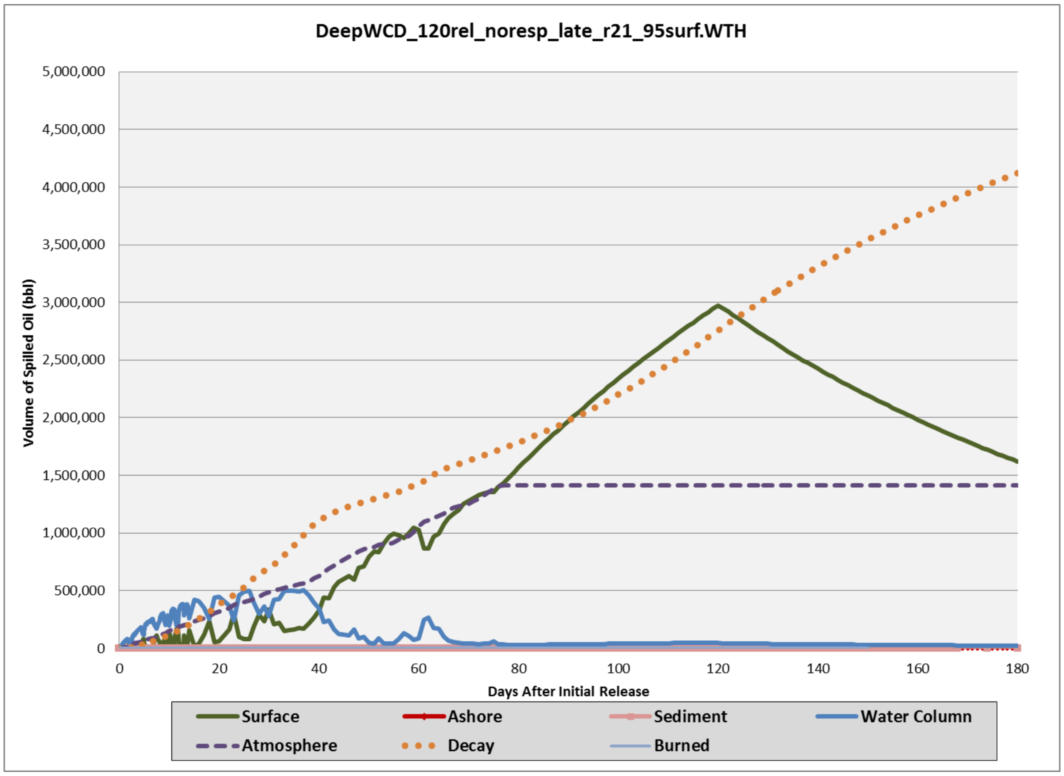

Figure 172. DeepWCD_120rel_noresp_late_r21_95surf - Mass balance chart. Start date: 8/16/2009.

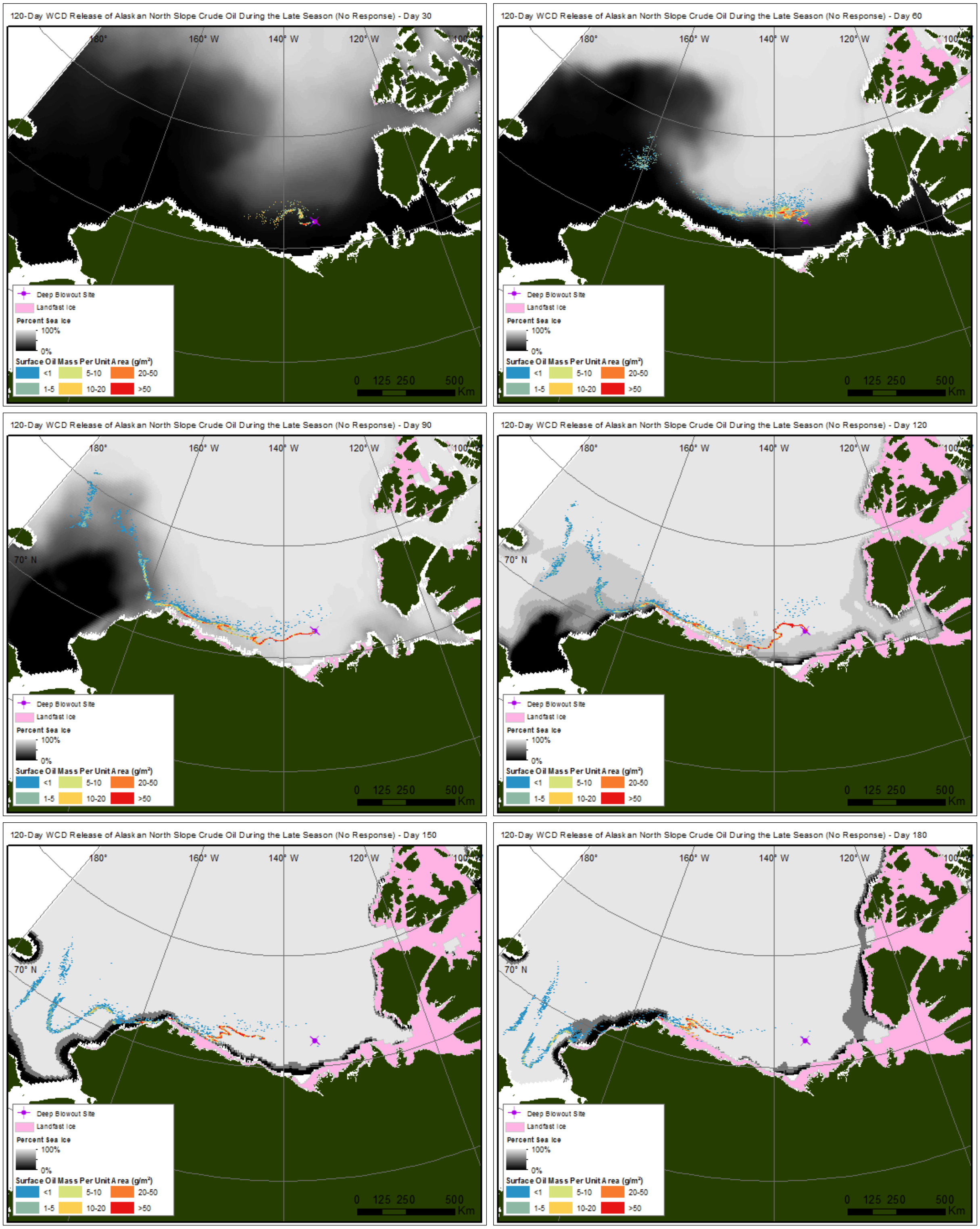

Figure 173. DeepWCD_120rel_noresp_late_r21_95surf – Time series maps of spill floating surface oil mass per unit area (g/m^2) (day 30, 60, 90, 120, 150, 180; September 2009 – February 2010). Pink polygons represent monthly average landfast ice. Grey scale contours represent ice percent coverage for that month from TOPAZ4 model. White indicates areas of no data for ice coverage. Start date: 8/16/2009.

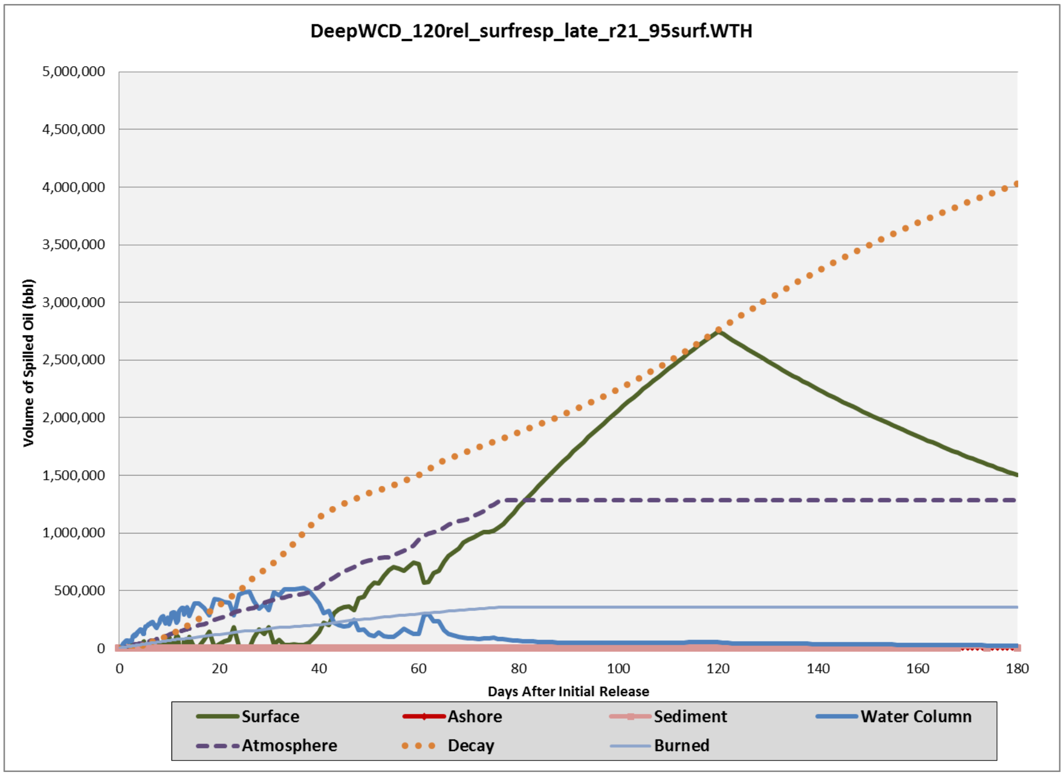

Figure 174. DeepWCD_120rel_surfresp_late_r21_95surf - Mass balance chart. **Surface response case including dispersant application and *in situ* burning**. Start date: 8/16/2009.

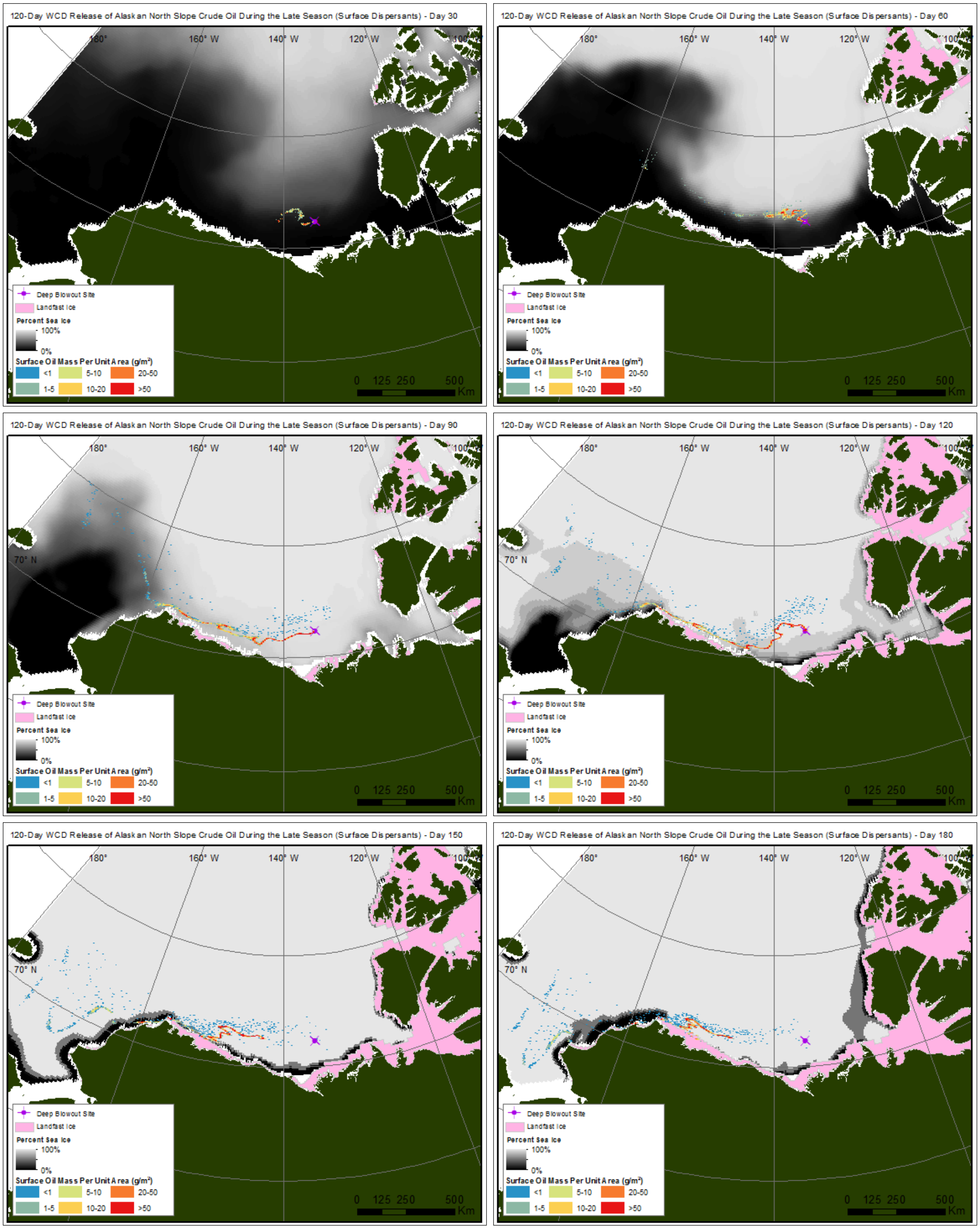

Figure 175. DeepWCD_120rel_surfresp_late_r21_95surf – Time series maps of spill floating surface oil mass per unit area (g/m^2) (day 30, 60, 90, 120, 150, 180; September 2009 – February 2010). **Surface response case including dispersant application and *in situ* burning**. Pink polygons represent monthly average landfast ice. Grey scale contours represent ice percent coverage for that month from TOPAZ4 model. White indicates areas of no data for ice coverage. Start date: 8/16/2009.

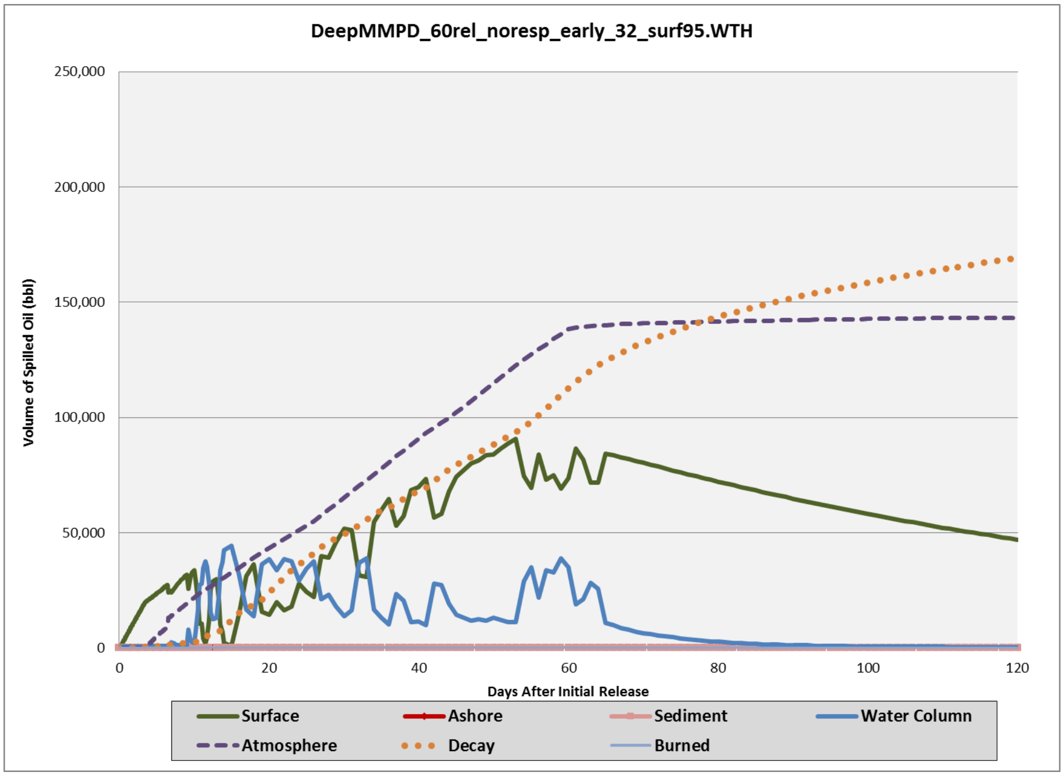

Figure 176. DeepMMPD_60rel_noresp_early_r32_95surf - Mass balance chart. Start date: 6/3/2009.

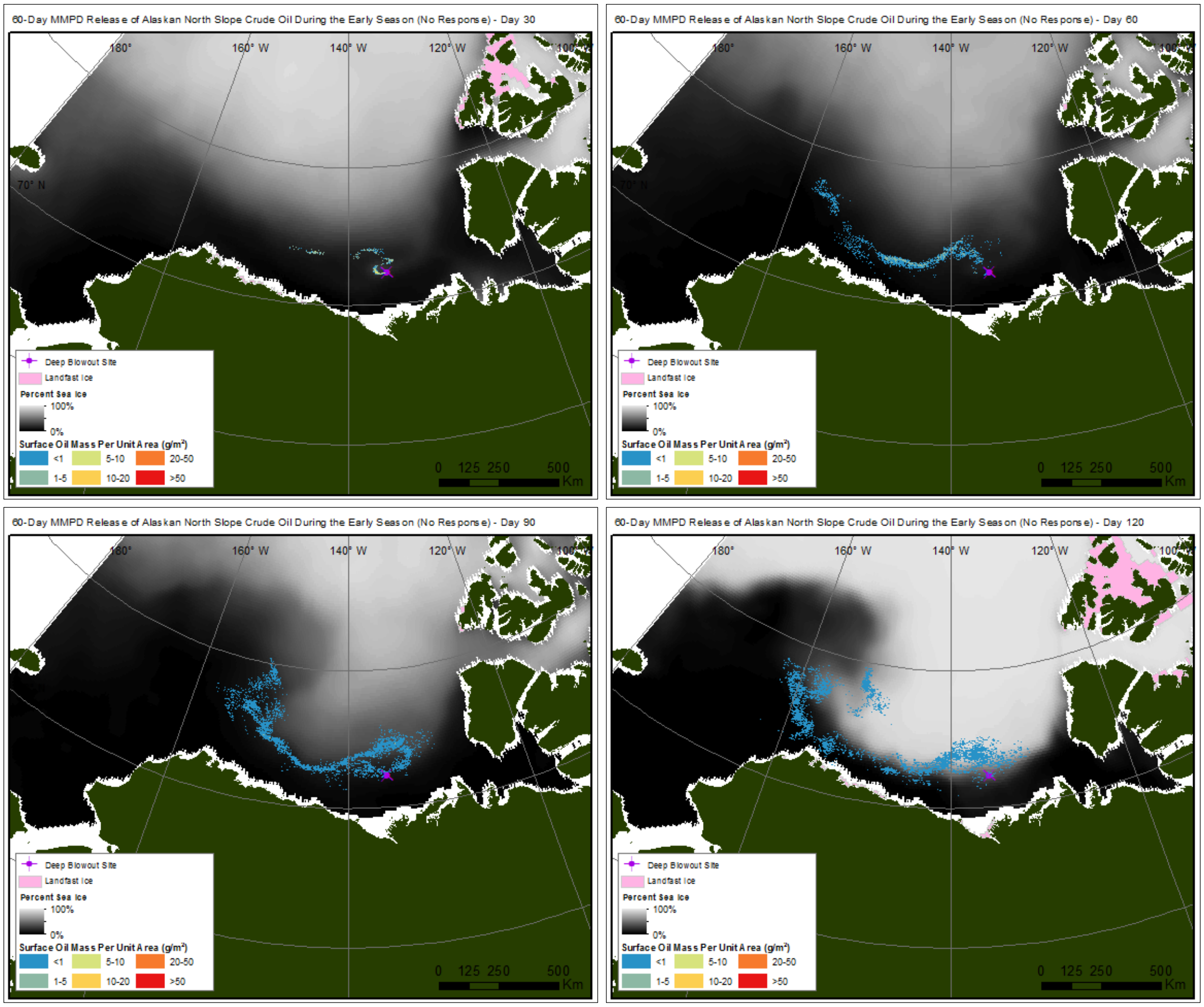

Figure 177. DeepMMPD_60rel_noresp_early_r32_95surf – Time series maps of spill floating surface oil mass per unit area (g/m^2) (day 30, 60, 90, 120; July – October 2009). Pink polygons represent monthly average landfast ice. Grey scale contours represent ice percent coverage for that month from TOPAZ4 model. White indicates areas of no data for ice coverage. Start date: 6/3/2009.

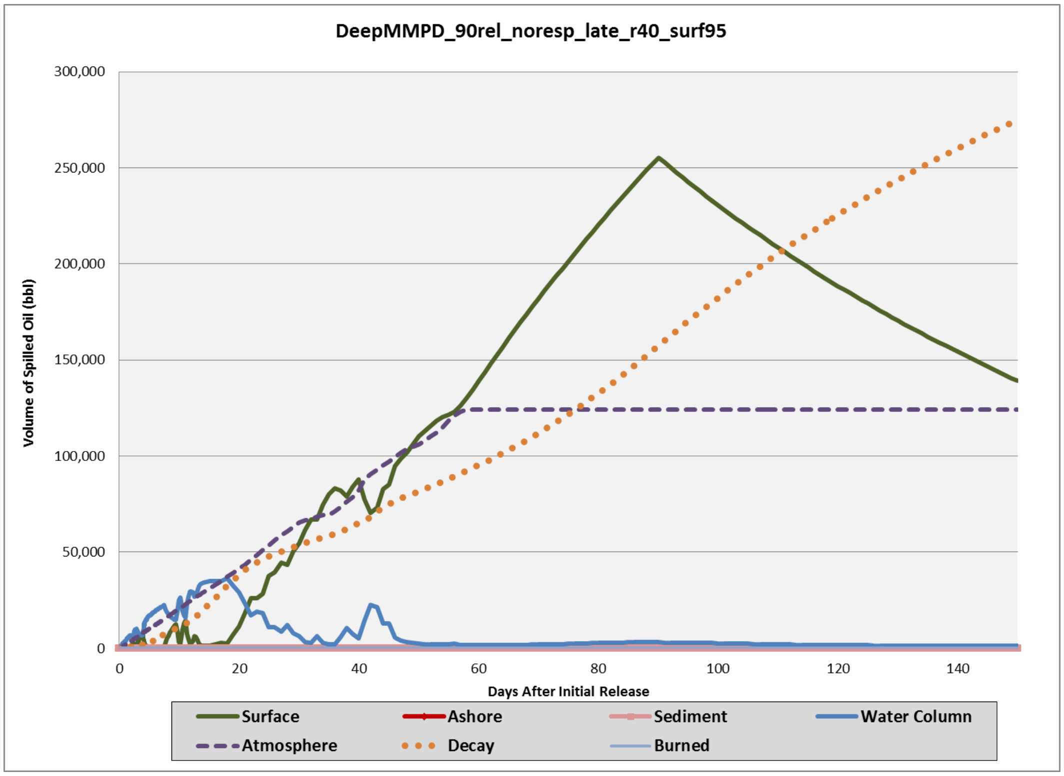

Figure 178. DeepMMPD_90rel_noresp_late_r40_95surf - Mass balance chart. In this scenario, oil becomes trapped under ice after about 60 days. The end of the release at 90 days is evident, as floating oil no longer accumulates under the ice and oil already trapped degrades over time. Start date: 9/4/2009.

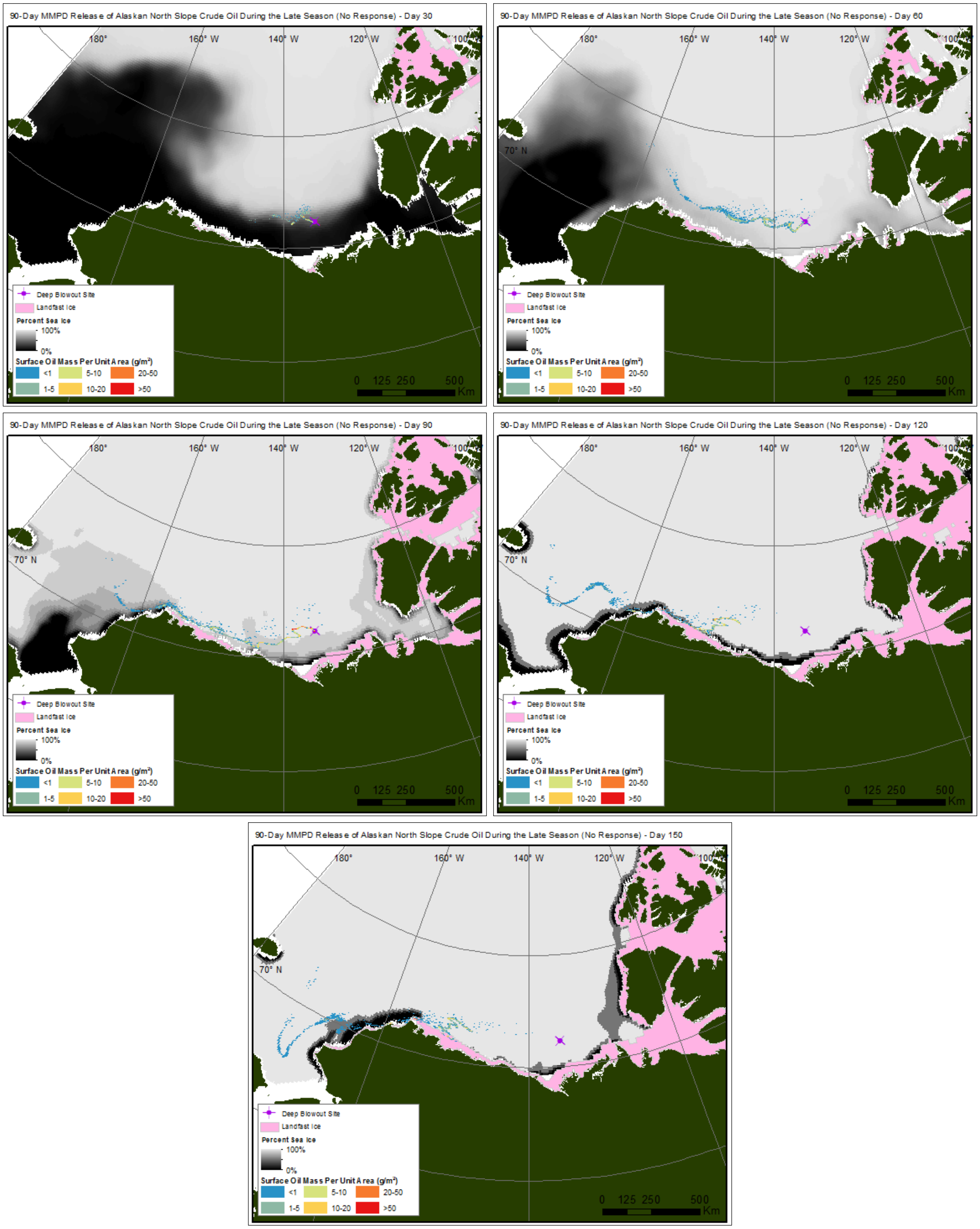

Figure 179. DeepMMPD_90rel_noresp_late_r40_95surf – Time series maps of spill floating surface oil mass per unit area (g/m^2) (day 30, 60, 90, 120, 150; October 2009 – February 2010). Pink polygons represent monthly average landfast ice. Grey scale contours represent ice percent coverage for that month from TOPAZ4 model. White indicates areas of no data for ice coverage. Start date: 9/4/2009.

95th Percentile Shoreline Oiling

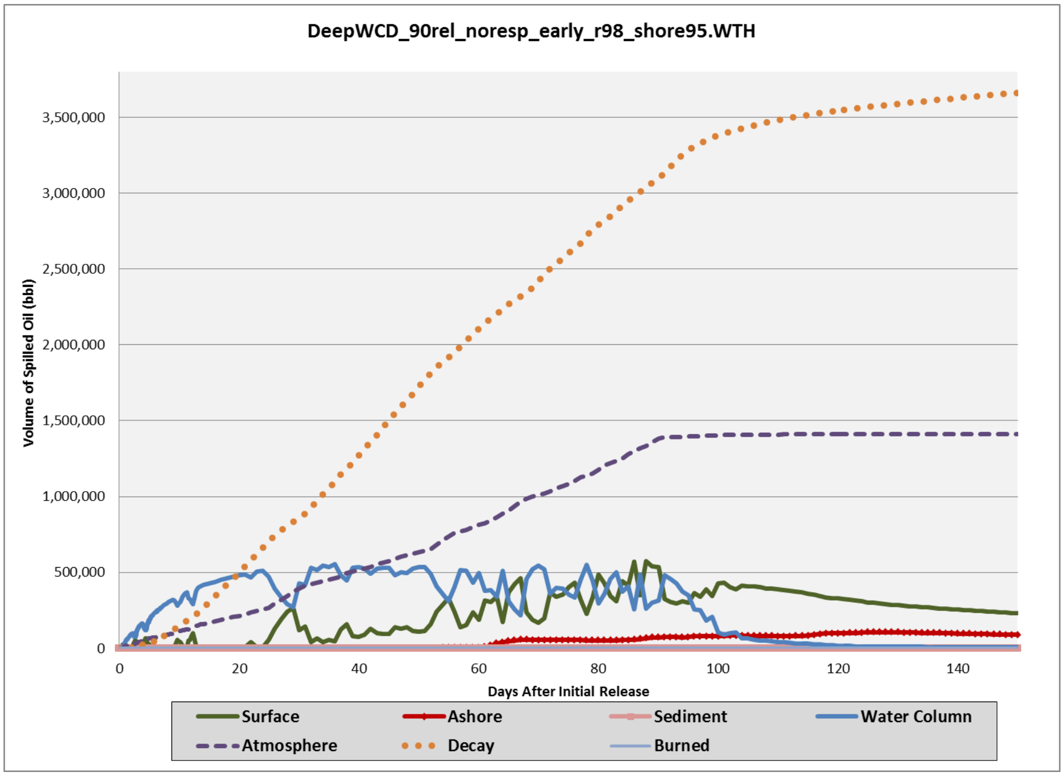

Figure 180. DeepWCD_90rel_noresp_early_r98_95shore - Mass balance chart. Start date: 6/18/2008.

Table 29. DeepWCD_90rel_noresp_early_r98_95shore – Shoreline length oiled (km) by habitat type, for both shore oiling thresholds. Start date: 6/18/2008.

Shore Type	Shore Length Oiled (km)	
	> 100 micrometers	> 1 micrometer
Seaward Rocky Shore	95.8	95.8
Seaward Gravel Beach	630.1	630.1
Seaward Sand Beach	524.3	539.4
Seaward Fringing Mud Flat	408.3	413.4
Seaward Fringing Wetland	10.1	35.3
Seaward Intertidal Macroalgal Bed	146.2	146.2
Total Shoreline	**1,814.8**	**1,860.2**

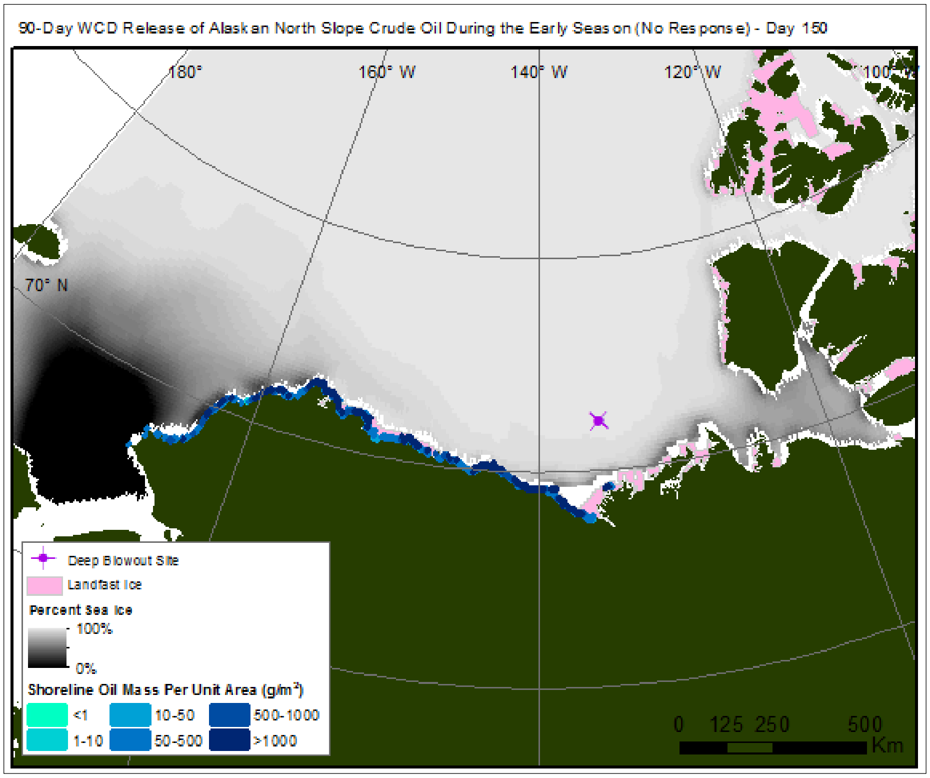

Figure 181. DeepWCD_90rel_noresp_early_r98_95shore – Map of overall effects to shorelines as mass of oil deposited on shore per unit of area (g/m^2) (day 180 – December 2008). Pink polygons represent monthly average landfast ice. Grey scale contours represent ice percent coverage for that month from TOPAZ4 model. White indicates areas of no data for ice coverage. Start date: 6/18/2008.

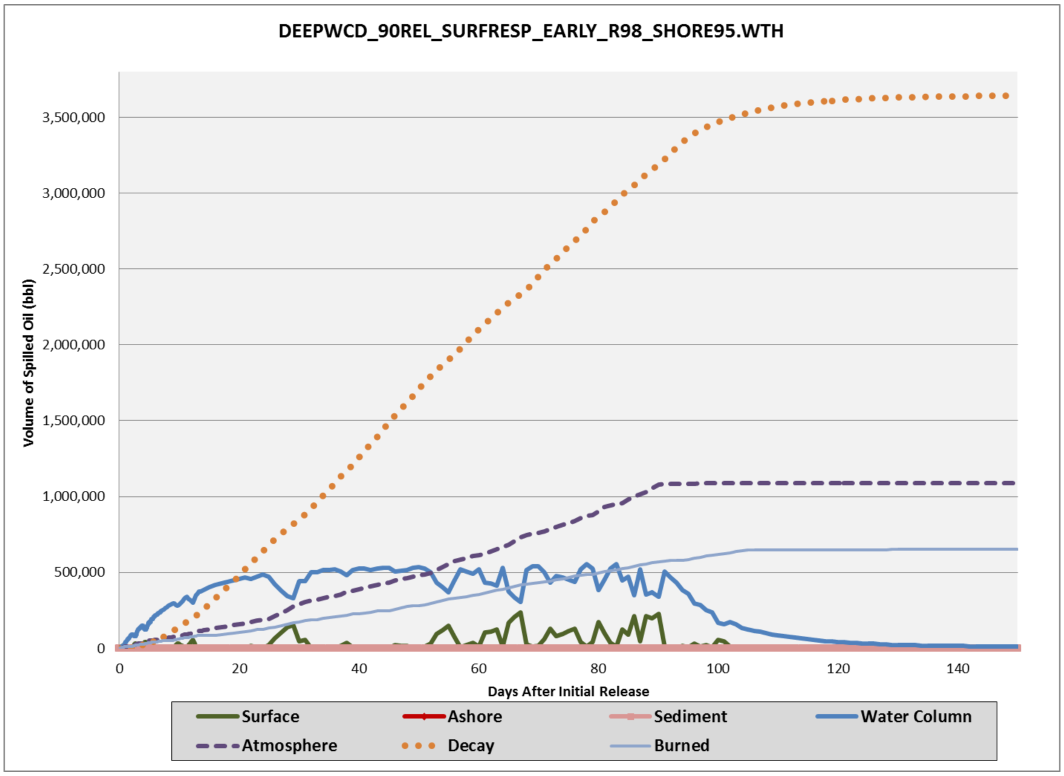

Figure 182. DeepWCD_90rel_surfresp_early_r98_95shore - Mass balance chart. **Surface response case including dispersant application and *in situ* burning**. Start date: 6/18/2008.

Table 30. DeepWCD_90rel_surfresp_early_r98_95shore – Shoreline length oiled (km) by habitat type, for both shore oiling thresholds. **Surface response case including dispersant application and *in situ* burning**. Start date: 6/18/2008

Shore Type	Shore Length Oiled (km)	
	> 100 micrometers	> 1 micrometer
Seaward Rocky Shore	5.0	5.0
Seaward Gravel Beach	15.1	15.1
Seaward Sand Beach	35.3	45.4
Seaward Fringing Mud Flat	15.1	20.2
Seaward Fringing Wetland	0.0	5.0
Seaward Intertidal Macroalgal Bed	45.4	45.4
Total Shoreline	**115.9**	**136.1**

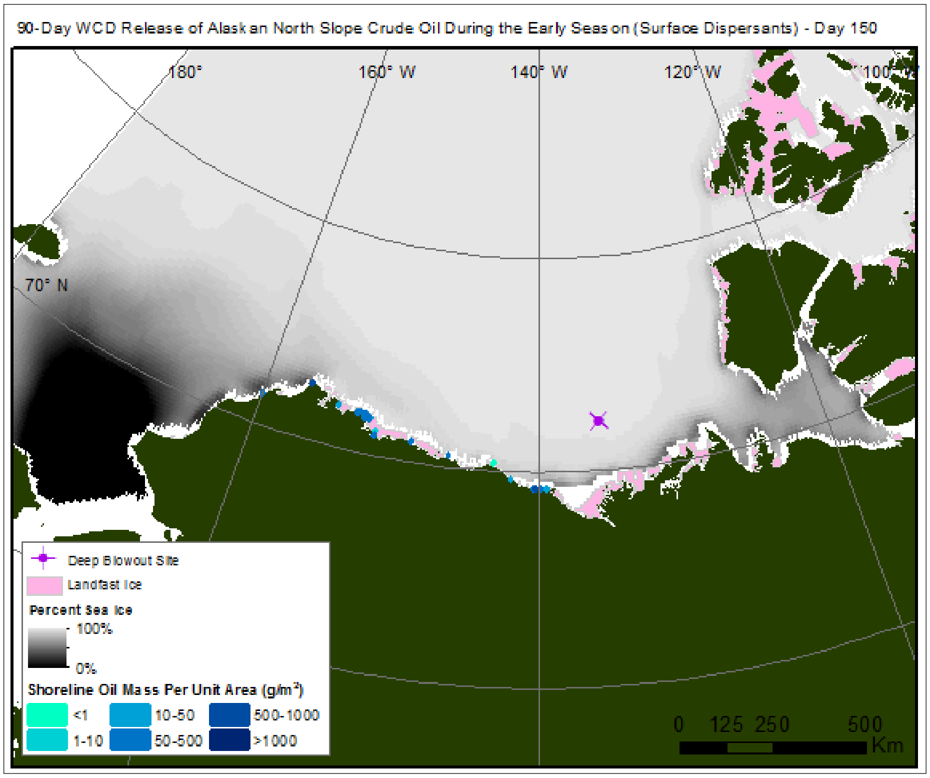

Figure 183. DeepWCD_90rel_surfresp_early_r98_95shore – Map of overall effects to shorelines as mass of oil deposited on shore per unit of area (g/m^2) (day 150 – November 2008). **Surface response case including dispersant application and *in situ* burning**. Pink polygons represent monthly average landfast ice. Grey scale contours represent ice percent coverage for that month from TOPAZ4 model. White indicates areas of no data for ice coverage. Start date: 6/18/2008.

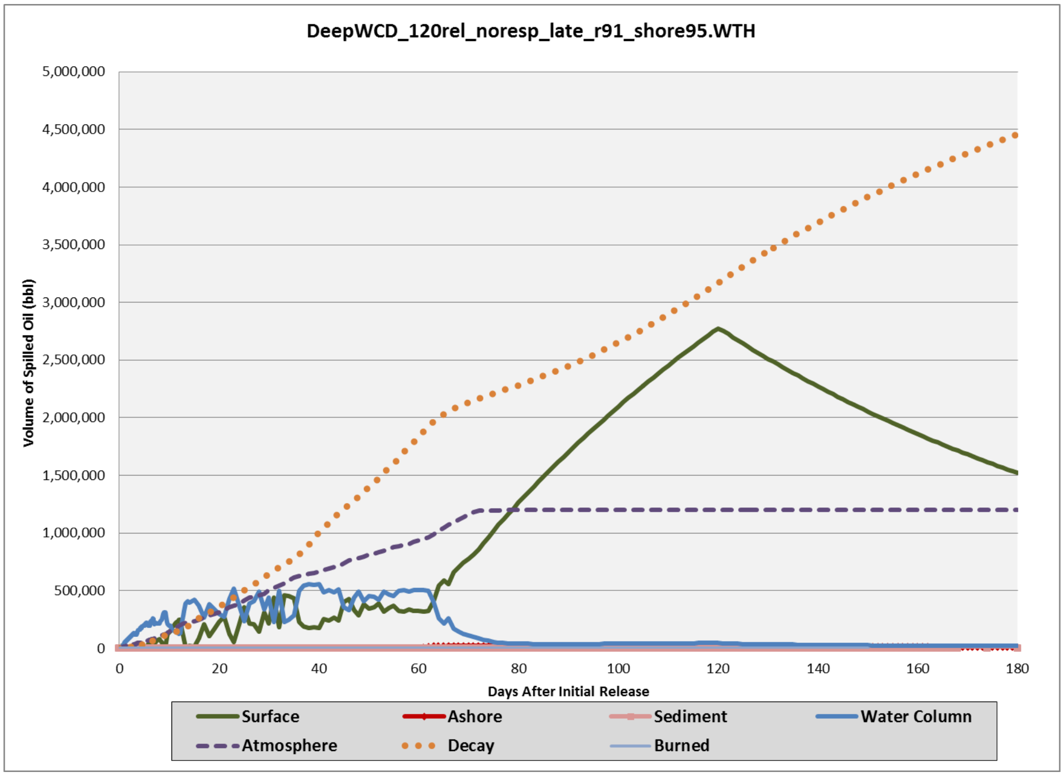

Figure 184. DeepWCD_120rel_noresp_late_r91_95shore - Mass balance chart. Start date: 8/12/2008.

Table 31. DeepWCD_120rel_noresp_late_r91_95shore – Shoreline length oiled (km) by habitat type, for both shore oiling thresholds. Start date: 8/12/2008.

Shore Type	Shore Length Oiled (km)	
	> 100 micrometers	> 1 micrometer
Seaward Gravel Beach	90.7	90.7
Seaward Sand Beach	90.7	95.8
Seaward Fringing Mud Flat	80.7	85.7
Seaward Fringing Wetland	0.0	5.0
Seaward Intertidal Macroalgal Bed	75.6	75.6
Total Shoreline	**337.7**	**352.8**

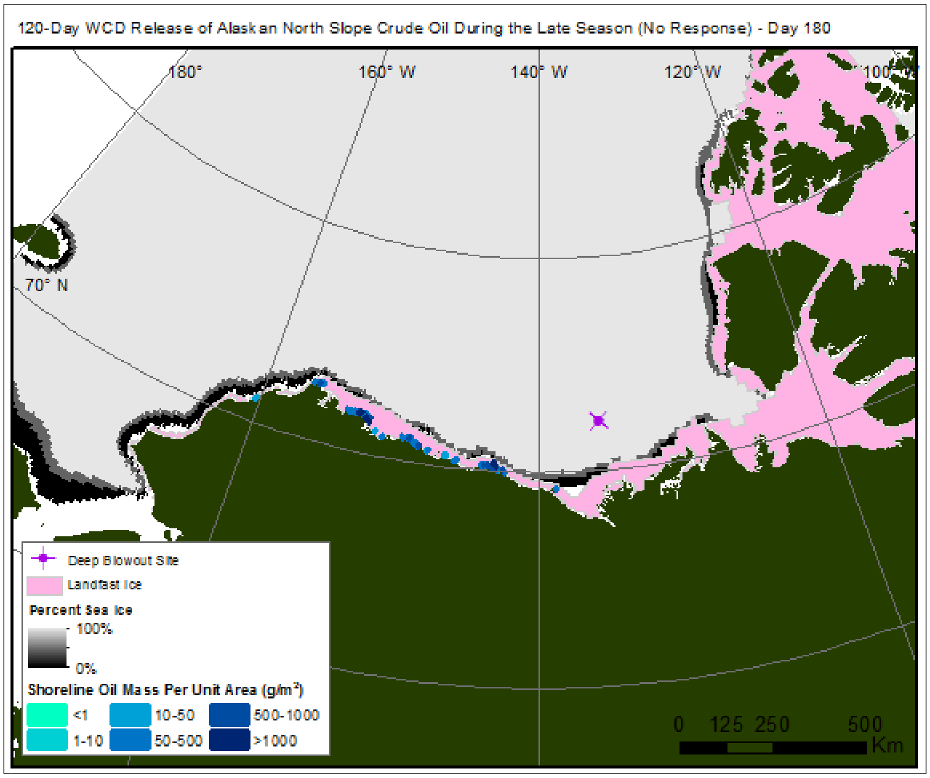

Figure 185. DeepWCD_120rel_noresp_late_r91_95shore – Map of overall effects to shorelines as mass of oil deposited on shore per unit of area (g/m^2) (day 180 – February 2009). Pink polygons represent monthly average landfast ice. Grey scale contours represent ice percent coverage for that month from TOPAZ4 model. White indicates areas of no data for ice coverage. Start date: 8/12/2008.

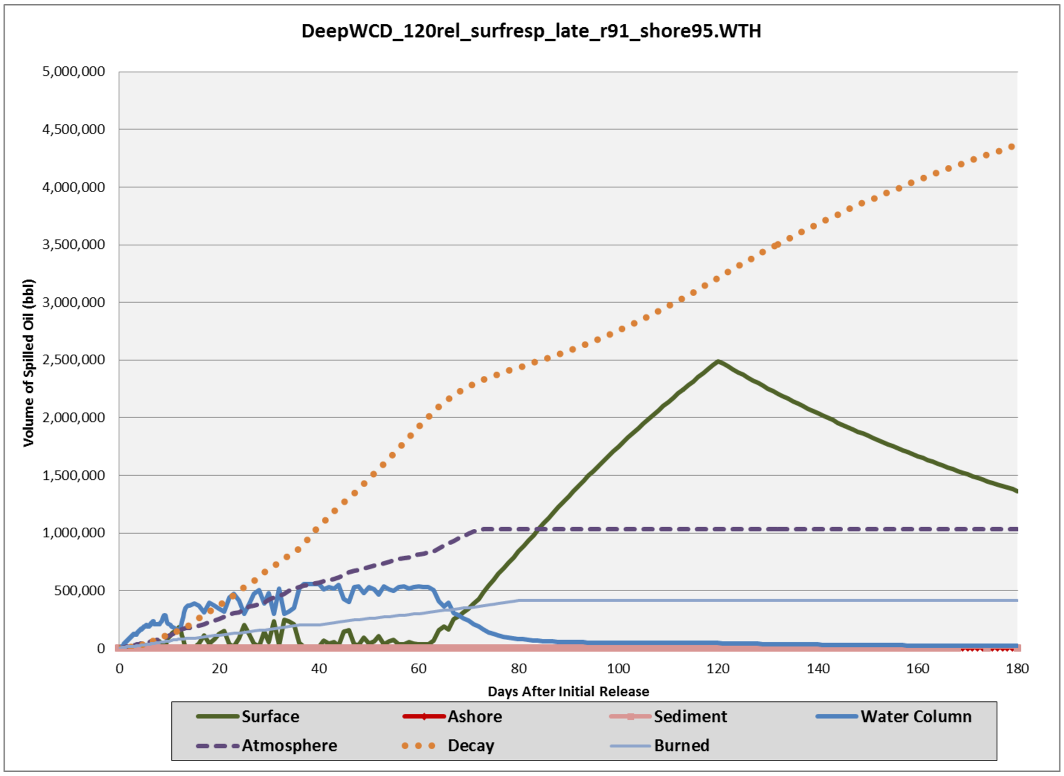

Figure 186. DeepWCD_120rel_surfresp_late_r91_95shore - Mass balance chart. **Surface response case including dispersant application and *in situ* burning**. Start date: 8/12/2008.

Table 32. DeepWCD_120rel_surfresp_late_r91_95shore – Shoreline length oiled (km) by habitat type, for both shore oiling thresholds. **Surface response case including dispersant application and *in situ* burning**. Start date: 8/12/2008.

Shore Type	Shore Length Oiled (km)	
	> 100 micrometers	> 1 micrometer
Seaward Gravel Beach	25.2	25.2
Seaward Sand Beach	30.2	35.3
Seaward Fringing Mud Flat	20.2	20.2
Total Shoreline	**75.6**	**80.7**

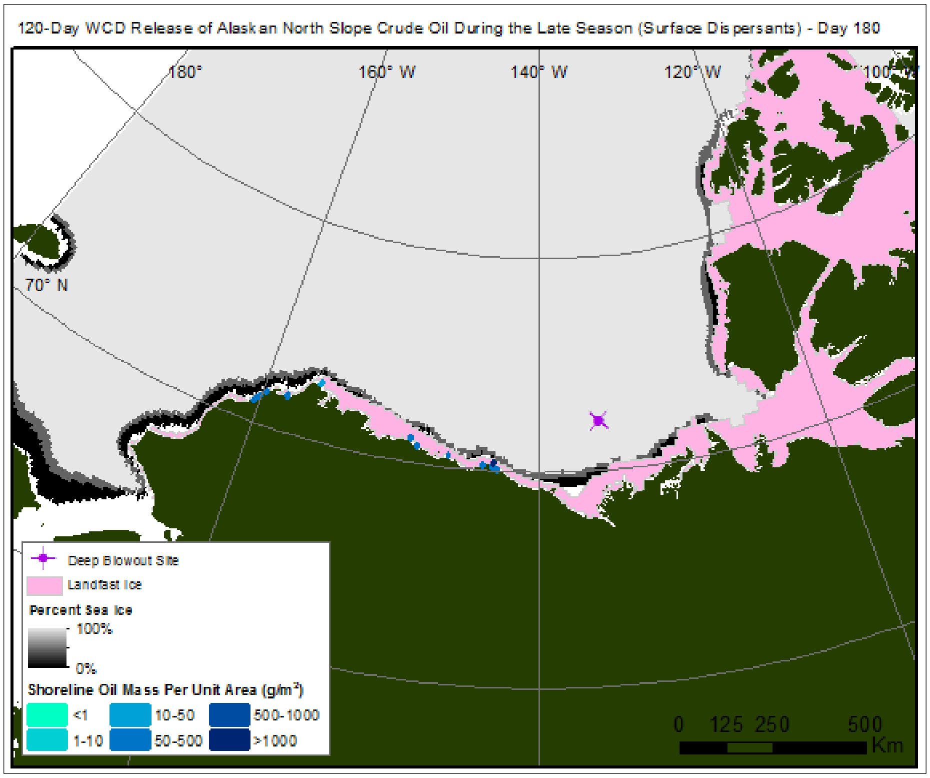

Figure 187. DeepWCD_120rel_surfresp_late_r91_95shore – Map of overall impact to shorelines as mass of oil deposited on shore per unit of area (g/m^2) (day 180 – February 2009). **Surface response case including dispersant application and *in situ* burning**. Pink polygons represent monthly average landfast ice. Grey scale contours represent ice percent coverage for that month from TOPAZ4 model. White indicates areas of no data for ice coverage. Start date: 8/12/2008.

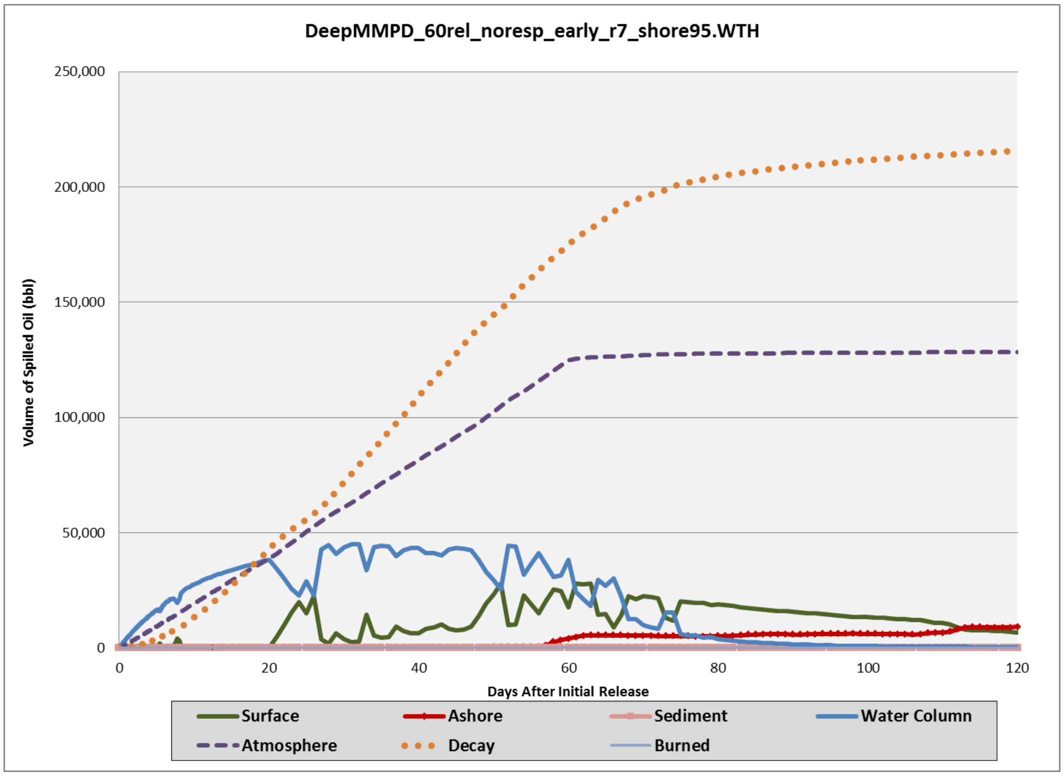

Figure 188. DeepMMPD_60rel_noresp_early_r7_95shore - Mass balance chart. Start date: 6/22/2008.

Table 33. DeepMMPD_60rel_noresp_early_r7_95shore – Shoreline length oiled (km) by habitat type, for both shore oiling thresholds. Start date: 6/22/2008.

Shore Type	Shore Length Oiled (km)	
	> 100 micrometers	> 1 micrometer
Seaward Rocky Shore	50.4	50.4
Seaward Gravel Beach	423.4	463.8
Seaward Sand Beach	307.5	448.6
Seaward Fringing Mud Flat	181.5	292.4
Seaward Fringing Wetland	0.0	15.1
Seaward Intertidal Macroalgal Bed	115.9	126.0
Total Shoreline	**1,078.7**	**1,396.3**

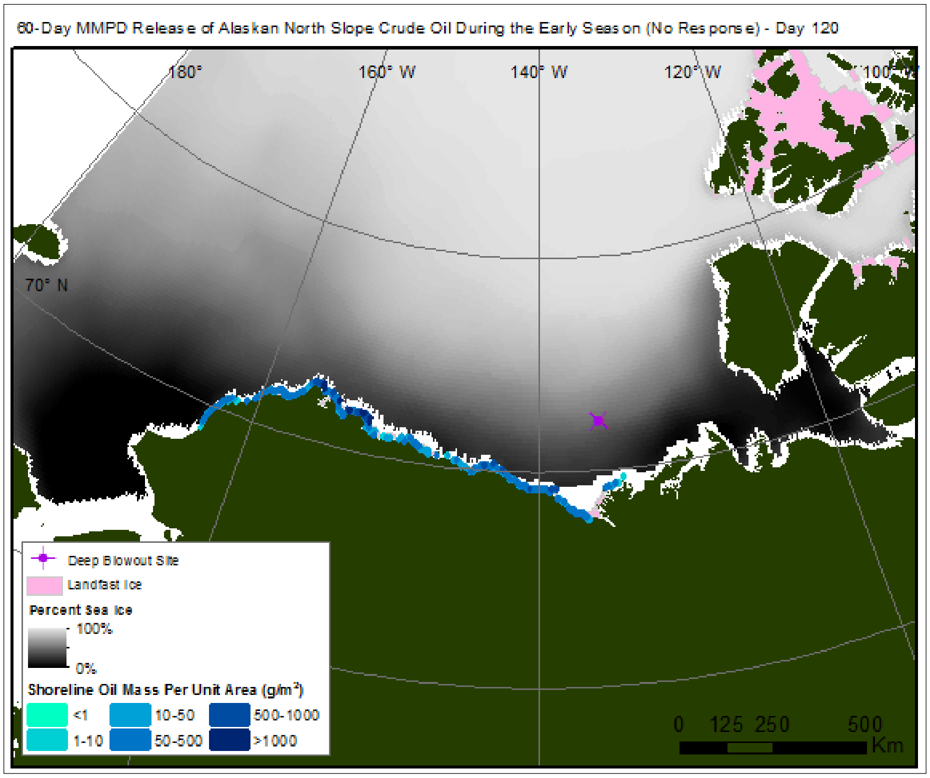

Figure 189. DeepMMPD_60rel_noresp_early_r7_95shore – Map of overall effects to shorelines as mass of oil deposited on shore per unit of area (g/m^2) (day 120 – October 2008). Pink polygons represent monthly average landfast ice. Grey scale contours represent ice percent coverage for that month from TOPAZ4 model. White indicates areas of no data for ice coverage. Start date: 6/22/2008.

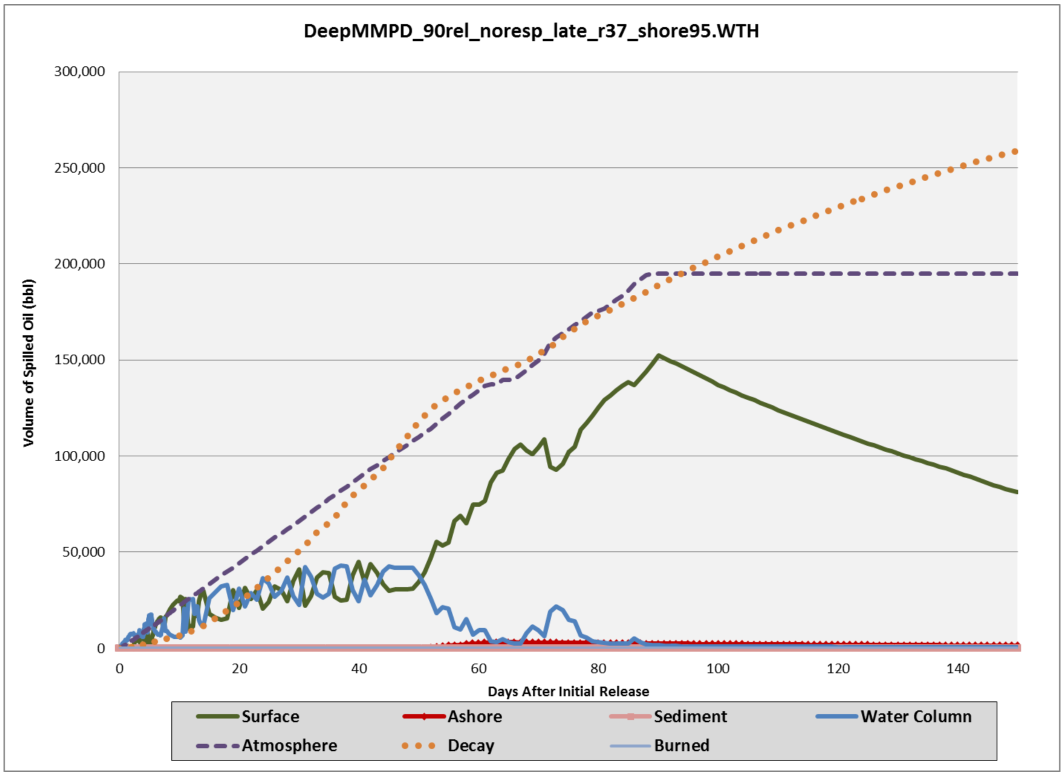

Figure 190. DeepMMPD_90rel_noresp_late_r37_95shore - Mass balance chart. Start date: 8/4/2009.

Table 34. DeepMMPD_90rel_noresp_late_r37_95shore – Shoreline length oiled (km) by habitat type, for both shore oiling thresholds. Start date: 8/4/2009.

Shore Type	Shore Length Oiled (km)	
	> 100 micrometers	> 1 micrometer
Seaward Gravel Beach	35.3	40.3
Seaward Sand Beach	50.4	95.8
Seaward Fringing Mud Flat	30.2	65.5
Seaward Intertidal Macroalgal Bed	90.7	90.7
Total Shoreline	**206.6**	**292.3**

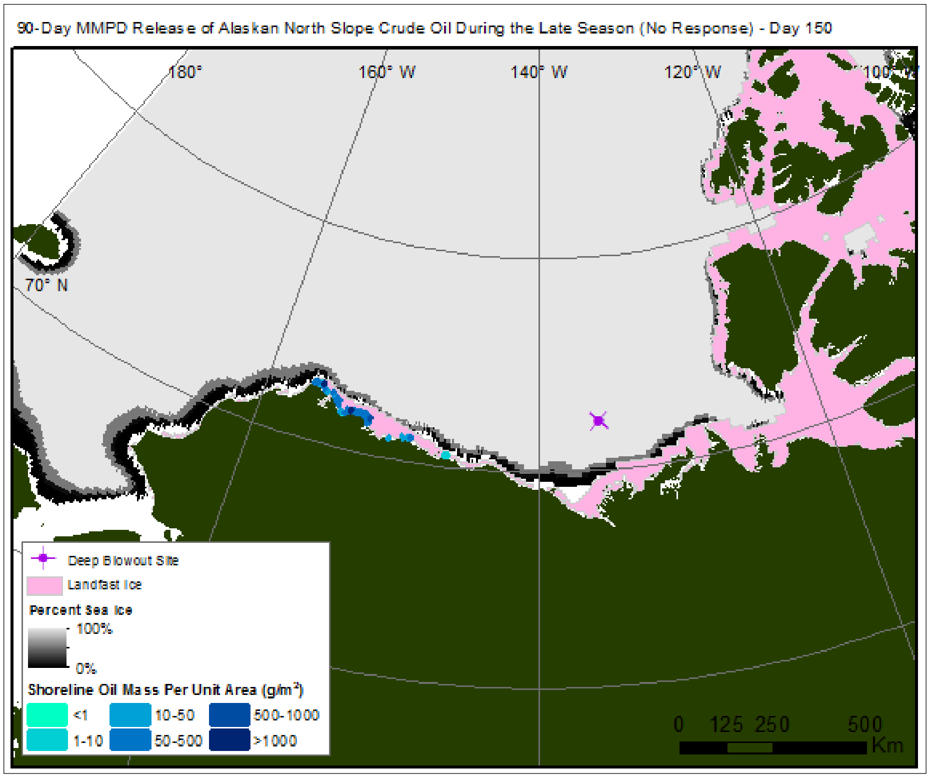

Figure 191. DeepMMPD_90rel_noresp_late_r37_95shore – Map of overall impact to shorelines as mass of oil deposited on shore per unit of area (g/m^2) (day 150 – January 2010). Pink polygons represent monthly average landfast ice. Grey scale contours represent ice percent coverage for that month from TOPAZ4 model. White indicates areas of no data for ice coverage. Start date: 8/4/2009.

95th Percentile Water Column Contamination

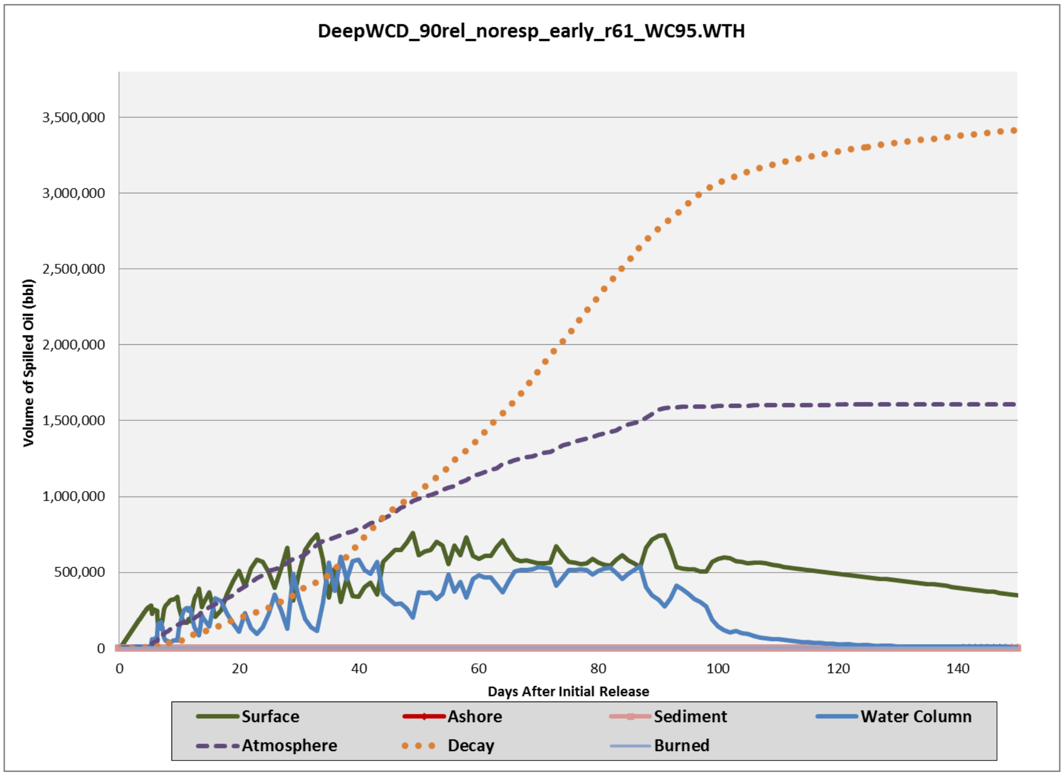

Figure 192. DeepWCD_90rel_noresp_early_r61_95WC - Mass balance chart. Start date: 6/2/2010.

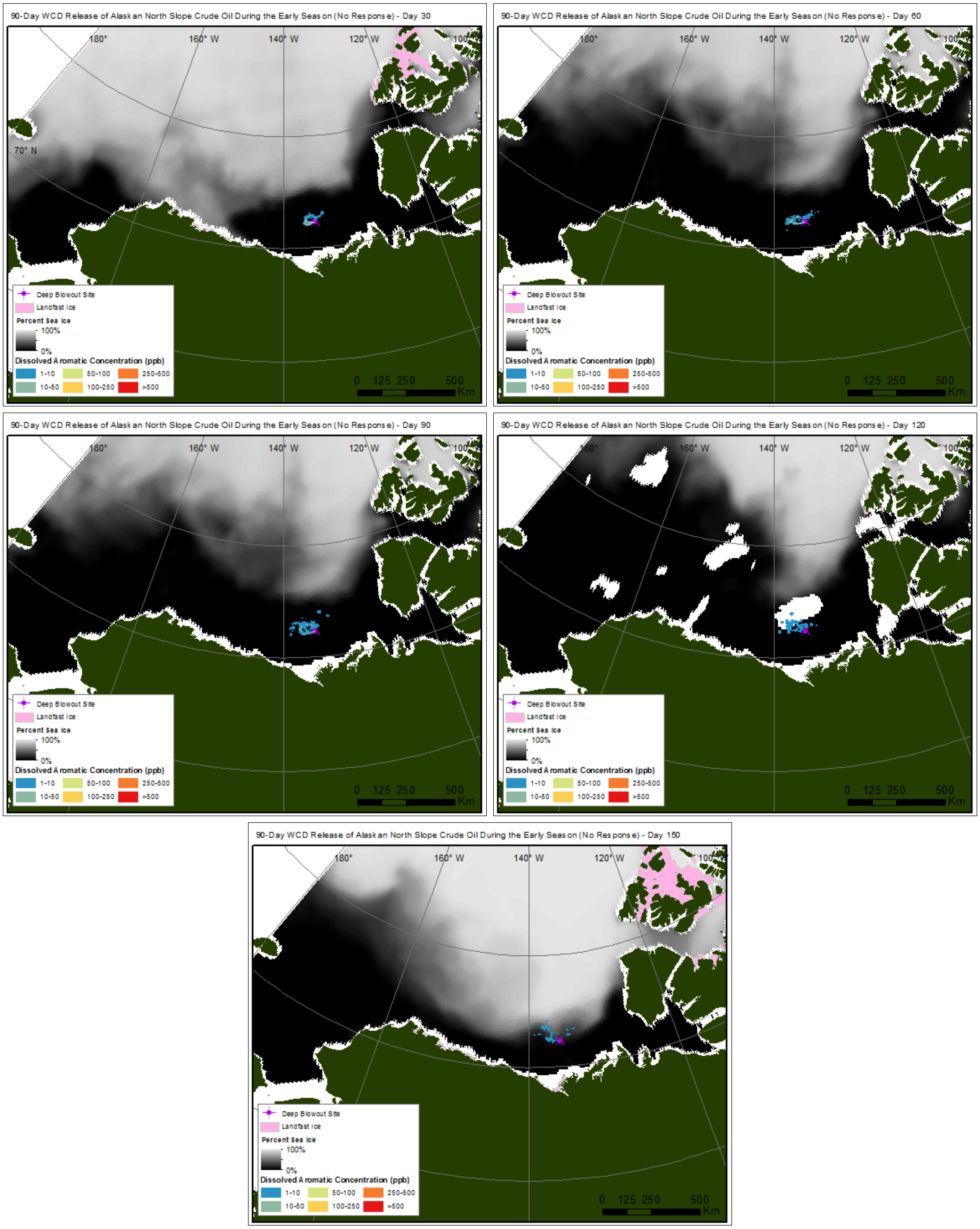

Figure 193. DeepWCD_90rel_noresp_early_r61_95WC – Time series maps of spill dissolved aromatics ≥1 ppb (day 30, 60, 90, 120, 150; June – October 2010). Pink polygons represent monthly average landfast ice. Grey scale contours represent ice percent coverage for that month from TOPAZ4 model. White indicates areas of no data for ice coverage. Start date: 6/2/2010.

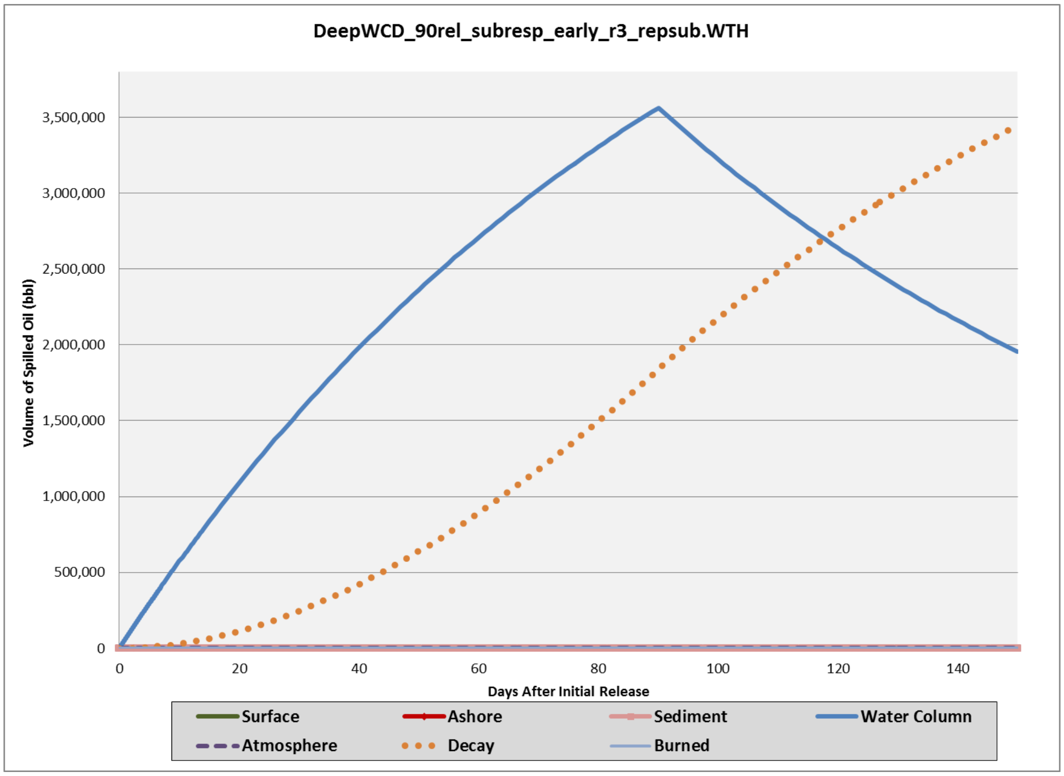

Figure 194. DeepWCD_90rel_subresp_early_r3_repsub - Mass balance chart. **Subsurface response case including subsea dispersant application, assumed 100% effective**. Start date: 7/29/2008.

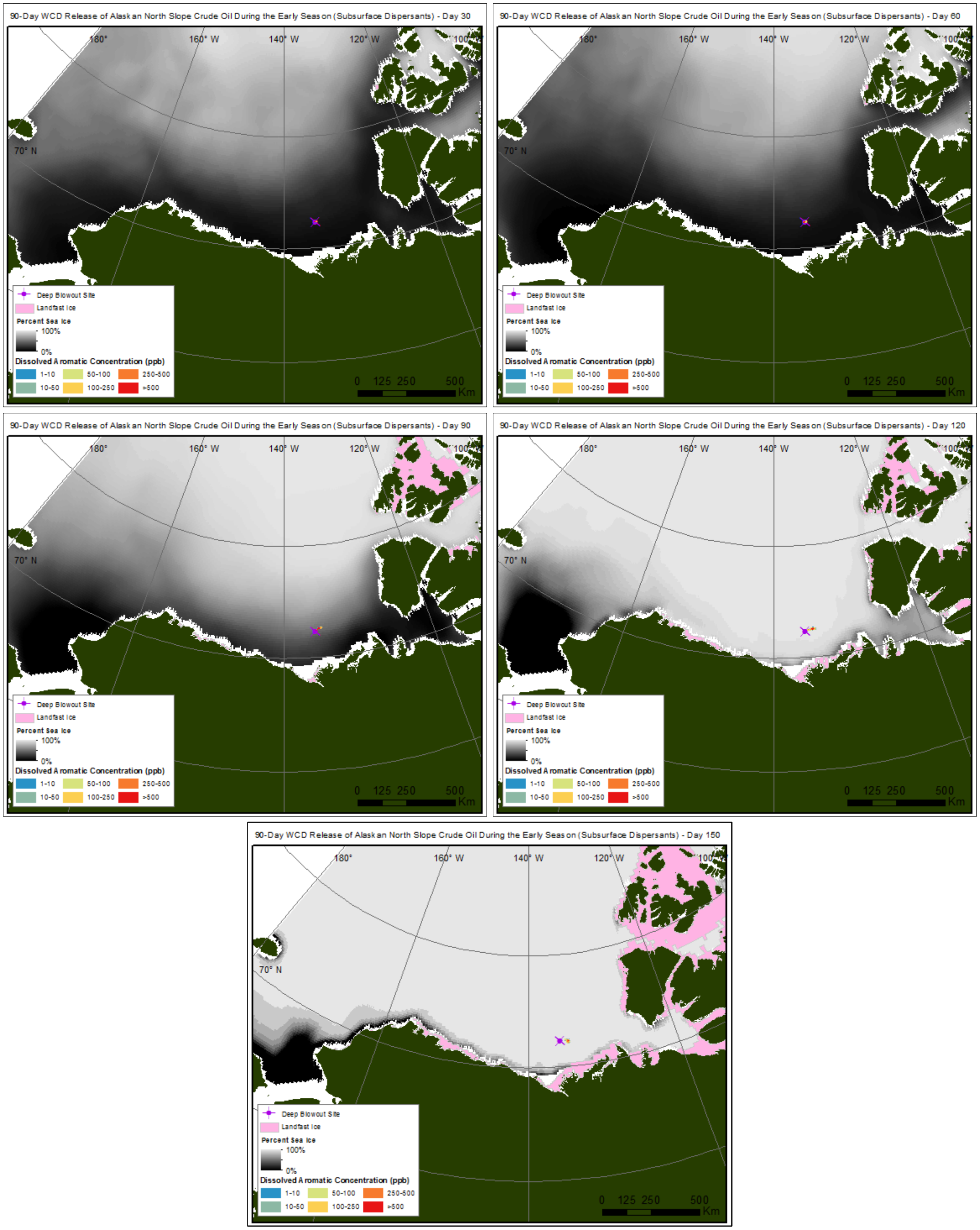

Figure 195. DeepWCD_90rel_subresp_early_r3_repsub – Time series maps of spill dissolved aromatics ≥1 ppb (day 30, 60, 90, 120, 150; August – December 2008). **Subsurface response case including subsea dispersant application**. Pink polygons represent monthly average landfast ice. Grey scale contours represent ice percent coverage for that month from TOPAZ4 model. White indicates areas of no data for ice coverage. Start date: 7/29/2008.

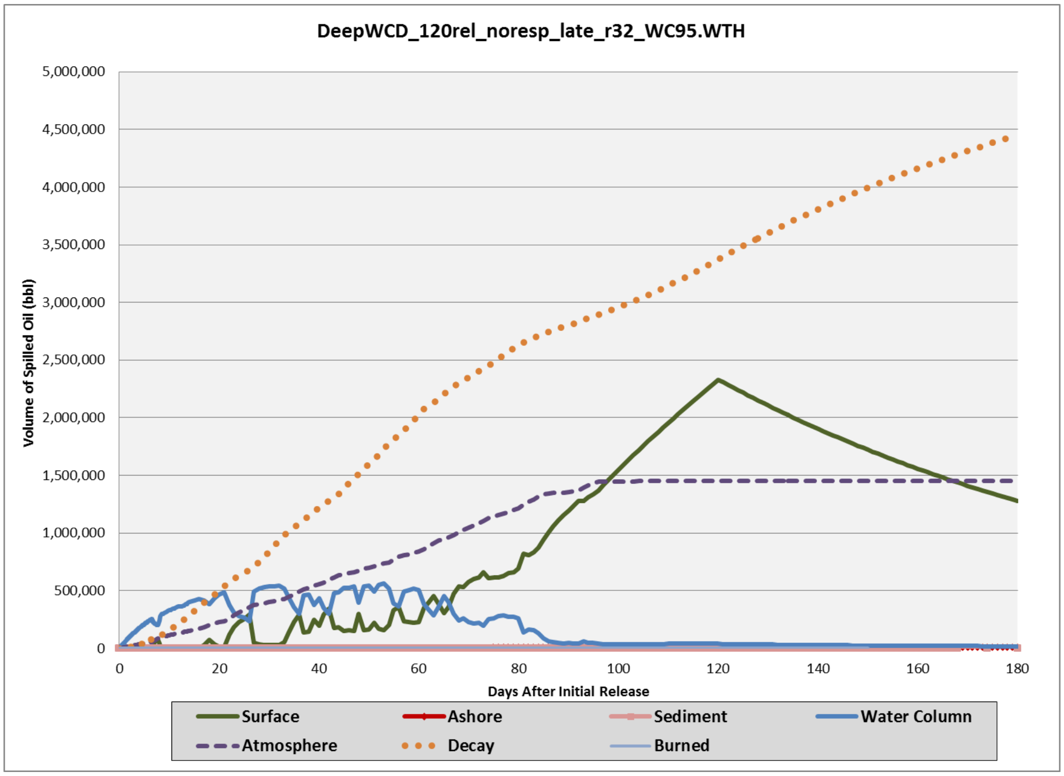

Figure 196. DeepWCD_120rel_noresp_late_r32_95WC - Mass balance chart. Start date: 8/7/2010.

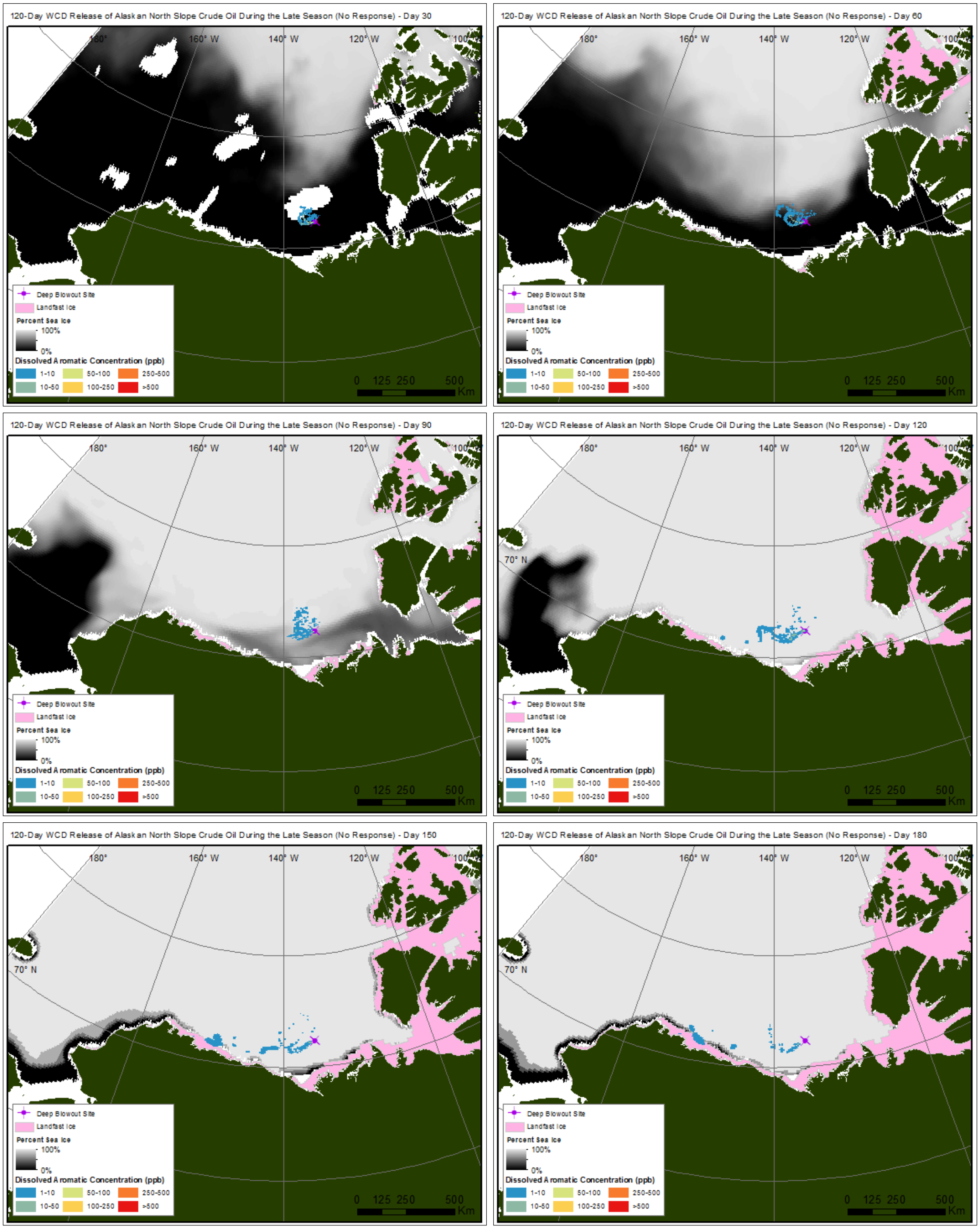

Figure 197. DeepWCD_120rel_noresp_late_r32_95WC – Time series maps of spill dissolved aromatics ≥1 ppb (day 30, 60, 90, 120, 150, 180; September 2010 – February 2011). Pink polygons represent monthly average landfast ice. Grey scale contours represent ice percent coverage for that month from TOPAZ4 model. White indicates areas of no data for ice coverage. Start date: 8/7/2010.

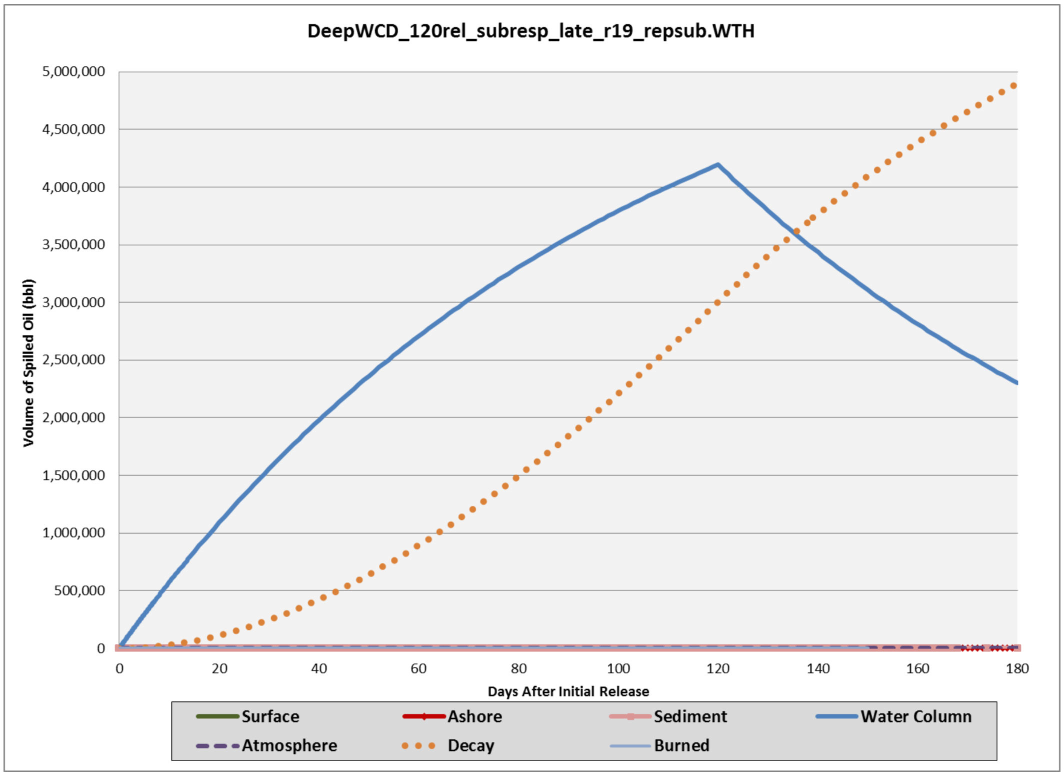

Figure 198. DeepWCD_120rel_subresp_late_r19_repsub - Mass balance chart. **Subsurface response case including subsea dispersant application, assumed 100% effective**. Start date: 9/2/2010.

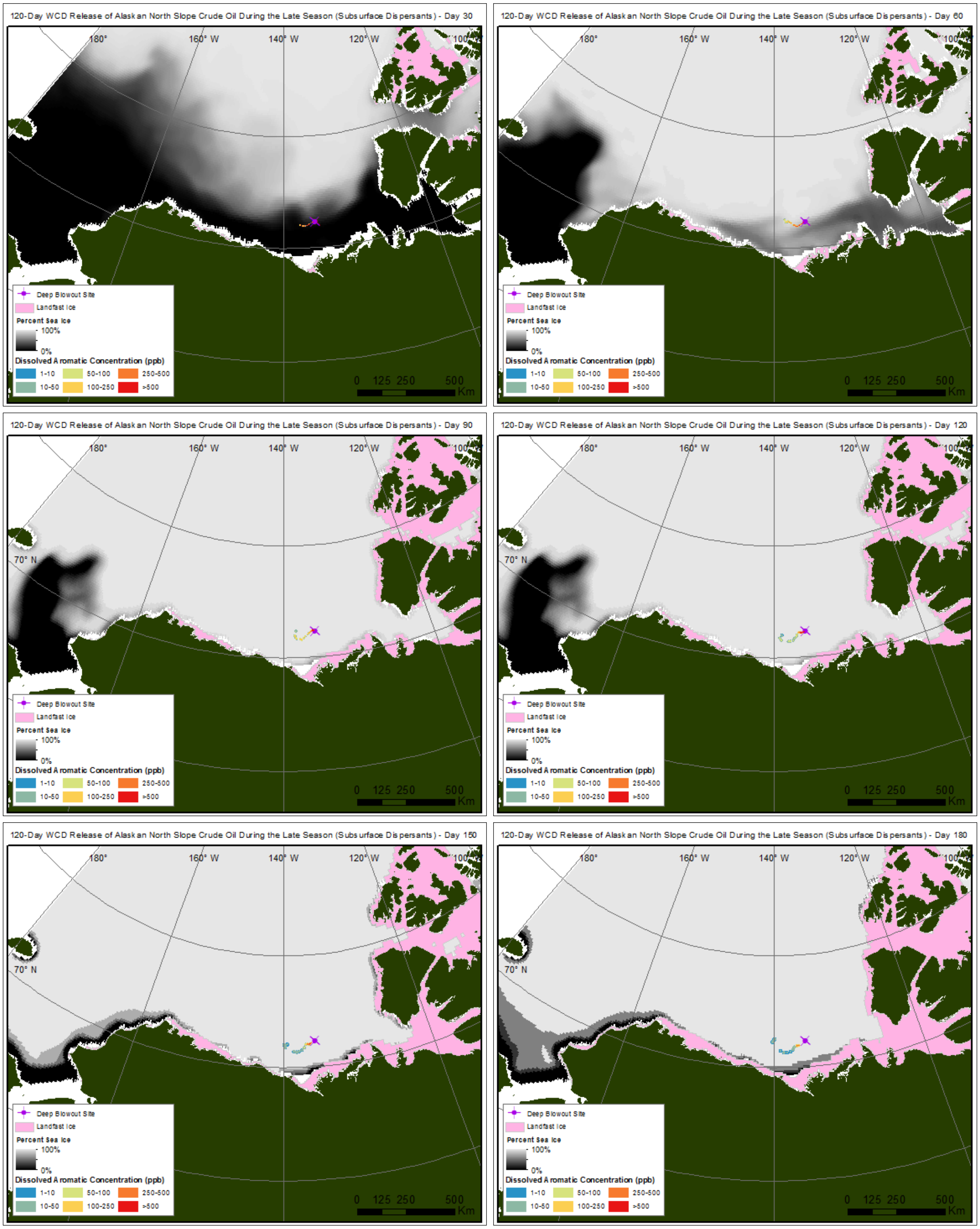

Figure 199. DeepWCD_120rel_subresp_late_r19_repsub – Time series maps of spill dissolved aromatics ≥1 ppb (day 30, 60, 90, 120, 150, 180; October 2010 – March 2011). **Subsurface response case including subsea dispersant application**. Pink polygons represent monthly average landfast ice. Grey scale contours represent ice percent coverage for that month from TOPAZ4 model. White indicates areas of no data for ice coverage. Start date: 9/2/2010.

8 Discussion and Conclusions

Stochastic footprints from the lower thresholds investigated (surface oil ≥0.01 g/m^2, shoreline oil ≥1 g/m^2) were fairly large for most of the scenarios and suggest that transport of oil over long distances in the region is possible. Stochastic output corresponding to these lower thresholds included surface oil as thin as sheen. Stochastic footprints (Appendix E) from the higher thresholds investigated (surface oil ≥10 g/m^2, shoreline oil ≥100 g/m^2) are much less expansive and represent the probable extent of thicker oil.

Larger volume spills (WCDs) exhibited higher probabilities of oiling further from the spill site (extensive *higher* probability contours). Whereas lower volume spills (MMPDs) exhibited overall lower probabilities of oiling further from the spill site (extensive *lower* probability contours). For the lower volume scenarios (MMPDs), higher probability contours, tended to be more localized around the spill sites. Oil weathering processes, including spreading, evaporation, emulsification, entrainment, and volatilization were slowed as higher ice coverage was encountered. This inherently increased the residence time of oil on the sea surface, which undoubtedly contributed to increased distance traveled while “trapped” in and/or under moving sea ice, even for lower volume spills. In open water conditions where wind strongly influences oil transport and fate, residence time of oil at the surface would be shorter.

The cell resolution of the grid used to generate stochastic probabilities was relatively large, given the vast extent of the region of interest. This coarse grid resolution may have also slightly exaggerated the overall extent of stochastic footprints. Gridding for individual trajectory results was at a finer scale and was based around the total extent of that particular spill event and not on the entire region of interest. Therefore, the individual trajectories provide a refined and more accurate representation of a potential spill’s areal coverage. The stochastic model results merely serve as a predictive modelled surface showing frequency of presence/absence of oil (above a certain oil contamination threshold) for that grid cell.

The most common surface oil trajectory pattern observed across the 5-year (spring 2008-spring 2013) wind and current record at all spill sites evaluated in this region of the Beaufort, was transport to the west with the westward flowing Beaufort Gyre current along the shelf break. This movement pattern coincides with the observed prevailing wind pattern as well (coming from the east, blowing towards the west). Even spill sites closer to the coast, located in the shallower areas of the shelf often followed a westward track. The Beaufort Shelf is relatively narrow continental shelf, and the slope has a steep narrow drop off. Therefore, the Beaufort Gyre current appeared to be influential even in areas close to the coast. It should be noted that the TOPAZ4 hydrodynamic model does not resolve complex coastal circulation features such as the influence of the Mackenzie River discharge. Models that do capture finer scale features may yield overall different trajectory results. Please refer to Section 5.4.2 for further discussion of TOPAZ4 model limitations.

Net sea ice flow followed the prevailing westward surface current near and on the shelf. Many of the spill analyses investigated began in open water conditions (summer) and continued throughout months where ice coverage increased (fall into winter). In most cases oil collected or became trapped in areas of high percent ice coverage in the late fall. Oil was modelled as travelling long distances from the Canadian Beaufort west to the Alaskan coast and Chukchi Sea throughout the entire simulation because of being trapped under high ice cover, which moved westward at a relatively fast rate according to the TOPAZ4 ice current data. However, Sakov et al. (2012) found that modelled ice drift velocities in TOPAZ4, when compared to field data, were generally too fast by approximately 3 km/day. This overestimation may have exaggerated the total distance that oil traveled. Even though distance traveled and extent of shore oiling may be slightly exaggerated in the modelling results due to uncertainty of the forcing data sources, these results suggest that spills originating from the Canadian Beaufort and resulting coastal oiling could be an international issue.

Sea ice coverage in the Canadian Beaufort was typically lowest in August and September. The decent of increasing ice coverage from the North Pole began in October, with close to full ice coverage up to the coast occurring in mid-November. From December to May almost 100% sea ice coverage was observed in the entire Beaufort Sea. The ice starts to break up and retreat North in June and July.

The spreading of oil on the water surface was limited as ice coverage increased. This was apparent in model output starting in open water and continuing throughout the freeze up. Oil released in open water spread into larger and wider surface slicks than when surfacing in ice. When subsequently encountering high ice coverage, these wider slicks continued to be transported in the ice in a more spread out patchy pattern. Oil that was directly released into high sea ice coverage appeared as long thin continuous and highly concentrated streaks of oil contained in ice floes.

Although net sea ice movement was westward, some longitudinal movement (northward/southward) of surface oil slicks was observed as sea ice coverage descended or ascended from the pole. Oil tended to collect or follow along the edges of the higher ice coverage contours. This was most apparent in the longer, higher volume scenarios. This was due to the inability to spread and northward/southward sea ice velocities.

With respect to inter-annual variability, the wind, current, and ice patterns in 2012 were somewhat different from other years. A positive shift in the Arctic Oscillation has been reported for the years 2011-2012 (NSIDC), which may in part account for the observed variation. Variable wind direction and speed, departing from the prevailing east to west pattern, typically observed during the summer months, was slightly offset and observed into early fall in 2012. The eastward flowing coastal counter current did occur in the modelled TOPAZ4 data but was variable in speed and direction and its presence was highly erratic. Direction fluctuated often throughout the years. This current tended to be more present and influential in 2012 as compared to other years. The timing of the decent of the polar ice pack in 2012, and increase of sea ice coverage up to the coastline, occurred later in 2012 as compared to previous years. This occurred late November into December in 2012, whereas in previous years this transition was observed late October to mid-November. There were some less common trajectories observed that flowed to the north and eastward, and traveled into the channels between the islands in the Canadian archipelago. These trajectories, though less likely, often resulted in high shoreline oiling. Many of the less common eastward and northward trajectories occurred in 2012, although some were also observed in 2009.

Similar to sea ice, landfast ice was least present in the months of August and September. It began to build out from the coast in October, mainly in areas of Mackenzie Bay and along the North Slope up to Point Barrow. Landfast ice growth increased throughout the fall and winter months, peaking in extent from the coastline in March, and began to recede in May. Shoreline oiling was highest in cases that started early in the summer when coastlines were the most free of landfast ice. For cases that continued into or started in the landfast freeze up period, oil coming in contact with this “artificial shoreline” became “entrapped” in the ice. As the ice built over the months and extended out from shore, new oil encountering the newly established ice edge would become trapped. Oil from previous months still appeared trapped at the previous ice edge. These cases ultimately resulted in lower overall shoreline oiling, as oil was not allowed to reach the actual shore, although when reviewing model results accumulation of oil along the coast looked relatively high.

For all oils and scenarios modelled, assumed degradation (decay) rates were based on those applied to the Alaska province of the CERCLA Type A Natural Resource Damage Assessment Model for Coastal and Marine Environments (NRDAM/CME) (French et al., 1996). Degradation may occur as the result of photolysis, which is a chemical process energized by ultraviolet light from the sun, and by biological breakdown, termed biodegradation. Generally speaking, little reliable data exists on the true decay rate of oil hydrocarbons in the ocean. Several factors can affect decay including temperature and chemical composition. Overall, by the end of the simulations, decay represented a relatively high percentage of the oil, and in some cases accounted for up to 67% of the oil in the mass balance. This result is further highlighted in cases having high oil and ice interactions where most of the other fates processes, represented in the mass balance, have been supressed. However, the rates used are relatively low compared to some literature estimates, available for lower molecular weight compounds.

8.1 Eastern Shipping Analysis

The IFO spill stochastic probability footprint (lower surface oiling threshold ≥0.01 g/m^2) was much larger, and extended further to the west, as compared to the Diesel in the Eastern Shipping Analysis, although both cases exhibited relatively low percent probabilities overall. IFO is a very heavy viscous product that typically does not readily entrain into the water column, doing so only under highly turbulent conditions. In open water IFO surface slicks may travel long distances. If IFO trajectories encounter ice, such as those occurring in the later months of the active shipping season, this travel time can be extended. However, results suggest there was a very low probability 1-10% that spills would travel as far as the international dateline. Some trajectories did travel outside of the model's western boundary (i.e, the straight line where stochastic footprint cuts off). There was 25-50% probability of oiling occurring within 300-600 km west of the spill site, which corresponded to approximately a 0-14 day minimum travel time.

Diesel will entrain into the water column much easier than a heavier oil product such as IFO. Highest probabilities of surface oiling were localized around the spill site. Stochastic subsurface contamination results showing presence of total oil in the water column suggest that many trajectories exhibited entrainment to some degree. Surface and shoreline oiling of the diesel cases was less extensive due to overall lower volume released, the high evaporation associated with light fuel oils, and the tendency of the oil to entrain into the water and disperse.

Both stochastic cases exhibited some less common eastward trajectories resulting in surface and shoreline oiling in the channels of the Canadian Archipelago. The 95th worst case shoreline oiling trajectory for IFO resulted in over 400 km of oiled shoreline (at the lower threshold examined ≥1 g/m^2 or 1 µm, causing socio-economic impacts) along coastline to the east of the spill site. Though this run was identified as a worst case, its probability of occurrence was relatively low.

Spills of the IFO oil type resulted in greater distance travelled and more extensive shoreline oiling to the west, as opposed to spills of Diesel. In both cases the areas closest to the spill site, around Bailee Island and the Amundsen Gulf, were the greatest affected.

8.2 Trans-boundary Analysis

Stochastic output showing probability of surface oiling (lower surface oiling threshold ≥0.01 g/m^2) for all shipping scenarios (crude volume, IFO volume, active shipping season releases, year round releases, US release region, Canadian release region) was very similar in overall extent and pattern. Shipping scenarios were all surface releases, having release durations less than a day. Most trajectories travelled to the west, 25-50% probability occurring approximately 600-800 km from either spill site region. This probability contour was associated with approximate minimum travel times of 0-14 days. There was approximately 1-10% probability of surface oil traveling eastward as far as the Canadian archipelago. The crude shipping release from the US release region for 95th percentile surface oiling was a trajectory that travelled eastward (although having a low probability of occurrence). Overall the crude tanker scenario stochastic footprint extended further to the north, as compared to the IFO. This was due to higher volume of crude released as compared to the IFO, as well as the crude’s lower viscosity allowing it to spread further than IFO. Individual crude trajectories exhibited much higher surface oiling concentrations, and larger surface slicks, further away from the spill site. Smaller slicks of high concentration IFO on the surface were observed closer to the spill release region.

IFO stochastic shoreline oiling probabilities from the US and Canadian release regions extended east to Balliee Island and west to the Chukchi coast of Alaska, although these were primarily low probabilities (1-10%). Shoreline oiling probability results for crude spills from the US and Canadian release regions were similar in extent and probability percentage, but had more consistent coverage along coastlines (not as patchy). Minimum travel times to shore where lowest along coastlines nearest to spill regions. The individual 95th percentile run for highest shoreline oiling effects for the IFO and crude shipping releases ranged approximately from 400 to 500 km of oiled shoreline above the lower threshold evaluated ≥ 1 g/m^2 (1 µm). Individual 95th percentile runs for IFO from US and Canadian release regions and for the crude from the US release region, oiled areas to the west up the North Slope. Whereas the crude run from the Canadian release site resulted in shoreline oiling from areas just west of the border all the way east to the Mackenzie River delta.

Subsurface contamination was much higher in the crude shipping spills, as IFO does not readily entrain (previously discussed in Section 8.1). Subsurface stochastic output mirrored surface oiling patterns (movement primarily to the west), although extent was much less. Subsurface contamination of crude oil components due to surface entrainment would be expected given the large volume released in the trans-boundary crude shipping spills (533,000 bbls).

Overall, the stochastic output showing probability of surface oiling (lower surface oiling threshold ≥0.01 g/m^2) for both crude pipeline release scenarios (US and Canadian release regions) were very similar to each other in extent and pattern, as well as to the shipping scenarios in the trans-boundary analysis. One subtle difference was that for both pipeline releases the higher probability contour (50-75%) extended further from each spill region approximately 150 - 300 km west. This was due to the longer release period of the pipeline leaks (6 days) and most likely because these were subsurface releases, potentially increasing over all spreading extent.

Shoreline oiling probabilities for pipeline releases followed similar patterns and extent along coastlines as the shipping scenarios. The individual 95th percentile run for shoreline oiling effects for the crude pipeline leaks ranged approximately from 500 to 600 km of oiled shoreline above the lower threshold evaluated ≥ 1 g/m^2 (1 µm). Subsurface stochastic output mirrored surface oiling patterns (movement primarily to the west), although extent was drastically reduced.

The Trans-boundary analysis confirmed that most oil from spills originating from around the US/Canadian border would travel westward and affect the Alaskan coastline. The results suggested that some eastward movement of oil was possible along the Canadian coast and Mackenzie River Delta, but this would be much less probable than the prevailing westward drift. Regardless of varying release periods and years, the general probability patterns of all scenarios investigated were similar suggesting that the surface current, ice current, and wind regime throughout the year, and between years, exhibited low variability and were relatively consistent.

8.3 Shallow Blowout Analysis

Like the other analyses investigated in this study, 60- to 120-day spills from the shallow blowout site primarily travelled westward towards Alaska and into the Chukchi Sea. There were some trajectories (low occurrence) that travelled eastward into the channels of the Canadian archipelago. For all scenarios some surface oil exited the western boundary of the model domain. Model output appears to be cut-off in a straight line were oil left the boundary.

Late season stochastic surface oil footprints (lower surface oiling threshold ≥0.01 g/m^2) from the shallow blowout were narrower, or did not extend northward as much as the early season blowout scenarios. This reduction in overall footprint was due to limited spreading in the late season runs as they encountered more and higher ice coverage. The surface oil footprint of the late season WCD and the MMPD were similar in overall shape and extent, although the WCD was slightly larger. The inner probability contours varied between WCD and MMPD. As expected the higher volume scenario had higher probabilities of surface oiling further from the spill site. Probabilities of 50-75% for the MMPD scenario extended approximately 600 km to the west, whereas WCD extended up to approximately 1000 km to the west. Highest probabilities (75-100%) of oiling were observed closer to the spill site for both late season scenarios. Landfast ice extent intersected with the shallow blowout spill site in December and into the winter months. Some late season spills that started in October would have been releasing when landfast ice coverage above the spill site was growing. This trapped oil and kept it localized around the spill site.

The overall surface oil footprint (lower surface oiling threshold ≥0.01 g/m^2) for the MMPD early season scenario was smaller as compared to the WCD, although total westward extent was comparable. This was due to the shorter release period of the MMPD, as well as the lower spill volume. In both cases, the higher probability of surface oiling contours (75-100%) extended great distances from the spill site and ran parallel and close to the coastline. The WCD high probability contours extended approximately 1,200 km to just west of Point Barrow.

Early season scenarios (both WCD and MMPD) had higher probability of oiling the shoreline as compared to the late season. This was attributed to landfast ice growth in the fall and winter months prohibiting landfall of oil. Early season shoreline probabilities were often in the 50-75% range south of the spill site (Mackenzie River delta) and to the west along the Canadian Beaufort coastline. In all scenarios, the extent of shoreline oiling probabilities >1% was from the Point Barrow east to shorelines of the Amundsen Gulf, and also the southwest coast of Banks Island.

The individual 95th percentile run for shoreline oiling in the early season (WCD) oiled up to 1,900 km of shoreline above the lower threshold evaluated ≥1 g/m^2 (1 µm). The MMPD early season individual 95th percentile run for shoreline oiling resulted in approximately 1,300 km of oiled shoreline ≥ 1 g/m^2 (1 µm thick on average). The individual 95th percentile run for shoreline oiling in the late season (WCD) oiled over 800 km of shoreline above the lower threshold evaluated (≥ 1 g/m^2, 1 µm). The MMPD late season individual 95th percentile run for shoreline oiling resulted in approximately 1,100 km of oiled shoreline ≥ 1 g/m^2 (1 µm).

Surface response scenarios in the early season showed dramatic differences in surface and shoreline effects as compared to the no response base cases. This was primarily due to the efficiency of *in situ* burning. Favourable and beneficial response assumptions were incorporated into the modelling (see Section 6.5). Up to 26% of the total mass released was removed from burning in the early season. In June and July in the Arctic there is between 21-24 hours of daylight. This allowed for “around the clock” response during the first few months of the early season cases. More response effort was also possible in the early season before the October 31st response cut off. Shoreline effects differed by orders of magnitude in the early season; no response 1,966 km (>1 g/m^2, 1 µm) verses response 136 km (>1 g/m^2, 1 µm) of affected shoreline. The amount removed from burning for the late season cases was lower (16%) due to less response time before October 31st and from fewer hours of daylight in the later summer and fall months. Oil also became trapped in ice in the late season and was not available for response. Shoreline effects in the late season for the no response case was 857 km (>1 g/m^2, 1 µm), whereas it was reduced to 272 km (>1 g/m^2, 1 µm) for the response case.

The amount of mass in the water column was similar between the response and non-response cases. Although, the response cases for the most part had slightly higher peaks due to increased entrainment from surface dispersant application. Overall, surface dispersant (increased entrainment) had less of an effect on mass balance as compared to removal from *in situ* burning. This was primarily driven by thresholds for surface dispersant effectiveness.

Oil released at the subsurface shallow spill site surfaced very quickly. Subsurface contamination was primarily from surface oil entraining from wind stress as it travelled with the surface currents. Subsurface stochastic output mirrored surface oiling patterns (movement primarily to the west), although extent was much less. Dissolved aromatic concentrations, as modelled in the individual 95th percentile runs for water column contamination, were observed in relatively close proximity to the spill site (within 250 km) with highest concentration nearest to spill site. General movement of the contamination was to the west, and it was present throughout each scenario’s release duration as fresh oil was entering into the system. In some cases dissolved aromatic concentrations >1 ppb lingered for up to 30 days after the end of the release. 95th percentile dissolved aromatic concentrations for early season (WCD) primarily ranged between 1 and 100 ppb, with some occasional spikes up to 200 ppb. 95th percentile dissolved aromatic concentrations for late season (WCD) primarily ranged between 1 and 100 ppb. The contamination was localized around the spill site as oil was trapped in and under landfast ice.

Modelling results suggested that 90- to 120-day WCD and 60-day MMPD blowouts originating from the shallow spill site located in the Amauligak lease area, early in the operating season would result in extensive surface oiling to the west, as far as Point Barrow. There was a high probability that shorelines to the south of the spill site along the Mackenzie River delta, and to the west along the Canadian Beaufort coast up the North Slope would get moderately to heavily oiled. Blowouts occurring later in the operating season would exhibit extensive westward surface oiling, although less extensive to the north as compared to spills spreading for longer periods of time in ice free open water (early season). Late season spills would result in lower shoreline oiling due to landfast ice build-up into the winter months. Persistent water contamination by dissolved aromatics (1-100 ppb) may result from long blowout releases, but these would be relatively localized around the spill site area.

8.4 Deep Blowout Analysis

Like the shallow blowout analysis, spills from the 60- to 120-day deep blowout site primarily travelled westward towards Alaska and into the Chukchi Sea. There were some trajectories (low occurrence) that travelled eastward into the channels of the Canadian archipelago. Some trajectories exhibited northward movement before travelling west. The deep blowout site was located just south of a shelf break eddy feature. In several trajectories, oil was initially swept up into this feature and swirled before getting transported to the west (or east, lower occurrence). In general, deep blowout scenarios resulted in higher surface oiling probabilities and slightly higher overall extent as compared to the shallow blowout scenarios. The deeper location allowed for oil to spread in wider slicks that extended to the west, especially during the early season when there was more open water. For all scenarios some surface oil exited the western boundary of the model domain. Model output appears to be cut-off in a straight line were oil left the boundary.

Late season stochastic surface oil footprints from the deep blowout were narrower, or did not extend northward as much as the early season blowout scenarios. This reduction in overall footprint was due to limited spreading in the late season runs as they encountered more and higher ice coverage. The surface oil footprint of the late season WCD and the MMPD were similar in overall shape and extent, although the WCD was slightly larger. The inner probability contours varied between WCD and MMPD. As expected the higher volume scenario had higher probabilities of surface oiling further from the spill site. Probabilities of 50-75% for the MMPD scenario extended approximately 600 km to the west, whereas WCD extended up to approximately 1,100 km to the west. Highest probabilities (75-100%) of oiling were observed closer to the spill site for both late season scenarios.

The overall surface oil footprint for the MMPD early season scenario was slightly smaller as compared to the WCD, although total westward extent was comparable. This was due to the shorter release period of the MMPD, as well as the lower spill volume. In both cases, the higher probability of surface oiling contours (75-100%) extended great distances from the spill site and ran parallel and close to the coastline. The WCD high probability contours extended approximately 1300 km to just west of Point Barrow.

Early season scenarios (both WCD and MMPD) had higher probability of shoreline oiling as compared to the late season. This was attributed to landfast ice growth in the fall and winter months prohibiting landfall of oil. Early season WCD shoreline probabilities (50-75%) were observed along the US North Slope coast, in and around Prudhoe Bay to Point Barrow. Higher probabilities of shoreline oiling (75-100%) were observed only near Point Barrow. Highest probabilities for the MMPD early scenario also occurred around Point Barrow.

The individual 95th percentile run for shoreline oiling in the early season (WCD) oiled approximately 1,800 km of shoreline above the lower threshold evaluated ≥ 1 g/m^2 (1 µm). The MMPD early season individual 95th percentile run for shoreline oiling resulted in approximately 1,400 km of oiled shoreline ≥ 1 g/m^2 (1 µm). The individual 95th percentile run for shoreline oiling in the late season (WCD) oiled over 300 km of shoreline above the lower threshold evaluated ≥ 1 g/m^2 (1 µm). The MMPD late season individual 95th percentile run for shoreline oiling resulted in approximately 290 km of oiled shoreline ≥ 1 g/m^2 (1 µm).

Surface response scenarios in the early season showed differences in surface and shoreline effects as compared to the no response base cases. This was primarily due to the efficiency of *in situ* burning.

Favourable and beneficial response assumptions were incorporated into the modelling (see Section 6.5). Up to 13% of the total mass released was removed from burning in the early season. In June and July in the Arctic there is between 21-24 hours of daylight. This allowed for “around the clock” response during the first few months of the early season cases. More response effort was also possible in the early season before the October 31st response cut off. Shoreline effects differed by orders of magnitude in the early season; no response 1,860 km (>1 g/m^2, 1 µm) verses response 136 km (>1 g/m^2, 1 µm) of affected shoreline. The amount removed from burning for the late season cases was lower (16%) due to less response time before October 31st and from fewer hours of daylight in the later summer and fall months. Oil also became trapped in ice in the late season and was not available for response. Shoreline effects in the late season for the no response case was 353 km (>1 g/m^2, 1 µm), whereas it was reduced to 81 km (>1 g/m^2, 1 µm) for the response case.

The amount of mass in the water column was similar between the response and non-response cases. Although, the response cases for the most part had slightly higher peaks due to increased entrainment from surface dispersant application. Overall, surface dispersant (increased entrainment) had less of an effect on mass balance as compared to removal from *in situ* burning. This was primarily driven by thresholds for surface dispersant effectiveness.

Oil released at the subsurface deep spill site surfaced in less than a day. Subsurface contamination was from both fresh oil ascending to the surface, and from surface oil entraining from wind stress as it travelled with the surface currents. Subsurface stochastic output primarily mirrored surface oiling patterns (movement to the west), although extent was much less. However, subsurface oil contamination was observed entering into the channel north of Banks Island in the early and late WCD scenarios. This did not correspond to surface oiling, suggesting that subsurface currents occasionally transported oil in the water column, freshly released from the spill site, considerable distances.

Dissolved aromatic concentrations, as modelled in the individual 95th percentile runs for water column contamination for WCD early season, were observed relatively close to the spill site (within 250 km) with highest concentrations nearest to spill site. Dissolved aromatic concentrations, as modelled in the individual 95th percentile runs for water column contamination for WCD late season, were observed further distances from the spill site (within 500 km) again with highest concentrations nearest to spill site. General movement of the contamination was to the west, although some transport to the north and east was observed. Contamination was present throughout each scenario’s release duration as fresh oil was entering into the system. In some cases dissolved aromatic concentrations >1ppb lingered for up to 30 days after the end of the release. 95th percentile dissolved aromatic concentrations for early season (WCD) primarily ranged between 1 and 100 ppb, with some occasional spikes up to 200 ppb. 95th percentile dissolved aromatic concentrations for late season (WCD) primarily ranged between 1 and 100 ppb.

Subsurface dispersant response cases showed the highest overall water column contamination. It was assumed that all oil was 100% effectively treated by subsurface dispersant application; therefore, all oil remained subsurface broken up into tiny oil droplets. For both the early and late subsurface response scenarios, the oil droplet contamination lingered and was transported between the depths of 300 and 500 m. The area having the highest probability of subsurface oil contamination was to the southwest of the spill site along the shelf edge near the Mackenzie trough. The subsurface oil droplets tended to build up along the shelf at depth (approximately 300-400 m). Often dissolved aromatic concentration was observed between 100-500 ppb, in areas near to the spill site (within 250 km).

Modelling results suggested that 90- to 120-day WCD and 60-day MMPD blowouts originating from the deep spill site located in the Pokak lease area, early in the operating season would result in extensive surface oiling to the west, as far as Point Barrow (occasionally further west). There is a high probability that shorelines along the US coast of the North Slope and Point Barrow would get moderately to heavily oiled. Blowouts occurring later in the operating season would exhibit extensive westward surface oiling. Contamination from later season blowouts would be less extensive to the north when compared to spills spreading for longer periods of time in ice free open water (early season). Late season spills would result in lower shoreline oiling due to landfast ice build-up into the winter months. Persistent water contamination by dissolved aromatics (1-100 ppb) may result from long blowout releases, and could travel far distances from the spill site. If no dispersants were used, oil surfaced within a day and became trapped in sea ice in the later operating season and winter. Use of subsea dispersants at the deep release site may cause subsurface oil to concentrate at depth along the Beaufort shelf.

9 References

Aagaard, K., Pease, C. H., Roach, A. T., and Salo, S. A. (1989). Beaufort Sea Mesoscale Circulation Study, NOAA Technical Memorandum ERL PMEL-90, Pacific Marine Environmental Laboratory, Seattle, WA.

American Petroleum Institute (API), National Oceanic and Atmospheric Administration (NOAA), U.S. Coast Guard (USCG), and U.S. Environmental Protection Agency (USEPA), Characteristics of Response Strategies: A Guide for Spill Response Planning in Marine Environments, Joint Publication of API, NOAA, USCG, and USEPA, June 2001, 80p., 2001.

AXYS, (2004). Environmental Atlas for Beaufort Sea Oil Spill Response. Provided as PDF to RPS ASA from WWF Fall 2013.

Barry, R.G., Moritz, R.E., and Rogers, J.C., (1979). The fast ice regimes of the Beaufort and Chukchi Sea coasts, Alaska. *Cold Regions Science and Technology* (1) 129-152.

Beaufort Regional Environmental Assessment (BREA), Trudel, K. SL Ross Environmental Research Ltd. (2012). Annual Progress Report 2011-2012: Biological Data to Assess the Net Environmental Benefits and Costs of Dispersants and In-Situ Burning in Oil Spill Response, 2011-2013. p. 7.

Bentsen, M., Evensen, G., Drange, H., and Jenkins, A. D., (1999). Coordinate transformation on a sphere using conformal mapping. *Mon. Weather Rev*. (127) 2733–2740.

Bishnoi, P.R. and Mainik B.B. (1979). Laboratory study of behaviour of oil and gas particles in salt water, relating to deepwater blowouts, Spill Technology Newsletter, Vol. 4 (1), pp. 24-36.

Bleck, R. (2002). An oceanic general circulation model framed in hybrid isopycnic-cartesian coordinates. *Ocean Modelling* (4) 55-88.

Boyer, T., Levitus, S., Garcia, H., Locarnini, R. A., Stephens, C., and J. Antonov, (2004). Objective Analyses of Annual, Seasonal, and Monthly Temperature and Salinity for the World Ocean on a ¼ E Grid. *International Journal of Climatology* (25) 931-945.

Carmack, E. C., and Kulikov, E. A. (1998). Wind-forced upwelling and internal Kelvin wave generation in Mackenzie Canyon, Beaufort Sea. *Journal of Geophysical Research* (96) 21,989 – 22,008.

Carmark, E. C., and Macdonald, R. W. (2002). Oceanography of the Canadian Shelf of the Beaufort Sea: a setting for marine life. *Arctic* (55, Supp. 1) 29-45.

Coachman, L. K., Aagaard, K., and Tripp, R. B. (1975). Bering Strait: The Regional Physical Oceanography, 172pp., University of Washington Press, Seattle.

Conkright, M.E., Antonov, J.I., Baranova, O., Boyer, T.P., Garcia, H.E., Gelfeld, R., Johnson, D., Locarnini, R.A., Murphy, P.P., O'Brien, T.D., Smolyar, I., and Stephens, C. (2002). World Ocean Database 2001, Volume 1: Introduction. Sydney Levitus (ed.). NOAA Atlas NESDIS 42, U.S. Government Printing Office, Washington, D.C., 167 pp.

Davies, K. F. (1975). Mackenzie River Input to the Beaufort Sea, Technical Report #15, Department of the Environment, Victoria, B.C.

Divine, D. V., Korsnes, R., and Makshtas, A. P. (2004). Temporal and spatial variation of shore-fast ice in the Kara Sea. *Continental Shelf Research* (24) 1717-1736.

Dobbins, E., "Chukchi & Western Beaufort Circulation Study Data Tool." University of Alaska, 1 Oct. 2013. Web. http://dm.sfos.uaf.edu/chukchi-beaufort

Drozdowski, A., Nudds, S., Hannah, C. G., Niu, H., Peterson, I., and Perrie, W. (2011). Review of Oil Spill Trajectory Modelling in the Presence of Ice. Can. Tech. Rep. Hydrogr. Ocean Sci. 274: vi + 84 pp.

Eicken, H., Shapiro, L.H., Gens, R., Meyer, F., Heninrichs, T., Mahoney, A.R., Gaylord, A., and P. W. Cotter (2006). Mapping and Characterization of Recurring Spring Leads and Landfast Ice in the Beaufort and Chukchi Seas. U.S. Department of the Interior, Minerals Management Service (MMS), Alaska Outer Continental Shelf Region, Anchorage, AK. Final Report, OCS Study MMS 2005-068.

Environmental Technology Centre, Environment Canada (2004). Spills Technology Databases. Oil Properties database. http://www.etc-cte.ec.gc.ca/databases/OilProperties/Default.aspx (27 August 2004).

Evensen, G. (1994). Sequential data assimilation with nonlinear quasi-geostrophic model using Monte Carlo methods to forecast error statistics. *Journal of Geophysical Research* (99) 10,143-10,162.

French McCay, D., J. Rowe, N. Whittier and C. Santos, 2013. Modeling the M/T Prestige Oil Spill and Alternative Scenarios if Towed to a Port of Refuge. In Proceedings of the 36th AMOP Technical Seminar on Environmental Contamination and Response, Emergencies Science Division, Environment Canada, Ottawa, ON, Canada.

French McCay, D., Reich, D., Rowe, J., Schroeder, M., and Graham, E. (2011). Oil Spill Modelling Input to the Offshore Environmental Cost Model (OECM) for US-BOEMRE's Spill Risk and Cost Evaluations. In: Proceedings of the 34th Arctic and Marine Oil Spill Program (AMOP) Technical Seminar, Emergencies Science Division, Environment Canada, Ottawa, ON, Canada.

French-McCay, D.P. (2009). State-of-the-Art and Research Needs for Oil Spill Impact Assessment Modelling. In Proceedings of the 32nd AMOP Technical Seminar on Environmental Contamination and Response, Emergencies Science Division, Environment Canada, Ottawa, ON, Canada, pp. 601-653.

French McCay, D.P. (2003). Development and Application of Damage Assessment Modelling: Example Assessment for the North Cape Oil Spill. *Marine Pollution Bulletin* (47: 9-12): 341-359.

French, D., Reed, M., Jayko, K., Feng, S., Rines, H., Pavignano, S., Isaji, T., Puckett, S., Keller, A., French III, F. W., Gifford, D., McCue, J., Brown, G., MacDonald, E., Quirk, J., Natzke, S., Bishop, R., Welsh, M., Phillips, M., and Ingram, B.S. (1996). The CERCLA Type A Natural Resource Damage Assessment Model for Coastal and Marine Environments (NRDAM/CME), Technical Documentation, Vol. I -VI, Final Report, submitted to the Office of Environmental Policy and Compliance, U.S. Dept. of the Interior, Washington, D.C., Contract No. 14-0001-91-C-11, April, 1996.

Hunke, E.C. and Dukowicz, J.K. (1997). An Elastic-Viscous-Plastic model for sea ice dynamics. *Journal of Physical Oceanography* (27) 1849-1867.

Imperial Oil Resources Ventures Limited (IORVL), (2013). Beaufort Sea Exploration Joint Venture Drilling Program, *Environmental Impact Screening Committee*.

IOC, IHO and BODC (GEBCO), (2009). Centenary Edition of the GEBCO Digital Atlas, published on behalf of the Intergovernmental Oceanographic Commission (IOC) and the International Hydrographic Organization (IHO) as part of the General Bathymetric Chart of the Oceans; British Oceanographic Data Centre (BODC), Liverpool.

Isaji, T., Howlett, E., Dalton, C., and Anderson, E.L. (2001a). Stepwise continuous-variable rectangular grid hydrodynamics model. In: Proceedings of the Twenty-fourth Arctic and Marine Oil spill Program (AMOP) Technical Seminar, Edmonton (Alberta) Canada, pp. 597- 610, June 12, 2001.

Isaji, T., Howlett, E., Dalton, C., and Anderson, E.L. (2001b). Stepwise continuous-variable rectangular grid hydrodynamics model. In Proceedings of the 7th International Conference on Estuarine and Coastal Modelling, St. Pete Beach, FL, November 5-7, 2001.

Jia, W., Mizobata, K., Haoguo, H., Meibing, J., Sheng, Z., Johnson, W., Shimada, K., and Ikeda, M. (2008). Modelling seasonal variations of ocean and sea ice circulation in the Beaufort and Chukchi Seas: A model-data fusion study. *Chinese Journal of Polar Science* (19, No. 2) 168-184.

Jokuty, P., Whiticar, S., Wang, Z., Fingas, M., Fieldhouse, B., Lambert, P., Mullin, J. (1999). Properties of Crude Oils and Oil Products. Manuscript Report EE-165, Environmental Protection Service, Environment Canada, Ottawa, ON, Canada, 13pp. + appendices.

Kasper, J. L., and Weingartner, T. J. (2012). Modelling winter circulation under landfast ice: The interaction of winds with landfast ice. *Journal of Geophysical Research*, submitted.

Khelifa, A. and So, L.L.C. (2009). Effects of chemical dispersants on oil-brine interfacial tension and droplet formation. In: 32nd Proceedings of Arctic and Marine Oil Spill Program Technical Seminar, Environment Canada, Ottawa, Canada, pp. 383-396.

Kolpack, R.L., Plutchak, N.B., and Stearns, R.W. (1977). Fate of oil in a water environment - Phase II, a Dynamic model of the mass balance for released oil. University of Southern California, prepared for American Petroleum Institute, API Publication 4313, Washington, D.C.

Konig Beatty, C. S. (2012). Arctic Landfast Sea Ice 1953-1998. Boulder, Colorado USA: National Snow and Ice Data Center. http://dx.doi.org/10.7265/N5ZW1HV4.

Lansard, B., Mucci, A., Miller, L. A., Macdonald, R. W., and Gratton, Y. (2012). Seasonal variability of water mass distribution in the southeastern Beaufort Sea determined by total alkalinity and d18O. *Journal of Geophysical Research,* (117) C03003, doi: 10.1029/2011JC007299.

Lee, L.S., Hagwall, M., Delfino J.J., and Rao, P.S.C. (1992). Partitioning of Polycyclic Aromatic Hydrocarbons from Diesel Fuel into Water. *Environ. Sci. Technol.* (26):2104-2110.

Macdonald, R. W., Carmack, E. C., and McLaughlin, F. A. (1999). Connections among ice, runoff and atmospheric forcing in the Beaufort Gyre. *Geophysical Research Letters* (26, No. 15) 2223-2226.

Mahoney, A., H. Eicken, A. G. Gaylord, and Shapiro L. (2007). Alaska landfast sea ice: Links with bathymetry and atmospheric circulation. *Journal of Geophysical Research Oceans* (112).

Mahoney, A.R., Eicken, H., Shapiro, L.H., Gens, R., Heinrichs, T., Meyer, F.J., and Graves Gaylord, A. (2012). Mapping and Characterization of Recurring Spring Leads and Landfast Ice in the Beaufort and Chukchi Seas. U.S. Dept. of the Interior, Bureau of Ocean Energy Management, Alaska Region, Anchorage, AK. OCS Study BOEM 2012-067. 179pp.

McAuliffe, C.D. (*1987*). Organism Exposure to Volatile/Soluable Hydrecarbons from Crude Oil Spills – A Field Laboratory Comparison. International Oil Spill Conference Proceedings: April 1987, Vol. 1987, No. 1, pp. 275-288.

McDougall, T.J. (1978). Bubble plumes in stratified environments, Journal of Fluid Mechanics, Vol. 85, Part 4, pp. 655-672.

Melling, H. (1993). The formation of a haline shelf front in wintertime in an ice-covered arctic sea. *Continental Shelf Research* (13) 1123-1147.

Melling, H., Riedel, D.A., and Gedalof, Z. (2005). Trends in the draft and extent of seasonal pack ice, Canadian Beaufort Sea. *Geophysical Research Letters* (32) doi:10.1029/2005GL024483.

Moore, G. W. K., and Pickart, R. S. (2012). The Wrangel Island Polynya in early summer: Trends and relationship to other polynyas and the Beaufort Sea high. *Geophysical Research Letters* (39) 5 p.

National Energy Board (NEB) (2011). Review of Offshore Drilling in the Canadian Arctic. Technical report.

National Incident Command (NIC) Oil Budget Calculator Deepwater Horizon (2010). Technical Documentation, Federal Interagency Solutions Group, Oil Budget Calculator Science and Engineering Team.

Nikolopoulos, A., Pickart, R. S., Fratantoni, P. S., Shimada, K., Torres, D. J., and Jones, E. P. (2009). The western Arctic boundary current at 152oW: Structure, variability, and transport. *Deep Sea Research Part II* (56) 1164 – 1181.

Osborne, P. D., Fissel, D., Mudge, T., Lowings, M. G., Hawkins, J., Darlow, N., Gratton, Y., Pyc, C., Driver, D., Fortier, M., and Levesque, K. (2012). Observations of currents, salinity and temperature in the Ajurak and Pokak exploration license areas of the Canadian Beaufort Sea, July 2009 to September 2012. Abstract and poster presentation, US –Canada Northern Oil and Gas Research Forum, Anchorage, AK.

Owen, A. (1980). A three-dimensional model of the Bristol Channel. *Journal of Physical Oceanography* (10) 1290-1302.

Peterson, I.K., Prinsenberg, S., and Holladay, J.S. (2008). Observations of sea ice thickness, surface roughness and ice motion in Amundsen Gulf. *Journal of Geophysical Research* (113) doi: 10.1029/2007JC004456.

Pickart, R. S. (2004). Shelfbreak circulation in the Alaskan Beaufort Sea: Mean structure and variability, Journal of Geophysical Research (109) C04024, doi:10.1029/2003JC001912.

Pickart, R. S., Moore, G. W. K., Torres, D. J., Frantantoni, P. S., Goldsmith, R. A., Yang, J. (2009). Upwelling on the continental slope of the Alaskan Beaufort Sea: Storms, ice, and oceanographic response. *Journal of Geophysical Research* (114).

Pickart, R. S., Spall, M. A., Moore, G. W. K., Weingartner, T. J., Woodgate, R. A., Aagaard, K., and Shimada, K. (2011). Upwelling in the Alaskan Beaufort Sea: Atmospheric forcing and local versus on-local response. *Progress in Oceanography* (88) 78 – 100.

Potter, S., Buist, I., Trudel, K., Dickens, D., and Owens, E. (2012). Spill Response in the Arctic Offshore. Report prepared for the American Petroleum Institute and the Joint Industry Programme on Oil Spill Recovery in Ice. February 2, 2012: FINAL.

Proshutinsky, A., Bourke, R. H., and McLaughlin, F. A. (2002). The role of the Beaufort Gyre in Arctic climate variability: Seasonal to decadal climate scales. *Geophysical Research Letters* (29).

Proshutinsky, A., Krishfield, R., Timmermans, M.-L., Carmack, E. McLaughlin, F., Williams, W. J., Zimmermann, S., Itoh, M., and Shimada, K. (2009). Beaufort Gyre freshwater reservoir: State and variability from observations. *Journal of Geophysical Research* (114).

Sakov, P., Counillon, F., Bertino, L., Lisaeter, K.A., Oke, P.R., and Korablev, A. (2012). TOPAZ4: an ocean-sea ice data assimilation system for North Atlantic and Arctic. *Ocean Science* (8) 633-656.

Samuelson, A., and Bertino, L. (2013). Lofoten and versteralen currents, Mid-term Report. NERSC Technical Report no. 312. Nansen Environmental and Remote Sensing Center.

Schulze, L. M., Pickart, R. S. (2012), Seasonal variation of upwelling in the Alaskan Beaufort Sea, *Journal of Geophysical Research (*117).

SL Ross Environmental Research Ltd., DF Dickins Associates LLC., Envision Planning Solutions Inc. (2010). Beaufort Sea Oil Spills State of Knowledge Review and Identification of Key Issues. Environmental Studies Research Funds Report No. 177. Calgary. 126p.

Sørstrøm, S. E., Brandvik, P.J., Buist, I., Daling, P., Dickins, D., Faksness, L.-G., Potter, S., Fritt Rasmussen, J., and Singsaas, I. (2010). Joint industry program on oil spill contingency for Arctic and ice covered waters, SINTEF report.

Spaulding, M.L. (1988). A state-of-the-art review of oil spill trajectory and fate modelling. *Oil and Chemical Pollution (*4): 39-55.

Venkatesh, S., H. El-Tahan, G. Comfort, and Abdelnour, R. (1990). Modelling the Behaviour of Oil Spills in Ice-Infested Waters. *Atmosphere-Ocean*. Canadian Meteorological and Oceanographic Society (28:3) 303-329.

Whiticar, S., Bobra, M., Fingas, M., Jokuty, P., Liuzzo, P., Callaghan, S., Ackerman, F., and Cao, J. (1994). A catalogue of crude oil and oil product properties, 1992 edition with 1994 data files. Unpublished report of Environment Canada.

World Wildlife Fund (WWF) and EcoJustice (2011). Letter of Comment to NEB: Arctic Offshore Drilling Review, NEB File: OF-EP-Gen-AODR 01., S.L. Ross Spill Response Gap Study for the Canadian Beaufort Sea and the Canadian Davis Straight.

Youssef, M. (1993). The behavior of the near ocean surface under the combined action of waves and currents in shallow water. PhD Dissertation, Department of Ocean Engineering, University of Rhode Island, Narragansett, RI.

Youssef, M. and Spaulding, M. L. (1993). Drift current under the action of wind waves, in *Proceedings of the 16th Arctic and Marine Oil Spill Program Technical Seminar*, Calgary, Alberta, Canada, 587-615.

Youssef, M. and Spaulding, M.L. (1994). Drift Current under the Combined Action of Wind and Waves in Shallow Water, in *Proceedings of the 17th Arctic and Marine Oil Spill Program (AMOP) Technical Seminar*, Vancouver, British Columbia, 767-784.

Appendix A: SIMAP Model Description

SIMAP is a computer Modelling software application that estimates physical fates and biological effects of releases of oil. In SIMAP, both the physical fates and biological effects models are three-dimensional. There is also a two-dimensional oil spill model for quick trajectories and screening of scenarios and a three-dimensional stochastic model for risk assessment and contingency planning applications. The models are coupled to a geographic information system (GIS), which contains environmental and biological data, and also to databases of physical-chemical properties and biological abundance, containing necessary inputs for the models.

SIMAP was derived from the physical fates and biological effects submodels in the Natural Resource Damage Assessment Models for Coastal and Marine and Great Lakes Environments (NRDAM/CME and NRDAM/GLE), which were developed for the U.S. Department of the Interior (USDOI) as the basis of Comprehensive Environmental Response, Compensation and Liability Act of 1980 (CERCLA) Natural Resource Damage Assessment (NRDA) regulations for Type A assessments (French et al., 1996; Reed et al., 1996). The physical fates model has been validated with more than 20 case histories, including the *Exxon Valdez* and other large spills (French McCay, 2003, 2004; French McCay and Rowe, 2004), as well as test spills designed to verify the model's transport algorithms (French et al., 1997). The wildlife mortality model has been validated with more than 20 case histories, including the *Exxon Valdez* and other large spills, verifying that these values are reasonable (French and Rines, 1997; French McCay 2003, 2004; French McCay and Rowe, 2004). The technical documentation for SIMAP is in French McCay (2003, 2004, 2009).

Applications for SIMAP include impact assessment; hindcast/forecast of spill response; Natural Resource Damage Assessment (NRDA); contingency planning; ecological risk assessment; cost-benefit analysis, and drills and education. The model may be run for a hindcast/forecast of a specific release, or be used in stochastic mode to evaluate the probable distribution of contamination. SIMAP contains several major components:

- The physical fates model estimates surface distribution and subsurface concentrations of the spilled oil and its components over time.
- The biological effects model estimates effects resulting from a spill scenario on fish, shellfish, wildlife, and for each of a series of habitats (environments) affected by the spill.
- The probability of effects from an oil discharge is quantified using the three-dimensional stochastic model.
- Currents that transport contaminant(s) and organisms are entered using the graphical user interface or generated using a (separate) hydrodynamic model. Alternatively, existing current data sets may be imported.
- Environmental, chemical, and biological databases supply required information to the model for computation of fates and effects.
- The user supplies information about the spill (time, place, oil type, and amount spilled) and some limited environmental conditions at the time (such as temperature and wind data).

As with RPS ASA's other modelling systems, SIMAP is easily applied to a wide variety of conditions. It is set up and runs within RPS ASA's standard Geographic Information system (GIS) or ESRI's ArcView GIS, and can be applied to any aquatic environment (fresh or salt) in the world. It uses any of a variety of hydrodynamic data file formats (1-, 2- and 3-dimensional; time varying or constant) and allows 2-d vertically-averaged current files to be created within the program system when modelled currents are not available. Outputs include easily interpreted visual displays of dissolved and particulate concentrations and trajectories over time, as appropriate to the properties of the chemical being simulated. An optional biological exposure model is available to evaluate areas and volumes exposed above concentrations of concern and to predict effects on exposed fish and wildlife.

SIMAP specifically simulates the following processes:

- slick spreading, transport, and entrainment of floating oil
- evaporation and volatilization (to atmosphere)
- transport and dispersion of entrained oil and dissolved aromatics in the water column
- dissolution and adsorption of entrained oil and dissolved aromatics to suspended sediments
- sedimentation and re-suspension
- natural degradation
- shoreline entrainment, and
- boom and dispersant effectiveness.

The physical and biological models require environmental, oil and biological data as inputs. One of RPS ASA's strengths is the ability to synthesize data from disparate sources. The data come from many sources including government and private data services, field studies and research. Modelling techniques are used to fill in "holes" in the observational data, thus allowing complete specification of needed data. The environmental database is geographical, including data of the following types: coastline, bathymetry, shoreline type, ecological habitat type, and temporally varying ice coverage and temperature. This information is stored in the simplified geographic information system (GIS). The chemical database includes physical-chemical parameters for a wide variety of oils and petroleum products. Data have been compiled by RPS ASA from existing, but diffuse, sources.

An oil spill is simulated using site-specific wind, current, and other environmental data gathered from existing information, on-line services, and/or field studies. Shoreline and habitat types, as well as bathymetry, are mapped and gridded for use as model input. The physical, chemical, and toxicological properties of the spilled oil are provided by the oil database or updated to the specific conditions of the release. The model estimates the fate of the oil over time. The model outputs are time-varying concentrations and mass per unit area on surfaces (i.e., water surface, shoreline, sediments), which quantifies exposure to aquatic biota and habitats. Atmospheric loading in space and time is also computed, and provides input to air dispersion models.

SIMAP References

French, D., M. Reed, K. Jayko, S. Feng, H. Rines, S. Pavignano, T. Isaji, S. Puckett, A. Keller, F. W. French III, D. Gifford, J. McCue, G. Brown, E. MacDonald, J. Quirk, S. Natzke, R. Bishop, M. Welsh, M. Phillips and B.S. Ingram, 1996. The CERCLA type A natural resource damage assessment model for coastal and marine environments (NRDAM/CME), Technical Documentation, Vol. I - V. Final Report, submitted to the Office of Environmental Policy and Compliance, U.S. Dept. of the Interior, Washington, DC, April, 1996; Available from National Technical Information Service, 5285 Port Royal Road, Springfield, VA 22161, PB96-501788.

French, D.P., and H. Rines, 1997. Validation and use of spill impact Modelling for impact assessment. In: *Proceedings, 1997 International Oil Spill Conference*. Fort Lauderdale, Florida, American Petroleum Institute Publication No. 4651, Washington, DC, pp.829-834.

French, D.P., H. Rines and P. Masciangioli, 1997. Validation of an Orimulsion spill fates model using observations from field test spills. In: *Proceedings of 20th Arctic and Marine Oil Spill Program (AMOP) Technical Seminar*. Vancouver, Canada, June 10-13, 1997, Emergencies Science Division, Environment Canada, Ottawa, ON, Canada, pp. 933-961.

French McCay, D.P., 2003. Development and Application of Damage Assessment Modelling: Example Assessment for the *North Cape* Oil Spill. *Marine Pollution Bulletin* 47 (9-12): 341-359.

French McCay, D.P., 2004. Oil spill impact Modelling: development and validation. *Environmental Toxicology and Chemistry* 23(10): 2441-2456.

French McCay, D.P, 2009. State-of-the-Art and Research Needs for Oil Spill Impact Assessment Modelling. In *Proceedings of the 32nd AMOP Technical Seminar on Environmental Contamination and Response*, Emergencies Science Division, Environment Canada, Ottawa, ON, Canada, pp. 601-653.

French McCay, D.P., and J.J. Rowe, 2004. Evaluation of Bird Impacts in Historical Oil Spill Cases Using the SIMAP Oil Spill Model. In: *Proceedings of the 27th Arctic and Marine Oil Spill Program (AMOP) Technical Seminar*, Emergencies Science Division, Environment Canada, Ottawa, ON, Canada, pp. 421-452.

Reed, M., D.P. French, S.Feng, F.W. French III, E. Howlett, K, Jayko, W.Knauss, J. McCue, S. Pavignano, S. Puckett, H. Rines, R.Bishop, M. Welsh, and J. Press, 1996. The CERCLA type a natural resource damage assessment model for the Great Lakes environments (NRDAM/GLE), Vol. I - III. Final report, submitted to Office of Environmental Policy and Compliance, U.S. Department of the Interior, Washington, DC, by Applied Science Associates, Inc., Narragansett, RI, April 1996, Contract No. 14-01-0001-88-C-27.

Appendix B: OILMAPDeep Model Description

As offshore oil development proceeds into deeper water, the possibility of blowouts becomes of increasing concern. The principal issues are the difficulty in mounting effective containment and cleanup for such spills and of the effects of dispersed, subsurface oil that may travel many kilometers in the water column. As an example, oil released from the IXTOC blowout (Gulf of Mexico, September 1979) was dispersed throughout the water column and resulted in high concentrations of petroleum hydrocarbons in the vicinity of the well.

To address this issue, RPS ASA's OILMAPDeep was developed to serve as a tool to evaluate potential accidental releases of oil and gas from a deepwater well blowout, and furthermore to be able to evaluate spill response activities such as subsurface dispersant application.

OILMAPDeep contains two sub-models, a plume model and a droplet size model. The plume model predicts the evolution of buoyant plume position, geometry, centerline rise velocity and oil and gas concentrations until either surfacing or reaching a terminal height at which point the plume is no longer buoyant and so is trapped. The droplet model predicts the size and volume (mass) distribution of oil droplets. The plume dynamics transport released oil to the plume termination height, after which point the transport of the oil is dominated by the ambient environmental conditions. The near field blowout model results calculated in OILMAPDeep define the initial conditions for the far field simulations, where the oil mass is initially released at the plume trap height in droplets defined by the calculated size distribution.

The OILMAPDeep blowout model is based on the work of McDougall (gas plume model, 1978), Fanneløp and Sjøen (1980a, plume/free surface interaction), Spaulding (1982, oil concentration model), Kolluru, (1993, World Oil Spill Model implementation), Spaulding et.al. (2000, hydrate formation) and Zheng et.al., (2002, 2003, gas dissolution). A simplified integral jet theory is employed for the vertical as well as for the horizontal motions of the gas-oil plume. Oil and gas buoyancy are incorporated based on their respective densities and for gas include the effects of compression based on methane characteristics. The necessary model parameters defining the rates of entrainment and spreading of the jet are obtained from laboratory studies (Fanneløp and Sjøen, 1980a). The gas plume analysis is described in McDougall (1978), Spaulding (1982), and Fanneløp and Sjøen (1980a). Gas dissolution is included based on formulations originally from Johnson et al. (1969) and Clift et al. (1978). The dissolution algorithm is a function of initial gas bubble size, the appropriate gas saturation depending on the temperature and the estimated water column concentration of dissolved gas in the plume water. The formulation includes a calculation of the mass transfer coefficient as a function of bubble size. The bubbles are approximated as spheres for small size, ellipsoids for intermediate size, and spherical-caps for large size. Consistent with Zheng (2003) the critical diameter between small and intermediate size ranges is 5 mm and between intermediate and large size ranges is 13 mm. A hydrate formation and dissociation model is formulated based on a unique equilibrium kinetics model developed by R. Bishnoi (1989) and colleagues at the University of Calgary.

Oil droplet size distribution calculations are based on the methodology presented by Yapa and Zheng (2001b), which uses a maximum diameter (d_{95}) calculation and the associated volumetric droplet size distribution. The maximum diameter formulation is based on Hinze (1955), and the droplet size distribution is described utilizing a Rosin-Rammler (1933) distribution.

Description of a Blowout

In a well blowout, discharged materials consisting of a mixture of gaseous and liquid hydrocarbon, go through three phases:

1) Momentum jet

The immediate pressure difference between inside the well and the ambient water drives the discharge. Due to the relative high-density of the deep ocean water, this jet momentum dissipates relatively quickly and is confined to the vicinity of the release point (on the order of meters).

2) Buoyant density plume

As the discharge moves upward, the density difference between the expanding gas bubbles in the plume and the receiving water results in a buoyant force which drives the plume. As the plume rises, it continues to entrain sea water, reducing the plume's velocity and buoyancy and increasing its radius.

The oil in the release is rapidly mixed due to turbulence in the plume, resulting in a break up into small droplets. These droplets (typically a few micrometers to millimeters in diameter) are transported upward by the rising plume; their individual rise velocities contributing little to their upward motion in this region.

3) Free rise and advection-diffusion.

As the plume reaches the sea surface or its *termination height* (when all momentum is lost), it can be deflected in a radial pattern within a horizontal / surface flow zone without appreciable loss of momentum. This radial jet carries the oil particles rapidly away from the center of the plume, while the velocity and oil concentrations in this surface flow zone decrease.

Plumes that do not reach the surface terminate within the water column and the plume acts to transport the oil droplets to this termination height. Subsequently (in the so-called far field), oil particles ascend to the surface solely by their own buoyancy. Rise velocities of oil droplets are much slower than the velocity of a buoyant gas-liquid plume, resulting in particle transport that may take considerably longer to reach the surface and result in transport farther (horizontally) from the release site due to ambient currents.

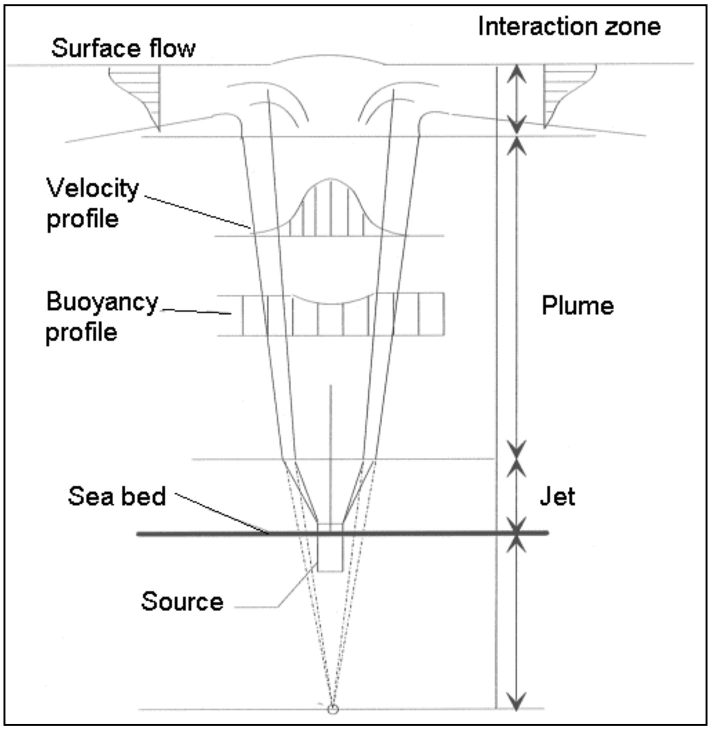

In order to reproduce this dynamic and complex process, blowout simulations are performed in two steps:

A. Near-field analysis, describing the oil/gas plume generated by the blowout that typically evolves vertically due to vertical processes (momentum and relative buoyancy), and

B. Far-field analysis, describing the long term transport and weathering of the released oil mixture, that typically evolves as a horizontal process due to currents and winds

The near-field model results provide the initial conditions for both the stochastic and deterministic modes of the far-field modelling. The near-field results depend more on the blowout conditions (flow rate, GOR, and pipe diameter), and less on the environmental conditions (e.g., seasonality). Conversely, the far-field modelling is highly dependent on the environmental conditions such as winds and currents as the main the drifting/driving forces.

OILMAPDeep References:

Bishnoi, P.R. and Mainik B.B. (1979). Laboratory study of behaviour of oil and gas particles in salt water, relating to deepwater blowouts, Spill Technology Newsletter, Vol. 4 (1), pp. 24-36.

Clift, R., Grace, J.R., and Weber, M.E. (1978). Bubbles, Drops and Particles. New York, NY. Academic Press, Inc.

Fanneløp, T.K. and Sjoen , K. (1980a). Hydrodynamics of underwater blowouts, AIAA 8th Aerospace Sciences Meeting, January 14-16, Pasadena, California, AIAA paper, pp. 80-0219.

Hinze, J. O. (1955). Fundamentals of the hydrodynamics mechanisms of splitting in dispersion process. AIChE J. (1): 289–295.

Johansen, O. (2002). "Estimates of Droplet Size from Subsea Oil and Gas Leaks or Blowouts," SINTEF document.

Johnson, A. I., Besik. F., and Hamielec, A. (1969). Mass Transfer from a Single Rising Bubble. *A. E. Can. J. Cheril. Eng*. (47): 559-564.

Kolluru, V.S. (1993). Oil blowout model, Applied Science Associates, Inc., Narragansett, RI 02882.

McDougall, T.J. (1978). Bubble plumes in stratified environments, Journal of Fluid Mechanics. (85: Part 4): 655-672.

Rosin, P. and Rammler, E. (1933). The Laws Governing the Fineness of Powdered Coal. *Journal of the Institute of Fuel* (7): 29–36.

Spaulding, M.L. (1982). User's manual for a simple gas blowout plume model, Continental Shelf Institute, Trondheim, Norway.

Spaulding, M.L., Bishnoi, P.R., Anderson, E., and Isaji, T. (2000). An Integrated Model for Prediction of Oil Transport from a Deep Water Blowout. 23 rd Arctic and Marine Oil Spill Program (AMOP) Technical Seminar, June 14-16, 2000, Vancouver, British Columbia, Canada, pp.611-636.

Yapa, P. D., and Chen, F. H. (2003). CDOG 2 Clarkson Deepwater Oil and Gas Model Users Guide. Dep. Civ. and Env. Eng., Clarkson University, Potsdam, NY.

Yapa, P. D., Zheng, L., and Chen, F. H. (2001a). A model for deepwater oil/gas blowouts. *Mar. Pollution Bull.* (43): 234–241.

Yapa, P. D., Zheng, L., and Chen, F. H. (2001b). Clarkson deepwater oil & gas ~CDOG model. Rep. No. 01–10, Dept. of Civil and Environmental Engineering, Clarkson Univ., Potsdam, N.Y.

Zheng, L. and Yapa, P.D. (2002). Modelling Gas Dissolution in Deepwater Oil/Gas Spills, Journal of Marine Systems, Elsevier, the Netherlands, March, 299-309

Zheng, L., Yapa, P.D. and Chen, F.H. (2003). A Model for Simulating Deepwater Oil and Gas Blowouts - Part I: Theory and Model Formulation. *Journal of Hydraulic Research* (41:4): 339-351.

Appendix C: Spill Scenario Development and Probability Analysis

Please see external electronic document file titled:

“13-235_WWF_Spill Scenario Development and Probability Analysis_Appendix C_Revised2”

Appendix D: Full Scenario List and Naming Convention

This Appendix contains tables of scenario names and the naming convention followed for each. Tables are organized by analysis and scenario type (stochastic or individual trajectory).

Table 35. Eastern Shipping Analysis – list of stochastic scenarios and naming convention.

Scenario Name	Release Location	Oil Type
EastShip_IFO	EastShip	IFO
EastShip_Diesel	EastShip	Diesel

Table 36. Eastern Shipping Analysis – list of individual trajectories and naming convention.

Scenario Name	Release Location	Oil Type	Individual Run Number in Stochastic Ensemble	Run Type - 95th percentile for shore/surface/water column oil contamination
EastShip_IFO_r98_95surf	EastShip	IFO	r98	95surf
EastShip_IFO_r59_95shore	EastShip	IFO	r59	95shore
EastShip_Diesel_r60_95surf	EastShip	Diesel	r60	95surf
EastShip_Diesel_r22_95shore	EastShip	Diesel	r22	95shore

Table 37. Trans-boundary Analysis – list of stochastic scenarios and naming convention (TB = Trans-boundary).

Scenario Name	Release Type	Release Location	Oil Type
TB_Ship_IFO_CAN	Ship	CAN	IFO
TB_Ship_Crude_CAN	Ship	CAN	Crude
TB_Ship_IFO_US	Ship	US	IFO
TB_Ship_Crude_US	Ship	US	Crude
TB_Pipeline_CAN	Pipeline	CAN	Crude
TB_Pipeline_US	Pipeline	US	Crude

Table 38. Trans-boundary Analysis – list of individual trajectories and naming convention (TB=Trans-boundary).

Scenario Name	Release Type	Release Location	Oil Type	Individual Run Number in Stochastic Ensemble	Run Type - 95th percentile for shore/surface/water column oil contamination
TB_Ship_IFO_CAN_r85_95surf	Ship	CAN	IFO	r85	95surf
TB_Ship_IFO_CAN_r87_95shore	Ship	CAN	IFO	r87	95shore
TB_Ship_Crude_CAN_r80_95surf	Ship	CAN	Crude	r80	95surf
TB_Ship_Crude_CAN_r71_95shore	Ship	CAN	Crude	r71	95shore
TB_Ship_Crude_CAN_r70_95WC	Ship	CAN	Crude	r70	95WC
TB_Ship_IFO_US_r65_95surf	Ship	US	IFO	r65	95surf
TB_Ship_IFO_US_r23_95shore	Ship	US	IFO	r23	95shore
TB_Ship_Crude_US_r65_95surf	Ship	US	Crude	r65	95surf
TB_Ship_Crude_US_r33_95shore	Ship	US	Crude	r33	95shore
TB_Ship_Crude_US_r60_95WC	Ship	US	Crude	r60	95WC
TB_Pipeline_CAN_r57_95surf	Pipeline	CAN	Crude	r57	95surf
TB_Pipeline_CAN_r15_95shore	Pipeline	CAN	Crude	r15	95shore
TB_Pipeline_CAN_r60_95WC	Pipeline	CAN	Crude	r60	95WC
TB_Pipeline_US_r23_95surf	Pipeline	US	Crude	r23	95surf
TB_Pipeline_US_r54_95shore	Pipeline	US	Crude	r54	95shore
TB_Pipeline_US_r85_95WC	Pipeline	US	Crude	r85	95WC

Table 39. Shallow Blowout Analysis – list of stochastic scenarios and naming convention (Shal = Shallow Blowout Site).

Scenario Name	Release Volume	Release Duration (Days)	Response Measures	Season
ShalWCD_60rel_noresp_early	WCD	60rel	noresp	early
ShalWCD_90rel_noresp_late	WCD	90rel	noresp	late
ShalMMPD_30rel_noresp_early	MMPD	30rel	noresp	early
ShalMMPD_60rel_noresp_late	MMPD	60rel	noresp	late

Table 40. Shallow Blowout Analysis – list of individual trajectories and naming convention (Shal = Shallow Blowout Site).

Scenario Name	Release Volume	Release Duration (Days)	Response Measures	Season	Individual Run Number in Stochastic Ensemble	Run Type - 95th percentile for shore/surface/water column oil contamination
ShalWCD_60rel_noresp_early_r32_95surf	WCD	60rel	noresp	early	r32	95surf
ShalWCD_60rel_noresp_early_r98_95shore	WCD	60rel	noresp	early	r98	95shore
ShalWCD_60rel_noresp_early_r81_95WC	WCD	60rel	noresp	early	r81	95WC
ShalWCD_60rel_surfresp_early_r32_95surface	WCD	60rel	surfresp	early	r32	95surface
ShalWCD_60rel_surfresp_early_r98_95shore	WCD	60rel	surfresp	early	r98	95shore
ShalWCD_90rel_noresp_late_r72_95surf	WCD	90rel	noresp	late	r72	95surf
ShalWCD_90rel_noresp_late_r8_95shore	WCD	90rel	noresp	late	r8	95shore
ShalWCD_90rel_noresp_late_r30_95WC	WCD	90rel	noresp	late	r30	95WC
ShalWCD_90rel_surfresp_late_r72_95surf	WCD	90rel	surfresp	late	r72	95surf
ShalWCD_90rel_surfresp_late_r8_95shore	WCD	90rel	surfresp	late	r8	95shore
ShalMMPD_30rel_noresp_early_r31_95surf	MMPD	30rel	noresp	early	r31	95surf
ShalMMPD_30rel_noresp_early_r20_95shore	MMPD	30rel	noresp	early	r20	95shore
ShalMMPD_60rel_noresp_late_r13_95surf	MMPD	60rel	noresp	late	r13	95surf
ShalMMPD_60rel_noresp_late_r50_95shore	MMPD	60rel	noresp	late	r50	95shore

Table 41. Deep Blowout Analysis – list of stochastic scenarios and naming convention (Deep = Deep Blowout Site).

Scenario Name	Release Volume	Release Duration (Days)	Response Measures	Season
DeepWCD_90rel_noresp_early	WCD	90rel	noresp	early
DeepWCD_90rel_subresp_early	WCD	90rel	subresp	early
DeepWCD_120rel_noresp_late	WCD	120rel	noresp	late
DeepWCD_120rel_subresp_late	WCD	120rel	subresp	late
DeepMMPD_60rel_noresp_early	MMPD	60rel	noresp	early
DeepMMPD_90rel_noresp_late	MMPD	90rel	noresp	late

Table 42. Deep Blowout Analysis – list of individual trajectories and naming convention (Deep = Deep Blowout Site).

Scenario Name	Release Volume	Release Duration (Days)	Response Measures	Season	Individual Run Number in Stochastic Ensemble	Run Type - 95th percentile for shore/surface/water column oil contamination
DeepWCD_90rel_noresp_early_r97_95surf	WCD	90rel	noresp	early	r97	95surf
DeepWCD_90rel_noresp_early_r98_95shore	WCD	90rel	noresp	early	r98	95shore
DeepWCD_90rel_noresp_early_r61_95WC	WCD	90rel	noresp	early	r61	95WC
DeepWCD_90rel_surfresp_early_r97_95surf	WCD	90rel	surfresp	early	r97	95surf
DeepWCD_90rel_surfresp_early_r98_95shore	WCD	90rel	surfresp	early	r98	95shore
DeepWCD_90rel_subresp_early_r3_repsub	WCD	90rel	subresp	early	r3	repsub*
DeepWCD_120rel_noresp_late_r21_95surf	WCD	120rel	noresp	late	r21	95surf
DeepWCD_120rel_noresp_late_r91_95shore	WCD	120rel	noresp	late	r91	95shore
DeepWCD_120rel_noresp_late_r32_95WC	WCD	120rel	noresp	late	r32	95WC
DeepWCD_120rel_surfresp_late_r21_95surf	WCD	120rel	surfresp	late	r21	95surf
DeepWCD_120rel_surfresp_late_r91_95shore	WCD	120rel	surfresp	late	r91	95shore
DeepWCD_120rel_subresp_late_r19_repsub	WCD	120rel	subresp	late	r19	repsub*
DeepMMPD_60rel_noresp_early_r32_95surf	MMPD	60rel	noresp	early	r32	95surf
DeepMMPD_60rel_noresp_early_r7_95shore	MMPD	60rel	noresp	early	r7	95shore
DeepMMPD_90rel_noresp_late_r40_95surf	MMPD	90rel	noresp	late	r40	95surf
DeepMMPD_90rel_noresp_late_r37_95shore	MMPD	90rel	noresp	late	r37	95shore

*representative run for subsurface contamination along the Beaufort Shelf.

Appendix E: Stochastic Analysis Results for Higher Thresholds

In addition to the lower threshold stochastic results (Section 7), surface and shoreline oiling exceeding higher thresholds were examined. Higher threshold stochastic results are presented in this Appendix. The higher thresholds and significance of each value is summarized in the below outline. Oil in the water column was not evaluated with a threshold, therefore no subsurface contamination results are presented in this Appendix.

- Floating Surface Oil Thickness Threshold: **≥10 g/m^2**
    - Dark brown oil
    - Potential effects on ecological resources on the water surface (coating, smothering)
    - French McCay (2009); French McCay et al. (2011)
- Shoreline Thickness Threshold: **≥100 g/m^2**
    - Black Oil
    - Potential effects on ecological resources on the shoreline (coating, smothering)
    - French McCay (2009); French McCay et al. (2011)

Eastern Shipping Analysis

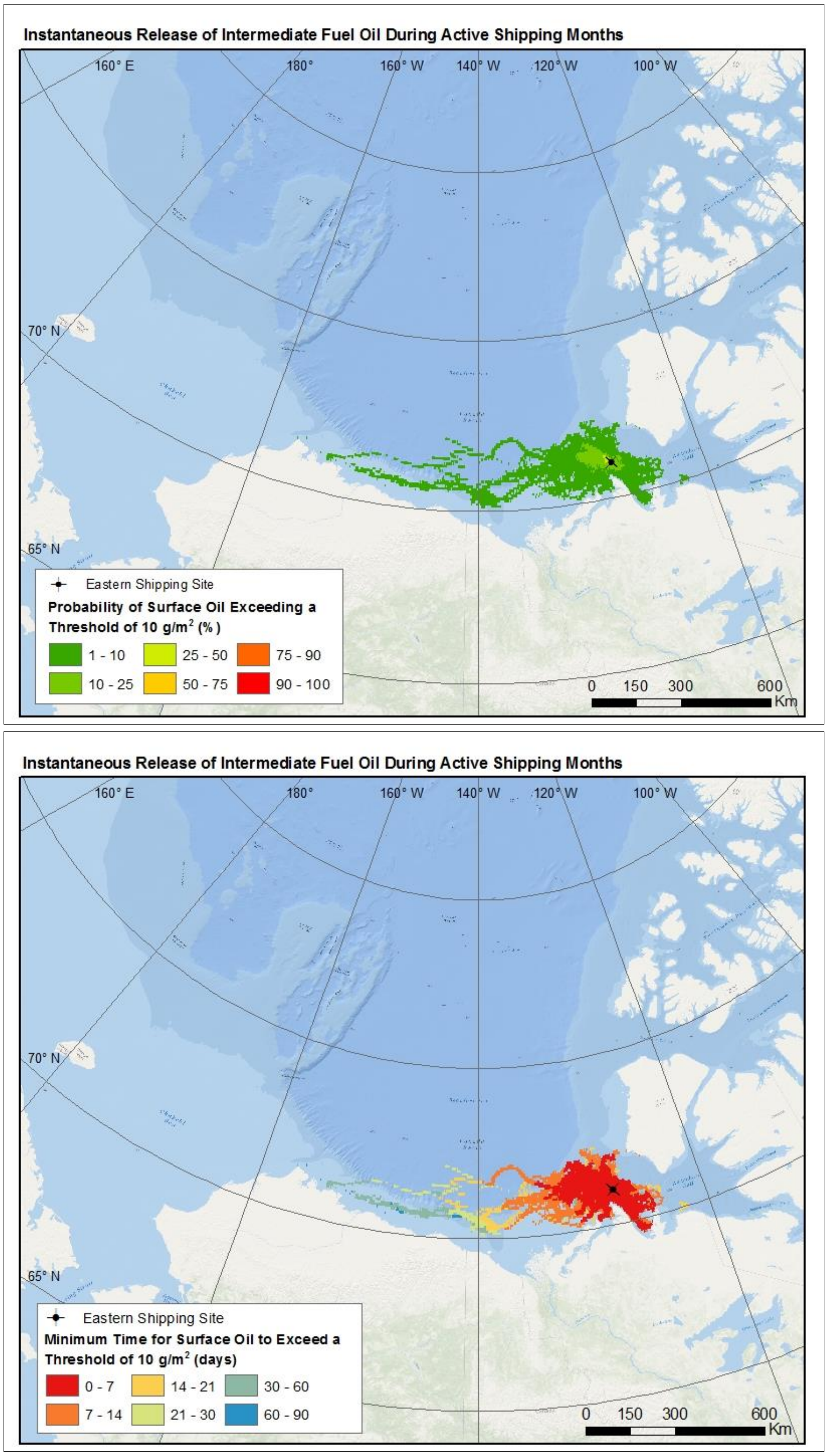

Figure 200. EastShip_IFO - Water surface oiling probabilities and minimum travel times for floating oil ≥10 g/m^2.

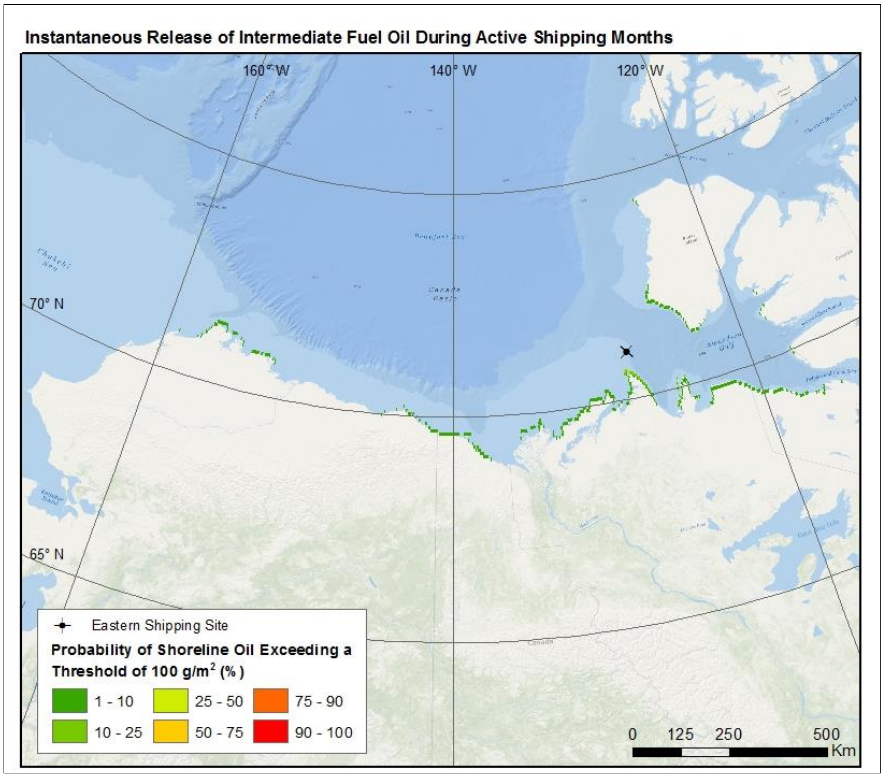

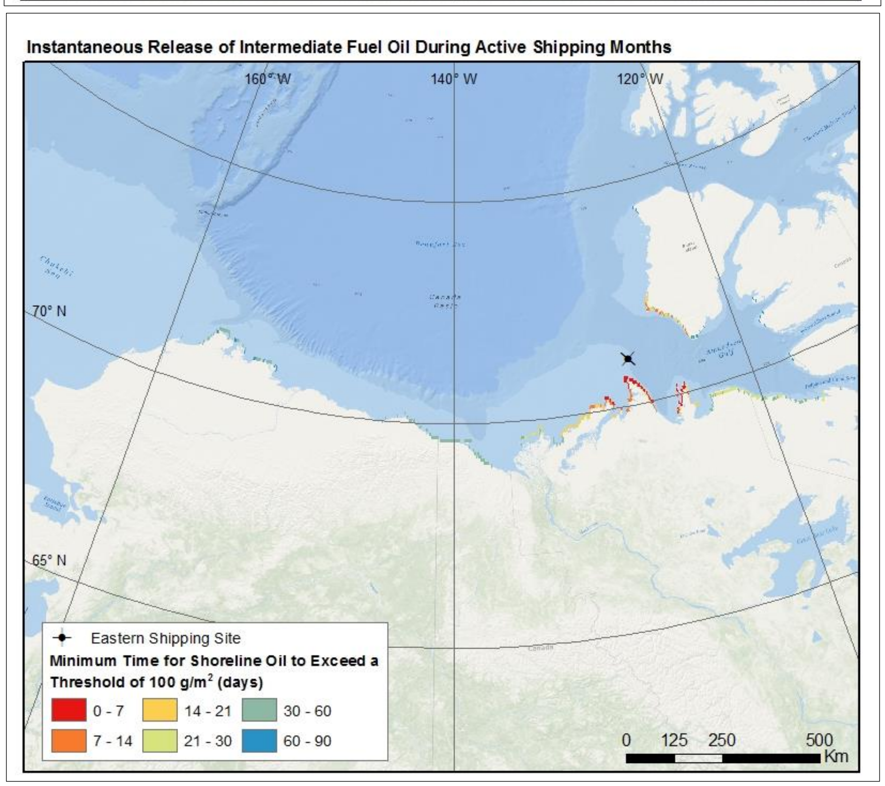

Figure 201. EastShip_IFO - Shoreline oiling probabilities and minimum travel times for shoreline oil ≥100 g/m^2.

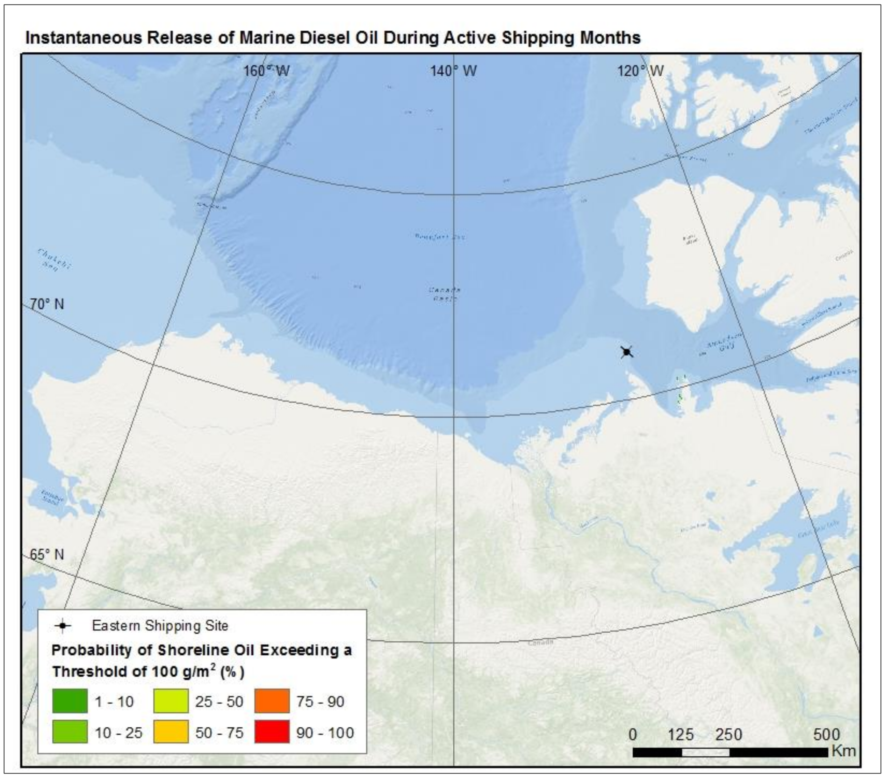

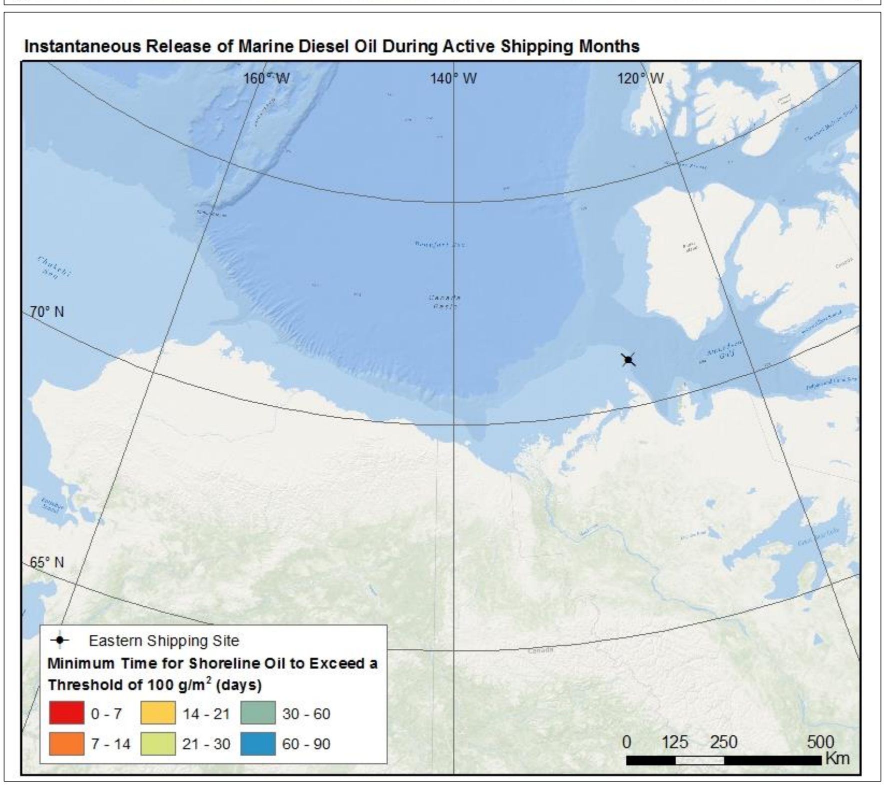

Figure 202. EastShip_Diesel - Shoreline oiling probabilities and minimum travel times for shoreline oil ≥100 g/m^2.

Trans-boundary Analysis

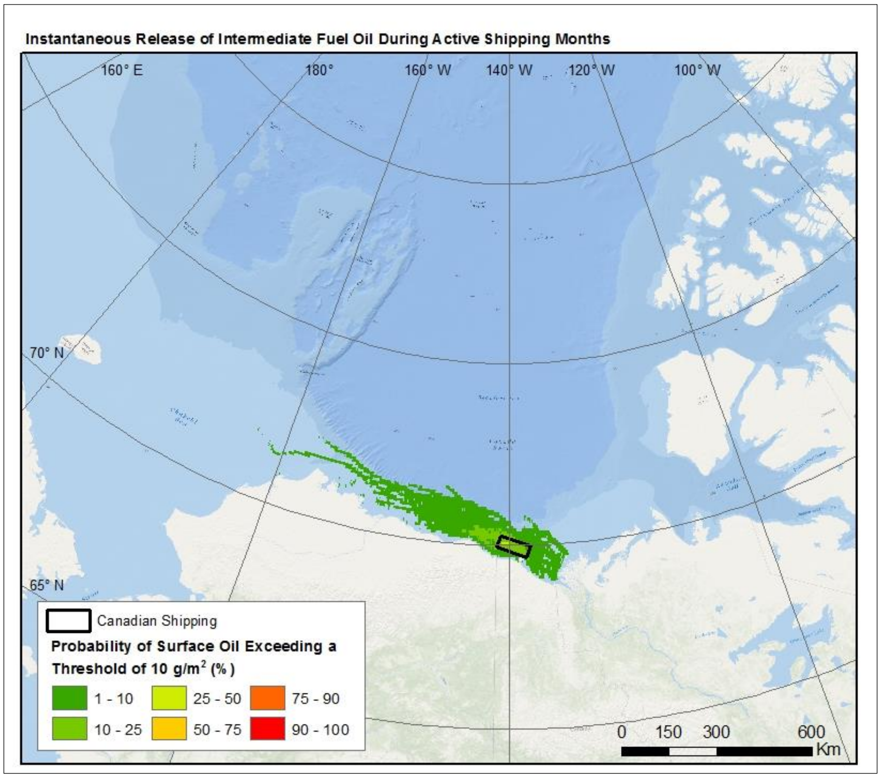

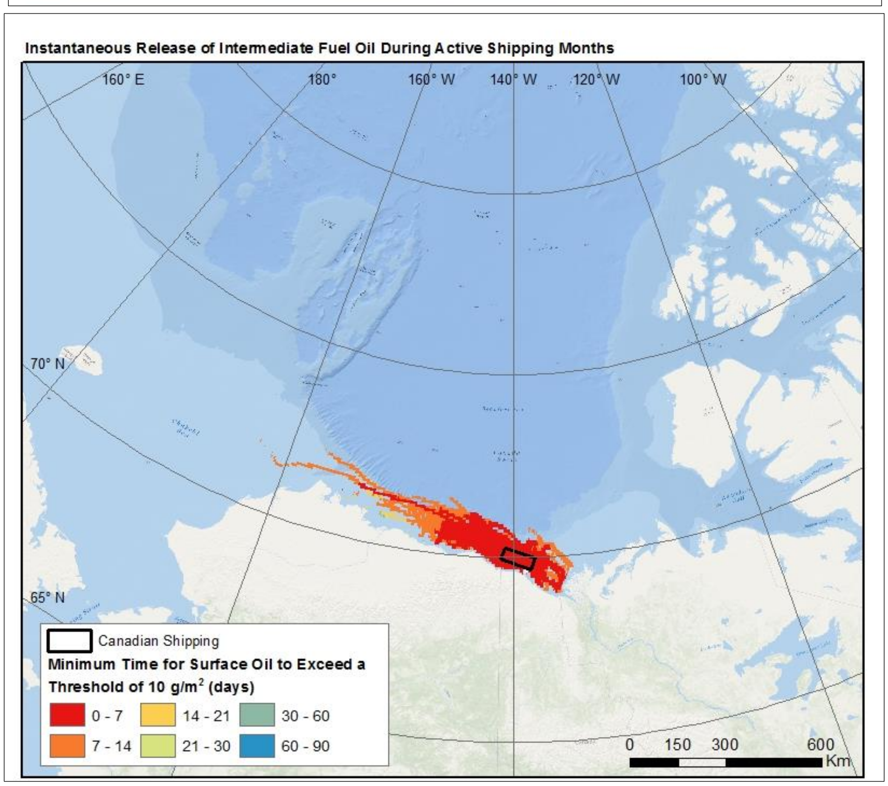

Figure 203. TB_Ship_IFO_CAN - Water surface oiling probabilities and minimum travel times for floating oil ≥10 g/m^2.

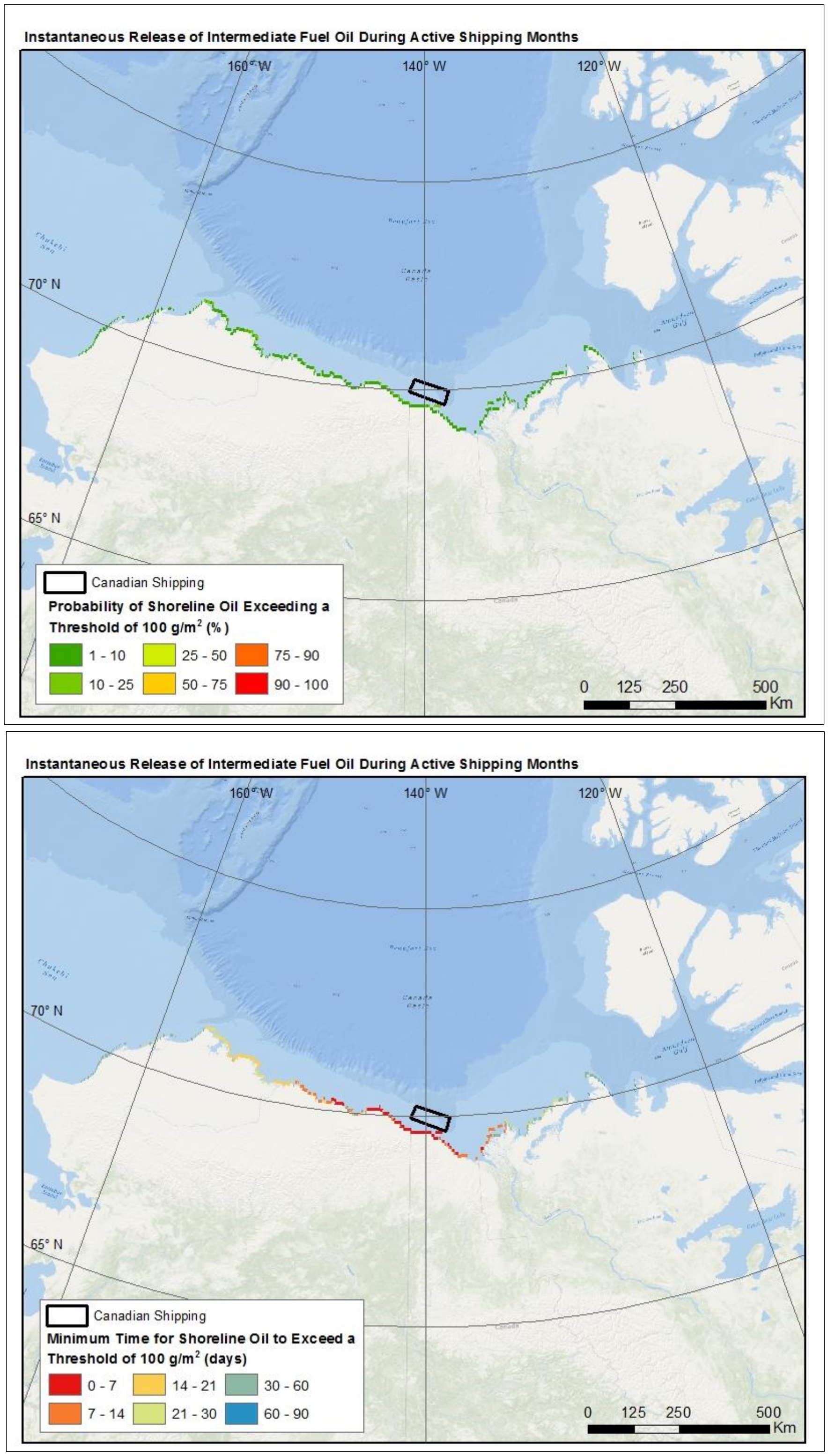

Figure 204. TB_Ship_IFO_CAN - Shoreline oiling probabilities and minimum travel times for shoreline oil ≥100 g/m^2.

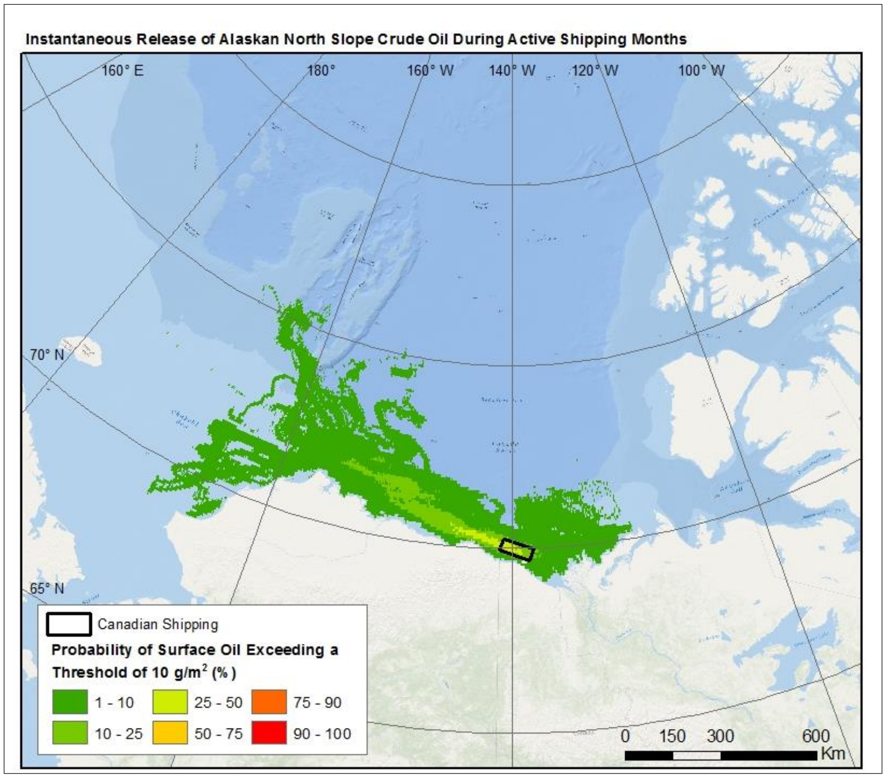

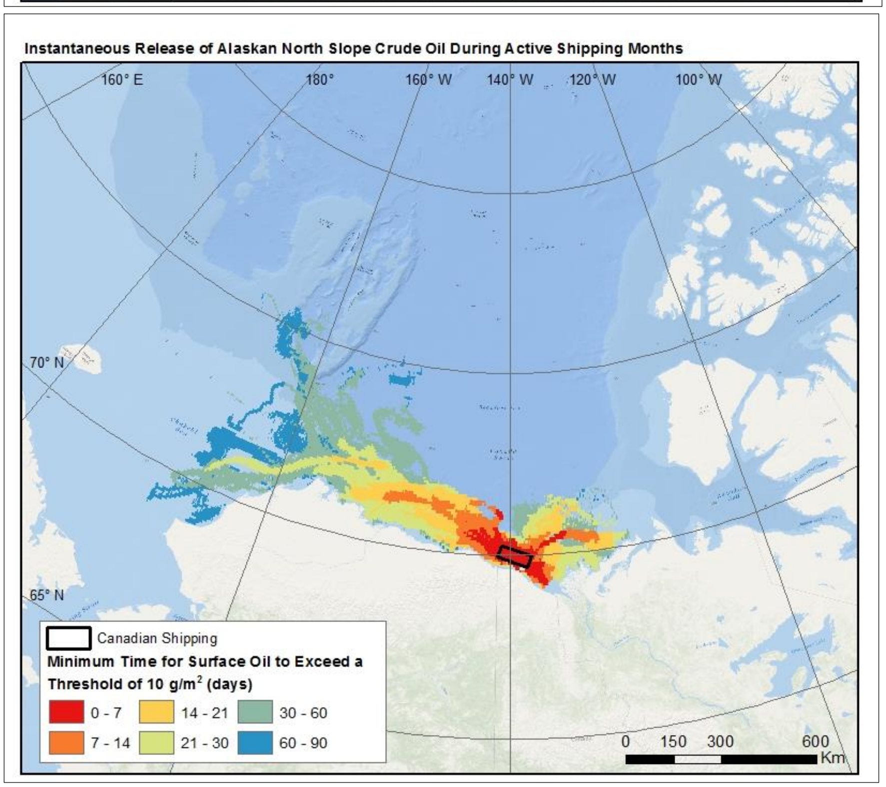

Figure 205. TB_Ship_Crude_CAN - Water surface oiling probabilities and minimum travel times for floating oil ≥10 g/m^2.

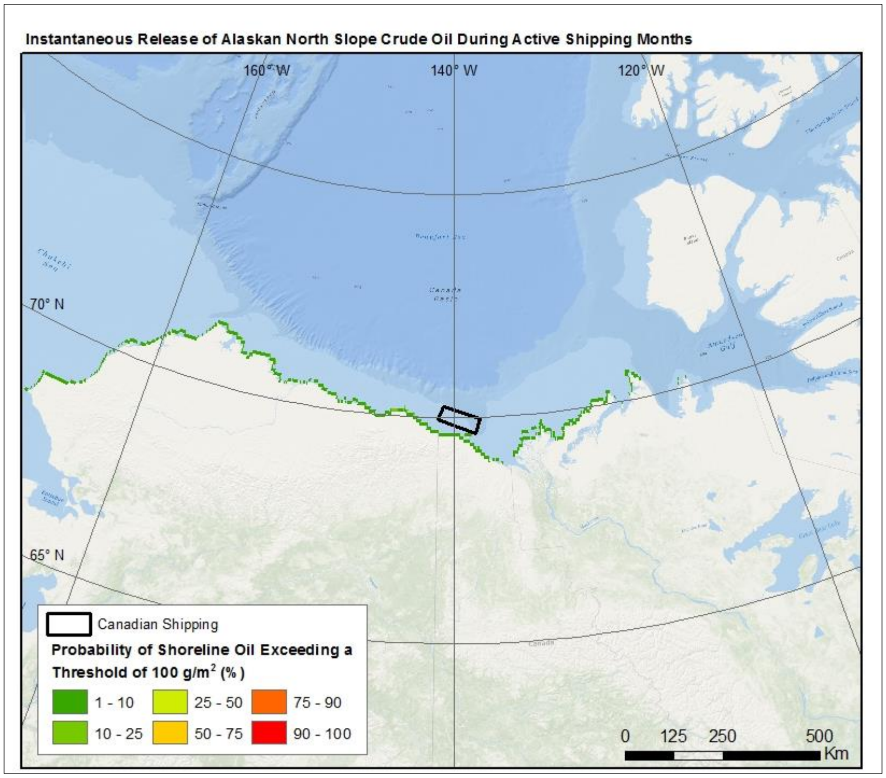

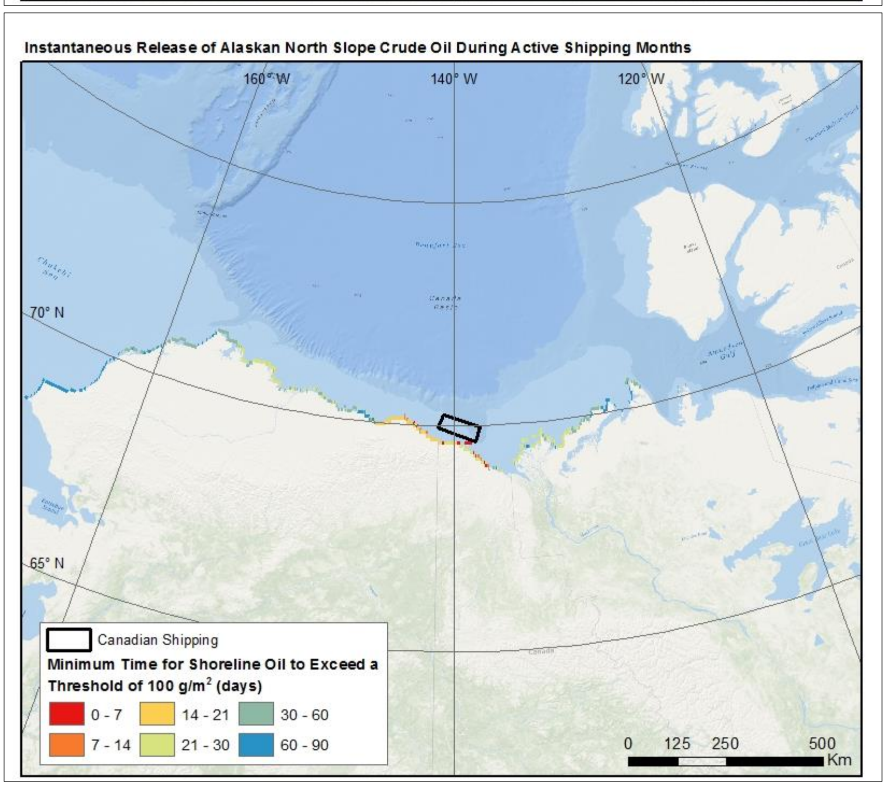

Figure 206. TB_Ship_Crude_CAN - Shoreline oiling probabilities and minimum travel times for shoreline oil ≥100 g/m^2.

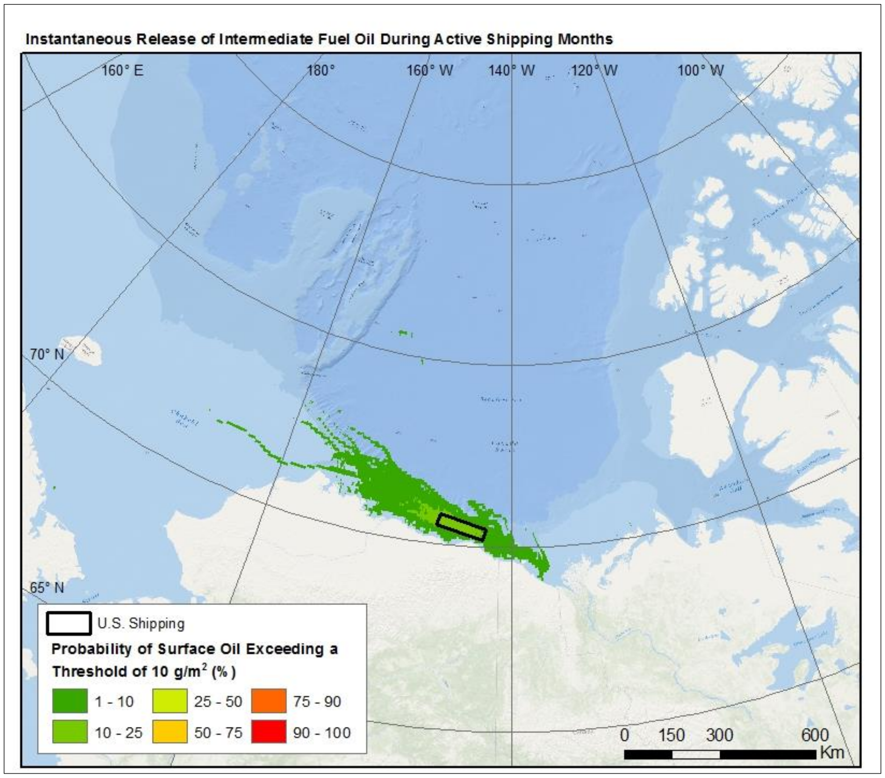

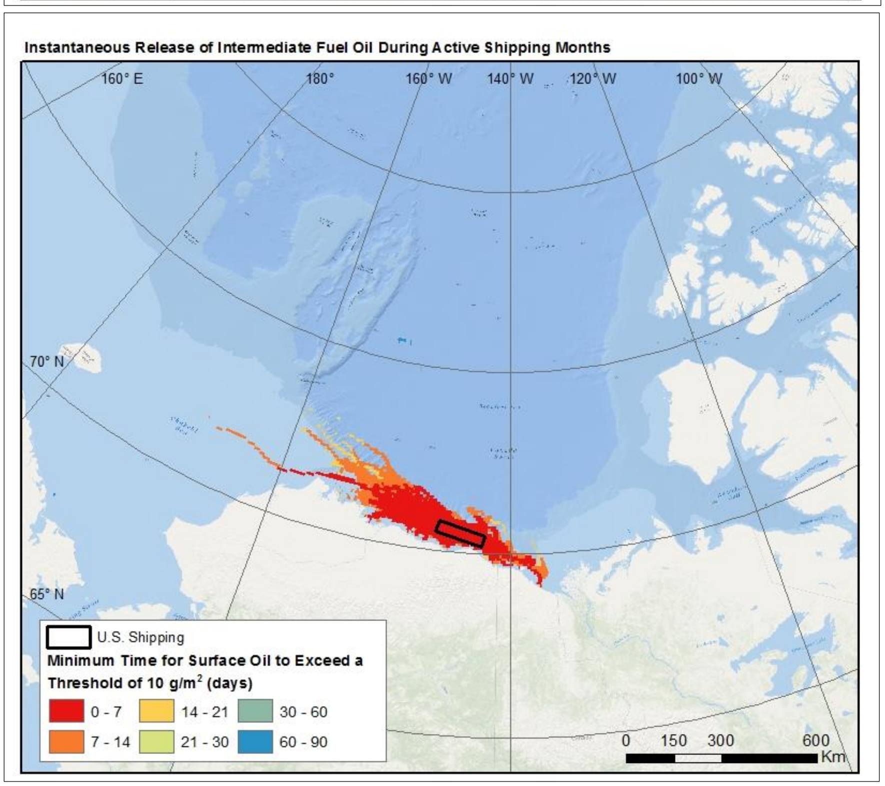

Figure 207. TB_Ship_IFO_US - Water surface oiling probabilities and minimum travel times for floating oil ≥10 g/m^2.

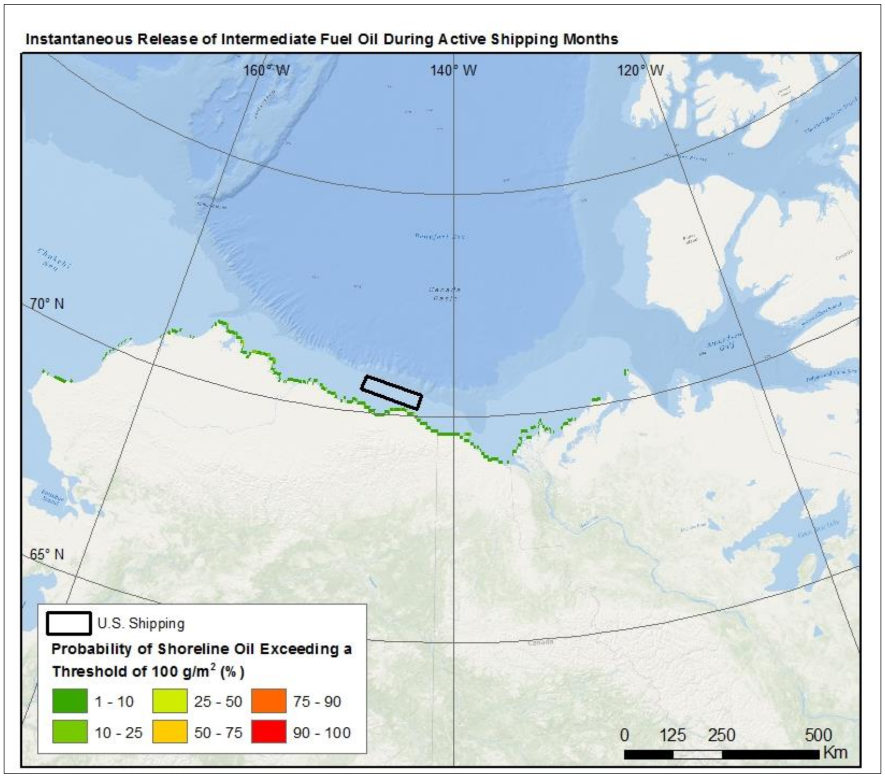

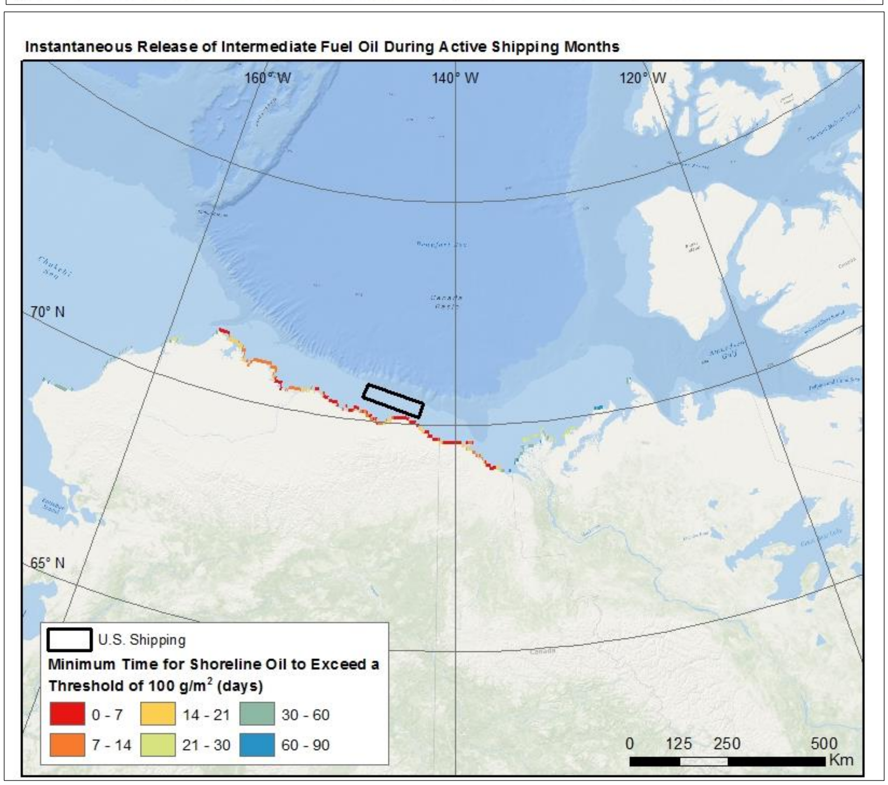

Figure 208. TB_Ship_IFO_US - Shoreline oiling probabilities and minimum travel times for shoreline oil ≥100 g/m^2.

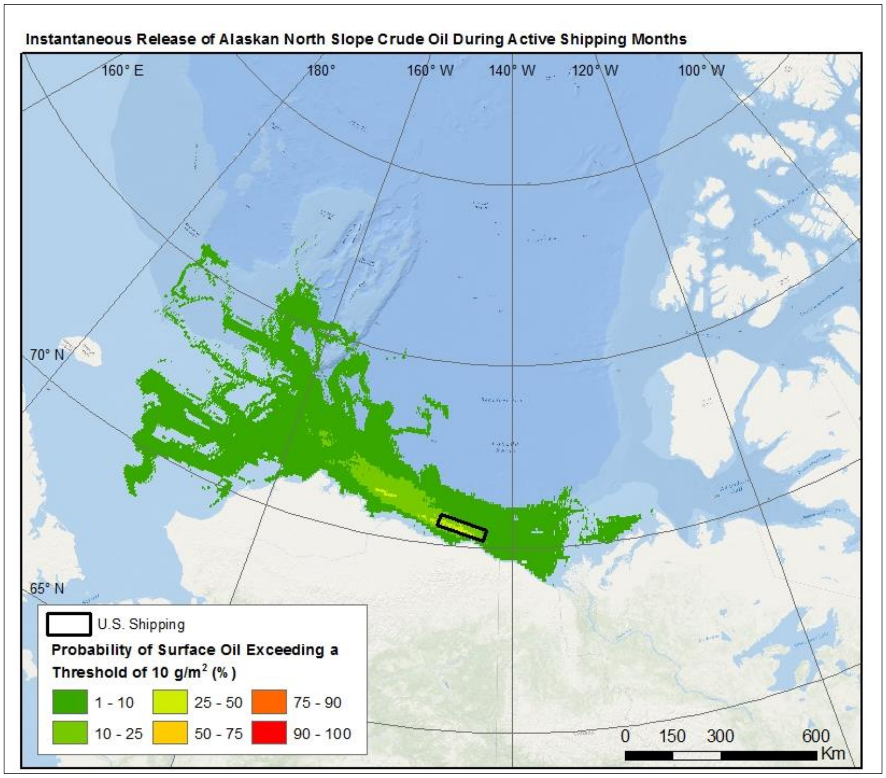

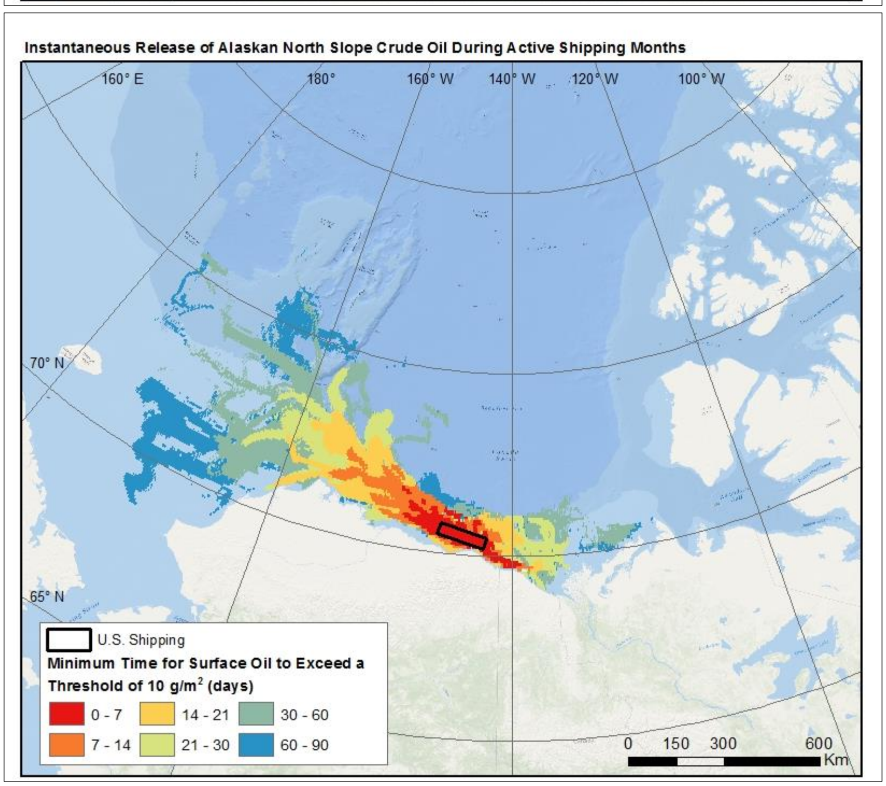

Figure 209. TB_Ship_Crude_US - Water surface oiling probabilities and minimum travel times for floating oil ≥10 g/m^2.

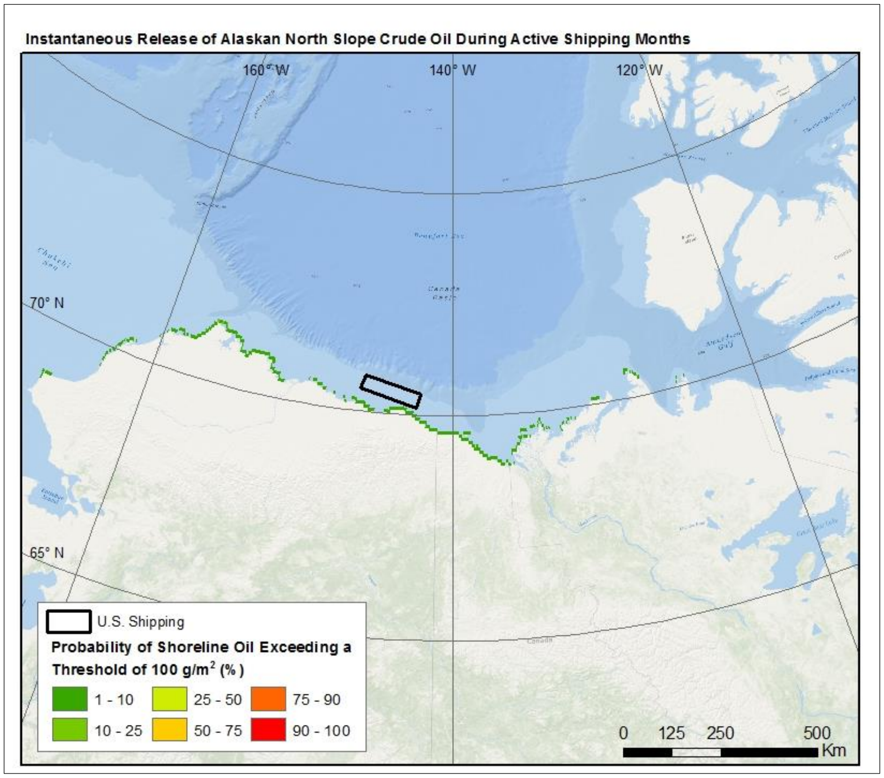

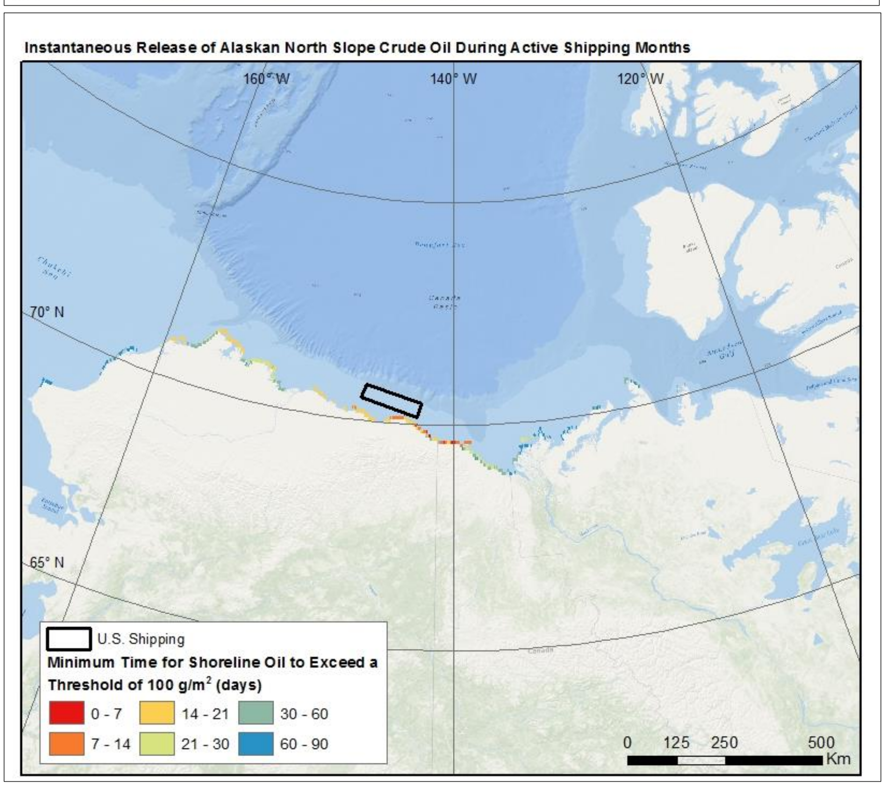

Figure 210. TB_Ship_Crude_US - Shoreline oiling probabilities and minimum travel times for shoreline oil ≥100 g/m^2.

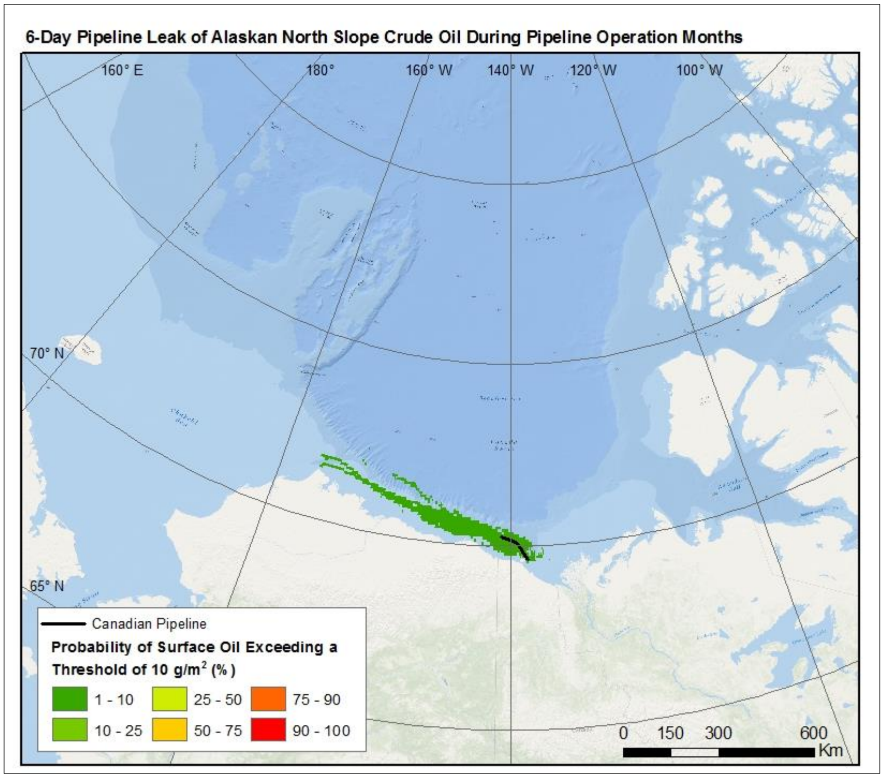

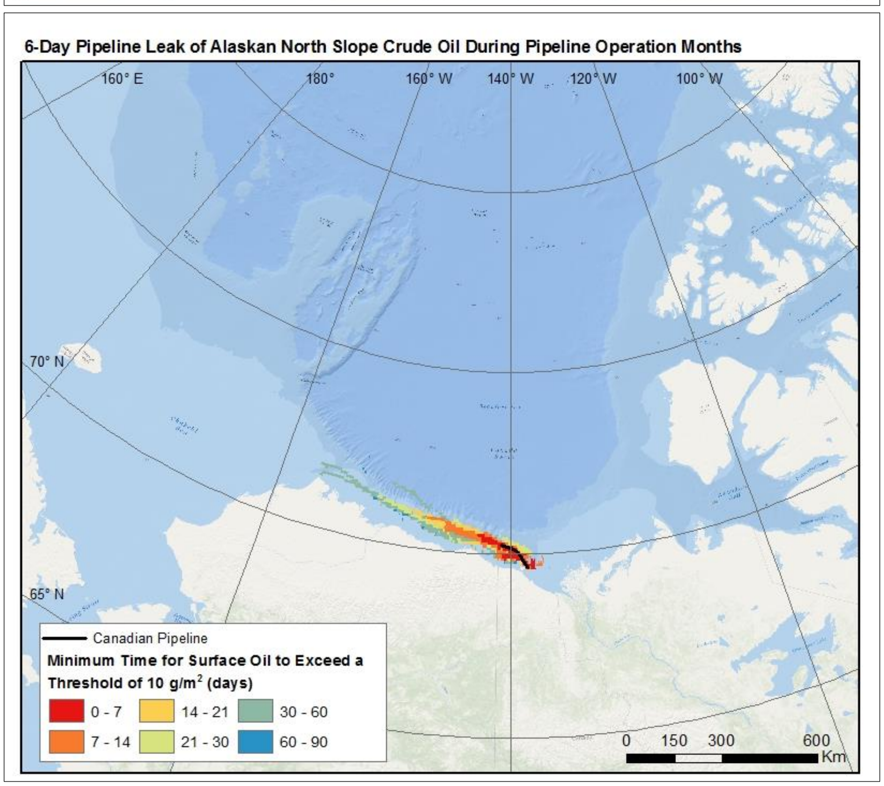

Figure 211. TB_Pipeline_CAN - Water surface oiling probabilities and minimum travel times for floating oil ≥10 g/m^2.

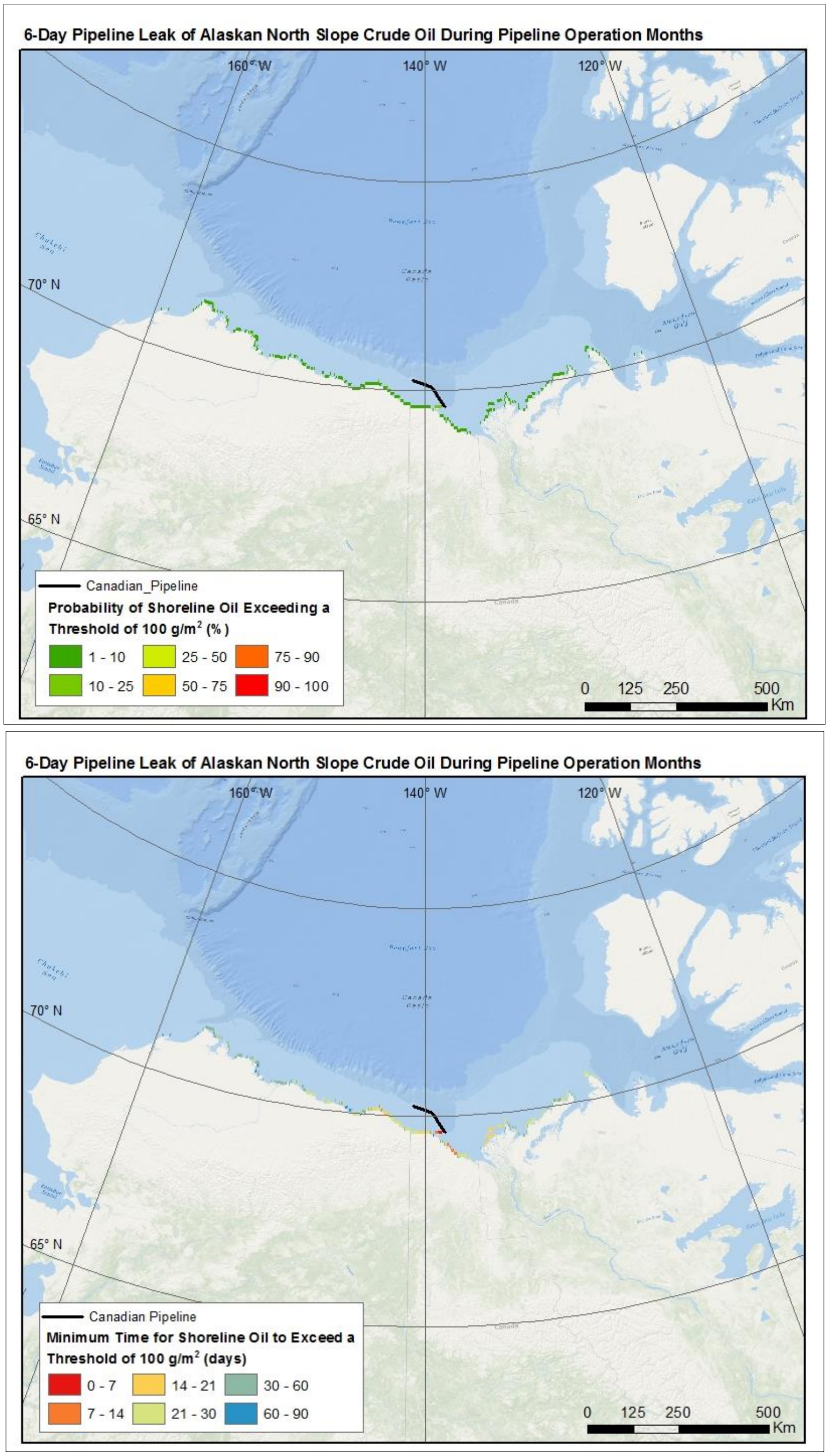

Figure 212. TB_Pipeline_CAN - Shoreline oiling probabilities and minimum travel times for shoreline oil ≥100 g/m^2.

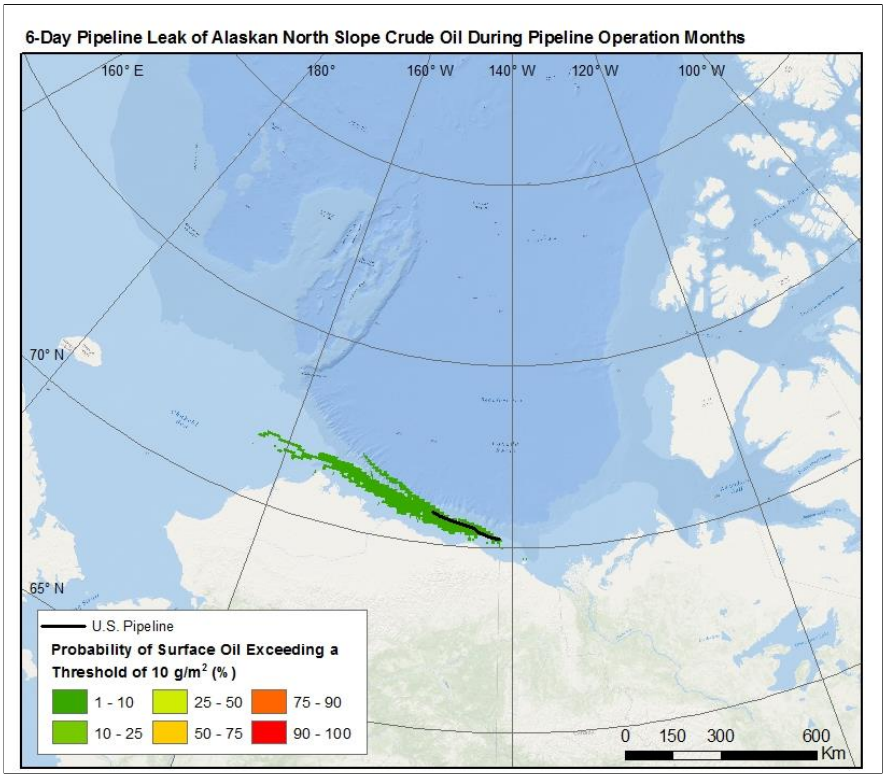

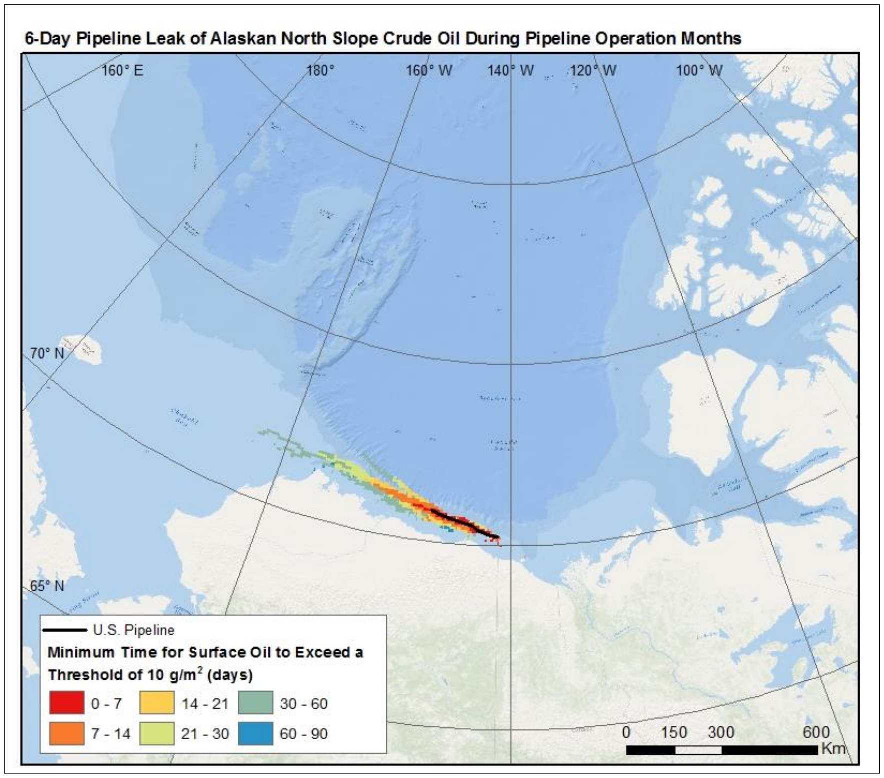

Figure 213. TB_Pipeline_US - Water surface oiling probabilities and minimum travel times for floating oil ≥10 g/m^2.

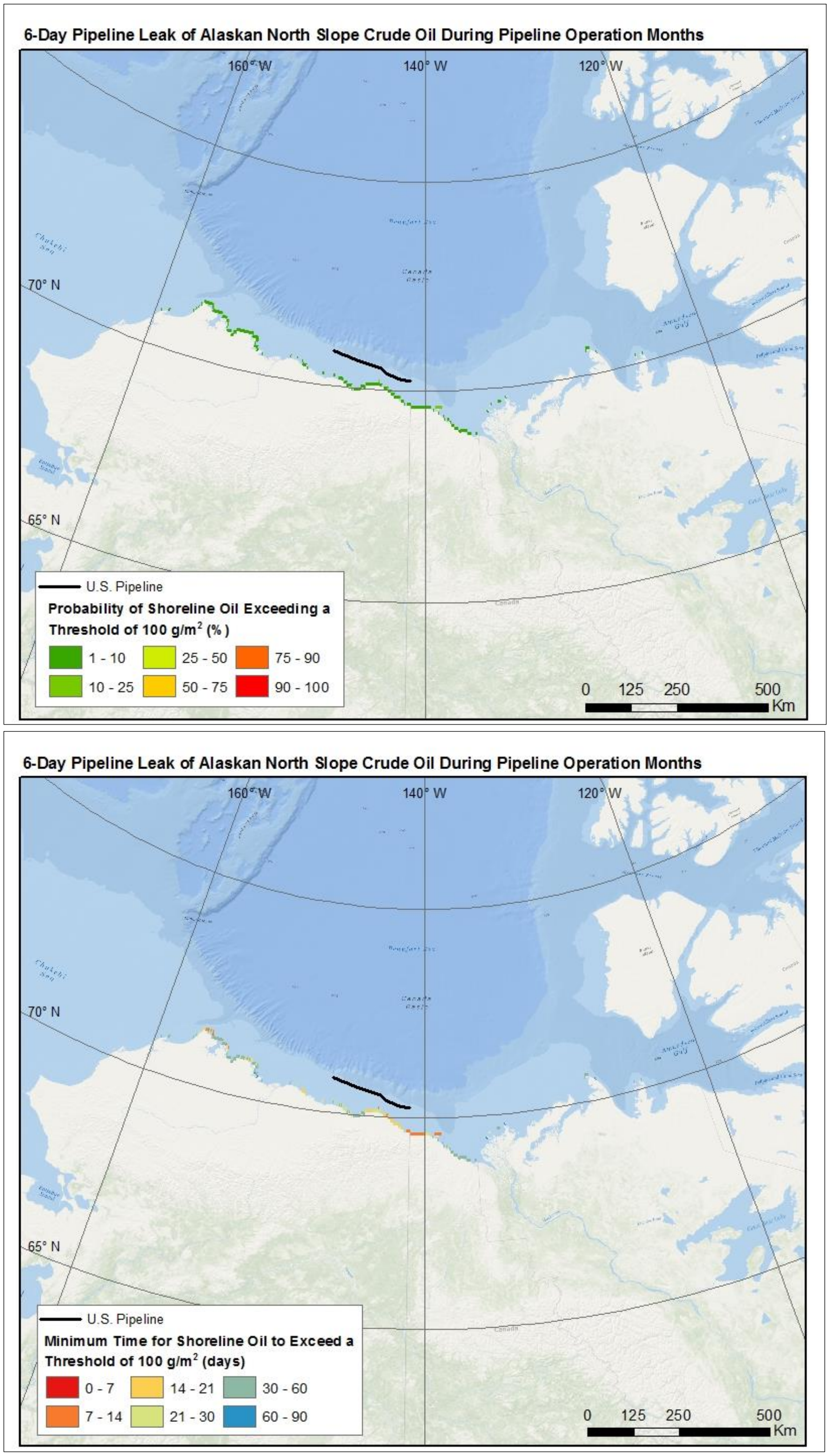

Figure 214. TB_Pipeline_US - Shoreline oiling probabilities and minimum travel times for shoreline oil ≥100 g/m^2.

Shallow Blowout Analysis

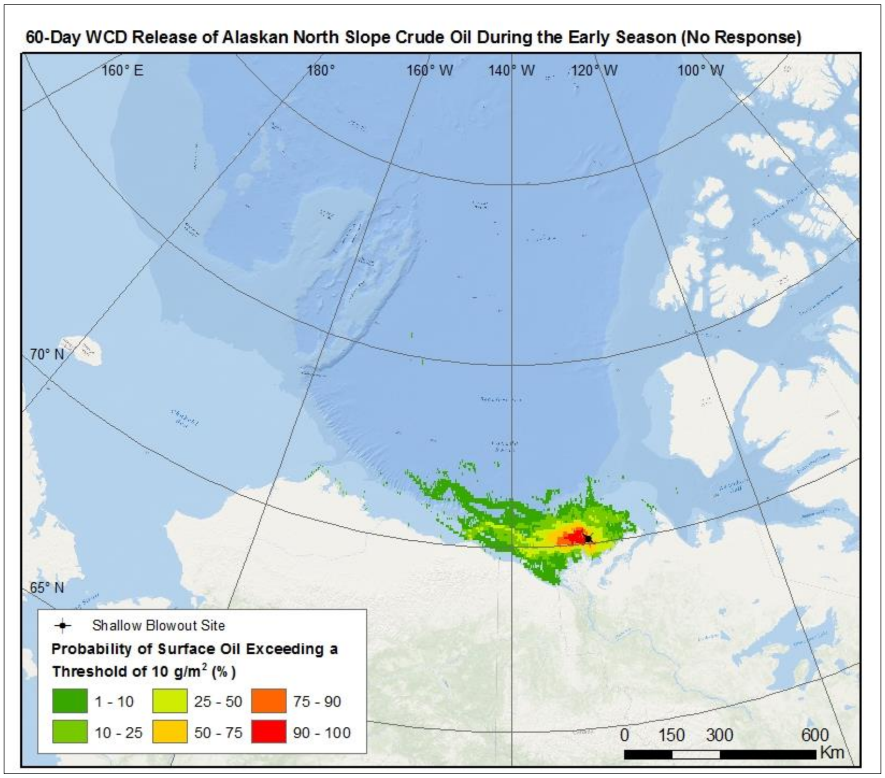

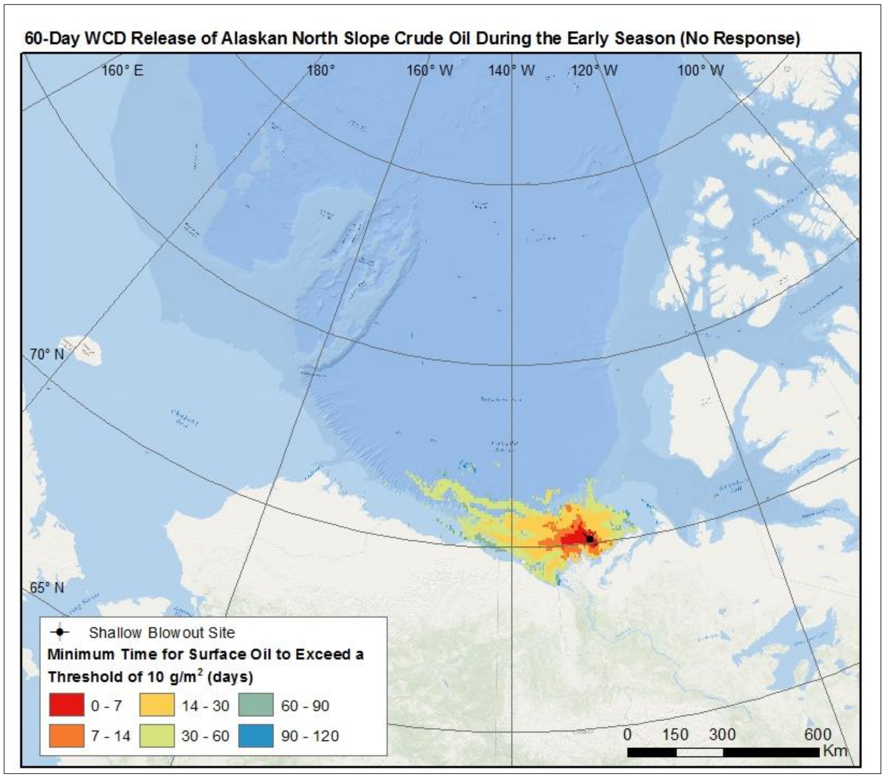

Figure 215. ShalWCD_60rel_noresp_early - Water surface oiling probabilities and minimum travel times for floating oil ≥10 g/m^2.

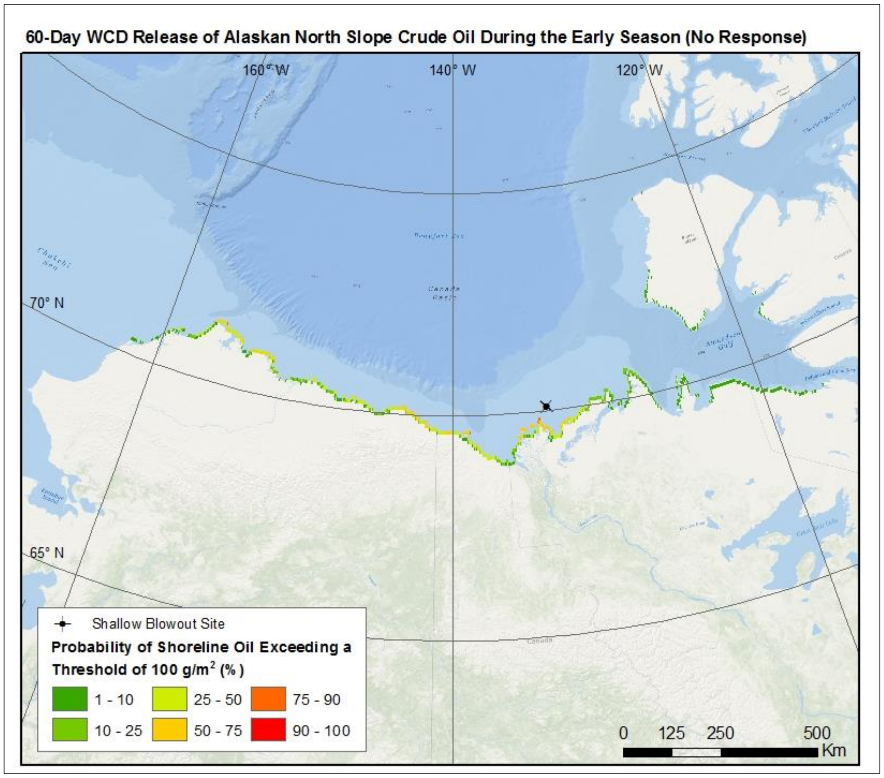

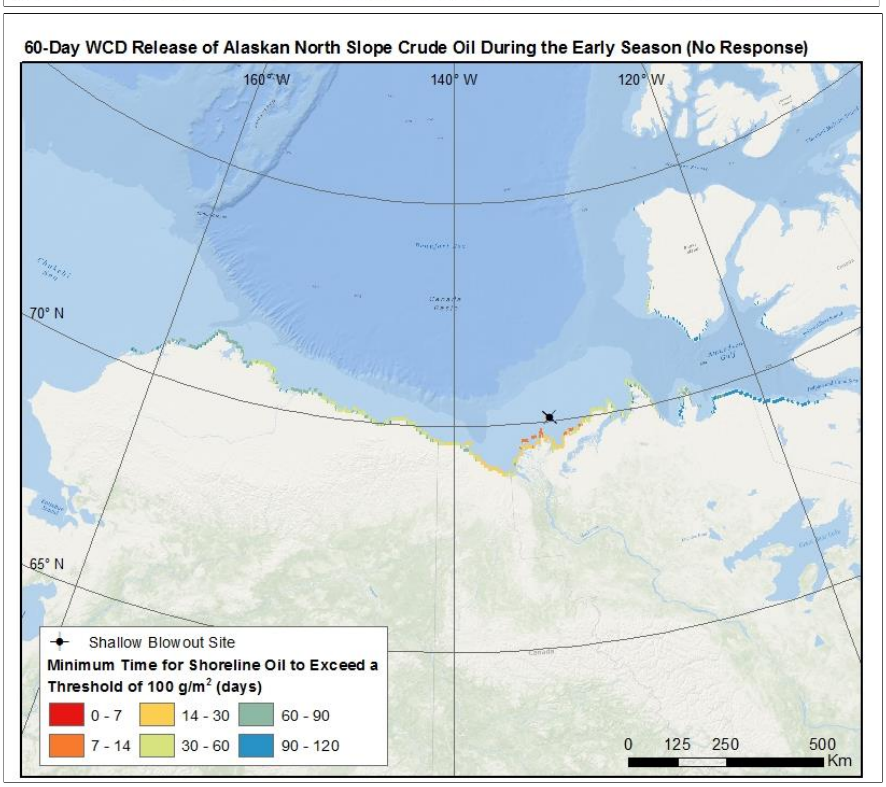

Figure 216. ShalWCD_60rel_noresp_early - Shoreline oiling probabilities and minimum travel times for shoreline oil ≥100 g/m^2.

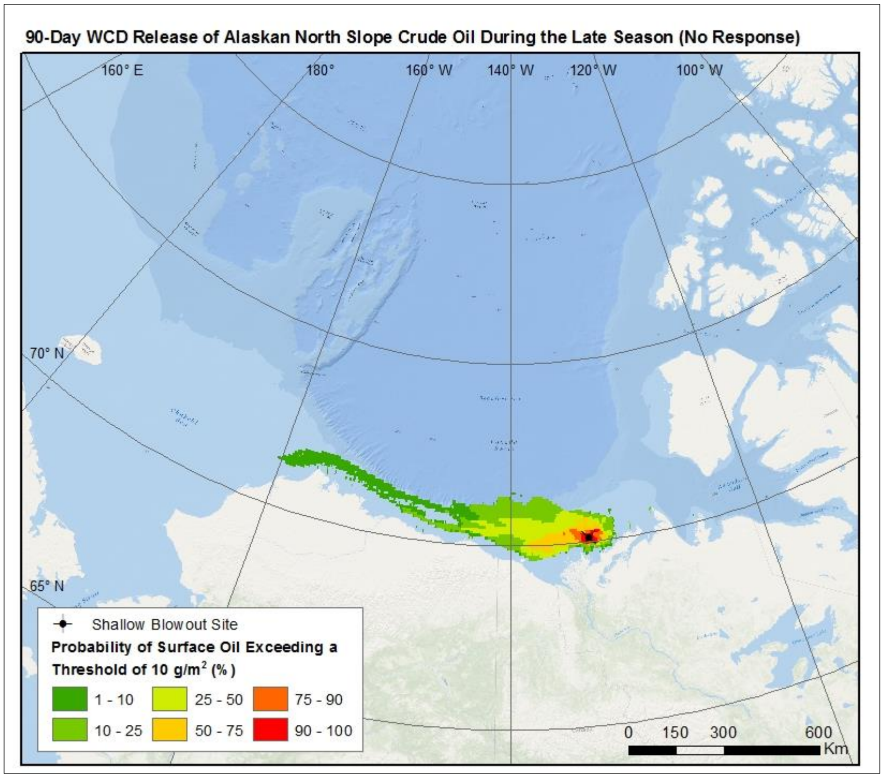

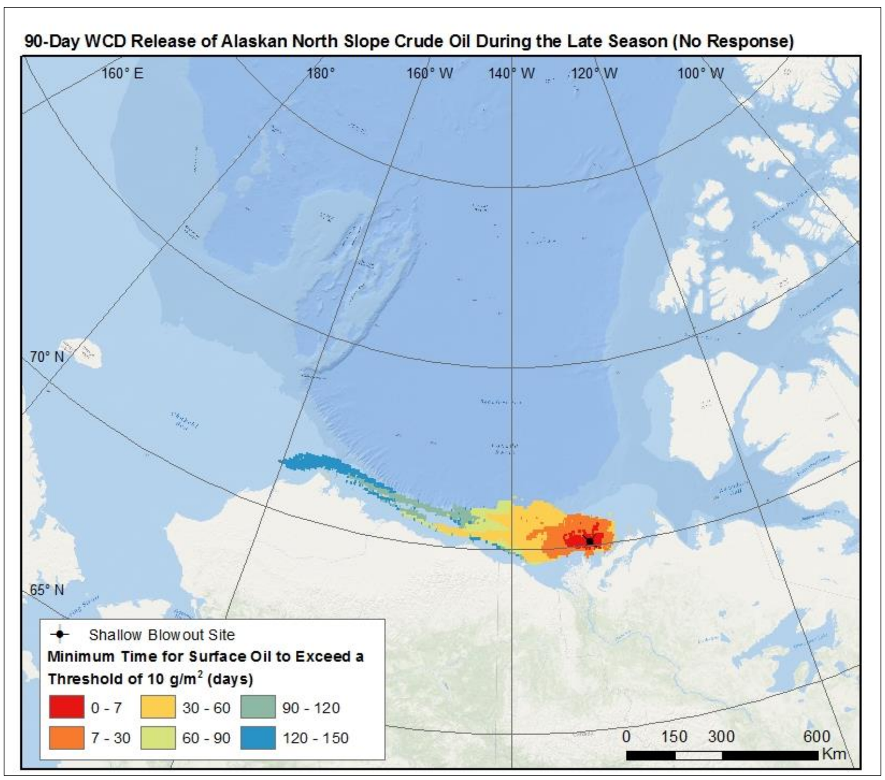

Figure 217. ShalWCD_90rel_noresp_late - Water surface oiling probabilities and minimum travel times for floating oil ≥10 g/m^2.

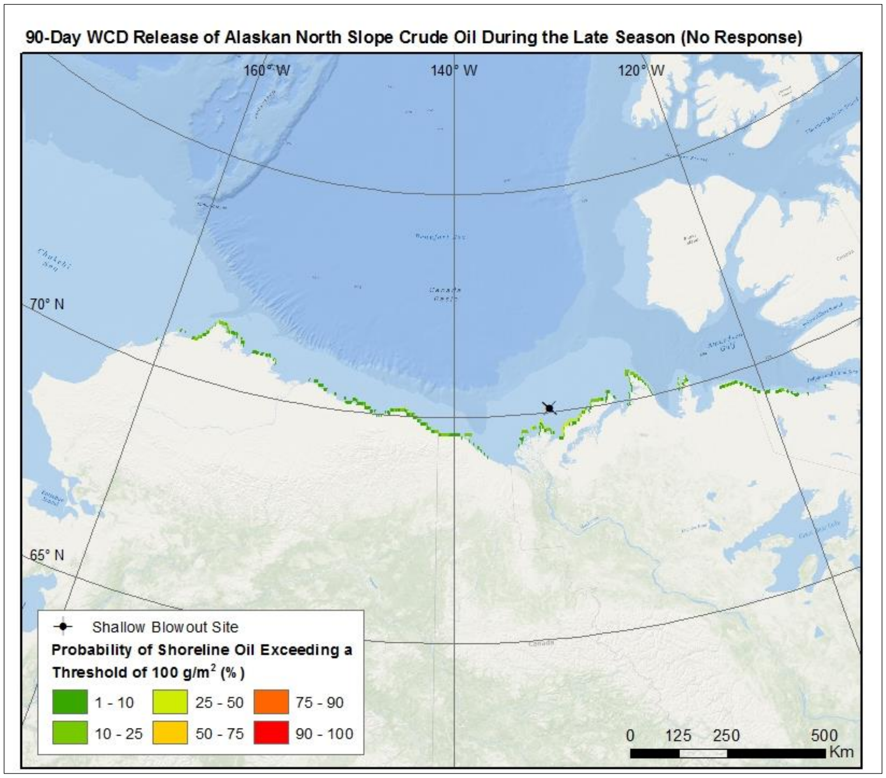

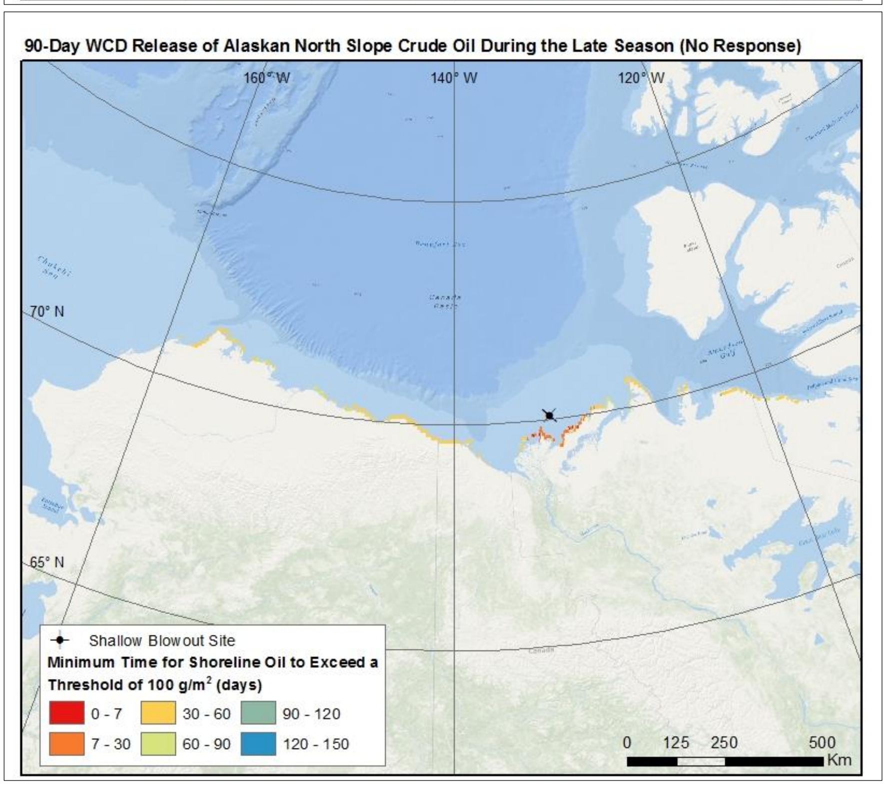

Figure 218. ShalWCD_90rel_noresp_late - Shoreline oiling probabilities and minimum travel times for shoreline oil ≥100 g/m^2.

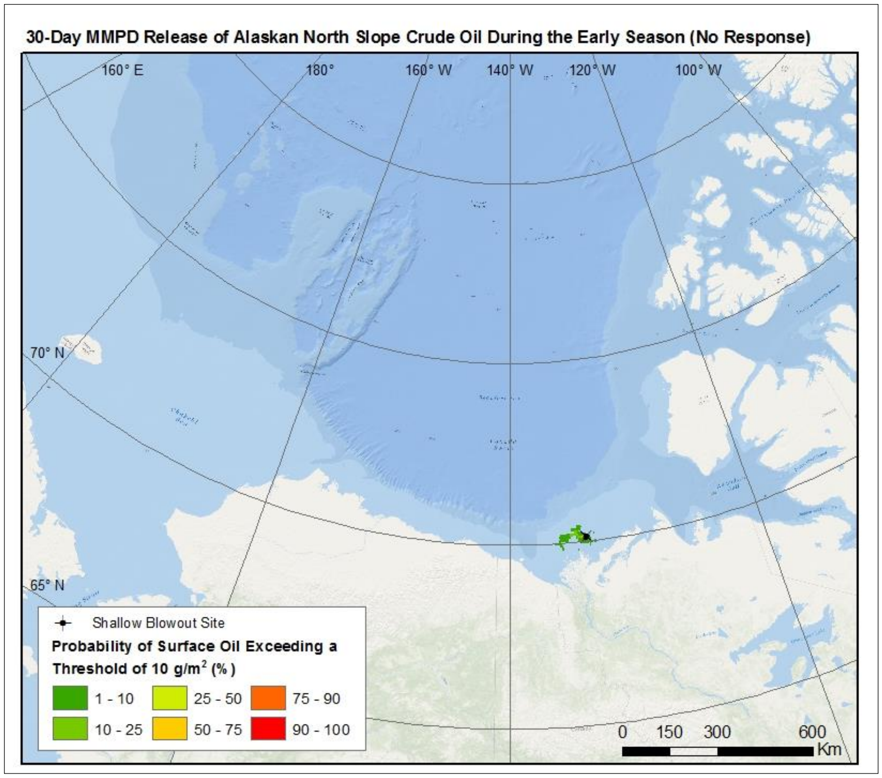

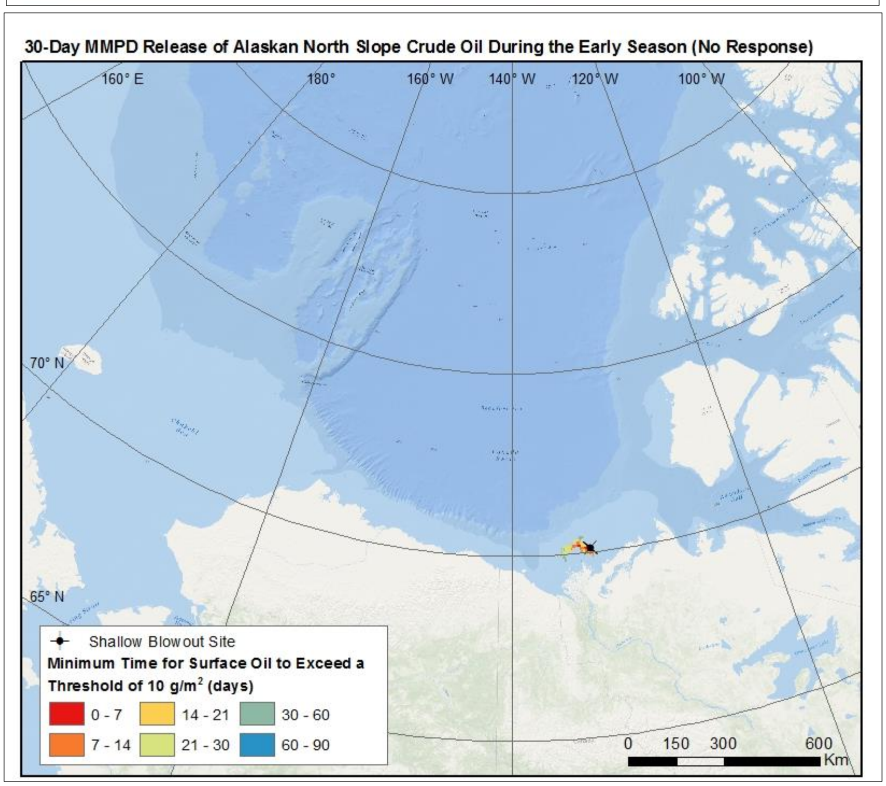

Figure 219. ShalMMPD_30rel_noresp_early - Water surface oiling probabilities and minimum travel times for floating oil ≥10 g/m^2.

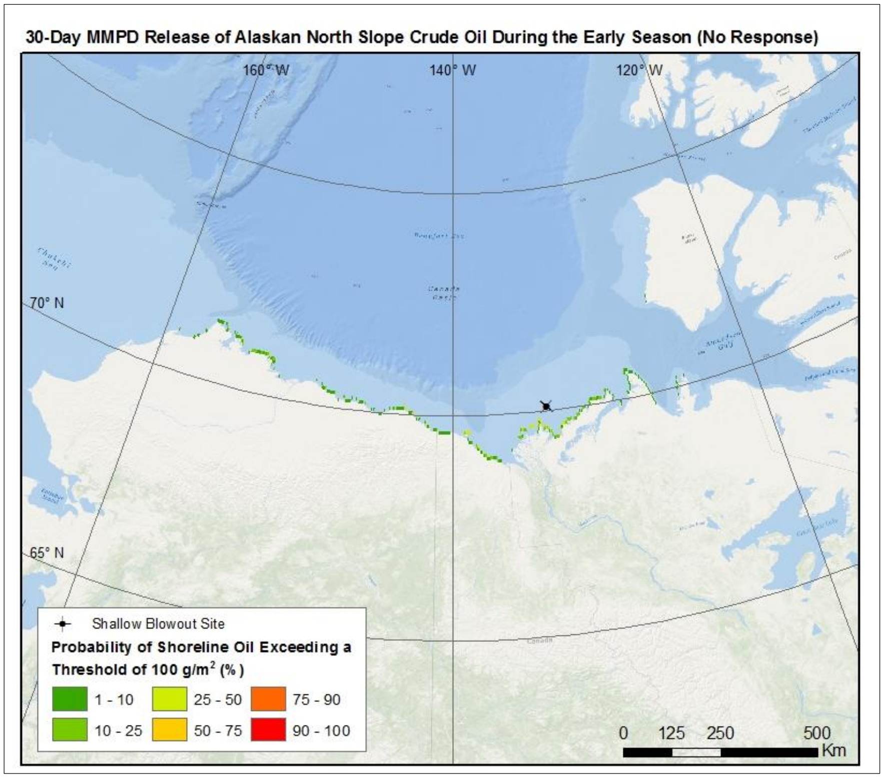

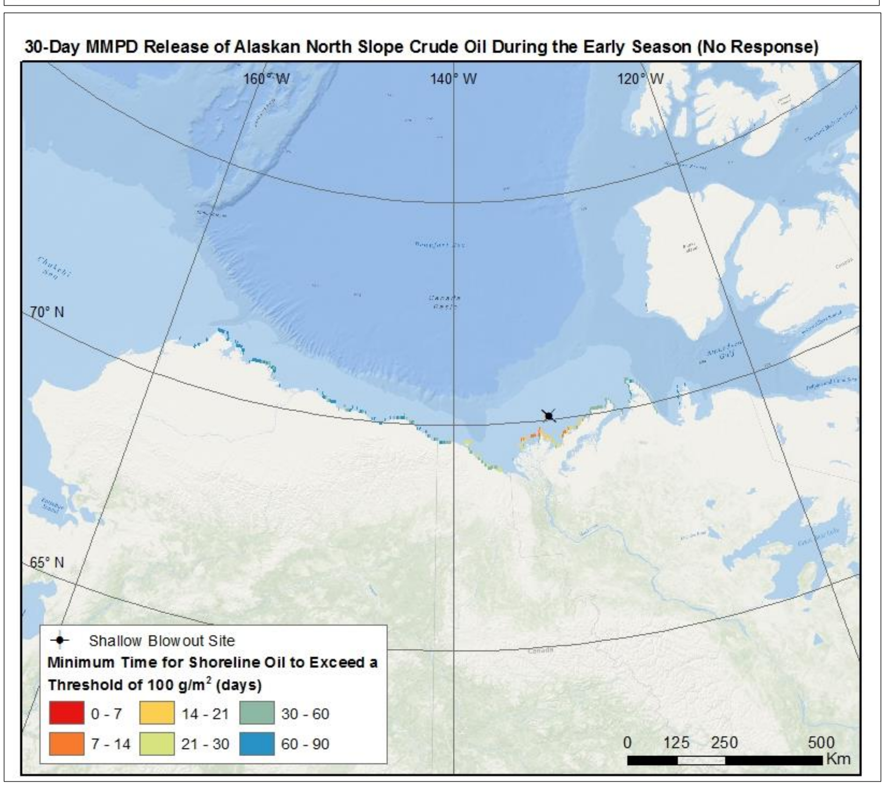

Figure 220. ShalMMPD_30rel_noresp_early - Shoreline oiling probabilities and minimum travel times for shoreline oil ≥100 g/m^2.

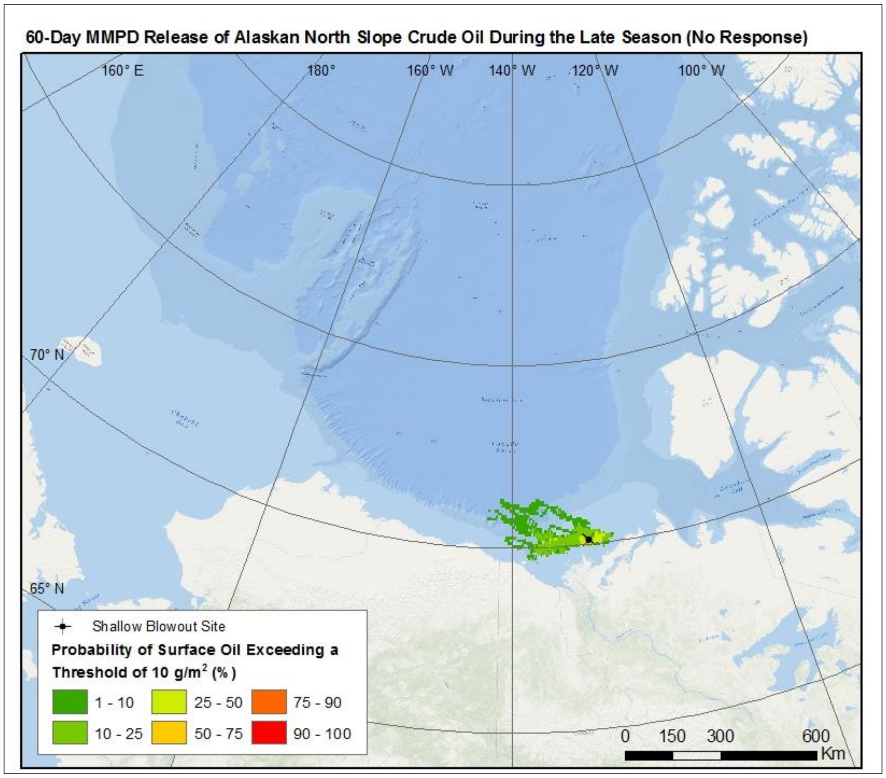

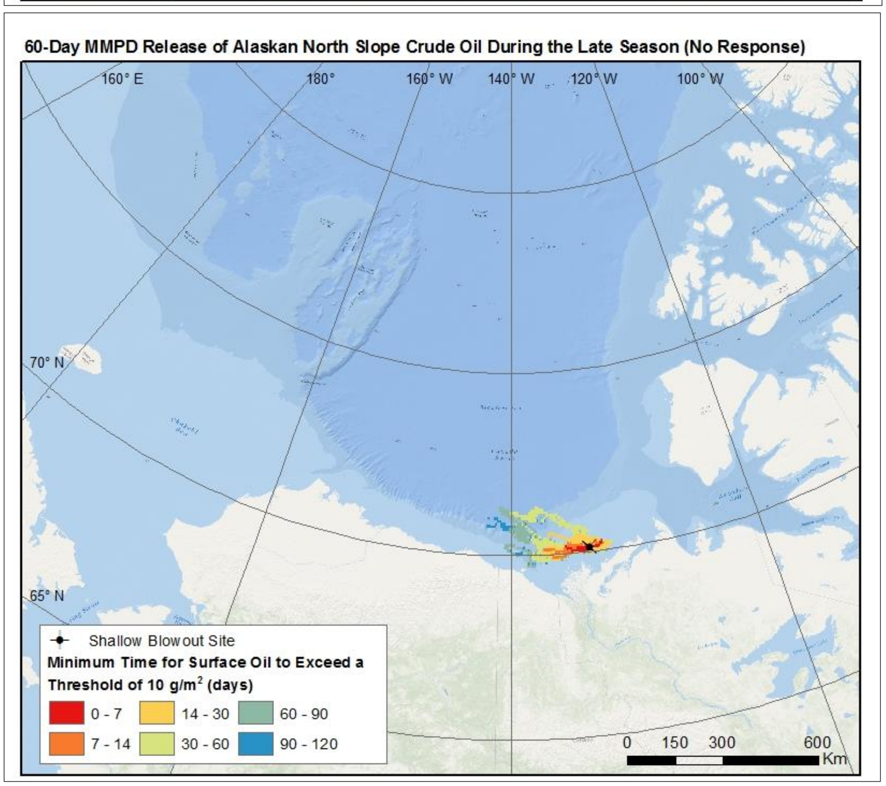

Figure 221. ShalMMPD_60rel_noresp_late - Water surface oiling probabilities and minimum travel times for floating oil ≥10 g/m^2.

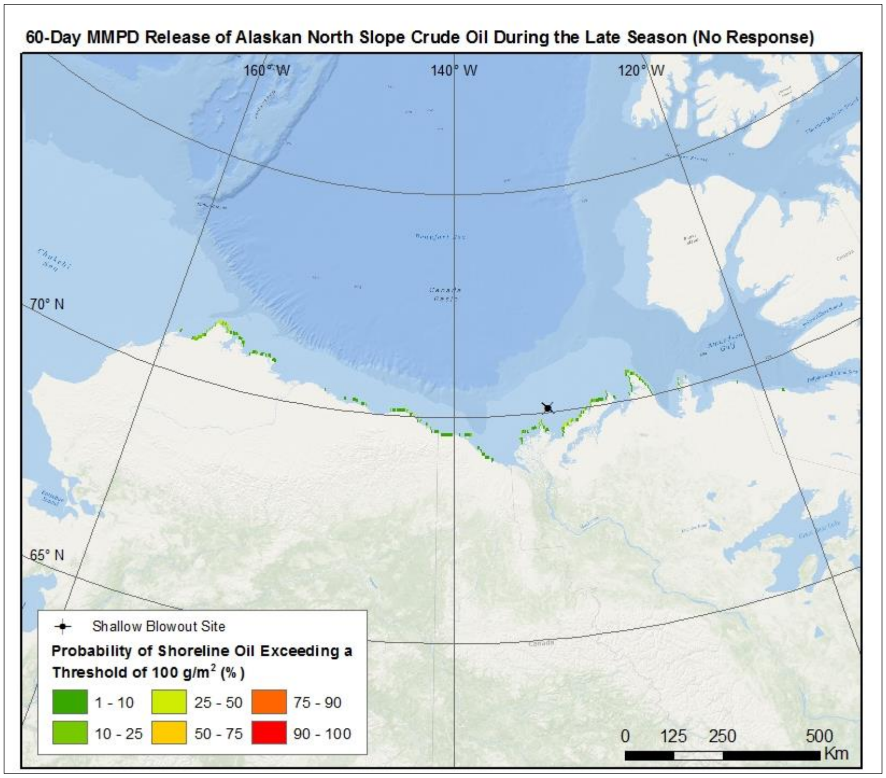

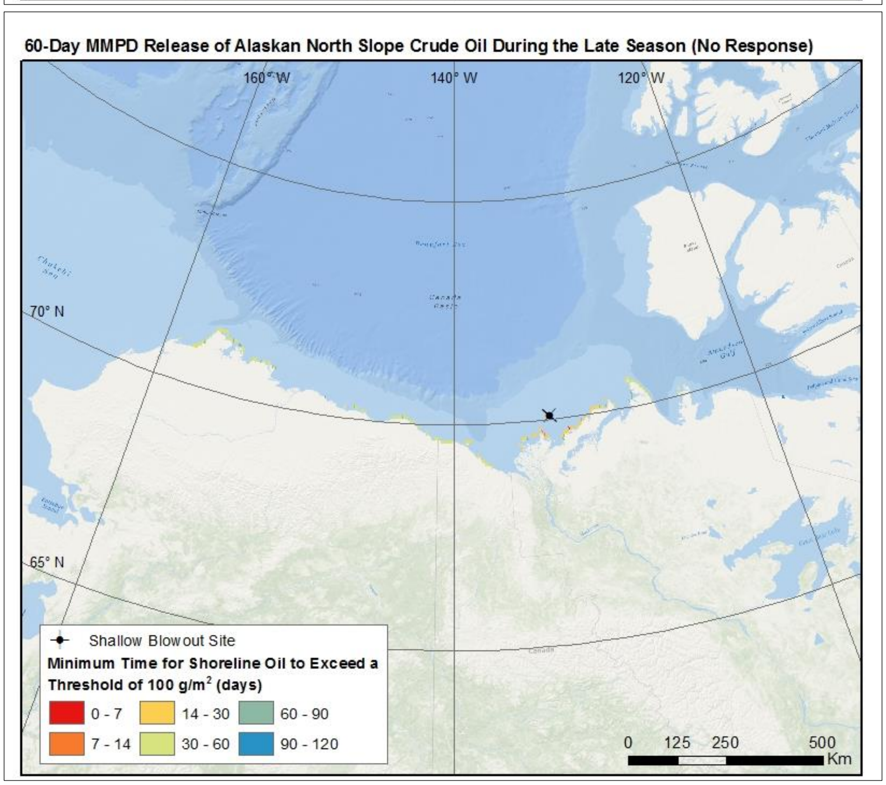

Figure 222. ShalMMPD_60rel_noresp_late - Shoreline oiling probabilities and minimum travel times for shoreline oil ≥100 g/m^2.

Deep Blowout Analysis

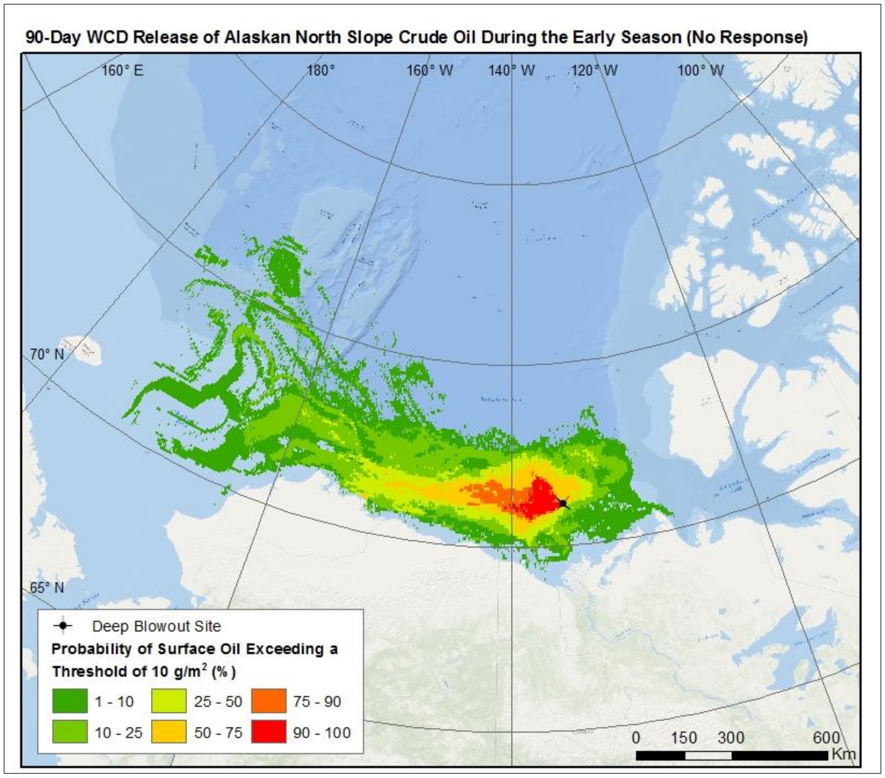

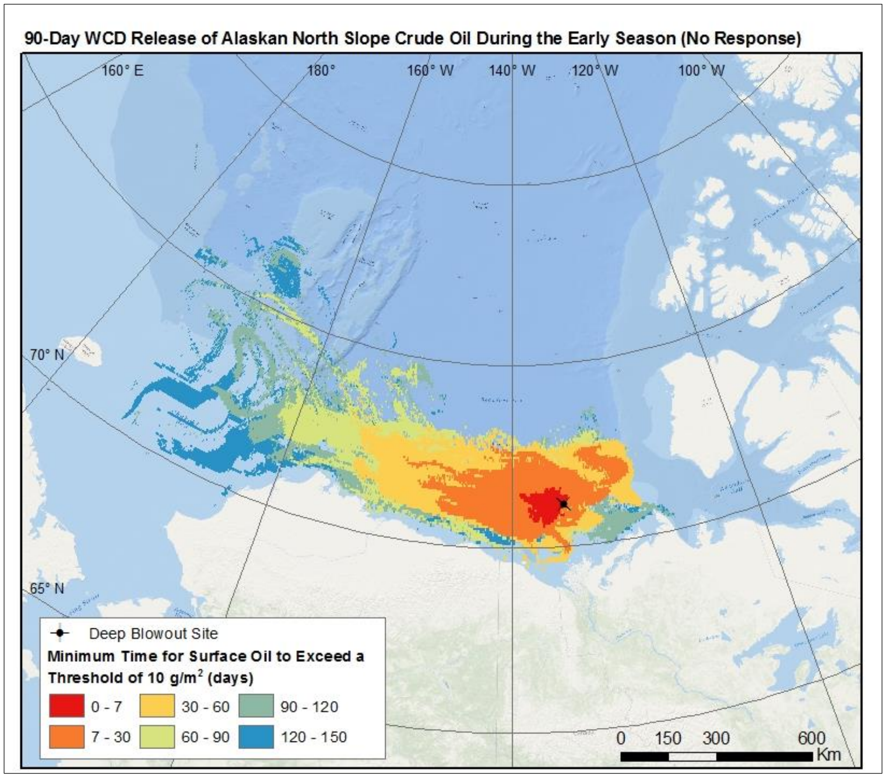

Figure 223. DeepWCD_90rel_noresp_early - Water surface oiling probabilities and minimum travel times for floating oil ≥10 g/m2.

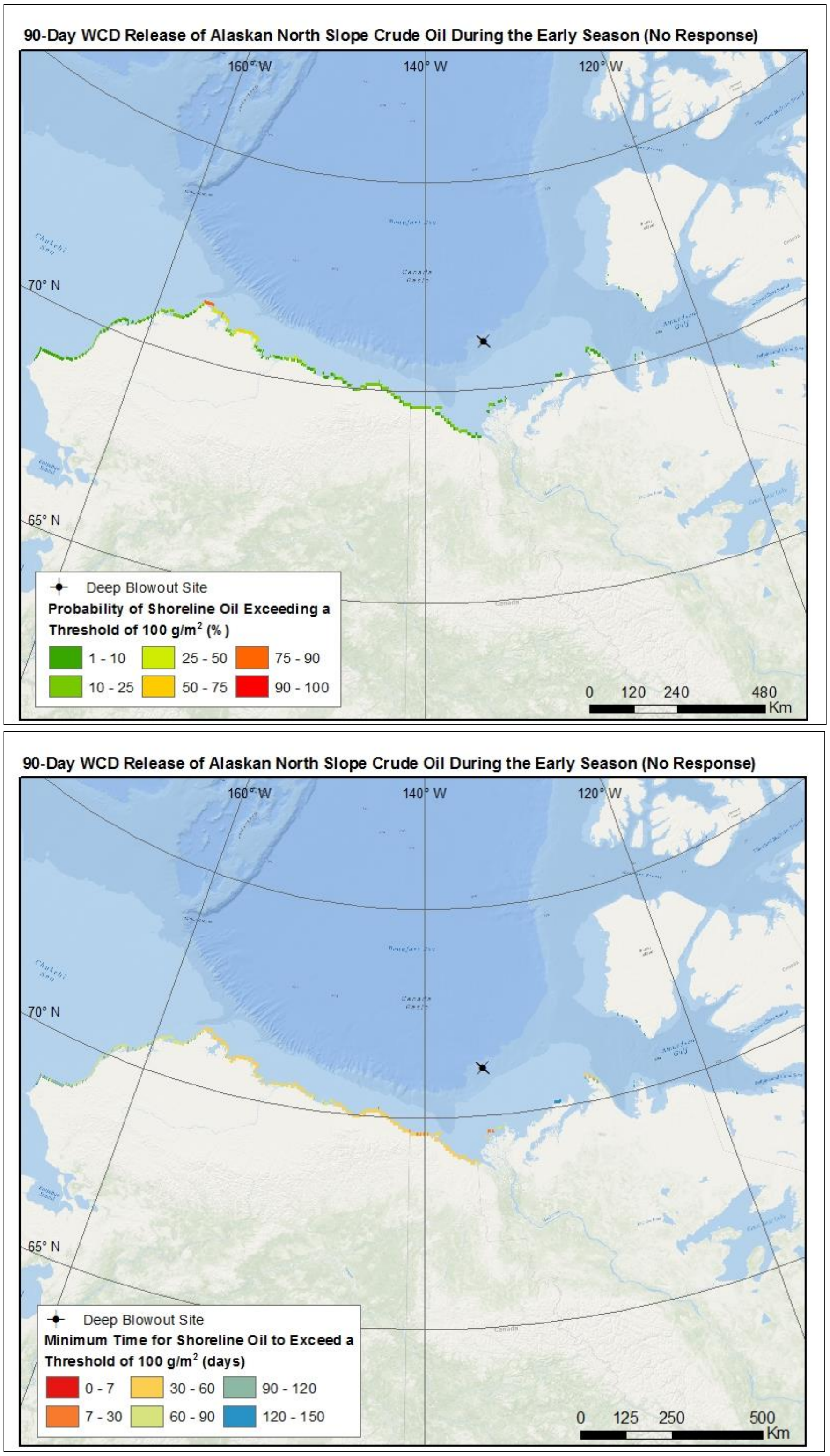

Figure 224. DeepWCD_90rel_noresp_early - Shoreline oiling probabilities and minimum travel times for shoreline oil ≥100 g/m2.

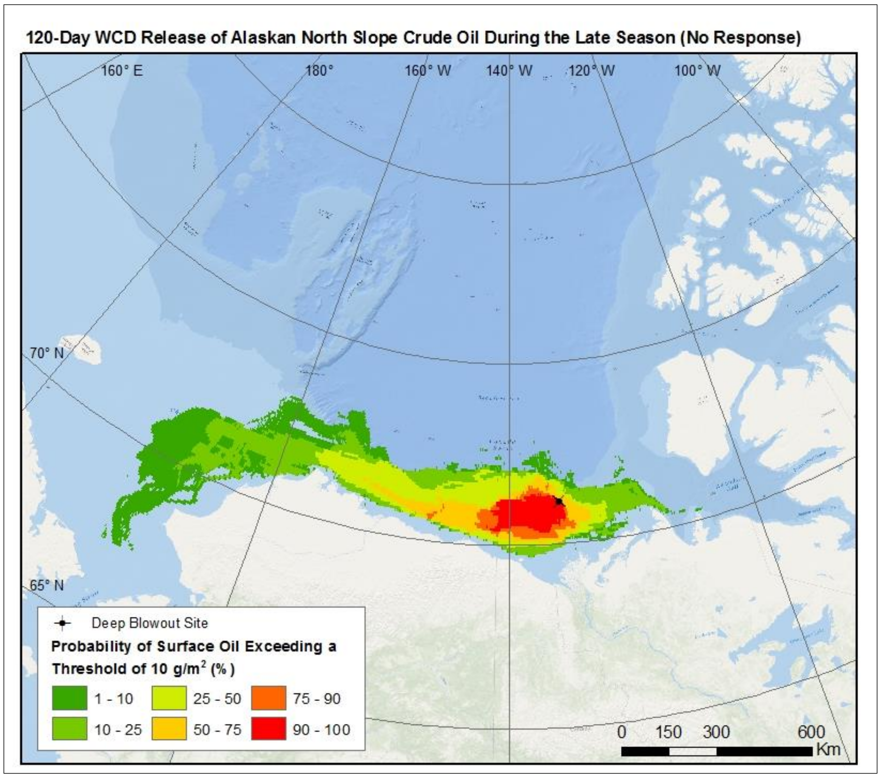

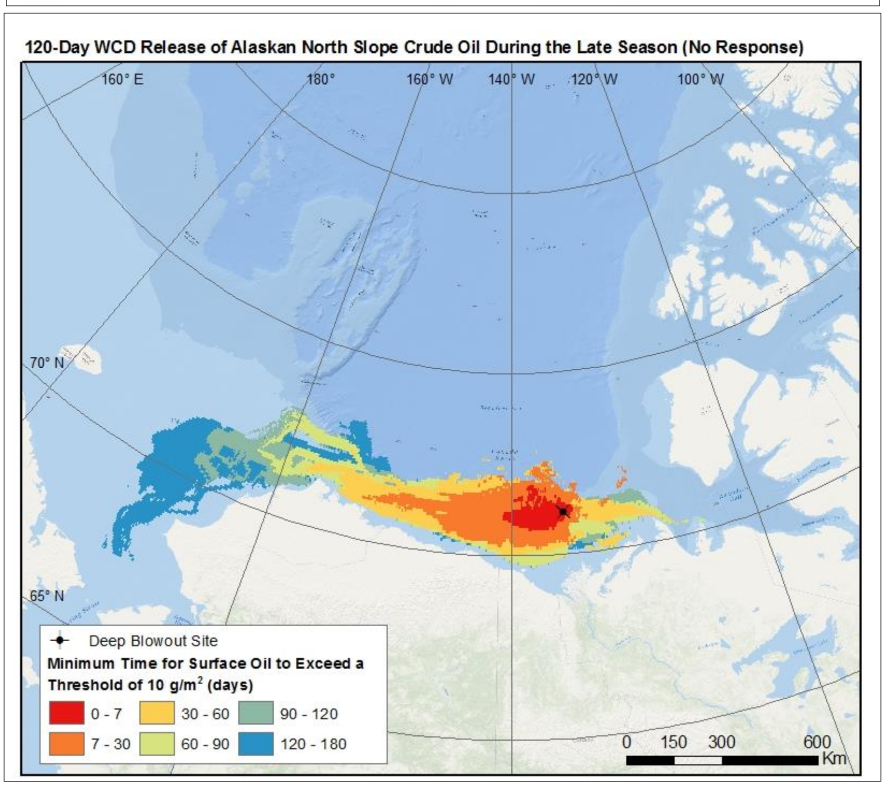

Figure 225. DeepWCD_120rel_noresp_late - Water surface oiling probabilities and minimum travel times for floating oil ≥10 g/m2.

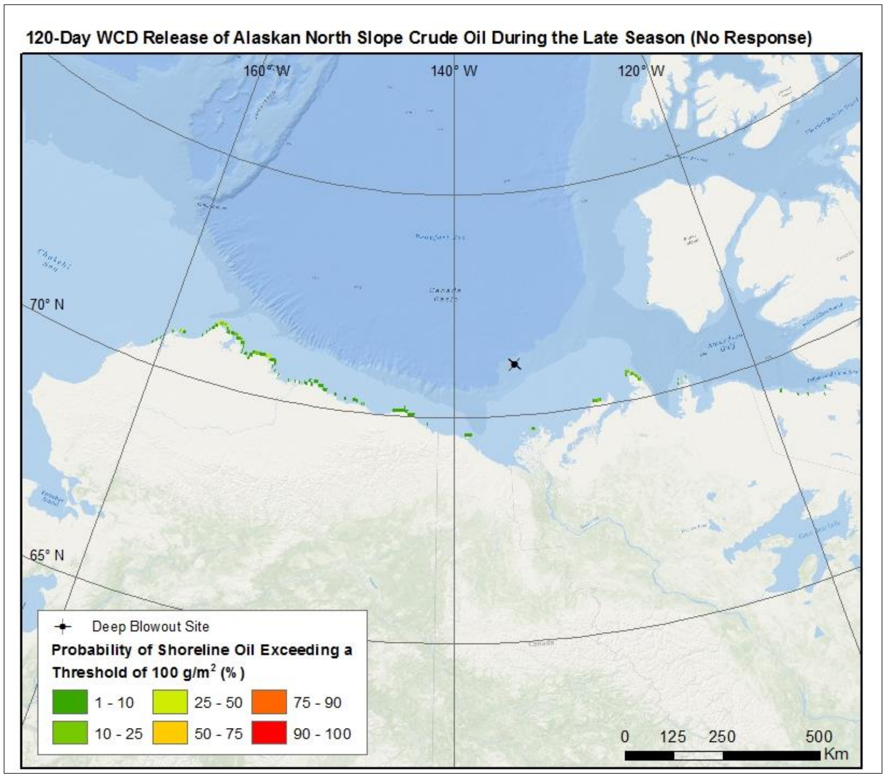

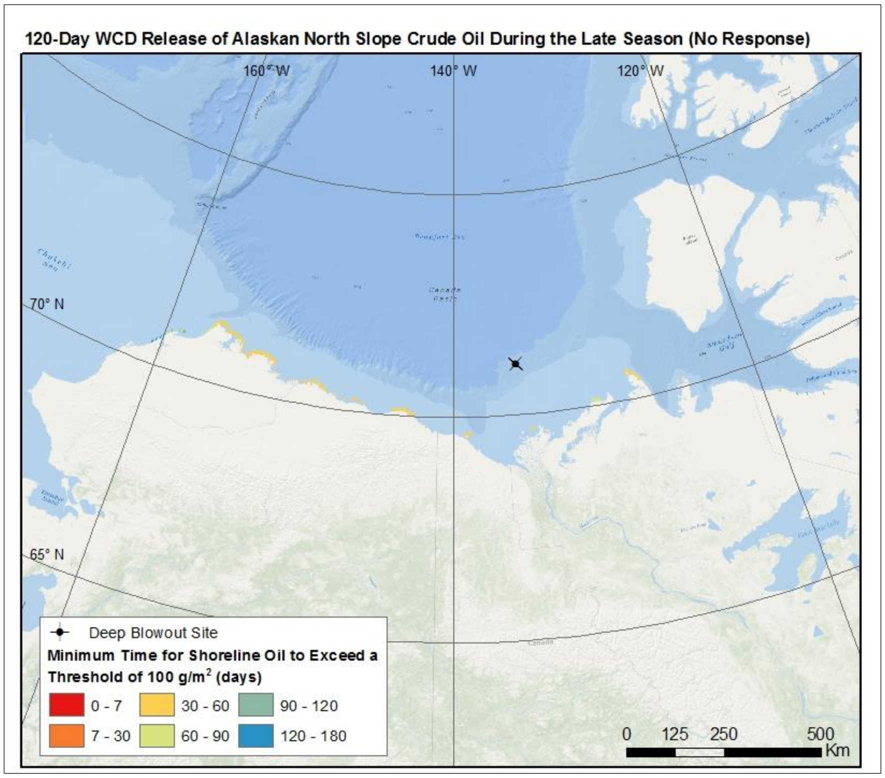

Figure 226. DeepWCD_120rel_noresp_late - Shoreline oiling probabilities and minimum travel times for shoreline oil ≥100 g/m2.

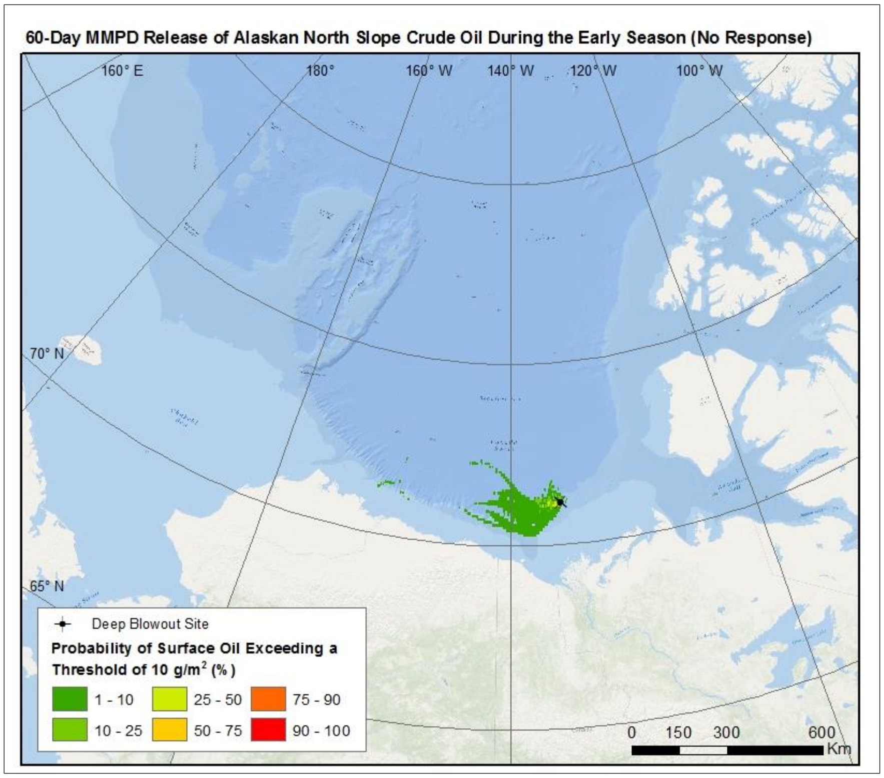

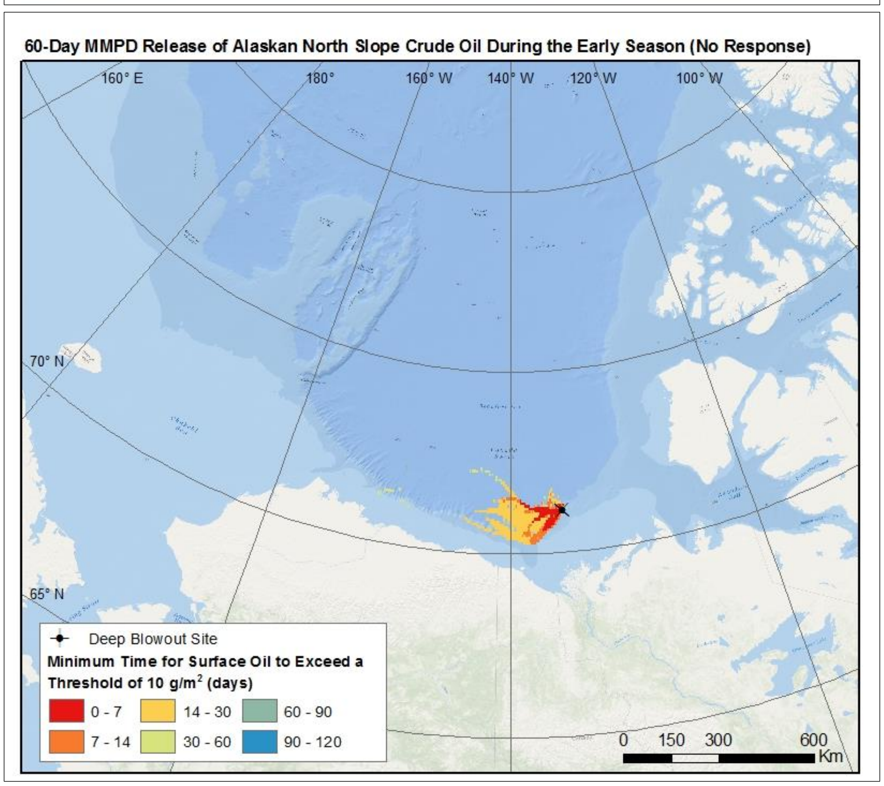

Figure 227. DeepMMPD_60rel_noresp_early - Water surface oiling probabilities and minimum travel times for floating oil ≥10 g/m^2.

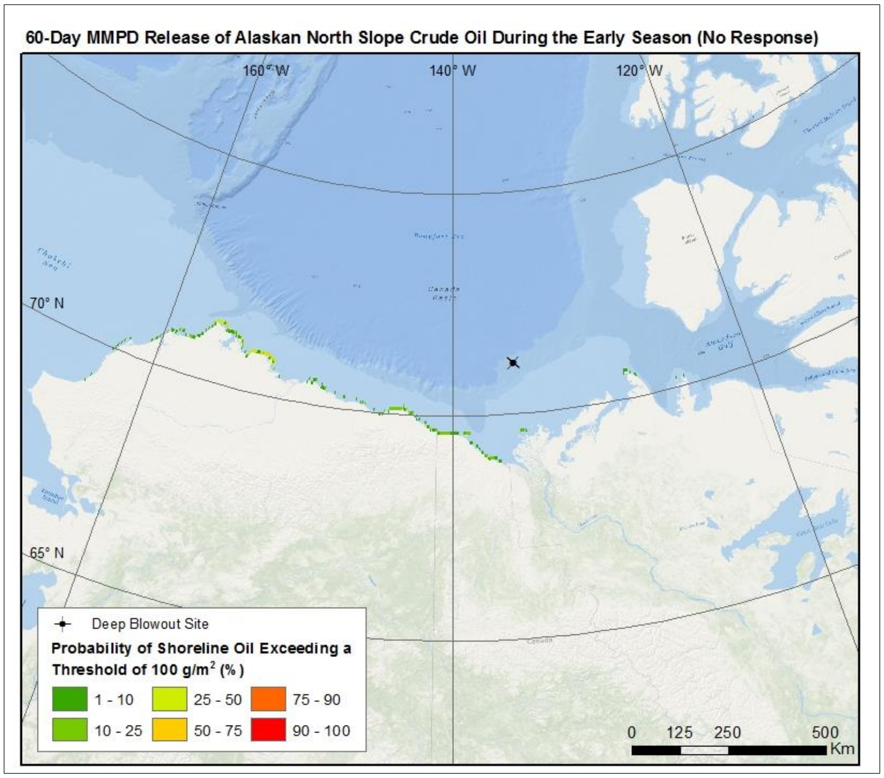

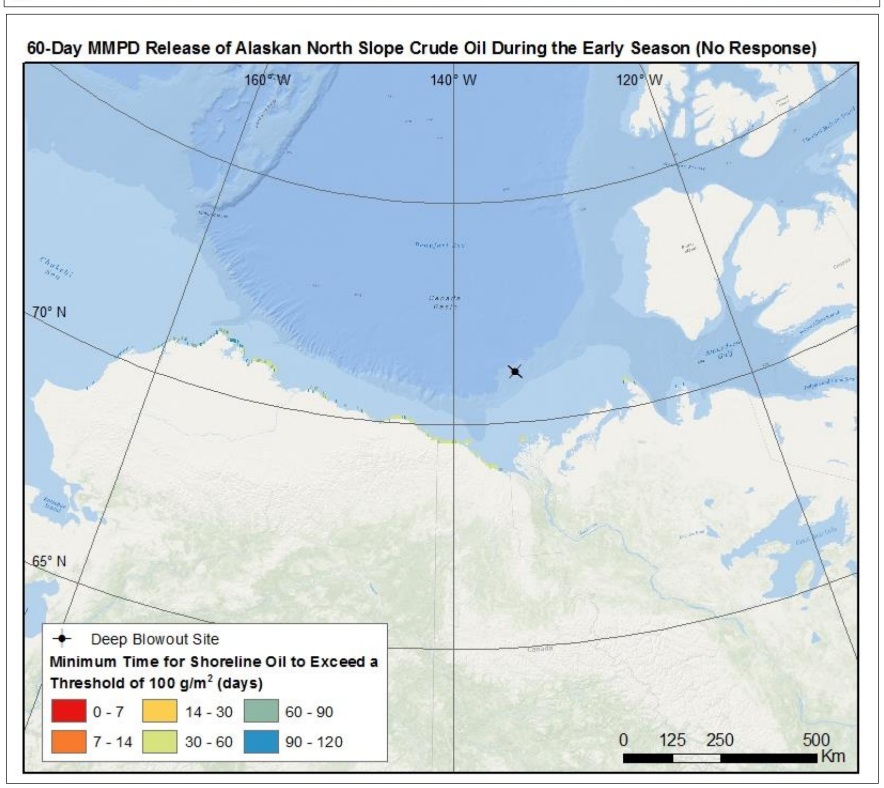

Figure 228. DeepMMPD_60rel_noresp_early - Shoreline oiling probabilities and minimum travel times for shoreline oil ≥100 g/m^2.

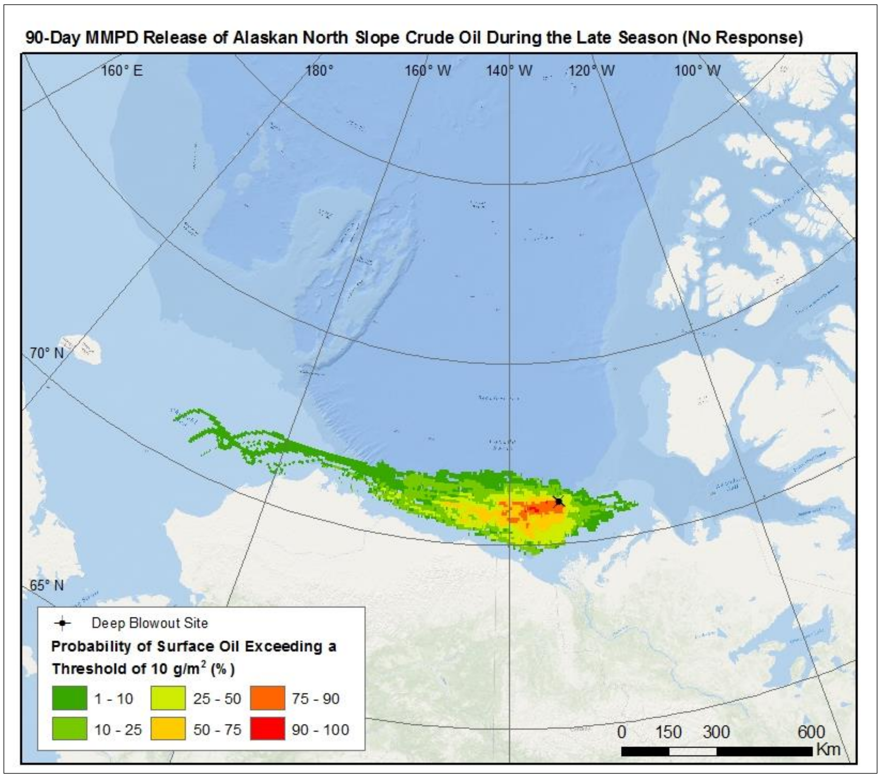

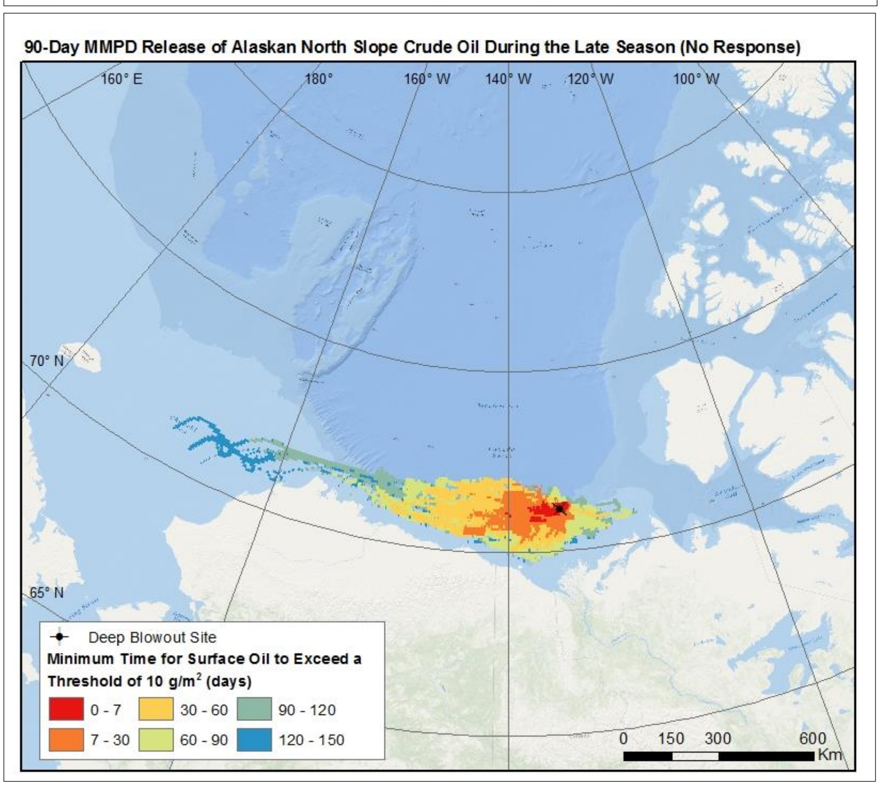

Figure 229. DeepMMPD_90rel_noresp_late - Water surface oiling probabilities and minimum travel times for floating oil ≥10 g/m^2.

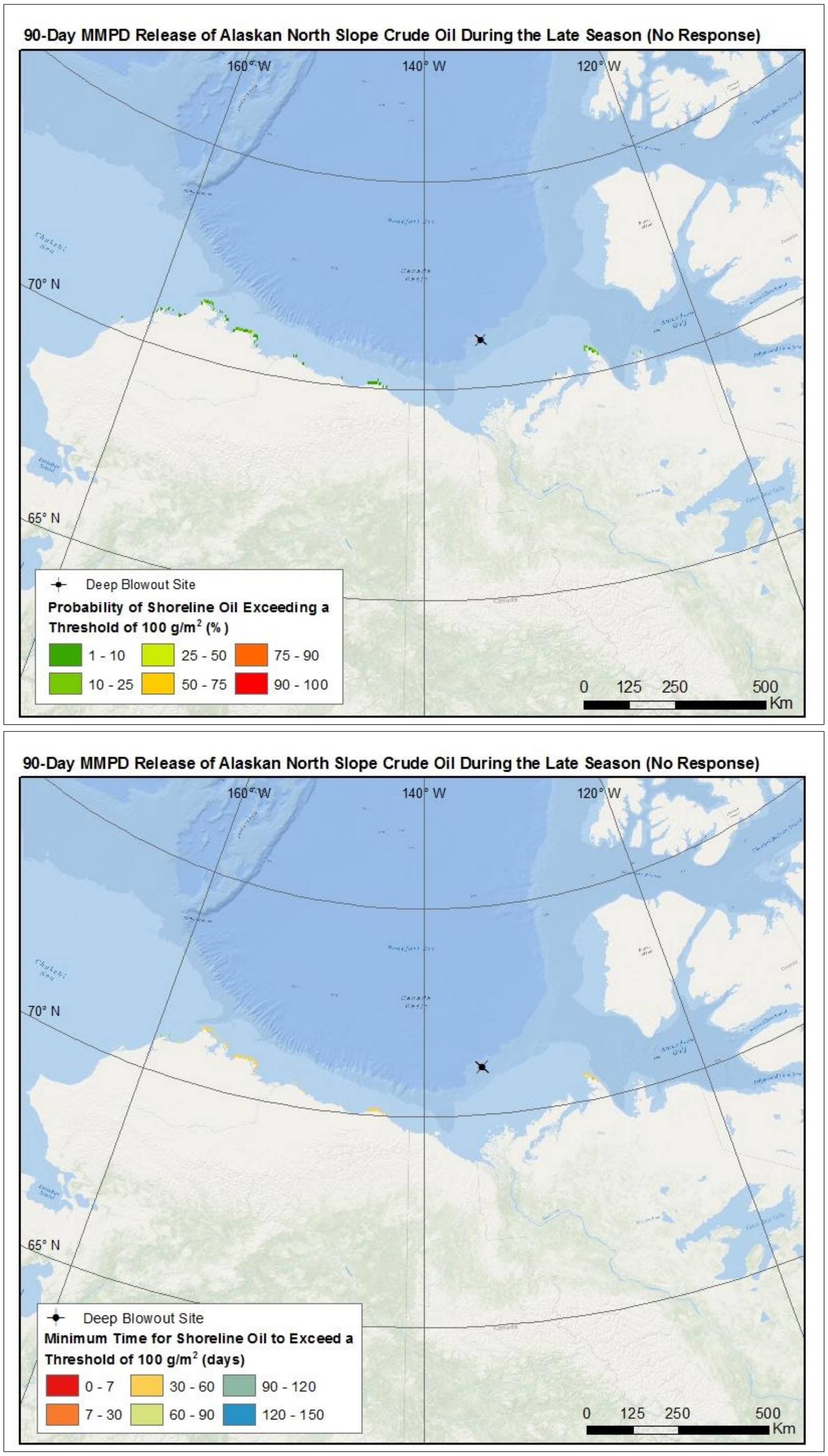

Figure 230. DeepMMPD_90rel_noresp_late - Shoreline oiling probabilities and minimum travel times for shoreline oil ≥100 g/m^2.